ISSN 1816-8957

Volume 33, issue 2

Scientific Drilling

Reports on Deep Earth Sampling and Monitoring

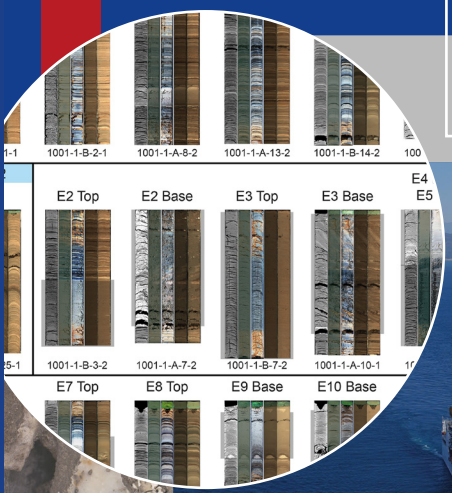

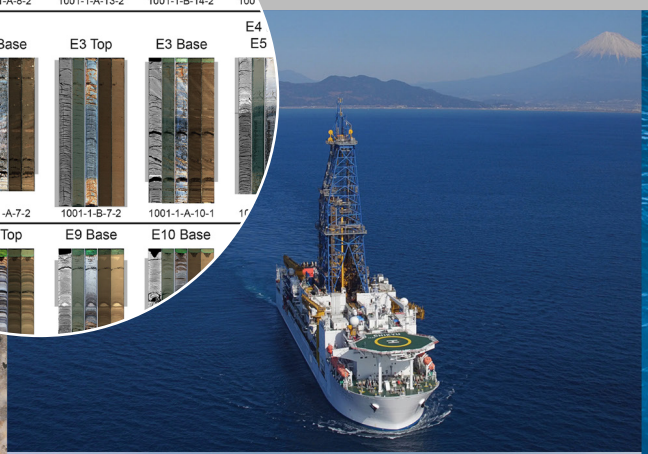

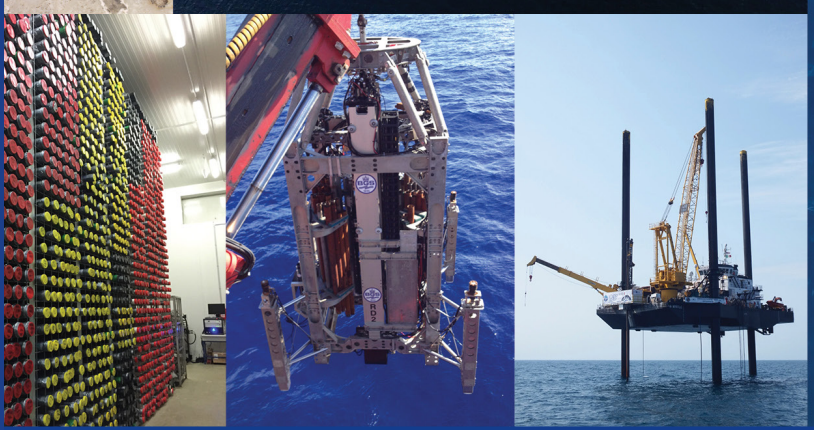

ICDP workshop on the Deep Drilling in the Turkana Basin 93

Paleozoic Equatorial Records of Melting Ice Ages (PERMIA) 109

Drilling of Barberton Archean Surface Environments (BASE) 129

A borehole strainmeter array along the Alto Tiberina Fault 173

Drilling the Overdeepened Valleys (DOVE): results from the Tannwald Basin site 191

Workshop report on Afar Dallol Drilling 207

Active seismic surveys in preparation for Drilling the Ivrea–Verbano zonE (DIVE) 219

Crosshole seismic experiments at the ICDP DOVE site Tannwald Basin 237

ICDP workshop on the Fucino paleolake project 249

Aims & scope

Scientific Drilling (SD) is a multidisciplinary journal focused on bringing the latest science and news from the scientific drilling and related programmes to the geosciences community. Scientific Drilling delivers peer-reviewed science reports from recently completed and ongoing international scientific drilling projects. The journal also includes reports on engineering developments, technical developments, workshops, progress reports, and news and updates from the community.

Editorial board

Additional information

ISSN 1816-8957 | eISSN 1816-3459

Copernicus Publications
Bahnhofsallee 1e
37081 Göttingen
Germany
Phone: +49 551 90 03 39 0
Fax: +49 551 90 03 39 70

editorial@copernicus.org
production@copernicus.org

https://publications.copernicus.org

View the online library or learn more about Scientific Drilling on:
www.scientific-drilling.net

Cover figure: The International Ocean Drilling Programme (IODP[3]) (p. 89).
Insert 1: Compilation of drilling core images from L. Hallstatt (p. 1).
Insert 2: Electron backscatter images of spherules from Wilson Lake and Millville (p. 47).

Contents

93 **ICDP workshop on the Deep Drilling in the Turkana Basin project: exploring the link between environmental factors and hominin evolution over the past 4 Myr**
Catherine C. Beck et al.

109 **Paleozoic Equatorial Records of Melting Ice Ages (PERMIA): calibrating the pace of paleotropical environmental and ecological change during Earth's previous icehouse**
Jonathan M. G. Stine et al.

129 **BASE (Barberton Archean Surface Environments) – drilling Paleoarchean coastal strata of the Barberton Greenstone Belt**
Christoph Heubeck et al.

173 **A strainmeter array as the fulcrum of novel observatory sites along the Alto Tiberina Near Fault Observatory**
Lauro Chiaraluce et al.

191 **Shaped and filled by the Rhine Glacier: the overdeepened Tannwald Basin in southwestern Germany**
Bennet Schuster et al.

207 **Workshop report: Afar Dallol Drilling – ONset of sedimentary processes in an active rift basin (ADD-ON)**
Anneleen Foubert et al.

219 **Active seismic surveys for drilling target characterization in Ossola Valley: International Continental Scientific Drilling Program (ICDP) project Drilling the Ivrea–Verbano zonE (DIVE) phase I**
Andrew Greenwood et al.

237 **A comprehensive crosshole seismic experiment in glacial sediments at the ICDP DOVE site in the Tannwald Basin**
Sarah Beraus et al.

249 **International Continental Scientific Drilling Program (ICDP) workshop on the Fucino paleolake project: the longest continuous terrestrial archive in the MEditerranean recording the last 5 Million years of Earth system history (MEME)**
Biagio Giaccio et al.

Sci. Dril., 33, 93–108, 2024
https://doi.org/10.5194/sd-33-93-2024

Scientific Drilling
Open Access

ICDP workshop on the Deep Drilling in the Turkana Basin project: exploring the link between environmental factors and hominin evolution over the past 4 Myr

Catherine C. Beck[1], Melissa Berke[2], Craig S. Feibel[3,4], Verena Foerster[5], Lydia Olaka[6,7], Helen M. Roberts[8], Christopher A. Scholz[9], Kat Cantner[10], Anders Noren[10], Geoffery Mibei Kiptoo[11], James Muirhead[12], and the Deep Drilling in the Turkana Basin (DDTB) project team✚

[1]Geosciences Department, Hamilton College, Clinton, NY 13323, USA
[2]Department of Civil and Environmental Engineering and Earth Sciences, University of Notre Dame, Notre Dame, IN 46556, USA
[3]Department of Earth and Planetary Sciences, Rutgers University, Piscataway, NJ 08854, USA
[4]Department of Anthropology, Rutgers University, New Brunswick, NJ 08901, USA
[5]Institute of Geography Education, University of Cologne, 50931 Cologne, Germany
[6]Department of Geoscience and Environment, School of Physics and the Environment, The Technical University of Kenya, P.O. Box 52428-00200, Nairobi, Kenya
[7]Department of Earth and Climate Sciences, Faculty of Science and Technology, University of Nairobi, P.O. Box 30197, Nairobi, Kenya
[8]Department of Geography and Earth Sciences, Aberystwyth University, Aberystwyth, Wales, SY23 3DB, UK
[9]Department of Earth and Environmental Sciences, Syracuse University, Syracuse, NY 13244, USA
[10]Continental Scientific Drilling Facility, University of Minnesota, Minneapolis, MN 55455, USA
[11]National Renewable Energy Laboratory, Golden, CO 80401, USA
[12]School of the Environment, University of Auckland, Tāmaki Makaurau / Auckland, New Zealand
✚A full list of authors appears at the end of the paper.

Correspondence: Catherine C. Beck (ccbeck@hamilton.edu)

Received: 2 December 2023 – Revised: 3 April 2024 – Accepted: 11 April 2024 – Published: 17 June 2024

Abstract. Scientific drill cores provide unique windows into the processes of the past and present. In the dynamic tectonic, environmental, climatic, and ecological setting that is eastern Africa, records recovered through scientific drilling enable us to look at change through time in unprecedented ways. Cores from the East African Rift System can provide valuable information about the context in which hominins have evolved in one of the key regions of hominin evolution over the past 4 Myr. The Deep Drilling in the Turkana Basin (DDTB) project seeks to explore the impact of several types of evolution (tectonic, climatic, biological) on ecosystems and environments. This includes addressing questions regarding the region's complex and interrelated rifting and magmatic history, as well as understanding processes of sedimentation and associated hydrothermal systems within the East African Rift System. We seek to determine the relative impacts of tectonic and climatic evolution on eastern African ecosystems. We ask the follow questions: what role (if any) did climate change play in the evolution of hominins? How can our understanding of past environmental change guide our planning for a future shaped by anthropogenic climate change?

To organize the scientific community's goals for deep coring in the Turkana Basin, we hosted a 4 d ICDP supported workshop in Nairobi, Kenya, in July 2022. The team focused on how a 4 Myr sedimentary core from the Turkana Basin will uniquely address key scientific research objectives related to basin evolution, paleoclimate, paleoenvironment, and modern resources. Participants also discussed how DDTB could collaborate with community partners in the Turkana Basin, particularly around the themes of access to water and education. The team concluded that collecting the proposed Pliocene to modern record is best accomplished through a two-phase

drilling project with a land-based transect of four cores spanning the interval from 4 Ma to the Middle–Late Pleistocene (< 0.7 Ma) and a lake-based core targeting the interval from ∼ 1 Ma to present. The second phase, while logistically more challenging due to the lack of drilling infrastructure currently on Lake Turkana, would revolutionize our understanding of a significant interval in the evolution and migration of *Homo sapiens* for a time period not currently accessible from the Kenyan part of the Turkana Basin. Collectively, the DDTB project will provide exceptional tectonic and climatic data directly associated with one of the world's richest hominin fossil localities.

1 Introduction

Questions of who we are, where we came from, and why we are the way we are as a species are among the most fundamental of scientific enquiries. Eastern Africa is crucial for understanding the story of hominin evolution and dispersal due to the richness and extent of the archaeological and fossil records. The Turkana Basin, located in the East African Rift System (EARS) (Fig. 1), is of particular significance with more than 500 hominin fossil discoveries from the region (Wood and Leakey, 2011). Hominin evolution and dispersal has taken place against a backdrop of dramatic changes in the Earth's climate (e.g., Bergström et al., 2021; Mounier and Mirazón Lahr, 2019), resulting in major changes to the environment in which our human ancestors were living. Links between environmental change and human evolution have long been hypothesized (e.g., Vrba et al., 1989), including specific climatic shifts and key events in human evolution, such as early human speciation patterns, brain expansion, and species dispersal (e.g., Shultz and Maslin, 2013), and major revolutions in tool making technology (e.g., deMenocal, 2011; Potts et al., 2020). However the relationship between paleoclimate, paleoenvironment, and hominin evolution and dispersal remains unclear and is a matter of ongoing debate (e.g., Faith et al., 2021). Furthermore, in settings such as the EARS, tectonic influences exert a confounding influence on the record of environmental change. The major factor impeding the exploration of links between the changing environment due to climate and tectonic influences and the existing record of hominin evolution and dispersal is the lack of continuous, high-resolution sedimentary records documenting the changing environment over long timescales, commensurate with those relevant to hominin evolution (Cohen et al., 2022; Russell et al., 2012). Through the proposed Deep Drilling in the Turkana Basin (DDTB) project, we seek to build upon the promising advances made in the past decade by other eastern African continental deep drilling projects with the ambitious goal of recovering a composite core record from 4 Ma to present for the Turkana Basin without temporal gaps. The proposed core record would address major research questions including how tectonic extension in the East African Rift System has shaped the environment and climate of the region through time, the effects of cyclical climatic changes on the environment, and how the evolution of hominins and the ecosystems surrounding them has been shaped by climatic and tectonic drivers.

The primary research goals of the project are as follows:

1. To establish a continuous high-resolution record of climate and environmental variability for the past 4 Myr in the Turkana Basin. This will allow direct comparison with trends and events recorded in the rich paleontological and archaeological record recovered from the basin.

2. *To investigate linkages between tectonic evolution and magmatic development in the basin*. A better understanding of the tectono-magmatic evolution in Turkana will have broad implications for our understanding of this continental rift setting.

3. *To chronicle long-term evolution of the Turkana hydrographic system*. This has critical implications for water development issues in the present and for the development of the Turkana hydrologic network in the past.

4. *To expand our understanding of geothermal systems within the basin*. This is a key area for potential development in the basin and is of significance to understanding thermal signatures in the rock and fossil record.

5. *To track the dynamics of ecological systems within both lacustrine and terrestrial communities in Turkana*. This will help better understand current responses to environmental change, human resource demands, and the broader pattern of long-term response to environmental drivers.

1.1 Tectonic evolution

Extensional tectonic processes in the Turkana Basin play a key role in driving the local topographic variations that affect the distribution of the surface and subsurface hydrology and associated ecosystems in the region. In addition to addressing questions of our own origins in the context of a changing climate, a long core retrieved from the Turkana Basin would give unique insight into the complex tectonic development, fault geometries, and hydrothermal systems within the EARS. Extension in the Turkana Basin is linked to NW–SE-trending Mesozoic–Paleogene rifts overprinted by the younger Oligocene–Miocene to Recent N–S-trending EARS

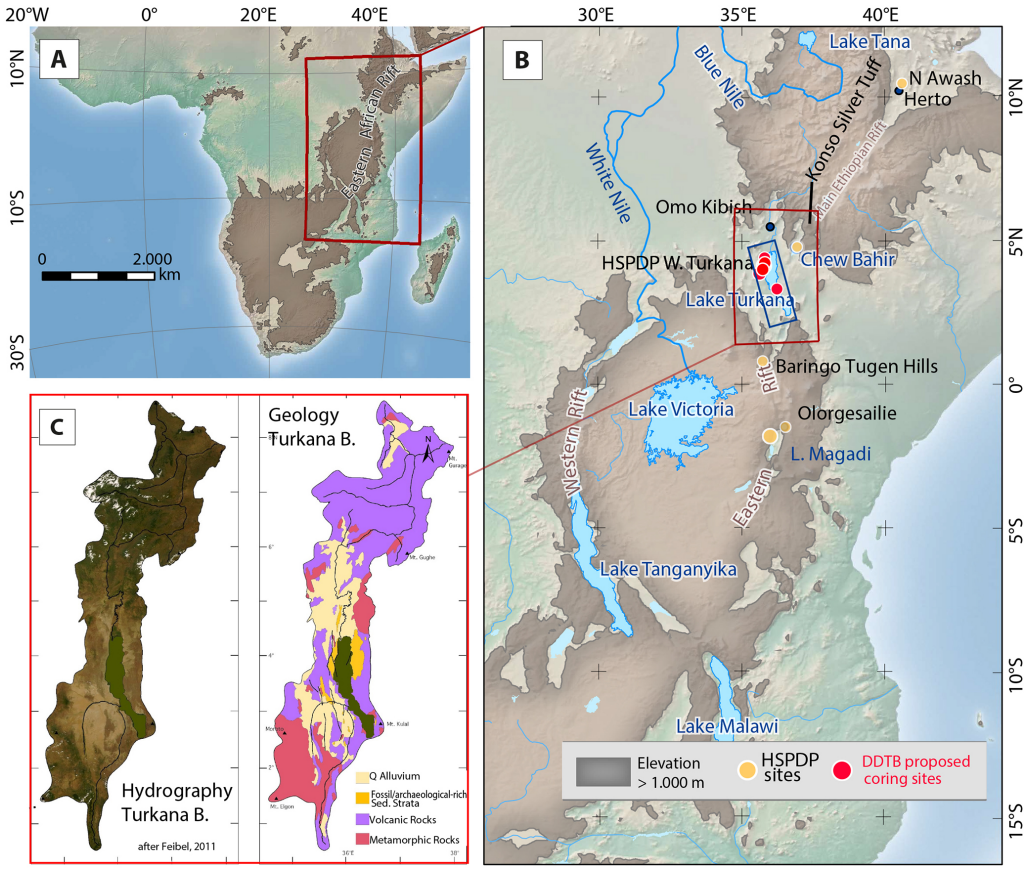

Figure 1. Map of the Turkana Basin (TB) and its location. **(a)** Rift systems and highland areas in excess of 1000 m elevation. **(b)** East African Rift System with major lakes, key archaeological sites, and former HSPDP coring sites discussed in the text. The proposed DDTB drilling sites are marked with red circles. The blue box marks the Turkana region for which seismic reflection profile tracklines are available (Fig. 3). **(c)** The modern Lake Turkana catchment with hydrography and simplified geology (modified after Feibel, 2011).

(Boone et al., 2018a). Thermochronology studies in the region provide evidence for tectonic activity in the Turkana Basin that predates all other sectors of the EARS (Reeves et al., 1987; Foster and Gleadow, 1996; Torres Acosta et al., 2015; Boone et al., 2018a, b), with early volcanism dated at 39.2 Ma prior to the ∼ 31 Ma Ethiopia flood basalt eruptions (Rooney, 2017). Today the Turkana Basin continues to experience rifting (Knappe et al., 2020) and is a classic example of extension in a magma-rich setting, where magmatic activity has been essential in promoting and modulating continental extension and crustal thinning (Muirhead et al., 2022; Rooney et al., 2022). Border faults segment the rift into a series of linked half-graben basins, each ∼ 30–50 km long (Dunkelman et al., 1989). Deep sedimentary sections observed in multichannel seismic (MCS) reflection data thicken towards the border faults, and shallow Late Quaternary sediments thicken towards recently developed axial magmatic segments in the center of rift (Muirhead et al., 2022), indicating ongoing syn-rift sedimentation (Fig. 1).

The Turkana region is a tectonic anomaly within the EARS overall, in that it is a broadly rifted zone that has experienced complex episodes of rifting and magmatism spanning more than 30 Myr (Baker and Wohlenberg, 1971; Cerling and Powers, 1977; Morley et al., 1992, 1999; Haileab et al., 2004; Furman et al., 2004, 2006; Rooney, 2017). Unlike most sectors of the EARS, it is underlain by thin crust and shallow Moho and presumably high heat flow (Wheidon et al., 1994), which makes it an active target for geothermal exploration (Dunkley et al., 1993). Whereas faults elsewhere in the EARS are generally steep and planar, older basins in Turkana (e.g., the Lokichar Basin) display evidence of listric and potentially detachment faulting in places (Morley et al., 1999). The length scales of proposed rift segments are also generally shorter than other areas in the EARS (Ebinger et al., 1999), possibly reflecting the comparatively thinner, warmer crust in the region (Rosendahl et al., 1992). Finally, models for mature continental rifts in the eastern branch (e.g., Ethiopia) suggest that rifting initiates on border faults, but later migrates to intra-rift structures with time (Corti, 2009; Ebinger and Casey, 2001; Keranen et al., 2004; Nutz et al., 2020). This standard model of rift evolution, however, does not apparently apply to older (> 10 Ma) rift segments in Turkana,

which also lack evidence for persistent axial magmatism (e.g., Lokichar and Kerio basin segments; Morley, 2020).

However, recent investigations into fault behavior in the South Turkana Basin reveal evidence for strain focusing into intra-rift fault populations in association with developing axial magmatism beginning in the Middle to Late Pleistocene, consistent with volcano–tectonic patterns observed across the eastern branch generally (Muirhead et al., 2016; Rooney, 2020; Muirhead et al., 2022; Rooney et al., 2022). Although these observations suggest that magmatism has played a critical role in driving the distribution of faulting and development of rift topography in the Turkana Basin in the Late Quaternary, the majority of earlier tectonic activity recorded in Lake Turkana (i.e., prior to 20 ka) is poorly resolved (Morrissey and Scholz, 2014; Muirhead et al., 2022), due in part to the absence of samples of the deep sedimentary section below the lake. Though reflection seismic data reveal that the history and tectonic evolution of continental rifting is likely contained within the stratigraphic sequences of the Turkana Basin (e.g., Dunkelman et al., 1989; Morley et al., 1999; Muirhead et al., 2022), analysis of drill cores, in conjunction with seismic stratigraphic analyses, will enhance and refine our understanding of the tectonic history of this rift system over the last ~ 4 Myr.

1.2 Water and ecological resources

The story of water as a resource in the past and present is at the heart of the Turkana Basin record. The lake has varied in size throughout its existence, regulated by tectonics, volcanism, and climate change, which in turn combine to shape the hydrology and ecosystem functions through time. Modern Lake Turkana is the world's largest desert lake (Ojwang et al., 2016). While the water is not potable for humans (Avery and Eng, 2012; Ojwang et al., 2016) due to a high pH (8.6–9.5) and salinity (ca. 3500 $\mu S\,cm^{-1}$), the health of this water body is essential to the ecosystems services that sustain humans today in the region. In particular, the fisheries industry has become a significant source of food and revenue for the region (Gownaris et al., 2015, and references therein). While traditionally the indigenous people have been pastoralists (Leslie and Fry, 1989), beginning in 1961 and continuing today, Lake Turkana supports a large fishing industry born out of a need to diversify the local economy (Avery, 2010; Bayley, 1982). Overfishing and fishing of juveniles have already stressed key fish species, reducing their resiliency and making populations more vulnerable to the impacts of climate change and human disturbance, particularly in crucial breeding grounds such as Ferguson's Gulf (Hopson, 1982; Avery, 2010; Gownaris et al., 2015). Data on the fish stocks in Lake Turkana are sparse, given the size of the lake and the scant resources available for monitoring efforts (Obiero et al., 2022). Coupling decreasing lake levels with already stressed ecosystems could decimate the fish populations many of the local communities have come to rely upon for food and income (Velpuri et al., 2012; Beck et al., 2021).

A better baseline assessment of how ecosystems have responded to changes in water and sediment input through time is necessary to assess and predict how Lake Turkana will respond to future changes in fluvial input and climate shifts. This information would help inform policy makers and draw attention to the serious issues facing the lake system today. By comparing proxy records of lake conditions, particularly ostracod assemblages, from pre- and post-onset of industrial-scale fishing in 1961 and the Gibe Dam Project construction in 1998, it is possible to evaluate the lake's response to both natural and anthropogenic changes (Beck et al., 2021). Our paleo-baseline from the proposed coring activity would help quantify the hydrological budget to better constrain the role of climate change vulnerability and dry–wet oscillations on human-scale ecosystems through time. Sub-Saharan Africa is one of the most vulnerable regions to future climate change, with widespread and until now uncertain impacts on African environments and society, as predicted by the IPCC reports (IPCC, 2014). The "deep time" perspective allows significant opportunities to test the sensitivity of systems to lake level variability.

Groundwater resources are important in this arid to semi-arid landscape. Groundwater in some regions of the Turkana Basin has been mapped through subsurface geophysics (Gramling, 2013; Nyaberi et al., 2019) but has not yet yielded the much anticipated fresh water resources as the quality does not meet the health guidelines (Rusiniak et al., 2021; Mbugua et al., 2022). In addition, the quality of shallow groundwater in areas of settlement is impacted by anthropogenic contamination (Tanui et al., 2020). Understanding of the groundwater system in the Turkana Basin is complicated by the fact that the tectonic, environmental, and volcanic processes have created discontinuous and heterogeneous aquifers (Olaka et al., 2022). This necessitates using multiple techniques (geophysical, geochemical, and geological) to determine the factors that control groundwater quality, quantity and dynamics. Our project has the potential to contribute to a comprehensive analytical approach which will not only ensure location and sustainable management of groundwater resources for the different needs (domestic, agriculture, industrial) but also help inform the hydrogeological recharge models related to hydrothermal systems, thereby supporting the exploration of geothermal resources.

Deep drilling in the Turkana Basin will provide the archives essential for constraining regional climate controls and hydrological responses, linking the dynamics of faunal/floral communities and cultural development with environmental parameters and spanning the entire range of hominin evolution from ~ 4 Ma to present, covering the full diversity of hominin/human technological (i.e., stone tool) development. A Turkana record of the past also could help the regional and global communities prepare for the challenges

that lie ahead in a future dramatically shaped by unprecedented climate change.

1.3 Geothermal resources

The intricate interplay of volcanism and tectonism in the EARS provides a suitable environment for high heat flow and fault-controlled deep fluid circulation. This is the main reason that the EARS is associated with abundant geothermal resources. Because of the early (39.2 Ma; Rooney, 2017) volcanism and the rifting that followed, the Turkana Basin is a key geothermal resource area of interest in Kenya. Five Quaternary volcanic centers occur in Turkana, including the Korath range; the North Island, Central Island, and South Islands; and the Barrier complex (Bloomer et al., 1989). The Barrier volcanic center is of particular interest to geothermal exploration due to its location and numerous geothermal manifestations including altered ground, fumaroles, caldera structures, and recent volcanic eruptions (Njau et al., 2020).

Exploration of geothermal potential is actively ongoing in the Turkana Basin as Olsuswa Energy owns the geothermal exploration license in the Barrier and has begun surface exploration in the area. The present scientific deep drilling project would be of immense importance to geothermal exploration in the area in several ways. The drill cores obtained will provide high-resolution stratigraphic information of the Turkana Basin, including micro- and macro-subsurface structures. This will guide the development of a quality geothermal drilling prognosis and a better understanding of subsurface permeability through structural analysis from direct core information. The resulting boreholes could also provide important information for calculation of geothermal gradient building on the earlier regional data by Wheildon et al. (1994). In addition, water samples from the drill wells would be key in fluid chemical characterization, geothermometry, and possibly age information, further assisting in understanding the geothermal reservoirs and the areas geothermal conceptual models and hence facilitating geothermal exploration programs. Furthermore, understanding the regional structural and volcanic history is significant as the Turkana Basin is potentially the only region within the Kenya Rift where extensive basalt flows occur, and thus it could provide opportunities in other energy and environmental projects like carbon storage research. As a result, there is a natural linkage between potential scientific drilling and geothermal resource development in the Turkana Basin.

2 Rationale for drilling

The goal of obtaining a long core record linked closely to human origins in Turkana has deep roots, beginning with a US National Science Foundation (NSF) workshop in 1978 (Lewin, 1981). More recently, a continental drilling workshop held in 2011 prioritized drilling of Lake Turkana as one of the most important future targets for addressing outstanding scientific questions in eastern Africa (Russell et al., 2012). The report from this 2011 workshop concluded that future deep drilling of Turkana would integrate well with the then-planned (now successfully executed) Hominin Sites and Paleolake Drilling Project (HSPDP), which cored a short window of the Early Pleistocene lacustrine-dominated sequence in West Turkana (WTK13) (Fig. 1). In April 2018 a workshop supported by the NSF-funded Research Coordination Network (RCN) EarthRates outlined objectives for the next phase of scientific drilling and coring in the Turkana Basin. The goal of the 2018 workshop was to define potential coring targets in the Turkana Basin of interest to the broader scientific community that could contribute to the next decade of scientific discovery about the paleoclimatic and paleoenvironmental context in which our ancestors evolved. The workshop attendees consisted of 12 scientists from the USA (9 participants) and Kenya (3 participants), and an additional 13 participants joined the live stream of the workshop over the 2 workshop days. The group quickly coalesced around the idea of prioritizing recovery of the entire Plio-Pleistocene record in the Turkana Basin. The rationale for this is that the richness of the Turkana Basin fossil record provides the unique opportunity to study the paleoclimatic and paleoenvironmental context surrounding continuous occupation by hominin groups. This has implications for both physical and cultural evolution. Whilst outcrops expose short windows into the archives of the past, they are complicated by their limited temporal range for any given location and obscured through modern soil processes. Only deep drilling can capture the entire, and minimally altered, sedimentary sequence describing the climate and environmental conditions throughout the last 4 Myr of hominin evolution, migration and dispersal.

Data from existing Turkana Basin sediment cores are narrowly focused in terms of temporal scope, coming from three sources (Fig. 2):

1. The Hominin Sites and Paleolakes Drilling Project (HSPDP) drilled a 216 m record from West Turkana (WTK13), recovering an interval from 1.9–1.4 Ma (Cohen et al., 2016; Sier et al., 2017; Lupien et al., 2018, 2020). The cores showed a progression from a deep basin to a lake margin to a delta plain (Beck, 2015). The WTK core provided an unparalleled view of deposition on a dynamic lake margin, enhancing the community's understanding of the scale of hydrologic variability (Beck et al., 2017; Feibel et al., 2017), its impact on hominin evolution (Campisano et al., 2017), and the implications of climate versus tectonic evolution for rift basins (Lupien et al., 2018). There is also thought to be a connection of lake level and enhanced/weakened Indian Ocean monsoon variability. Lupien et al. (2018) found fairly stable hydroclimate conditions responding to changes in insolation using leaf wax δD values during the Early Pleistocene, through previously described fluctuations in lake level at Lake Turkana (e.g., Lepre et

al., 2007; Morrissey and Scholz, 2014). Ultimately, the impact of this 500 000-year core record has been significant, despite its limited duration, highlighting the immense potential and feasibility of additional scientific drilling in the Turkana Basin.

2. A series of terminal Pleistocene and Holocene-aged cores have been collected from modern Lake Turkana (Halfman et al., 1994; Johnson and Malala, 2009; Morrissey and Scholz, 2014; Morrissey et al., 2018). Much past work has focused on trying to connect climate conditions to lake level. While today it is a closed basin lake, during wetter times, including the African Humid Period (Owen et al., 1982; Junginger and Trauth, 2013; Morrissey and Scholz, 2014), the lake likely overflowed at times to the Indian Ocean (> 1.9 Ma; Feibel, 1994; Bruhn et al., 2011) and subsequently into the Nile drainage basin (latest Pleistocene; Johnson and Malala, 2009). Late Pleistocene and Holocene sedimentary reconstructions also show a temperature response to the end of the African Humid Period, linked to local insolation changes (Berke et al., 2012; Morrissey et al., 2018). Seismic reflection data suggest that there may have been multiple episodes of lake level draw-down and desiccation in the Quaternary (Dunkelman et al., 1989; Morrissey and Scholz, 2014; Hargrave et al., 2014), perhaps similar to Pleistocene low lake stages in other parts of Africa (e.g., Cohen et al., 2007; Scholz et al., 2007). The timing of these low stages and any relationship to those major climate episodes identified elsewhere in eastern Africa are however unknown.

3. Finally, active oil exploration has led to the drilling of numerous deep wells in the Turkana Basin. However, the target of these wells was Miocene- to Oligocene-aged sediments, and for cost reasons, these wells were not cored, so only cuttings exist. However, in 2021, team member Isaiah Nengo (deceased) facilitated a non-disclosure agreement, allowing the DDTB team access to the extensive seismic data collected between 2011 and 2014 across the basin (Fig. 3).

Ultimately, only by returning to Turkana through the proposed Deep Drilling in the Turkana Basin project can the record of climate and landscape evolution be fully resolved (Fig. 2). By targeting a continuous 4 Myr of sediment, this project will enable us to minimize the complicating factors of both spatial variability and modification by modern soil forming processes inherent in using outcrops to reconstruct change through time.

3 Turkana Basin: an unparalleled link to paleoanthropology and humans

For more than half a century the Turkana Basin has been central to our understanding of hominin evolution and cultural development in eastern Africa (Isaac and Isaac, 1997; Roche et al., 2004; Wood and Leakey, 2011). The extremely rich fossil assemblages spanning the Plio-Pleistocene include the earliest australopithecines from around 4 Ma; early examples of the *Paranthropus* lineage from ca. 2.5 Ma; and a diverse assemblage of early *Homo* fossils beginning prior to 2 Ma, including the nearly complete skeleton of *Homo erectus*, the Turkana Boy at 1.4 Ma. These hominin specimens are complemented by a suite of archaeological assemblages ranging from the earliest known stone tools at Lomekwi (3.3 Ma; Harmand et al., 2015); early Acheulean at Kokiselei (1.7 Ma; Lepre et al., 2011); and a wide variety of lithic traditions from Koobi Fora, the lower Omo Valley, and West Turkana. This unsurpassed record of early human development is associated with a huge collection of fossils representing the savanna community in the basin throughout the Plio-Pleistocene (Bobe, 2011). The entire record has been contextualized by complex sedimentary records from extensive outcrops (Brown and Feibel, 1991; Harris et al., 1988) and the limited coring efforts to date. Capping off the unique nature of the Turkana Basin record, the Plio-Pleistocene sequence is punctuated by abundant widespread tephra markers which can be geochemically correlated and many of which have associated radiometric dates (Brown et al., 2006). Thus

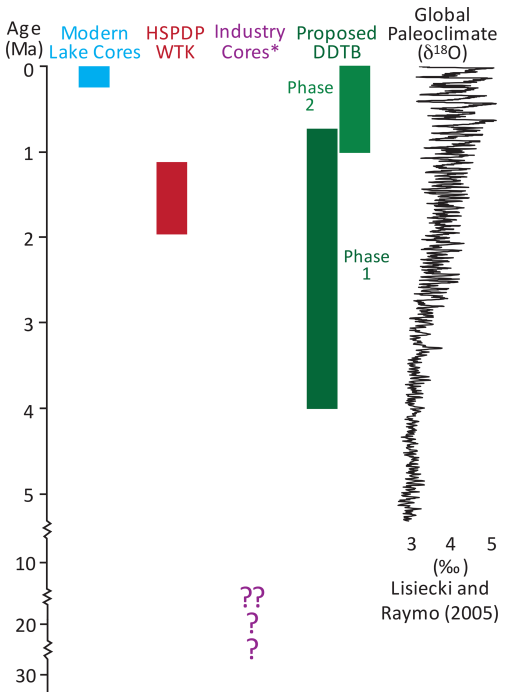

Figure 2. Summary of time periods covered by existing cores from the Turkana Basin and those spanned by the proposed DDTB record plotted with the global paleoclimate benthic stack (Lisiecki and Raymo, 2005). The proposed DDTB record will fill significant gaps in the understanding of the continental paleoclimate response to global forcing in the Turkana Basin. * Note that industry data are predominantly cuttings, not continuous core.

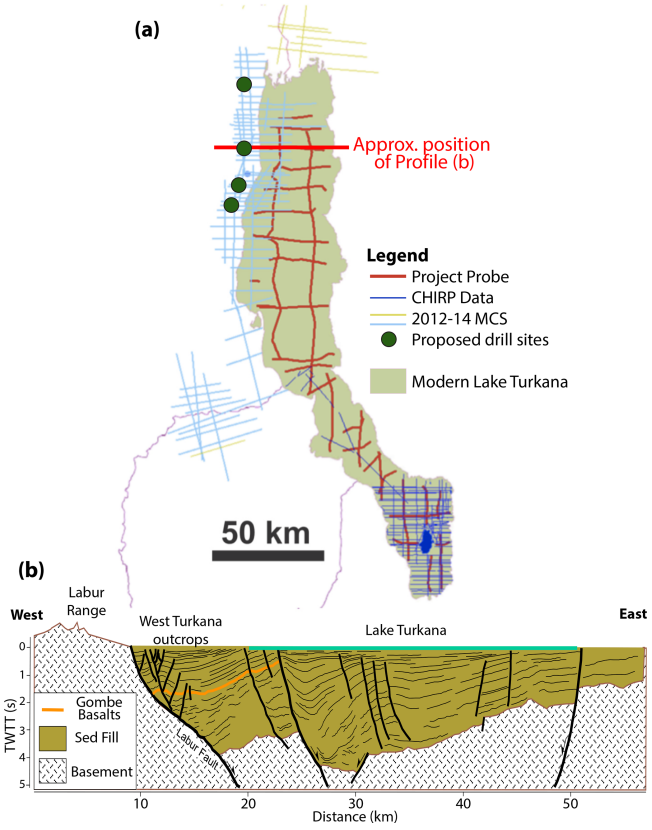

Figure 3. **(a)** Outline of Lake Turkana with locations of available seismic reflection tracklines. Red lines denote legacy offshore multichannel seismic reflection profiles collected in 1984 by Project PROBE of Duke University. Dark-blue lines indicate high-resolution CHIRP seismic reflection profiles acquired by Syracuse University in 2009–2011. Light-blue lines are commercial seismic profiles acquired during hydrocarbon exploration in the Turkana Rift and include land, transition-zone, and offshore reflection data. **(b)** Interpreted seismic profile across the basin. Profile redrawn and simplified from Nutz et al. (2022). The targeted sequence for onshore drilling will exploit the West Turkana outcrop belt, with staggered holes extending down to ca. 4 Ma (Gombe Basalts).

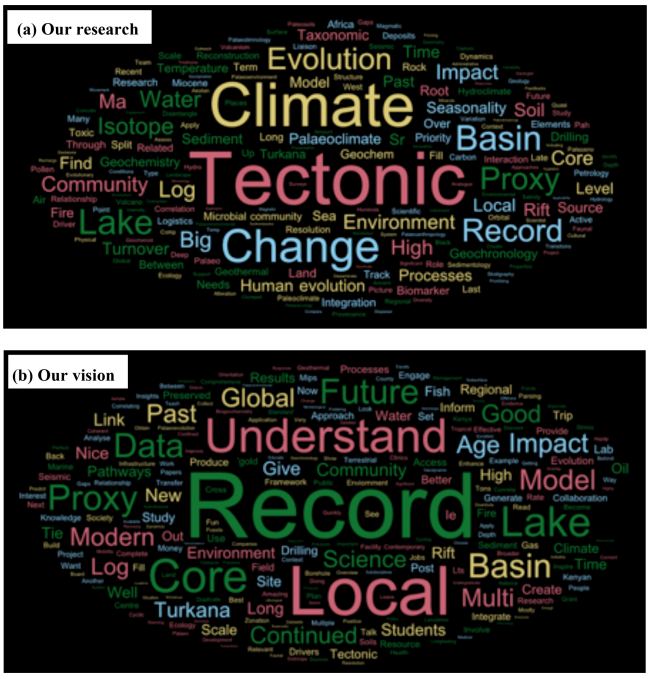

Figure 4. Word clouds reflecting **(a)** the broad variety of scientific topics and expertise in the community represented during the ICDP workshop and **(b)** the aims of participants along the five key topics in the project applied to DDTB, namely (i) basin evolution; (ii) paleoclimate; (iii) paleoenvironment; (iv) modern systems; and (v) outreach, capacity building and education.

the legacy of crucial discoveries in hominin evolution can be directly and precisely integrated with a high-resolution continuous core record and all of the signals of climatic drivers, tectonic effects, and landscape evolution we can extract from that sediment archive.

4 Workshop structure and findings

We convened a series of three events to solicit input on defining scientific priorities and strategies from the broader scientific community. With the repercussions of COVID still making travel complicated, particularly from certain countries/regions, and seeking to be as inclusive as possible even beyond those impacted by COVID restrictions, we opted to bracket our in-person workshop with online meetings. The online meetings enabled all interested applicants to initiate potential key discussions before the meeting, revise central themes right after the meeting, and also to incorporate team members who could not attend in-person, thereby expanding the participation base for DDTB.

The in-person International Continental Scientific Drilling Program (ICDP) workshop was held in Nairobi, Kenya, between 11–14 July 2022. It was attended by 38 participants from nine countries, representing 30 institutions/organizations (universities, government agencies, and private sector, etc.) and the broad variety of research foci in the community (outlined in Fig. 4a). Of this group, 52 % of the participants were women, and 32 % were Kenyan. We discussed the unique opportunities for cutting-edge science offered by a long, continuous sedimentary core from Turkana Basin and developed hypotheses that can be advanced and tested only through long scientific drill cores. These hypotheses focus primarily on the ICDP theme of environmental change, but the community also engaged in discussion of georesources, specifically potable water, fisheries, and geothermal energy. Logistics and potential drill sites were discussed, as were technical requirements and strategies to prepare for full drilling and scientific funding proposals. The first day of the workshop began with presentations on the evolution of the paleoenvironment, paleoclimate, tectonics, and hominins as

recorded in the Turkana Basin. The modern limnology and its relationship to ecosystems were also discussed. From there, we tasked participants with "dreaming big" ("our vision" in Fig. 4b) through a series of breakout activities to imagine what the ideal project and collaboration structure would look like from both a science and outreach perspective in order to make sure all perspectives and approaches were heard at this stage. This culminated in collecting feedback and compiling that feedback into clusters centered around emerging themes, both in terms of scientific goals but also broader impacts and project team structure (Fig. 4). The five major topics addressed by DDTB and worked on by breakout groups during the workshop were (i) basin evolution; (ii) paleoclimate; (iii) paleoenvironment; (iv) modern systems; and (v) outreach, capacity building and education. These thematic topics and the research questions that could be addressed through the strategic acquisition of deep scientific drill cores from Turkana Basin are discussed further in the following sections.

The in-person workshop in Nairobi also included an excursion to the National Museums of Kenya where we saw and learned more about the significant paleoanthropological finds that originated from the Turkana Basin. As centering the theme of environmental change around the rich hominin fossil record and associated ecosystems from the Turkana Basin is one of the unique elements of DDTB, seeing the actual fossils helped the team more fully develop the linkages between the disciplines of paleoanthropology and the geosciences.

4.1 Drilling plan

The goal of DDTB is to drill a continuous, high-resolution sedimentary record from the Pliocene to present (4–0 Ma) through strata of the Omo Group (Plio-Pleistocene) and Turkana Group (Late Quaternary). Sediment accumulation rates in the basin are spatially variable but average 15 cm kyr^{-1}, up to 100 cm kyr^{-1}, in thickened sequences on shore (Feibel, 1988) and more than 1 m kyr^{-1} in offshore Late Quaternary cores (Morrissey and Scholz, 2014). We will target the thicker packages as interpreted from seismic data, while avoiding settings prone to discontinuities and sedimentary gaps. Based on comparative composite sections from outcrop (Feibel, 2011) and the newly acquired industry seismic reflection data (Fig. 3), a $\sim$ 1500 m composite core length is required to recover this interval. From our DDTB scientific workshop, we developed a two-phase drilling plan to recover the sedimentary record from 4 Ma to present from the Turkana Basin. Phase 1 of DDTB is focused on the time interval from 4 to < 0.7 Ma from an on-land offset drilling transect of cores along the northwestern edge of modern Lake Turkana (Fig. 1). This transect will sample the full sedimentary section of the Turkana Basin and enable the team to apply a multi-proxy approach to reconstructing the paleoenvironment, paleovegetation, and paleoclimate during a period of great diversity in hominins. Because much of this interval is also exposed in weathered outcrops which yield fossils and archaeology, we will be able to directly tie the proposed high-resolution proxy records in with known paleoanthropological sites. This will be achieved through a sequence of four single- or double-cored $\sim$ 400 m holes, positioned youngest to oldest from north to south (Fig. 1b). This transect will enable the project to recover this interval most cost-effectively by minimizing operational costs, as smaller rigs, shallower boreholes, and industry-standard coring tools will allow recovery of a complete sequence in offset locations. The project will leverage the experience from HSPDP in 2013 (Cohen et al., 2016) to design a drilling program with significantly improved likelihood of success. This approach avoids major cost increases associated with the engineering and operational requirements to drill fewer, deeper boreholes and the potential for compromised core datasets due to high geothermal gradients in this region. Long seismic reflection survey lines along structural strike provide the basis for determining the depth needed at each location to yield the overlap in core sequences for correlation and integration. The team will leverage the well-documented tephrostratigraphic record from Turkana (Brown and McDougall, 2011) and multi-proxy core scanning data to correlate this transect of cores into a synthetic record that ties tightly with the archaeological and paleoanthropological record from the Turkana Basin.

Phase 2 of DDTB targets the most recent $\sim$ 1 Myr of sediment from a core drilled in modern Lake Turkana that extends to the present day (Fig. 1b) and provides a $\sim$ 300 kyr overlap with the land based record from Phase I of DDTB to ensure a continuous record when the drill cores from both phases are combined. This record will provide a hitherto unseen look into the Turkana Basin during the interval of time from $\sim$ 700–20 kyr which is rarely exposed in outcrops from the Kenyan sedimentary record (McDougall et al., 2008; Manthi et al., 2018). We know very little about what the Turkana Basin looked like (including fundamental questions like whether a lake was present) for this key corridor of hominin migration and the evolution of *Homo sapiens* (Cohen et al., 2022; Foerster et al., 2022). A record of the past million years from Turkana will also create opportunities to incorporate this critical region into broader Afro-Syrian Rift synthesis, leveraging a wealth of data from other completed and planned ICDP projects. Phase 2 will be accomplished through drilling at one or more sites double- or triple-cored to $\sim$ 400–500 m sediment depth, positioned in the Central Basin of Lake Turkana in 20–60 m water depth, using drilling tools and protocols proven in numerous past ICDP lake drilling campaigns. Both legacy and new seismic reflection data from industry, including continuous onshore-offshore lines (Fig. 3), confirm the continuity of subsurface units and provide confidence that the stratigraphy can be correlated between these locations to allow a complete sequence

to be developed most effectively through an offset drilling program.

4.2 Scientific agenda

Continental drilling for core retrieval is essential in the Turkana Basin in order to advance the state of the science, particularly to constrain the paleoenvironmental and paleoclimatic context in which our hominin ancestors survived and thrived. But a composite deep drill core located in Turkana Basin would also give insight into other key topics identified by the PI team and workshop participants, including basin evolution, tectonics, and magmatism. Through the proposed drilling plan, we seek to pursue a series of research topics and hypotheses related to the thematic breakout groups formed through the online and in-person meetings. A summary of the key take-home messages from these workshop discussions is summarized in the sections that follow.

4.2.1 Basin evolution

The basin evolution breakout group focused on how DDTB could contribute to constraining the interplay between tectonics, magmatism, and climate in continental rift systems. The Turkana Basin, with its magmatically active system and early onset of rifting, is an ideal location to integrate studies of eruptive history with sedimentary and structural archives of basin evolution. Recent modeling and field studies reveal that surface processes, including erosion and sediment and water column loading, can impact rates and styles of extensional deformation in rifts, as well as magma body inflation and deflation (Albino et al., 2010; Sternai, 2020; Egger et al., 2021; Xue et al., 2023). Utilizing only shallow sedimentary cores, critical feedbacks between the magmatic, tectonic, hydrologic, and sedimentary systems have been revealed on 1000- to 10 000-year timescales (Muirhead and Scholz, 2017); however, a rich (>1 Myr) and first-of-its-kind history of the feedbacks between these key processes operating at continental rifts can only be obtained through a deep drilling project. Key to this story would be compiling data from both Phase 1 and Phase 2 of this project as both offer unique but independent opportunities to synthesize the proposed DDTB record with existing structural data. To achieve these objectives, the project would undertake facies analysis and provenance studies, which could be used to reconstruct basin extension, paleoenvironment evolution, and eruptive history. Results from the core would be spatially integrated using core–seismic outcrop integration, which can allow reconstruction of the temporal history of fault slip through careful mapping of displaced seismic horizons of known age (e.g., Wright et al., 2023). By comparing the interpreted fault slip history with the ~ 4 Myr chronology of volcanism and lake-level change revealed by the deep drilling record, we can explore how climate-driven hydrological changes in the region have influenced the structural development of the basin. Ultimately, this would enable DDTB to constrain the critical feedbacks between the tectonic, magmatic, climatic, and hydrologic processes that have driven the Plio-Pleistocene evolution of ecosystems in the Turkana Basin.

4.2.2 Paleoclimate

The paleoclimate breakout group focused on the potential scientific advances that could be achieved from a 4 Myr record from the Turkana Basin. Much of our current understanding of eastern African climate for this time comes from outcrops, providing snapshots of climate variability, and nearby marine sediment cores (deMenocal, 1995). While marine drill cores are more continuous, questions remain about how well these distal archives actually reconstruct conditions in continental settings (Cohen et al., 2016). Continuous Pliocene to present records of proxy-derived paleoclimate from eastern Africa would be the first of their kind, with resolution and continuity currently unavailable from a single region in Africa. The ability to reconstruct the regional climate for the last 4 Myr would allow us to better frame the environmental changes underway both across the landscape and within the lake itself. These records of climate variability, obtained directly for the region where the fossil record is one of the richest, would also provide context for hominin evolution. This new record would provide a continental signal of tropical climate variability from northern hemispheric eastern Africa. The proposed DDTB record could be directly compared to marine records (e.g., Castañeda et al., 2016; Taylor et al., 2021), existing southern hemispheric continental paleoclimate records spanning the last ~ 1.4 Ma (e.g., Lake Malawi; Scholz et al., 2007; Lyons et al., 2015; Johnson et al., 2016), and/or other southern hemispheric continental records proposed to ICDP (e.g., ~ 10 Ma to modern from Lake Tanganyika; Russell et al., 2020). We will examine spatiotemporal coherence of eastern and southern African climate change through quantitative comparisons of the Turkana Basin drill cores with these other records. New sedimentary records produced through deep-drilling will span important Plio-Pleistocene global climate changes and allow us to examine how these events shaped the paleoenvironment. By examining the amount and degree of climatic variability in the region and how sensitive the Turkana Basin is to global climate events including glaciation, circulation changes, and oceanic gateway changes in a high CO_2 world, we can provide important Pliocene climate model constraints.

4.2.3 Paleoenvironment and impacts of paleoecology

An understanding of eastern African paleoenvironmental changes during the last 4 Myr would enable the scientific community to tackle key questions on the ecological structure through time, including the tempo and mode of change.

The breakout group on paleoenvironments emphasized that this would be crucial to finally understand more about eastern African habitat transformations and how these might have been associated with the rate of evolutionary change. The unique location of Lake Turkana within the EARS would facilitate parsing the impacts of tectonic versus climatic drivers and extend the knowledge on the role that basin evolution might have played in reaching milestones in faunal evolution. Environmental reconstruction could be achieved through a multi-proxy approach including but not limited to diatoms, invertebrate fossils (ostracods, molluscs, etc.), pollen, phytoliths, paleosol-based proxies, and organic compound-specific stable isotope records, all of which have comparable records both from HSPDP and outcrop-based studies (Brown and Feibel, 1991). Although numerous significant fragments of this story are available (e.g., Yost et al., 2021), the discontinuity of these records in space and time complicates the ability to parse the impacts of climate from those of tectonic drivers on paleoenvironments and their associated ecosystems. Those gaps could finally be filled by the DDTB record, and, moreover, a continuous paleoenvironmental record from the Turkana Basin would offer the unique opportunity to directly tie in with the robust paleontological, paleoanthropological, and archaeological record in the Turkana Basin. It also creates opportunities to compare with other basins across the African continent, leveraging the work from other ICDP projects, both completed (e.g., Lake Bosumtwi (Koeberl et al., 2005), Lake Malawi (Scholz et al., 2011), and HSPDP (Cohen et al., 2016)) and proposed (e.g., Lake Tanganyika (Russell et al., 2020), Lake Victoria (Berke et al., 2024), and Afar Dallol Drilling (Foubert et al., 2021)).

4.2.4 Modern systems

The modern lake systems' breakout group focused on the activities and changes that have recently occurred in Lake Turkana driven by anthropogenic activities on the lake and its catchments and by natural climate variability. The group recognized that a robust understanding of the modern lake system is key to understanding responses in paleo-proxy records. The modern lake is experiencing pressure from the catchment that directly impacts the hydrochemistry and water influx. This transboundary lake has its main source of inflow coming from the Ethiopian highlands via the Omo River, and thus activities such as the recent construction of hydroelectric dams (e.g., Gibe Dam series) on the Omo River perturb the annual cycle of sediments and nutrient input into the lake and flood regimes. There are a number of data gaps and unknowns within the modern systems that need monitoring, including in situ lake level and evaporation monitoring, river level and physicochemical parameter monitoring, groundwater monitoring, and monitoring of the climatic parameters (winds, solar insolation, rainfall, humidity) at different elevation within the catchments. The team is actively working to address these gaps by working in close conjunction with local partners including colleagues at the Kenyan Marine and Fisheries Research Institution, Earth Observation Systems (satellites), and accessing wind data from The Trans-African Hydro-Meteorological Observatory (van de Giesen et al., 2014). Collaboration with colleagues focused on the fact that the modern system serves two significant purposes. The first is leveraging this partnership to advance our mutual research interests. The second, extremely significant, opportunity here is to collaborate to successfully design and implement Phase 2 of the DDTB. We continue to work on integrating modern climate, hydrology, and limnological data in ways that inform the reconstruction of the past climates, environments, and ecosystems, as well as the resource focus of this project.

4.2.5 Outreach, capacity building, and education

The workshop was structured to maximize input from all participants, regardless of their area of expertise, career stage, or role on the team. In this way all participant perspectives were heard, and their feedback was documented. Centering our working groups around emerging themes co-created with the workshop participants cultivated new interpersonal connections that resulted in a sense of shared responsibility toward broader impacts. This intentionality opened the door for discussions around the societal impact of coring and drilling work such as the critical role of water in community social structure.

With this foundation, ongoing development of strategies for outreach, education, and capacity building has been facilitated by the US Continental Scientific Drilling Facility's Science and Outreach Coordinator, Kat Cantner, with community partners through the Turkana Basin Institute, Kenya. Access to water is essential for drilling operations. There is also a direct connection between water access and girls' education since girls are responsible for transporting water to the household. Girls are prevented from attending school if water is not readily available since they must spend many hours supplying the home. Stigma around menstruation and lack of universal support for women's education are also a challenge in local communities. Based on assessment of need and interest through partnership with the Turkana Basin Institute, we proposed funding outreach to communities regarding the value of girls' education, providing sanitary products for girls (where not already covered by national programs) and sponsoring local students. The project team will co-create science content and educational activities for the Turkana Basin Institute's student science clubs and will also generate age-appropriate material for primary-, secondary-, and university-age learners to increase awareness of geoscience career opportunities and build capacity for a stronger geoscience workforce. The international drilling campaign and subsequent research also offer opportunities to support future capacity building, particularly for Kenyan students. The implementation of well-established concepts like international

summer school provides unique synergies and networking opportunities for both experienced scientists involved and future generations of scientists and students (e.g., Wiersberg et al., 2021). The involvement of international experts with a range of expertise around scientific drilling, being both on-site for several weeks and/or in close dialogue with cooperating institutions (e.g., universities, national museum, industry), also offers a unique opportunity for interdisciplinary knowledge transfer and hands-on experience across disciplines and national borders.

5 Conclusions and recommendations

Based on the need to expand understanding of the tectonic, climatic, and biologic evolution in eastern Africa and the opportunities to leverage collaboration between research and industry (fisheries and geothermal), we recommend a two-phase drilling campaign to recover a continuous sedimentary record from the Turkana Basin extending from 4 Ma to present. We propose that Phase 1 will recover an on-shore transect of cores along the northwestern margin of Lake Turkana spanning the interval from 4 to 0.7 Ma, expanding upon the success for the WTK13 drill core drilled as part of HSPDP. Phase 2 of the DDTB project will focus on the record from 1 Ma to modern, and targeting the Central Basin of Lake Turkana. DDTB will leverage existing outcrop research from the Turkana Basin and regional lacustrine cores. When combined, the two phases of this unprecedented record will enable researchers to parse the relative impacts of tectonics, volcanism, and climate on biological and ecological evolution, including the physical and cultural origins of our own ancestors.

Data availability. No datasets were used in this article.

Team list. In addition to the named co-authors on this paper, the following individuals make up the Deep Drilling in the Turkana Basin (DDTB) project team through their participation in the meetings that shaped this project. This team contributed to the ideas presented in this workshop report: Meshack Owira Amimo (Water Resources Authority, Nairobi, Kenya), Omondi Everlyne Apondi (University of Albany, Albany, NY, USA), Christopher Campisano (Arizona State University, Tempe, AZ, USA), Patrick Gathogo (Stony Brook University, Stony Brook, NY, USA), John Greenlee (Syracuse University, Syracuse, NY, USA), Sonia Harmand (CRNS, Paris, France), Annett Junginger (University of Tübingen, Tübingen, Germany), Benjamin Keenan (McGill University, Montreal, Canada), James Last Keyombe (Kenya Marine and Fisheries Institute, Kisumu, Kenya), Rahab Kinyanjui (National Museums of Kenya, Nairobi, Kenya; Max Planck Institute for Geoanthropology, Jena, Germany), Simon Kübler (Ludwig Maximilian University Munich, Munich, Germany), Rachel Lupien (Aarhus University, Aarhus, Denmark), John Malala (Kenya Marine and Fisheries Institute, Kalokol, Kenya), Fredrick Kyalo Manthi (National Museums of Kenya, Nairobi, Kenya), Marta Marchegiano (University of Granada, Granada, Spain), Inka Meyer (Ghent University, Ghent, Belgium), Veronica Muiruri (National Museums of Kenya, Nairobi, Kenya), Dennis Njagi (Dedan Kimathi University, Nyeri, Kenya), Julian Ogondo (Maseno University, Kisumu, Kenya), Samson Omondi (Water Resources Authority, Nairobi, Kenya), Ayan Hassan Omar (National Oil Corporation of Kenya, Nairobi, Kenya), Christina Omuombo (University of Nairobi and Technical University of Kenya, Nairobi, Kenya), Simona Pierdominici (GFZ-Potsdam, Potsdam, Germany), Robert Raynolds (Denver Natural History Museum, Denver, CO, USA), Carolina Rosca (Andalusian Institute of Earth Sciences (IACT – CSIC), Granada, Spain), Christian Rowan (Lamont-Doherty Earth Observatory, Palisades, NY, USA), Sara Shedroff (University of Massachussetts, Amherst, MA, USA), Andrew Steen (University of Tennessee, Knoxville, TN, USA), Jeroen van der Lubbe (Vrije Universiteit Amsterdam, Amsterdam, the Netherlands), Thomas Wiersberg (ICDP, Potsdam, Germany), Marcella Winget (Hamilton College, Clinton, NY, USA), and Christian Zeeden (Leibniz Institute for Applied Geophysics, Hanover, Germany).

Author contributions. CCB, MB, KC, CSF, VF, AN, LO, HMR, and CAS organized the workshop and co-facilitated it. CCB was lead author for the workshop report with significant contributions from co-authors MB, KC, CSF, VF, GMK, JM, AN, LO, HMR, and CAS. The content of this report was generated by the whole DDTB project team and participants from two online meets which complemented the in-person workshop.

Competing interests. The contact author has declared that none of the authors has any competing interests.

Disclaimer. Publisher's note: Copernicus Publications remains neutral with regard to jurisdictional claims made in the text, published maps, institutional affiliations, or any other geographical representation in this paper. While Copernicus Publications makes every effort to include appropriate place names, the final responsibility lies with the authors.

Acknowledgements. We recognize the collaboration of the Geothermal Development Company (GDC) and the National Museums of Kenya during the workshop. We acknowledge the contributions from the National Oil Corporation of Kenya; the Turkana Basin Institute; Africa Oil; and the late Isaiah Nengo (Turkana Basin Institute, Kenya, and Stony Brook University, USA), who facilitated the transfer of industry seismic data that support the site selection. Thanks are expressed to Christian Rowan (Lamont-Doherty Earth Observatory, USA) for his efforts on seismic interpretation and site selection.

Financial support. This research has been supported by the NSF-funded Research Coordination Network EarthRates (which funded the initial 2017 planning workshop leading to the creation of

DDTB) and the International Continental Scientific Drilling Program (ICDP) which funded the 2022 workshop in Nairobi.

Review statement. This paper was edited by Ulrich Harms and reviewed by Thomas Wagner and one anonymous referee.

References

Albino, F., Pinel, V., and Sigmundsson, F.: Influence of surface load variations on eruption likelihood: application to two Icelandic subglacial volcanoes, Grímsvötn and Katla, Geophys. J. Int., 181, 1510–1524, https://doi.org/10.1111/j.1365-246X.2010.04603.x, 2010.

Avery, S.: Hydrological impacts of Ethiopia's Omo Basin on Kenya's Lake Turkana water levels & fisheries, African Development Bank Group, https://www.afdb.org/fileadmin/uploads/afdb/Documents/Compliance-Review/REPORT_NOV_2010_S_AVERY_TURKANA_Small_file.pdf (last access: 5 December 2023), 2010.

Avery, S. and Eng, C.: Lake Turkana & the Lower Omo: hydrological impacts of major dam and irrigation developments, African Studies Centre, the University of Oxford, 2012.

Baker, B. H. and Wohlenberg, J.: Structure and evolution of the Kenya rift valley, Nature, 229, 538–542, https://doi.org/10.1038/229538a0, 1971.

Bayley, P. B.: The Commercial Fishery of Lake Turkana, in: Report on the Findings of the Lake Turkana Project, 1972–75, edited by: Hopson, A. J., 2, 351–554, 1982.

Beck, C. C.: The terrestrial climate record from the Turkana Basin, Kenya: a multiproxy approach, PhD dissertation, Rutgers University, USA, 170 pp., https://doi.org/10.7282/T3ZS2ZGB, 2015.

Beck, C. C., Feibel, C. S., Lupien, R., Yost, C. L., Rucina, S., Russell, J. M., Deino, A., Sier, M., Cohen, A. S., and Campisano, C. J.: Paleoenvironmental change as seen from a multiproxy perspective in the West Turkana Kaitio core (WTK13), Kenya, AGU Annual Meeting, 11–15 December 2017, New Orleans, LA, USA, https://agu.confex.com/agu/fm17/meetingapp.cgi/Paper/292581 (last access: 5 December 2023), 2017.

Beck, C. C., Feibel, C. S., Mortlock, R. A., Quinn, R. L., and Wright, J. D.: Little Ice Age to modern lake-level fluctuations from Ferguson's Gulf, Lake Turkana, Kenya, based on sedimentology and ostracod assemblages, Quaternary Res., 101, 129–142, https://doi.org/10.1017/qua.2020.105, 2021.

Bergström, A., Stringer, C., Hajdinjak, M., Scerri, E. M. L., and Skoglund, P.: Origins of modern human ancestry, Nature 590, 229–237, https://doi.org/10.1038/s41586-021-03244-5, 2021.

Berke, M. A., Johnson, T. C., Werne, J. P., Grice, K., Schouten, S., and Damsté, J. S. S.: Molecular records of climate variability and vegetation response since the Late Pleistocene in the Lake Victoria basin, East Africa, Quaternary Sci. Rev., 55, 59–74, https://doi.org/10.1016/j.quascirev.2012.08.014, 2012.

Berke, M. A., Peppe, D. J., and the LVDP team: ICDP workshop on the Lake Victoria Drilling Project (LVDP): scientific drilling of the world's largest tropical lake, Sci. Dril., 33, 21–31, https://doi.org/10.5194/sd-33-21-2024, 2024.

Bloomer, S. H., Curtis, P. C., and Karson, J. A.: Geochemical variation of Quaternary basaltic volcanics in the Turkana Rift, northern Kenya, J. Afr. Earth Sci., 8, 511–532, 1989.

Bobe, R.: Fossil mammals and paleoenvironments in the Omo-Turkana Basin, Evol. Anthropol., 20, 254–263, https://doi.org/10.1002/evan.20330, 2011.

Boone, S. C., Seiler, C., Kohn, B. P., Gleadow, A. J. W., Foster, D. A., and Chung, L.: Influence of Rift Superposition on Lithospheric Response to East African Rift System Extension: Lapur Range, Turkana, Kenya, Tectonics, 37, 182–207, https://doi.org/10.1002/2017TC004575, 2018a.

Boone, S. C., Kohn, B. P., Gleadow, A. J., Morley, C. K., Seiler, C., Foster, D. A., and Chung, L.: Tectono-thermal evolution of a long-lived segment of the East African Rift System: Thermochronological insights from the North Lokichar Basin, Turkana, Kenya, Tectonophysics, 744, 23–46, https://doi.org/10.1016/j.tecto.2018.06.010, 2018b.

Brown, F. H. and Feibel, C. S.: Stratigraphy, depositional environments and paleogeography of the Koobi Fora Formation, in: Koobi Fora Research Project, Volume 3. Stratigraphy, artiodactyls and paleoenvironments, edited by: Harris, J. M., Clarendon Press, Oxford, UK, 1–30, https://doi.org/10.1093/oso/9780198573999.003.0001, 1991.

Brown, F. H. and McDougall, I.: Geochronology of the Turkana depression of northern Kenya and southern Ethiopia, Evol. Anthropol., 20, 217–227, https://doi.org/10.1002/evan.20318, 2011.

Brown, F. H., Haileab, B., and McDougall, I.: Sequence of tuffs between the KBS Tuff and the Chari Tuff in the Turkana Basin, Kenya and Ethiopia, J. Geol. Soc. Lond., 163, 185–204, https://doi.org/10.1144/0016-764904-165, 2006.

Bruhn, R. L., Brown, F. H., Gathogo, P. N., and Haileab, B.: Pliocene volcano-tectonics and paleogeography of the Turkana Basin, Kenya and Ethiopia, J. Afr. Earth Sci., 59, 295–312, https://doi.org/10.1016/j.jafrearsci.2010.12.002, 2011.

Campisano, C. J., Cohen, A. S., Arrowsmith, J. R., Asrat, A., Behrensmeyer, A. K., Brown, E. T., Deino, A. L., Deocampo, D. M., Feibel, C. S., Kingston, J. D., Lamb, H. F., Lowenstein, T. K., Noren, A., Olago, D. O., Owen, R. B., Pelletier, J. D., Potts, R., Reed, K. E., Renaut, R. W., Russell, J. M., Russell, J. L., Schäbitz, F., Stone, J. R., Trauth, M. H., and Wynn, J. G.: The Hominin Sites and Paleolakes Drilling Project: high-resolution paleoclimate records from the East African Rift System and their implications for understanding the environmental context of hominin evolution, PaleoAnthropology, 2017, 1–43, https://doi.org/10.4207/PA.2017.ART104, 2017.

Castañeda, I. S., Caley, T., Dupont, L., Kim, J. H., Malaizé, B., and Schouten, S.: Middle to Late Pleistocene vegetation and climate change in subtropical southern East Africa, Earth Planet. Sci. Lett., 450, 306-316, https://doi.org/10.1016/j.epsl.2016.06.049, 2016.

Cerling, T. E. and Powers, D. W.: Paleorifting between the Gregory and Ethiopian rifts, Geology, 5, 441–444, https://doi.org/10.1130/0091-7613(1977)5<441:PBTGAE>2.0.CO;2,1977.

Cohen, A., Campisano, C., Arrowsmith, R., Asrat, A., Behrensmeyer, A. K., Deino, A., Feibel, C., Hill, A., Johnson, R., Kingston, J., Lamb, H., Lowenstein, T., Noren, A., Olago, D., Owen, R. B., Potts, R., Reed, K., Renaut, R., Schäbitz, F., Tiercelin, J.-J., Trauth, M. H., Wynn, J., Ivory, S., Brady, K.,

O'Grady, R., Rodysill, J., Githiri, J., Russell, J., Foerster, V., Dommain, R., Rucina, S., Deocampo, D., Russell, J., Billingsley, A., Beck, C., Dorenbeck, G., Dullo, L., Feary, D., Garello, D., Gromig, R., Johnson, T., Junginger, A., Karanja, M., Kimburi, E., Mbuthia, A., McCartney, T., McNulty, E., Muiruri, V., Nambiro, E., Negash, E. W., Njagi, D., Wilson, J. N., Rabideaux, N., Raub, T., Sier, M. J., Smith, P., Urban, J., Warren, M., Yadeta, M., Yost, C., and Zinaye, B.: The Hominin Sites and Paleolakes Drilling Project: inferring the environmental context of human evolution from eastern African rift lake deposits, Sci. Dril., 21, 1–16, https://doi.org/10.5194/sd-21-1-2016, 2016.

Cohen, A. S., Stone, J., Beuning, K., Park, L., Reinthal, P., Dettman, D., Scholz, C. A., Johnson, T., King, J. W., Talbot, M., Brown, E., and Ivory, S.: Ecological Consequences of Early Late-Pleistocene Megadroughts in Tropical Africa, P. Natl. Acad. Sci. USA, 104, 16422–16427, https://doi.org/10.1073/pnas.0703873104, 2007.

Cohen, A. S., Campisano, C. J., Arrowsmith, J. R., Asrat, A., Beck, C. C., Behrensmeyer, A. K., Deino, A.L., Feibel, C.S., Foerster, V., Kingston, J. D., Lamb, H. F., LOwenstein, T. K., Lupien, R. L., Muiruri, V., Olago, D. O., Owen, R. B., Potts, R., Russel, J. M., Schaebitz, F., Stone, J. R., Trauth, M. H., and Yost, C. L.: Reconstructing the Environmental Context of Human Origins in Eastern Africa Through Scientific Drilling, Annu. Rev. Earth Pl. Sc., 50, 451–476, https://doi.org/10.1146/annurev-earth-031920-081947, 2022.

Corti, G.: Continental rift evolution: from rift initiation to incipient break-up in the Main Ethiopian Rift, East Africa, Earth-Sci. Rev., 96, 1–53, https://doi.org/10.1016/j.earscirev.2009.06.005, 2009.

deMenocal, P. B.: Plio-Pleistocene African Climate, Science, 270, 53–59, https://doi.org/10.1126/science.270.5233.53, 1995.

deMenocal, P. B.: Climate and human evolution, Science, 331, 540–542, https://doi.org/10.1126/science.1190683, 2011.

Dunkelman, T. J., Rosendahl, B. R., and Karson, J. A.: Structure and stratigraphy of the Turkana rift from seismic reflection data, J. Afr. Earth Sci., 8, 489–510, https://doi.org/10.1016/S0899-5362(89)80041-7, 1989.

Dunkley, P. N., Smith, M., Allen, D. J., and Darling, W. G.: The geothermal activity of the northern sector of the Kenya Rift Valley, British Geological Survey, Research Report no. SC/93/1, 185, https://nora.nerc.ac.uk/id/eprint/507920 (last access: 15 December 2023), 1993.

Ebinger, C. J. and Casey, M.: Continental breakup in magmatic provinces: An Ethiopian example, Geology, 29, 527–530, https://doi.org/10.1130/0091-7613(2001)029<0527:CBIMPA>2.0.CO;2, 2001.

Ebinger, C. J., Jackson, J. A., Foster, A. N., and Hayward, N. J.: Extensional basin geometry and the elastic lithosphere, Philos. T. Roy. Soc. A, 357, 741–765, https://doi.org/10.1098/rsta.1999.0351, 1999.

Egger, A. E., Ibarra, D. E., Weldon, R., Langridge, R. M., Marion, B., and Hall, J.: Influence of pluvial lake cycles on earthquake recurrence in the northwestern Basin and Range, USA, in: From Saline to Freshwater: The Diversity of Western Lakes in Space and Time, edited by: Starratt, S. W. and, Rosen, M. R., Geol. Soc America Special Paper 536, https://doi.org/10.1130/2018.2536(07), 2021.

Faith, J. T., Du, A., Behrensmeyer, A. K., Davies, B., Patterson, D. B., Rowan, J., and Wood, B.: Rethinking the ecological drivers of hominin evolution, Trends Ecol. Evol., 36, 797–807, https://doi.org/10.1016/j.tree.2021.04.011, 2021.

Feibel, C. S.: Paleoenvironments of the Koobi Fora Formation, Turkana Basin, northern Kenya, PhD dissertation, University of Utah, USA, 330 pp., 1988.

Feibel, C. S.: Freshwater stingrays from the Plio-Pleistocene of the Turkana Basin, Kenya and Ethiopia, Lethaia, 26, 359–366, https://doi.org/10.1111/j.1502-3931.1993.tb01542.x, 1994.

Feibel, C. S.: A geological history of the Turkana Basin, Evol. Anthropol., 20, 206–216, https://doi.org/10.1002/evan.20331, 2011.

Feibel, C. S., Beck, C. C., Lupien, R., Russell, J. M., Deino, A., Sier, M. J., Campisano, C., and Cohen, A. S.: Environmental dynamics on an Early Pleistocene lake margin: the WTK13 core at Kaitio, West Turkana, Kenya, Geological Society of America, Abstracts with Programs, Volume 49, No. 6,https://gsa.confex.com/gsa/2017AM/webprogram/Paper303947.html (last access: 5 December 2023), 2017.

Foerster, V., Asrat, A., Bronk Ramsey, C., Brown, E. T., Chapot, M. S., Deino, A., Duesing, W., Grove, M., Hahn, A., Junginger, A., Kaboth-Bahr, S., Lane, C. S., Opitz, S., Noren, A., Roberts, H. M., Stockhecke, M., Tiedemann, R., Vidal, C. M., Vogelsang, R., Cohen, A. S., Lamb, H. F., Schaebitz, F., and Trauth, M. H.: Pleistocene climate variability in eastern Africa influenced hominin evolution, Nat. Geosci., 15, 805–811, https://doi.org/10.1038/s41561-022-01032-y, 2022.

Foster, D. A. and Gleadow, A. J.: Structural framework and denudation history of the flanks of the Kenya and Anza Rifts, East Africa, Tectonics, 15, 258–271, https://doi.org/10.1029/95TC02744, 1996.

Foubert, A., Kidane, T., Keir, D., Atnafu, B., and ADD-ON Team, T. I.: Afar Dallol Drilling – ONset of sedimentary processes in an active rift basin (ADD-ON): Scientific drilling targets in the Afar (Ethiopia), EGU General Assembly 2021, online, 19–30 Apr 2021, EGU21-14486, https://doi.org/10.5194/egusphere-egu21-14486, 2021.

Furman, T., Bryce, J. G., Karson, J., and Iotti, A.: East African Rift System (EARS) plume structure: insights from Quaternary mafic lavas of Turkana, Kenya, J. Petrol., 45, 1069–1088, https://doi.org/10.1093/petrology/egh004, 2004.

Furman, T., Kaleta, K. M., Bryce, J. G., and Hanan, B. B.: Tertiary Mafic Lavas of Turkana, Kenya: Constraints on East African Plume Structure and the Occurrence of High-μ Volcanism in Africa, J. Petrol., 47, 1221–1244, https://doi.org/10.1093/petrology/egl009, 2006.

Gownaris, N. J., Pikitch, E. K., Ojwang, W. O., Michener, R., and Kaufman, L.: Predicting species' vulnerability in a massively perturbed system: the fishes of Lake Turkana, Kenya, PLoS One, 10, 1–24, https://doi.org/10.1371/journal.pone.0127027, 2015.

Gramling, C.: Kenyan find heralds new era in water prospecting, Science, 341, 1327, https://doi.org/10.1126/science.341.6152.1327, 2013.

Haileab, B., Brown, F. H., McDougall, I., and Gathogo, P. N.: Gombe Group basalts and initiation of Pliocene deposition in the Turkana depression, northern Kenya and southern Ethiopia, Geol. Mag., 141, 41–53, https://doi.org/10.1017/S001675680300815X, 2004.

Halfman, J. D., Johnson, T. C., and Finney, B. P.: New AMS dates, stratigraphic correlations and decadal climatic cycles for the past 4 Ka at Lake Turkana, Kenya, Palaeogeogr.

Palaeocl. Palaeoecol, 111, 83–98, https://doi.org/10.1016/0031-0182(94)90349-2, 1994.

Hargrave, J. E., Hicks, M. K., and Scholz, C. A.: Lacustrine Carbonates From Lake Turkana, Kenya: A Depositional Model of Carbonates in an Extensional Basin, J. Sediment. Res., 84, 224–237, https://doi.org/10.2110/jsr.2014.22, 2014.

Harmand, S., Lewis, J. E., Feibel, C. S., Lepre, C. J., Prat, S., Lenoble, A., Boes, X., Quinn, R. L., Brenet, M., Arroyo, A., Taylor, N., Clement, S., Daver, G., Brugal, J. P., Leakey, L., Mortlock, R. A., Wright, J. D., Lokorodi, S., Kirwa, C., Kent, D. V., and Roche, H.: 3.3-million-year-old stone tools from Lomekwi 3, West Turkana, Kenya, Nature, 521, 310–315, https://doi.org/10.1038/nature14464, 2015.

Harris, J. M., Brown, F. H., and Leakey, M. G.: Geology and paleontology of Plio-Pleistocene localities west of Lake Turkana, Kenya, Contributions in Science, 399, 1–128, 1988.

Hopson, A. J. (Ed.): Lake Turkana: a report on the findings of the Lake Turkana Project 1972–1975, Overseas Development Administration, https://doi.org/10.5962/bhl.title.137758, 1982.

IPCC: Mitigation of climate change: Contribution of Working Group III to the Fifth Assessment Report of the Intergovernmental Panel on Climate Change, edited by: Edenhofer, O., Pichs-Madruga, R., Sokona, Y., Minx, J. C., Farahani, E., Kadner, S., Seyboth, K., Adler, A., Baun, I., Brunner, S., Eickemeier, P., Kriemann, B., Savolainen, P., Schlömer, S., von Stechow, C., Zwickel, T., and Working Group III Technical Support Unit, Cambridge University Press, ISBN 978-1-107-05821-7, p. 1454, 2014.

Isaac, G. L. and Isaac, B. (Eds.): Koobi Fora Research Project, Volume 5, Plio-Pleistocene archaeology, Oxford University Press, Oxford, ISBN 978-0198575017, 596 pp., 1997.

Johnson, T. C. and Malala, J. O.: Lake Turkana and Its Link to the Nile, in: The Nile, edited by: Dumont, H. J., Springer, Dordrecht, Monog. Biol., 89, 287–304, https://doi.org/10.1007/978-1-4020-9726-3_15, 2009.

Johnson, T. C., Werne, J. P., Brown, E. T., Abbott, M., Berke, M., Steinman, B. A., Halbur, J., Contreras, S., Grosshuesch, S., Deino, A., Scholz, C. A., Lyons, R. P., Schouten, S., and Sinninghe Damsté, J. S.: A progressively wetter climate in southern East Africa over the past 1.3 million years, Nature, 537, 20–224, https://doi.org/10.1038/nature19065, 2016.

Junginger, A. and Trauth, M. H.: Hydrological constraints of paleo-Lake Suguta in the Northern Kenya Rift during the African humid period (15–5 ka BP), Global Planet. Change, 111, 174–188, https://doi.org/10.1016/j.gloplacha.2013.09.005, 2013.

Keranen, K., Klemperer, S. L., Gloaguen, R., and Group, E. W.: Three-dimensional seismic imaging of a protoridge axis in the Main Ethiopian rift, Geology, 32, 949–952, https://doi.org/10.1130/G20737.1, 2004.

Knappe, E., Bendick, R., Ebinger, C., Birhanu, Y., Lewi, E., Floyd, M., King, R., Kanji, G., Mariita, N., Temtime, T., Waktola, B., Deresse, B., Musila, M., Kanoti, J., and Perry, M.: Accommodation of East African Rifting across the Turkana Depression, J. Geophys. Res.-Sol. Ea., 125, e2019JB018469, https://doi.org/10.1029/2019JB018469, 2020.

Koeberl, C., Peck, J., King, J., Milkereit, B., Overpeck, O., and Scholz, C.: The ICDP Lake Bosumtwi Drilling Project: A First Report, Sci. Dril., 1, 23–27, https://doi.org/10.2204/iodp.sd.1.04.2005, 2005.

Lepre, C. J., Quinn, R. L., Joordens, J. C., Swisher III, C. C., and Feibel, C. S.: Plio-Pleistocene facies environments from the KBS Member, Koobi Fora Formation: implications for climate controls on the development of lake-margin hominin habitats in the northeast Turkana Basin (northwest Kenya), J. Hum. Evol., 53, 504–514, https://doi.org/10.1016/j.jhevol.2007.01.015, 2007.

Lepre, C. J., Roche, H., Kent, D. V., Harmand, S., Quinn, R. L., Brugal, J. P., Texier, P. J., Lenoble, A., and Feibel, C. S.: An earlier origin for the Acheulian, Nature, 477, 82–85, https://doi.org/10.1038/nature10372, 2011.

Leslie, P. W. and Fry, P. H.: Extreme seasonality of births among nomadic Turkana pastoralists, Am. J. Phys. Anthropol., 79, 103–115, https://doi.org/10.1002/ajpa.1330790111, 1989.

Lewin, R.: Lake bottoms linked with human origins, Science, 211, 564–566, 1981.

Lisiecki, L. E. and Raymo, M. E.: A Pliocene-Pleistocene stack of 57 globally distributed benthic $\delta^{18}O$ records, Paleoceanography, 20, PA1003, https://doi.org/10.1029/2005PA001164, 2005.

Lupien, R. L., Russell, J. M., Feibel, C., Beck, C., Castaneda, I., Deino, A., and Cohen, A. S.: A leaf wax biomarker record of early Pleistocene rainfall from West Turkana, Kenya, Quaternary Sci. Rev., 186, 225–235, https://doi.org/10.1016/j.quascirev.2018.03.012, 2018.

Lupien, R. L., Russell, J. M., Grove, M., Beck, C. C., Feibel, C. S., and Cohen, A. S.: Abrupt climate change and its influences on hominin evolution during the early Pleistocene in the Turkana Basin, Kenya, Quaternary Sci. Rev., 245, 106531, https://doi.org/10.1016/j.quascirev.2020.106531, 2020.

Lyons, R. P., Scholz, C. A., Cohen, A. S., King, J. W., Brown, E. T., Ivory, S. J., Johnson, T. C., Deino, A. L., Reinthal, P. N., McGlue, M. M., and Blome, M. W.: Continuous 1.3-million-year record of East African hydroclimate, and implications for patterns of evolution and biodiversity, P. Natl. Acad. Sci. USA, 112, 15568–15573, https://doi.org/10.1073/pnas.1512864112, 2015.

Manthi, F. K., Brown, F. H., Plavcan, M. J., and Werdelin, L.: Gigantic lion, *Panthera leo*, from the Pleistocene of Natodomeri, eastern Africa, J. Paleontol., 92, 305–312, https://doi.org/10.1017/jpa.2017.68, 2018.

Mbugua, D., Makokha, M. K., and Shisanya, C. A.: Assessment of physicochemical properties of groundwater near oil well pads in Lokichar Basin, Turkana County, Kenya, Open Access Library Journal, 9, 1–17, https://doi.org/10.4236/oalib.1108487, 2022.

McDougall, I., Brown, F. H., and Fleagle, J. G.: Sapropels and the age of hominins Omo I and II, Kibish, Ethiopia, J. Hum. Evol., 55, 409–420, https://doi.org/10.1016/j.jhevol.2008.05.012, 2008.

Morley, C. K.: Early syn-rift igneous dike patterns, northern Kenya Rift (Turkana, Kenya): Implications for local and regional stresses, tectonics, and magma-structure interactions, Geosphere, 16, 890–918, https://doi.org/10.1130/GES02107.1, 2020.

Morley, C. K., Wescott, W. A., Stone, D. M., Harper, R. M., Wigger, S. T., and Karanja, F. M.: Tectonic evolution of the northern Kenyan Rift, J. Geol. Soc. Lond., 149, 333–348, https://doi.org/10.1144/gsjgs.149.3.0333, 1992.

Morley, C. K., Wescott, W. A., Stone, D. M., Harper, R. M., Wigger, S. T., Day, R. A., and Karanja, F. M.: Geology and geophysics of the Western Turkana Basins, Kenya, in: Geoscience of rift systems: evolution of East Africa, edited by: Morley, C. K., American Association of Petroleum Geologists Studies in Geology, 44, 19–54, https://doi.org/10.1306/St44623C2, 1999.

Morrissey, A. and Scholz, C. A.: Paleohydrology of Lake Turkana and its influence on the Nile River system, Palaeogeogr. Palaeocl., 403, 88–100, https://doi.org/10.1016/j.palaeo.2014.03.029, 2014.

Morrissey, A., Scholz, C. A., and Russell, J. R.: Late-Quaternary TEX86 paleotemperatures from the world's largest desert lake, Lake Turkana, Kenya, J. Paleolimnol., 59, 103–117, https://doi.org/10.1007/s10933-016-9939-6, 2018.

Mounier, A. and Mirazón Lahr, M.: Deciphering African late middle Pleistocene hominin diversity and the origin of our species, Nat. Commun., 10, 3406, https://doi.org/10.1038/s41467-019-11213-w, 2019.

Muirhead, J. D. and Scholz, C. A.: The temporal and spatial distribution of upper crustal faulting and magmatism in the south Lake Turkana rift, East Africa, in: American Geophysical Union Fall Meeting, 11–15 December 2017, New Orleans LA, USA, T51B-0447, https://agu.confex.com/agu/fm17/meetingapp.cgi/Paper/242875 (last access: 5 December 2023), 2017.

Muirhead, J. D., Kattenhorn, S. A., Lee, H., Mana, S., Turrin, B. D., Fischer, T. P., Kianji, G., Dindi, E., and Stamps, D. S.: Evolution of upper crustal faulting assisted by magmatic volatile release during early-stage continental rift development in the East African Rift, Geosphere, 12, 1670–1700, https://doi.org/10.1130/GES01375.1, 2016.

Muirhead, J. D., Scholz, C. A., and Rooney, T. O.: Transition to magma-driven rifting in the South Turkana Basin, Kenya: Part 1, J. Geol. Soc. Lond., 179, 159, https://doi.org/10.1144/jgs2021-159, 2022.

Njau, K., Kimani, F., and Wambugu, J.: Geothermal Exploration of the Barrier Volcanic Complex, Kenya, Proceedings, 8th African Rift Geothermal Conference, 2–8 November 2020, Nairobi, Kenya, 2020.

Nutz, A., Schuster, M., Barboni, D., Gassier, G., Van Bocxlaer, B., Robin, C., Ragon, T., Ghienne, J. F., and Rubino, J. L.: Plio-Pleistocene sedimentation in West Turkana (Turkana Depression, Kenya, East African Rift System): Paleolake fluctuations, paleolandscapes and controlling factors, Earth-Sci. Rev., 211, 103415, https://doi.org/10.1016/j.earscirev.2020.103415, 2020.

Nutz, A., Ragon, T., and Schuster, M.: Cenozoic tectono-sedimentary evolution of the northern Turkana Depression (East African Rift System) and its significance for continental rifts, Earth Planet. Sci. Lett., 81, 299–311, https://doi.org/10.1016/j.epsl.2021.117285, 2022.

Nyaberi, D. M., Basweti, E., Barongo, J. O., Ogendi, G. M., and Kariuki, P. C.: Mapping of Groundwater through the Integration of Remote Sensing and Vertical Electrical Sounding in ASALs: A Case Study of Turkana South Sub-County, Kenya, Journal of Geoscience and Environment Protection, 7, 229–243, https://doi.org/10.4236/gep.2019.711017, 2019.

Obiero, K., Wakjira, M., Gownaris, N., Malala, J., Keyombe, J. L., Ajode, M. Z., Smith, S., Lawrence, T., Ogello, E., Getahun, A., and Kolding, J.: Lake Turkana: Status, challenges, and opportunities for collaborative research, J. Great Lakes Res., 46, 102120, https://doi.org/10.1016/j.jglr.2022.10.007, 2022.

Ojwang, W., Obiero, K. O., Donde, O. O., Gownaris, N. J., Pikitch, E. K., Omondi, R., Agembe, S., Malala, J., and Avery, S. T.: Lake Turkana: World's Largest Permanent Desert Lake (Kenya), in: The Wetland Book, edited by: Finlayson, C., Milton, G., Prentice, R. and Davidson, N., Springer, Dordrecht, https://doi.org/10.1007/978-94-007-6173-5_254-1, 2016.

Olaka, L. A., Kasemann, S. A., Sültenfuß, J., Wilke, F. D. H., Olago, D. O., Mulch, A., and Musolff, A.: Tectonic control of groundwater recharge and flow in faulted volcanic aquifers, Water Resour. Res., 58, e2022WR032016, https://doi.org/10.1029/2022WR032016, 2022.

Owen, R. B., Barthelme, J. W., Renaut, R. W., and Vincens, A.: Palaeolimnology and archaeology of Holocene deposits north-east of Lake Turkana, Kenya, Nature, 298, 523–529, https://doi.org/10.1038/298523a0, 1982.

Potts, R., Dommain, R., Moerman, J. W., Behrensmeyer, A. K., Deino, A. L., Riedl, S., Beverly, E. J., Brown, E. T., Deocampo, D., Kinyanjui, R., Lupien, R., Owen, R. B., Rabideaux, N., Russell, J. M., Stockhecke, M., deMenocal, P., Faith, J. T., Garcin, Y., Noren, A., Scott, J. J., Western, D., Bright, J., Clark, J. B., Cohen, A. S., Keller, C. B., King, J., Levin, N. E., Brady, S. K., Muiruri, V., Renaut, R. W., Rucina, S. M., and Uno, K.: Increased ecological resource variability during a critical transition in hominin evolution, Science Advances, 6, 8975, https://doi.org/10.1126/sciadv.abc8975, 2020.

Reeves, C. V., Karanja, F. M., and MacLeod, I. N.: Geophysical evidence for a failed Jurassic rift and triple junction in Kenya, Earth Planet. Sci. Lett., 81, 299–311, https://doi.org/10.1016/0012-821X(87)90166-X, 1987.

Roche, H., Brugal, J.-P., Delagnes, A., Feibel, C., Harmand, S., Kibunjia, M., Prat, S., and Texier, P. -J.: Plio-Pleistocene archaeological sites in the Nachukui Formation, West Turkana, Kenya: synthetic results 1997–2001, C. R. Palevol., 2, 663–673, https://doi.org/10.1016/j.crpv.2003.06.001, 2004.

Rooney, T. O.: The Cenozoic magmatism of East-Africa: Part I – Flood basalts and pulsed magmatism, Lithos, 286–287, 264–301, https://doi.org/10.1016/j.lithos.2017.05.014, 2017.

Rooney, T. O.: The Cenozoic magmatism of East Africa: part V – magma sources and processes in the East African Rift, Lithos, 360, 105296, https://doi.org/10.1016/j.lithos.2019.105296, 2020.

Rooney, T. O., Wallace, P. J., Muirhead, J. D., Chiasera, B., Steiner, R. A., Girard, G., and Karson, J. A.: Transition to magma-driven rifting in the South Turkana Basin, Kenya: Part 2, J. Geol. Soc., 179, 160, https://doi.org/10.1144/jgs2021-160, 2022.

Rosendahl, B. R., Kilembe, E., and Kaczmarick, K.: Comparison of the Tanganyika, Malawi, Rukwa and Turkana Rift zones from analyses of seismic reflection data, Tectonophysics, 213, 235–256, https://doi.org/10.1016/0040-1951(92)90261-4, 1992.

Rusiniak, P., Sekuła, K., Sracek, O., and Stopa, P.: Fluoride ions in groundwater of the Turkana County, Kenya, East Africa, Acta Geochim., 40, 945–960, https://doi.org/10.1007/s11631-021-00481-3, 2021.

Russell, J. M., Cohen, A. S., Johnson, T. C., and Scholz, C. A.: Scientific Drilling in the East African Rift Lakes: A Strategic Planning Workshop, Sci. Dril., 14, 49–54, https://doi.org/10.2204/iodp.sd.14.08.2012, 2012.

Russell, J. M., Barker, P., Cohen, A., Ivory, S., Kimirei, I., Lane, C., Leng, M., Maganza, N., McGlue, M., Msaky, E., Noren, A., Park Boush, L., Salzburger, W., Scholz, C., Tiedemann, R., Nuru, S., and the Lake Tanganyika Scientific Drilling Project (TSDP) Consortium: ICDP workshop on the Lake Tanganyika Scientific Drilling Project: a late Miocene–present record of climate, rifting, and ecosystem evolution from the world's oldest tropi-

cal lake, Sci. Dril., 27, 53–60, https://doi.org/10.5194/sd-27-53-2020, 2020.

Scholz, C. A., Johnson, T. C., Cohen, A. S., King, J. W., Peck, J., Overpeck, J. T., Talbot, M. R., Brown, E. T., Kalindekafe, L., Amoako, P. Y. O, Lyons, R. P., Shanahan, T. M., Castaneda, I. S., Heil, C. W., Forman, S. L., McHargue, L. R., Beuning, K. R., Gomez, J., and Pierson, J.: East African megadroughts between 135–75 kyr ago and bearing on early-modern human origins, P. Natl. Acad. Sci. USA, 104, 16416–16421, https://doi.org/10.1073/pnas.0703874104, 2007.

Scholz, C. A., Cohen, A. S., Johnson, T. C., King, J., Talbot, M. R., and Brown, E. T.: Scientific drilling in the Great Rift Valley: The 2005 Lake Malawi Scientific Drilling Project – An overview of the past 145 000 years of climate variability in Southern Hemisphere East Africa, Palaeogeogr. Palaeocl., 303, 3–19, https://doi.org/10.1016/j.palaeo.2010.10.030, 2011.

Shultz, S. and Maslin, M.: Early Human Speciation, Brain Expansion and Dispersal Influenced by African Climate Pulses, PLoS One, 8, e76750, https://doi.org/10.1371/journal.pone.0076750, 2013.

Sier, M. J., Langereis, C. G., Dupont-Nivet, G., Feibel, C. S., Joordens, J. C. A., van der Lubbe, J. H. J. L., Beck, C. C., Olago, D., and Cohen, A.: The top of the Olduvai Subchron in a high-resolution magnetostratigraphy from the West Turkana core WTK13, hominin sites and Paleolakes Drilling Project (HSPDP), Quat. Geochronol., 42, 117–129, https://doi.org/10.1016/j.quageo.2017.08.004, 2017.

Sternai, P.: Surface processes forcing on extensional rock melting, Sci. Rep., 10, 1, 7711, https://doi.org/10.1038/s41598-020-63920-w, 2020.

Tanui, F., Olago, D., Dulo, S., Ouma, G., and Kuria, Z.: Hydrogeochemistry of a strategic alluvial aquifer system in a semi-arid setting and its implications for potable urban water supply: The Lodwar Alluvial Aquifer System (LAAS), Groundwater for Sustainable Development, 11, 100451, https://doi.org/10.1016/j.gsd.2020.100451, 2020.

Taylor, A. K., Berke, M. A., Castañeda, I. S., Koutsodendris, A., Campos, H., Hall, I. R., Hemming, S. R., LeVay, L. J., Sierra, A. C., O'Connor, K., and Expedition 361 Scientists: Plio-Pleistocene continental hydroclimate and Indian ocean sea surface temperatures at the southeast African margin, Paleoceanography and Paleoclimatology, 36, e2020PA004186, https://doi.org/10.1029/2020PA004186, 2021.

Torres Acosta, V., Bande, A., Sobel, E. R., Parra, M., Schildgen, T. F., Stuart, F., and Strecker, M. R.: Cenozoic extension in the Kenya Rift from low-temperature thermochronology: Links to diachronous spatiotemporal evolution of rifting in East Africa, Tectonics, 34, 2367–2386, https://doi.org/10.1002/2015TC003949, 2015.

van de Giesen, N., Hut, R., and Slker, J.: The Trans-African Hydro-Meteorological Observatory (TAHMO), WIREs Water, 1, 341–348, https://doi.org/10.1002/wat2.1034, 2014.

Velpuri, N. M., Senay, G. B., and Asante, K. O.: A multi-source satellite data approach for modelling Lake Turkana water level: calibration and validation using satellite altimetry data, Hydrol. Earth Syst. Sci., 16, 1–18, https://doi.org/10.5194/hess-16-1-2012, 2012.

Vrba, E. S., Denton, G. H., and Prentice, M. L.: Climatic influences on early hominid behavior, Ossa, 14, 127–156, 1989.

Wheildon, J., Morgan, P., Williamson, K. H., Evans, T. R., and Swanberg, C. A.: Component parts of the World Heat Flow Data Collection, PANGAEA, https://doi.org/10.1594/PANGAEA.806192, 1994.

Wiersberg, T., Zens, J., Kück, J., Pierdominici, S., and Conze, R.: Training, Outreach, and ICDP Support, 5th, ICDP Primer – Planning, Managing, and Executing Continental Scientific Drilling Projects, edited by: Harms, U., GFZ German Research Centre for Geosciences, https://doi.org/10.48440/icdp.2021.001, 2021.

Wood, B. and Leakey, M.: The Omo-Turkana Basin fossil hominins and their contribution to our understanding of human evolution in Africa, Evol. Anthropol., 20, 264–292, https://doi.org/10.1002/evan.20335, 2011.

Wright, L. J. M., Scholz, C. A., Muirhead, J. D., and Shillington, D. J.: Heterogeneous Strain Distribution in the Malawi (Nyasa) Rift, East Africa: Implications for Rifting in Magma-Poor, Multi-Segment Rift Systems, Tectonics, 42, e2022TC007486, https://doi.org/10.1029/2022tc007486, 2023.

Xue, L., Muirhead, J. D., Moucha, R., Wright, L. J. M., and Scholz, C. A.: The Impact of Climate-Driven Lake Level Changes on Mantle Melting in Continental Rifts, Geophys. Res. Lett., 50, e2023GL103905, https://doi.org/10.1029/2023gl103905, 2023.

Yost, C. L., Lupien, R. L., Beck, C., Feibel, C. S., Archer, S. R., and Cohen, A. S.: Orbital influence on precipitation, fire, and grass community composition from 1.87 to 1.38 Ma in the Turkana Basin, Kenya, Front. Earth Sci., 9, 568646, https://doi.org/10.3389/feart.2021.568646, 2021.

Sci. Dril., 33, 109–128, 2024
https://doi.org/10.5194/sd-33-109-2024

Scientific Drilling
Open Access

Paleozoic Equatorial Records of Melting Ice Ages (PERMIA): calibrating the pace of paleotropical environmental and ecological change during Earth's previous icehouse

Jonathan M. G. Stine[1,2], Joshua M. Feinberg[1,2], Adam K. Huttenlocker[3], Randall B. Irmis[4,5], Declan Ramirez[1,2], Rashida Doctor[1,2], John McDaris[1,2], Charles M. Henderson[6], Michael T. Read[7], Kristina Brady Shannon[1,8], Anders Noren[1,8], Ryan O'Grady[1,8], Ayva Sloo[9], Patrick Steury[10], Diego P. Fernandez[5], Amy C. Henrici[11], and Neil J. Tabor[12]

[1]Department of Earth & Environmental Sciences, University of Minnesota – Twin Cities, 116 Church Street SE, Minneapolis, MN 55455, USA
[2]Institute for Rock Magnetism, University of Minnesota – Twin Cities, 116 Church Street SE, Minneapolis, MN 55455, USA
[3]Department of Integrative Anatomical Sciences, University of Southern California, 1333 San Pablo Street, Los Angeles, CA 90033, USA
[4]Natural History Museum of Utah, University of Utah, 301 Wakara Way, Salt Lake City, UT 84108-1214, USA
[5]Department of Geology & Geophysics, University of Utah, 115 South 1460 East, Salt Lake City, UT 84112, USA
[6]Department of Earth, Energy and Environment, University of Calgary, 2500 University Drive NW, Calgary, Alberta, T2N 1N4, Canada
[7]Department of Earth Sciences and Geologic Resources, Stephen F. Austin State University, 1901 N. Raguet St, Nacogdoches, TX 75962, USA
[8]Continental Scientific Drilling Facility, University of Minnesota, 116 Church Street SE, Minneapolis, MN 55455, USA
[9]Geology Department, Occidental College, 1600 Campus Road, Los Angeles, CA 90041, USA
[10]Department of Marine, Earth, and Atmospheric Sciences, North Carolina State University, Jordan Hall, 2800 Faucette Dr, Raleigh, NC 27607, USA
[11]Carnegie Museum of Natural History, 4400 Forbes Avenue, Pittsburgh, PA 15213, USA
[12]Roy M. Huffington Department of Earth Sciences, Southern Methodist University, 3225 Daniel Ave Suite 207, Dallas, TX 75205, USA

Correspondence: Jonathan M. G. Stine (jstine@umn.edu)

Received: 15 December 2023 – Revised: 27 March 2024 – Accepted: 11 April 2024 – Published: 18 June 2024

Abstract. The upper Paleozoic Cutler Group of southern Utah, USA, is a key sedimentary archive for understanding the Earth-life effects of the planet's last pre-Quaternary icehouse–hothouse state change: the Carboniferous–Permian (C–P) transition, between 304 and 290 million years ago. Within the near-paleoequatorial Cutler Group, this transition corresponds to a large-scale aridification trend, loss of aquatic habitats, and ecological shifts toward more terrestrial biota as recorded by its fossil assemblages. However, fundamental questions persist. (1) Did continental drift or shorter-term changes in glacio-eustasy, potentially driven by orbital (Milankovitch) cycles, influence environmental change at near-equatorial latitudes during the C–P climatic transition? (2) What influence did the C–P climatic transition have on the evolution of terrestrial ecosystems and on the diversity and trophic structures of terrestrial vertebrate communities?

Published by Copernicus Publications on behalf of the IODP and the ICDP.

The Paleozoic Equatorial Records of Melting Ice Ages (PERMIA) project seeks to resolve these issues in part by studying the Elk Ridge no. 1 (ER-1) core, complemented by outcrop studies. This legacy core, collected in 1981 within what is now Bears Ears National Monument, recovered a significant portion of the Hermosa Group and the overlying lower Cutler Group, making it an ideal archive for studying paleoenvironmental change during the C–P transition. As part of this project, the uppermost ∼450 m of the core were temporarily transferred from the Austin Core Repository Center to the Continental Scientific Drilling Facility at the University of Minnesota for splitting, imaging, and scanning for geophysical properties and spectrophotometry. Here we (1) review the history of this legacy core, (2) introduce recently obtained geophysical and lithologic datasets based on newly split and imaged core segments to provide a sedimentological and stratigraphic overview of the Elk Ridge no. 1 core that aligns more accurately with the currently recognized regional lithostratigraphic framework, (3) establish the position of the boundary between the lower Cutler beds and the overlying Cedar Mesa Sandstone in the core, and (4) outline our ongoing research goals for the core.

In-progress work on the core aims to refine biostratigraphic and chemostratigraphic age constraints, retrieve the polarity stratigraphy, interrogate preserved cyclostratigraphy, analyze sedimentary structures and paleosol facies, investigate stable isotope geochemistry, and evaluate elemental abundance data from X-ray fluorescence (XRF) scanning. Together with outcrop studies throughout Bears Ears National Monument and its vicinity, these cores will allow the rich paleontological and paleoenvironmental archives recorded in the continental Carboniferous–Permian transition of western North America to be confidently placed in a robust chronologic context that will help test hypotheses relating ecosystem evolution to the Carboniferous rainforest collapse, initial decline of the Late Paleozoic Ice Age, and long-wavelength astronomical cycles pacing global environmental change.

1 Introduction and motivation

As global climate change impacts our present day, understanding the intricate feedback mechanisms that regulate Earth's climate has become a focal point across geoscience disciplines. In the geological past, the Late Paleozoic Ice Age (LPIA) has a special relevance to current climate studies because it serves as our only deep-time analog for comprehending "climate change in an icehouse on a vegetated Earth" (Gastaldo et al., 1996; Montañez and Soreghan, 2006). This unique episode coincided with the highest rates of organic carbon burial in the past half billion years, resulting in low atmospheric pCO_2 and high pO_2 levels. These conditions likely sustained the longest-lived icehouse of the Phanerozoic Eon and may have catalyzed significant evolutionary innovations in terrestrial life, including such traits as insect flight and gigantism (Berner et al., 2007; Montañez, 2016).

Towards the end of the LPIA, during the C–P transition (∼304–290 Ma), a climatic shift to substantially more arid conditions resulted in the dramatic recession of the formerly vast paleotropical wetlands of low-latitude western and central Pangea (Sahney et al., 2010; Pardo et al., 2019). This loss of freshwater and classic "coal swamp" habitats, conceptualized as the Carboniferous rainforest collapse hypothesis, marked a profound shift in continental ecosystems. Indeed, many paleontological studies of Late Paleozoic central Pangea repeatedly demonstrate a stark contrast between Late Carboniferous paleoequatorial ecosystems, characterized by a blend of aquatic and terrestrial species and Cisuralian (Early Permian) environments dominated by more terrestrial faunal and floral assemblages (Figs. 1–2) (Vaughn, 1966, 1970; Olson and Vaughn, 1970; Frederiksen, 1972; Rowley et al., 1985; Gastaldo et al., 1996; Cleal and Thomas, 1999; Cleal and Thomas, 2005; Pardo et al., 2019). These changes also coincide with the emergence of the first large-bodied tetrapod herbivores, a pervasive feature of terrestrial ecosystems from the Permian through to the present day (Sues and Reisz, 1998; Reisz and Sues, 2000; Pearson et al., 2013; Reisz and Fröbisch, 2014; Brocklehurst et al., 2015).

Although at first glance this may suggest a mass extinction event, quantitative analysis of late Paleozoic equatorial fossil assemblages, as detailed by Pardo et al. (2019), supports the notion that this environmental and ecological shift was protracted and spatially diachronous, corroborating earlier hypotheses (Vaughn, 1966, 1970; Olson and Vaughn, 1970). This in turn led to the development of the Vaughn–Olson model (Pardo et al., 2019), which posits that the proliferation of terrestrial faunas during the C–P transition occurred earlier in western equatorial Pangea (Fig. 2) in the area roughly corresponding to the modern Colorado Plateau of southwestern North America.

Located within the hypothesized epicenter of dryland vertebrate expansion (Pardo et al., 2019), the Cutler Group in southeastern Utah, USA (Figs. 1–3), is ideal for studying this environmental and ecological transition. This unit's abundant fossil record (Fig. 1) and extensive outcrops of interbedded marine and continental "redbed" sediments preserve a diverse suite of depositional environments and associated biota spanning the C–P transition (Fig. 3), properties which make them a valuable resource for understanding the effects of this

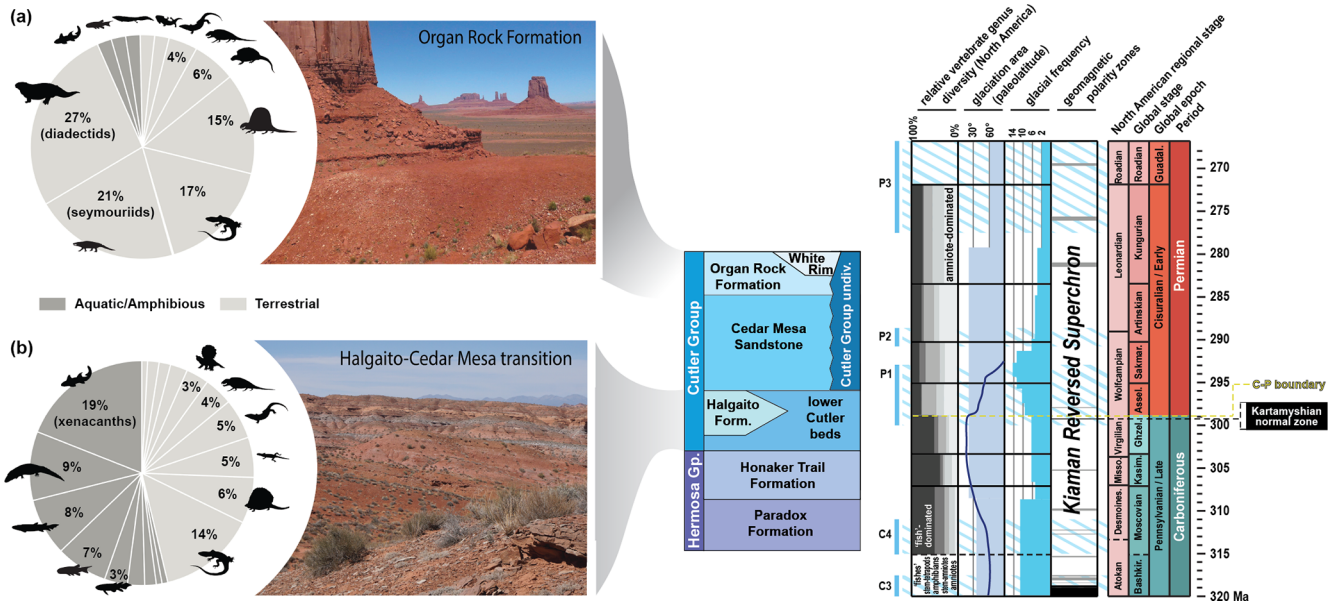

Figure 1. Climate-associated shifts in paleoequatorial vertebrate diversity within the Cutler Group during the C–P transition. Vertebrate abundance in C–P Halgaito Formation **(b)** is biased toward aquatic taxa, whereas the Permian Organ Rock assemblage **(a)** is less even (differential relative abundance of each clade) and dominated by terrestrial stem-amniote herbivores (diadectids) and amniotes. This compositional change broadly coincided with the final phases of Gondwanan glaciation and desertification of western Pangea, but the ages and positions of stage boundaries in these units are poorly constrained (glacial data from Fielding et al., 2008, and Montañez and Poulsen, 2013).

climatic transition on paleoequatorial ecosystems. Nevertheless, limited marine-biostratigraphic and geochronologic control (Fig. 3b) hinders a comprehensive paleoenvironmental reconstruction of these sediments and confident comparison to other contemporaneous fossil assemblages.

This collaborative research project, titled PERMIA (Paleozoic Equatorial Records of Melting Ice Ages), seeks to address these issues by studying the Elk Ridge no. 1 core (ER-1). This legacy core, collected in 1981 within what is now part of Bears Ears National Monument (Fig. 3a), recovered a significant portion of the lower Cutler Group and underlying units, making it an ideal archive for studying paleoenvironmental change during this critical period in terrestrial vertebrate evolution. Work is ongoing, yet much has been learned about the stratigraphic and geophysical properties through initial core processing. The purpose of this contribution is to introduce the project, share preliminary lithologic and geophysical results from the analysis of a legacy core (Elk Ridge no. 1), revise the position of lithostratigraphic boundaries within that core to align more accurately with the currently recognized regional stratigraphic framework, and discuss ongoing work with the core and complementary outcrop sites.

1.1 Motivation for studying the core

Few sites outside of the southwestern United States preserve a record complete enough to explore the relative contributions of paleoenvironmental change driven by global climate and continental drift in paleoequatorial C–P terrestrial ecosystems. Given the quality of its fossil record and expansive outcrops of shallow marine and continental rocks spanning the C–P transition, the canyon country of southeastern Utah is an ideal testing ground for these timely research questions (Reese, 2019; Gay et al., 2020). The rare juxtaposition of continental vertebrate-bearing fluvial and eolian redbeds interbedded with marine carbonate beds in a relatively continuous stratigraphic sequence makes southeastern Utah a unique window for studying synchronous, glacio-eustasy-driven oceanic and terrestrial events. In southern San Juan County, the lower Cutler Group include the fossiliferous terrestrial redbeds of the Halgaito Formation, which form the skirts and pedestals of the isolated buttes in Valley of the Gods (Fig. 3b) and the overlying eolian Cedar Mesa Sandstone. However, large portions of the Cutler Group in the region (including Valley of the Gods) are restricted to exposures along vertical cliff faces, rendering them inaccessible to outcrop-based, high-resolution paleoclimatic sampling.

The ER-1 core, collected ~25 km north of Valley of the Gods (Fig. 3a), contains a relatively complete and minimally altered record of the Hermosa Group through the Cedar Mesa Sandstone, both of which were deposited in a position more proximal to the center of Paradox Basin (Fig. 4). The crucial paleogeographic position of ER-1, located further from the late Carboniferous uplift of the "Ancestral Rocky Mountains" (Fig. 4a) (Moore et al., 2008; Sweet et al., 2021), reduces tectonic autocyclic influences, thus enhancing the pos-

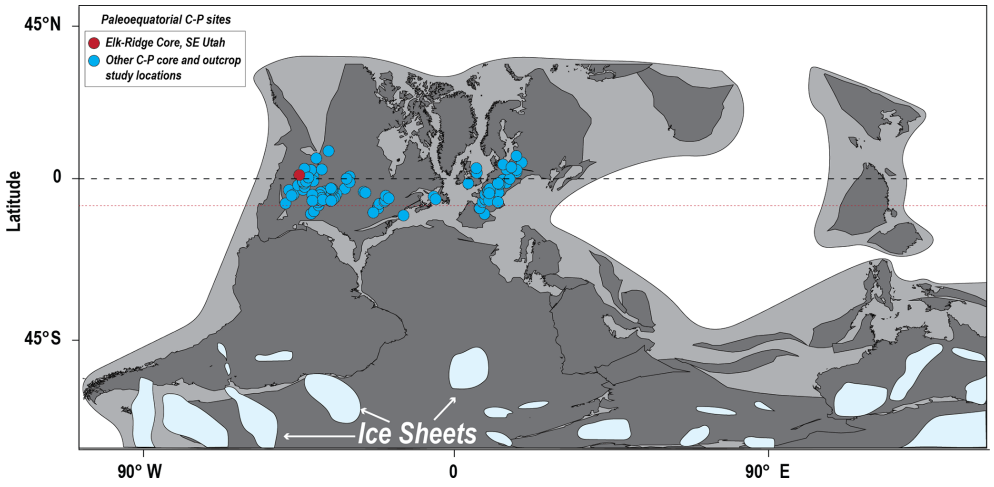

Figure 2. Plate configuration of Pangea during the Late Carboniferous Period (Late Pennsylvanian), modified from Pardo et al. (2019). The red circle represents the paleogeographic location of our study area, including the Elk Ridge no. 1 core (ER-1). The light-blue circles represent other important paleoequatorial Late Carboniferous to Early Permian fossil sites (Pardo et al., 2019). Approximate paleogeographic locations and extents of the late Paleozoic ice sheets are modified from Isbell et al. (2012) and Kent and Muttoni (2020). The red dotted line shows the approximate position of the equator in the early Permian (Pardo et al., 2019), which is meant to show that many of the C–P localities would have been transported north of the Equator at this later time.

sible preservation of orbital climate signals. Furthermore, ER-1 exhibits a higher proportion of carbonate interlayers compared to southern outcrop sites (Figs. 3–4), offering a promising opportunity to utilize biostratigraphic methods for core dating. Therefore, ER-1 is one of the best opportunities to collect high-resolution paleoclimatic data from a nearly complete record of the C–P transition within the uppermost Hermosa Group (Honaker Trail Formation) and the overlying lower Cutler Group.

1.2 Geologic setting

In southern Utah's Paradox Basin, the C–P transition is encompassed by the lower portion of the Cutler Group (Scott, 2013; Huttenlocker et al., 2018), a ∼600 m thick succession of marginal-to-shallow marine and distal floodplain sediments deposited between rising salt anticlines (Condon, 1997). In the Colorado Plateau region, most early authors subdivided the Cutler Group into approximately four subunits, which they originally named the Halgaito tongue, Cedar Mesa Sandstone, Organ Rock tongue, and De Chelly Sandstone (Fig. 5) (Baker and Reeside Jr., 1929; Baker, 1936; Orkild, 1955; Sears, 1956; Baars, 1962; O'Sullivan, 1965). Wengerd (1958, 1963) revised the nomenclature, incorporating "Rico" as the basal-most unit and elevating Cutler and Halgaito to group and formation status, respectively. In the northern part of the basin, Baars (1962) raised the Organ Rock to formation status and considered lower Cutler-like units to be assignable to the Elephant Canyon Formation. In contrast, Loope et al. (1990) argued that all units below the Cedar Mesa Sandstone be redefined as the informal "lower Cutler beds" until regional correlations could be clarified, removing the Elephant Canyon Formation and calling into question the validity of strata assigned to Rico, given that its type section is located in western Colorado (Cross and Spencer, 1900). Nevertheless, the term "Halgaito" has continued to be used among researchers studying the Valley of the Gods and Mexican Hat region (Murphy, 1987; G. S. Soreghan et al., 2002; M. J. Soreghan et al., 2002; DiMichele et al., 2014; Golab, 2016; Huttenlocker et al., 2018, 2021; Golab et al., 2018; Tobey, 2020) (Fig. 5).

In the northwest–southeast-trending Paradox Basin, located on the western margin of the Pangean supercontinent (Fig. 4a–b), the Carboniferous–Permian units of the Cutler Group consist of three parallel and time-successive facies belts – the southwestern carbonate shelf, the northeastern siliciclastic wedge, and the mid-basin erg and evaporite belt (Fig. 4c). The group ultimately terminated with the expansion of coastal dune and loessite facies, indicative of pronounced seasonal aridity (Loope, 1984; Murphy, 1987; Condon, 1997; Doelling, 2002; Doelling et al., 2002; G. S. Soreghan et al., 2002; Dubiel et al., 2009; Jordan and Mountney, 2010, 2012; Scott, 2013; Golab et al., 2018; Tobey, 2020).

Near the Monument Upwarp, around the present-day Valley of the Gods, the Halgaito Formation represents a southern wedge of terrestrial redbeds that formed during the early phases of this aridity trend (Figs. 1, 3–5). Farther north, near the ER-1 core and the Bears Ears buttes (Fig. 3a), the basal Cutler unit consists of fluvial, aeolian, and shallow-marine facies informally known as the "lower Cutler beds" (Murphy, 1987; Condon, 1997). The Halgaito Formation intertongues with and is laterally equivalent to the lower Cut-

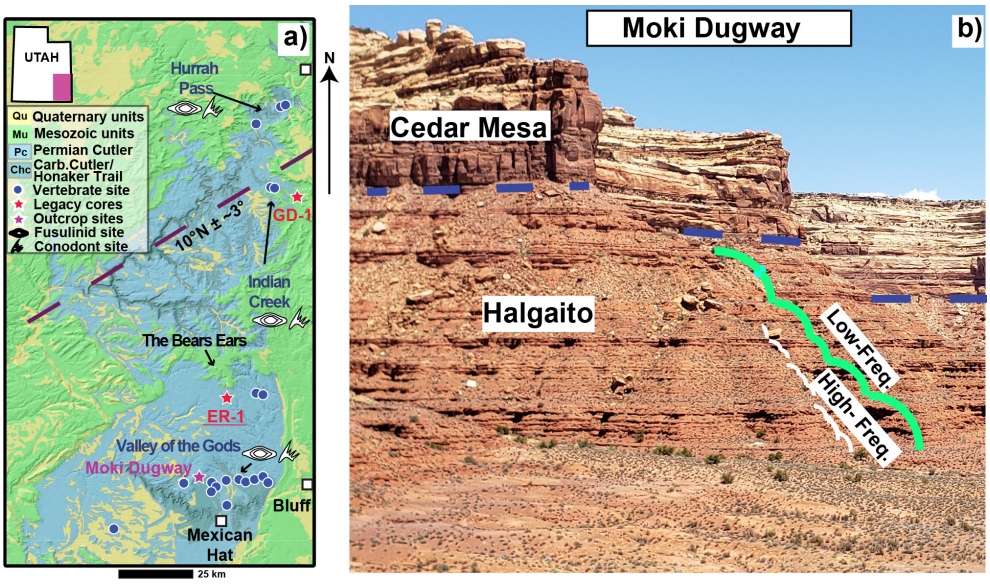

Figure 3. **(a)** Map showing the extent of Cutler Group exposures in the study area, modified from Hintze et al. (2000) with paleolatitude estimates from van Hinsbergen et al. (2015) using the 300 Ma paleopole. Moki Dugway is represented with a purple star, while red stars designate the approximate locations of the Gibson Dome (GD-1) and Elk Ridge (ER-1) cores. Blue circles represent known vertebrate sites. Fossil sites with conodont and fusulinid occurrences are designated with their respective symbols. **(b)** Exposures of the Halgaito Formation (lower Cutler beds) and Cedar Mesa Sandstone at Moki Dugway; lithologic cycles in Halgaito are highlighted.

ler beds (Figs. 4–5), both of which display evidence of progressively drier climates during the late Paleozoic (Murphy, 1987; Condon, 1997; G. S. Soreghan et al., 2002; Jordan and Mountney, 2010, 2012). This steady shift ultimately culminated in deposition of the overlying Cedar Mesa Sandstone, a set of thick, extensive, and predominantly eolian deposits overlying the lower Cutler beds throughout much of Paradox Basin, including the eponymous Cedar Mesa, greater Canyonlands area, and Indian Creek areas (Fig. 3a). By contrast, in the Hurrah Pass area southwest of Moab (Kane Creek Anticline), the Cutler Group only consists of the lower Cutler beds and an upper arkosic facies that is undivided but that may be equivalent to the Cedar Mesa and Organ Rock formations farther to the south and west (Billingsley and Huntoon, 1982; Langford and Chan, 1988; Condon, 1997; Carpenter and Ottinger, 2018).

Despite local variation, previous workers have observed that the strata across these areas show pronounced cyclicity (Doelling, 2002; G. S. Soreghan et al., 2002; Jordan and Mountney, 2010, 2012). Within the Halgaito Formation, these lithologic cycles occur as alternating sequences of loessite–paleosol couplets (Murphy, 1987) with accompanying cyclicities observed in rock magnetic properties (G. S. Soreghan et al., 2002), whereas in the overlying Cedar Mesa Sandstone they consist of alternating dune–interdune couplets (Mountney and Jagger, 2004). Traditionally, the cyclic nature of the Cutler Group has been speculated to record long eccentricity Milankovitch cycles (G. S. Soreghan et al., 2002; Jordan and Mountney, 2012), whereas the larger-scale transition from the fluvial or marine lower Cutler beds to the eolian Cedar Mesa Sandstone is commonly interpreted as representing a longer-term desertification event of ambiguous origin (Soreghan and Soreghan, 2007; Soreghan et al., 2008, 2020, 2023; Tabor and Poulsen, 2008).

Evidence for large-scale aridification during the Carboniferous–Permian is not restricted to Paradox Basin; indeed, coeval basins throughout Pangea all display a decline in lithologic characteristics associated with wet climates (i.e., coal, laterite, and bauxites) and an increase in those that indicate arid climates (calcrete, evaporites, and eolianites) (Soreghan and Soreghan, 2007; Soreghan et al., 2008, 2020, 2023; Tabor and Poulsen, 2008; Pardo et al., 2019). This environmental shift is also reflected in paleoequatorial fossil sites (blue circles in Fig. 2), which show a shift to more abundant terrestrial taxa in the early Permian (Pardo et al., 2019). Due to the widespread nature of central Pangean arid lithologies and terrestrial life during the Late Carboniferous–Cisuralian, it is not unreasonable to postulate that the aridity trend exhibited by the lower Cutler Group is related to a near-global climatic shift as opposed to an autocyclic event or lateral migration of facies independent of climate. Nevertheless, uncertainty persists with regards to inter-basinal temporal correlation between the Cutler Group and other C–P assemblages, such as the classically studied mid-continental and Texas–Oklahoma regions in North America, the Dunkard Group in West Virginia and Pennsylvania, the Lodève Basin in France, and the Saar–Nahe Basin in Germany (blue circles in

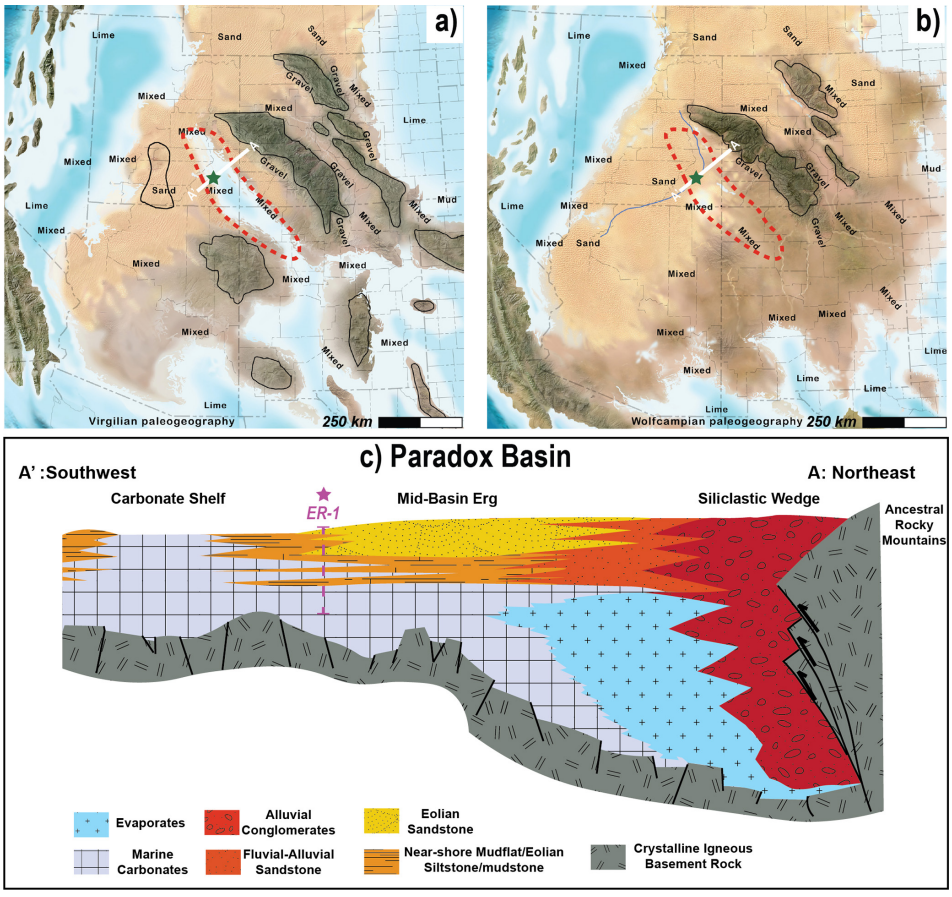

Figure 4. **(a)** and **(b)**: paleogeography of Paradox Basin (red outline) during the Virgilian and Wolfcampaian, respectively (modified from Blakey, 2019); green stars are the locations of ER-1. **(c)** Southwest–northeast cross section of Paradox Basin during the C–P. Note the three successive facies of the Cutler Group: siliciclastic wedge, mid-basin erg, and carbonate shelf. The vertical green dashed line to the left represents ER-1. Figure 4c is modified from Baars and Stevenson (1981), Goldhammer et al. (1991), Guthrie and Bohacs (2009), and Whidden et al. (2014). The location of line A–A' is shown in Fig. 4a–b.

Fig. 2) (Romer, 1945; Parrish, 1978; Boy and Fichter, 1982; Craddock et al., 1989; Eberth et al., 2000; Uhl et al., 2004; Tabor and Poulsen, 2008; Michel et al., 2015; Pfeifer et al., 2020). Therefore, one of the goals of PERMIA is to analyze the ER-1 core with the goal of building a robust dataset of biostratigraphic and geochronological age controls and paleoclimate proxies with unambiguous superposition, allowing for the correlation between the lower Cutler Group and these other late Paleozoic records. Additionally, this work complements the ongoing Deep Dust Project targeting mid-continent and European sites recording the Early to Middle Permian collapse of the Late Paleozoic Ice Age (blue circles in Fig. 2) (Soreghan et al., 2020).

2 ER-1

2.1 Historical context and selection by PERMIA

The ER-1 core was collected in the early 1980s as part of a national study for determining potential subsurface storage sites for high-level radioactive waste. This federal project, named the National Waste Terminal Storage Program, was founded in 1976 by the Energy Research and Development Administration (ERDA), a precursor to the United States Department of Energy (DOE) (Woodward-Clyde Consultants, 1982b). This initiative aimed to identify suitable locations for the permanent, long-term disposal of high-level radioactive waste arising from nuclear weapons production and electricity generation (Interagency Review Group on Nuclear Waste Management, 1978; Woodward-Clyde Consultants, 1982a, b; Thackston et al., 1984). Due to the long half-life of radioactive waste, ideal long-term geologic storage necessitates that the toxic materials be relocated to tectonically inactive areas where they will be completely sealed and isolated from adjacent hydrologic units over geologic timescales (i.e., ~ 100 000 years) (European Commission, 2004; Ahn and Apted, 2010). At the time, subsurface salt deposits, which are highly impermeable, were considered one of the best candidates for deep geologic repositories (Pierce and Rich,

1962; Hansen and Leigh, 2011). This led to the investigation of several evaporite-bearing basins in the continental United States, including Paradox Basin in southern Utah (Fig. 4). To better understand both the properties of the Paradox evaporites and the overlying hydrogeologic system, at least two rock cores were collected by Woodward-Clyde Consultants, the ER-1 and Gibson Dome no. 1 (GD-1) cores (Fig. 3a) (Woodward-Clyde Consultants, 1982a, b; Thackston et al., 1984). After several years of investigation, the Elk Ridge site was abandoned in favor of the Yucca Mountain, Nevada, site (Blanchard, 1985; U.S. Department of Energy, 1986; Keeney, 1987; Merkhofer and Keeney, 1987; McCleary, 1989; Stuckless and Levich, 2016), but the ER-1 and GD-1 cores were archived at the Austin Core Research Center and have become available for scientific study.

For the PERMIA project, the decision to prioritize the ER-1 core over the GD-1 core was primarily influenced by the need to minimize the potential influence of salt tectonics. Despite their shared penetration of formations of interest and biostratigraphic controls, GD-1's proximity to regions characterized by significant salt-tectonic activity (Fig. 4) raised concerns about potential alteration to the sedimentary record. In contrast, ER-1 is situated in a more geologically stable area, making it the most favorable choice for conducting precise paleoclimatic analyses and preserving the integrity of the sedimentary data required for PERMIA. In addition, the ER-1 site is more centrally located between rich outcrop archives of paleontological and paleoenvironmental information that are also part of our project, between the Valley of the Gods–Mexican Hat area to the southwest and the Indian Creek and greater Canyonlands areas to the north.

2.2 Drilling, initial handling, and storage of ER-1

The ER-1 core is a continuous 933.5 m long 6.35 cm diameter (HQ) core which was collected by operators Woodward-Clyde Consultants from San Juan County, Utah, USA (Fig. 3), between 5 August and 30 September 1981. Woodward-Clyde Consultants contracted Zimmerman Well Service for the drilling and installation of a 127.7 m (419 ft) surface casing, which was prepared using an 8 ton well drilling rig. Woodward-Clyde Consultants then contracted Boyles Brothers for coring operations, employing a Chicago-Pneumatic Model 50 rig (additional details available in Woodward-Clyde Consultants, 1982a).

The core was collected from an initial depth of 127.7 m (419 ft) to a final depth of 1061.2 m (3481.6 ft). To prevent dissolution of Paradox Formation evaporites, the drilling fluid consisted of a cellulose polymer mixed with "Moab brine", a salt-saturated fluid produced by pumping freshwater into the Paradox Formation at Moab, Utah (Woodward-Clyde Consultants, 1982a; Thackston et al., 1984). The cellulose polymer, specified in Woodward-Clyde (1982a) as Mark IV and Hi-Vis, was provided by Western Mud Company (Woodward-Clyde Consultants, 1982a), which is now known as GEO Drilling Fluids, Inc (GEO Drilling Fluids Inc., 2023). Unfortunately, during the drilling process, substantial amounts of lost circulation were encountered while drilling through the Middle Pennsylvanian Pinkerton Trail Formation at ∼ 1061 m depth, preventing the penetration of the underlying Mississippian Leadville Limestone as originally planned (Thackston et al., 1984; Woodward-Clyde Consultants, 1982a). Nevertheless, the successful collection of the Carboniferous–Permian lower Cutler Group, which comprises the top ∼ 313 m of the ER-1 core, makes it ideal for accomplishing the research objectives of PERMIA. Geologic mapping of the area indicates that beds have a regional dip of no more than 1–3 ° (Lewis et al., 2011). This, in conjunction with the minimally reported borehole deviation (Woodward-Clyde, 1982a), suggests that the cores represent a near-vertical cross section of the rock formations under study.

Detailed descriptions of core collection and handling are provided in Woodward-Clyde (1982a). To briefly summarize, the wire-line diamond coring method and split inner-core barrels were utilized to minimize damage to the core. Core runs, measured by Woodward-Clyde in feet, were continuously collected at ∼ 10 ft (∼ 3.05 m) intervals. Once brought to the surface, core runs were transported to an on-site core handling building, where they were opened, placed onto roller tracks, fitted together at breaks, examined for core loss, washed, measured, and directly marked with depth measurements (in feet) at 1 ft (∼ 30.5 cm) intervals. Subsections of individual core runs were completely sampled on the occasion that said portions exhibited notable amounts of hydrocarbons. Otherwise, the core runs were cut into 2 ft (∼ 61 cm) sections with a diamond saw, wrapped in plastic, and placed into cardboard core boxes. Depth measurements, run numbers, locations, dates, and, if present, core loss and/or complete removal of sampled subsections were noted directly on the box lid as well as on labels taped to the box bottom.

The cores were shipped to an interim storage facility known as the "ONWI core storage facility", which was in Lakewood, Colorado (Woodward-Clyde, 1982a). The cores were eventually transferred to the Austin Core Research Center (CRC), part of the Bureau of Economic Geology in Austin, Texas. As of 2022, 98.3 % of the top 451.1 m of ER-1 remained in storage at the CRC. This exceptional level of preservation can be attributed to a combination of factors, including a high initial drilling recovery rate of 99.8 % (450.3 m recovered out of 451.1 m drilled) and a relatively minor amount of sampling from previous studies, totaling approximately 6.98 m, or 1.5 %, of removal of whole-core (unsplit) samples.

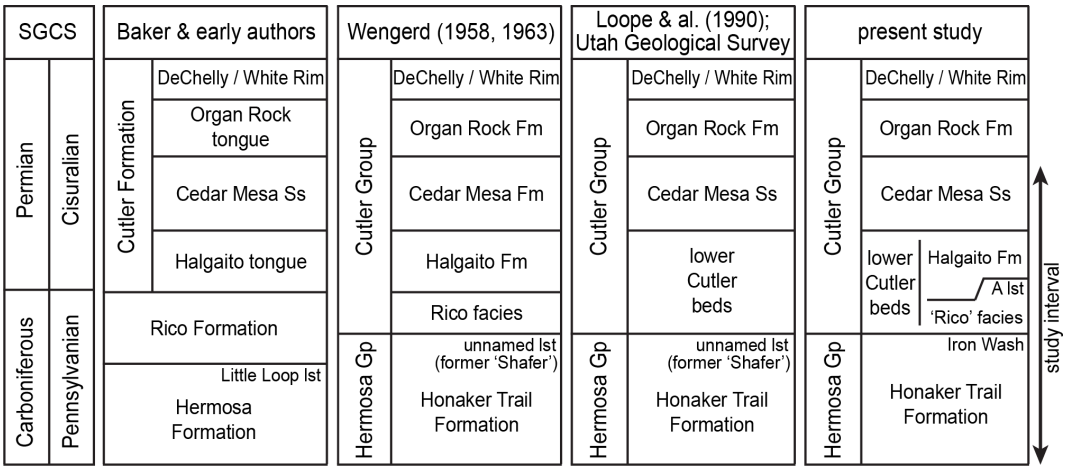

Figure 5. Stratigraphic subdivisions of the Carboniferous–Permian Cutler Group exposed in Valley of the Gods and its vicinity, southeastern Utah, USA. Abbreviations: Ss, Sandstone; Gp, Group; lst, limestone; Fm, Formation. Modified from Huttenlocker et al. (2018).

2.3 Previous research

2.3.1 Geologic descriptions from Woodward-Clyde

Originally described by Woodward-Clyde (1982b), the ER-1 core recovered ~ 933.5 m of late Paleozoic sediment, encompassing the lower portion of the Cedar Mesa Sandstone down to the Middle Pennsylvanian Pinkerton Trail Formation. The incomplete recovery of the Cedar Mesa Sandstone is a result of the ER-1 borehole being drilled and cased to a depth of 127.7 m (419 ft) prior to coring. This interval included Cenozoic surficial sediments directly overlying exposures of the upper portion of the Cedar Mesa Sandstone. Therefore, though the original report measured the total thickness of the Cedar Mesa Sandstone at the drilling site at 252.98 m, the ER-1 core only recovered the lowermost 128.3 m of this unit.

In the original lithologic description, the Cedar Mesa Sandstone is generally described as a sequence of light-colored, well-sorted, quartz-rich, carbonate-cemented, and primarily cross-bedded sandstones. Though primarily comprising sandstone, a limited number of thin reddish siltstone and sandy siltstone interbeds were also observed. Below the Cedar Mesa Sandstone is a heterogeneous collection of siltstone, sandy siltstone, and sandstone with occasional limestone interbeds. Measured to a thickness of 138.9 m, Woodward-Clyde (1982b) referred to this section as the "Elephant Canyon Formation", a now obsolete name roughly equivalent to what are currently referred to as the "lower Cutler beds" (Loope et al., 1990; Jordan and Mountney, 2012).

Underlying the Elephant Canyon Formation is the Upper Carboniferous Hermosa Group, which consists of the Honaker Trail, Paradox, and Pinkerton Trail formations in descending order. In ER-1, the Honaker Trail Formation was measured to a thickness of ~ 374.3 m and primarily consists of calcite-rich carbonate rocks (primarily limestones and cherty limestones). Nevertheless, ~ 30 % of the Honaker Trail in ER-1 is described as consisting of siliciclastics (siltstones and sandstones) and dolomitic interbeds. Woodward-Clyde noted a gradational contact between the Honaker Trail and the underlying Paradox Formation, the latter of which was measured to a thickness of 291.4 m; 29 % of the Paradox Formation in ER-1 is described as halite, with the remainder consisting of siltstone, shale, anhydrite, limestone, and dolomite. Woodward-Clyde described this unit as highly cyclical with four to six sequences correlated with the regionally recognized salt cycles of the Paradox Formation (specifically, cycles 6, 7, 9, and 13 and potentially cycles 15 and 16) (Peterson and Hite, 1969; Hite and Buckner, 1981; Woodward-Clyde Consultants, 1982a, b). The lowest unit of the Hermosa Group and the deepest deposit recovered by ER-1 is the Pinkerton Trail Formation. Woodward-Clyde (1982b) describes the formation as primarily consisting of limestone and calcareous siltstone, with some minor units of dolomite and anhydrite. Though drilling plans originally intended to recover both the underlying Molas and Leadville formations, substantial drilling fluid loss forced the termination of drilling activities after recovering only 51.8 m of the Pinkerton Trail (Woodward-Clyde Consultants, 1982a, b).

2.3.2 Previous age control

Since recovery, various researchers have examined portions of the ER-1 core for biostratigraphic analysis, sedimentological analysis, and regional stratigraphic correlations (Loope and Watkins, 1989; Atchley, 1990; Nail et al., 1994, 1996; Tromp, 1995; Raup and Hite, 1996; Tuttle et al., 1996; Nail, 1996; Atchley and Loope, 1993; Petrychenko et al., 2012; Rasmussen and Rasmussen, 2018). The identification of Late Carboniferous conodonts and fusulinids within ER-1 by Nail et al. (1996) implies a late Missourian through middle Virgilian age for the Honaker Trail Formation and a late Virgilian age for the lowermost limestones of the lower part

of the lower Cutler beds (Fig. 7). These age constraints are consistent with outcrop work in nearby Arch Canyon and Valley of the Gods, where Huttenlocker et al. (2021) identified the conodont *Adetognathus* sp. B in the upper part of the lower Cutler beds. The presence of this conodont species, now referred to as *Adetognathus carlinensis* (see Beauchamp et al., 2022), which is known from the C–P interval (latest Gzhelian–early Asselian) of the Canadian Arctic and eastern–central British Columbia (Henderson et al., 1995), suggests that the C–P transition can be identified in the lower Cutler beds, including the ER-1 site. To this end, see the "Continuing science plans" section of this paper for ongoing research on the biostratigraphy of the ER-1 core.

3 PERMIA core analysis

In early 2023, the top 450 m (corresponding to a depth of 127.77–581 m) of the ER-1 core was transported from the Austin Core Research Center to the Continental Scientific Drilling Facility at the University of Minnesota for preparation and analysis. Upon arrival, all core sections were photographed in their respective boxes and placed in transparent plastic core liners with end-caps indicating the stratigraphic top and bottom of each core section. The liners enabled detailed scanning and processing workflows aligned with best practices established in numerous recent scientific drilling projects (e.g., Clyde et al., 2013; Cohen et al., 2016; Olsen et al., 2018). Evidence of core degradation was minimal, limited to salt crystals from dried drilling fluid on the surface of some sandstone core segments. The geophysical properties of the whole cores were measured using a Geotek Standard Multisensor Core Logger and included magnetic susceptibility (loop), gamma density, p-wave velocity and amplitude, natural gamma radiation, and electrical resistivity.

Using a diamond-blade rock saw with continuous deionized water flush, the core was split lengthwise into two halves: an archive half which was placed into storage and a work half which was subjected to further analysis and subsampling. To eliminate saw marks and enhance the clarity of the split core face, the working halves were polished using either dry or wet rock polishers. This step was necessary to more clearly image sedimentary structures and microfossils that were obscured by the cutting process. The polished working halves were imaged at 20 pixels per millimeter resolution using the Geotek Core Imaging System. Additionally, high-resolution point magnetic susceptibility and color reflectance spectrophotometry of the core face were measured using a Geotek XYZ Multisensor Core Logger. Core depth scales were generated by applying a linear compression factor for core runs to fit the drilled interval when recovery wad $> 100\,\%$ (equivalent to the CSF-B depth scale used in scientific ocean drilling, e.g., Expedition 337 Scientists, 2013).

Employing Corelyzer software, the PERMIA team directly compared the physical core sections with their high-resolution images and accompanying geophysical datasets (Ito et al., 2023). These visual representations enabled comprehensive lithologic descriptions of each core section, which were recorded using the PSICAT software program (Reed et al., 2007).

4 Initial results

One of the initial goals of PERMIA was to refine the stratigraphy of ER-1 within an updated regional stratigraphic framework using currently accepted terms (Loope et al., 1990; Fig. 5). Examination of the polished split cores and high-resolution core images (e.g., Fig. 6) in the stratigraphic context using the Corelyzer visualization environment (Ito et al., 2023) allowed for more accurate determinations of lithology, stratigraphic contacts, sedimentary structures, and microfossils. By comparing this new dataset to recent stratigraphic work (Loope et al., 1990; Dubiel et al., 1996, 2009; Condon, 1997; Ritter et al., 2002; Mountney and Jagger, 2004; Jordan and Mountney, 2012), PERMIA updated the stratigraphy of the upper core to reflect more accurately the accepted lithostratigraphic nomenclature (Fig. 5) and associated boundaries (Fig. 7). Specifically, we place the Cedar Mesa Sandstone–lower Cutler beds contact at 318.9 m depth and the lower Cutler beds–Honaker Trail Formation (Cutler Group–Hermosa Group) boundary at 442.6 m depth. These placements are consistent with the lithostratigraphic boundaries as observed in nearby outcrops (e.g., the Arch Canyon and Valley of the Gods area) and descriptions in the published literature.

Our placement of the Cutler–Honaker Trail boundary is at a marked change to redder, predominantly non-calcareous siltstone with less abundant and much thinner marine carbonate layers and more common sandstone layers. This is consistent with the lithologic changes observed in outcrops along the southern margin of Cedar Mesa (e.g., Valley of the Gods and Goosenecks of the San Juan State Park areas), where a mixed siliciclastic–carbonate succession with abundant marine limestones (the Honaker Trail Formation) is overlain by siltstone and sandstone redbeds with rare, thin marine limestones (the local equivalent of the lower Cutler beds called the Halgaito Formation) (Baker, 1936; G. S. Soreghan et al., 2002; Ritter et al, 2002; Huttenlocker et al., 2021). The color change associated with this boundary is apparent in the core line scan image stack (Fig. 7), where our boundary placement also marks a change from drab brown and tan colors below to darker reddish-brown colors above. Also notable is that our placement of the Honaker Trail–Cutler boundary is just above three sandstone units associated with marine limestones (sandstones otherwise being rare in the Honaker Trail Formation), a lithologic association also observed in outcrops in the uppermost Honaker Trail Formation at its eponymous locality just south of Cedar Mesa (Ritter et al., 2002: Figs. 3, 5). Some previous stratigraphic studies em-

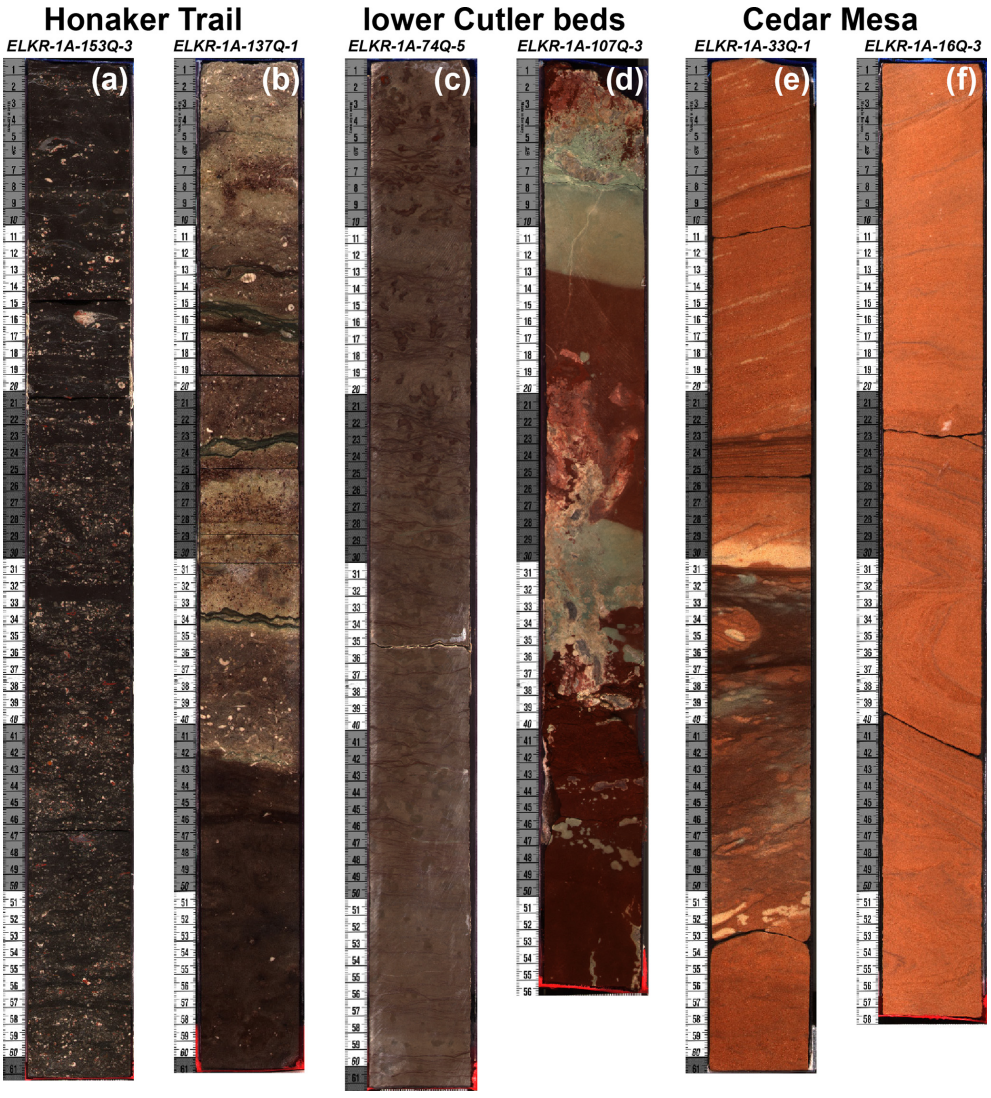

Figure 6. Representative facies in core segments from the ER-1 core. **(a)** Fossiliferous limestone layer from the Honaker Trail Formation. **(b)** Contact between a carbonaceous siltstone (lower darker unit) and a lighter-colored fossiliferous limestone unit (upper light-grey unit) in the Honaker Trail Formation. **(c)** Calcareous siltstone with abundant burrows in the lower Cutler beds. **(d)** Siltstone redbed units in the lower Cutler beds, with abundant reduction zones. **(e)** Cross-bedded sandstone unit from the Cedar Mesa Sandstone with a dark-brown siltstone interbed. **(f)** Cross-bedded sandstone unit from the Cedar Mesa Sandstone.

phasize that the contact in this area forms a change in the weathering profile from the canyon or cliff down-section to the slope and pillar-forming lower Cutler above (e.g., Baker, 1936; Gregory, 1938), but this cannot be evaluated in the core.

We place the lower Cutler beds–Cedar Mesa Sandstone boundary at the base of the first thick (> 20 m) cross-bedded sandstone, marking a rather abrupt change from strata dominated by dark reddish-brown siltstone with less common thin (typically < 5 m thick) sandstone packages, to thick (> 10 m), predominately cross-bedded light-colored sandstones separated by occasional thin reddish-brown siltstones (all < 5 m thick and often less than 1 m thick). This boundary placement is just above the highest unambiguous marine unit, a wavy-laminated dark reddish-brown sandy siltstone between 323 and 318.9 m depth containing abundant disarticulated echinoderm elements. Locating the lower Cutler–Cedar Mesa boundary above the last marine unit and at the base of the first thick sandstone sequence is also consistent with its placement in outcrops by recent stratigraphic studies (e.g., Stanesco and Campbell, 1989; Loope et al., 1990; Dubiel et al., 1996, 2009; Jordan and Mountney, 2012; Huttenlocker et al., 2021; Pettigrew et al., 2021). Our boundary placement is also associated with a noticeable decrease in magnetic susceptibility, gamma density, and natural gamma radiation values (Fig. 7), which other authors have observed

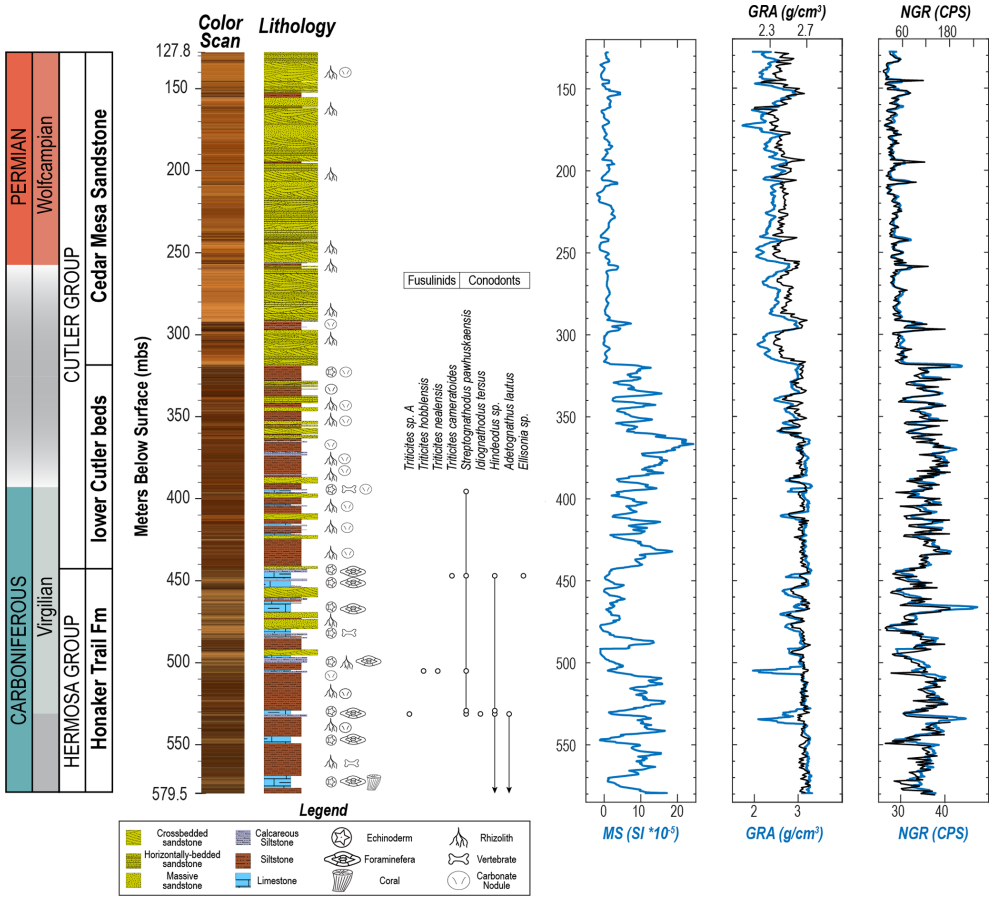

Figure 7. Generalized stratigraphic column of the top 450 m of the ER-1 core. Left to right: color profile from spectrophotometry, lithology, published biostratigraphic controls (from Nail et al., 1996), core magnetic susceptibility (MS), gamma ray attenuation density (GRA) from both core (blue) and well log (black), and natural gamma radiation from both core (blue) and well log (black). Though all three lithologic units are present throughout the core, limestones, siltstones, and sandstones are thickest and most common within the Honaker Trail, lower Cutler beds, and Cedar Mesa formations, respectively. Moreover, there is a notable negative secular trend in both the magnetic susceptibility and gamma density values as the lower Cutler beds transition into the Cedar Mesa Sandstone. Note that the geologic timescale uses the regional terms Virgilian and Wolfcampian, which roughly correspond to the Gzhelian and Asselian stages, respectively. Grey zones between chronostratigraphic terms indicate uncertainty in boundary placement.

at this contact from wells in the same area (Fig. 8 in Condon, 1997).

Overall, the core is dominated by a relatively small number of lithologies. Carbonate layers are typically either sandy to silty limestones containing abundant marine fossils (echinoderms, brachiopods, bivalves, fusulinids) or thin carbonate layers devoid of visible fossils and with mostly nodular textures. The fossiliferous marine carbonate facies are only observed in the Honaker Trail Formation and lower Cutler beds, whereas the non-fossiliferous carbonates are found throughout the core and appear to be mostly non-marine in origin (i.e., they are associated with pedogenically modified siltstones). Carbonate-rich siltstones are often associated with both of these limestone facies and are also present as thin layers associated with dark reddish-brown siltstones within the Cedar Mesa Sandstone. Brown to dark reddish-brown siltstones and sandy siltstones are either parallel-bedded and are sometimes laminated or massive. The latter are often both mottled and contain carbonate nodules. These siltstone facies comprise the majority of the Honaker Trail Formation and lower Cutler beds but also form thin (< 5 m thick) layers between the thick sandstones of the Cedar Mesa Sandstone. Predominantly orange, tan, and pinkish-grey fine- to medium-grained sandstones are typically trough cross-bedded or parallel-bedded, though a small number of units are apparently massive (acknowledging the restricted lateral view of a core). Sandstones are rare in the Honaker Trail Formation, except for an interval between 440 and 500 m depth, more common (but still subordinate to siltstone) in the lower Cutler beds, and dominate the Cedar Mesa Sandstone. In the latter, they are mostly trough cross-bedded, but parallel-bedded and massive units are present, particularly just above

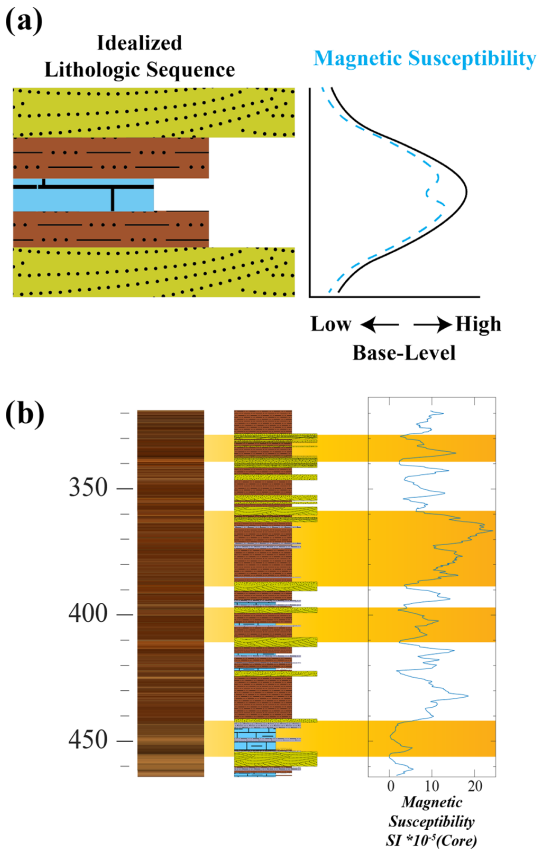

Figure 8. **(a)** Idealized lithologic sequence and associated response in MS. In this model lower base levels correspond to more arid conditions, resulting in sandstones composed of relatively weakly magnetic to non-magnetic minerals (i.e., hematite). As base levels rise, conditions become wetter, corresponding to finer and more magnetic minerals. However, fully marine environments (limestone) correspond to a magnetic decrease. As the base level lowers and arid conditions return, sandstones composed of weak magnetic material are deposited once again. **(b)** ER-1 from 460 to 320 m CSF-B, with certain cycles highlighted in orange. Note that each cycle is book-ended by sandstone layers.

and below silty layers. The fact that we often observe gradational transitions between lithologies (i.e., sandy siltstones between sandstones and siltstones, calcareous siltstones between carbonates and siltstones) and a lack of observable erosive contacts supports our inference that the core lacks any significant discontinuities.

This variety of lithologies can be grouped into three informal lithofacies associations: (1) clastic to silty fossiliferous limestones; (2) massive to horizontally bedded calcareous and non-calcareous siltstone; and (3) massive, horizontally bedded, and cross-bedded fine-grained sandstone (Figs. 6–7). Siltstones in all three formations show extensive evidence of pedogenic modification (e.g., mottling, carbonate nodules) (Fig. 6). Though all three rock types are present within each formation, limestones become less abundant up-section, being most common and thickest in the Honaker Trail Formation, siltstones are most common in the Honaker Trail Formation and lower Cutler beds, whereas cross-bedded sandstones dominate the Cedar Mesa Sandstone.

Cyclic variation both within and among these three rock types is common throughout the core, regardless of stratigraphic unit. In the Honaker Trail Formation, this cyclicity is manifested predominantly as siltstone–limestone couplets, whereas in the overlying lower Cutler beds it consists of siltstone–sandstone couplets, with occasional limestone or calcareous siltstone layers in the middle of the siltstones. In the Cedar Mesa Sandstone, the main cyclicity is an alternation between trough cross-bedded sandstone, parallel-bedded or massive sandstone, and thin siltstone beds. These lithologic cycles match those observed by other authors in equivalent outcrops in Paradox Basin (e.g., Ritter et al., 2002; Mountney, 2006; Williams, 2009; Jordan and Mountney, 2012; Langford and Salsman, 2014; Olivier et al., 2023). Comparing these lithologic cycles to the geophysical data, siltstones generally have a much higher magnetic susceptibility than either sandstone or limestone layers. This results in a distinct cyclical pattern in the magnetic susceptibility data (Figs. 7–8), which aligns with corresponding cycles in the lithostratigraphy. On a larger scale, the magnetic data exhibit a negative secular trend as the lower Cutler beds transition into the more sandstone-dominated Cedar Mesa Sandstone (Fig. 7).

5 Continuing science plans

With initial core processing completed, the micropaleontological, geochemical, and paleomagnetic properties of ER-1 are currently being analyzed, the primary goal being the construction of a robust paleoenvironmental reconstruction anchored by reliable geochronologic controls. Though no known volcanic ash layers (and few juvenile detrital zircons) have yet to be identified in the lower Cutler Group, several approaches are available to date the core effectively. First, Nail et al. (1996) already recovered biostratigraphically useful fusulinids and conodonts from several levels within the core, and polished split core segments of ER-1 revealed highly fossiliferous carbonate layers in the Honaker Trail Formation (Fig. 6) and the lower Cutler Group (Fig. 7); together, this implies that the core can be precisely dated using biostratigraphic methods. Such an approach has been applied successfully to the underlying Carboniferous Hermosa Group (Ritter et al., 2002) as well as outcrop exposures of the lower Cutler beds in the region, where widespread presence of conodonts in marine carbonate layers (Figs. 3, 4) allowed for correlation with well-resolved marine biochronologies from elsewhere (Fig. 7) (Huttenlocker et al., 2021). Indeed, conodont biostratigraphy is the gold standard used to define the C–P boundary at both the Asselian GSSP (Usolka, Ural Mountains) (Chernykh and Ritter, 1997; Chernykh et al.,

1997) and North American mid-continental sections (Ritter, 1995; Wardlaw, 2005; Boardman et al., 2009; Wardlaw and Nestell, 2014; Henderson, 2018). Formal identification of the C–P boundary within the Cutler Group remains critical for correlating Utah's rock record with the geologic timescale as well as other relevant C–P paleoenvironmental and paleontological archives across Pangea. Complementary to the biostratigraphic approach, the global marine $^{87}Sr/^{86}Sr$ record – a proxy for Phanerozoic seawater Sr (Veizer, 1989; McArthur et al., 2020) – shows a steep decrease from base-Ghzelian (latest Carboniferous) values of 0.7081–0.7087 to 0.7079–0.7081 by the end of the Asselian (earliest Permian) (Korte et al., 2006; Korte and Ullmann, 2018; Chen et al., 2018). Thus, a time series of $^{87}Sr/^{86}Sr$ isotope values from marine carbonates and the associated conodont bioapatite should accurately place the Cutler sequence along the C–P strontium reference curve. Therefore, we sampled all major marine limestone units in the studied portion of the core for conodonts, fusulinids, and $^{87}Sr/^{86}Sr$ isotopes.

Previous attempts at dating through paleomagnetic methods confirmed that deposition of the Cutler Group coincides with the Kiaman-reversed superchron (Gose and Helsley, 1972; Scott, 1975) (Fig. 1). This interval should also include the short-lived "Kartamyshian event", a normal polarity magnetozone dated to ∼ 299 Ma (Fig. 1), and if found within this core and outcrop, it would serve as a useful maximum age constraint and datum for the top of the Carboniferous (Hounslow and Balabanov, 2016). Previous work (Gose and Helsley, 1972; Scott, 1975) indicates that the lower Cutler beds preserve a primary magnetic remanence, and we therefore should be able to identify the Kartamyshian event if it is present.

Furthermore, cyclic sedimentation patterns established in the Cutler Group (G. S. Soreghan et al., 2002; Jordan and Mountney, 2012; Golab, 2016; Golab et al., 2018; Tobey, 2020) strongly suggest that astronomically tuned geochemical and magnetic cyclostratigraphy can provide high-resolution age models for these deposits. Various studies have shown that long-term eccentricity cycles (∼ 405–413 kyr) have been stable throughout Earth's history (Olsen and Kent, 1999; Horton et al., 2012; Kent et al., 2017, 2018; Lantink et al., 2019; Olsen et al., 2019). Indeed, in the Canyonlands area, Jordan and Mountney (2012) identified lithologic cycles in the lower Cutler beds, which they hypothesized were reflective of long eccentricity cycles. The magnetic susceptibility record of ER-1 (Figs. 7–8), along with previous environmental–magnetic studies of the Halgaito Formation near Mexican Hat (G. S. Soreghan et al., 2002), demonstrate that cyclic facies changes correspond to variations in magnetic properties (Fig. 8). This provides strong evidence that it is possible to construct a magnetic cyclostratigraphic framework anchored by biostratigraphic, strontium isotope, and paleomagnetic age constraints.

This high-resolution geochronological dataset will be constructed in tandem with the measurement of various geophysical and geochemical paleoclimatic proxies. This will include the whole-core geophysical data presented in this paper (e.g., MS, NGR, color scans) (Fig. 7), high-resolution XRF core scans (in progress), and environmental magnetic (Verosub and Roberts, 1995; Evans and Heller, 2003; Liu et al., 2012) measurements of discrete specimens. Furthermore, similar datasets will be collected from outcrop sites (Fig. 3a), enabling the development of a robust and temporally constrained paleoenvironmental framework for this region during the C–P transition. Finally, this model will be correlated with a high-resolution dataset of georeferenced vertebrate sites and specimens (in progress) as a means of testing the Vaughn–Olson model (Pardo et al., 2019) and other important questions regarding the C–P transition.

1. Do independent paleoenvironmental proxies and magnetic mineral assemblages record a secular drying trend across the lower Cutler bed–Cedar Mesa Sandstone transition?

2. Is this transition rapid and concurrent with the established LPIA maximum (Gzhelian), or does it instead follow a longer-term trend that matches the paleomagnetically determined northward drift of North America into a more arid paleolatitudinal climate belt?

3. What effect, if any, did these paleoclimatic changes have on the evolution of C–P vertebrate communities?

6 Broader impacts

Our analysis of the ER-1 core will improve the geochronological and paleoenvironmental context for the important paleontological and geological archives of the C–P transition preserved within Bears Ears National Monument. Thus, these core data enrich and elevate the global importance of the at-risk scientific resources preserved within the monument (Gay et al., 2020). By clarifying the processes driving equatorial climate and biotic change during the Late Paleozoic Ice Age, the study of the ER-1 core strengthens our ability to use the LPIA and its decline as a natural deep time analog that can be compared with ongoing anthropogenically driven global warming and ecological change. Data and conclusions from our ER-1 studies will be integrated into all levels of education and public engagement, from informal settings such as public exhibits in local communities in southeastern Utah to K-12 public school and higher-education classrooms. We are working with education experts at the Natural History Museum of Utah to develop curriculum resources, and the core images and associated data will be investigated and analyzed by undergraduate students, as one of us (RBI) has done with similar data from the CPCP project (Olsen et al., 2018).

7 Summary

By continuing to analyze the ER-1 core, we expect to gain further insight into the precise timing of regional late Paleozoic drying and its relationship with the collapse of the LPIA, ca. 304–280 million years ago. Furthermore, by correlating this new dataset with planned paleontological field work, we intend to enhance our comprehension of the biotic impacts resulting from Earth's last pre-Quaternary icehouse–hothouse state change. As present-day anthropogenic climate change threatens to destabilize a multitude of environments, improvements in our understanding of how major climate processes have impacted biomes in the past are increasingly relevant. To this end, the outcome of this study will benefit climate modelers, policy makers, ecologists, and the many communities impacted by climate change.

Data availability. The archive and work halves of the ER-1 cores are permanently stored at the Austin Core Research Center (CRC), run by the Bureau of Economic Geology (BEG) in Austin, Texas.

Author contributions. JMGS, JMF, AKH, RBI, DR, RD, JM, KBS, RO, AS, and PS helped process the core, conduct measurements, and collect images. JMGS drafted Figs. 2, 4, 5, 6 and 7. AKH drafted Figs. 1 and 4. RBI and JMGS co-drafted Fig. 3. JMF and JMGS co-drafted Fig. 8. JMGS, JMF, AKH, RBI, CMH, MTR, and AN contributed to editing the final versions of the figures. All the authors have read and approved the current version of the manuscript and figures.

Competing interests. The contact author has declared that none of the authors has any competing interests.

Disclaimer. Publisher's note: Copernicus Publications remains neutral with regard to jurisdictional claims made in the text, published maps, institutional affiliations, or any other geographical representation in this paper. While Copernicus Publications makes every effort to include appropriate place names, the final responsibility lies with the authors.

Acknowledgements. The authors thank the personnel at the CSD facility for their support. The authors would also like to thank the UT-Austin Bureau of Economic Geology – Core Research Center for providing access to the core. We are grateful to Don Rasmussen for originally suggesting we examine the ER-1 core. We would also like to thank Carolyn Bishoff and the library staff at Interlibrary Loan (ILL) at the University of Minnesota for acquiring the various reports by Woodward-Clyde Consultants (1982a, b). We are grateful to Judith Totman Parrish, an anonymous reviewer, and editor Ulrich Harms for comments that significantly improved the quality of the manuscript.

The University of Minnesota is built on the ancestral lands of the Wahpekute band that was ceded to the United States by the Treaty of Traverse des Sioux in July of 1851, in an agreement that was not paid in full and whose underlying aim was the dissolution of the Dakota culture. The university has also benefited from Chippewa and Dakota (Mdewakanton, Wahpekute, Wahpeton, and Sisseton bands) land ceded by treaty and given to the University of Minnesota via the Morrill Act. Due to its land-grant status, the infrastructure, financial foundations, faculty, students, and staff at the University of Minnesota all continue to benefit directly from these ceded lands, and we wish to acknowledge this support in our research.

Financial support. This research has been supported by the National Science Foundation Division of Earth Sciences (grant nos. NSF-2221050, NSF-2219902, NSF-2219947, NSF-2153786, and NSF-1951112) and the College of Science and Engineering, University of Minnesota (grant no. UMN GIA-#500130).

Review statement. This paper was edited by Ulrich Harms and reviewed by Judith Totman Parrish and one anonymous referee.

References

Ahn, J. and Apted, M. J.: Geological repository systems for safe disposal of spent nuclear fuels and radioactive waste, Woodhead Publishing, 792 pp., First Edition, https://doi.org/10.1533/9781845699789, 2010.

Atchley, S. C.: Influence of lowstand eolian erosional processes on stratigraphic completeness: sequence stratigraphy of the upper member of the Hermosa Formation (Upper Pennsylvanian), Paradox Basin, southeast Utah, Dissertation, University of Nebraska, Lincoln, Nebraska, 1–135 pp., ISBN 979-8-207-75988-3, 1990.

Atchley, S. C. and Loope, D. B.: Low-stand aeolian influence on stratigraphic completeness: upper member of the Hermosa Formation (latest Carboniferous), southeast Utah, USA, Special Publications of the International Association of Sedimentologists, 16, 127–149, https://doi.org/10.1002/9781444303971.ch9, 1993.

Baars, D. L.: Permian System of Colorado Plateau, Am. Assoc. Pet. Geol. Bull., 46, 149–218, https://doi.org/10.1306/BC74376F-16BE-11D7-8645000102C1865D, 1962.

Baars, D. L. and Stevenson, G. M.: Tectonic evolution of the Paradox Basin, Utah & Colorado, in: Rocky Mountains Association of Geologists, edited by: Wiegand, D. L., Geology of the Paradox Basin, 23–31 pp., ISSN 01675648, 1981.

Baker, A. A.: Geology of the Monument Valley- Navajo Mountain region, San Juan County, Utah, U.S. Geological Survey Bulletin, 865, 1–106, https://doi.org/10.3133/b865, 1936.

Baker, A. A. and Reeside Jr., J. B.: Correlation of the Permian of southern Utah, northern Arizona, northwestern New Mexico, and southwestern Colorado, Am. Assoc. Pet. Geol. Bull., 13, 1413–1448, https://doi.org/10.1306/3D932893-16B1-11D7-8645000102C1865D, 1929.

Beauchamp, B., Henderson, C. M., Dehari, E., Waldbott von Bassenheim, D., Elliot, S., and González, D. C.: Carbonate sed-

imentology and conodont biostratigraphy of late Pennsylvanian-early Permian stratigraphic sequences, Carlin Canyon Nevada: new insights into the tectonic and oceanographic significance of an iconic succession of the Basin and Range, SEPM Spec. Pub., 113, 34–71, https://doi.org/10.2110/sepmsp.113.14, 2022.

Berner, R. A., VandenBrooks, J. M., and Ward, P. D.: Oxygen and evolution, Science, 316, 557–558, https://doi.org/10.1126/science.1140273, 2007.

Billingsley, G. H. and Huntoon, P. W.: Geologic map of Canyonlands National Park and vicinity, Utah, edited by: Breed, W. J., Canyonlands Natural History Association, 1982.

Blakey, R. C.: Pennsylvanian-Jurassic sedimentary basins of the Colorado Plateau and southern Rocky Mountains, in: The Sedimentary Basins of the United States and Canada, Elsevier, 315–367, https://doi.org/10.1016/B978-0-444-63895-3.00007-3, 2019.

Blanchard, B.: Dept of the Interior Comments on Environmental Assessments for the Davis Canyon Site, Washington D.C., 1–64 pp., https://www.nrc.gov/docs/ML0320/ML032050695.pdf (last access: 11 October 2023), 1985.

Boardman, D. R., Wardlaw, B. R., and Nestell, M. K.: Stratigraphy and conodont biostratigraphy of the uppermost Carboniferous and Lower Permian from the North American Midcontinent, Kansas Geological Survey Bulletin, 255, 1–146, 2009.

Boy, J. A. and Fichter, J.: Stratigraphy of the Saar-Nahe Rotliegendes (? Upper Carboniferous – Lower Permian; Germany), Z. Dtsch. Geol. Ges., 133, 607–642, https://doi.org/10.1127/ZDGG/133/1982/607, 1982.

Brocklehurst, N., Ruta, M., Müller, J., and Fröbisch, J.: Elevated extinction rates as a trigger for diversification rate shifts: early amniotes as a case study, Sci. Rep., 5, 17104, https://doi.org/10.1038/srep17104, 2015.

Carpenter, K. and Ottinger, L.: Permo-Pennsylvanian shark teeth from the lower Cutler beds near Moab, Utah, Geol. Intermount. West, 5, 105–116, https://doi.org/10.31711/giw.v5.pp105-116, 2018.

Chen, J., Montañez, I. P., Qi, Y., Shen, S., and Wang, X.: Strontium and carbon isotopic evidence for decoupling of pCO_2 from continental weathering at the apex of the late Paleozoic glaciation, Geology, 46, 395–398, https://doi.org/10.1130/G40093.1, 2018.

Chernykh, V. V. and Ritter, S. M.: *Streptognathodus* (Conodonta) succession at the proposed Carboniferous-Permian boundary stratotype section, Aidaralash Creek, northern Kazakhstan, J. Paleontol., 71, 459–474, https://doi.org/10.1017/S0022336000039470, 1997.

Chernykh, V. V., Ritter, S. M., and Wardlaw, B. R.: *Streptognathodus isolatus* new species (Conodonta): proposed index for the Carboniferous-Permian boundary, J. Paleontol., 71, 162–164, https://doi.org/10.1017/S0022336000039068, 1997.

Cleal, C. J. and Thomas, B. A.: Palaeozoic tropical rainforests and their effect on global climates: is the past the key to the present?, Geobiology, 3, 13–31, https://doi.org/10.1111/j.1472-4669.2005.00043.x, 2005.

Cleal, C. L. and Thomas, B. A.: Tectonics, tropical forest destruction and global warming in the late Palaeozoic, Acta Palaeobotanica, Supplement, 39, 17–19, 1999.

Clyde, W. C., Gingerich, P. D., Wing, S. L., Röhl, U., Westerhold, T., Bowen, G., Johnson, K., Baczynski, A. A., Diefendorf, A., McInerney, F., Schnurrenberger, D., Noren, A., Brady, K., and the BBCP Science Team: Bighorn Basin Coring Project (BBCP): a continental perspective on early Paleogene hyperthermals, Sci. Dril., 16, 21–31, https://doi.org/10.5194/sd-16-21-2013, 2013.

Cohen, A., Campisano, C., Arrowsmith, R., Asrat, A., Behrensmeyer, A. K., Deino, A., Feibel, C., Hill, A., Johnson, R., Kingston, J., Lamb, H., Lowenstein, T., Noren, A., Olago, D., Owen, R. B., Potts, R., Reed, K., Renaut, R., Schäbitz, F., Tiercelin, J.-J., Trauth, M. H., Wynn, J., Ivory, S., Brady, K., O'Grady, R., Rodysill, J., Githiri, J., Russell, J., Foerster, V., Dommain, R., Rucina, S., Deocampo, D., Russell, J., Billingsley, A., Beck, C., Dorenbeck, G., Dullo, L., Feary, D., Garello, D., Gromig, R., Johnson, T., Junginger, A., Karanja, M., Kimburi, E., Mbuthia, A., McCartney, T., McNulty, E., Muiruri, V., Nambiro, E., Negash, E. W., Njagi, D., Wilson, J. N., Rabideaux, N., Raub, T., Sier, M. J., Smith, P., Urban, J., Warren, M., Yadeta, M., Yost, C., and Zinaye, B.: The Hominin Sites and Paleolakes Drilling Project: inferring the environmental context of human evolution from eastern African rift lake deposits, Sci. Dril., 21, 1–16, https://doi.org/10.5194/sd-21-1-2016, 2016.

Condon, S. M.: Geology of the Pennsylvanian and Permian Cutler Group and Permian Kaibab Limestone in the Paradox Basin, southeastern Utah and southwestern Colorado, U.S. Geological Survey Bulletin, 2000-P, 1–59, https://doi.org/10.3133/b00P, 1997.

Craddock, K. W., Hook, R. W., Cummins, W. F., Sternberg, C. H., and Olson, E. C.: An overview of vertebrate collecting in the Permian System of north-central Texas, in: Permo-Carboniforous Vertebrate Paleontology, Lithostratigraphy, and Depositional Environments of North-Central Texas, 40–46, Society of Vertebrate Paleontology, 1989.

Cross, W. and Spencer, A. C.: Geology of the Rico Mountains, Colorado, 21st Annual Report of the United States Geological Survey to the Secretary of the Interior, 1899–1900: Part II – General Geology, Economic Geology, Alaska, Government Printing Office, Washington, D.C, 1900.

DiMichele, W. A., Cecil, C. B., Chaney, D. S., Elrick, S. D., and Nelson, W. J.: Fossil floras from the Pennsylvanian-Permian Cutler Group of southeastern Utah, in: Geology of Utah's Far South: Utah Geological Association Publication, Vol. 43, 491–504, 2014.

Doelling, H. H.: Geologic map of the Fisher Towers 7.5' quadrangle, Grand County, Utah, Utah Geological Survey Map, 183, 1–26, https://doi.org/10.34191/m-183, 2002.

Doelling, H. H., Ross, M. L., and Mulvey, W. E.: Geologic map of the Moab 7.5' quadrangle, Grand County, Utah, Utah Geological Survey Map, 181, 1–38, https://doi.org/10.34191/m-181, 2002.

Dubiel, R. F., Huntoon, J. E., Condon, S. M., and Stanesco, J. D.: Permian deposystems, paleogeography, and paleoclimate of the Paradox Basin and vicinity, in: Paleozoic Systems of the Rocky Mountain Region. Society of Economic Paleontologists and Mineralogists, Rocky Mountain Section, edited by: Longman, M. W. and Sonnenfeld, M. D., Denver, 427–443 pp., 1996.

Dubiel, R. F., Huntoon, J. E., Stanesco, J. D., and Condon, S. M.: Cutler Group alluvial, eolian, and marine deposystems: Permian facies relations and climatic variability in the Paradox Basin, Rocky Mountain Association of Geologists, Denver, The Paradox Basin Revisited, 265–308, edited by: Houston, W. S., Wray, L. L., and Moreland, P. G., 2009.

Eberth, D. A., Berman, D. S., Sumida, S. S., and Hopf, H.: Lower Permian terrestrial paleoenvironments and vertebrate paleoecology of the Tambach Basin (Thuringia, central Germany): the upland holy grail, Palaios, 15, 293–313, https://doi.org/10.1669/0883-1351(2000)015<0293:LPTPAV>2.0.CO;2, 2000.

European Commission: Geological Disposal of Radioactive Wastes Produced by Nuclear Power. From Concept to Implementation, Belgium, 43 pp., ISBN 9789289480901, 2004.

Evans, M. and Heller, F.: Environmental Magnetism: Principles and Applications of Enviromagnetics, 1st ed., Elsevier Science, San Diego, CA, 1–299 pp., ISBN 9780080505787, 2003.

Expedition 337 Scientists: in: Methods, edited by: Inagaki, F., Hinrichs, K.-U., Kubo, Y., and the Expedition 337 Scientists, Proc. IODP, 337: Tokyo (Integrated Ocean Drilling Program Management International, Inc.). https://doi.org/10.2204/iodp.proc.337.102.2013, 2013.

Fielding, C. R., Frank, T. D., and Isbell, J. L.: The late Paleozoic ice age – a review of current understanding and synthesis of global climate patterns, Geol. Soc. Am. Spec. Paper, 441, 343–354, https://doi.org/10.1130/2008.2441(24), 2008.

Frederiksen, N. O.: The rise of the mesophytic flora, Geosci. Man, 4, 17–28, https://doi.org/10.2307/3687204, 1972.

Gastaldo, R. A., DiMichele, W. A., and Pfefferkorn, H. W.: Out of the icehouse into the greenhouse: a late Paleozoic analog for modern global vegetational change, GSA Today, 6, 1–7, 1996.

Gay, R. J., Huttenlocker, A. K., Irmis, R. B., Stegner, M. A., and Uglesich, J.: Paleontology of Bears Ears National Monument (Utah, USA): history of exploration, study, and designation, Geol. Intermount. West, 7, 205–241, https://doi.org/10.31711/giw.v7, 2020.

GEO Drilling Fluids, Inc.: About us, https://geodf.com/about-us/ (last access: 22 September 2023), 2023.

Golab, J. A.: The use of ichnofossils in geological and petrophysical characterizations of aquifers and reservoirs: examples from south-central Texas and southeast Utah, Dissertation, University of Kansas, Lawrence, Kansas, 1–195 pp., http://hdl.handle.net/1808/25778 (last access: 10 November 2023), 2016.

Golab, J. A., Smith, J. J., and Hasiotis, S. T.: Paleoenvironmental and paleogeographic implications of paleosols and ichnofossils in the Upper Pennsylvanian Halgaito Formation, southeastern Utah, Palaios, 33, 296–311, https://doi.org/10.2110/palo.2017.074, 2018.

Goldhammer, R. K., Oswald, E. J., and Dunn, P. A.: Hierarchy of stratigraphic forcing: example from Middle Pennsylvanian shelf carbonates of the Paradox Basin, Kansas Geological Survey Bulletin, 233, 361–413, 1991.

Gose, W. A. and Helsley, C. E.: Paleomagnetic and rock-magnetic studies of the Permian Cutler and Elephant Canyon formations in Utah, J. Geophys. Res., 77, 1534–1548, https://doi.org/10.1029/JB077i008p01534, 1972.

Gregory, H. E.: The San Juan country: a geographic and geologic reconnaissance of southeastern Utah, U.S. Geological Survey Professional Paper 188, 1–123, 1938.

Guthrie, J. M. and Bohacs, K. M.: Spatial variability of source rocks: a critical element for defining the petroleum system of Pennsylvanian carbonate reservoirs of the Paradox Basin, SE Utah, RMAG Special Publication, Denver, edited by: Houston, W. S., Wray, L. L., and Moreland, P. G., 2009.

Hansen, F. D. and Leigh, C. D.: Salt Disposal of Heat-Generating Nuclear Waste, Albuquerque, New Mexico, U.S. Department of Energy Office of Scientific and Technical Information Technical Report, 1–110 pp., https://doi.org/10.2172/1005078, 2011.

Henderson, C. M.: Permian conodont biostratigraphy, Geological Society of London Special Publications, 450, 119–142, https://doi.org/10.1144/SP450.9, 2018.

Henderson, C. M., Pinard, S., and Beauchamp, B.: Biostratigraphic and sequence stratigraphic relationships of Upper Carboniferous conodont and foraminifer distribution, Canadian Arctic Archipelago, Bull. Can. Petrol. Geol., 43, 226–246, https://doi.org/10.35767/GSCPGBULL.43.2.226, 1995.

Hintze, L. F., Willis, G. C., Laes, D. Y. M., Sprinkel, D. A., and Brown, K. D.: Digital geologic map of Utah, Utah Geological Survey, 2000.

Hite, R. J. and Buckner, D. H.: Stratigraphic correlations, facies concepts, and cyclicity in Pennsylvanian rocks of the Paradox Basin, in: Rocky Mountain Association of Geologists, Geology of the Paradox Basin, edited by: Wiegand, D. L., 147–159, 1981.

Horton, D. E., Poulsen, C. J., Montañez, I. P., and DiMichele, W. A.: Eccentricity-paced late Paleozoic climate change, Palaeogeogr. Palaeoclimatol. Palaeoecol., 331–332, https://doi.org/10.1016/j.palaeo.2012.03.014, 2012.

Hounslow, M. W. and Balabanov, Y. P.: A geomagnetic polarity timescale for the Permian, calibrated to stage boundaries, Geological Society of London Special Publications, 450, 63–103, https://doi.org/10.1144/SP450.8, 2016.

Huttenlocker, A. K., Henrici, A., Nelson, W. J., Elrick, S., Berman, D. S., Schlotterbeck, T., and Sumida, S. S.: A multitaxic bonebed near the Carboniferous–Permian boundary (Halgaito Formation, Cutler Group) in Valley of the Gods, Utah, USA: vertebrate paleontology and taphonomy, Palaeogeogr. Palaeoclimatol. Palaeoecol., 499, 72–92, https://doi.org/10.1016/j.palaeo.2018.03.017, 2018.

Huttenlocker, A. K., Henderson, C. M., Berman, D. S., Elrick, S. D., Henrici, A. C., and Nelson, W. J.: Carboniferous–Permian conodonts and the age of the lower Cutler Group in the Bears Ears National Monument and vicinity, Utah, USA, Lethaia, 54, 330–340, https://doi.org/10.1111/let.12405, 2021.

Interagency Review Group on Nuclear Waste Management: Report to the President by the Interagency Review Group on Nuclear Waste Management, Washington, DC (USA), 90 pp., 1978.

Isbell, J. L., Henry, L. C., Gulbranson, E. L., Limarino, C. O., Fraiser, M. L., Koch, Z. J., Ciccioli, P. L., and Dineen, A. A.: Glacial paradoxes during the late Paleozoic ice age: evaluating the equilibrium line altitude as a control on glaciation, Gondwana Research, 22, 1–19, https://doi.org/10.1016/j.gr.2011.11.005, 2012.

Ito, E., Higgins, S., Jenkins, C., Leigh, J., Johnson, A., and Grivna, B.: Corelyzer. v2.2.2, Continental Scientific Drilling Facility, Minneapolis, https://github.com/corewall/corelyzer (last access: 15 January 2024), 2023

Jordan, O. D. and Mountney, N. P.: Styles of interaction between aeolian, fluvial and shallow marine environments in the Pennsylvanian to Permian lower Cutler beds, south-east Utah, USA, Sedimentology, 57, 1357–1385, https://doi.org/10.1111/j.1365-3091.2010.01148.x, 2010.

Jordan, O. D. and Mountney, N. P.: Sequence stratigraphic evolution and cyclicity of an ancient coastal desert sys-

tem: the Pennsylvanian-Permian lower Cutler beds, Paradox Basin, Utah, U.S.A., J. Sediment. Res., 82, 755–780, https://doi.org/10.2110/jsr.2012.54, 2012.

Keeney, R. L.: An analysis of the portfolio of sites to characterize for selecting a nuclear repository, Risk Anal., 7, 195–218, https://doi.org/10.1111/j.1539-6924.1987.tb00982.x, 1987.

Kent, D. V. and Muttoni, G.: Pangea B and the Late Paleozoic Ice Age, Palaeogeogr. Palaeoclimatol. Palaeoecol., 553, 109753, https://doi.org/10.1016/j.palaeo.2020.109753, 2020.

Kent, D. V., Olsen, P. E., and Muttoni, G.: Astrochronostratigraphic polarity time scale (APTS) for the Late Triassic and Early Jurassic from continental sediments and correlation with standard marine stages, Earth Sci. Rev., 166, 153–180, https://doi.org/10.1016/j.earscirev.2016.12.014, 2017.

Kent, D. V., Olsen, P. E., Rasmussen, C., Lepre, C., Mundil, R., Irmis, R. B., Gehrels, G. E., Giesler, D., Geissman, J. W., and Parkerh, W. G.: Empirical evidence for stability of the 405-kiloyear Jupiter-Venus eccentricity cycle over hundreds of millions of years, P. Natl. Acad. Sci. USA, 115, 6153–6158, https://doi.org/10.1073/pnas.1800891115, 2018.

Korte, C. and Ullmann, C. V.: Permian strontium isotope stratigraphy, Geological Society of London Special Publications, 450, 105–118, https://doi.org/10.1144/SP450.5, 2018.

Korte, C., Jasper, T., Kozur, H. W., and Veizer, J.: $^{87}Sr/^{86}Sr$ record of Permian seawater, Palaeogeogr. Palaeoclimatol. Palaeoecol., 240, 89–107, https://doi.org/10.1016/j.palaeo.2006.03.047, 2006.

Langford, R. and Chan, M. A.: Flood surfaces and deflation surfaces within the Cutler Formation and Cedar Mesa Sandstone (Permian), southeastern Utah, Bull. Geol. Soc. Am., 100, 1541–1549, https://doi.org/10.1130/0016-7606(1988)100<1541:FSADSW>2.3.CO;2, 1988.

Langford, R. P. and Salsman, A.: Facies geometries and climatic influence on stratigraphy in the eolian-sabkha transition in the Permian Cedar Mesa Sandstone, SE Utah, Utah Geological Association Publication 43, 275–294, 2014.

Lantink, M. L., Davies, J. H. F. L., Mason, P. R. D., Schaltegger, U., and Hilgen, F. J.: Climate control on banded iron formations linked to orbital eccentricity, Nat. Geosci., 12, 369–374, https://doi.org/10.1038/s41561-019-0332-8, 2019.

Lewis, R. Q., Campbell, R. H., Thaden, R. E., Krummel, W. J. Jr., Willis, G. C., and Matyjasik B.: Geologic map of Elk Ridge and vicinity, San Juan County, Utah (modified from U.S. Geological Survey Professional Paper 474-B), Utah Geological Survey Miscellaneous Publication, 11–1DM, 1–13, https://doi.org/10.34191/mp-11-1dm, 2011.

Liu, Q., Roberts, A. P., Larrasoaa, J. C., Banerjee, S. K., Guyodo, Y., Tauxe, L., and Oldfield, F.: Environmental magnetism: principles and applications, Rev. Geophys., 50, RG4002, https://doi.org/10.1029/2012RG000393, 2012.

Loope, D. B.: Eolian origin of Upper Paleozoic sandstones, southeastern Utah, J. Sediment. Petrol., 54, 563–580, https://doi.org/10.1306/212F846D-2B24-11D7-8648000102C1865D, 1984.

Loope, D. B. and Watkins, D. K.: Pennsylvanian fossils replaced by red chert: early oxidation of pyritic precursors, J. Sediment. Petrol., 59, 375–386, https://doi.org/10.1306/212F8F99-2B24-11D7-8648000102C1865D, 1989.

Loope, D. B., Sanderson, G. A., and Verville, G. J.: Abandonment of the name "Elephant Canyon Formation" in southeastern Utah: physical and temporal implications, Mountain Geologist, 27, 119–130, 1990.

McArthur, J. M., Howarth, R. J., Shields, G. A., and Zhou, Y.: Strontium isotope stratigraphy, in: Geologic Time Scale 2020, edited by: Gradstein, F. M., Ogg, J. G., Schmitz, M. D., and Ogg, G. M., 211–238, Elsevier, Amsterdam, 2020.

McCleary, J.: Characterization of the Davis Canyon site, San Juan County, Utah, as a potential repository for the disposal of high level nuclear waste and spent fuel, Utah Geologic Association: Geology and Hydrology of Hazardous-Waste, Mining-Waste, Water-Waste, and Repository Sites in Utah, 209–222, https://doi.org/10.1016/0148-9062(91)91093-7, 1989.

Merkhofer, M. W. and Keeney, R. L.: A multiattribute utility analysis of alternative sites for the disposal of nuclear waste, Risk Anal., 7, 173–194, https://doi.org/10.1111/j.1539-6924.1987.tb00981.x, 1987.

Michel, L. A., Tabor, N. J., Montañez, I. P., Schmitz, M. D., and Davydov, V. I.: Chronostratigraphy and paleoclimatology of the Lodève Basin, France: evidence for a pan-tropical aridification event across the Carboniferous–Permian boundary, Palaeogeogr. Palaeoclimatol. Palaeoecol., 430, 118–131, https://doi.org/10.1016/J.PALAEO.2015.03.020, 2015.

Montañez, I. and Soreghan, G. S.: Earth's fickle climate: lessons learned from deep-time ice ages, Geotimes, 51, 24–27, http://www.geotimes.org/mar06/feature_deeptimeiceages.html (last access: 10 November 2023), 2006.

Montañez, I. P.: A Late Paleozoic climate window of opportunity, P. Natl. Acad. Sci. USA, 113, 2334–2336, https://doi.org/10.1073/pnas.1600236113, 2016.

Montañez, I. P. and Poulsen, C. J.: The late Paleozoic ice age: an evolving paradigm, Annu. Rev. Earth Planet Sci., 41, 629–656, https://doi.org/10.1146/annurev.earth.031208.100118, 2013.

Moore, K. D., Soreghan, G. S., and Sweet, D. E.: Stratigraphic and structural relations in the proximal Cutler Formation of the Paradox Basin: implications for timing of movement on the Uncompahgre Front, Mountain Geologist, 45, 49–68, 2008.

Mountney, N. P.: Periodic accumulation and destruction of aeolian erg sequences in the Permian Cedar Mesa Sandstone, White Canyon, southern Utah, USA, Sedimentology 53, 789–823, 2006.

Mountney, N. P. and Jagger, A.: Stratigraphic evolution of an aeolian erg margin system: the Permian Cedar Mesa Sandstone, SE Utah, USA, Sedimentology, 51, 713–743, https://doi.org/10.1111/j.1365-3091.2004.00646.x, 2004.

Murphy, K.: Eolian origin of upper Paleozoic red siltstones at Mexican Hat and Dark Canyon, southeastern Utah, Master's Thesis, University of Nebraska-Lincoln, Lincoln, Nebraska, 1–138 pp., 1987.

Nail, R. S.: Middle-Late Pennsylvanian fusulinid faunas from midcontinent North America and the Paradox Basin, Utah and Colorado, Dissertation, Texas Tech University, Lubbock, Texas, 1–371 pp., ISBN 9798641029290, 1996.

Nail, R. S., Barrick, J. E., and Williams, M. R.: Fusulinid and conodont biostratigraphy of sedimentary cycles in the middle and upper Pennsylvanian Honaker Trail Formation, western Paradox Basin, GSA Abstracts with Programs, 26, 56, 1994

Nail, R. S., Barrick, J. E., and Ritter, S. M.: Preliminary fusulinid and condodont biostratigraphy of the Honaker Trail Formation (late Middle Pennslvanian-Late Pennsylvanian) in the Gibson Dome 1 and Elk Ridge 1 cores, Paradox Basin, Utah Geological Association Guidebook, 25, 303–312, https://archives.datapages.com/data/uga/data/067/067001/303_ugs670303.htm (last access: 10 November 2023), 1996.

Olivier, M., Bourquin, S., Desaubliaux, G., Ducassou, C., Rossignol, C., Daniau, G., and Chaney, D.: The Late Paleozoic Ice Age in western equatorial Pangea: context for complex interactions among aeolian, alluvial, and shoreface sedimentary environments during the Late Pennsylvanian – early Permian, Gondwana Res., 124, 305–338, 2023.

Olsen, P. E. and Kent, D. V.: Long-period Milankovitch cycles from the Late Triassic and Early Jurassic of eastern North America and their implications for the calibration of the Early Mesozoic time–scale and the long–term behaviour of the planets, Philos. Trans. Roy. Soc. London A, 357, 1761–1786, https://doi.org/10.1098/rsta.1999.0400, 1999.

Olsen, P. E., Geissman, J. W., Kent, D. V., Gehrels, G. E., Mundil, R., Irmis, R. B., Lepre, C., Rasmussen, C., Giesler, D., Parker, W. G., Zakharova, N., Kürschner, W. M., Miller, C., Baranyi, V., Schaller, M. F., Whiteside, J. H., Schnurrenberger, D., Noren, A., Brady Shannon, K., O'Grady, R., Colbert, M. W., Maisano, J., Edey, D., Kinney, S. T., Molina-Garza, R., Bachman, G. H., Sha, J., and the CPCP team: Colorado Plateau Coring Project, Phase I (CPCP-I): a continuously cored, globally exportable chronology of Triassic continental environmental change from western North America, Sci. Dril., 24, 15–40, https://doi.org/10.5194/sd-24-15-2018, 2018.

Olsen, P. E., Laskar, J., Kent, D. V., Kinney, S. T., Reynolds, D. J., Sha, J., and Whiteside, J. H.: Mapping Solar System chaos with the geological orrery, P. Natl. Acad. Sci. USA, 116, 10664–10673, 2019.

Olson, E. C. and Vaughn, P. P.: The changes of terrestrial vertebrates and climates during the Permian of North America, Forma et functio, 3, 113–138, 1970.

Orkild, P. P.: Photogeologic map of the Bluff-6 quadrangle, San Juan County, Utah, U.S. Geological Survey IMAP, 53, https://doi.org/10.3133/i53, 1955.

O'Sullivan, R. B.: Geology of the Cedar Mesa-Boundary Butte area, San Juan County, Utah, U.S. Geological Survey Bulletin, 1186, 1–128, https://doi.org/10.3133/b1186, 1965.

Pardo, J. D., Small, B. J., Milner, A. R., and Huttenlocker, A. K.: Carboniferous–Permian climate change constrained early land vertebrate radiations, Nat. Ecol. Evol., 3, 200–206, https://doi.org/10.1038/s41559-018-0776-z, 2019.

Parrish, W. C.: Paleoenvironmental analysis of a Lower Permian bonebed and adjacent sediments, Wichita County, Texas, Palaeogeogr. Palaeoclimatol. Palaeoecol., 24, 209–237, https://doi.org/10.1016/0031-0182(78)90043-3, 1978.

Pearson, M. R., Benson, R. B. J., Upchurch, P., Fröbisch, J., and Kammerer, C. F.: Reconstructing the diversity of early terrestrial herbivorous tetrapods, Palaeogeogr. Palaeoclimatol. Palaeoecol., 372, 42–49, https://doi.org/10.1016/j.palaeo.2012.11.008, 2013.

Peterson, J. A. and Hite, R. J.: Pennsylvanian evaporite-carbonate cycles and their relation to petroleum occurrence, southern Rocky Mountains, Am. Assoc. Pet. Geol. Bull., 53, 884–908, https://doi.org/10.1306/5d25c807-16c1-11d7-8645000102c1865d, 1969.

Petrychenko, O. Y., Williams-Stroud, S. C., and Peryt, T. M.: The relationship of brine chemistry of the Pennsylvanian Paradox evaporite basin (southwestern USA) to secular variation in seawater chemistry, Geological Quarterly, 56, 25–40, 2012.

Pettigrew, R. P., Priddy, C., Clarke, S. M., Warke, M. R., Stüeken, E. E., and Claire, M. W.: Sedimentology and isotope geochemistry of transitional evaporitic environments within arid continental settings: from erg to saline lakes, Sedimentology, 68, 907–942, https://doi.org/10.1111/sed.12816, 2021.

Pfeifer, L. S., Hinnov, L., Zeeden, C., Rolf, C., Laag, C., and Soreghan, G. S.: Rock magnetic cyclostratigraphy of Permian loess in eastern equatorial Pangea (Salagou Formation, south-central France), Front. Earth Sci., 8, 241, 1–13, https://doi.org/10.3389/feart.2020.00241, 2020.

Pierce, W. G. and Rich, E. I.: Summary of rock salt deposits in the United States as possible storage sites for radioactive waste materials, US Geological Survey Bulletin 1148, 1–91, 1962.

Rasmussen, D. L. and Rasmussen, L.: Regional cross sections of the Paradox Basin, in: Subsurface Cross Sections of Southern Rocky Mountains, edited by: Rasmussen, L., Payne, J., and Curnella, S. P., Rocky Mountain Association of Geologists, Denver, 24–27, 2018.

Raup, O. B. and Hite, R. J.: Bromine geochemistry of chloride rocks of the Middle Pennsylvanian Paradox Formation of the Hermosa Group, Paradox Basin, Utah and Colorado, US Geological Survey Bulletin, 2000 M, 1–117, https://doi.org/10.3133/b00M, 1996.

Reed, J. A., Cervato, C., and Fils, D.: PSICAT: a new open-source core description application, in: The Paleontological Stratigraphic Interval Construction and Analysis Tool, Iowa State University, Ames, Iowa, 15–22, 2007.

Reese, A.: The bones of Bears Ears, Science, 363, 218–220, https://doi.org/10.1126/science.363.6424.218, 2019.

Reisz, R. R. and Fröbisch, J.: The oldest caseid synapsid from the late Pennsylvanian of Kansas, and the evolution of herbivory in terrestrial vertebrates, PLoS One, 9, e94518, https://doi.org/10.1371/journal.pone.0094518, 2014.

Reisz, R. R. and Sues, H.-D.: Herbivory in late Paleozoic and Triassic terrestrial vertebrates, in: Evolution of Herbivory in Terrestrial Vertebrates, Cambridge University Press, edited by: Sues, H.-D., 9–41, https://doi.org/10.1017/cbo9780511549717.003, 2000.

Ritter, S. M.: Upper Missourian–lower Wolfcampian (upper Kasimovian–lower Asselian) conodont biostratigraphy of the midcontinent, U.S.A., J. Paleontol., 69, 1139–1154, https://doi.org/https://doi.org/10.1017/S0022336000038129, 1995.

Ritter, S. M., Barrick, J. E., and Skinner, M. R.: Conodont sequence biostratigraphy of the Hermosa Group (Pennsylvanian) at Honaker Trail, Paradox Basin, Utah, J. Paleontol., 76, 495–517, https://doi.org/10.1017/S0022336000037331, 2002.

Romer, A. S.: The late Carboniferous vertebrate fauna of Kounova (Bohemia) compared with that of the Texas redbeds, Am. J. Sci., 243, 417–442, https://doi.org/10.2475/AJS.243.8.417, 1945.

Rowley, D. B., Raymond, A., Parrish, J. T., Lottes, A. L., Scotese, C. R., and Ziegler, A. M.: Carboniferous paleogeographic, phytogeographic, and paleoclimatic reconstructions, Int. J. Coal.

Geol., 5, 7–42, https://doi.org/10.1016/0166-5162(85)90009-6, 1985.

Sahney, S., Benton, M. J., and Falcon-Lang, H. J.: Rainforest collapse triggered Carboniferous tetrapod diversification in Euramerica, Geology, 38, 1079–1082, https://doi.org/10.1130/G31182.1, 2010.

Scott, G. R.: Paleomagnetism of Carboniferous and Triassic strata from cratonic North America, Dissertation, The University of Texas at Dallas, Dallas, 1–172 pp., ISBN 9781083468468, 1975.

Scott, K. M.: Carboniferous–Permian boundary in the Halgaito Formation, Cutler Group, Valley of the Gods and surrounding area, southeastern Utah, in: The Carboniferous–Permian Transition, New Mexico Museum of Natural History and Science Bulletin, 60, 398–409, 2013.

Sears, J. D.: Geology of Comb Ridge and vicinity north of San Juan River, San Juan County, Utah, U.S. Geological Survey Bulletin, 1021-D, 167–207, https://doi.org/10.3133/b1021E, 1956.

Soreghan, M. J. and Soreghan, G. S. (Lynn): Whole-rock geochemistry of upper Paleozoic loessite, western Pangaea: implications for paleo-atmospheric circulation, Earth Planet Sci. Lett., 255, 117–132, https://doi.org/10.1016/j.epsl.2006.12.010, 2007.

Soreghan, G. S., Elmore, R. D., and Lewchuk, M. T.: Sedimentologic-magnetic record of western Pangean climate in upper Paleozoic loessite (lower Cutler beds, Utah), Geol. Soc. Am. Bull., 114, 1019–1035, 2002a.

Soreghan, M. J., Soreghan, G. S. (Lynn), and Hamilton, M. A.: Paleowinds inferred from detrital-zircon geochronology of upper Paleozoic loessite, western equatorial Pangea, Geology, 30, 695–698, https://doi.org/10.1130/0091-7613(2002)030<0695:PIFDZG>2.0.CO;2, 2002b.

Soreghan, G. S., Soreghan, M. J., and Hamilton, M. A.: Origin and significance of loess in late Paleozoic western Pangaea: a record of tropical cold?, Palaeogeogr. Palaeoclimatol. Palaeoecol., 268, 234–259, https://doi.org/10.1016/j.palaeo.2008.03.050, 2008.

Soreghan, G. S., Beccaletto, L., Benison, K. C., Bourquin, S., Feulner, G., Hamamura, N., Hamilton, M., Heavens, N. G., Hinnov, L., Huttenlocker, A., Looy, C., Pfeifer, L. S., Pochat, S., Sardar Abadi, M., Zambito, J., and the Deep Dust workshop participants: Report on ICDP Deep Dust workshops: probing continental climate of the late Paleozoic icehouse–greenhouse transition and beyond, Sci. Dril., 28, 93–112, https://doi.org/10.5194/sd-28-93-2020, 2020.

Soreghan, G. S., Heavens, N. G., Pfeifer, L. S., and Soreghan, M. J.: Dust and loess as archives and agents of climate and climate change in the late Paleozoic Earth system, Geological Society, London, Special Publications, 535, 195–223, https://doi.org/10.1144/sp535-2022-208, 2023.

Stanesco, J. D. and Campbell, J. A.: Eolian and noneolian facies of the Lower Permian Cedar Mesa Sandstone Member of the Cutler Formation, southeastern Utah, U.S. Geological Survey Bulletin, 1808-F, 1–13 https://doi.org/10.3133/b1808EF, 1989.

Stuckless, J. S. and Levich, R. A.: The road to Yucca Mountain – evolution of nuclear waste disposal in the United States, Environ. Eng. Geosci., 22, 1–25, https://doi.org/10.2113/gseegeosci.22.1.1, 2016.

Sues, H. D. and Reisz, R. R.: Origins and early evolution of herbivory in tetrapods, Trends in Ecology & Evolution, 13, 141–145, https://doi.org/10.1016/S0169-5347(97)01257-3, 1998.

Sweet, D. E., Brotherton, J. L., Chowdhury, N. U. M. K., and Ramsey, C. E.: Tectonic subsidence analysis of the Ancestral Rocky Mountains from the interior to the southern margin, Palaeogeogr. Palaeoclimatol. Palaeoecol., 576, 110508, https://doi.org/10.1016/j.palaeo.2021.110508, 2021.

Tabor, N. J. and Poulsen, C. J.: Palaeoclimate across the Late Pennsylvanian-Early Permian tropical palaeolatitudes: a review of climate indicators, their distribution, and relation to palaeophysiographic climate factors, Palaeogeogr. Palaeoclimatol. Palaeoecol., 268, 293–310, https://doi.org/10.1016/j.palaeo.2008.03.052, 2008.

Thackston, J. W., Preslo, L. M., Hoexter, D. E., and Donnelly, N.: Results of hydraulic tests at Gibson Dome No. 1, Elk Ridge No. 1, and E. J. Kubat boreholes, Paradox Basin, Utah, Office of Nuclear Waste Isolation Technical Report, Battelle Memorial Institute, Columbus, 1–99, 1984.

Tobey, D. E.: Water and Wind: The fluvial and eolian forces behind the Pennsylvanian-Permian Halgaito Formation, Utah, Dissertation, Dalhousie University, Halifax, Nova Scotia, 1–103 pp., http://hdl.handle.net/10222/79933 (last access: 10 November 2023), 2020.

Tromp, D. E.: Clays as indicators of depositional and diagenetic conditions in Pennsylvanian black shales, Paradox Basin, Utah and Colorado, Dissertation, Colorado School of Mines, Golden, Colorado, 1–168 pp., https://hdl.handle.net/11124/176268 (last access: 10 November 2023), 1995.

Tuttle, M. L., Klett, T. R., Richardson, M., and Breit, G. N.: Geochemistry of two interbeds in the Pennsylvanian Paradox Formation, Utah and Colorado – a record of deposition and diagenesis of repetitive cycles in a marine basin, US Geological Survey Bulletin, 2000-N, 1–86, https://doi.org/10.3133/b00N, 1996.

Uhl, D., Lausberg, S., Noll, R., and Stapf, K. R. G.: Wildfires in the late Palaeozoic of central Europe – an overview of the Rotliegend (Upper Carboniferous–Lower Permian) of the Saar–Nahe Basin (SW-Germany), Palaeogeogr. Palaeoclimatol. Palaeoecol., 207, 23–35, https://doi.org/10.1016/J.PALAEO.2004.01.019, 2004.

U.S. Department of Energy: Environmental Assessment Overview: Davis Canyon Site, Utah, Washington D.C., 38 pp., 1986.

van Hinsbergen, D. J. J., de Groot, L. V, van Schaik, S. J., Spakman, W., Bijl, P. K., Sluijs, A., Langereis, C. G., and Brinkhuis, H.: A paleolatitude calculator for paleoclimate studies, PLoS One, 10, e0126946, https://doi.org/10.1371/journal.pone.0126946, 2015.

Vaughn, P. P.: Comparison of the Early Permian vertebrate faunas of the Four Corners region and north-central Texas, Los Angeles County Museum Contributions in Science, 105, 1–13, https://doi.org/10.5962/p.241094, 1966.

Vaughn, P. P.: Lower Permian vertebrates of the Four Corners and the Midcontinent as indices of climatic differences, in: Proceedings of the North American Paleontological Congress, edited by: Yochelson, E. L., Vol. 1969, Allen Press, Lawrence, KS, USA, 388–408, 1970.

Veizer, J.: Strontium isotopes in seawater through time, Annu. Rev. Earth Planet Sci., 17, 141–167, https://doi.org/10.1146/annurev.ea.17.050189.001041, 1989.

Verosub, K. L. and Roberts, A. P.: Environmental magnetism: past, present, and future, J. Geophys. Res., 100, 2175–2192, https://doi.org/10.1029/94JB02713, 1995.

Wardlaw, B. R.: Age assignment of the Pennsylvanian-Early Permian succession of north central Texas, Permophiles, 46, 21–22, 2005.

Wardlaw, B. R. and Nestell, M. K.: The first appearance of *Streptognathodus isolatus* in the Permian of Texas, Permophiles, 59, 17–20, 2014.

Wengerd, S. A.: Pennsylvanian Stratigraphy, Southwest Shelf, Paradox Basin, Intermountain Association of Petroleum Geologists: Guidebook to the Geology of the Paradox Basin, 109–134, 1958.

Wengerd, S. A.: Stratigraphic section at Honaker Trail, San Juan Canyon, San Juan County, Utah, Four Corners Geological Society Guidebook, 4, 236–243, 1963.

Whidden, K. J., Lillis, P. G., Anna, L. O., Pearson, K. M., and Dubiel, R. F.: Geology and total petroleum systems of the Paradox Basin, Utah, Colorado, New Mexico, and Arizona, The Mountain Geologist, 51, 119–138, 2014.

Williams, M. R.: Stratigraphy of Upper Pennsylvanian cyclic carbonate and siliciclastic rocks, western Paradox Basin, Utah, in: The Paradox Basin Revisited – New Developments in Petroleum Systems and Basin Analysis, edited by: Houston, W. S., Wray, L. L., and Moreland, P. G., Rocky Mountain Association of Geologists, Denver, 381–435, 2009.

Woodward-Clyde Consultants: Completion report for Elk Ridge no. 1 borehole, Elk Ridge study area of the Paradox Basin region, San Juan County, Utah: Topical Report, San Francisco, California, 1–803 pp., 1982a.

Woodward-Clyde Consultants: Geologic Characterization Report for the Paradox Basin Study Region Utah Study Areas – Volume III: Elk Ridge, Woodward-Clyde Consultants, 1–172 pp., 1982b.

Sci. Dril., 33, 129–172, 2024
https://doi.org/10.5194/sd-33-129-2024

Scientific Drilling
Open Access

BASE (Barberton Archean Surface Environments) – drilling Paleoarchean coastal strata of the Barberton Greenstone Belt

Christoph Heubeck[1], Nic Beukes[2,†], Michiel de Kock[2], Martin Homann[3,a], Emmanuelle J. Javaux[4], Takeshi Kakegawa[5], Stefan Lalonde[6], Paul Mason[7], Phumelele Mashele[8,b], Dora Paprika[8,c], Chris Rippon[9], Mike Tice[10], Rodney Tucker[11], Ryan Tucker[11], Victor Ndazamo[12], Astrid Christianson[13], and Cindy Kunkel[14]

[1]Department of Geosciences, Friedrich-Schiller-Universität Jena, Burgweg 11, 07749 Jena, Germany
[2]Department of Geology, University of Johannesburg, Cnr. Kingsway and University Road, Auckland Park 2006, South Africa
[3]Department of Earth Sciences, University College London, 5 Gower Place, London WC1E 6BS, UK
[4]Bât. B22 Early Life Traces & Evolution-Astrobiology, Quartier Vallée 1, Chemin de la Vallée 4, 4000 Liège, Belgium
[5]402 Geosciences Building, Graduate School of Science, Tohoku University, Aramaki 6-3, Sendai, Japan
[6]UMR 6538 Laboratoire Géosciences Océan, Institut Universitaire Européen de la Mer, Brest, France
[7]Department of Earth Sciences, Utrecht University, Princetonlaan 8A, 3584 CB, Utrecht, the Netherlands
[8]Department of Geology, University of Johannesburg, Johannesburg, South Africa
[9]independent researcher: 10 Amethys Street, Mbombela 1200, South Africa
[10]Department of Geology & Geophysics, Texas A&M University, College Station, Texas 77843, USA
[11]Wildlife Estate, 367 Kierrieklapper Street, Hoedspruit 1380, Limpopo, South Africa
[12]Barberton Mines (Pty.) Ltd., Kaapmuiden Road, Barberton 1300, South Africa
[13]Barberton Community Tourism, Market Square, Barberton 1300, South Africa
[14]ICDP, Helmholtz-Zentrum Potsdam, Deutsches GeoForschungsZentrum GFZ, Telegrafenberg, 14473 Potsdam, Germany
[a]current address: Division of Geological and Planetary Sciences, California Institute of Technology, Pasadena, 91125 California, USA
[b]now at: School of Geosciences, University of the Witwatersrand, Johannesburg, South Africa
[c]now at: The MSA Group, Henley House, Greenacres Office Park, Victory Road, Victoria Park, Randburg, Johannesburg 2195, South Africa
†deceased, 9 January 2023

Correspondence: Christoph Heubeck (christoph.heubeck@uni-jena.de)

Received: 19 February 2024 – Revised: 8 April 2024 – Accepted: 15 April 2024 – Published: 18 June 2024

Abstract. The BASE (Barberton Archean Surface Environments) scientific drilling project aimed at recovering an unweathered continuous core from the Paleoarchean Moodies Group (ca. 3.2 Ga), central Barberton Greenstone Belt (BGB), South Africa. These strata comprise some of the oldest well-preserved sedimentary strata on Earth, deposited within only a few million years in alluvial, fluvial, coastal-deltaic, tidal, and prodeltaic settings. They represent a very-high-resolution record of Paleoarchean surface conditions and processes. Moodies Group strata consist of polymict conglomerates, widespread quartzose, lithic and arkosic sandstones, siltstones, shales, and rare banded-iron formations (BIFs) and jaspilites, interbedded with tuffs and several thin lavas. This report describes objectives, drilling, and data sets; it supplements the operational report.

Eight inclined boreholes between 280 and 495 m length, drilled from November 2021 through July 2022, obtained a total of 2903 m of curated core of variable quality through steeply to subvertically dipping, in part over-

turned stratigraphic sections. All drilling objectives were reached. Boreholes encountered a variety of conglomerates, diverse and abundant, mostly tuffaceous sandstones, rhythmically laminated shale-siltstone and banded-iron formations, and several horizons of early-diagenetic silicified sulfate concretions. Oxidative weathering reached far deeper than expected. Fracturing was more intense, and BIFs and jaspilites were thicker than anticipated. Two ca. 1 km long mine adits and a water tunnel, traversing four thick stratigraphic sections within the upper Moodies Group in the central BGB, were also sampled. All boreholes were logged by downhole wireline geophysical instruments. The core was processed (oriented, slabbed, photographed, described, and archived) in a large, publicly accessible hall in downtown Barberton. A geological exhibition provided background explanations for visitors and related the drilling objectives to the recently established Barberton Makhonjwa Mountains World Heritage Site. A substantial education, outreach, and publicity program addressed the information needs of the local population and of local and regional stakeholders.

1 Introduction and geologic setting

1.1 The Archean

The Archean eon encompasses the fundamental events of building a habitable planet, evident from comparing the state of Earth at the beginning of that eon at 4 Ga and 1500 million years later. However, we know little about this critical time period, such as the temperature and composition of the oceans and the atmosphere, continental freeboard, nature of the geomagnetic field, consequences of a high spin rate and intense solar UV radiation, volcanism, meteorite impacts, tides, and the role shorelines played as biological laboratories for early life, to name a few (Fig. 1). This is due to a scarce rock record, considerable degree of deformation and metamorphism, and poor exposure of existing strata. The few Paleoarchean marine–terrestrial transitional strata preserve a unique and potentially valuable record which allows us to constrain the history of interaction between the geosphere, biosphere, and atmosphere. This includes conditions of paleosol formation, intensity, and type of weathering and processes of sediment generation and maturation. The oldest preserved (microbial) traces of early life on land have a bearing on fundamental geosphere–biosphere interactions such as the mechanism and degree of nutrient delivery, strategies of radiation avoidance, and atmospheric composition. Eolian strata may convey unique environmental parameters such as local wind strength and atmospheric density, with implications for aridity and circulatory systems. Lastly, terrestrial evaporites relate to temperature, evaporation, and groundwater movement.

BASE (Barberton Archean Surface Environments) set out to produce a comprehensive data set of unweathered continuous cores from marine–terrestrial transitional strata from one of the world's oldest, well-preserved Paleoarchean units, the Moodies Group of the Barberton Greenstone Belt. The Barberton Greenstone Belt (BGB; Viljoen and Viljoen, 1969a, b, c; Anhaeusser, 1984; de Wit et al., 1992; Lowe et al., 1999; Lowe and Byerly, 2007; Anhaeusser, 2014) (Figs. 2, 3) of South Africa and Eswatini represents one of the two best-preserved records of the early Earth's surface environments, the other being the greenstone belts of Western Australia's East Pilbara Terrane. Strata of the BGB, ca. 3.57 to ca. 3.21 Ga in age, offer excellent conditions to reconstruct Paleoarchean (> 3.2 Ga) tectonic processes and surface environments.

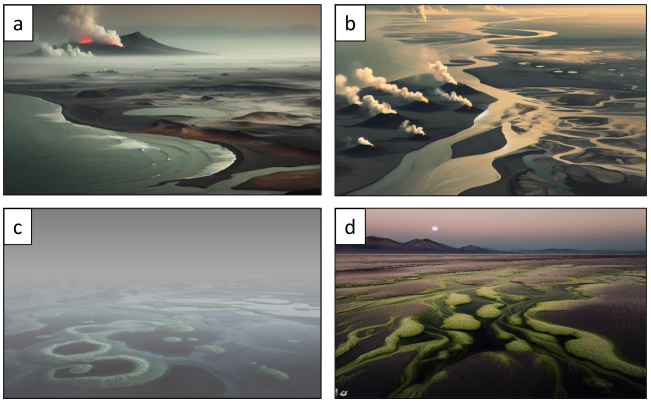

Figure 1. AI-generated visualizations (Image Creator from © Microsoft Designer, formerly Bing Image Creator) showing surface environments of the Paleoarchean, inspired by outcrop exposures from the Moodies and Onverwacht groups of the Barberton Greenstone Belt (BGB). BASE drilling had the objective to assess these settings and constraining the environments of early life. Text prompts to the software read as follows: **(a)** "An almost flat foggy dark landscape with a grey pale-orange sky, pale green sea, a sandy tidal coastline, one volcano, red lava and steam, a tidal estuary and the moonrise. photorealistic style"; **(b)** "Lava plain eruption fog coastline dark no volcanoes"; and **(c, d)** "A sandy tidal flat without mountains with hot springs and pale green microbial mats. Dark; low moon".

Because the stratigraphically coherent, mappable strata of the BGB exposed in good to excellent outcrops have been studied by numerous industry and government surveys and academic Honor's, MSc, and PhD theses, its rocks permit a deep understanding of local and regional stratigraphy. This, in turn, allows insights into Archean surface dynamics, e.g., weathering and erosion, tides, atmospheric composition and

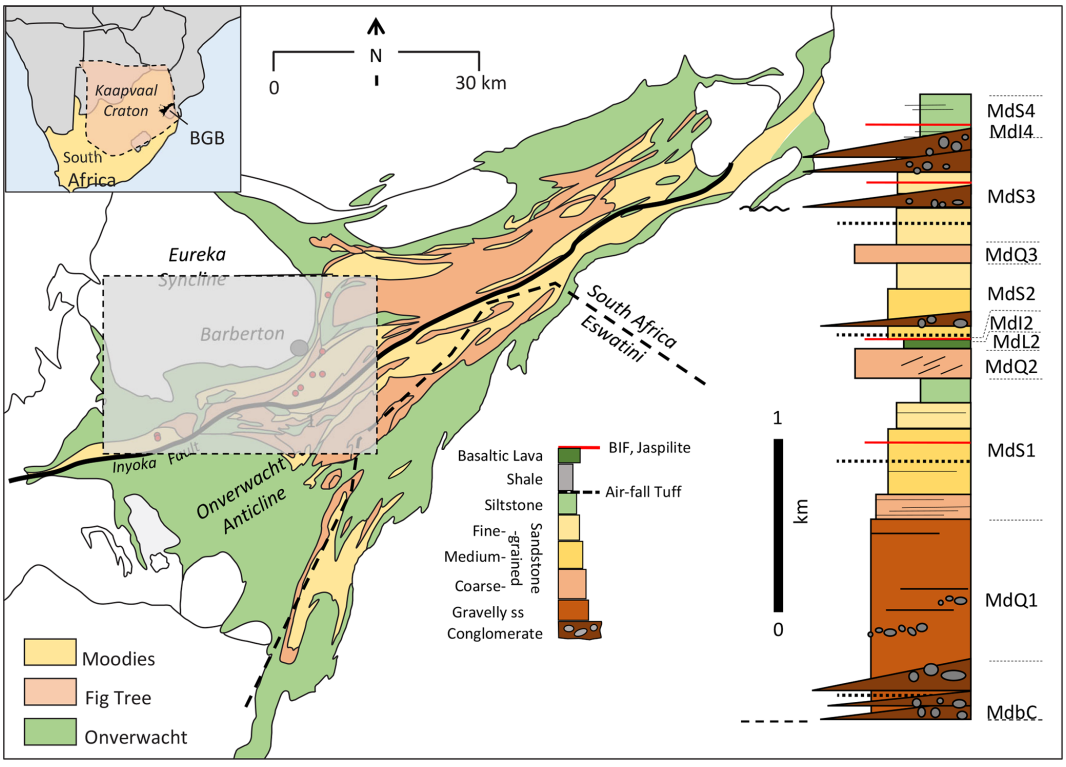

Figure 2. Generalized geologic map of the BGB. The inset shows the location in southern Africa. The stratigraphic column to the right measures ca. 3.7 km in thickness and represents first-order lithology of the Moodies Group strata north of the Inyoka Fault. The area shown in Fig. 2 is outlined by the grey-dashed rectangle.

Figure 3. Scenery of the central Barberton Greenstone Belt; the view is along the strike to the northeast. The region is partially covered by pine and eucalyptus plantations, interspersed by rocky and grassy hills which in part serve as natural fire breaks.

climate, the record of meteorite impacts, the early biosphere, and tectonic drivers.

1.2 Composition, stratigraphy, structure, and metamorphism of the Moodies Group

The Moodies Group (ca. 3223 ± 1 to 3219 ± 9 Ma; Anhaeusser, 1976, 1984, 2014; Eriksson, 1979; Eriksson et al., 2006; Heubeck, 2022; Heubeck et al., 2013; Heubeck, 2019; Heubeck et al., 2022b, and many others) is the uppermost stratigraphic unit of the BGB. It crops out over ca. 110 km length and 40 km width in the Barberton–Makhonjwa Mountains range with up to 1700 m relief. Strata reach up to ~ 3.7 km in thickness and are dominated by quartzose sandstones but locally also include thick sequences of siltstones and conglomerates. Shales, banded-iron formations (BIFs), and volcanic units are uncommon. Strata were probably deposited within only ~ 1 to 14 Myr (Heubeck et al., 2013; Heubeck et al., 2022b). They thus constitute a worldwide unique, very-high-resolution record of Paleoarchean surface processes, perhaps approximately comparable in overall temporal resolution to many Holocene geologic records.

All strata of the BGB, including those of the underlying Fig Tree and Onverwacht groups, are tightly folded and cut by major faults. The metamorphic grade is typically lower-greenschist facies (Toulkeridis et al., 1998; Tice et al., 2004). Maximum paleotemperatures from Raman spectroscopy of organic material reach ca. 320 to 380 °C. Widespread early-diagenetic silicification preserved microtextures and macro-

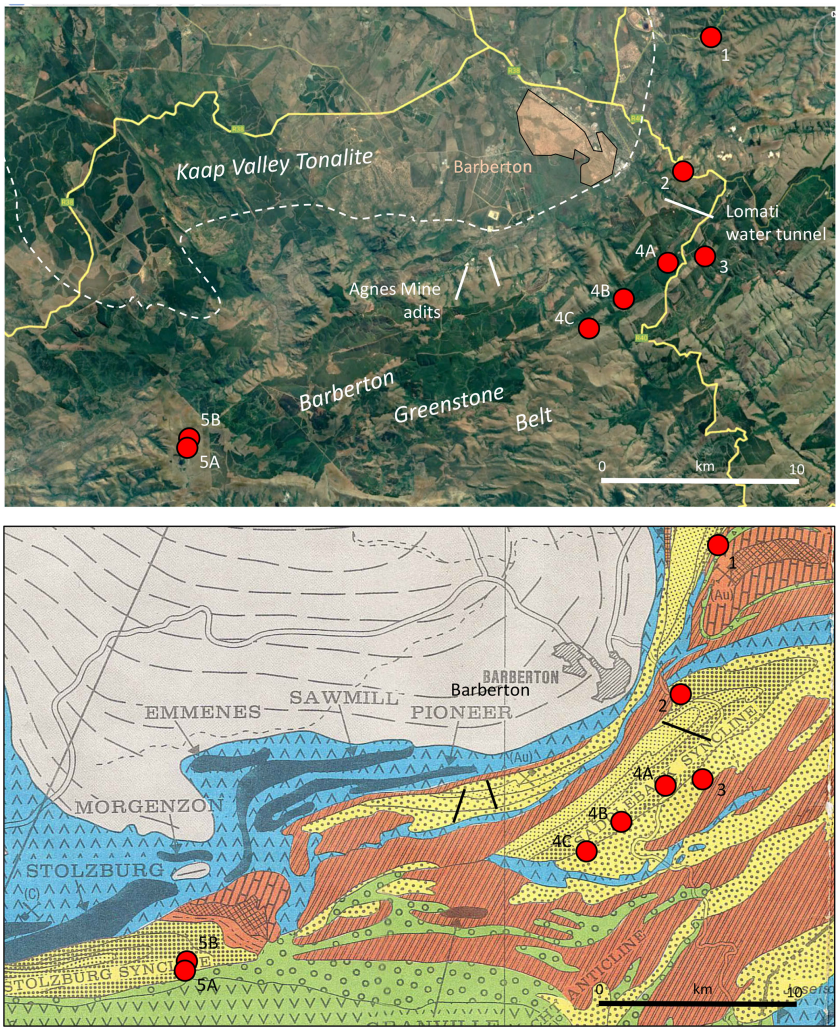

Figure 4. Satellite image (© Google Earth) and geologic map (Anhaeusser et al., 1981) of the northern–central Barberton Greenstone Belt, showing the drillsite locations. All sites except Site 5A and Site 5B lie within about 12 km from Barberton. See the text for site descriptions.

textures in many locations, virtually without strain. Most Moodies strata are preserved in subvertically dipping or overturned limbs of regional-scale (up to 15 km long, up to 5 km wide) synclines (Figs. 2, 4; Heubeck and Lowe, 1994b; Lowe et al., 2012). Regional geologic mapping at the 1 : 25 000 scale has covered the central BGB (e.g., Lowe et al., 2012); numerous unpublished geologic maps (e.g., Gribnitz et al., 1961; Herget, 1964; Viljoen, 1963; Büttner, 1983; Paris, 1984; Daneel, 1987; Hose, 1990; Heubeck, 1994; Stutenbecker, 2014) provide details for areas of special interest. A fully representative Moodies stratigraphy exists only north of the greenstone-belt-axial Inyoka Fault because strata south of that fault are thinner and mostly experienced a higher degree of hydrothermal alteration (Reimann et al., 2021). All BASE drill sites are located north of the Inyoka Fault (Fig. 2).

2 Scientific objectives

Most outcrops in the BGB, despite appearing fresh, have been affected by surficial oxidative weathering, the effects of surface- or near-surface biologic activity (e.g., by endolithic bacteria), and/or near-surface oxic (groundwater) alteration. Even seemingly fresh sample locations, usually limited to steep cliffs and isolated exposures along streambeds, have been subjected to oxidative alteration. Previous drilling showed that weathering extends up to ∼ 20 m depth. Analyzing short (and usually stratigraphically poorly located) underground drill core provided by producing gold mines along the northern margin of the BGB has occasionally been successful (Hessler et al., 2004; Hessler and Lowe, 2006; Javaux et al., 2010; Nwaila and Frimmel, 2019), but advanced and high-resolution geochemical research on mine material is commonly compromised by poor geographic and stratigraphic constraints and carries the risk of local hydrothermal

alteration or contamination by drilling fluids (Toulkeridis et al., 2015).

Analytical work in Moodies strata over the past 20 years, based on detailed field studies, has identified numerous geological features related to processes of the Archean biosphere, geosphere, atmosphere, and hydrosphere. These include extensive microbial mats in tidal and fluvial facies, concretions and biogenic reaction products in paleosols, weathering rinds, putative eolian strata, prodeltaic banded-iron formations, exquisitely preserved microfossils, and detailed reconstructions of shoreline and deltaic processes (Heubeck and Lowe, 1994a, b; Hessler and Lowe, 2006; Noffke et al., 2006; Javaux et al., 2010; Simpson et al., 2012; Heubeck et al., 2013, 2016, 2022b; Homann et al., 2015, 2016, 2018; Nabhan et al., 2016a, b; Nakajima et al., 2016; Stutenbecker et al., 2019; Janse van Rensburg et al., 2021; Eulenfeld and Heubeck, 2023; Heubeck et al., 2023; see Heubeck, 2019, for a review). Because of the straightforward lithostratigraphic correlation possible in Moodies strata north of the Inyoka Fault between terrestrial, transitional, and marine Moodies strata, physical, chemical, and biologic processes can be traced well beyond the marine record that usually obscures atmospheric processes.

The drillsite selection was based on previous detailed geological mapping by Heubeck and his students. Existing regional geophysical data (gravity and magnetics; Burley et al., 1970; Darracott, 1975; de Beer et al., 1988; de Beer and Stettler, 2009; Kütter et al., 2016) are handicapped by low resolution because the area has a mountainous topography, subvertically dipping strata, strongly varying unit thicknesses and lithologies, and diagenetic alteration fronts. Aerial and ground magnetic surveys had been scheduled for the five drill sites of the BARB International Continental Scientific Drilling Program (ICDP) project conducted in 2011 (Nick Arndt et al.: Peering into the Cradle of Life: Scientific Drilling in the Barberton Greenstone Belt, South Africa, ICDP Proposal, unpublished, 2009) but were never implemented because geological characterization proved sufficient. Geophysical data will nevertheless be crucial for future strategic projects intending to constrain the large-scale (e.g., shallow or deep, symmetric or asymmetric) structure of the BGB and to delineate major structural breaks at depth.

The aims of BASE were to study Archean surface environments which were crucial to forming the foundation of subsequent evolutionary, sedimentary, and tectonic processes. Major targets of investigations were

1. conformable terrestrial–marine transitions for environmental proxies;

2. diagnostic lithologies (such as various paleosols, nearshore BIFs, evaporites, and basaltic lavas) for their environmental significance;

3. the compositional, facies, and morphological variability of thick and laterally extensive microbial mats; and

4. sedimentary and mineralogical responses to surface variables, such as tides, climate, potential meteorite impacts, and radiation.

Principal questions included the following.

1. What were the ecology, 3-D morphology, and metabolism(s) of abundant (oxygenic photosynthetic?) microbial mats preserved in minimally compacted tidal-facies sandstones? Are these properties recorded in their C-isotope microstratigraphy? What were the preservation pathways, origins of early-diagenetic chert, and degrees of thermal overprint? Can we constrain net O_2 production rates and the early N cycle?

2. What is the (cyclo)stratigraphic and microfossil record of fine-grained marine and prodelta sediments? What is the origin of its clay minerals? How do coastal BIFs and jaspilites relate to nearby tidal microbial mats? What does the paleomagnetic record imply about the nature and strength of the Paleoarchean geomagnetic field?

3. What global surface conditions can be inferred? What was the redox state (sulfate, redox-sensitive metal isotopes), temperature and composition of ocean water, of early-diagenetic fluids, and of the atmosphere?

4. What can we infer about the role and significance of terrestrial weathering from proxies of physical and geochemical weathering, the composition of variable paleosols, the architecture of eolian strata, and the traces of evaporites and microbial metabolism(s) in terrestrial sediment?

3 Drilling strategy

Site selection

Site selection took place during an ICDP-funded field workshop from 5 to 10 October 2017 outside Barberton which was attended by 48 scientists from 11 countries and 10 local stakeholders. Sites had to (1) provide information that could not be obtained from surface outcrops (contacts, unweathered material, facies transitions); (2) record environmental and geochemical processes related to surface conditions of the Archaean Earth through key sedimentary and geochemical proxies; (3) be chosen on the basis of significant prior field studies and laboratory work; (4) minimize structural complexity and avoid zones of known hydrothermal alteration; and (5) allow technically feasible drilling at economically reasonable costs.

The full ICDP proposal included detailed site characterization which spelled out borehole-specific scientific issues, specific targets, and logistical aspects, along with geologic strip maps and predicted geologic profiles along the drill paths. All boreholes were oriented perpendicular to the strike

of bedding, drilled at an inclination of 45° from the horizontal and against the dip of bedding in order to maximize the stratigraphic thickness intersected by the borehole. Drilling in overturned sections was stratigraphically base-up, progressing from older into younger strata. Because the central objective of the drilling program was to obtain a continuous and unweathered core (rather than the identification of facies from diagnostic sedimentary structures, better done on outcrop strata), drilling the bulk of the sections was done at a comparatively thin core diameter (PQ3 = 83 mm diameter core with a 122.3 mm diameter hole).

The five stratigraphic sections selected for drilling are all located within a ca. 30 by 20 km area close to Barberton (Fig. 4; Tables 1, 2) and can be stratigraphically correlated (Fig. 5).

4 Technical operations

4.1 Permitting and stakeholder buy-in

Christoph Heubeck started contacting and briefing local stakeholders (World Heritage Site administration, mining companies, local and regional government, and local associations) in 2015 and 2016. The briefing was to ensure that these entities were aware first-hand and early of the scientific and non-commercial objectives of the proposed drilling program. Stakeholders were invited to and attended the Barberton workshop in 2017. While funding was organized from 2018 through 2021, the coordinator obtained formal letters of approval from relevant property holders and letters of support from professional societies and government agencies. Astrid Christianson at Barberton Community Tourism led a "grassroots" movement in Barberton by keeping municipality and district officials informed. Christoph Heubeck held (usually while conducting yearly field work) public evening talks to the Barberton Mountain Land branch of the Geological Society of South Africa, chaired by Chris Rippon. Drilling was originally planned to begin in winter 2020 to take advantage of the climate, but obtaining landowner approval for drilling proved to be more time-consuming than anticipated. Nic Beukes at the Centre of Excellence for Integrated Mineral and Energy Resource Analysis (CIMERA) in Johannesburg published a drilling tender, "Scope of Drilling Services Required", in June 2021. Bids were received in July, and a selection was made by a committee in August 2021.

Nic Beukes obtained documents certifying the non-commercial, tax-free status of the project from the South African government and set up the accounting infrastructure at the CIMERA office at the Department of Geology, University of Johannesburg. He also lobbied in Pretoria to have South Africa rejoin the ICDP.

On 7 and 8 April 2021, approximately half a year prior to the scheduled start-up, Nic Beukes and Christoph Heubeck briefed all stakeholders on the objectives and structure of the drilling program, followed by a field inspection of all eight proposed drill sites (Table 1). This also served to clarify practical questions of access, security, clearing of trees, fencing, water supply, location of the field office, and crisis protocols.

The Barberton region has had a long history of exploration for (and mining of) gold from the hydrothermal mineralization in deep-reaching subvertical ductile–brittle shear zones, mostly along the northern margin of the greenstone belt. The mines make up the economic backbone of the town's economy. Many residents are thus familiar with drilling as part of gold exploration. For these reasons, the scientific, non-commercial, curiosity-driven nature of this project had to be made widely known, an unfamiliar concept for many. Because seven of the eight BASE boreholes were located within the newly declared Barberton Makhonjwa World Heritage Site, it was also essential to communicate that this project was linked to the objectives and philosophy of the World Heritage Site. The Education–Outreach–Publicity (EOP) component of BASE was large and is spelled out in detail in the operational report (Heubeck et al., 2024a). The drilling and scientific crews devoted considerable resources to this aspect, including a permanent legacy in the form of a new room added to the Barberton regional museum after the end of operations.

4.2 Site inspections

Site 1 was located on an active mine property with more than 100 years of continuous operations involving heavy moving equipment. Site 2A was in a sandy flood retention depression immediately next to a parking lot adjacent to the paved R40 road. Sites 3A, 4A, 4B, and 4C were on or next to forest roads in commercial pine and eucalyptus plantations. Sites 5A and 5B were in grassland near an abandoned homestead (Fig. 6).

The Ecological Control Officer (ECO) conducted a baseline environmental survey for each site, inspected sites using a previously agreed-upon checklist, inducted drilling staff, visited the sites during drilling operations to conduct audits, conducted site visits to clear any remaining issues after completion of the rehabilitation program, and wrote final reports on all the sites. (Site 1 did not receive a final report because its location in a hairpin of a mining road made any changes moot.) Each site was handed back following a final joint inspection by a drilling contractor's representative, the ECO, and the landowner's representative.

4.3 Preparation of core processing and local infrastructure

Nic Beukes, Christoph Heubeck, and Astrid Christianson started to actively look for a site to process the core in March 2021. The BIAS (Barberton Iron And Steel Inc.) Hall, a large former industrial hall in downtown Barberton, caught our attention. The owner, the Department of Arts, Sports and Culture of Mpumalanga Province, granted free use of about one-third of the underused central segment of the hall for core

Table 1. Drillsite locations.

Name	Location/tectonic element	Setting		Coordinates		Along-drillhole length	Approximately true stratigraphic thickness of the Moodies section	Drilling activity shown in Google Earth® image of . . .
				Latitude	Longitude	(m)	(m)	
BASE boreholes								
1A	Eureka Syncline	Elephant's Kloof		25°44′2.63″ S	31°5′50.65″ E	496.85	350	Ops. ongoing 4 July 2022
2A	Dycedale Syncline	"Tidal Sandstones"		25°47′37.78″ S	31°5′1.50″ E	367.80	290	Ops. ongoing 11 February 2022
3A	Saddleback Syncline	Microbial laminations		25°49′48.39″ S	31°5′26.88″ E	280.2	218	Vacated site 4 July 2022
4A		Distal	Lomati Delta	25°49′52.60″ S	31°4′41.69″ E	340.1	230	Vacated site 4 July 2022
4B		Medial	Complex	25°51′11.70″ S	31°2′54.70″ E	355.5	300	Vacated site 9 August 2022
4C		Proximal		25°51′39.40″ S	31°2′3.11″ E	351.49	295	Vacated site 9 August 2022
5A	Stolzburg Syncline	Upper section		25°54′13.97″ S	30°50′44.83″ E	451.3	360	Ops. ongoing 31 May 2022
5B		Lower section		25°54′2.80″ S	30°50′49.06″ E	489.9	400	Ops. ongoing 11 June 2022
						3133	2443	
Tunnel sections								
Lomati water tunnel		Entrance		25°48′40.23″ S	31°5′58.36″ E			
		Exit		25°48′6.32″ S	31°4′26.43″ E			
Agnes Mine	Ben Lomond adit	Entrance		25°50′3.60″ S	30°58′56.70″ E			
	22-level adit	Entrance		25°49′28.39″ S	31°0′7.62″ E			

Table 2. Borehole orientations and depths.

Borehole number	Final borehole position from the origin (m)		Direction from true north (°)	Distance from the origin (m)	Borehole tilt from the horizontal (beginning/end) (°)
	N	W			
1A	165.03	346.79	295	384.06	44.7/57.1
2A	180.50	190.90	313	262.72	44.8/49.2
3A	151.74	132.87	319	201.54	44.7/49.9
4A	188.49	149.00	322	240.27	45.8/54.1
4B	245.49	108.76	336	268.50	45.4/53.0
4C	236.84	107.75	336	260.20	44.4/52.7
5A	308.16	155.84	27	345.32	45.7/58.7
5B	366.29	87.06	13	376.49	45.0/56.0

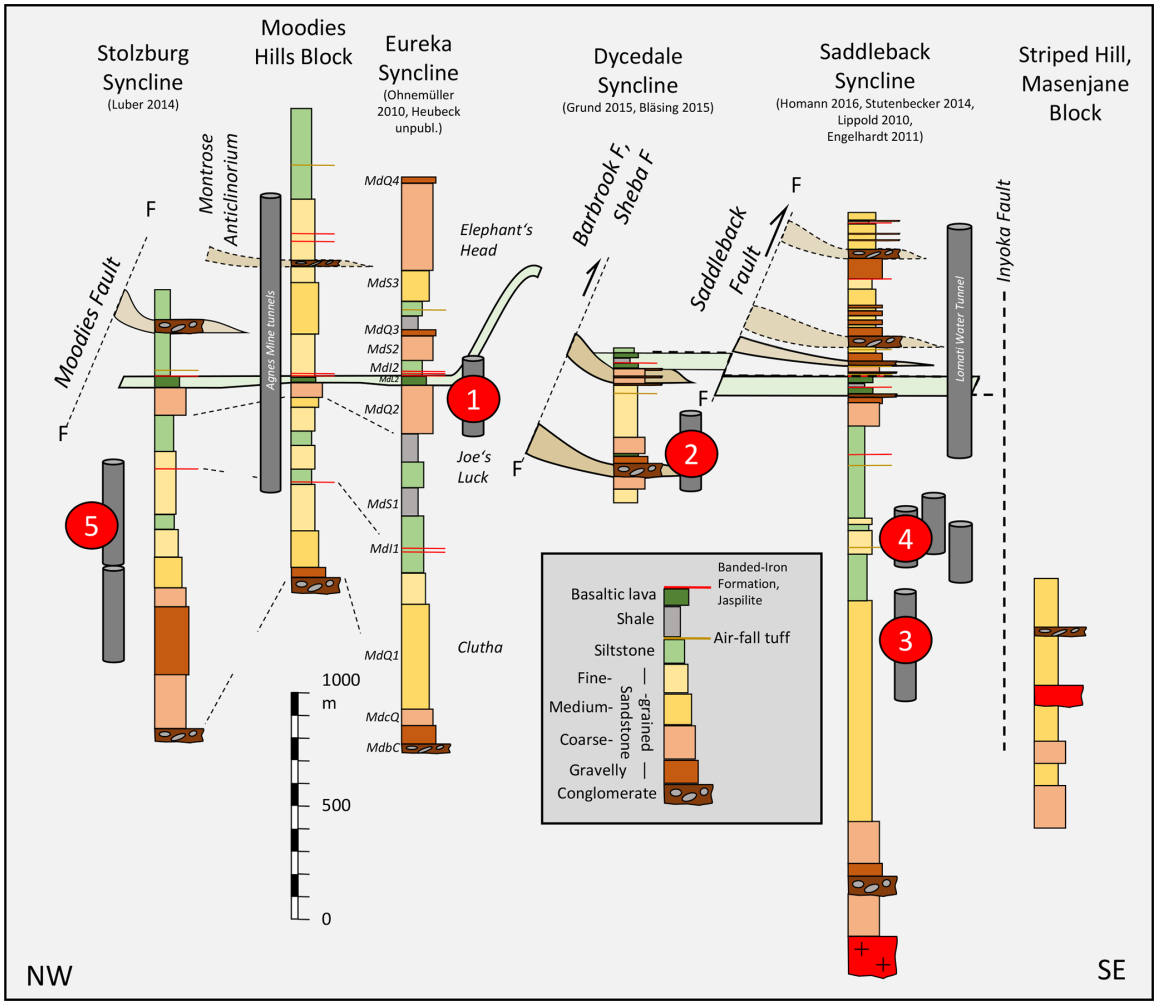

Figure 5. Schematic stratigraphic columns of the Moodies Group, showing the architecture of the Moodies Group and correlation of the sections (modified after Heubeck et al., 2016).

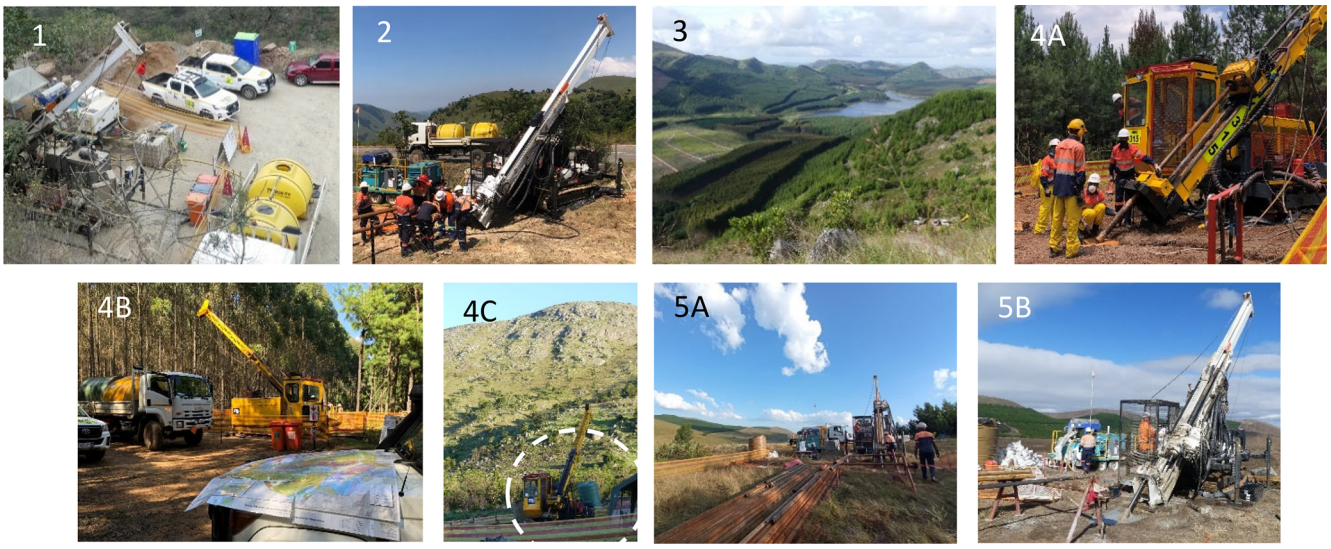

Figure 6. Locations of drill sites (numbered photographs). Site 1 is located in the hairpin turn of a mining road, Site 2 next to a parking lot of the paved R40 road. Sites 3, 4A, 4B, and 4C are located within commercial plantations, Sites 5A and 5B on open grassland.

processing. The hall turned out to be an excellent location for core processing and outreach.

Christoph Heubeck arrived about a month prior to the start of drilling to set up accommodation and the processing center and to speak personally with landowners. Water, electricity, Internet, and site security were quickly installed in September and October 2021. Nic Beukes arranged for a core rock saw and associated equipment (tables, a steel cabinet, field chairs, etc.) to be delivered from UJ stores in September 2021. The front half of our space was set up as an informative geological exhibition (Fig. 10).

4.4 Initial mobilization, water, accommodation, site preparation, and crew

The drilling contractor initially assigned two track-mounted drill rigs (MDX 315 from 15 November 2021, MDX 318 from 26 November 2021) to the task. They were delivered by flatbed truck to an offloading site as close as possible to the drill site and then usually driven under its own power to the drill site along forest roads, up to a distance of a few kilometers. That drill site had been set up a few days before (flagging, limits, safe area, parking, toilets, staffing board identifying responsibilities and contact information, tent; Fig. 7). Upon arrival of the rig at the site, the geologists marked the precise drilling direction.

A compact, trailer-mounted Solid Removal Unit (SRU) was installed at the site to process the drilling mud (Fig. 7e). The SRU centrifuged the sludge-like cuttings, which were bagged and removed as solids. They were never studied and were considered of no use to the project.

The contractor supplied a water truck capable of carrying 5 t of water. Each borehole had an assigned water extraction point, typically a 15 to 30 min drive away. Water consumption was far higher than anticipated due to the numerous fractures encountered, making more water runs necessary. The roads, softened by the unusually long and intense rainy season of 2021/2022, were occasionally too slippery to safely drive, causing additional delays.

The on-site drilling site manager, together with his rig supervisors, actively searched for crew accommodation close to the drill sites. SAPPI kindly made some of their forestry brick houses available. At these sites, the contractor also parked one or two short containers to store tools, trays, electrical equipment, and occasionally cores.

Each site was cleared of stumps and flammable vegetation. The site was leveled and delimited with flagging tape; parking, safe area, smoking area, and work area were marked and the equipment placed and connected. Signs were installed, a sump was dug, and the toilet was installed. Fifty-five-gallon drums with secure, clamped lids and oil-absorbent pads were put ready for oil or solvent spill clean-up. All drums and barrels were placed in a tray. The SRU was installed and hooked up to the generator.

Each rig was headed by a site supervisor and had a crew of five with specific functions (operator, rig assistant, scribe, assistant, safety representative, first aider, snake handler; Figs. 6–8). Operations, particularly core handling on site, were done exclusively by the drilling crew; visitors stayed outside the fenced perimeter. The conspicuous Site 2, next to the paved road R40 and only a few kilometers from Barberton, was fenced with a construction-site-quality fence by a local contractor and guarded overnight by security (Fig. 7a).

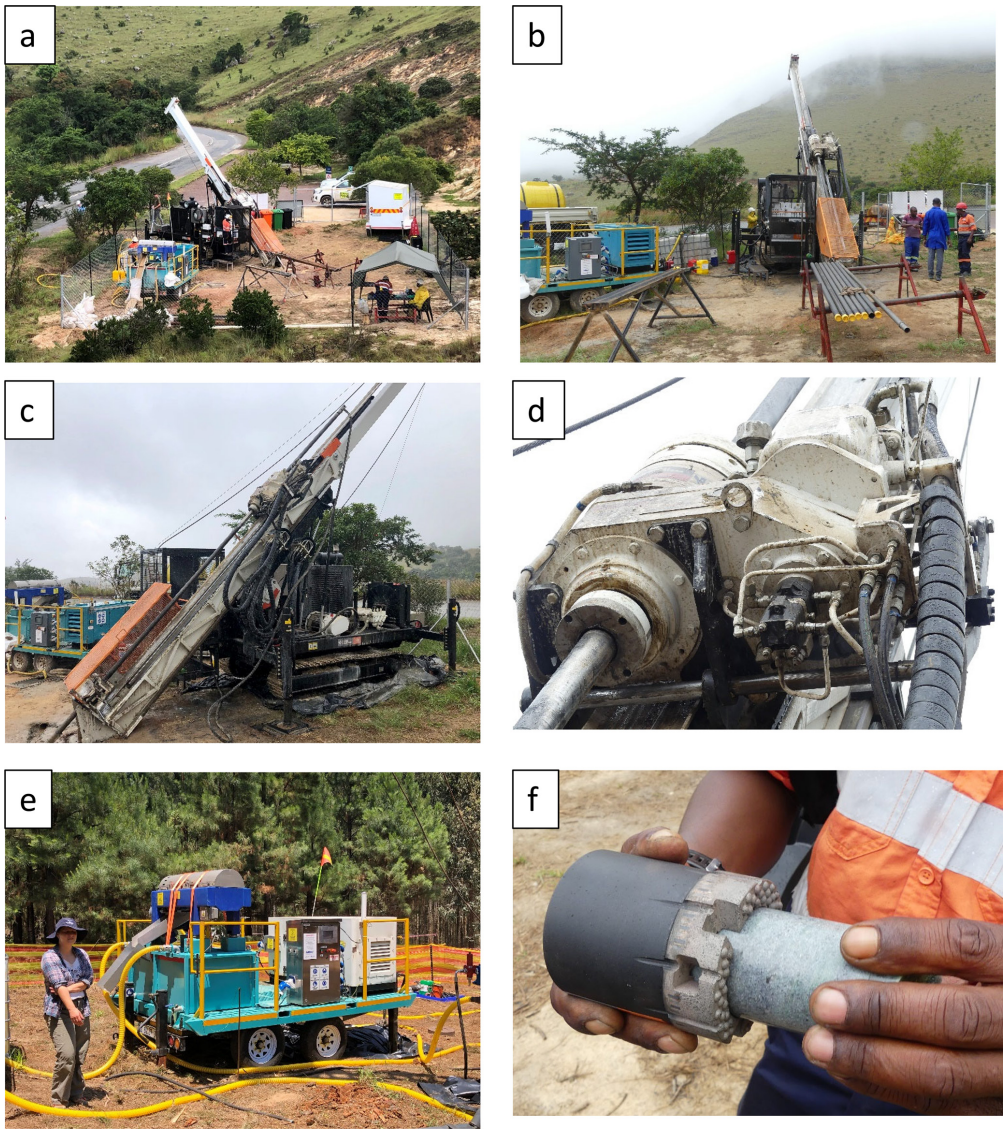

Figure 7. Drilling setup at Site 2. **(a)** Overview of the site: from left, bagged sludge, trailer-mounted Solid Removal Unit (SRU), drill rig MDX317, and the tressels and workbench for the drill pipes, tented work area, and storage trailer. The entire site is fenced. **(b)** Site overview. **(c)** Track-mounted drill rig. **(d)** "Top drive". **(e)** SRU. **(f)** Rotary drill bit with a piece of core.

5 Coring and downhole logging

5.1 Coring plan, drilling schedule, and progress

BASE boreholes were drilled using water-based hydrocarbon-free drilling mud. Drilling at each site started with PQ3 core size (83 mm core and 122.6 mm hole diameter) to allow installation of surface casing for groundwater protection. Once the weathered zone had been drilled through, the casing was set, typically between 60 and 100 m depth. Drilling continued from there for some depth on HQ3 (63.5 mm core and 96 mm hole diameter) before switching to NQ3 (47.6 mm core and 75.7 mm hole diameter) to improve drilling rates. The contractor's drilling operations manager decided the depth at which the drill pipe diameter was changed (Table 3).

The variable core diameters PQ3, HQ3, and NQ3 corresponded to core trays with four, five, and six grooves, respectively, each 1 m long. While trays with four PQ-diameter cores had to be carried by two persons, the large majority of core trays handled during processing could be readily handled by a single person because they contained only six half NQ diameter cores. This significantly eased the workflow.

The core was drilled with conventional diamond-impregnated bits, giving a core diameter which would fit into wireline inner tubes (the wireline diamond drilling method). The core is extracted by sending a wire cable down through the rod string with a spear-shaped overshot device at the end.

Figure 8. Core retrieval at Site 2.

Table 3. Drilling and casing plan.

Borehole and rig	Casing down to (m)	PQ3 down to (m)	HQ3 down to (m)	NQ2 or NQ3 down to the total depth (m)
BASE 1A (MDX900)	108.44	31.65	108.44	496.85
BASE 2A (MDX901)	138.2	40.9	138.2	367.8
BASE 3A (MDX 317)	Less than 11	16.65	73.63	280.2
BASE 4A (MDX315)		At least 24.15	101.85	340.1
BASE 4B (MDX315)	66.6	28.50	65.9	355.5
BASE 4C (MDX317)	90.84	37.12	92.99	351.49
BASE 5A (MDX901)	107.79	34.46	106.76	451.30
BASE 5B (MDX901)	96.00	17.90	94.71	489.9

This device would clip itself over the swivel head assembly, essentially a spike at the top of the core barrel. This action disengages the latches of the inner barrel assembly from the outer barrel and the drill pipe, freeing the inner tube with the core inside. Thus, the core barrel could be rapidly winched up to the surface. Only when the bit needed to be replaced was the entire rod string brought to the surface ("tripped").

The initial drilling progress of ca. 5 to 8 m d^{-1} was far slower than the contractor had predicted, so that the contractor assigned a third, new drill rig (MDX 317) on 3 February 2022. These measures and continuous optimization in the drilling parameters significantly improved the core recovery and drilling rate. However, logistical problems with moving the rigs between locations due to the low availability of flatbed trucks, washed-out tricky roads, and lack of an adequate water supply, together with the very rainy summer of early 2022, caused additional delays. Drilling ended on 26 July 2022, with a total of 3135 m drilled and 2903 m of core recovered. All scientific objectives of the project

were achieved; all boreholes had reached their planned total depths.

Moving rigs between sites from the end of drilling to collaring at a new site took approximately 10 d, including weekends. This included pulling the drilling assembly, flushing the hole, filling the hole with clean water, conducting geophysical logging, extracting the surface casing, driving the rig on its own tracks to a location where a flatbed truck could load the rig, transferring it to an offloading point, driving it on its own power to the new site, setting it up there, and properly orienting the rig.

5.2 On-site core handling

The 3 m long core barrel was laid on tressels and the drill bit screwed off (Fig. 8). The barrel was opened at its lower end and its upper end hooked to a cable which was slowly raised using the winch, causing the core to slide out of the core barrel under its own weight. The core, usually in several pieces and caught by two helpers, slid into a 3 m long V-shaped angle iron laid on the grooved tressel. All the core pieces were carefully moved together. The full length of the core was accurately measured with a steel tape. This length is the "core recovery" (as opposed to the drilled depth, the length of which is called the "advance"). Once the core barrel had been emptied, the core was washed and transferred to a plastic core tray, taking care to maintain the right order and correct orientation of each piece. If the last piece was too long to fit in the row, it was broken with a hammer tap. The driller's depth for each run was demarcated by a plastic depth-marker block. The driller recorded the end-of-run depth, drilling advance, and core recovery on this plastic block and included these numbers in the daily drilling report.

Core was recovered each time the core barrel was full, if the bit had worn out, or if the water channels in the bit had become blocked. The depths were always calculated on a run-by-run basis. The core depth was calculated by the "stick-up" procedure. The data for this calculation were recorded for every run, whether it was a full or partial core barrel. The latter would apply if, for example, the drilling had to be prematurely stopped because of a bit failure or water blockage.

Accurate depth measurements were recorded by the rig supervisor in his daily report sheet by adding the lengths of all rods, couplings, core barrels, shells, and crowns in the hole and subtracting the length of the rod string protruding from the hole and above a base reference plate or mark. This system worked well.

A drilling rig produced between three and six core trays per day, amounting to between 12 and 36 m of core. Because friable cores were particularly susceptible to breaking by vibration during transport, core trays had to be tightly stacked, covered by a lid, and securely strapped down in the vehicle. The driver had to drive carefully and take care to avoid the many potholes.

5.3 Rock quality

The quality of the drilled cores varied more than anticipated for several reasons: (1) the weathering zone was thicker than predicted, causing the rock to be clayey and friable; (2) the degree of natural fracturing was higher than predicted; (3) deep oxidation along fractures and faults reduced rock strengths, even at depth; (4) the drill crews were inexperienced with this type of rock; and (5) the first cores, already affected by faults or hairline fractures, were transported over potholed dirt roads and were not fully secured. This caused some additional breakage. As a result, a substantial number of drill cores arrived broken. Such core had to be time-consumingly rearranged, taped, and marked. The rock quality index (RQI) was entered into the database to describe an aspect of rock quality.

5.4 Activities after reaching the total depth; logging

Downhole geophysical logging was done by Wireline Africa Inc. A wireline unit logged each cleaned and fluid-filled borehole, usually the day after the rig had pulled the drill string (Fig. 9a, b). Logging usually took 2 d. The final few meters of casing were left in the hole, and the annulus was sealed using a viscous bentonite clay mixed with cement. The borehole was then covered by an oval steel cap with the borehole name (Fig. 9c, d) which was welded on in June and July 2022. These caps were mounted a few decimeters below ground level to be completely unobtrusive. At an inspection in March 2023, no caps or signs of drilling were visible.

After departure of the drilling rig and loading of the remaining site equipment, the ground was cleaned and raked (Fig. 9e, f). Minor spills were taken care of by absorption material.

6 Scientific operations

6.1 Core handling workflow

We had set up a core processing workflow in BIAS Hall by stations, arranged clockwise. Each station had at least one principal attendant, a working area, and a waiting area (Fig. 10a, b). The regular crew consisted of five scientists and three operators (Fig. 11).

6.2 Reception, repacking, labeling, mobile Drilling Information System (mDIS) entry, and photography

After offloading from the vehicle, core trays were briefly inspected for completeness and order and stacked by drill site. Sections and individual core pieces were then moved up to the last (usually partially empty) core tray of the previous day. Repacking was done to create a continuum and to avoid having long empty rows in core trays. The black plastic core trays were neatly labeled using a white marker (box numbers, core run numbers, "START", arrows).

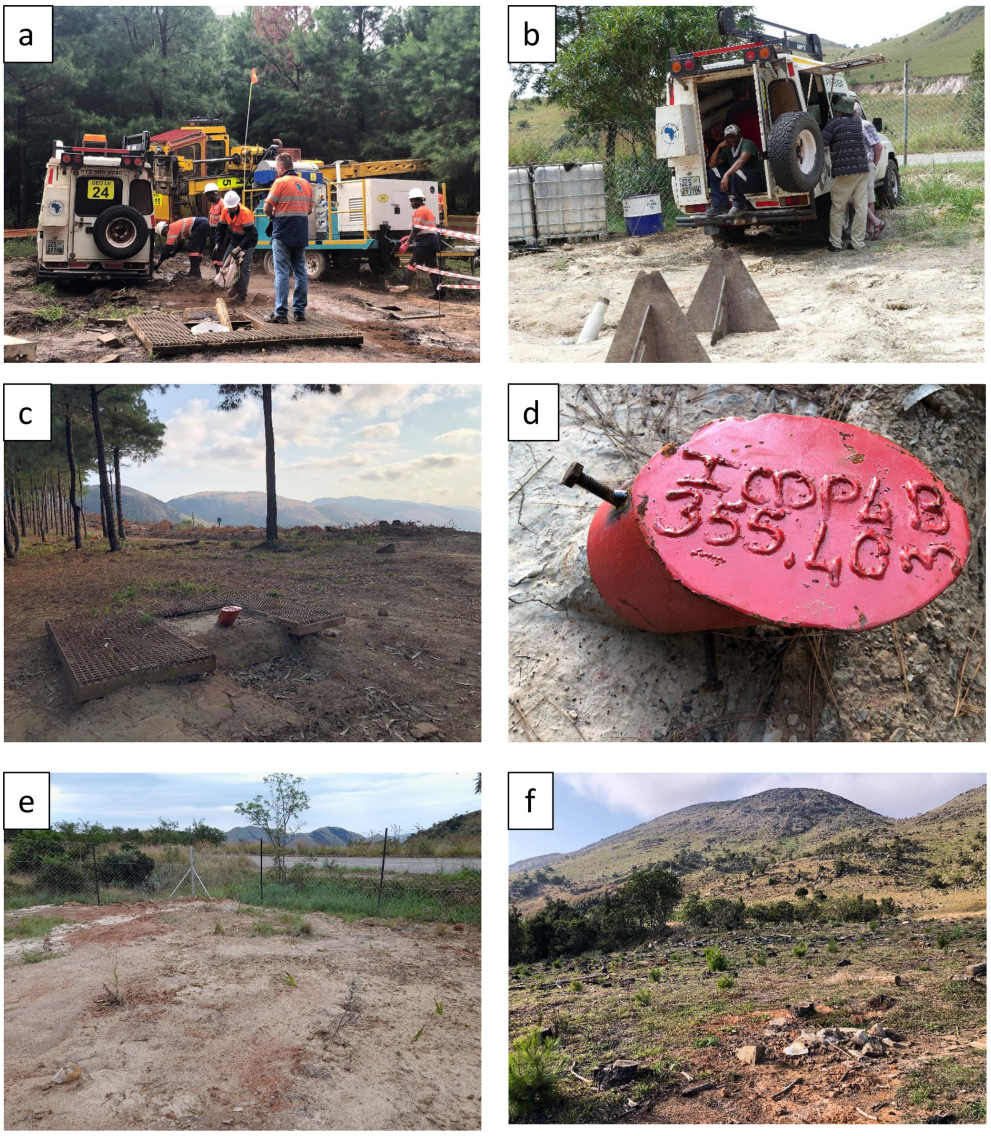

Figure 9. Post-drilling site operations. **(a, b)** Logging. **(c, d)** Site 4B with the cap welded on; the steel grating is yet to be removed. **(e)** Site 2 with the equipment removed; the site still needs to be raked and the fence removed. **(f)** Site 4C rehabilitated.

Basic core and section data, e.g., I lengths of each core, their sections, and their number of pieces were entered into the ICDP's mDIS, a database system for capturing and curating basic data generated during the project's operational phase (Fig. 11a). Notably, the mDIS is not based on absolute depth values (which can change during a project's lifetime due to adjustments) but on "core number" – the "section number of the core in the core tray" and "number of a piece of core within a section". Only then are core sections measured and labeled with lengths; the system automatically adds all section lengths to arrive at dynamic depth values. Several report forms allow data output in tabular, graphic, or digital formats and printing of QR code labels for sampling.

Immediately after repacking, the full core trays were photographed dry and wet to record presence, core continuity, and rock quality. The existence of these "book-in" photos proved helpful later when core segments disintegrated, were occasionally mishandled, or were misplaced during processing.

The photography station was located on a trolley next to a lifting frame which had been fabricated from a tripod and a horizontal outlier, the end of which held a smartphone at a fixed location and height (Fig. 11d). The trolley could easily be reoriented to optimize illumination. The core and tray were wiped clean, and a data bar showing the hole number, scale, and reference color bar was placed below the core tray.

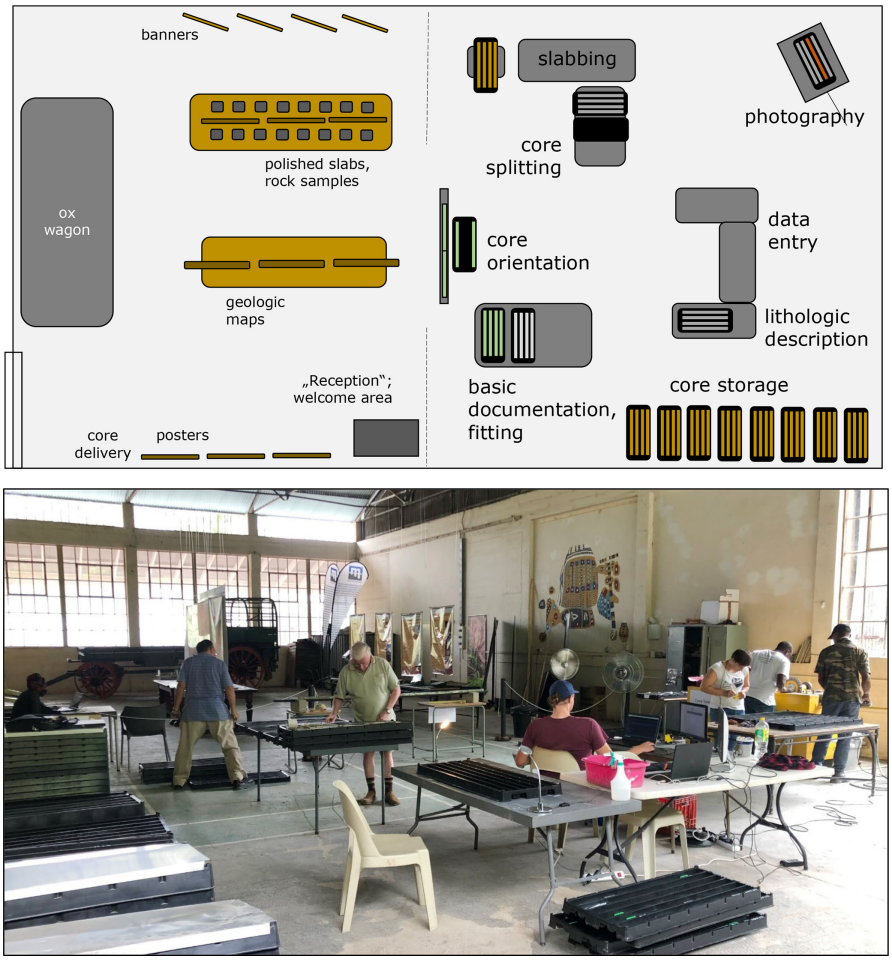

Figure 10. Workflow of core processing in BIAS Hall. The "reception desk" is visible to the left, staffed by Phumelele Mashele. The exhibition area and the museum's ox wagon are visible in the background. Chris Rippon, with his back to the camera, is working on core orientation, Rod Tucker on basic documentation and fitting. Derick Dludlu and Musa Mavimbela (far right) are slabbing core at the yellow core saw. Dora Paprika is in front of them, slabbing and labeling the core. The photography stand is out of view to the right. Ryan Tucker is entering data into the mDIS. The lithology description table in the foreground is usually occupied by Christoph Heubeck.

6.3 Orientation

After returning from book-in photography, core pieces were taken from their tray and placed on a 4 m long V-shaped angle iron which had been set on nudged bricks between two tables. The core was rotated and moved together for a best fit between pieces (Fig. 11b). We oriented core by hand based on the angle at which the regional bedding inclination (known from outcrops) intersected the borehole, which was inclined at 45° below the horizontal. Chris Rippon oriented all core segments on the angle iron such that the bedding low-point faced downhole. Where the bedding was poorly distinguishable, estimates of proper fits were made from the end pieces of previous core pieces. Where core was badly broken, pieces were taped together. Once oriented, a yellow "cut line" was drawn on top of the horizontally resting core using a 1 m steel ruler. This defined the left and right halves of the core. Yellow arrow marks (< < < < <) were drawn on the top of the core to indicate the direction to the drill rig. Parallel red and blue lines were drawn on the left and right halves. Full meter numbers were marked on the outside of the core in black. The core was returned to its tray and transferred to the core saw waiting area.

6.4 Slabbing, tray labeling, separation of archive and working halves, and repeat photography

The core saw operators took a marked core segment from its tray, shortened it if necessary with a hammer to fit in the 30 cm long slotted cradle, and placed the core such that the yellow cut line faced upward. The tray was automatically drawn into the (housed) saw blade by a toothed pulley (Fig. 11c). An operator retrieved the slabbed core in its cradle on the other end of the saw blade housing and returned both halves, still placed next to each other, into the core tray. A self-made sump with a pool pump, bought from a local hard-

Figure 11. Stations of core processing in BIAS Hall: **(a)** re-packing; **(b)** orientation; **(c)** slabbing and splitting; **(d)** photography; **(e)** data entry; **(f)** lithological description and close-up photography.

ware store, circulated water which was laced with a diamond saw cutting-fluid additive.

Once core from a tray had been completely slabbed, it was placed on a large table next to an empty core tray. A helper carefully duplicated all markers from the original core tray to the other tray using a white permanent marker and added a "W" (working) and an "A" (archive), respectively, to the core tray number. Usually, the left half of the split core and any core pieces too broken to be moved remained in the original tray (now labeled "A": archive). The right half of the split core was transferred to the new core tray (labeled "W"), which became the working half destined for shipping to Germany. At this point, both trays also received handwritten labels on the front and depth information on the side. Finally, and prior to photography, the black full meter markings from the outside of the core were duplicated on the slabbed core faces.

Both the archive and working halves and their trays with the data bar were cleaned and photographed again wet and dry (Fig. 11d). Then, the tray with the working half moved to the storage section, the archive half into the lithology waiting area.

6.5 Geological core description and close-up photography

For its initial geological description, a core tray was placed on a table, illuminated by two high-powered LED desktop lamps; the core was sprayed with water. A 90° seating arrangement between the describing geologist and the data entry operator turned out to be most effective at transmitting the information while the very noisy diamond saw was running (Fig. 11e).

Core description used the ICDP's mDIS. Information was entered in two categories: lithofacies and special features. The lithofacies terminology included lithologic units (e.g., sandstones, interbedded sandstone-shale couplets, conglomerates) combined with specific subsets of sedimentary structures (laminated, cross-bedded, with microbial mats, mudchip-bearing, grain size trends, etc.). We attempted to transfer these terms between boreholes but found that dif-

ferences in primary depositional facies, degree of weathering and fracturing, cementation, and hydrothermal alteration were large enough to change lithofacies appearances significantly, making new definitions a common necessity. This approach reduced comparability between borehole lithologies but allowed detailed recording of subtle lithologic and textural changes. If workload and core variability allowed, we identified all lithofacies units > 2 cm in thickness. They differed from each other by lithofacies, contact type, grain size, sorting, and/or code from the Munsell rock color chart. Typical units, however, were 7 to 12 cm thick; unusually thick units reached up to 40 cm.

The category "Special Features" included non-pervasive primary sedimentary features of a lithofacies such as isolated clasts of various types and sedimentary structures (e.g., mud cracks, mud clasts, rhythmic bedding, shale coatings, load structures, fluid-escape structures, cross-bedding, erosional scours, slump folds, microbial mats, concretions). Post-depositional features in this category recorded slump folds, fractures, faults, veins, and (pyrite) mineralization which were not or insufficiently included in the definition of the lithofacies nomenclature (e.g., lithofacies: cross-bedded medium-grained sandstone; special feature: quartz-veined). Dora Paprika, our principal data manager, oversaw the database and kept digital order.

Many close-up photographs of the freshly slabbed and sprayed core on the lithology description desk were taken (Fig. 11f). Each photograph included a small handwritten label stating the borehole, core, section, piece, arrow pointing in the stratigraphic younging direction, and depth; the stated depth on that label was always the measured depth which was marked in handwriting on the core. It constituted the depth of the label, not of the feature. The text of the label was always oriented so as to face stratigraphically upward. These close-up photographs proved to be useful in subsequent core description.

6.6 Archiving, preparation for shipping, and shipping

Once cores had completely dried again, trays were stacked about 20 trays high in separate stacks (working, archive). We checked whether labeling was complete. Inexpensive pallets were ordered locally. Trays fit snugly on top of each other such that they immobilized cores. Only the topmost trays received a lid. Tight steel band strapping prevented the jostling of trays during transport.

A total of 29 pallets, each with two stacks of about 12 core trays each, were shipped to the CGS's National Core Repository in Donkerhoek in August 2022. This archive is the legislated custodian of all geoscience data in South Africa. It provides accessible, safe storage for the core and is a resource for future research.

Twenty-eight pallets from the boreholes loaded with 503 core trays plus one pallet with boxed samples from the tunnels left Barberton on 30 September en route to Germany and arrived at the Berlin Core Repository of the Bundesanstalt für Geowissenschaften and Rohstoffe (BGR), a federal agency, on 30 November 2022.

The working core is currently stored at the Nationales Bohrkernlager für kontinentale Forschungsbohrungen, Wilhelmstr. 25–30, 13593 Berlin (Spandau), Germany.

The samples from the probed tunnel sections were shipped to Jena and processed there. Chips and thin sections are archived in the departmental archive, care of Christoph Heubeck.

7 Basic data and preliminary scientific results

7.1 General remarks

The drilling campaign drilled a total of 3135 m, recovering 2903 m of core and yielding a recovery rate of 93 % (Figs. 12–20). Lost core material consisted of sections in the weathering zone which were not cored (5–70 m thick) and core broken due to oxidative weathering or due to extensive fracturing at depth.

The coring program encountered several surprises.

1. Unexposed strata overlying and underlying the weathering-resistant Lomati Delta Complex of the Saddleback Syncline in BASE 4A, BASE 4B, and BASE 4C did not consist of (deep-water) shale as predicted, but of friable, cross-bedded tuffaceous sandstones. This will require a reassessment of facies.

2. Virtually all boreholes encountered a high degree of fractured rock, resulting in excessive water consumption; oxidation along fractures was encountered up to 250 m depth.

3. The jaspilite unit MdI1 in the Stolzburg Syncline was found to be significantly thicker at depth than mapped at the surface (Luber, 2014) because finely interbedded shale-jaspilite was found to overlay and underlay the silica-rich central section.

4. BASE 2A encountered a thick association of cobble conglomerates interbedded with and reworking carbonaceous microbial mats, confirming the interpretations from nearby roadside outcrops (Heubeck et al., 2016) and supporting previous claims of continental, not entirely marine sedimentation.

5. BASE 3A, drilling a sandy tidal-flat facies (Homann et al., 2015), encountered repetitively stacked, ca. −20 –90 cm thick, fining-upward genetic units. They consisted of microbial-chip conglomerate at the erosive base, overlain by massive sandstone, overlain by horizontally stratified and faintly microbially laminated sandstone, and capped by fully developed "crinkly" microbially laminated sandstone.

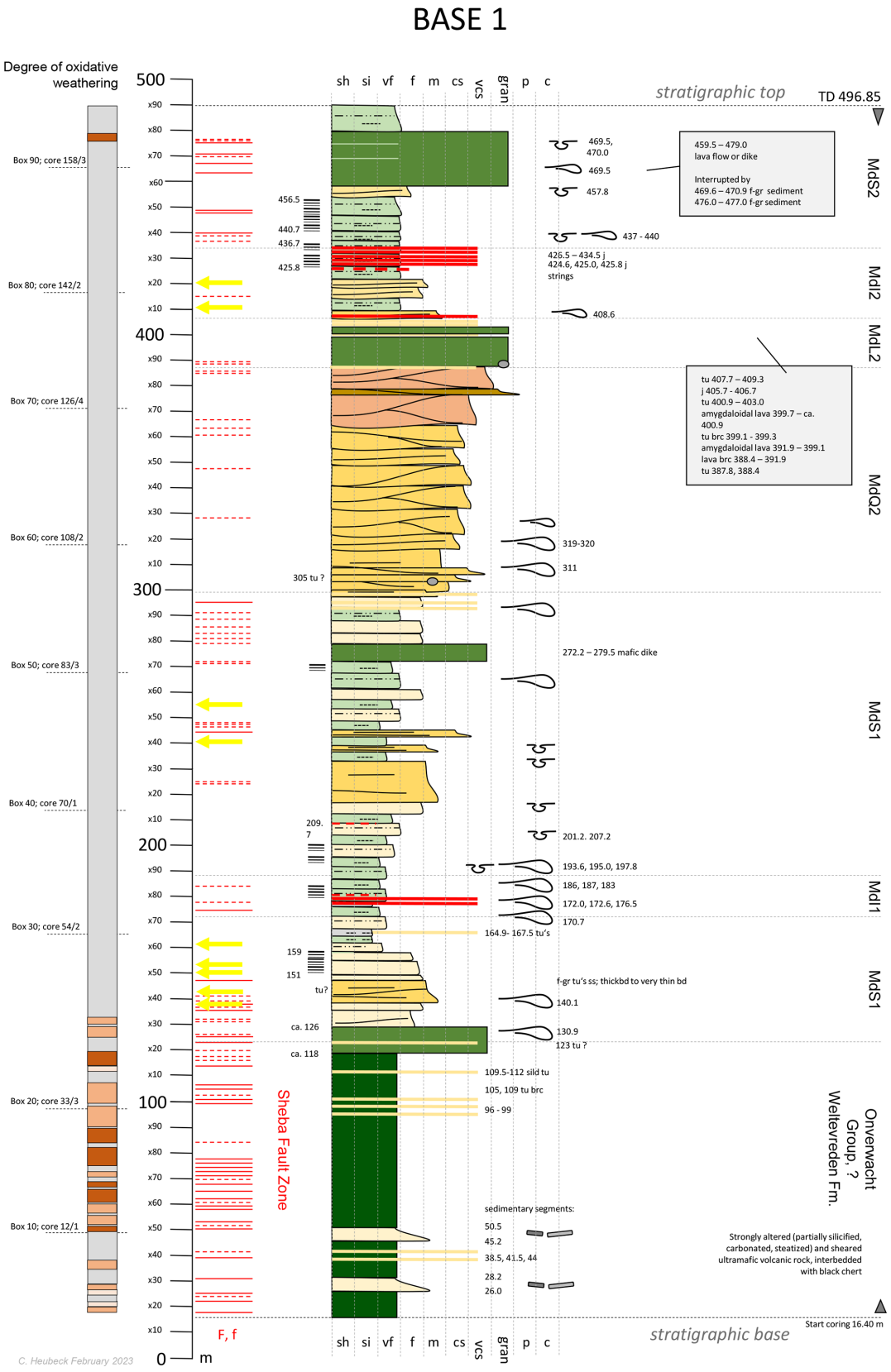

Figure 12. BASE 1A drilled 295° from true north and base-up through the eastern, west-facing limb of the Eureka Syncline on the grounds of Fairview Mine. The borehole spudded in the Sheba Fault Zone at 25°44′2.48″ S, 31°5′51.08″ E and was drilled from 16 May through 26 July 2022.

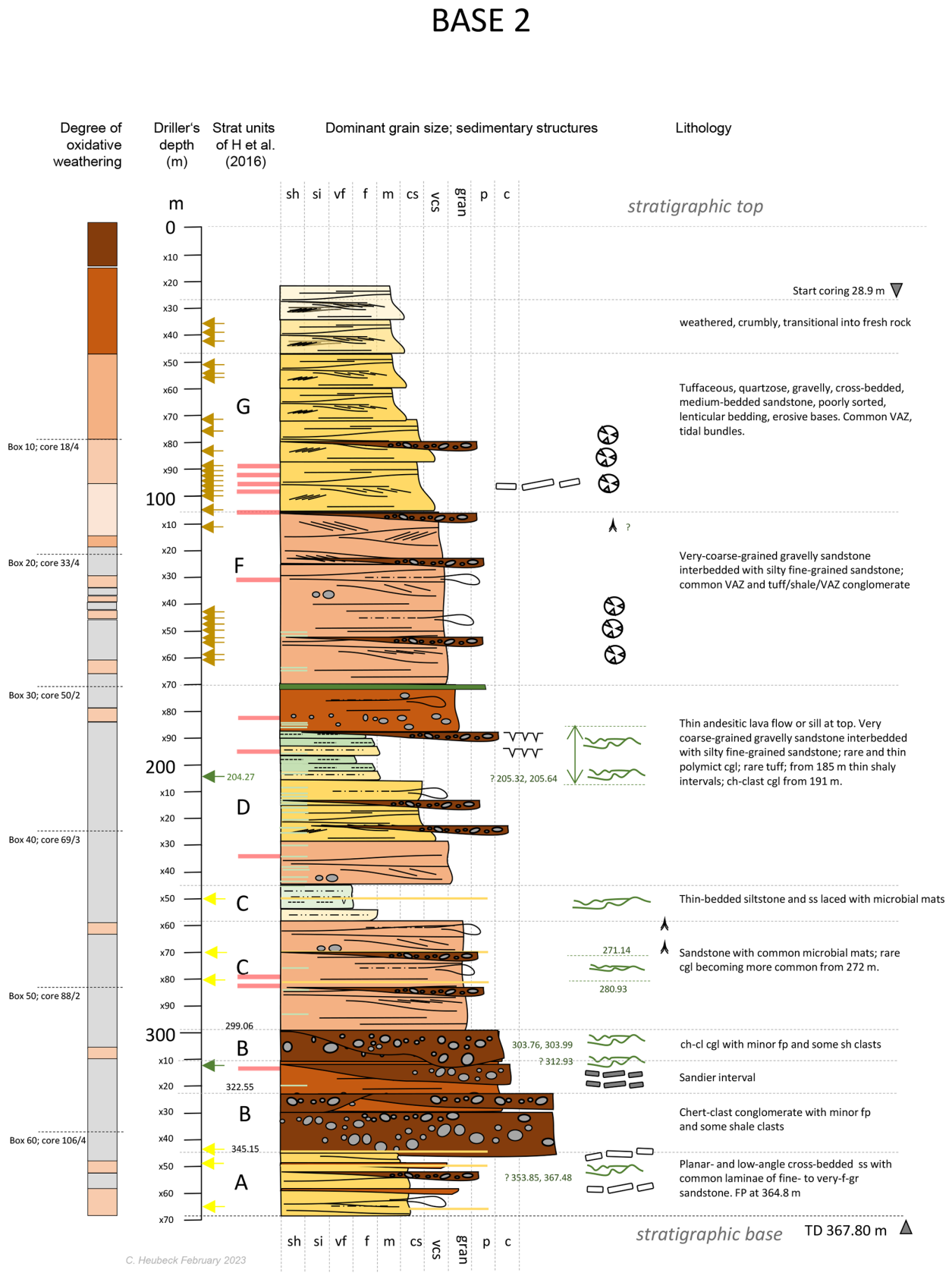

Figure 13. BASE 2A drilled top-down, 313° from true north on the southeast-dipping limb of the Dycedale Syncline. The borehole spudded just north of the R40 Geotrail "Tidal Sandstone" parking lot at −25.793817° S, 31.083763° E and was drilled from 3 February through 15 March 2022.

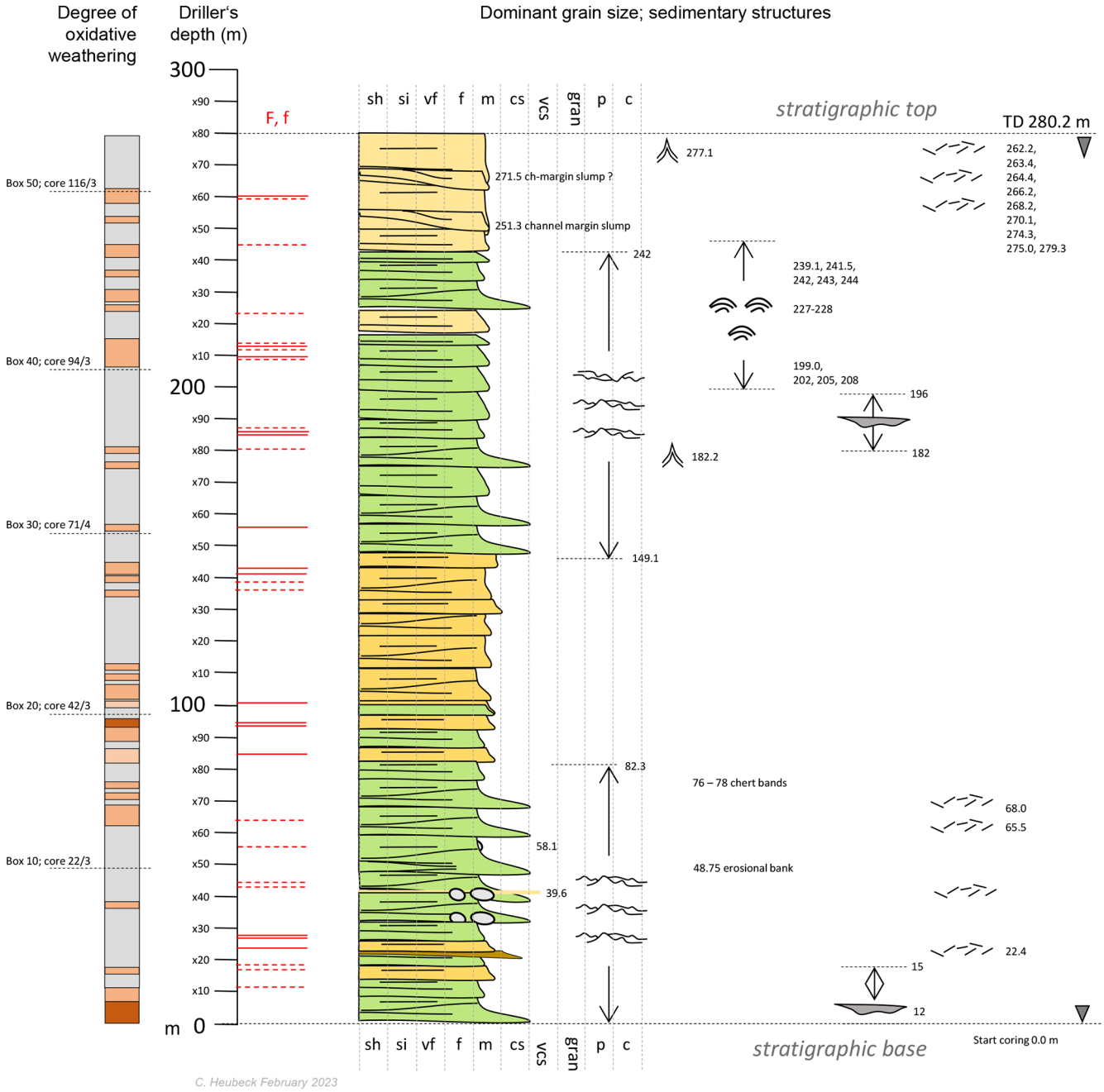

Figure 14. BASE 3A drilled 319° from true north and base-up on the south-dipping southern limb of the NE–SW-trending Saddleback Syncline. The borehole spudded at 25°49′48.39″ S, 31°5′26.88″ E and was drilled from 25 November 2021 through 26 January 2022.

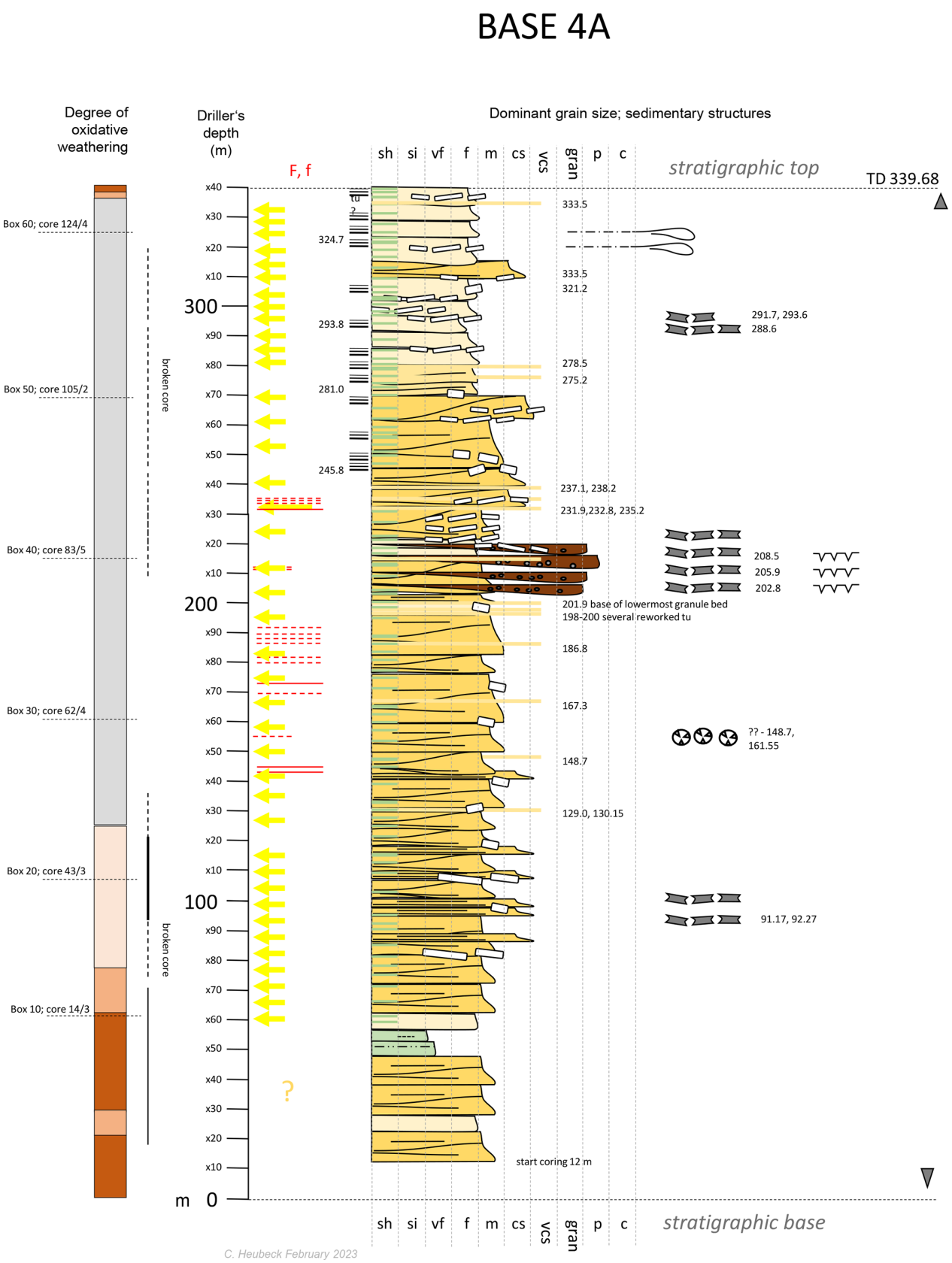

Figure 15. BASE 4A drilled toward 319° from true north and base-up through the overturned southern limb of the Saddleback Syncline. The borehole spudded at 25°44′2.48″ S, 31°5′51.08″ E and was drilled from 17 November 2021 through 26 January 2022.

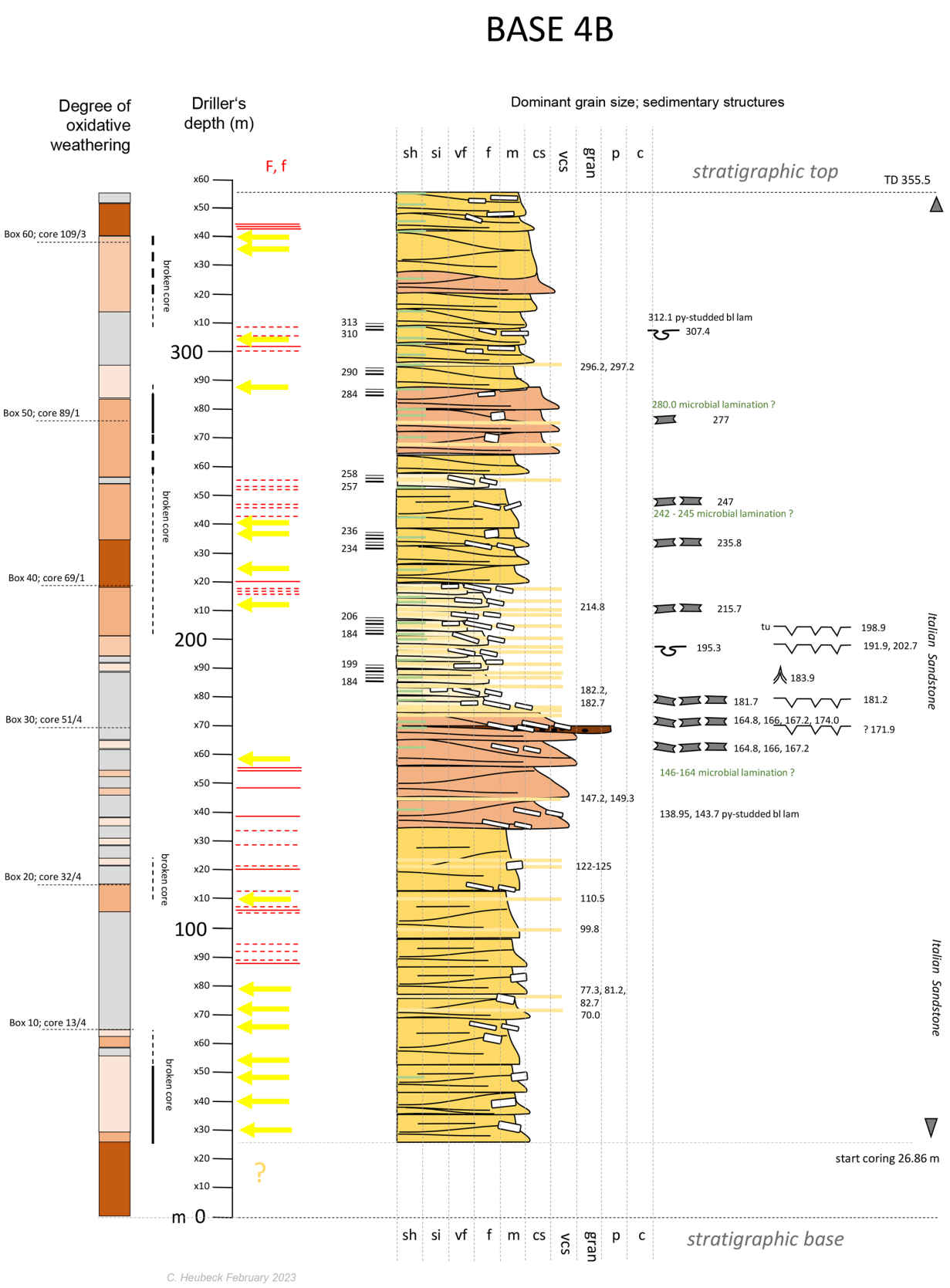

Figure 16. BASE 4B drilled toward 336° from true north and base-up through the overturned southern limb of the Saddleback Syncline. The borehole spudded at 25°51′11.77″ S, 31°2′54.81″ E and was drilled from 9 February through 23 March 2022.

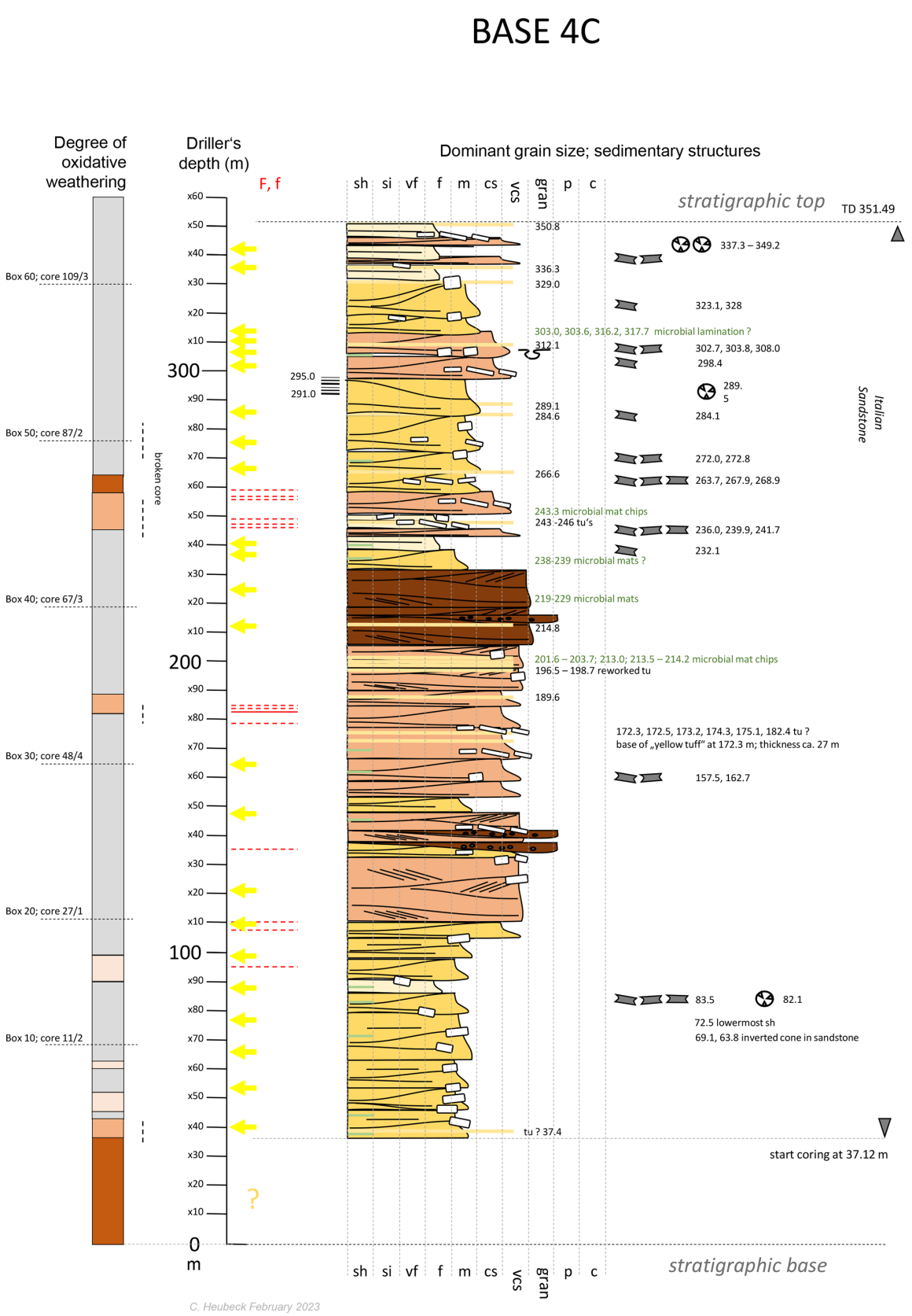

Figure 17. BASE 4C drilled toward 336° from true north and base-up through the overturned southern limb of the Saddleback Syncline. The borehole spudded at 25°51′39.38″ S, 31°2′3.41″ E and was drilled from 11 February through 22 April 2022.

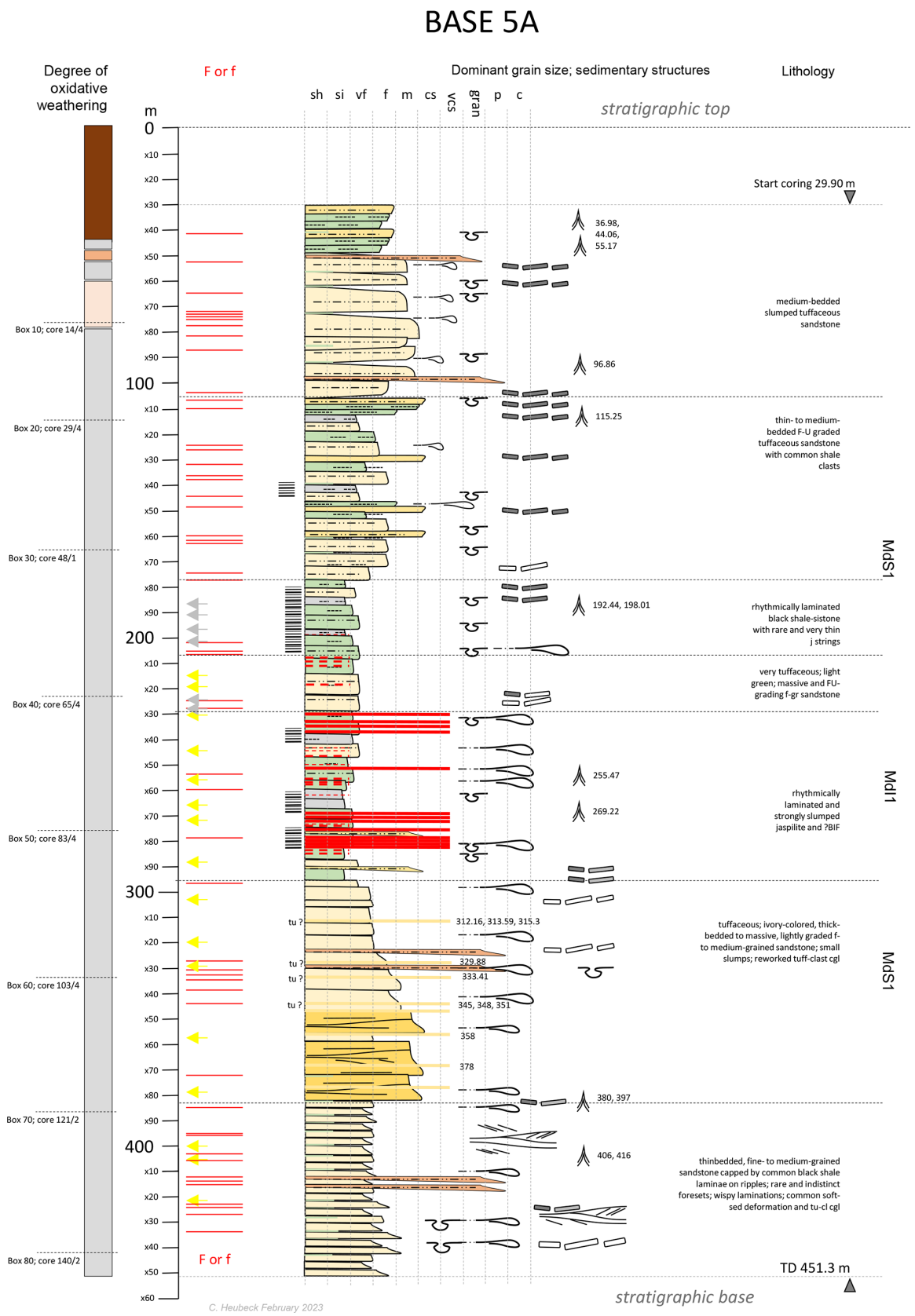

Figure 18. BASE 5A drilled northward (009°) and top-down on the south-dipping northern limb of the E–W-trending Stolzburg Syncline. The borehole spudded at 25°54′13.32″ S, 30°50′44.68″ E and was drilled from 5 April through 18 May 2022.

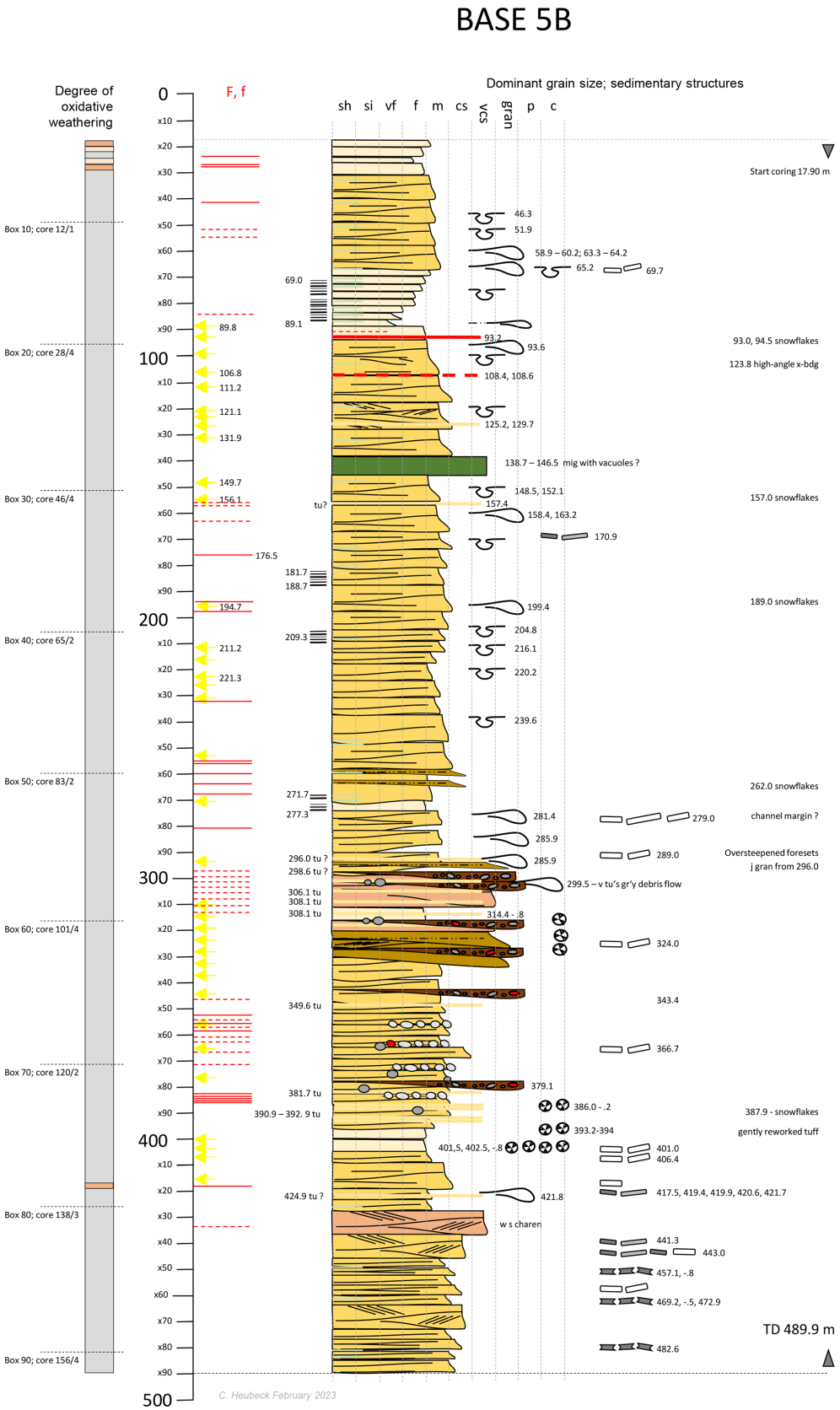

Figure 19. BASE 5B drilled northward (013°) and top-down on the south-dipping northern limb of the E–W-trending Stolzburg Syncline. The borehole spudded at 25°54′2.80″ S, 30°50′49.06″ E and was drilled from 3 June through 17 July 2022.

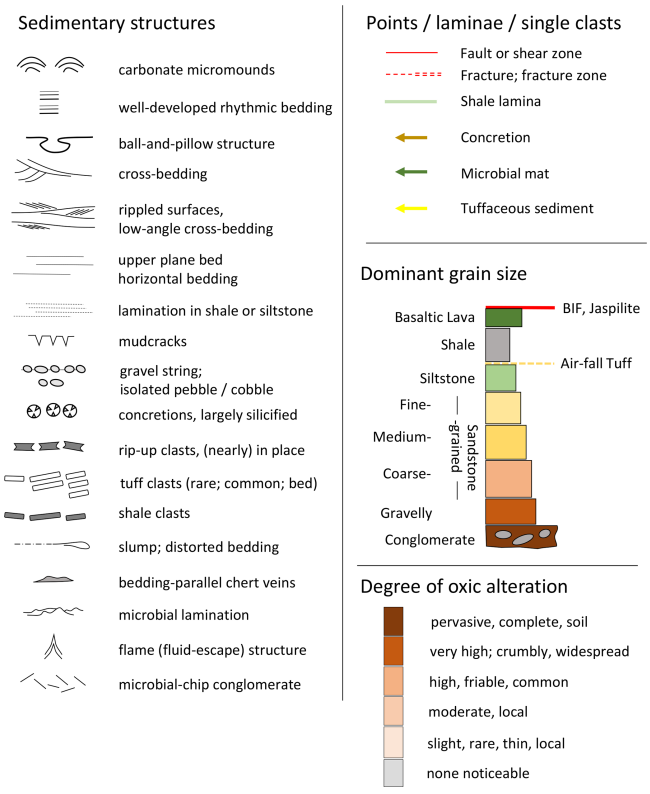

Figure 20. Legend to Figs. 13–19.

6. Virtually all boreholes encountered some felsic volcanic tuff (Heubeck et al., 2013, 2022b), but most are very thin and consisted of off-white fine-grained ash (not accretionary lapilli); most were slightly to fully reworked.

The preliminary stratigraphic columns of Figs. 12–20 provide a framework for lithologic and stratigraphic research. Fault zones, tuffs or tuffaceous horizons, and segments of abundant microbial mats or of well-developed laminations are marked. The locations of symbols representing sedimentary structures are approximate. On each log, a thin stratigraphic column qualitatively illustrates rock quality, thus indicating the extent of weathering near the surface and along fracture or fault zone networks.

7.2 Brief description of each borehole

Drill site **BASE 1A** was located in Elephant's Kloof valley on the grounds of Fairview Mine, ca. 10 km northeast of Barberton (25°44′2.63″ S, 31°5′50.65″ E). The borehole probed the overturned (inner) limb of the arcuate Eureka Syncline of the northern–central BGB. The drill site had to be moved from its originally planned location along a mine road due to space constraints to a stratigraphically lower position in a wide turnout of a hairpin turn. The hole was collared in altered schistose ultramafic rocks of the Weltevreden Formation of the Onverwacht Group in an anticlinal shear zone (locally known as the Zwartkoppie horizon of the Sheba Fault Zone). BASE 1A drilled, after having reached the faulted base of the Moodies Group at ca. 126 m depth, stratigraphically up-section. Drilling started on 19 May and ended on 27 July 2022, for a total depth of 496.85 m. The true stratigraphic thickness of cored Moodies strata is approximately 350 m.

This section targeted thick fine-grained siliciclastic strata of MdS1 and MdS2 in deep-water facies (delta slope turbidites of MdS1 and MdS2, offshore jaspilites and BIFs of MdI1 and MdI2). These units are also intermittently exposed in the Clutha Creek drainage ca. 4 km to the north (Christoph Heubeck, unpublished field notes) and along the slopes and ridges paralleling Elephant's Kloof valley. A second target was the progradational coarsening-upward or shallowing-upward sandstone complex of MdQ2, abruptly overlain by the regional Moodies basaltic lava (MdL2) and in turn overlain by jaspilites of unit MdI2 and fine-grained deep-water strata of MdS2. All targets were reached. The mine geologists examined all cores before they left Fairview Mine.

BASE 2A (25°47′37.78″ S, 31°5′1.50″ E) was located ca. 5 km from Barberton next to a parking lot of a geoscience stop ("Tidal Sandstones") along the paved R40 route. This road, the "Geotrail", winds its way across the central BGB from Barberton to the Josefsdal–Bulembu border post with Eswatini. The borehole targeted a retrogradational (deepening- and fining-upward) fluvial–coastal–estuarine section partially exposed on the northern, south-dipping limb of the Dycedale Syncline, described by Homann et al. (2018) and Heubeck et al. (2016). This site has spectacular outcrops in deeply eroded ("badland"-type) friable tuffaceous sandstones next to the parking lot on grassland slopes adjacent to the drill site and in good but weathered roadside outcrops north of the drill site; neither of these allows geochemical sampling. The borehole spudded on 3 February and reached total depth on 15 March 2022. It was drilled using a tracked rig on its first deployment and drilled for 367.80 m top-down. The true stratigraphic thickness of cored Moodies strata is approximately 290 m. This section was of great interest to the paleoenvironment, sedimentary, and life groups: from base to top, the units included fluvial sandstones with several intervals of microbial mats in channelized conglomerates ("life on land"; weathering rinds on clasts), coastal (lagoonal, sabkha) sandstones with abundant, partially rock-forming vadose-zone sulfate concretions (now largely silicified), interrupted by at least one Aridisol (*terrestrial weathering*) with teepee structures and a single andesitic lava flow (*weathering intensity*). These units are overlain by thick estuary sandstones (*tidal dynamics*) with significant tuffaceous contributions. Because key marker units known from outcrop (the top of the thick cobble conglomerate and the 1 m thick andesitic lava) were encountered ca. 40 m earlier than anticipated from the extrapolation of the surface dip angle, the post-drill cross section shows numerous out-of-syncline ac-

commodation thrust faults. At least one such low-angle thrust fault is prominently visible in roadside outcrop.

BASE 2A was the most conspicuous and visited site of the drilling campaign; these aspects are described below.

BASE 3A (25°49′48.39″ S, 31°5′26.88″ E) was located on the north-facing rocky slope in the central Saddleback Syncline, stratigraphically at the top of unit MdQ1. The borehole had originally been planned ca. 200 m further uphill (further down-section), approximately on top of the ridge, but had to move downslope (up-section) to the wide dead end of a forest road on a steep rocky slope to occupy a suitable drilling location. From this "platform", the rig drilled a 45° inclined borehole in young pine growth in the downslope direction. It spudded on 25 November 2021 and reached a total depth of 280.2 m on 26 January 2022, after having drilled base-to-top (up-section) through a thick low-relief tidal platform with abundant signs of microbial life. The true stratigraphic thickness of cored Moodies strata is approximately 218 m. The primary objective was to investigate stratigraphic patterns (rhythmicity, stacking) of microbial mats and their sandy host rock, to obtain continuous sections of microbial-mat-bearing sandstones and to investigate a thick tidal channel and a ca. 30 m thick unit of abundant calcareous "minimounds" resembling small stromatolites within the kerogenous-laminae-laced tidal sandstones (Heubeck et al., 2023).

All these objectives were reached. The borehole initially cored slightly gravelly sandstone of a coastal-plain facies (ca. 0–50 m) and then reached a sandstone unit (ca. 50–100 m) of numerous, stacked, ca. 0.2–0.7 m thick, fining-upward units consisting of (base-up) erosionally based microbial-chip conglomerate, massive sandstone, flat microbial mats, and tufted microbial mats. A cross-bedded sandstone unit ca. 50 m thick (100–149 m drilled depth) may represent an estuarine channel. The "minimound" unit, mapped in the eucalyptus plantation at the base of the slope, was encountered at ca. 199–239 m depth. The borehole surprised by its numerous fractures, many of them lined with oxidative halos.

Of all the BASE sites, this core offers the most detailed insight into how early life handled the challenges of exposure, tides, and abrasion. It is unique worldwide. This section is of central interest to the scientists interested in early life and paleoenvironmental conditions.

The three boreholes of Site BASE 4 (A, B, C) investigated the Lomati Delta Complex (LDC), a wedge-shaped coarse-clastic body extending over ca. 8 km strike length in the central Saddleback Syncline, by drilling one borehole each in its distal (BASE 4A), medial (BASE 4B), and proximal (BASE 4C) facies. The proximal part of this wedge, ca. 300 m thick, is well exposed as a prominent ridge in grasslands southwest of SAPPI plantations; the medial (ca. 150 m thick) and distal (ca. 12 m thick) segments are poorly exposed in extensive, mature pine and eucalyptus plantations occupying the wide Lomati Valley. The region is easily accessible by the Ameide Road, a major forestry road along the valley axis. The wedge, interpreted as an estuarine delta complex and named the LDC, was studied stratigraphically, sedimentologically, and petrographically by Laura Stutenbecker for her MSc (2014); the results were published in Stutenbecker et al. (2019). Microbial mats had been mapped in the distal and proximal outcrop sections, making this site an ideal candidate for investigating microbial life in a terrestrial–marine transition zone. The microbial mats in the distal location drilled by BASE 4A are probably erroneously identified in outcrop, but microbial mats were newly documented in BASE 4B and overlying outcrop. Their occurrence in the proximal outcrops was confirmed by BASE 4C. Approximately stratigraphically midway in the wedge-shaped units, a distinct thick yellow tuff provides a sound stratigraphic marker. Sedimentary structures (mud cracks, mud-chip conglomerates, cross-bedding, mud coating on ripples, fluid-escape structures, etc.) abound in outcrop. Overlying and underlying unexposed and weathering-susceptible strata had been assumed to be shaly and to represent deep-water deposits, analogous to stratigraphically equivalent units in the Stolzburg and Eureka synclines. Preliminary assessment of the core, however, suggests that these strata represent highly tuffaceous, poorly cemented sandstones in estuarine facies. All three boreholes were drilled stratigraphically upwards (northwards to northwestwards) but physically downwards and at an angle of 45° through the overturned, ca. 70–75° southward-dipping, northward-younging strata on the >3 km thick overturned limb of the Saddleback Syncline (Heubeck and Lowe, 1994a). Drilling in the fractured, tuffaceous, medium- to coarse-grained tuffaceous sandstones was accompanied by frequent loss of circulation. As a result, drilling parameters were occasionally not optimally adjusted. Long sections of the recovered core, particularly in the friable sandstones, show densely spaced drilling-induced stress fractures.

The three boreholes at Site 4 were expected to provide firm proximal-to-distal and marine-to-terrestrial correlations through a highly dynamic but systematic stratigraphic sequence of units to address the questions of microbial life in the transition zone (exposure to the atmosphere, radiation, resilience, metabolism) and basin dynamics (subsidence, sedimentation rates, tides, currents, paleogeography).

BASE 4A (25°49′52.60″ S, 31°4′41.69″ E) was the first borehole of the BASE drilling campaign. The rig arrived on site on 15 November 2021, and the borehole spudded 2 d later and reached a total depth of 340.1 m on 26 January 2022. The true stratigraphic thickness of cored Moodies strata is approximately 230 m. The rig had to overcome several difficulties: (1) the rig crew was initially inexperienced with the rock types and the operating parameters required to obtain high-quality core in friable sandstones; (2) the thickness of the fully weathered soil zone, assumed to be minor, was ca. 62 m thick; unweathered core was not reached until 125 m depth (ca. 90 m vertical depth); and (3) the summer rainy season was particularly intense. The borehole initially penetrated a

seemingly monotonous sequence of medium-grained, tuffaceous, horizontal- and cross-bedded friable tuffaceous sandstones with thin shale coatings, carrying rare angular shale mud chips and common white tuff clasts and interbedded with numerous centimeter-thin (largely aqueously reworked) air-fall tuff beds. The distal equivalent of the LDC was encountered between 201.9 and ca. 219 m drilled depth. It is represented by a spectacular repetitive sequence of very-high-energy coarse-granule sandstone interbedded with shale–clast conglomerates and some (in-place) mud-cracked shale beds. In places (e.g., ca. 88–305 m), green shale laminae, white tuff clasts, and red jaspilite sand grains result in a colorful sandstone. Rhythmically bedded sandstone–(green) shale couplets on bedding planes and foresets are common.

BASE 4B (25°51′11.70″ S, 31°2′54.70″ E) was set up at the junction of several secondary forest roads just upslope of (and stratigraphically below) a prominent forested ridge, ca. 1670 m downdip from BASE 4C and ca. 3820 m updip from BASE 4A. Drilling started on 9 February 2022 and ended at 355.5 m depth on 23 March 2022. The true stratigraphic thickness of cored Moodies strata in the borehole is approximately 300 m. Drilling progress was good through evenly firm rock at ca. 10 to 15 m d^{-1}. The borehole started coring after leaving the zone of profound weathering at 27 m. It penetrated a lithologically similar sequence to BASE 4A. The high-energy, very-coarse-grained and mudchip-carrying units extended over ca. 150 m thickness (ca. 135–284 m), with several indications of (reworked?) microbial laminations. A highly tuffaceous unit, approximately midway in the target unit, occurred between 175 and 219 m depth. Rhythmic (tidal?) bedding was commonly encountered. The quality of the core was affected by extensive oxidative alteration and fracturing between 188 and 288 m and from 315 to 350 m depth. The reasons for this alteration at significant vertical depth are unknown; possibly, these are expressions of a wide alteration zone associated with a brittle shear zone along Lomati Valley, of vertical fractures extending to this depth, or of a hydrothermal halo surrounding a porphyritic mafic dike mapped ca. 50 m beyond the location of the end of the borehole in an unusual, approximately bedding-parallel orientation. Also, the core shows several zones of an unusual, evenly dark-grey discoloration (e.g., 151–176 m).

The drill site for **BASE 4C** (25°51′39.40″ S, 31°2′3.11″ E) was originally intended to be located in grasslands just outside (southwest of) the SAPPI plantation in order to obtain the best possible correlation with well-exposed sandstone ridges of the proximal-facies LDC; however, the site was moved a few tens of meters to the northeast to be located just within SAPPI property on recently harvested pine plantation land. This was decided to keep environmental disturbance to a minimum and to avoid the necessity of negotiations with the owner MTPA, a provincial state agency. The plantation stands on the ridge in that section had been recently harvested, so that rock exposures were excellent and ubiquitous. Drilling took place from 11 February through 22 April 2022 and reached 351.49 m depth. The true stratigraphic thickness of cored Moodies strata is approximately 295 m. The rock quality was generally good. The base of the LDC was reached at ca. 105 m; its top is gradational fining-upward and was not encountered in the core. Key correlative units are as follows: (1) base of yellow tuff, ca. 25 m thick, at ca. 172 m; (2) microbial mats, ca. 10 m thick, ca. 5 m above the top of the yellow tuff; (3) base of the mud-crack-bearing unit, ca. 10–30 m above the top of microbial mats. Concretions were recorded between 337 and 349 m.

Site BASE 5 (A, B) cored top-down a ca. 860 m thick section; this required two offset boreholes in which the bottom of BASE 5A correlated with the top of BASE 5B. It targeted a conformable deepening-upward (transgressive) sequence top in the eastern Stolzburg Syncline from a fluvial–evaporitic floodplain at the stratigraphic base to a prodelta facies at the stratigraphic top (Luber, 2014). The site was chosen to be located approximately midway between a major, obliquely crosscutting dolerite dike to the west and the tight curvature encountered in the fold hinge of the Stolzburg Syncline in the east; it also attempted to avoid mapped faults of minor offset and relied on good but weathered and intermittent surface outcrop for stratigraphic and structural control. The true stratigraphic thickness of cored Moodies strata, combined from both boreholes, is approximately 740 m. The stratigraphic base of BASE 5A overlaps the cored stratigraphic top of BASE 5B by about 20 m (cf. Fig. 28).

BASE 5A (25°54′13.97″ S, 30°50′44.83″ E) spudded on 5 April 2022 and reached its TD of 451.3 m on 18 May. It started coring at 30 m depth. Basal strata probably overlap with those at the top of BASE 5B by about 20 m and represent rhythmically bedded tuffaceous and shaly (green) fine-grained sandstones with common slump, dewatering, and load structures. This is indicative of high rates of deposition, largely below wave base (451–385 m) in a distal delta mouth bar and upper-prodelta setting. A minor sandy delta lobe was intersected between ca. 385 m (base) and 320 m (top). Lower-slope prodelta sedimentation style dominates the remaining, overlying section (ca. 320–30 m core depth). Spectacular intervals of rhythmically bedded (e.g., 180–206 m) and slumped, micro-laminated BIF, jaspilite, and shale occur between 230 and 290 m. The ferruginous section, stratigraphically known as MdI1, was significantly thicker than predicted from its surface exposure of 10 to 15 m; it correlates lithostratigraphically with a jaspilitic interval mapped as MdI1 near 180 m depth in BASE 1A, more than 31 km to the northeast. The interval 175–295 m (MdS1) probably represents the finest-grained, deepest-water, most distal facies encountered during the BASE drilling program, alongside a similarly fine-grained section in BASE 1A at 160–270 m depth. The true stratigraphic thickness of cored Moodies strata in BASE 5A was approximately 360 m.

BASE 5B (25°54′2.80″ S, 30°50′49.06″ E) started drilling on 3 June 2022 and terminated at 489.9 m depth on 17 July 2022. Coring started at 17.9 m depth. The section (base to

top) begins in tuffaceous, cross-bedded, slightly gravelly floodplain sandstones with common early-diagenetic silicified sulfate concretions (ca. 500–350 m depth), probably representing vadose-zone diagenesis of sulfate-bearing tuffaceous sediments. They contain evidence of microbial sulfate reduction ("life on land", Nabhan et al., 2016b). This zone is overlain by coarse-sandy and gravelly shoreline-facies sandstones, ca. 350 to 300 m, possibly interrupted by lagoonal sediments consisting of reworked tuffaceous (lapilli) siltstones (ca. 315–306 m). Overlying thick, green, monotonous medium-grained tuffaceous sandstones with common load structures may represent shoreline and upper delta mouth bar facies with extensive reworking, slumps, load structures, and shale-free foresets (ca. 306–100 m), gradually grading into finer-grained sandstones with some rhythmically bedded segments (150–18 m). Thin shaly jaspilites were encountered at 108 and 93 m depth, the latter reworked as chip clasts. Microbial mat sandstones were not encountered in either core. The section is generally rich in tuffaceous material. The true stratigraphic thickness of cored Moodies strata was approximately 400 m.

7.3 The tunnel sections

Three tunnels which traverse relevant Moodies strata in the central BGB at approximately right angles to strike were made accessible for sampling. They were (1) the Lomati water tunnel below Saddleback Hill of the Saddleback Syncline, ca. 2 km south of Barberton (van Wyk, 1985); and (2) the Ben Lomond (a.k.a. Princeton) and 22-level adits of Agnes Mine in the Moodies Hills Block, ca. 8 km west of Barberton. The data obtained from those tunnels add significantly to the stratigraphic extent of unweathered Moodies samples and can easily be integrated into BASE data. We include a basic description of this data set in the operational report. A more detailed description was the topic of two BSc theses completed in 2023 at the University of Jena under the supervision of Christoph Heubeck (Seifert, 2023; Bender, 2023). Visual inspection and point counting of medium-grained sandstones show that samples from all three tunnels are fresher than virtually all surface outcrop samples above the tunnels. Samples were relabeled, photographed, packed, and shipped to the Department of Geosciences, FSU Jena.

7.4 Description of BASE basic data sets

7.4.1 Data sets originating from drilling operations

Table 4 shows an example of the daily Driller's Report.

7.4.2 Data sets based on the drill core

All basic data sets generated during drilling up to the end of the second sampling workshop in March 2024 are compiled, described, and curated following ICDP conventions (operational report in Heubeck et al., 2024a; data sets in Heubeck et al., 2024b; explanatory remarks to the data sets in Heubeck et al., 2024c). The basic data sets are available at https://doi.org/10.5880/ICDP.5069.001 (Heubeck et al., 2024b). International Generic Sample Numbers (IGSNs) were assigned to all the holes, cores, sections, and samples and will be registered. After the expiry of the moratorium on 15 September 2025, 2 years after the end of the first sampling workshop, all the data sets and IGSNs will become publicly available.

Photography

BASE photographs are organized by borehole and then by core tray. All full (unslabbed) cores in their trays were photographed in wet and dry states unless the core was too crumbly. Similarly, all working halves and archive halves of the slabbed core were photographed wet and dry, with a few exceptions. Each photograph also shows a data bar at its base (Fig. 21).

At the Spandau core facility, most core trays (containing five core sections of approximately 1 m each) of BASE 5A, BASE 2A, and BASE 3A were scanned using a DMT core scanner to preserve their sedimentary textures in detail. This generated high-resolution (11 000 × 4000 px; ca. 160 MB) images, which allows 1 : 1-scale printouts of the images without pixelation.

Lithology and structures: conventions, depth, and lithologic description

Core naming conventions followed ICDP protocol (Expedition – Site-Hole – Core – Section – Split – Lithology/Facies Units/Special Geol. Features/Sample).

Expedition	Project name, expedition no.	BASE, 5069
Site	One or more boreholes in a specific area	4
Hole	Borehole number	A, B, C
Run	Drilling run number	Run with the core barrel
Core	A single piece of drill core retrieved from the run (up to 3 m length)	
Section	A row of core in a core tray or box (up to 1 m length)	
Split	A: archive half (to Pretoria) W: working half (to Berlin)	
Advance	Run start less run end (hole depths)	
Recovery	Length of core recovered in a run	
Gain/loss	Advance – recovery	
Depth	Drill hole depth below the reference base plate	

All depths represent handwritten marked depths (by the Onsite Geoscience Team) on the core, not the drillers' depths marked on the yellow or green plastic blocks. These drillers' depths usually only deviate by centimeters to several decime-

Table 4. Daily drilling report (example).

Date 10 June 2022	Borehole 1A	Report no. 14571	Operator Thabo	Contract Barberton	Bit code Grey	Rig no. MDX900	Machine LF90	Shift Day
Run number	Units	50	51	52	53	54	55	56
Core size		HQ2	HQ2	HQ2	HQ2	HQ2	HQ2	HQ2
Core barrel	m	4.00	4.00	4.00	4.00	4.00	4.00	4.00
Quill	m	6.00	6.00	6.00	6.00	6.00	6.00	6.00
No. of stands	No.	18.00	18.00	19.00	19.00	20.00	20.00	20.00
Odd	m		3.00		3.00			3.00
Unit rod length	m	6.00	6.00	6.00	6.00	6.00	6.00	6.00
$\sum$ = total stands	m	108.00	108.00	114.00	114.00	120.00	120.00	120.00
$\sum$ rod strings	m	118.00	121.00	124.00	127.00	130.00	130.00	133.00
Stick-up	m	2.45	2.45	2.45	2.45	3.25	2.45	2.45
Hole depth	m	115.55	118.55	121.55	124.55	126.75	127.55	130.55
Last depth	m	113.90	115.55	118.55	121.55	124.55	126.75	127.55
Drilling advance	m	1.65	3.00	3.00	3.00	2.20	0.80	3.00
Core recovered	m	1.30	2.35	3.05	2.87	2.20	0.80	3.00
Gain/loss	m	−0.35	−0.65	0.05	−0.13	0.00	0.00	0.00
Formation state		Broken	Broken	Solid	Solid	Solid	Solid	Solid
Core box no.	No.	21	21	21	21, 22	22, 23	23	23, 24
Risk assessment		Y	Y	Y	Y	Y	Y	Y
Remarks		Broken	Broken	Solid	Solid	Solid	Solid	Solid

ters from measured and marked core depths. We used and accepted drillers depths, however, where there was core loss or bad ground. We found that the drillers' depth and the measured depth were balanced within a few decimeters at the end of each borehole, after 280 to 498 m of drilling. Lithologic descriptions were entered into the mDIS using the predefined sets of labels described above.

7.4.3 Data sets based on downhole logging

All boreholes were geophysically surveyed (log depth, true depth, hole tilt and azimuth, axial and polar coordinates) to check for agreement with planned azimuth and inclination. We initially intended to do most geophysical logging (GR, magnetic susceptibility) on the core and thus did not log the first two boreholes BASE 4A and BASE 3A, except for surveying. We soon realized, however, that this approach was erroneous because the fractured and broken core in core trays would have made laboratory logging difficult or impossible. All subsequent boreholes (BASE 1A, BASE 2A, BASE 4B, BASE 4C, BASE 5A, BASE 5B) were therefore logged with GR, magnetic susceptibility, temperature, caliper, and a borehole acoustic televiewer (ATV) (Tables 5, 6). ATV logging provided continuous, high-resolution ultrasound images of the borehole wall for detection and characterization of fracture-network and geologic characterization. Porosity and resistivity logs were not run because they did not contribute recognizably to the objectives of the drilling campaign. The geophysical contractor, Wireline Africa, provided log data in raw and processed format.

7.4.4 Geochemical reference data set

All working halves were sampled in January and February 2023 at the BGR core repository in Berlin, Germany, to construct a combined geochemical reference data set composed of major elements, trace elements, and mineralogy using X-ray fluorescence (XRF) scanning (Spandau, Brest), XRF bulk rock fusion disk analysis (Utrecht), and X-ray diffraction (XRD) on pressed powder pellets (Paris), respectively (Table 7).

A brief description of each method follows.

1. All cores were scanned using the Avaatech core scanner at the BGR core repository in Spandau. This instrument records characteristic X-ray spectra of a ca. 1 cm^2 sized area for elemental composition. Core samples were therefore selected about 1 m apart (i.e., about one sample per core box groove or approximately five samples per tray) and sequentially arranged in the instrument tray. In regions of medium interest, scanning was done in steps of 5 to 10 cm and, in the zones of highest interest, in steps as low as 3 cm. Measurements took about 6 weeks of full-time work. Table 7 shows the chosen intervals of high, normal, and low sampling density.

2. At the same facility, core was (destructively) sampled for powdering and bulk rock geochemical analysis. Segments ca. 10 cm long were selected approximately every 5 m (i.e., approximately one sample per core box) and slabbed in half, cutting parallel to the core long axis using a core saw. The unused half of the slab (a quar-

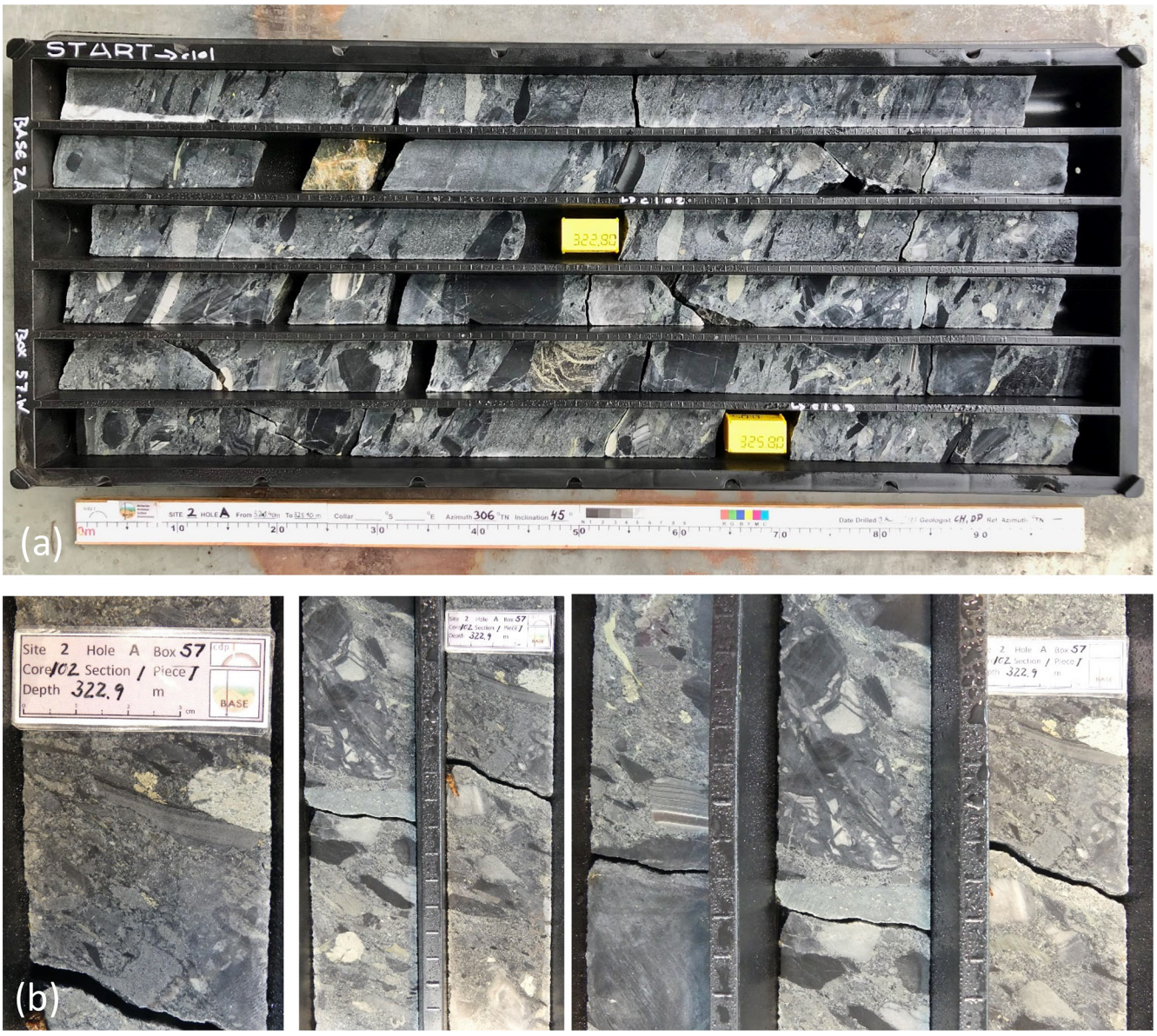

Figure 21. Examples of core photographs. **(a)** Slabbed and wet core of box 57 of borehole BASE 2A, showing ca. 2.5 m of core 101, all 3 m of core 102, and 0.4 m of core 103. The stratigraphic top is to the upper left. The data bar provides information about the depth, date, and staff. **(b)** Examples of handheld close-up photographs of the same core tray, showing textures of the cobble conglomerate and composition of individual clasts, mostly latite ("feldspar porphyries") and chert.

ter core) was returned to the core tray. Selected samples were crushed and powdered by two technicians at Brest in April 2023. Because the powders were more voluminous than anticipated, aliquots of the reference set and some remaining rock chips from the saw cut are available upon request from Stefan Lalonde (Brest) and Paul Mason (Utrecht). Amandine Migeon processed the pressed powders for high-precision whole-rock trace-element analysis by high-resolution inductively coupled plasma mass spectrometry (HR-ICP-MS).

3. Whole-rock powders were analyzed at Utrecht University for major elements by XRF. Wavelength-dispersive XRF measurements for major elements were carried out sequentially using a Thermo Scientific ARL Perform'X 4200W. Loss on ignition (LOI) was measured by thermogravimetric analysis at 1000 °C. Fusion beads were prepared using 0.6 g sample and 6 g flux consisting of 66 % lithium tetraborate, 34 % lithium metaborate, and 0.5 % lithium iodide.

Table 5. Logging tools deployed.

Borehole	Gamma ray from the three-arm caliper	Magnetic susceptibility	Borehole fluid temperature	Three-arm caliper	Borehole acoustic televiewer
	GRC	MSUS	GTMP	CC01	ATV
1A	•	•	•	•	•
2A	•	•	•	•	•
3A					
4A					
4B	•	•	•	•	•
4C	•	•	•	•	•
5A	•	•	•	•	•
5B	•	•	•	•	•

Table 6. Logging depths.

Borehole	Steel casing to (m)	Top log (m)	Logging to (m)
1A	108.44	9	496.85
2A	138.2	9	367.20
3A			280.20
4A			320.01
4B	66.60	9	355.00
4C	90.84	9	351.49
5A	107.79	9	451.00
5B	96	9	489.92

4. Stefan Lalonde wrote MATLAB code to plot large numbers of core-scan XRF data points usable for custom plots, e.g., for choosing a core interval to plot geochemical profiles as high-quality Adobe Illustrator-editable PDF files.

5. Powders were analyzed for quantitative mineralogy by X-ray diffraction at the Museum d'Histoire Naturelle in Paris in May and June 2023.

7.4.5 Borehole and wellsite documentation

Pre- and post-drill geologic cross sections

Detailed geologic maps of the regions around the drill site had provided the basis for predictive cross sections which were updated and annotated as drilling progressed. Their principal purpose was to check the progress in reaching borehole objectives by correlating the stratigraphic sequence encountered in the borehole with surface geology. Once total depth was reached, final cross sections were prepared (Figs. 22–28).

The final borehole sections generally differ from the predictive boreholes by showing (usually unexpectedly thick) weathering zones and much greater stratigraphic detail. They do not contain major inconsistencies, except at BASE 2A, where the top of the conglomerate was encountered about 30 m earlier than predicted from outcrop data. This offset was interpreted in the BASE 2A post-drill cross section by postulating a series of nearly horizontal, out-of-syncline accommodation faults, each with a minor offset. At least one such fault is well documented in roadside outcrop north of the drill site (cf. Heubeck et al., 2016; their Fig. 7).

Stratigraphic logs

The overview lithostratigraphic logs (Figs. 12–20) are based on the evaluation of core tray and close-up photographs. The scale of each log is such that the entire log occupies a single A3-sized printed page; the vertical resolution is thus approximately 2 m. Thinner units are not or only selectively represented. Because five of the eight BASE boreholes were drilled stratigraphically upwards (base to top), the depth scale increases upwards on these logs, so that the stratigraphic column can be displayed in the correct (youngest unit on top) orientation.

Hyperspectral data set

The three-camera hyperspectral scanner at the Donkerhoek National Core Storage Facility was used to image the complete core in 2023. The RGB camera provides natural color images at high spatial resolution, while the spectral cameras provide mineralogical information in the visible near-infrared (VNIR), shortwave infrared (SWIR), and longwave infrared (LWIR) electromagnetic spectra. We are currently trying to make this data set accessible from the BASE ICDP webpage.

7.4.6 Subsequent analyses

A first sampling workshop was conducted at the BGR core repository facilities in Berlin–Spandau from 11 to 14 September 2023; it was attended by 41 scientists. Ample space and favorable weather allowed us to lay out all 503 core boxes in the spacious parking lot. This made for efficient and

https://doi.org/10.5194/sd-33-129-2024

Table 7. Locations of the samples and intervals taken for the geochemical reference data set.

Borehole information			XRF scanning					Reference powders			
			High-resolution intervals (3 cm steps)		Medium-resolution intervals (8 cm steps)		Low-resolution (50 cm steps)		High-resolution sampling (ca. every 2.6 m)	Medium-resolution sampling (ca. every 6 m)	Low-resolution sampling (ca. every 14.5 m)
Borehole	Drilled depth (m)	Length analyzed (m)	Length of sections (m)	Intervals (m)	Length of sections (m)	Intervals (m)	Length of sections (m)	Total no. of samples	Intervals (m)		
1A	497	399	27	175 to 180, 404 to 426	17	387 to 404	355	37	175 to 180, 404 to 426	387 to 404	98 to 175, 180 to 387, 404 to 497
2A	368	264	21	140 to 161	39	161 to 210	204	28	140 to 161	161 to 210	104 to 140, 210 to 368
3A	280	269			35	215 to 250	234	22	–	215 to 250	11 to 215, 250 to 280
4A	340	264			8	154 to 162	256	19	–	154 to 162	76 to 154, 162 to 340
4B	355	150			7	85 to 92	143	11	–	85 to 92	50 to 85, 92 to 200
4C	350	306			24	208 to 232	282	23	–	208 to 232	44 to 208, 232 to 350
5A	451	411	117	178 to 295			294	64	178 to 295		40 to 178, 295 to 451
5B	490	460			145	300 to 445	315	46	–	300 to 445	30 to 300, 445 to 490
Total		2523	165		275		2083	250			

convenient sampling on the following days. About 1100 samples were taken. Documentation for internal use was placed on the BASE ICDP webpages. For each sample an IGSN was automatically generated in the mDIS and also printed on the sample label. All IGSNs for holes, cores, splits, and samples will be registered and publicly available after the moratorium period has ended.

8 Conclusions

The project ended slightly under budget because the education–outreach–publicity activities had been lower than estimated and because no borehole had drilled beyond 500 m. Drilling took about 9 instead of the estimated 6 months because of frequent rig breakdowns in the first 6 weeks of operations and weather-related delays during an unusually wet summer rainy season. The primary objective, to obtain a significant length of continuous and unweathered core through sections of siliciclastic sedimentary facies changes and pertaining to the surface conditions of early Earth, was fully reached. Surficial weathering reached deeper, and fracturing of the rock was higher than predicted. Initial inspection of core and logs does not show evidence of major deviations from predictions but rather confirms and clarifies several assumptions. The project had a high and lasting societal impact.

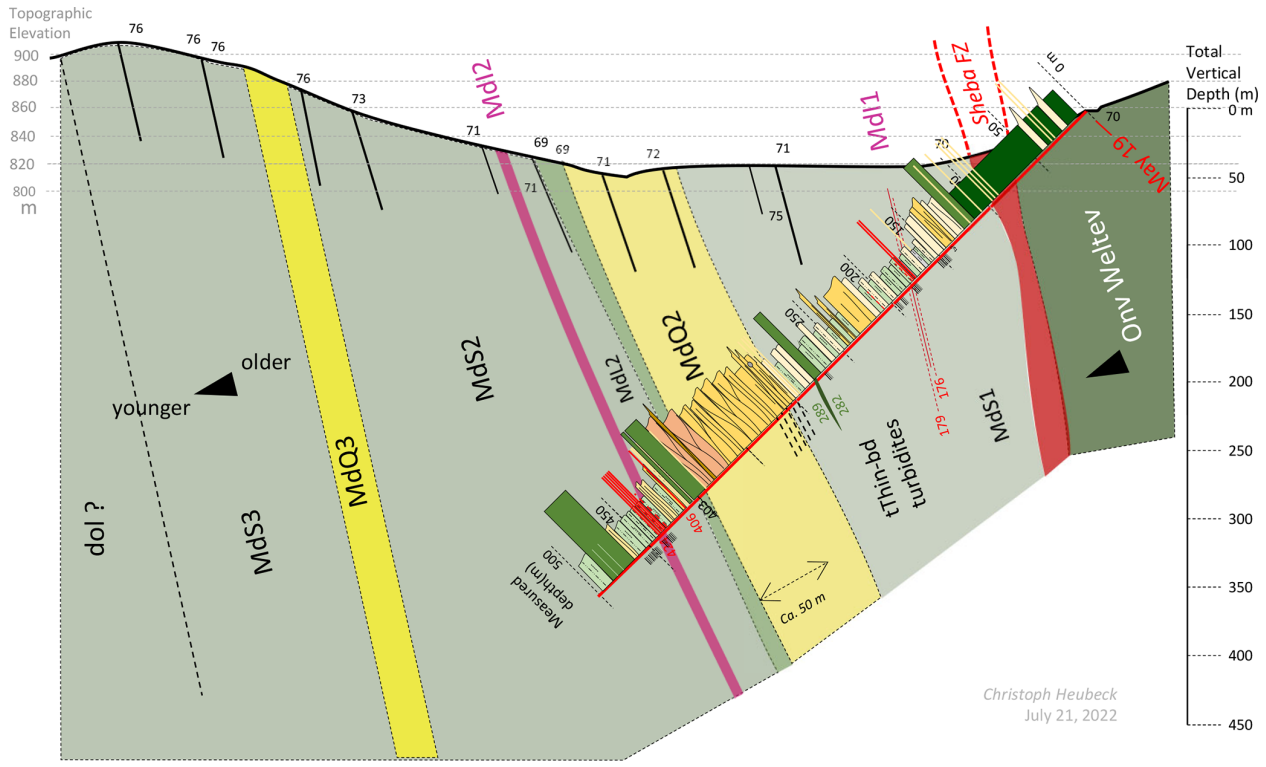

Figure 22. Post-drill geological cross section of Site 1 (Fairview Mine, Eureka Syncline).

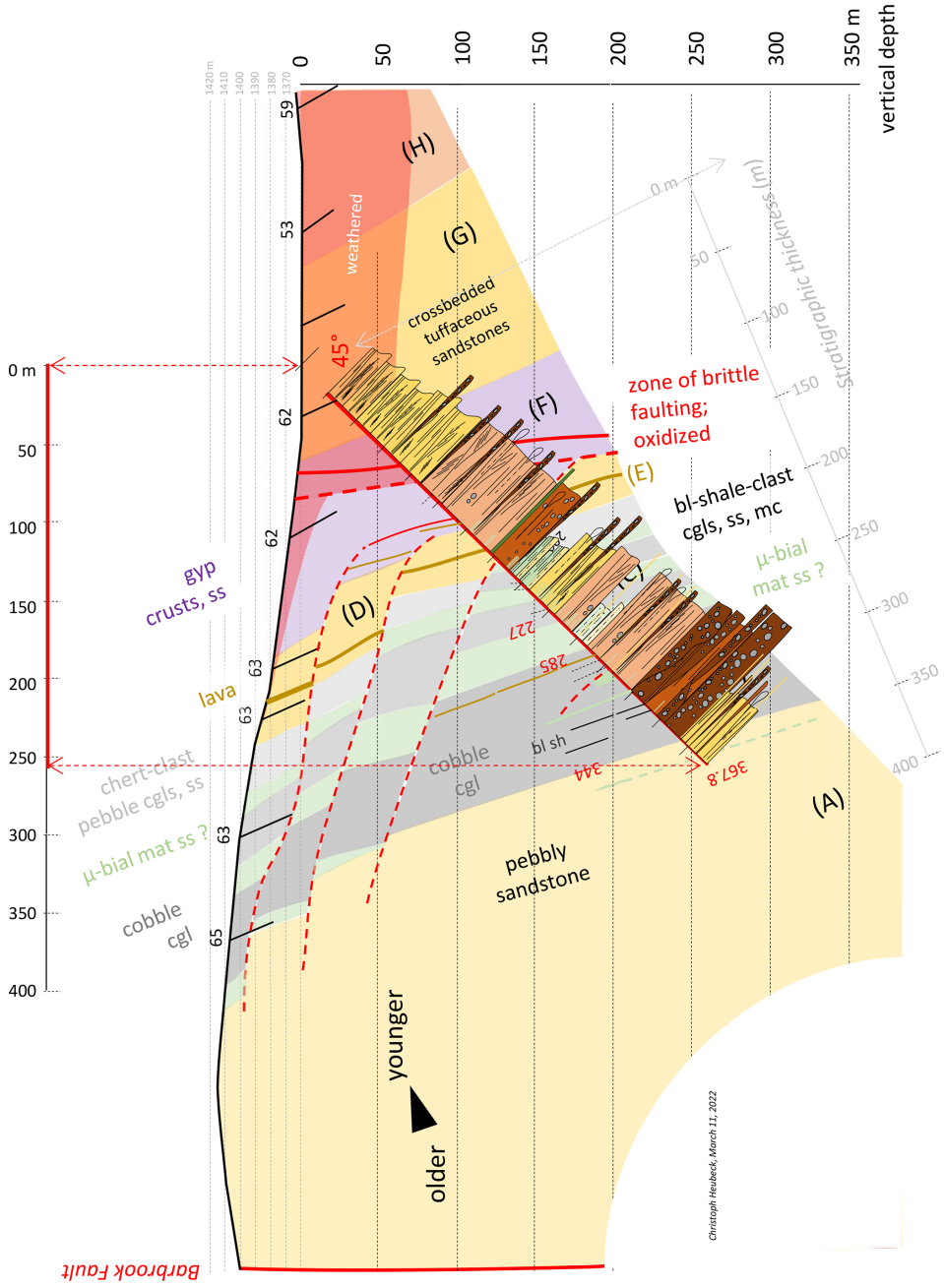

Figure 23. Post-drill geological cross section of Site 2 (Dycedale Syncline).

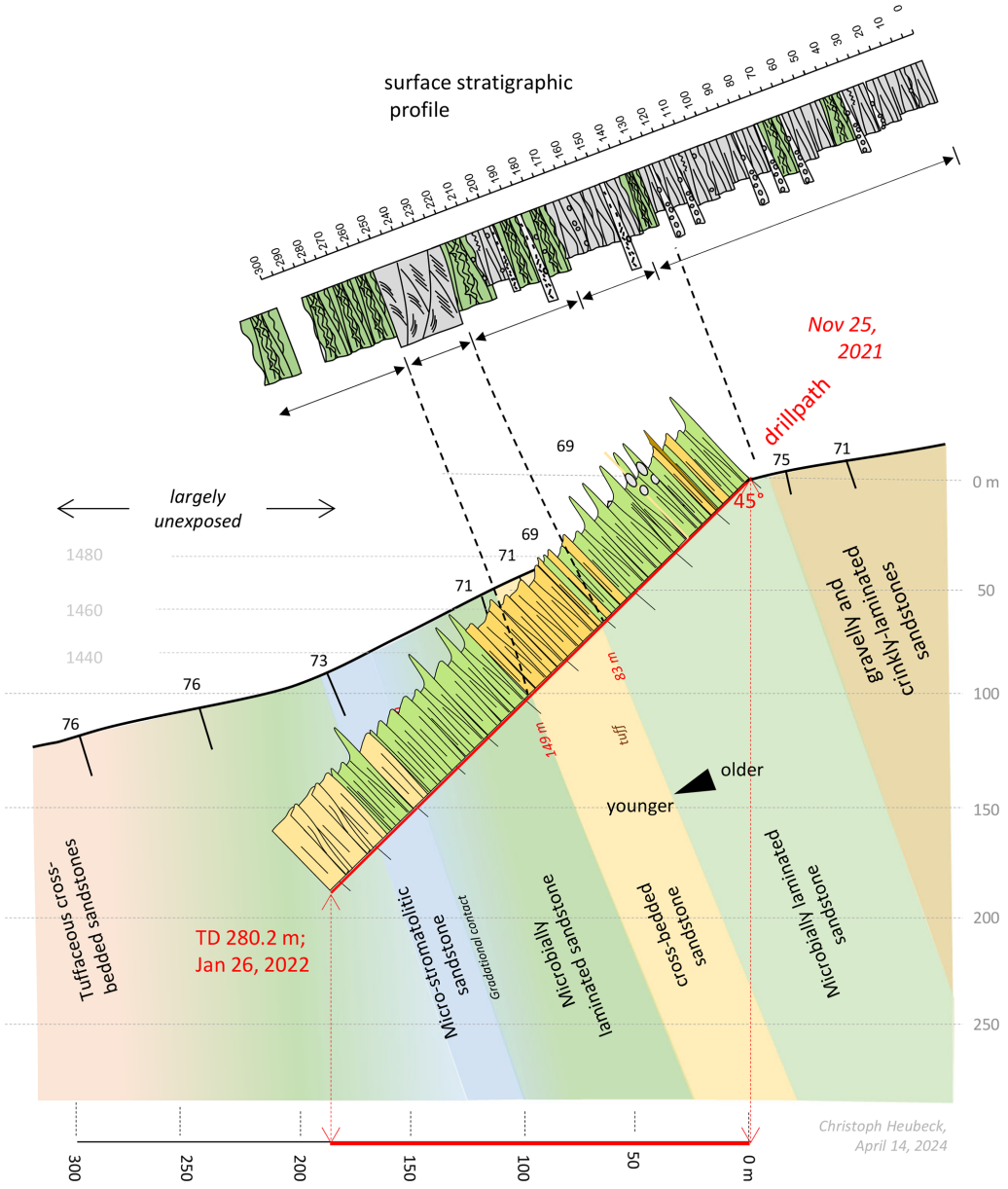

Figure 24. Post-drill geological cross section of Site 3 (MdQ1, Saddleback Syncline).

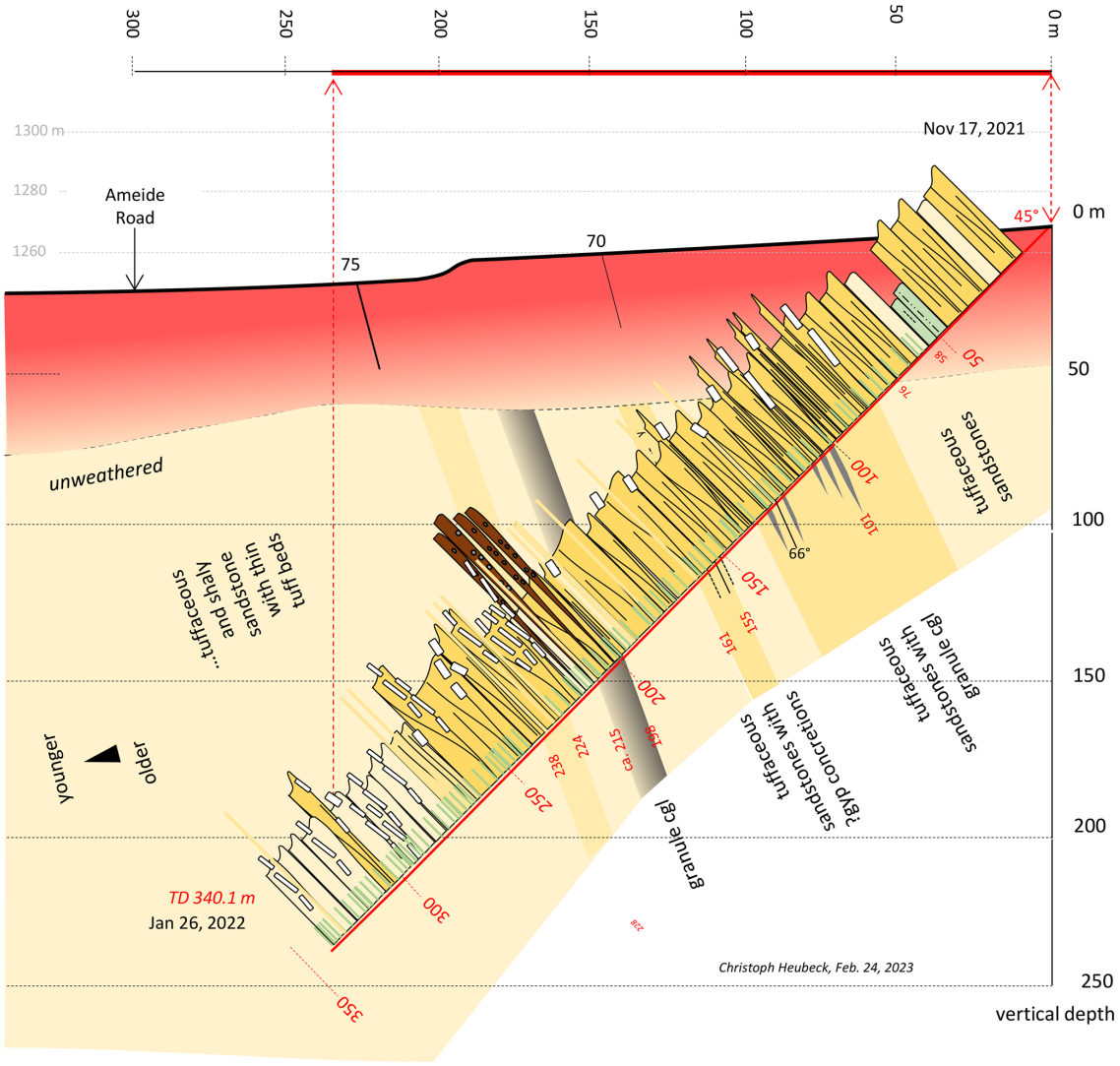

Figure 25. Post-drill geological cross section of Site 4A (distal Lomati Delta Complex, Saddleback Syncline).

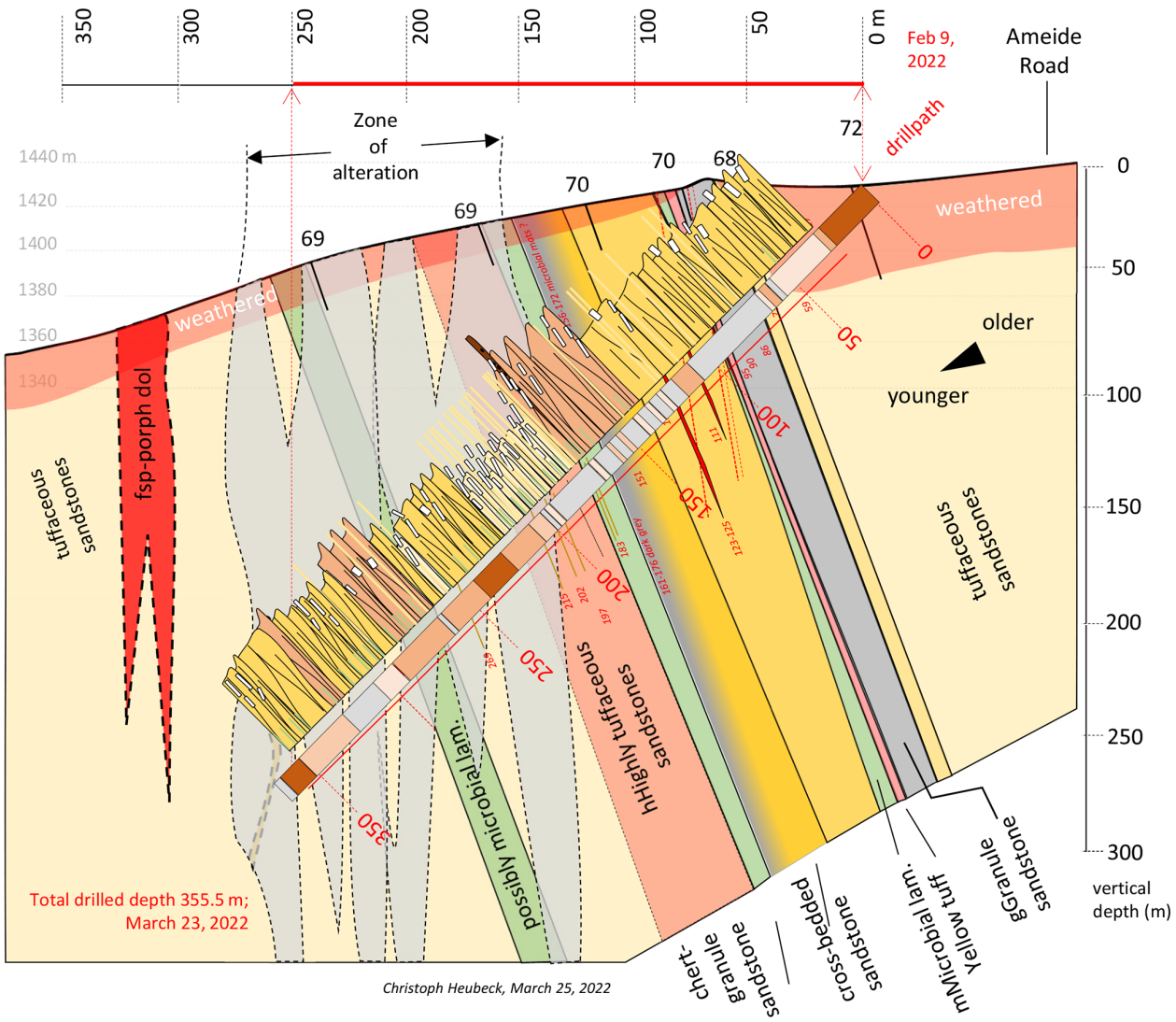

Figure 26. Post-drill geological cross section of Site 4B (medial Lomati Delta Complex, Saddleback Syncline).

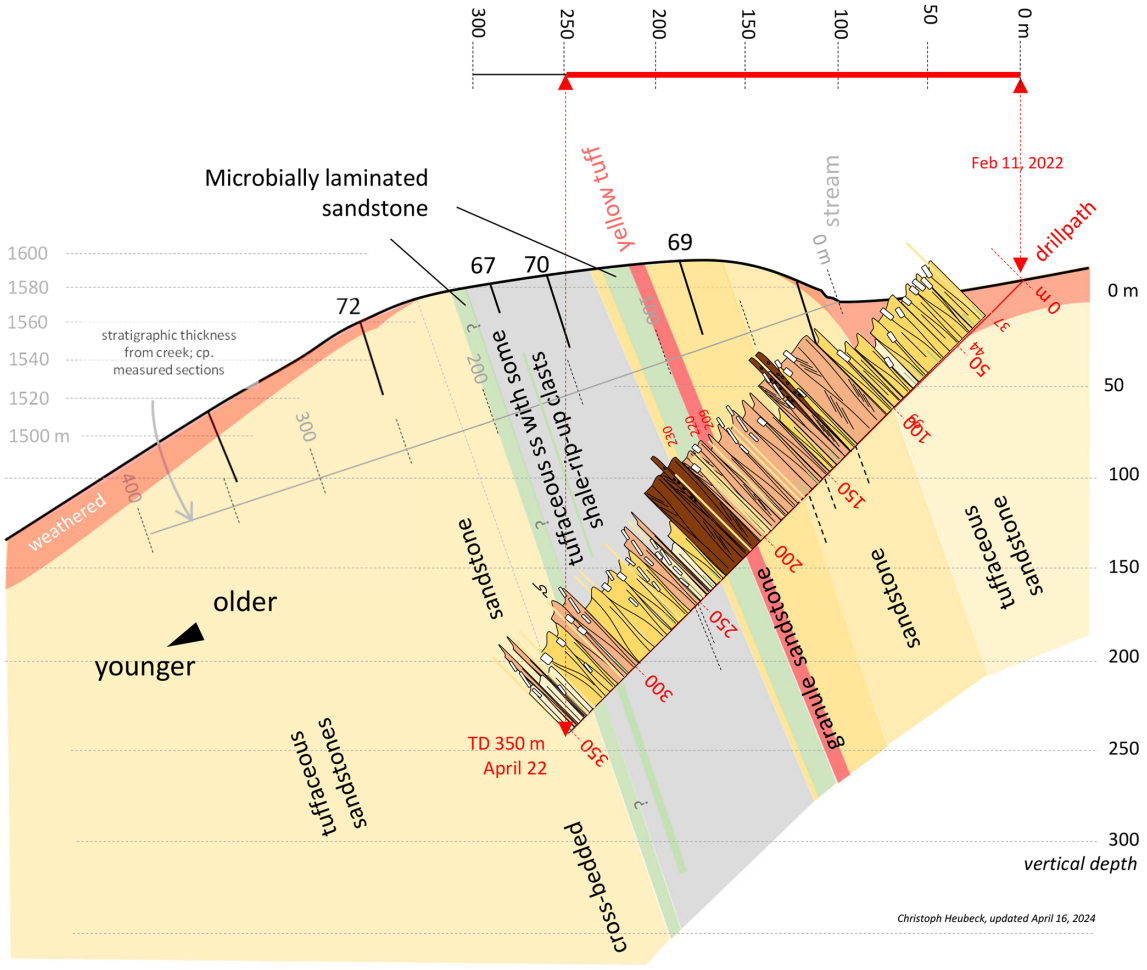

Figure 27. Post-drill geological cross section of Site 4C (proximal Lomati Delta Complex, Saddleback Syncline).

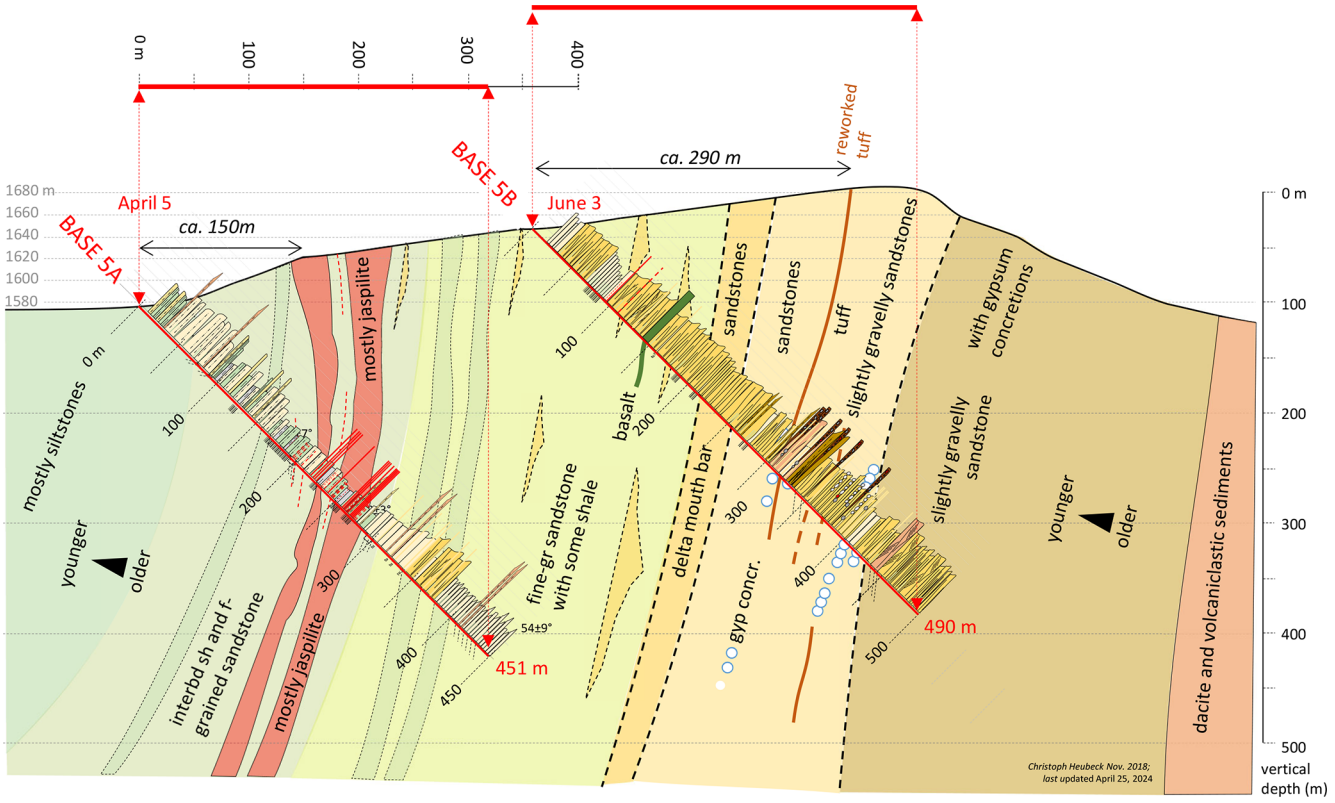

Figure 28. Post-drill geological cross section of Site 5 (eastern Stolzburg Syncline).

Appendix A: Glossary

AI	Artificial intelligence
BARB	Barberton Drilling Project
BASE	Barberton Archean Surface Environments
BGB	Barberton Greenstone Belt
BIAS	Barberton Iron and Steel
BIF	Banded-iron formation
CGS	Council for Geoscience (South Africa's national geologic survey)
CIMERA	Centre of Excellence for Integrated Mineral and Energy Resource Analysis
DSI-NRF	Department of Science and Innovation, National Research Foundation
ECO	Ecological Control Officer
EOP	Education–outreach–publicity
FSU Jena	Friedrich-Schiller-Universität Jena
GR	Gamma ray
GSSA	Geological Society of South Africa
HSE	Health, safety, and environment
ICDP	International Continental Scientific Drilling Program
IGSN	International Generic Sample Number
KLCBT	Kruger Lowveld Chamber of Business and Tourism
LDC	Lomati Delta Complex
MTPA	Mpumalanga Tourism and Parks Agency
mDIS	mobile Drilling Information System
PI	Principal investigator
ROP	Rate of penetration
SRU	Solid Removal Unit
TUT	Tshwane University of Technology
UJ	University of Johannesburg

Code and data availability. The DALL-E generative AI software, incorporated into Microsoft's Bing Internet browser (https://www.bing.com/images/create, Microsoft Inc, 2023a) or accessible through https://openai.com/index/dall-e-2/ (Microsoft Inc, 2023b), was used to generate the images of Fig. 1. This Scientific Report refers to Heubeck et al. (2024a, b, c). The data set is available at https://doi.org/10.5880/ICDP.5069.001 (Heubeck et al., 2024b).

Author contributions. The authors are either members of the BASE Science Management Board or contributed substantially to core processing during drilling operations. CH conceptualized the drilling program, supervised operations, wrote the original draft, and visualized the results. CH, NB, EJJ, TK, PaM, and MT acquired funds. MH, CH, EJJ, TK, SL, PaM, and MT contributed investigation methods and concepts. NB, CH, and AC contributed resources. NB was the project's administrative leader, assisted by PhM, CH, MdK, and AC. MdK, VN, PaM, MT, EJJ, MH, CH, and CK reviewed and edited the manuscript, and CH and CK curated and validated voluminous data. CH, PhM, DP, CR, RoT, RyT, and VN processed the core.

Competing interests. The contact author has declared that none of the authors has any competing interests.

Disclaimer. Publisher's note: Copernicus Publications remains neutral with regard to jurisdictional claims made in the text, published maps, institutional affiliations, or any other geographical representation in this paper. While Copernicus Publications makes every effort to include appropriate place names, the final responsibility lies with the authors.

Acknowledgements. We enthusiastically thank the ICDP Operations Support Group for continued help and advice through speedy advice, software and infrastructure over many years. The project would have been impossible to run without the legal, administrative, and financial guidance and activities of CIMERA (South Africa's consortium for research drilling) and its staff, led by its former chair, the late Nic Beukes. We thank the University of Johannesburg for logistic support. The Council for Geoscience, South Africa, provided in-kind support by hyperspectral imaging. The goodwill and permits by the authorities of Barberton, Mbombela Municipality, Mpumalanga Province, the WHS administration, and the local development company BATOBIC are gratefully acknowledged. Landowners, including the Mountainland Trust, SAPPI, Barberton Mines, and the Vos Brothers are thanked for allowing access to and drilling on their private land. Many members of the Barberton community, including schools, businesses, and private citizens, provided excellent and timely services, volunteered their services, and were gracious and interested hosts. We thank the drilling contractor and its team for its dedication in the face of adversity. The BIAS Hall, owned by the Mpumalanga Province Department of Arts, Sports, and Culture and administered by the Barberton Regional Museum, was a perfect location to combine core processing with outreach activities. Staff of the Barberton Community Tourism office helped and advised in many day-to-day questions. Astrid Christianson provided professional community hospitality and made sure that all of us found in Barberton a "home from home". A full list of the BASE staff is available in the operational report (Heubeck et al., 2024a).

Financial support. This research was financially supported by the ICDP (03_2019 BASE), the NASA Exobiology program (grant no. 80NSSC21K0443 to Mike M. Tice), the Deutsche Forschungsgemeinschaft (He2418/25-1 to Christoph Heubeck), the National Research Foundation of South Africa to Nic Beukes, the Japan Society for the Promotion of Science (KAKENHI grant no. 20H00184 to Tsubasa Otake and co-PIs), the Fonds National de la Recherche Scientifique (FNRS) de la Fédération Wallonie-Bruxelles, Belgium (FNRS PDR T.0137.20 to Emmanuelle Javaux), the Dutch Research Council NOW (Open Competition Domain Science – XS to Paul Mason), by Desiree Roerdink through the University of Bergen, Norway (SPIRE 2020), funding from Roger Fu through the Harvard University Origins of Life Initiative, and from Johanna Marin-Carbonne through a Université de Lausanne starting grant. A detailed listing of funding sources and amounts can be found in the Operational Report (Heubeck et al., 2024a).

Review statement. This paper was edited by Nadine Hallmann and reviewed by Gary Byerly and Brian Pratt.

References

Anhaeusser, C. R.: The geology of the Sheba Hills area of the Barberton Mountain Land, South Africa, with particular reference to the Eureka Syncline, Transactions of the Geological Society of South Africa, 79, 253–280, 1976.

Anhaeusser, C. R.: Structural elements of Archaean granite-greenstone terranes as exemplified by the Barberton Mountain Land, southern Africa, in: Precambrian Tectonics Illustrated, edited by: Kröner, A. and Greiling, R., Schweizerbart, Stuttgart, 57–78, 1984.

Anhaeusser, C. R.: Archaean greenstone belts and associated granitic rocks – A review, J. Afr. Earth Sci., 100, 684–732, 2014.

Anhaeusser, C. R., Robb, L. J., and Viljoen, M. J.: Provisional geological map of the Barberton greenstone belt and surrounding granitic terrane, eastern Transvaal and Swaziland scale 1 : 250 000, Geological Society of South Africa, https://doi.org/10.1016/j.jafrearsci.2014.07.019, 1981.

Bender, J.: Stratigraphie und Petrographie der Moodies-Gruppe in der Saddleback Synklinale, Barberton Grünsteingürtel, BSc thesis, Friedrich-Schiller-Universität Jena, 51 pp., 2023.

Bläsing, S.: Petrography and sedimentology of selected sandstones of the westernmost Dycedale Syncline, Barberton Greenstone Belt, South Africa, B.Sc.-Thesis, Freie Universität Berlin, 38 p., 2015.

Burley, A. J., Evans, R. B., Gillingham, J. M., and Masson Smith, D.: Gravity anomalies in Swaziland, Bulletin of the Geological Survey of Swaziland, 7, 4–16, 1970.

Büttner, W.: Geologische und geochemische Untersuchungen zur Genese der Msauli-Asbest-Lagerstätte, Barberton Greenstone Belt, Südafrika, PhD thesis, Universität zu Köln (Germany), 245 pp., 1983.

Daneel, G. J.: The Structural Controls of Gold Mineralization in the Moodies Hills which surround the Agnes Gold Mine, Barberton Greenstone Belt, MSc thesis, University of Natal, Durban, 129 pp., 1987.

Darracott, B. W.: The interpretation of the gravity-anomaly over the Barberton Mountain Land, South Africa, Transactions of the Geological Society of South Africa, 78, 123–128, 1975.

de Beer, J. and Stettler, E.: Geophysics and the deep structure of the Barberton Belt: a review, European Association of Geoscientists & Engineers Earthdoc online database, 11th SAGA Biennial Technical Meeting and Exhibition, Royal Swazi Spa, Ezulwini, Swaziland, 16–18 September 2009, 2–6, https://doi.org/10.3997/2214-4609-pdb.241.debeer_paper1, 2009.

de Beer, J. H., Stettler, E. H., du Plessis, J. G., and Blume, J.: The deep structure of the Barberton Greenstone Belt, S. Afr. J. Geol., 91, 184–197, 1988.

de Wit, M. J., de Ronde, C. E., Tredoux, M., Roering, C., Hart, R. J., Armstrong, R. A., Green, R. W. E., Peberdy, E., and Hart, R. A.: Formation of an Archaean continent, Nature, 357, 553–565, 1992.

Engelhardt, J. F.: Constraints from high-resolution zircon geochronology on age and provenance of the Archean Moodies Group, Barberton Greenstone Belt, South Africa, M.Sc.-Thesis, Freie Universität Berlin, 82 pp., 2012.

Eriksson, K. A.: Marginal marine depositional processes from the Archaean Moodies Group, Barberton Mountain Land, South Africa: Evidence and significance, Precambrian Res., 8, 153–182, 1979.

Eriksson, K. A., Simpson, E. L., and Mueller, W.: An unusual fluvial to tidal transition in the meso-Archaean Moodies Group, South Africa: A response to high tidal range and active tectonics, Sediment. Geol., 190, 13–24, 2006.

Eulenfeld, T. and Heubeck, C.: Constraints on Moon's orbit 3.2 billion years ago from tidal bundle data, J. Geophys. Res.-Planet., 128, e2022JE007466, https://doi.org/10.1029/2022JE007466, 2023.

Gribnitz, K. H.: Notes on the Barberton Goldfield, in: The Geology of Some Ore Deposits in Southern Africa, edited by: Haughton, S. H., vol. II, Geol. Soc., South Africa, 77–90, 1964.

Grund, M.: Stratigraphy and structural geology of the westernmost Dycedale Syncline (Moodies Group, Barberton Greenstone Belt, South Africa, B.Sc.-Thesis, Freie Universität Berlin, 33 pp., 2015.

Herget, G.: Beitrag zur Tektonik archaischer Sedimente im Barberton Bergland (Transvaal-Südafrika, Geol. Rundsch., 55, 775–786, 1966.

Hessler, A. M. and Lowe, D. R.: Weathering and sediment generation in the Archaean: An integrated study of the evolution of siliciclastic sedimentary rocks of the 3.2 Ga Moodies Group, Barberton Greenstone Belt, South Africa, Precambrian Res,, 151, 185–210, 2006.

Hessler, A. M., Lowe, D. R., Jones, R. L., and Bird, D. K.: A lower limit for atmospheric carbon dioxide levels 3.2 billion years ago, Nature, 428, 736–738, 2004.

Heubeck, C.: Geology of the Archean Moodies Group, central Barberton Greenstone Belt, South Africa, PhD thesis, Stanford University, USA, 557 pp., 1994.

Heubeck, C.: The Moodies Group – A high-resolution archive of Archaean surface and basin-forming processes, in: The Archaean Geology of the Kaapvaal Craton, Southern Africa, edited by: Kröner, A. and Hofmann, A., Springer (Regional Geology Reviews), 203–241, https://doi.org/10.1007/978-3-319-78652-0_6, 2019.

Heubeck, C.: In welchen Umgebungen und unter welchen Bedingungen entwickelte sich Leben auf der frühen Erde?, GMit (Geowissenschaftliche Mitteilungen), June 2022, 22–23, 2022.

Heubeck, C. and Lowe, D. R.: Depositional and Tectonic Setting of the Archean Moodies Group, Barberton Greenstone Belt, South Africa, Precambrian Res., 68, 257–290, 1994a.

Heubeck, C. and Lowe, D. R.: Late Syndepositional Deformation and Detachment Tectonics in the Barberton Greenstone Belt, South Africa, Tectonics, 13, 1514–1536, 1994b.

Heubeck, C., Engelhardt, J., Byerly, G. R., Zeh, A., Sell, B., Luber, T., and Lowe, D. R.: Timing of deposition and deformation of the Moodies Group (Barberton Greenstone Belt, South Africa): Very-high-resolution of Archaean surface processes, Precambrian Res., 231, 236–262, 2013.

Heubeck, C., Bläsing, S., Drabon, N., Grund, M., Homann, M., and Nabhan, S.: Geological constraints on Archean (3.22 Ga) coastal-zone processes from the Dycedale Syncline, Barberton Greenstone Belt, S. Afr. J. Geol., 119, 495–518, 2016.

Heubeck, C., Beukes, N., and the BASE Onsite Geoscience Team: ICDP research drilling in the Moodies Group of the Barberton Greenstone Belt is underway, Geol. Soc. South Africa Bulletin, March 2022, 18–21, 2022a.

Heubeck, C., Drabon, N., Byerly, G., Leisgang, I., Linnemann, U., Lowe, D. R., Merz, R., Gonzalez-Pinzon, A., Thomsen, T., Zeh, A., Rojas Agramonte, Y., and Kröner, A.: Constraints by detrital zircons on the provenance of the Archean Moodies Group, Barberton Greenstone Belt, South Africa and Eswatini, Am. J. Sci., 322, 65–107, https://doi.org/10.2475/02.2022.01, 2022b.

Heubeck, C., Reimann, S., and Homann, M.: Stromatolite-like Structures Within Microbially Laminated Sandstones of the Paleoarchean Moodies Group, Barberton Greenstone Belt, South Africa, Astrobiology, 23, 926–935, https://doi.org/10.1089/ast.2023.0014, 2023.

Heubeck, C., Beukes, N., Homann, M., Javaux, E. J., Kakegawa, T., Lalonde, S., Mason, P., Tice, M. M., Mashele, P., Paprika, D., Rippon, C., Tucker, R., Tucker, R., Ndazamo, V., Christianson, A., and Kunkel, C.: Operational Report about drilling in the Moodies Group of the Barberton Greenstone Belt, BASE – Barberton Archean Surface Environments, GFZ German Research Centre for Geoscience, https://doi.org/10.48440/ICDP.5069.001, 2024a.

Heubeck, C., Beukes, N., Homann, M., Javaux, E. J., Kakegawa, T., Lalonde, S., Mason, P., Tice, M. M., Mashele, P., Paprika, D., Rippon, C., Tucker, R., Tucker, R., Ndazamo, V., Christianson, A., and Kunkel, C.: Operational Dataset about drilling in the Moodies Group of the Barberton Greenstone Belt (BASE – Barberton Archean Surface Environments), GFZ Data Services [data set], https://doi.org/10.5880/ICDP.5069.001, 2024b.

Heubeck, C., Beukes, N., Homann, M., Javaux, E. J., Kakegawa, T., Lalonde, S., Mason, P., Tice, M. M., Mashele, P., Paprika, D., Rippon, C., Tucker, R., Tucker, R., Ndazamo, V., Christianson, A., and Kunkel, C.: Explanatory Remarks on the Operational Dataset about Drilling in the Moodies Group of the

Barberton Greenstone Belt, BASE – Barberton Archean Surface Environments, GFZ German Research Centre for Geoscience, https://doi.org/10.48440/ICDP.5069.002, 2024c.

Homann, M.: Depositional setting and metabolism of microbial mats in the Archean Moodies Group, Barberton Greenstone Belt, South Africa, Ph.D.-Thesis, Freie Universität Berlin, 105 pp., 2016.

Homann, M., Heubeck, C., Airo, A., and Tice, M. M.: Morphological adaptations of 3.22 Ga-old microbial communities to Archean coastal habitats (Moodies Group, Barberton Greenstone Belt, South Africa), Precambrian Res., 266, 47–64, 2015.

Homann, M., Heubeck, C., Bontognali, T. R. R., Bouvier, A.-S., Baumgartner, L. P., and Airo, A.: Evidence for cavity-dwelling microbial life in 3.22 Ga tidal deposits, Geology, 44, 51–54, 2016.

Homann, M., Sansjofre, P., Van Zuilen, M., Heubeck, C., Gong, J., Killingsworth, B., Foster, I. S., Airo, A., Van Kranendonk, M. J., Ader, M., and Lalonde, S. V.: Microbial life and biogeochemical cycling on land 3220 million years ago, Nat. Geosci., 11, 665–671, 2018.

Hose, L. D.: The Geology and Stratigraphic Evolution of the North-Central Part of the Barberton Greenstone Belt, South Africa, PhD thesis, Louisiana State University, 382 pp., https://doi.org/10.31390/gradschool_disstheses.4922, 1990.

Janse van Rensburg, D., Heubeck, C., and Reimann, S.: Volcanoes in the estuaries: Insights into earth's oldest (3.22 Ga) terrestrial microbial habitats, Moodies Group, Barberton Greenstone Belt, Precambrian Res., 365, 106325, https://doi.org/10.1016/j.precamres.2021.106325, 2021.

Javaux, E. J., Marshall, C. P., and Bekker, A.: Organic-walled microfossils in 3.2-billion-year-old shallow-marine siliciclastic deposits, Nature, 463, 709–840, 2010.

Kütter, S., Weckmann, U., and de Wit, M. J.: A deep electrical conductivity structure of the southern Barberton Greenstone Belt, South Africa, derived from magnetotelluric measurements, S. Afr. J. Geol., 119, 273–290, 2016.

Lippold, W.: Geological map of the upper Moodies Group, Saddleback Syncline, Barberton Greenstone Belt, South Africa, Project Report, unpublished, Freie Universität Berlin, 2011.

Lowe, D. R. and Byerly, G. R.: An overview of the geology of the Barberton Greenstone Belt and vicinity: Implications for early crustal development, in: Earth's Oldest Rocks, edited by: van Kranendonk, M. J., Smithies, R. H., and Bennett, V. H., Elsevier, Developments in Precambrian Geology, 15, 481–526, https://doi.org/10.1016/s0166-2635(07)15053-2, 2007.

Lowe, D. R., Byerly, G. R., and Heubeck, C.: Structural divisions and development of the west-central part of the Barberton Greenstone Belt, in: Geologic Evolution of the Barberton Greenstone Belt, South Africa, edited by: Lowe, D. R. and Byerly, G. R., Geological Society of America Special Paper, 329, 37–82, https://doi.org/10.1130/0-8137-2329-9.37, 1999.

Lowe, D. R., Byerly, G. R., and Heubeck, C.: Geologic map of the west-central Barberton Greenstone Belt, South Africa, scale 1 : 25 000, Geological Society of America, Map and Chart Series, No. 103, 2012.

Luber, T.: Archaean Geology of the east-central Stolzburg Syncline, Barberton Greenstone Belt, South Africa, MSc thesis, Freie Universität Berlin, 2014.

MacAlauy, D.: Lithologic-structural sketch drawings of the Lomati Water tunnel walls, unpublished, Scanned, obtainable through C. Heubeck, 1987.

Microsoft Inc: Bing Internet Web browser, https://www.bing.com/images/create, last access: 23 November 2023a.

Microsoft Inc: DALL·E 2, https://openai.com/index/dall-e-2, last access: 23 November 2023b.

Nabhan, S., Wiedenbeck, M., Milke, R., and Heubeck, C.: Biogenic overgrowth on detrital pyrite in 3.2 Ga Archean paleosols, Geology, 44, 763–766, 2016a.

Nabhan, S., Luber, T., Scheffler, F., and Heubeck, C.: Climatic and geochemical implications of Archean pedogenic gypsum in the Moodies Group (∼ 3.2 Ga), Barberton Greenstone Belt, South Africa, Precambrian Res., 275, 119–134, 2016b.

Nakajima, R., Ohmoto, Y., Otake, T., Kakegawa, T., and Sato, T.: Biosignatures recorded in geochemical correlations between organic matter and Fe-bearing minerals in 3.2 Ga banded iron formations, Barberton Greenstone Belt, South Africa, Goldschmidt Conference 2016, 26 June–1 July, 2016 Geochemical Society (GS) and the European Association of Geochemistry (EAG), Yokohama, Japan, Abstract Volume, 2217, 2016.

Noffke, N., Eriksson, K. A., Hazen, R. M., and Simpson, E. L.: A new window into Early Archaean life: Microbial mats in Earth's oldest siliciclastic tidal deposits (3.2 Ga Moodies Group, South Africa), Geology, 34, 253–256, 2006.

Nwaila, G. and Frimmel, H.: Highly siderophile elements in Archaean and Palaeoproterozoic marine shales of the Kaapvaal Craton, South Africa, Miner. Petrol., 113, 307–327, https://doi.org/10.1007/s00710-018-0650-3, 2019.

Ohnemüller, F.: Implications of below-wavebase sedimentation in the Moodies Group, Barberton Greenstone Belt, South Africa, M.Sc.-Thesis (unpublished), Freie Universität Berlin, 2010.

Paris, I. A.: The geology of the farms Josefsdal, Dunbar and part of Diepgezet in the Barberton greenstone belt, PhD thesis, University of the Witwatersrand, Johannesburg, 258 pp., 1984.

Reimann, S., Heubeck, C., Janse van Rensburg, D. J., Fugmann, P., Serre, S. H., Thomsen, T. B., and Zametzer, A.: Syndepositional hydrothermalism selectively preserves records of one of the earliest benthic ecosystems, Moodies Group (3.22 Ga), Barberton Greenstone Belt, South Africa, S. Afr. J. Geol., 124, 253–278, 2021.

Seifert, F.: Oberflächen- zu Untertagekorrelation der archaischen Moodies-Gruppe, Moodies Hills Block, Barberton Grünsteingürtel, BSc thesis, Friedrich-Schiller-Universität Jena, 26 pp., 2023.

Simpson, E. L., Eriksson, K. A., and Mueller, W.: 3.2 Ga eolian deposits from the Moodies Group, Barberton Greenstone Belt, South Africa: Implications for the origin of first-cycle quartz sandstones, Precambrian Res., 214/215, 185–191, 2012.

Stutenbecker, L.: Sedimentology, petrography and provenance of the "Lomati Quartzite": Implications for syntectonic Moodies Group sedimentation, Barberton Greenstone Belt, South Africa, MSc thesis, Freie Universität Berlin, 70 pp., 2014.

Stutenbecker, L., Heubeck, C., and Zeh, A.: The Lomati Delta Complex: A prograding tidal delta in the Archean Moodies Group, Barberton Greenstone Belt, S. Afr. J. Geol., 122, 17–38, https://doi.org/10.25131/sajg.122.0002, 2019.

Tice, M. M., Bostick, B. C., and Lowe, D. R.: Thermal history of the 3.5–3.2 Ga Onverwacht and Fig Tree Groups, Barberton green-

stone belt, South Africa, inferred by Raman microspectroscopy of carbonaceous material, Geology, 32, 37–40, 2004.

Toulkeridis, T., Goldstein, S. L., Clauer, N., Kröner, A., Todt, W., and Schidlowski, M.: Sm–Nd, Rb–Sr and Pb–Pb dating of silicic carbonates from the early Archaean Barberton Greenstone Belt, South Africa: Evidence for post-depositional isotopic resetting at low temperature, Precambrian Res., 92, 129–144, 1998.

Toulkeridis, T., Clauer, N., Kröner, A., and Todt, W.: A Mineralogical, Chemical and Isotopic Investigation of Shales from the Barberton Greenstone Belt, South Africa, To Constrain Source Materials and Post-Deposition Evolution, S. Afr. J. Geol., 118, 389–410, 2015.

van Wyk, B. C.: Lomati Tunnel. Geotechnical investigation for the Barberton Town Council, Volume 1: Report; cross sections, unpublished, 86 pp., 1985.

Viljoen, M. J.: The geology of the Lily Syncline and portion of the Eureka Syncline between the Consort Mine and Joe's Luck Siding, Barberton Mountain Land, MSc thesis, University of the Witwatersrand, Johannesburg, South Africa, 1963.

Viljoen, M. J. and Viljoen, R. P.: An introduction to the geology of the Barberton granite-greenstone terrain, Special Publication, Geological Society of South Africa, 2, 9–28, 1969a.

Viljoen, M. J. and Viljoen, R. P.: The geology and geochemistry of the lower ultramafic unit of the Onverwacht Group and a proposed new class of igneous rocks, Special Publication, Geological Society of South Africa, 2, 55–85, 1969b.

Viljoen, R. P. and Viljoen, M. J.: The geological and geochemical significance of the upper formations of the Onverwacht Group, Special Publication, Geological Society of South Africa, 2, 113–151, 1969c.

Sci. Dril., 33, 173–190, 2024
https://doi.org/10.5194/sd-33-173-2024

Scientific Drilling
Open Access

A strainmeter array as the fulcrum of novel observatory sites along the Alto Tiberina Near Fault Observatory

Lauro Chiaraluce[1], Richard Bennett[2], David Mencin[3], Wade Johnson[3], Massimiliano Rinaldo Barchi[4], Marco Bohnhoff[5], Paola Baccheschi[1], Antonio Caracausi[6], Carlo Calamita[7], Adriano Cavaliere[8], Adriano Gualandi[1], Eugenio Mandler[8], Maria Teresa Mariucci[1], Leonardo Martelli[8], Simone Marzorati[7], Paola Montone[1], Debora Pantaleo[7], Stefano Pucci[1], Enrico Serpelloni[8], Mariano Supino[1], Salvatore Stramondo[1], Catherine Hanagan[2,3], Liz Van Boskirk[3], Mike Gottlieb[3], Glen Mattioli[3,4], Marco Urbani[4], Francesco Mirabella[4], Assel Akimbekova[4], Simona Pierdominici[5], Thomas Wiersberg[5], Chris Marone[9], Luca Palmieri[10], and Luca Schenato[10]

[1]Istituto Nazionale di Geofisica e Vulcanologia INGV, Rome, Italy
[2]Department of Geosciences, University of Arizona UA, Tucson, Arizona, USA
[3]EarthScope Consortium, Boulder, Colorado, USA
[4]Dipartimento di Fisica e Geologia, Università degli Studi di Perugia, Perugia, Italy
[5]Geomechanics & Scientific Drilling, GFZ German Research Centre for Geosciences, Telegrafenberg, 14473 Potsdam, Germany
[6]Istituto Nazionale di Geofisica e Vulcanologia INGV, Palermo, Italy
[7]Istituto Nazionale di Geofisica e Vulcanologia INGV, Ancona, Italy
[8]Istituto Nazionale di Geofisica e Vulcanologia INGV, Bologna, Italy
[9]Dipartimento di Scienze della Terra, La Sapienza, Università degli Studi Roma, Rome, Italy
[10]Dipartimento di Ingegneria dell'informazione, Università degli Studi di Padova, Padova, Italy

Correspondence: Mariano Supino (mariano.supino@ingv.it)

Received: 14 November 2023 – Revised: 15 March 2024 – Accepted: 23 April 2024 – Published: 24 June 2024

Abstract. Fault slip is a complex natural phenomenon involving multiple spatiotemporal scales from seconds to days to weeks. To understand the physical and chemical processes responsible for the full fault slip spectrum, a multidisciplinary approach is highly recommended. The Near Fault Observatories (NFOs) aim at providing high-precision and spatiotemporally dense multidisciplinary near-fault data, enabling the generation of new original observations and innovative scientific products.

The Alto Tiberina Near Fault Observatory is a permanent monitoring infrastructure established around the Alto Tiberina fault (ATF), a 60 km long low-angle normal fault (mean dip 20°), located along a sector of the Northern Apennines (central Italy) undergoing an extension at a rate of about 3 mm yr^{-1}. The presence of repeating earthquakes on the ATF and a steep gradient in crustal velocities measured across the ATF by GNSS stations suggest large and deep (5–12 km) portions of the ATF undergoing aseismic creep.

Both laboratory and theoretical studies indicate that any given patch of a fault can creep, nucleate slow earthquakes, and host large earthquakes, as also documented in nature for certain ruptures (e.g., Iquique in 2014, Tōhoku in 2011, and Parkfield in 2004). Nonetheless, how a fault patch switches from one mode of slip to another, as well as the interaction between creep, slow slip, and regular earthquakes, is still poorly documented by near-field observation.

With the strainmeter array along the Alto Tiberina fault system (STAR) project, we build a series of six geophysical observatory sites consisting of 80–160 m deep vertical boreholes instrumented with strainmeters and seismometers as well as meteorological and GNSS antennas and additional seismometers at the surface.

By covering the portions of the ATF that exhibits repeated earthquakes at shallow depth (above 4 km) with these new observatory sites, we aim to collect unique open-access data to answer fundamental questions about the relationship between creep, slow slip, dynamic earthquake rupture, and tectonic faulting.

Published by Copernicus Publications on behalf of the IODP and the ICDP.

1 Introduction

1.1 TABOO NFO – the infrastructure

The Alto Tiberina Near Fault Observatory (TABOO NFO; Chiaraluce et al., 2014; Caracausi et al., 2023) is a state-of-the-art geophysical network, managed by the Istituto Nazionale di Geofisica e Vulcanologia (INGV), composed of modern seismological, geodetic, and geochemical stations placed along an extending sector of the Northern Apennines of Italy containing fault systems recently activated by a series of moderate magnitude earthquakes ($5 < M_w < 6.5$; Fig. 1).

The fault system monitored by TABOO NFO is dominated at depth by the Alto Tiberina fault (ATF), an east-dipping low-angle normal fault (mean dip 20°; see the topmost section in Fig. 1), which, if activated along its entire surface (60×40 km, reaching 15 km of depth), could generate an earthquake of magnitude up to 7. It is worth noting that such an event is not present in the Italian catalog of historical earthquakes for that portion of the Northern Apennines, and this range of magnitude can be considered complete for the past 900 years (Visini et al., 2022).

Along the ATF, in the last 40 years, in terms of instrumental earthquakes, we have only recorded events smaller than M_w 3, occurring at a high and almost continuous rate (Chiaraluce et al., 2007; Valoroso et al., 2017; Cattaneo et al., 2017; Vuan et al., 2020), whilst on its hanging wall, along shallower and minor syn- and antithetic splays dipping at higher angle (up to 45–60°), we detect seismic sequences with mainshocks reaching up to M_w 4.5.

With a mean inter-distance of about 8 km between the sites (Fig. 2), starting from 2010, TABOO's multidisciplinary sensors deployed both at the surface and within shallow boreholes (< 250 m) collect near-fault data to capture a very broad range of signatures related to tectonic deformation processes. All TABOO NFO's seismic, geodetic, and geochemical sensors record and transmit in real time, via dedicated Wi-Fi technology. Seismic and geodetic raw data are discoverable and accessible in standard formats on dedicated repositories (e.g., https://eida.ingv.it/it/, last access: 17 June 2024, and https://gnssdata-epos.oca.eu/#/site, last access: 17 June 2024), while meteorological and geochemical data (Rn, CO_2) and all the derived multidisciplinary scientific products are discoverable on open-access thematic portals and accessible via dedicated web services on thematic portals (http://fridge.ingv.it, last access: 17 June 2024, and https://www.epos-eu.org/dataportal, last access: 17 June 2024).

1.2 ATF system and STAR project

Consistent with the existing TABOO NFO geodetic data (Vadacca et al., 2016), the interpretation of the seismic reflection profiles provided by the CROP03-NVR survey (Crosta Profonda Project Near Vertical Reflection; Pialli et al., 1998; Pauselli et al., 2006) shows that a significant amount of Neogene–Quaternary extension within the Northern Apennines brittle upper crust is accommodated by a system of east-dipping LANFs (low-angle normal fault) with associated high-angle antithetic structures. The ATF is the most easterly and most recently formed among the LANFs contributing to the distributed faulting responsible for a significant portion of the documented tectonic extension within the Apennines belt. A long-term aseismic slip rate of 1.7 mm yr^{-1} is reported by geodetic data, contributing to the total amount of 3 mm yr^{-1} of extension ongoing in this sector of the Apennines (Anderlini et al., 2016).

Existing data from TABOO NFO support the hypothesis that portions of the ATF creep aseismically.

Seismicity data reveal microseismic release at a consistently high rate occurring along the ATF plane, including repeating earthquakes (REs; Valoroso et al., 2017; Vuan et al., 2020). A steep gradient in crustal velocities measured by GNSS (Vadacca et al., 2016) and interpreted as the signature of creeping occurring below 5 km of depth along the ATF plane and transient motion detected by GPS arrays lasting for a few months and coinciding with seismic swarms (Gualandi et al., 2017).

Recent studies document that any given patch of a fault can creep, nucleate slow earthquakes, and host large earthquakes (e.g., Iquique earthquake, Ruiz et al., 2014; Tōhoku earthquake, Kato et al., 2012; and Parkfield earthquake, Veedu and Barbot, 2016). The hypothesis that a fault patch would switch from one sliding mode to another is contrary to ordinary theory. Thus, these observations are forcing a revolution in our way of thinking about how faults accommodate slip. However, the interaction between creep, slow, and regular earthquakes is still poorly documented by observation.

With STAR (strainmeter array along the Alto Tiberina fault system; https://www.icdp-online.org/projects/by-continent/europe/star-italy, last access: 17 June 2024), a project co-founded by ICDP, NSF-US, and INGV, we aim to collect the data required to address these topics. By installing a set of six strainmeters that will be part of the existing TABOO NFO infrastructure, STAR will provide unique open-access data to answer fundamental questions about the relationship between creep, slow slip, dynamic earthquake rupture, and tectonic faulting. The strainmeter array (STAR) instruments can resolve the full horizontal strain tensor for deformation on the order of the nano-strain, with temporal sampling (> 20 Hz) shorter than timescales typically explored by GNSS. TABOO NFO instrumentation will thus resolve the spatiotemporal pattern of slip on the ATF with sufficient resolution on timescales (minutes to days to months) that appear to characterize transient aseismic slip worldwide. Our goal is to obtain high-resolution observations of deformation processes to better understand

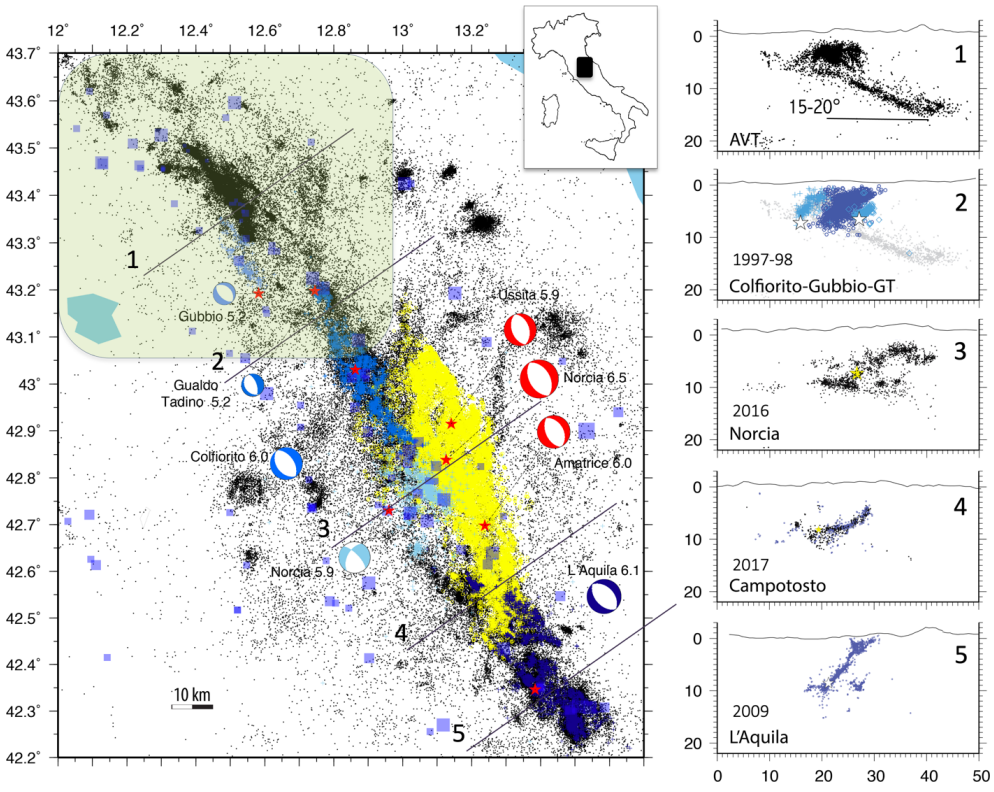

Figure 1. Map of the sector of the Northern Apennines, currently extending at about 3 mm yr^{-1} in the NE-trending direction. The southern portion was hit both recently and in historical times (light-blue squares represent historical earthquakes from CPTI15; Rovida et al., 2022) by a series of moderate magnitude earthquakes. From south to north, the seismic sequences are L'Aquila, 2009 (dark blue); the most recent 2016–2017 central Italy sequence (yellow); Norcia, 1979 (celestine); Colfiorito, 1997, and Gualdo Tadino, 1998 (blue); and Gubbio, 1984 (light blue). These sequences activated a 150 km long extensional fault system over the last 25 years. The TABOO study area is located north in the region highlighted in green where, differently from the southern area, we have no large historical earthquakes and a continuous release of microearthquakes with no events larger than M 4, occurring along an east-dipping fault at a very low angle (15–20°). This large and misoriented fault continuously generates microearthquakes along a structure dipping in the opposite direction relative to all the other segments activated during the large seismic sequences (see cross-sections).

the physical processes that enable both seismic and aseismic slip on a single fault patch, with potentially revolutionary implications for seismic hazard and risk assessment. Moreover, given the very local scale of our observatory network, we may bridge the gap between laboratory and natural-scale observations. Each observatory site is also equipped with surface GNSS, meteorological instruments, and additional seismic sensors. Moreover, the two deepest boreholes host fiber-optic cables for temperature and strain. Four out of six holes host pressure transducers to correct the strainmeter data.

An additional motivation for STAR is the presence in the ATF system volume of deep fluid circulation. The observed flux of natural CO_2 in central Italy, where the ATF is located, is comparable to that from worldwide active volcanic systems, making the ATF an ideal site for studying the relationship between fluids that move from the whole crust towards the atmosphere (e.g., Italiano et al., 2009), seismicity pattern, strain, and faulting. The existence of fluid transport processes is supported, as already highlighted, by the evidence that within deep boreholes drilled in this area and located in the ATF footwall (Pieve Santo Stefano 1 and San Donato 1; Fig. 2), fluid overpressure (CO_2) at about 85 % of lithostatic load has been encountered. In addition, the isotopic signature of fluids emitted in many local springs with gaseous emissions indicates that the whole area is affected by an extremely large flux of CO_2 from a deep source (e.g., Rogie et al., 2000; Chiodini et al., 2004; Italiano et al., 2009). The over-pressurization from below by deep derived CO_2 is proposed as being one of the primary triggering mechanisms of the Apennines earthquakes (Chiodini et al., 2004). That is why TABOO hosts four Rn and four CO_2 geochemical stations (Caracausi et al., 2023) that measure the output of these volatiles at high frequency and monitoring the high flux of CO_2 gas emissions at low frequency in order to investigate the sources of fluids (mantle vs. crust) and how secondary processes (e.g., rock–water–gas interaction) during the trans-

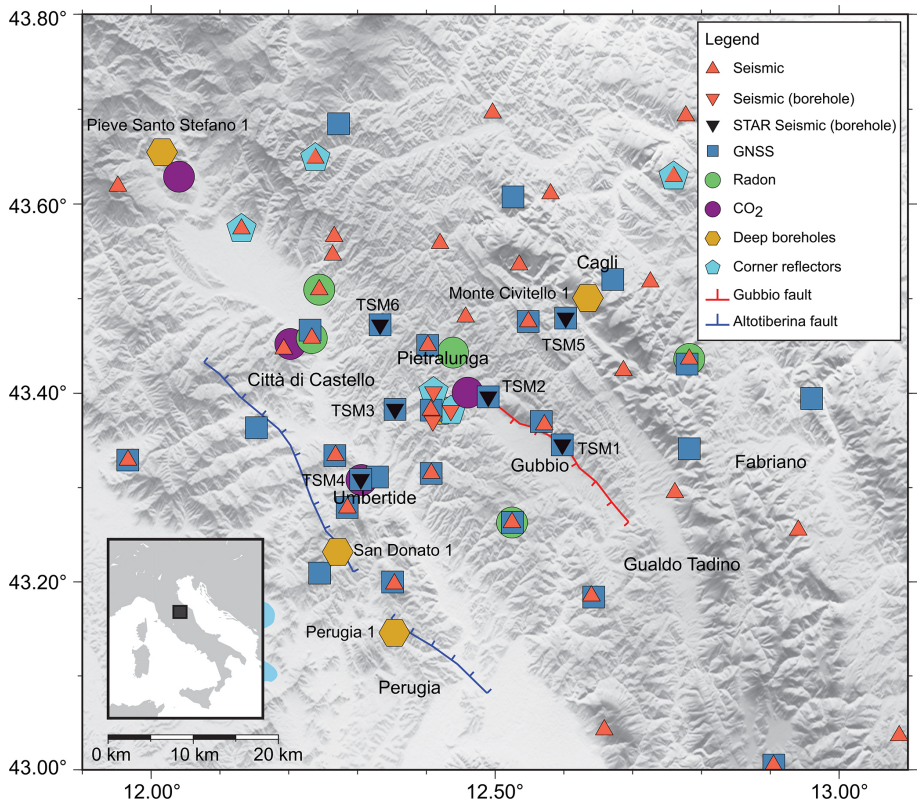

Figure 2. Map of TABOO NFO infrastructure and station distribution with respect to the ATF (blue line) and Gubbio fault (red line). Orange triangles are seismic stations deployed at the surface and within shallow boreholes. Blue squares and turquoise pentagons are GNSS stations and corner reflectors, respectively. Green and purple circles are, respectively, Rn and CO_2 monitoring sites, while the kilometer-deep boreholes are reported with yellow hexagons. The six observatory sites (STAR project, TSM1 to TSM6) are instead represented as black upside-down triangles. Figure generated with GMT (Generic Mapping Tools).

port and storage of the fluids within the crust can modify the chemistry of the fluids (Ventura Bordenca, 2020).

Thus, with the new observatory sites, TABOO NFO will acquire novel high-precision data, allowing for a quantitative characterization of ATF creep (~ 1 mm over < 1 km), enhanced monitoring of microseismicity (below M_c 0.5), and investigation of possible correlation between degassing (CO_2, Rn) measurements and subsurface deformation. Such unique near-fault data may illuminate the spatiotemporal characteristics of creep on the ATF, permitting detailed analysis of potential stress interactions with the overlying hanging wall faults known to host larger earthquakes. The interdisciplinary observations are needed to address key questions of global importance in the seismic hazards and risk assessment community about the physics that allows for both seismic and aseismic slip on a single fault patch.

After presenting the field campaigns, we give an overview of the new strainmeter and seismometer data, showing how they enable us to detect dynamic and static strain otherwise missed by other existing in situ instruments.

2 STAR field campaign

2.1 Site selection

The six boreholes of the STAR project (Fig. 2) were drilled in northern Umbria, in an area between the High Tiber Valley, bordered by the east-dipping ATF, and the western flank of the main ridge of the Umbria-Marche Apennines, a NE-verging, arc-shaped foreland fold-and-thrust belt, representing the eastern part of the Northern Apennines of Italy (Fig. 3a; Barchi, 2010).

The NNW–SSE-trending compressional structures (folds and thrusts) of this region were formed in the Late Miocene (Tortonian–Messinian age) and involve a Jurassic–Paleogene carbonate succession (Umbria-Marche succession; e.g., Cresta et al., 1989), deposited on the southern (African) margin of the Western Tethys, overlain by a thick succession of Neogene turbidites, marls, and sandstones, deposed in the foreland ramp and in the foredeep of the syntectonic, foreland basin of the Northern Apennines. The compressional structures are cut and displaced by later (Late Pliocene–Quaternary) normal faults, responsible for

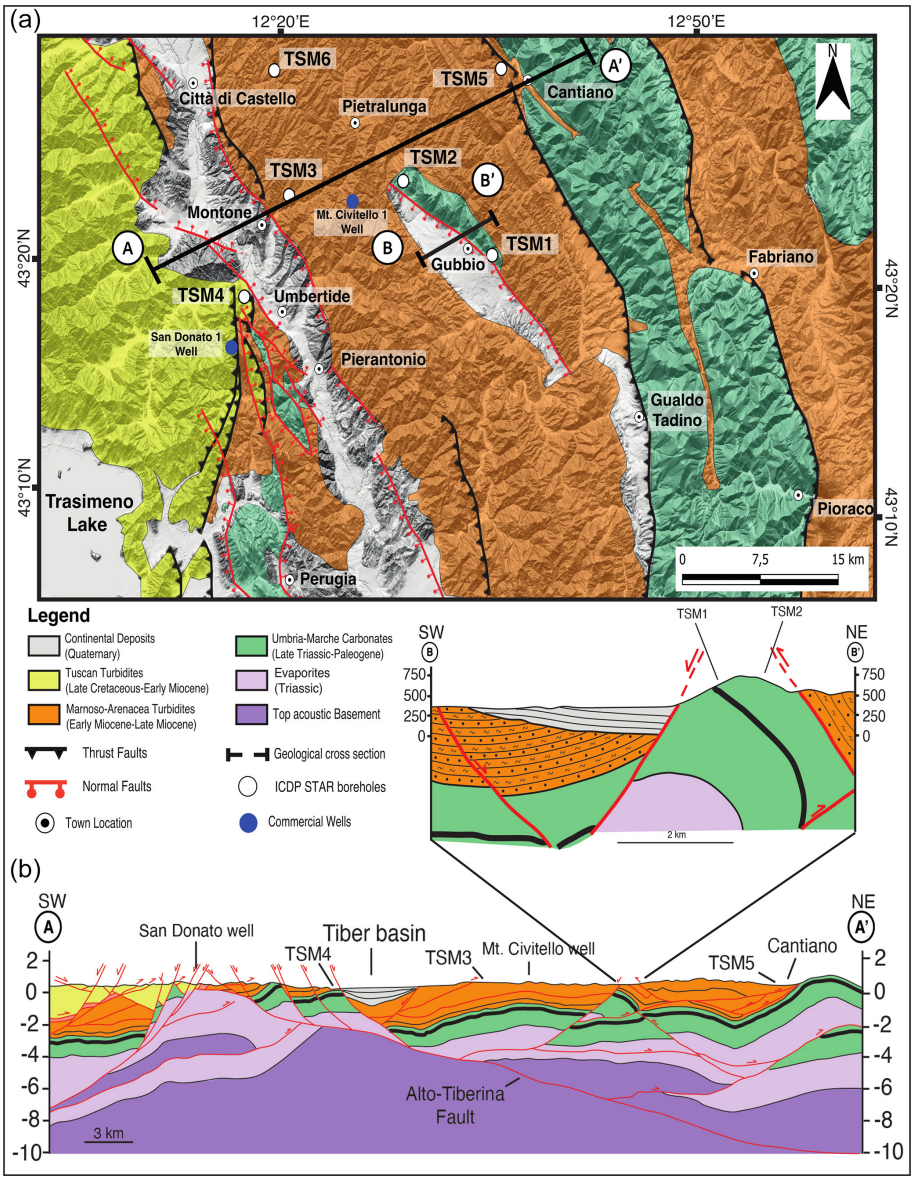

Figure 3. Schematic geological map **(a)** and geological sections **(b)** across the TABOO area. The map shows the locations of the six STAR boreholes (white circles) and of the two deep boreholes (San Donato 1 and Mt. Civitello 1, blue circles). The geological cross-sections A–A' and B–B' illustrate the geometry at depth of the major, contractional and extensional, tectonic structures affecting the study area, relative to the position of the STAR boreholes. The deep structures of section A–A' have been constrained through the interpretation of a set of seismic reflection profiles: the black layer within the Umbria-Marche carbonates represents the Marne a Fucoidi formation, which corresponds to a major seismic marker. Figure modified from Mirabella et al. (2011).

the present-day seismicity of the region, whose study and characterization are the main objective of the STAR project.

In the central part of the area, the Mesozoic carbonates are exposed at the core of the prominent Gubbio anticline, whose back limb is downthrown by the SW-dipping Gubbio fault, representing the most important antithetic splay of the ATF (e.g., Mirabella et al., 2004, 2011).

The stratigraphy of the six boreholes and their location with respect to the main geological structures are summarized in Table 1 and illustrated in the geological section of Fig. 3b.

Two sites (TSM1 and TSM2) were drilled across the late Mesozoic–early Tertiary carbonates, cropping out along the crest of the Gubbio anticline, which represents the maximum structural culmination of the study area. All the other wells were all drilled in the Neogene marls and sandstones: TSM4 is located at the ATF footwall block, west of the Tiber Valley; TSM2 and TSM6 were drilled in the ATF hanging wall

Table 1. List of key depths for the six boreholes.

Site	219 mm conductor casing depth	190.5 mm drilled depth	177.8 mm casing depth	Bottom of hole (152.5 mm below casing)
TSM1	9 m	99 m	99 m	133 m
TSM2	9 m	97 m	97 m	160.9 m
TSM3	9 m	32 m	32 m	80 m
TSM4	8 m	79.4 m	79.4 m	100.5 m
TSM5	7 m	82.4 m	82.4 m	117 m
TSM6	8 m	79 m	64 m	115.5 m

block, in the northern part of the study area; and TSM5 was drilled in the northeastern part, close to the western flank of the Umbria-Marche ridge (Fig. 3b).

Within the ATF seismicity, we observed that REs occur within the geodetically recognized creeping portions of the ATF, around an apparent locked asperity located in the northern portion of the fault placed between the settlements of Città di Castello and Gubbio (Valoroso et al., 2017; Anderlini et al., 2016). The rate of occurrence of REs has also been observed as synchronous with hanging wall swarms, suggesting that creeping may guide strain partitioning in the ATF system (Vuan et al., 2020). In detail, the seismic moment released from the ATF seismicity only accounts for about 30 % of the observed geodetic deformation, confirming the need for aseismic deformation (Gualandi et al., 2017). This implies that the ATF seismicity pattern is consistent with a mixed-mode (seismic and aseismic) slip behavior (as defined by Avouac, 2015). As pointed out above, the occurrence of slow and fast earthquakes on the same fault patch has revolutionized our thinking about how faults accommodate slip. However, the interaction between creep, slow, and regular earthquakes is still elusive, primarily due to the dearth of high-resolution observations across the spectrum of slip phenomena. In this context, the ATF is a particularly fruitful location for such an investigation at the local scale, as demonstrated in Gualandi et al. (2017), where the dense GNSS network allowed for the detection of a very small amplitude transient deformation signal, correlated in both space and time with an intense seismic swarm (maximum M_w 3.7) that occurred in the ATF hanging wall in 2013 (Vuan et al., 2020). Thus, the northern portion of the ATF that hosted the aseismic deformation, located primarily in the footwall of the antithetic (SW-dipping) Gubbio fault (Fig. 2), was identified as a STAR target zone for drilling and instrument deployment.

2.2 Drilling operations

We drilled the six 80–160 m deep boreholes surrounding the creeping portion of the ATF (named TABOO borehole strainmeter, acronym TSM1–6; see locations in Fig. 2), to deploy Gladwin Tensor strainmeters and short-period seismometers, in a two-step fieldwork campaign: during the fall of 2021 and spring of 2022.

Boreholes were drilled using a Casagrande C8 rig using mud rotary drilling. Mud was made using a polymer drilling fluid. The preferred method of drilling a strainmeter borehole is to use an air hammer for the cased section of the borehole and an air rotary for the open section of the borehole. Traditional bentonite mud can be difficult to clean out of the borehole and can leave a thin layer on the walls of the borehole, which can prevent the strainmeter from properly coupling with the host rock. Using the polymer drilling fluid allowed for a smaller drill rig while enabling complete flushing of the borehole.

Boreholes are drilled in two phases. Phase 1 consists of drilling to 7–9 m and setting 219 mm conductor casing to prevent loose surface material from falling into the borehole. After the conductor casing is set, a 190.5 mm section is drilled to a depth where the rock appears to be stable (32–99 m). After reaching our casing target depth, the drill rod is removed, and 177.8 mm steel casing is lowered into the borehole. Before casing, the inclination of the borehole was checked using an EZDip inclinometer, with a goal of maintaining no more than 5° vertical deviation. The casing protects the borehole from collapsing and is critical for the installation of the strainmeter. After the casing is installed, the anulus was cemented using Portland cement. After the downhole work is complete, the casing is used as a stable GNSS monument.

Phase 2 of the drilling uses a 152.5 mm tricone drill bit to drill down to the installation zone. While the boreholes are being drilled, the operation is closely monitored. We look for excessive vibration, changes in drilling speed, and water production. These can indicate fractures or changes in lithology. We also collected cutting samples every 9 m. Once we had passed through several sections of what appears to be consistent material (smooth drilling and lack of water production), we stopped drilling and prepared to log the hole. Before logging, the borehole is flushed with clean water while moving the drill rod up and down. Water is sampled until polymer is no longer be detected. After the borehole was cleaned, we ran geophysical logging gear in the open borehole.

2.3 Downhole logging

Upon completion of the drilling operations, a suite of downhole logging measurements was performed in each borehole. The main purpose of these acquisitions was to select the most ideal section of rock formation to deploy at depth seismometers and strainmeters. The selected interval had to be as stable as possible with unfractured, competent rocks and with a very smooth borehole wall for coupling between instruments and rock formation. Thus, it was crucial to detect fractures/-faults and weak zones intersecting the boreholes as well as their spatial distribution, characteristics, and connection with the geological structures mapped on the surface. Therefore, knowledge of petrophysical properties of drilled rock forma-

Table 2. Depth interval recorded by downhole logging sondes for each STAR borehole.

Site	Gamma ray (GR)	Acoustic image (ABI)	Optical image (OBI)	Full wave sonic (FWS)	E-log (Res and SPR)	Fluid temperature conductivity (FTC)	Caliper (CAL)
	Downhole logging interval (m)						
TSM1	0.9–132.5	97.8–132.4	98.4–132.0	97.0–132.0	–	1.8–133.3	96.1–130.7
TSM2	1.3–159.5	92.7–159.6	96.2–147.0	144.5–159.0	–	2.1–160.3	96.7–157.9
TSM3	1.1–79.9	31.6–79.9	30.9–79.4	33.0–78.0	33.0–78.0	1.8–80.8	29.4–77.8
TSM4	0.9–99.4	79.7–100.3	–	81.9–100.6	77.2–100.2	1.7–100.3	79.7–100.3
TSM5	0.7–116.2	82.2–117.1	79.5–117.1	80.7–117.5	80.1–116.9	1.5–117.0	82.2–117.1
TSM6	1.1–116.9	62.8–116.1	–	61.3–116.4	60.4–117.4	1.9–117.8	62.8–116.1

tion (i.e., Rider and Kennedy, 2011; Pierdominici and Kück, 2021) became key parameters for deep subsurface characterization, especially because no core material was available for further and more detailed geomechanical and structural analyses in laboratory.

Downhole logging measurements were acquired in fall 2021 and summer 2022 by a logging contractor (GEOLOGIN). All six shallow boreholes were logged by slim-hole sondes (Table 2), and the following downhole measurements only cover the open hole (OH; uncased): acoustic televiewer (ABI), optical borehole imager (OBI), full waveform sonic (FWS), E-log (resistivity, Res, and single-point resistance, SPR), fluid temperature conductivity (FTC), three-arm caliper (CAL), and total gamma ray (GR). The latter also ran in the cased hole (CH; Fig. 4). All logging measurements were depth-matched using the gamma ray as the reference logging present in all sondes.

Within this paper, a brief and preliminary analysis of the downhole logging data is presented (Table 3), which will be the main focus of a separate contribution. Downhole logging in the OH carbonate units of boreholes TSM1 (Fig. 4b) and TSM2 (Maiolica and Scaglia Rossa formations) shows no significance in the gamma ray (values less than 15 cps). P- and S-wave velocities have mean values of 5.3 and 2.9 km s^{-1}, respectively, for the Maiolica formation (TSM1) and 4.8 and 2.5 km s^{-1} for the Scaglia Rossa formation (TSM2). E-log has been not executed due to time constraints. In the sandstone–marly units (Marnoso-Arenacea formation), encountered in three boreholes (TSM3, 4, and 6), the gamma ray measurements provide higher values (about 80–100 cps), which are mainly correlated to marly intervals. In these three boreholes, P-wave velocities are similar, with values between 3.0 and 3.4 km s^{-1}, as are the S-wave velocities, which show constant values of about 1.9 km s^{-1}. E-log shows values less than 20 Ωm (Res) and 80 Ωm (SPR), with the exception of the TSM3 borehole, where a very hard and competent interval was encountered. In TSM5, the hemipelagic marls of the Schlier formation are characterized by a high gamma ray (mean value of 80 cps), by an average P- S wave velocity of about 3.5 and 1.9 km s^{-1}, and by low Res and SPR values. All six boreholes show fluid temperatures (T) between 12 and 10 °C. The fluid conductivity log (COND) has revealed values between 380 µS cm^{-1} in the carbonate formations of TSM1 and 694 µS cm^{-1} in the Marnoso-Arenacea formation of TSM4. The high value of COND recorded in TSM4 was ascribed to the proximity of a local spring (Fig. 4b, Table 3),

The televiewer and optical imager tools have delivered high-resolution images of the borehole wall. OBI was not performed in TSM4 and TSM6 boreholes. The televiewer sonde provides two 360° color-coded unwrapped images reflecting the roughness and shape of the borehole wall and its acoustic properties (Zemanek et al., 1969; Pierdominici and Kück, 2021). The analysis and evaluation of the OBI and ABI images allowed us to detect orientation and geometry of structures such as open or filled fractures and bedding planes but also additional geological features such as stylolites and cherts (Fig. 4c). Open and filled fractures were distinguished using purely OBI images, except for TSM4 and TSM6. For these two boreholes, the distinction between open and filled fractures was based on comparison of AMPL and TT images. Well-developed fractures visible in both images were classified as open, whereas those visible only in the AMPLs were defined as filled. Both fractures have on average a higher dip angle (Table 4) with a mean orientation of around NE–SW, while the bedding planes show a generally low dip angle and similar orientation.

The logging evaluation enabled the identification of intervals at depth not affected by fractures or weak zones that could affect the deployment of the instruments but especially the acquisition of seismic and deformation data.

2.4 Instrumenting

The primary STAR instrument is the Gladwin Tensor Strainmeter (GTSM). This instrument uses a capacitance bridge as a strain gauge to measure changes in length across a sensing volume. There are four horizontal strain gauges. The upper three gauges are oriented 120° from each other. The last gauge is 90° from the second gauge and 30° from the other

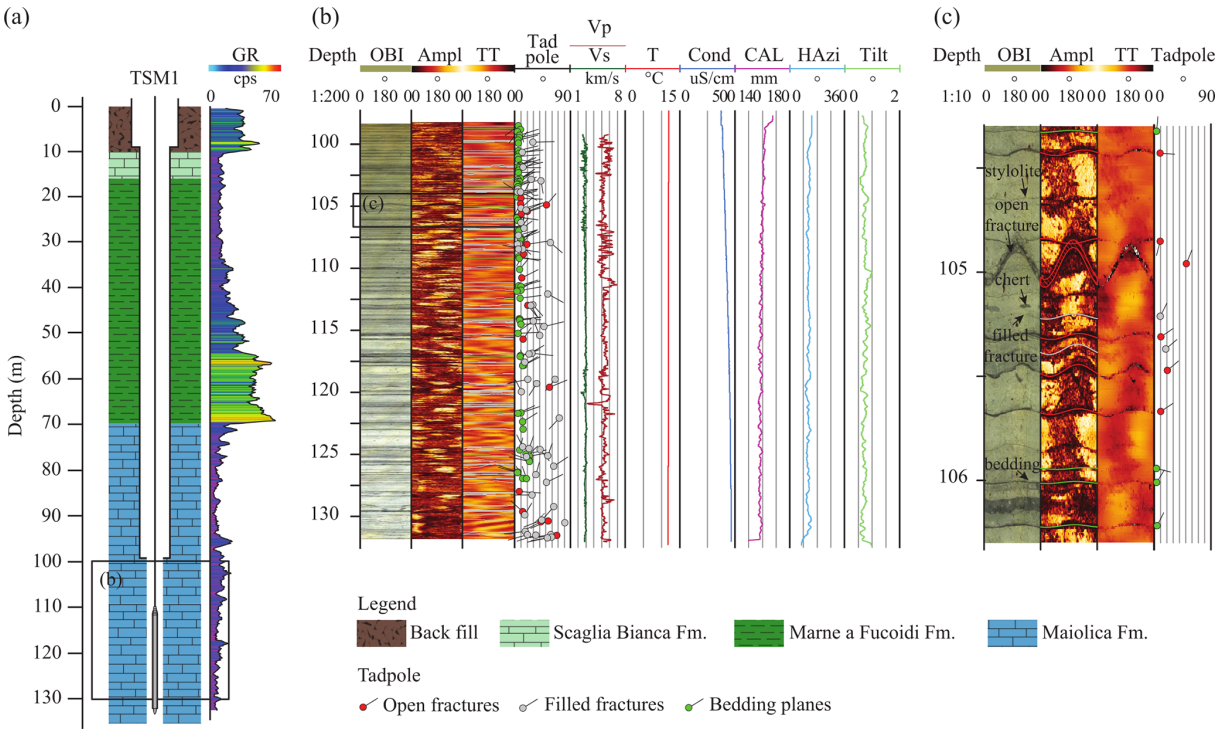

Figure 4. Downhole logging measurements executed in the borehole TSM1. **(a)** Lithological column with associated GR log acquired in both CH and OH. The GR shows a low signal in the carbonate rock (Maiolica formation) and higher values at the Marne a Fucoidi formation, especially between 60 and 70 m, where the GR reaches the highest values (around 60–70 cps) due to the higher clay contribution. **(b)** Geophysical logging measurements only in the OH: optical imager (OBI); borehole televiewer with amplitude and travel time images (Ampl and TT, respectively); Vp and Vs obtained from the analysis of the FWS, fluid temperature, and conductivity (T and Cond, respectively); and borehole geometry that includes the caliper (CAL) of the borehole calculated from TT, the hole azimuth (HAzi), and tilt from the three-arm caliper sonde. **(c)** An enlargement showing the geological structures identified on the borehole images. The tadpoles display their dip (colored dot) and dip azimuth (black tail).

Table 3. Geophysical properties of the rocks.

Sites	ICDP ID	GR cps		Vp km s^{-1}	Vs km s^{-1}	RES Ωm	SPR Ωm	T °C	COND µS cm^{-1}
		CH	OH						
TSM1	5070_1_A	17.9 ± 13.3	8.4 ± 4.4	5.3 ± 0.3	2.9 ± 0.1	–	–	12.3 ± 0.6	380.9 ± 39.9
TSM2	5070_2_A	11.7 ± 5.4	13.4 ± 5.6	4.8 ± 0.2	2.5 ± 0.5	–	–	14.7 ± 1.3	456.4 ± 61.5
TSM3	5070_3_B	61.5 ± 12.7	104.2 ± 15.9	3.2 ± 0.2	1.8 ± 0.1	29.2 ± 4.7	104.3 ± 10.4	13.6 ± 0.2	451.6 ± 7.4
TSM4	5070_1_A	61.5 ± 10.0	85.1 ± 13.2	3.0 ± 0.2	1.9 ± 0.1	8.6 ± 1.0	42.2 ± 4.6	16.2 ± 0.3	694.3 ± 91.7
TSM5	5070_5_A	48.6 ± 8.7	81.2 ± 9.3	3.5 ± 0.2	1.9 ± 0.1	11.5 ± 3.2	53.4 ± 7.2	16.5 ± 0.7	634.0 ± 8.2
TSM6	5070_6_A	62.4 ± 9.2	99.9 ± 10.5	3.4 ± 0.3	1.9 ± 0.1	19.2 ± 4.1	70.1 ± 13.9	16.7 ± 0.4	584.0 ± 187.9

two. This provides redundancy if a gauge fails. For proper coupling, the GTSM needs to be installed in competent rock without fractures and below any active aquifers. Once the suitable installation zone is selected based on the logging analysis, the borehole is prepared for installation. If the installation zone is more than a meter above the bottom of the borehole, it has to be lifted with Portland cement. If it is less than a meter above the bottom, gravel is used.

To properly couple the GTSM to the host rock, we used a cement able to expand. The preferred grout is BASF MasterFlow 1206 expansive grout (0 %–0.2 % expansion). The grout is mixed in a standard mortar mixer until completely hydrated with no lumps (20 s flow cone test). The grout is transferred to a dump baler. This is a 10.15 cm ID aluminum tube (9–12.5 m depending on rig tower height) with a valve on the bottom. The valve is opened when the baler hits the bottom of the borehole. The grout is released with minimum

Table 4. Structural analysis from OBI and ABI image logs.

Sites	Open fractures		Filled fractures		Bedding planes	
	strike	dip	strike	dip	strike	dip
TSM1	N320.3 ± 18.6	24.0 ± 19.5	N119.9 ± 26.6	30.8 ± 20.5	N328.2 ± 08.4	8.0 ± 4.5
TSM2	N331.1 ± 10.1	46.9 ± 17.8	N129.3 ± 08.8	50.3 ± 14.5	N327.6 ± 01.7	27.3 ± 8.6
TSM3	–	–	–	–	–	–
TSM4	N126.6 ± 24.4	32.8 ± 12.5	N076.9 ± 20.1	34.4 ± 15.9	–	–
TSM5	N325.8 ± 06.7	48.4 ± 17.0	N130.5 ± 07.1	35.8 ± 17.9	–	–
TSM6	N350.9 ± 16.7	36.7 ± 19.6	N031.0 ± 15.4	27.5 ± 13.2	N047.9 ± 02.1	7.0 ± 5.3

mixing with the fluids in the borehole. After the baler is removed from the borehole, the GTSM is lowered inside the hole using the same cable that carries the signal. Once the GTSM is lowered to the installation zone, its cable is tied off to the wellhead, and the installation equipment is cleaned up. No downhole work is done for the next 24 h to allow the grout to set.

The secondary instrument installed in the borehole is a three-component 2 Hz seismometer (see installation interval in Fig. 5), lowered on 50 mm PVC pipe. A section of slotted PVC is placed above the seismometer to sample an aquifer that is located using the geophysical logging data, usually 9–15 m above the seismometer. The seismometer is lowered until it reaches the top of the strainmeter grout. It is then pulled up by 1 m and finally cemented using the PVC pipe. The amount of cement is calculated to come up to the screen. The PVC is flushed with water to clear out the screen. TSM1 and TSM2 also have a loop of fiber-optic cable attached to the PVC pipe. Cement is allowed to cure until the next day. The final borehole work involves placing a sand pack around the screened section and a bentonite seal above the sand. After the bentonite hydrates, the hole is cemented up to the surface.

The top of the borehole is completed with an adapter and GNSS antenna. After several weeks to months, the water level is measured in the PVC tube. A pressure sensor is lowered in the PVC 3–4 m below the water level. Surface sensors include rain and barometric pressure sensors and a seismometer.

In Table 5 we report the key depths of the strainmeters and seismometers at installation.

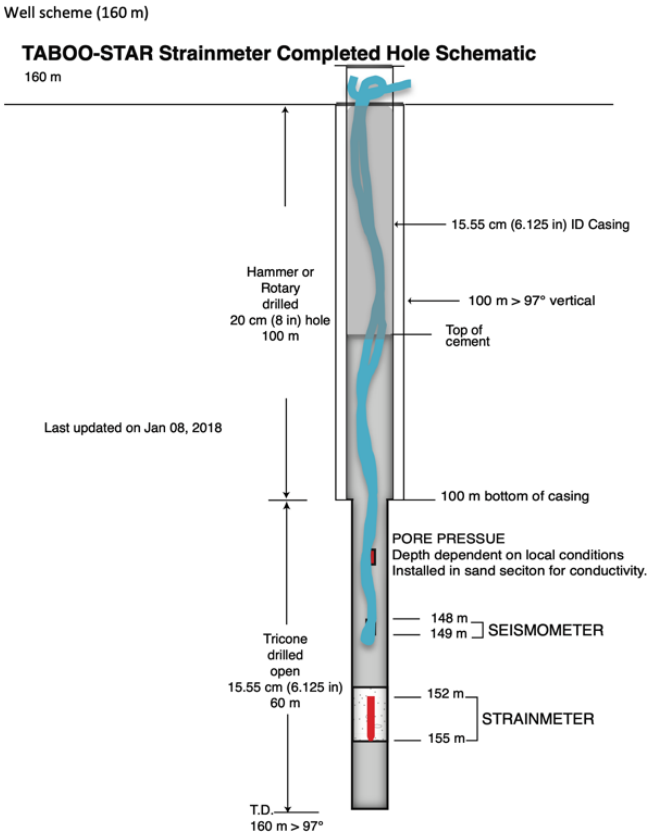

Figure 5. Schematic of the hole showing the strainmeter deployed in the deepest portion of the hole with the seismometer on top (see on the right side for details). The schematic also reports the adopted drilling techniques (see left side for details). The curved blue line represents the fiber-optic cable deployed only in the two deepest holes (see text for details).

3 Data acquisition

3.1 Strainmeters

Currently, about a year after installation, all strainmeters demonstrate signs of proper functionality. Following installation, initial grout curing transitions toward long-term borehole "relaxation", which typically manifests as a logarithmically decaying areal compression that persists through the lifetime of the station (Gladwin et al., 1987; Fig. 6). On the timescale of hours to days, the strainmeters respond to earth body tides and ocean loads, as well as atmospheric pressure changes, rainfall or groundwater flow (Fig. 6). The instruments likewise demonstrate superb capability for detecting high-rate dynamic strains, as depicted in Fig. 7 at TSM3 for the Umbertide M_w 4.3 earthquake ∼ 10 km away.

It is important to mention that the raw gauge signals must be properly calibrated to accurately represent rock formation

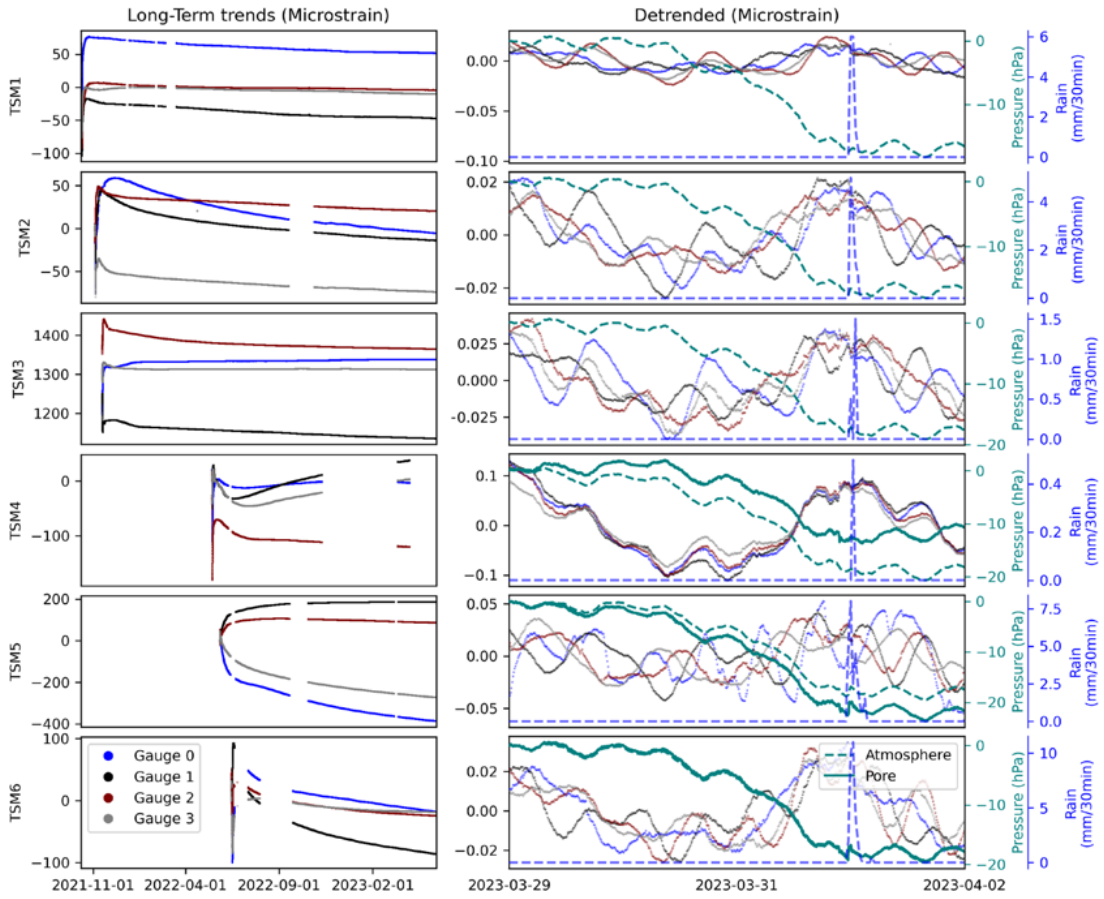

Figure 6. Demonstration of gauge strains for all STAR instruments. Plots on the left show the transition from initial grout curing following installation to long-term borehole relaxation. Plots on the right show the linearly detrended gauge strains, which are dominated by changes in atmospheric pressure changes and tidal strains. Pressure data from surface sensors and pore pressure sensors (TSM4, 5, and 6 because TSM3 was not recording pore pressure data at that time) are plotted on a separate y axis for comparison. All raw gauge data have been converted to units of linearized strain and plotted with different colors according to the figure legend shown in the bottom left. The pore pressure and barometric pressure data are plotted as solid and dashed teal lines, respectively. All data have had the first value of the time series subtracted. Raw strain records and pressure data are downloaded from EarthScope.

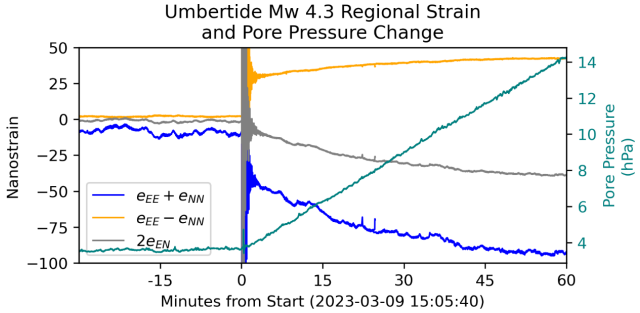

Figure 7. Demonstration of a high-rate (20 Hz) strain observations from the 9 March 2023 Umbertide M_W 4.3 earthquake at TSM3. The tidally calibrated regional strains are plotted for the areal (eEE + eNN), differential (eEE-eNN), and engineering shear (2eEN) strains according to the figure legend. The pore pressure data are plotted on the secondary y-axis in teal. Raw strain records and pore pressure data are downloaded from EarthScope.

Table 5. Instruments' depths of deployment.

Site	Strainmeter depth (m)	Seismometer depth (m)	Screen depth (m)	depth sensor (m)
TSM1	132	127.3	114–123	No water
TSM2	158.1	152.5	139.5–148	No water
TSM3	78.6	73	60–69	23
TSM4	100.3	95.1	85–91	20.12
TSM5	116.1	111	90–96	21.43
TSM6	115.5	110	82–91	17.6

strain, and additional signal corrections can further aid in isolating non-tectonic signals, depending on the timescale of interest. The long-term trend is easily filtered or removed from the strain record. The measured tidal signals (Fig. 6) are useful for calibrating the four-gauge system response to rock for-

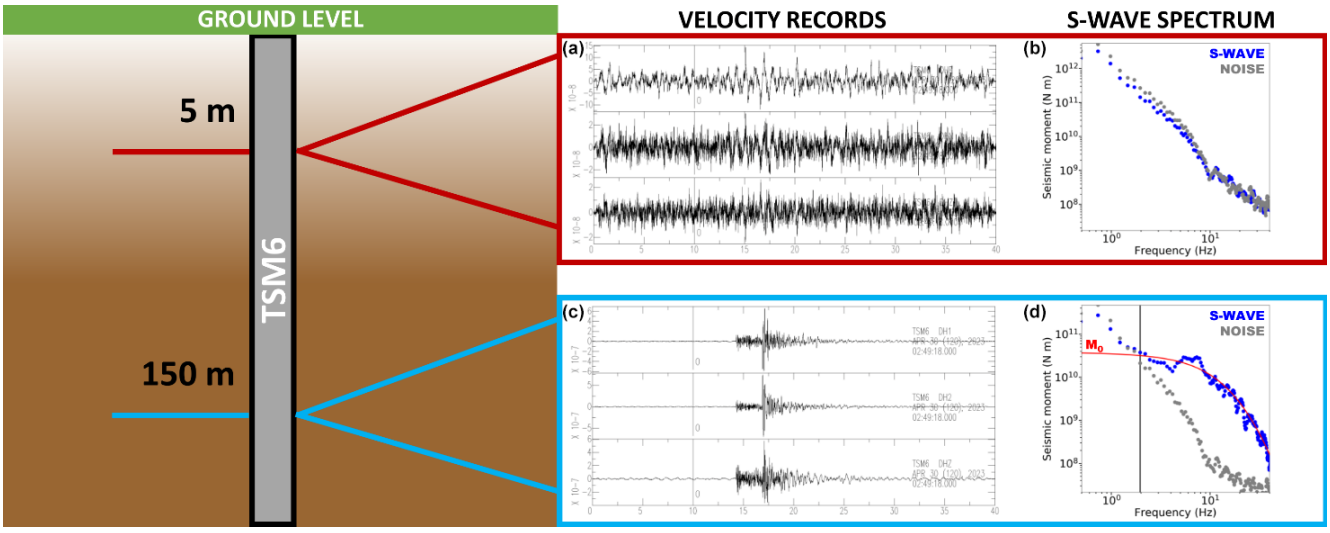

Figure 8. Small event recorded at the station TSM6 seismic instruments. **(a)** Three-component velocity signals recorded at the surface sensor. **(b)** Displacement spectrum of the expected (same time window observed in panel **(c)**) S-wave signal (blue circles) and of the noise (gray circles) recorded at the surface sensor. **(c)** As for panel **(a)**, for the borehole sensor. **(d)** As for panel **(b)**, for the borehole sensor; the black vertical bar is the minimum frequency used for the inversion, as defined by the SNR criterion of Supino et al. (2019). Event ID 34847211 (INGV catalog); the epicentral distance is 15.65 km, and the event depth is 1 km. The reference time in panels **(a)** and **(c)** is 30 April 2023 02:49:18 UTC.

mation strains in the east–north reference system by comparing the observed and modeled tides, which are approximately well-known (e.g., Canitano et al., 2018; Hodgkinson et al., 2013). These calibrations typically provide a more accurate characterization of tectonic strain than the standard manufacturer's calibrations (Hodgkinson et al., 2013; Roeloffs, 2010). The modeled tides can be removed from the time series, along with an estimated barometric pressure response derived from collocated surface atmospheric pressure data. Rain gauges at all stations and pore pressure transducers at TSM3, 4, 5, and 6 provide additional information related to strains induced by hydrologic changes (Figs. 6 and 7).

All strain data and data relevant to correcting the strain time series prior to geophysical analysis is available from the IRIS DMC (https://service.iris.edu/fdsnws/dataselect/1/, last access: 20 June 2024). Metadata for proper calibration and corrections are currently hosted by UNAVCO for each station (https://www.unavco.org/data/strain-seismic/bsm-data/bsm-data.html, last access: 20 June 2024).

3.2 Seismometers

We report an example of a small earthquake ($M_l = 0.7$) in Fig. 8, detected by the 2 Hz seismometers deployed within the TSM6 borehole. We can appreciate how the event is barely visible at the surface sensor (Fig. 8a) but provides a high signal-to-noise ratio (SNR) signal at depth (Fig. 8c). Such a clean signal allows us to constrain the earthquake source parameter seismic moment from the S-wave displacement spectrum (Fig. 8d), computed with the probabilistic approach of Supino et al. (2019). The estimated moment magnitude is $M_w = 1.0 \pm 0.1$.

3.3 GNSS antennas

Before the STAR project, the continuous GNSS (cGNSS) network across the Alto Tiberina fault zone was already dense with respect to the surrounding Italian regions (e.g., Devoti et al., 2017; Serpelloni et al., 2022), with average baselines among stations lower than the national average of 20 km. This is due to a relatively high number of GNSS stations, belonging to the INGV Rete Integrata Nazionale GNSS network (RING; http://ring.gm.ingv.it, last access: 20 June 2024), realized since the early 2000s (D'Agostino et al., 2009). When integrated with data from commercial and regional cGNSS networks, the spatial and temporal density allows for an estimate of high-resolution strain-rate measurements (e.g., Serpelloni et al., 2022), with important seismotectonic implications (Anderlini et al., 2016). However, it was necessary to improve the cGNSS network, which was originally designed as a linear array oriented in a direction perpendicular to the Apennine chain (D'Agostino et al., 2009). The implementation serves to increase both the spatial resolution of interseismic elastic coupling (see Anderlini et al., 2016) and our ability to detect small transient deformations of both tectonic and nontectonic origin (Gualandi et al., 2017; Mandler et al., 2021). Together with STAR, we benefit from the TECTONIC ERC project (https://cordis.europa.eu/project/id/835012, last access: 20 June 2024) that gives us the opportunity to deploy an additional 10 GNSS instru-

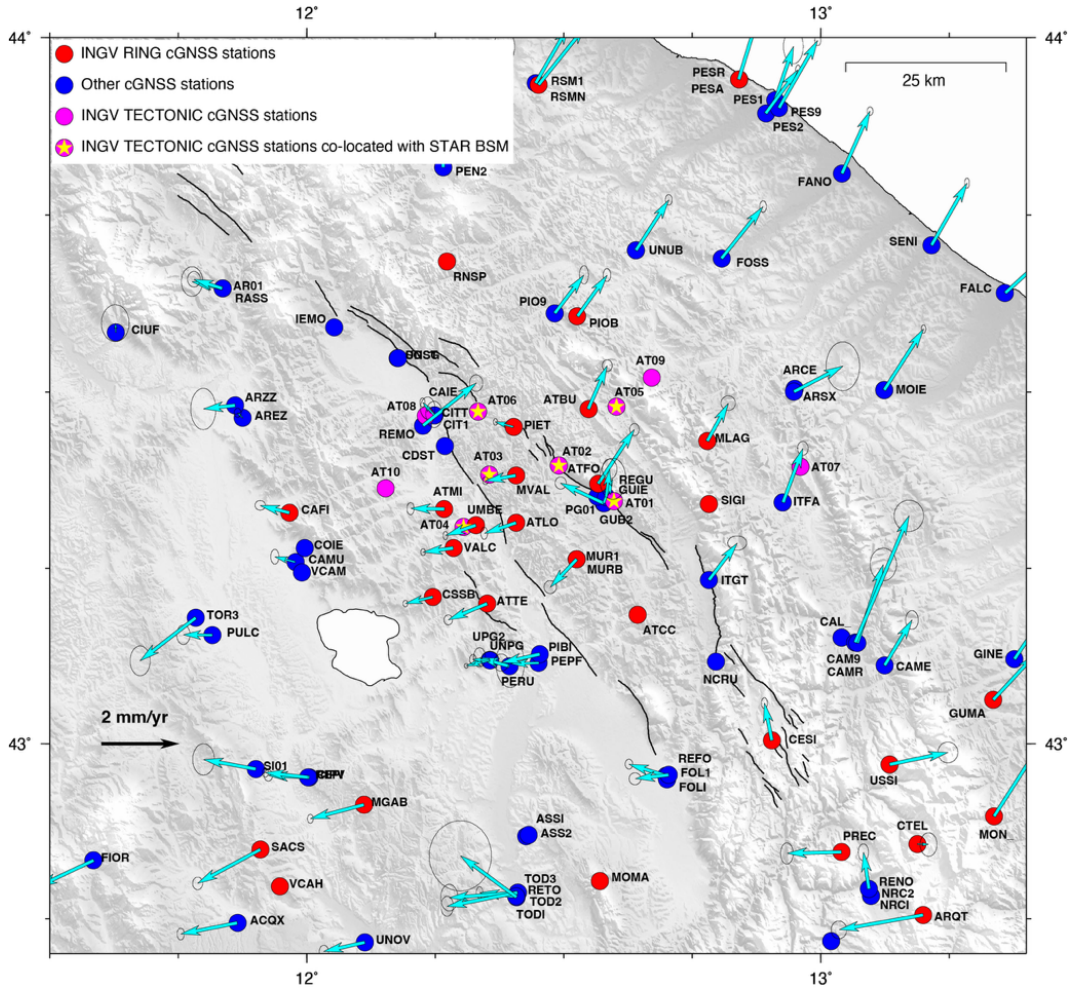

Figure 9. Map of the GNSS infrastructure. The cyan arrows show horizontal velocities, in an Apennines fixed reference frame for stations with more than 3.5 years of observation time span. Not all the blue stations are currently providing data.

ments with the goal of improving the geometry of the RING network in the area (see Fig. 9). Six instruments have been installed in correspondence with the borehole strainmeters, with the GNSS antenna mounted on top of the well heads. An additional four sites have been installed following the semi-continuous scheme developed and described in Serpelloni and Cavaliere (2010). Once dismounted, only the geodetic marker remains fixed in the substrate (bedrock or building). The four semi-continuous stations are powered by solar panels, and data are delivered to the acquisition center through an LTE modem. For the six stations installed on top of the strainmeters, data are instead transmitted through satellite carriers.

Table 6 lists the locations, GNSS instruments installed, and monument type for the 10 new cGNSS stations. Figure 10 shows photographs of the two types of installations adopted, while Fig. 11 shows the displacement time series obtained by processing the raw GNSS observations with the GAMIT/GLOBK software following the procedures described in Serpelloni et al. (2022). Given the still very limited temporal coverage (< 1.5 years) of the observations, the estimation of seasonal (annual, semi-annual, and multi-annual) components is still not accurate.

3.4 Pore pressure and meteorological data

As previously mentioned, several additional sensors have been deployed at each station to collect data useful in generating post-processed corrections for the strainmeter data. In addition to the four strain gauges, the GTSM instrument records 30 min sampled environmental channels including barometric pressure and rainfall. Additionally, Paros 8000 Series pressure transducers are installed in four of the boreholes to record 1 sps pore pressure and temperature. The full complement of extra sensors at each station is described in Table 7.

Pore pressure sensors were installed in a PVC pipe with a diameter of 5 cm, with a screened section (sampling depths listed in Table 4) sand-packed and capped with bentonite.

Table 6. Description of the 10 continuous GNSS stations; the first six stations are installed on top of the borehole strainmeter well, whereas the other four stations (AT07, AT08, AT09, and AT10) are installed on bedrock or stable buildings. Note that AT07 was first realized in the framework of the RETREAT project (Bennett et al., 2012) and measured in repeated campaigns in 2005, 2006 and 2007. The first epoch reported in the table refers to the first measurement collected as a continuous station.

Station ID	Longitude ° E Latitude ° N Height (m)	Monument type	Receiver model	Antenna model	Antenna height (m)	First epoch (yyyy/mm/dd)
AT01	12.5976 43.3453 600.42164	Top of BSM well head	TRIMBLE ALLOY	TRM115000.00	0.0083	2022/07/21
AT02	12.4899 43.3962 676.53991	Top of BSM well head	TRIMBLE ALLOY	TRM115000.00	0.0083	2021/12/02
AT03	12.3545 43.3830 386.52252	Top of BSM well head	TRIMBLE ALLOY	TRM115000.00	0.0083	2021/12/01
AT04	12.3046 43.3087 316.08221	Top of BSM well head	TRIMBLE ALLOY	TRM115000.00	0.0083	2022/12/31
AT05	12.6025 43.4797 425.98607	Top of BSM well head	TRIMBLE ALLOY	TRM115000.00	0.0083	2022/11/08
AT06	12.3328 43.4724 449.71935	Steel mast on bedrock	TRIMBLE ALLOY	TRM115000.00	0.0083	2022/11/08
AT07	12.9595 43.3944 836.99836	Steel mast on bedrock	TRIMBLE ALLOY	TRM115000.00	0.5	2022/04/20
AT08	12.2311 43.4668 330.51957	Steel mast on building	TRIMBLE ALLOY	TRM115000.00	0.3	2022/06/22
AT09	12.6711 43.5203 619.52707	Steel mast on bedrock	TRIMBLE ALLOY	TRM115000.00	0.5	2022/05/26
AT10	12.1534 43.3635 627.04682	Steel mast on bedrock	TRIMBLE ALLOY	TRM115000.00	0.5	2022/05/19

Table 7. Location and sample rates of pore pressure and meteorological data. n/a – not applicable.

Site	Paros 8000 sampling rate	Paros 8000 sensing depth (m)	Paros 8000 sensing depth (m)	Barometer sampling rate	Barometer sensing depth (m)	Rain gauge sampling rate	Rain gauge sensing depth (m)
TSM1	n/a	n/a	n/a	30 min	Surface	30 min	Surface
TSM2	n/a	n/a	n/a	30 min	Surface	30 min	Surface
TSM3	1 Hz	60–69	23	30 min	Surface	30 min	Surface
TSM4	1 Hz	85–91	20.12	30 min	Surface	30 min	Surface
TSM5	1 Hz	90–96	21.43	30 min	Surface	30 min	Surface
TSM6	1 Hz	82–91	17.6	30 min	Surface	30 min	Surface

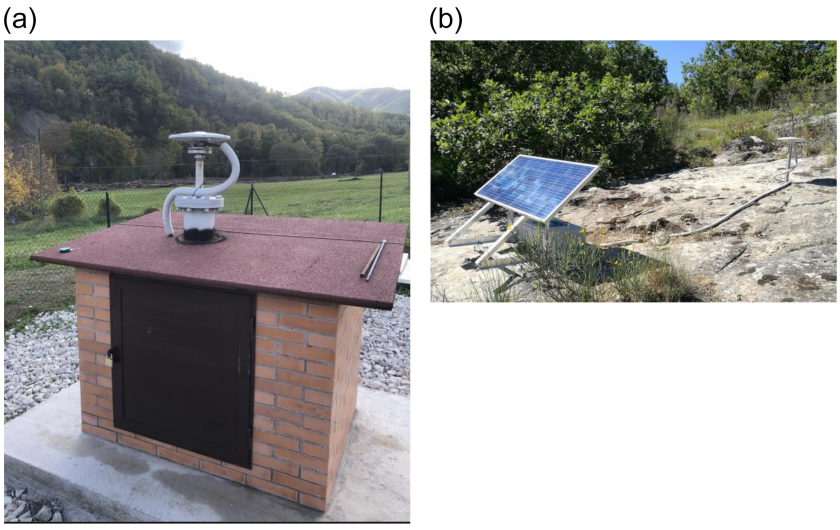

Figure 10. Photographs of GNSS station AT05 **(a)** installed on the well head at TSM3 site and GNSS station AT10 **(b)**. AT10 is installed as a semi-continuous station on bedrock with a 50 cm tall antenna mount fixed on a ∼ 50 cm founded and epoxide geodetic marker.

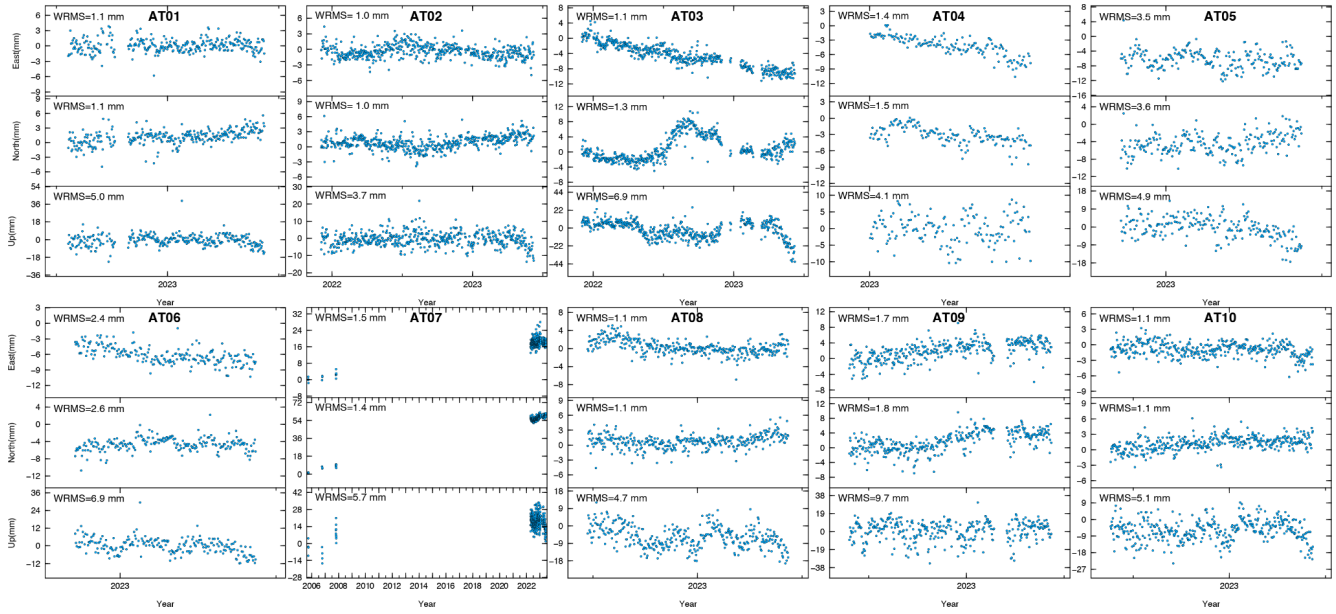

Figure 11. Displacement time series obtained from the analysis of GNSS observations using the GAMIT/GLOBK software, following the procedures described in Serpelloni et al. (2022). The horizontal components are rotated in a Eurasian fixed frame. Weighted root mean square (WRMS) values, from a linear fit of the time series, are indicators of daily repeatability for the east, north and vertical components.

Unfortunately, borehole conditions did not permit pore pressure installations at TSM1 and TSM2. The Paros sensors are connected to small board computers, which log 1 sps data into daily ascii files transmitted to EarthScope for archiving and distribution. The 30 min pressure and rainfall data are collected by the GTSM data logger and written into the daily bottle files. These data are translated to miniSEED and available as miniSEED or ascii formats from the EarthScope DMC. Figure 12 shows a time series of the currently available strain and correction data from each station.

4 Discussion and conclusions

The ATF is probably the best place in the world to understand the mechanisms and implications of the stress transfer process between seismic and aseismic fault segments at the local scale. By adding STAR to the existing TABOO NFO infrastructure, we realized one of the most complete and advanced system to investigate the complexities of fault slip processes at the local scale.

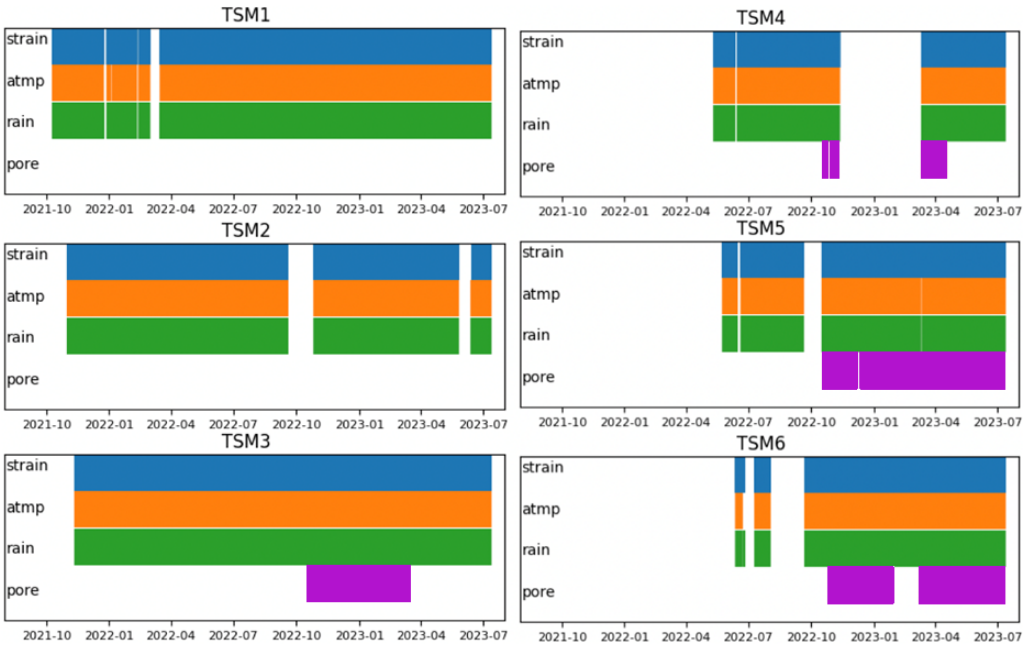

Figure 12. Time series of availability of data per station.

The ATF is an active low-angle normal fault that is directly related to the decades-long debate regarding the existence and mechanics of such structures in nature (e.g., Wernicke, 1995; Collettini and Sibson, 2001; Collettini, 2011).

The ATF is arguably the best location in the world for a BSM deployment targeting slip in a normal fault system because both steep and low-angle faults are present, and creep and episodic slip behavior are both known to occur (Chiaraluce et al., 2007; Hreinsdottir and Bennett, 2009; Gualandi et al., 2017; Anderlini et al., 2016). The greater ATF system is already among the best-instrumented fault systems in the world (e.g., Collettini and Chiaraluce, 2013; Chiaraluce et al., 2014). Consequently, the ATF has generated significant scientific interest internationally (e.g., MOLE workshop and report; EPOS NFO).

In addition to the ATF hazard problems of locally confined (even if crucial) importance, the STAR borehole array will allow us to address the global question of how aseismic slip relates to seismic slip. STAR data will also have implications for fault friction and crustal geodynamics that should be directly related to aseismic versus seismic fault slip more generally, including slip on transform faults, thrust and reverse faults, and subduction interfaces (e.g., Avouac, 2015). We anticipate that the strainmeter and other data we collect will have a broad impact on the global fault slip community, as testified by the international and definitively high profile of the colleagues ready to collaborate in the framework of the STAR scientific team. All data from TABOO are open to the international scientific community in standard format, available to inform studies of fault systems around the world. Data from STAR and other TABOO instruments will guide the interpretation of fault friction experiments from the laboratory (e.g., Collettini and Chiaraluce, 2013).

Data availability. The data collected within the STAR project are available to the scientific community. Seismic raw data are available at https://eida.ingv.it/it/ (EIDA, 2024). Geodetic raw data are available at https://gnssdata-epos.oca.eu/ (EPOS, 2024). Meteorological and geochemical data are available at http://fridge.ingv.it (Chiaraluce et al., 2022). The seismic data used in this study were provided within the framework of the Induced Seismicity European Plate Observing System (EPOS) under the data access portal https://www.epos-eu.org/dataportal (last access: 17 June 2024). Deformation data are available at https://service.iris.edu/fdsnws/dataselect/1/ (SAGE, 2024). Metadata for calibration and corrections are available at https://www.unavco.org/data/strain-seismic/bsm-data/bsm-data.html (GAGE, 2024). GNSS network data are available at https://doi.org/10.13127/RING (INGV RING Working Group, 2016). Catalogo Parametrico dei Terremoti Italiani (CPTI15) is available at https://doi.org/10.13127/cpti/cpti15.4 (Rovida et al., 2022). All data related to drilling, cuttings, and lithology acquired during the drilling operations can be found on the ICDP website: https://www.icdp-online.org/projects/by-continent/europe/star-italy/public-data (International Continental Scientific Drilling Program, 2024).

Author contributions. All authors contributed to the investigation and participated in the fieldwork. The paper was conceptualized and written by LC, MRB, MS, MG, WJ, SiP, and CH. All authors contributed to review and editing.

Competing interests. At least one of the (co-)authors is a member of the editorial board of *Scientific Drilling*. The peer-review process was guided by an independent editor, and the authors also have no other competing interests to declare.

Disclaimer. Publisher's note: Copernicus Publications remains neutral with regard to jurisdictional claims made in the text, published maps, institutional affiliations, or any other geographical representation in this paper. While Copernicus Publications makes every effort to include appropriate place names, the final responsibility lies with the authors.

Acknowledgements. The TABOO STAR (Alto Tiberina Near Fault Observatory strainmeter array) project is the result of a collaborative effort benefiting from funds and human resources from the International Continental Scientific Drilling Program (ICDP), the U.S. National Science Foundation (NSF), and the Italian National Institute of Geophysics and Volcanology (INGV).

This research was also funded in part by the European Research Council (ERC) grant agreement no. 835012 (TECTONIC) to Chris Marone. Chris Marone also acknowledges support from RETURN Extended Partnership and received funding from the European Union NextGenerationEU (National Recovery and Resilience Plan – NRRP, Mission 4, Component 2, Investment 1.3 – D.D. 1243 2/8/2022, PE0000005) and US Department of Energy projects DE-SC0020512 and DE-EE0008763.

Financial support. This research has been supported by the International Continental Scientific Drilling Program (ICDP-2018/05), the European Research Council (ERC; grant agreement no. 835012, TECTONIC), RETURN Extended Partnership, the European Union NextGenerationEU (National Recovery and Resilience Plan – NRRP, Mission 4, Component 2, Investment 1.3 – D.D. 1243 2/8/2022, PE0000005), and the US Department of Energy (projects DESC0020512 and DE-EE0008763).

Review statement. This paper was edited by Will Sager and reviewed by Matt Ikari and one anonymous referee.

References

Anderlini, L., Serpelloni, E., and Belardinelli, M.: Creep and locking of a low-angle normal fault: Insights from the Altotiberina fault in the Northern Apennines (Italy), Geophys. Res. Lett., 43, 4321–4329, https://doi.org/10.1002/2016GL068604, 2016.

Avouac, J.-P.: From geodetic imaging of seismic and aseismic fault slip to dynamic modeling of the seismic cycle, Annu. Rev. Earth Planet. Sci., 43, 233–271, https://doi.org/10.1146/annurev-earth-060614-105302, 2015.

Barchi, M. R.: The Neogene-Quaternary evolution of the Northern Apennines: crustal structure, style of deformation and seismicity, Journal of the Virtual Explorer, Electronic Edition, volume 36, paper 11, ISSN 1441-8142, 2010.

Bennett, R. A., Serpelloni, E., Hreinsdóttir, S., Brandon, M. T., Buble, G., Basic, T., Casale, G., Cavaliere, A., Anzidei, M., Marjonovic, M., Minelli, G., Molli, G., and Montanari, M.: Synconvergent extension observed using the RETREAT GPS network, northern Apennines, Italy, J. Geophys. Res., 117, B04408, https://doi.org/10.1029/2011JB008744, 2012.

Canitano, A., Hsu, Y. J., Lee, H. M., Linde, A. T., and Sacks, S.: Calibration for the shear strain of 3-component borehole strainmeters in eastern Taiwan through Earth and ocean tidal waveform modeling, J. Geodyn., 92, 223–240, https://doi.org/10.1007/s00190-017-1056-4, 2018.

Caracausi, A., Camarda, M., Chiaraluce, L., De Gregorio, S., Favara, R., and Pisciotta, A.: A novel infrastructure for the continuous monitoring of soil CO_2 emissions: a case study at the Alto Tiberina Near Fault Observatory in Italy, Front. Earth Sci., 11, 1172643, https://doi.org/10.3389/feart.2023.1172643, 2023.

Cattaneo, M., Frapiccini, M., Ladina, C., Marzorati, S., and Monachesi, G.: A mixed automatic-manual seismic catalog for Central-Eastern Italy: analysis of homogeneity, Ann. Geophys.-Italy, 60, S0667, https://doi.org/10.4401/ag-7333, 2017.

Chiaraluce, L., Chiarabba, C., Collettini, C., Piccinini, D., and Cocco, M.: Architecture and mechanics of an active low-angle normal fault: Alto Tiberina Fault, northern Apennines, Italy, J. Geophys. Res., 112, B10310, https://doi.org/10.1029/2007JB005015, 2007.

Chiaraluce, L., Amato, A., Carannante, S., Castelli, V., Cattaneo, M., Cocco, M., Collettini, C., D'Alema, E., Di Stefano, R., Latorre, D., Marzorati, S., Mirabella, F., Monachesi, G., Piccinini, D., Nardi, A., Piersanti, A., Stramondo, S., and Valoroso, L. : The Alto Tiberina Near Fault Observatory (northern Apennines, Italy), Ann. Geophys.-Italy, 57, S0327, https://doi.org/10.4401/ag-6426, 2014.

Chiaraluce, L., Festa, G., Bernard, P., Caracausi, A., Carluccio, I., Clinton, J. F., Di Stefano, R., Elia, L., Evangelidis, C. P., Ergintav, S., Jianu, O., Kaviris, G., Marmureanu, A., Šebela, S., and Sokos, E.: The Near Fault Observatory community in Europe: a new resource for faulting and hazard studies, Ann. Geophys.-Italy, 65, DM316, https://doi.org/10.4401/ag-8778, 2022 (data available at: http://fridge.ingv.it, last access: 17 June 2024).

Chiodini, G., Cardellini, C., Amato, A., Boschi, E., Caliro, S., Frondini, F., and Ventura, G.: Carbon dioxide Earth degassing and seismogenesis in central and southern Italy, Geophys. Res. Lett., 31, L07615, https://doi.org/10.1029/2004GL019480, 2004.

Collettini, C.: The mechanical paradox of low-angle normal faults: Current understanding and open questions, Tectonophysics, 510, 253–268, https://doi.org/10.1016/j.tecto.2011.07.015, 2011.

Collettini, C. and Chiaraluce, L.: Integrated laboratories to Study Aseismic and Seismic Faulting, EOS, 94, 97–104, https://doi.org/10.1002/2013EO100001, 2013.

Collettini, C. and Sibson, R. H.: Normal faults, normal friction? Geology, 29, 927–930, https://doi.org/10.1130/0091-7613(2001)029<0927:NFNF>2.0.CO;2, 2001.

Cresta, S., Monechi, S., and Parisi, G. (Eds.): Stratigrafia del Mesozoico al Cenozoico nell'area Umbro-Marchigiana, Mem. Descr. Carta Geol. Italia, 34, 185, ISBN 978-88-240-2295-5, 1989.

D'Agostino, N., Mantenuto, S., D'Anastasio, E., Avallone, A., Barchi, M., Collettini, C., Radicioni, F., Stoppini, A., and Fastellini G.: Contemporary crustal extension in the Umbria–Marche Apennines from regional CGPS networks and compar-

ison between geodetic and seismic deformation, Tectonophysics, 476, 3–12, https://doi.org/10.1016/j.tecto.2008.09.033, 2009.

Devoti, R., D'Agostino, N., Serpelloni, E., Pietrantonio, G., Riguzzi, F., Avallone, A., Cavaliere, A., Cheloni, D., Cecere, G., D'Ambrosio, C., Falco, L., Selvaggi, G., Métois, M., Esposito, A., Sepe, V., Galvani, A., and Anzidei, M.: A Combined Velocity Field of the Mediterranean Region, Ann. Geophys.-Italy, 60, S0215, https://doi.org/10.4401/ag-7059, 2017.

EIDA: Seismic raw data, European Integrated Data Archive [data set], https://eida.ingv.it/it/, last access: 17 June 2024.

European Plate Observing System (EPOS): Geodetic raw data, GNSS Data Gateway [data set], https://gnssdata-epos.oca.eu/, last access: 17 June 2024.

GAGE: Borehole Strainmeter Data, Geodetic Facility for the Advancement of Geoscience [data set], https://www.unavco.org/data/strain-seismic/bsm-data/bsm-data.html, last access: 20 June 2024.

Gladwin, M. T., Gwyther, R. L., Hart, R., Francis, M., and Johnston, M. J. S.: Borehole tensor strain measurements in California, J. Geophys. Res.-Sol. Ea., 92, 7981–7988, https://doi.org/10.1029/JB092iB08p07981, 1987.

Gualandi, A., Nichele, C., Serpelloni, E., Chiaraluce, L., Anderlini, L., Latorre, D., Belardinelli, M. E., and Avouac J.-P.: Aseismic deformation associated with an earthquake swarm in the northern Apennines (Italy), Geophys. Res. Lett., 44, 7706–7714, https://doi.org/10.1002/2017GL073687, 2017.

Hodgkinson, K., Langbein, J., Henderson, B., Mencin, D., and Borsa, A.: Tidal calibration of plate boundary observatory borehole strainmeters, J. Geophys. Res.-Sol. Ea., 118, 447–458, https://doi.org/10.1029/2012JB009651, 2013.

Hreinsdoìttir, S. and Bennett, R. A.: Active aseismic creep on the Alto Tiberina low-angle normal fault, Italy, Geology, 8, 683–686, https://doi.org/10.1130/G30194A.1, 2009.

International Continental Scientific Drilling Program: Public data and images, Project Acronym: STAR, State: Post Moratorium, Expedition ID: 5070, International Continental Scientific Drilling Program [data set], https://www.icdp-online.org/projects/by-continent/europe/star-italy/public-data, last access: 20 June 2024.

INGV RING Working Group: Rete integrata Nazionale GNSS, https://doi.org/10.13127/RING, 2016.

Italiano, F., Martinelli, G., Bonfanti, P., and Caracausi, A.: Long-term (1997–2007) geochemical monitoring of gases from the Umbria-Marche region, Tectonophysics, 476, 282–296, 2009.

Kato, A., Obara, K., Igarashi, T., Tsuruoka, H., Nakagawa, S., and Hirata, N.: Propagation of Slow Slip Leading Up to the 2011 Mw 9.0 Tohoku-Oki Earthquake, Science, 335, 6069, https://doi.org/10.1126/science.1215141, 2012.

Mandler, E., Pintori, F., Gualandi, A., Anderlini, L., Serpelloni, E., and Belardinelli, M. E.: Post-seismic deformation related to the 2016 Central Italy seismic sequence from GPS displacement time-series, J. Geophys. Res.-Sol. Ea., 126, e2021JB022200, https://doi.org/10.1029/2021JB022200, 2021.

Mirabella, F., Ciaccio, M. G., Barchi, M. R., and Merlini, S.: The Gubbio normal fault (Central Italy): geometry, displacement distribution and tectonic evolution, J. Struct. Geol., 26, 2233–2249, https://doi.org/10.1016/j.jsg.2004.06.009, 2004.

Mirabella, F., Brozzetti, F., Lupattelli, A., and Barchi, M. R.: Tectonic evolution of a low-angle extensional fault system from restored cross-sections in the Northern Apennines (Italy), Tectonics, 30, TC6002, https://doi.org/10.1029/2011TC002890, 2011.

Pauselli, C., Barchi, M. R., Federico, C., Magnani, M. B., and Minelli, G.: The crustal structure of the Northern Apennines (Central Italy): an insight by the CROP03 seismic line, Am. J. Sci., 306, 428–450, https://doi.org/10.2475/06.2006.02, 2006.

Pialli, G., Barchi, M., and Minelli G.: Results of the CROP03 deep seismic reflection profile, Mem. Soc. Geol. Ital., 52, 657 pp., Rome, ISSN 0375-9857, 1998.

Pierdominici, S. and Kück, J.: Borehole Geophysics, in: Encyclopedia of Geology, 2nd edn., Elsevier, 746–760, https://doi.org/10.1016/B978-0-08-102908-4.00126-0, 2021.

Rider, M. H. and Kennedy, M.: The Geological Interpretation of Well Logs, Rider-French, Scotland, 432 pp., ISBN 978-0-9541906-8-2, 2011.

Roeloffs, E.: Tidal calibration of Plate Boundary Observatory borehole strainmeters: Roles of vertical and shear coupling, J. Geophys. Res., 115, B06405, https://doi.org/10.1029/2009JB006407, 2010.

Rogie, J. D., Kerrick, D. M., Chiodini G., and Frondini, F.: Flux measurements of nonvolcanic CO_2 emission from some vents in central Italy, J. Geophys. Res., 105, 8435–844, 2000.

Rovida, A., Locati, M., Camassi, R., Lolli, B., Gasperini, P., and Antonucci, A.: Catalogo Parametrico dei Terremoti Italiani (CPTI15), versione 4.0, Istituto Nazionale di Geofisica e Vulcanologia (INGV) [data set], https://doi.org/10.13127/cpti/cpti15.4, 2022.

Ruiz, S., Metois, M., Fuenzalida, A., Ruiz, J., Leyton, F., Grandin, R., Vigny, C., Madariaga, R., and Campos, J.: Intense foreshocks and a slow slip event preceded the 2014 Iquique Mw 8.1 earthquake, Science, 345, 6201, https://doi.org/10.1126/science.1256074, 2014.

SAGE: NSF SAGE Facility FDSNWS dataselect Web Service Documentation, Seismological Facility for the Advancement of Geoscience, https://service.iris.edu/fdsnws/dataselect/1/, last access: 20 June 2024.

Serpelloni, E. and Cavaliere, A.: A Complementary GPS Survey Mode for Precise Crustal Deformation Monitoring: the Conegliano-Montello Active Thrust Semicontinuous GPS Network, Rapporti Tecnici INGV, no. 131, 44 pp., https://editoria.ingv.it/archivio_pdf/rapporti/130/pdf/rapporti_131.pdf (last access: 19 June 2024), 2010.

Serpelloni, E., Cavaliere, A., Martelli, L., Pintori, F., Anderlini, L., Borghi, A., Randazzo, D., Bruni, S., Devoti, R., Perfetti, P., and Cacciaguerra, S.: Surface Velocities and Strain-Rates in the Euro-Mediterranean Region From Massive GPS Data Processing, Front. Earth Sci., 10, 907897, https://doi.org/10.3389/feart.2022.907897, 2022.

Supino, M., Festa, G., and Zollo, A.: A probabilistic method for the estimation of earthquake source parameters from spectral inversion: application to the 2016–2017 Central Italy seismic sequence, Geophys. J. Int., 218, 988–1007, https://doi.org/10.1093/gji/ggz206, 2019.

Vadacca, L., Casarotti, E., Chiaraluce, L., and Cocco, M.: On the mechanical behaviour of a low-angle normal fault: the Alto Tiberina fault (Northern Apennines, Italy) system case study, Solid Earth, 7, 1537–1549, https://doi.org/10.5194/se-7-1537-2016, 2016.

Valoroso, L., Chiaraluce, L., Di Stefano, R., and Monachesi, G.: Mixed-mode slip behavior of the Altotiberina low-angle normal fault system (Northern Apennines, Italy) through high-resolution earthquake locations and repeating events, J. Geophys. Res.-Sol. Ea., 122, 10220–10240, https://doi.org/10.1002/2017JB014607, 2017.

Veedu, D. M. and Barbot, S.: The Parkfield tremors reveal slow and fast ruptures on the same asperity, Nature, 532, 7599, https://doi.org/10.1038/nature17190, 2016.

Ventura Bordenca, C.: Noble gas geochemistry in seismic (Umbria, Italy) and volcanic (Grand Comore Island, Indian Ocean) regions: New methodologies and implications, PhD thesis Università di Palermo, Italy, https://hdl.handle.net/10447/399971 (last access: 24 June 2024), 2020.

Visini, F., Meletti, C., Rovida, A., D'Amico, V., Pace, B., and Pondrelli, S.: An updated area-source seismogenic model (MA4) for seismic hazard of Italy, Nat. Hazards Earth Syst. Sci., 22, 2807–2827, https://doi.org/10.5194/nhess-22-2807-2022, 2022.

Vuan, A., Brondi, P., Sugan, M., Chiaraluce, L., Di Stefano, R., and Michele, M.: Intermittent slip along the Alto Tiberina low-angle normal fault in central Italy, Geophys. Res. Lett., 47, e2020GL08903, https://doi.org/10.1029/2020GL089039, 2020.

Wernicke, B.: Low-angle normal faults and seismicity: A review, J. Geophys. Res., 100, 20159–20174, https://doi.org/10.1029/95JB01911, 1995.

Zemanek, J., Caldwell, R. L., Glenn, E. E., Jr Holcomb, S. V., Nortom, L. F., and Siraus, A. D. J.: The borehole televiewer – A new logging concept for fracture location and other types of borehole inspection, J. Petrol. Technol., 264, 762–774, https://doi.org/10.2118/2402-pa, 1969.

Sci. Dril., 33, 191–206, 2024
https://doi.org/10.5194/sd-33-191-2024

Scientific Drilling
Open Access

Shaped and filled by the Rhine Glacier: the overdeepened Tannwald Basin in southwestern Germany

Bennet Schuster[1,2,3], Lukas Gegg[1], Sebastian Schaller[2,3], Marius W. Buechi[2,3], David C. Tanner[4], Ulrike Wielandt-Schuster[5], Flavio S. Anselmetti[2,3], and Frank Preusser[1]

[1]Institute of Earth and Environmental Sciences, University of Freiburg, Albertstr. 23b, 79104 Freiburg, Germany
[2]Institute of Geological Sciences, University of Bern, Baltzerstr. 1+3, 3012 Bern, Switzerland
[3]Oeschger Centre for Climate Change Research, University of Bern, Hochschulstr. 4, 3012 Bern, Switzerland
[4]Leibniz Institute for Applied Geophysics, Stilleweg 2, 30655 Hannover, Germany
[5]Baden-Württemberg State Office for Geology, Mineral Resources, and Mining, Albertstraße 5, 79104 Freiburg, Germany

Correspondence: Bennet Schuster (bennet.schuster@geologie.uni-freiburg.de)

Received: 21 December 2023 – Revised: 5 May 2024 – Accepted: 15 May 2024 – Published: 4 July 2024

Abstract. The Alpine region was shaped by repeated glaciations during the Quaternary, which led to the formation of overdeepened valleys and basins. These features today, hidden below the present-day land surface, host multiple stacked and nested glacial sequences and offer valuable insight into the environmental history and geomorphological evolution of the region. The project Drilling Overdeepened Alpine Valleys (DOVE) of the International Continental Scientific Drilling Program (ICDP) is dedicated to investigating such overdeepened structures around the Alps. Within DOVE, we here focus on the Tannwald Basin in southern Germany. Situated distally within the area formerly occupied by the Rhine Glacier piedmont lobe; it was shaped by multiple glaciations, yet it is located outside the Last Glacial Maximum (LGM) ice extent. Previous seismic imaging and the presence of interglacial pollen sequences indicate a multi-phase infill history. The complex sedimentary architecture observed in a newly drilled core allows for comparison with seismic data and lithological evidence from other sites. On the basis of a lithofacies model that introduces 17 lithotypes, we propose that the basin fill is composed of three lithostratigraphic units that reflect the glacial history of the basin. After the erosion of the Tannwald Basin, a cold-climate, stacked basin-infill sequence recorded sedimentation of two glacial advances, before it was covered by LGM outwash. The sedimentary record includes an extensive basal glacial shear zone with deformed bedrock and several overlying diamict horizons. Further upcore, deformation structures underscore the role of gravitational processes as well as profound glaciotectonics, deforming the sediment deep within the subsurface. While the sedimentary record indicates a rather rapid infill of the depression, further age constraints and detailed investigations of ice-contact sediments will clarify open questions regarding the temporal classification of the deposits.

1 Introduction

The northern Alpine foreland witnessed repeated glacial cycles during the Quaternary period, comprising glacier expansion and decay (e.g., Doppler et al., 2011; Ellwanger et al., 2011; Preusser et al., 2011). By eroding and redepositing large rock and sediment masses, glaciers created landscape features such as polished bedrock surfaces, high valley flanks, moraine ridges, and outwash terraces. Moreover, large-scale features of this dynamic landscape include overdeepened valleys and basins that are hidden below the present-day surface in the Alpine valleys and the Alpine foreland (Preusser et al., 2010; Gegg and Preusser, 2023). These overdeepened structures mainly represent deep and elongated troughs eroded by glaciers into the bedrock below

the fluvial base level (Cook and Swift, 2012). The formation process of overdeepening is under debate but presumably is a combination of ice-contact processes (i.e., abrasion and plucking) and pressurized subglacial (melt)water erosion (Huuse and Lykke-Andersen, 2000; Alley et al., 2019). Substantial overdeepening is not limited to topographically confined, inner-Alpine valleys with steep gradients but is also found in the lower-relief Alpine foreland (Preusser et al., 2010; Ellwanger et al., 2011; Ellwanger, 2015). An increased availability of basal water is believed to have enhanced the subglacial erosional potential far into the Alpine foreland, thus becoming a driving force for erosion (Alley et al., 1997; Dürst Stucki et al., 2010; Dürst Stucki and Schlunegger, 2013; Gegg et al., 2021).

Foreland overdeepenings offer large accommodation space upon deglaciation, capable of hosting multiple stacked and nested glacial sequences within subglacial to proglacial sediment successions, as well as post-glacial deposits (Schlüchter, 1989; Preusser et al., 2005; Anselmetti et al., 2010; Dehnert et al., 2012; Buechi et al., 2018). These formations serve as valuable archives that provide insight into the timing and extent, as well as the subglacial conditions and processes, of past glacier advances in the northern Alpine foreland (Preusser et al., 2010; Ellwanger et al., 2011; Gegg and Preusser, 2023). To unravel the complex glacial dynamics that produced overdeepened landforms and their sedimentary fillings, a combination of coring and geophysical analysis has proven indispensable (e.g., Dehnert et al., 2012; Pomper et al., 2017; Buechi et al., 2018; Gegg et al., 2021). Recent studies have also benefited significantly from advances in dating techniques, such as optically stimulated luminescence (OSL) dating, revolutionizing our ability to precisely determine the timing of glacial advances (e.g., Preusser et al., 2005; Dehnert et al., 2012; Fiebig et al., 2014; Buechi et al., 2018; Schwenk et al., 2022).

Unfortunately, such scientific investigations of sedimentary successions are still scarce, while records of commercial drillings, usually with cuttings only, often lack the necessary detail for comprehensive sedimentological interpretation and geochronological constrains. To address this gap, the pan-Alpine project Drilling Overdeepened Alpine Valleys (DOVE) was initiated, co-funded by the International Continental Scientific Drilling Program (ICDP). DOVE aims to conduct detailed investigations at several complementary sites along the northern (and potentially southern) Alpine foreland (Anselmetti et al., 2022). The primary objective of DOVE is to determine the timing and extent of past Alpine glaciations and to contribute to broader discussions on climate teleconnections and synchronization of glaciations across the Northern Hemisphere. This study aims to contribute data to evaluate patterns in glacial–interglacial paleoclimates and landscape evolution from a key overdeepening of the Alpine foreland: the Tannwald Basin. This basin stands out in several distinct aspects, leading to its identification as a high-potential location for the DOVE project (Anselmetti et al., 2022). Situated in the region that formerly occupied the Rhine Glacier piedmont lobe, it has been repeatedly covered by ice; however, this was without experiencing the direct impact of the Last Glacial Maximum (LGM) (Ellwanger et al., 1995, 2011; Ellwanger, 2015).

2 Geological setting

2.1 Lake Constance amphitheater

The Rhine piedmont–glacial landscape, which stretches from the northern Alpine front to the Swabian Jura, bears the distinct imprint of Quaternary erosion and deposition processes. These dynamic geological forces have sculpted the terrain into an amphitheater-like topography within the Alpine foreland Molasse Basin (Ellwanger et al., 1995, 2011; Lämmermann-Barthel et al., 2003), with Lake Constance at the heart of it. While different Quaternary stratigraphic systems are in use in the countries that border Lake Constance (Doppler et al., 2011; Preusser et al., 2011), a stratigraphic framework for the Lake Constance amphitheater has been introduced (Fiebig, 1995; Ellwanger et al., 1995, 2011; Geyer et al., 2011). This approach comprises four regional unconformity-bounded units that represent the three distinct generations of basin formation: the Steinental Fm., Dietmanns Fm., Illmensee Fm., and Hasenweiler Fm. The formation boundaries of the youngest three correlate with pleniglacial conditions during the Hosskirch, Riss (both Middle Pleistocene), and Würm (Late Pleistocene) glaciations, respectively (Ellwanger et al., 2011; Fig. 1). These lithostratigraphic investigations, in addition to the morphostratigraphic concept, have furthermore increased knowledge of changes in the erosion pattern and the identification of the reorientation of the branch glacial basins over time. While alignment of branch basins was originally northward towards the Danube, the direction later shifted into a westward direction towards the "Hochrhein" Rhine. This change in glacial direction also modified the fluvial drainage network orientation, i.e., the Alpine Rhine was connected to the lower parts of the Rhine drainage system (Ellwanger et al., 1995, 2011).

2.2 Previous drillings and geophysical surveys in the Tannwald Basin

Within the Lake Constance amphitheater, some overdeepened basins have been influenced by multiple glaciations (Ellwanger et al., 2011). One notable example of an overdeepened structure that has witnessed multiple glaciations is the Tannwald Basin, a distal overdeepened branch basin located ca. 45 km north of Lake Constance. It became of significant importance when pollen indicative of the Holsteinian Interglacial, the equivalent of Marine Isotope Stage (MIS) 11, were identified in a fine-grained lacustrine sediment succession of a research drilling in 1993/1994 ("Schneidermartin" drilling; Ellwanger et al., 1995, 2011;

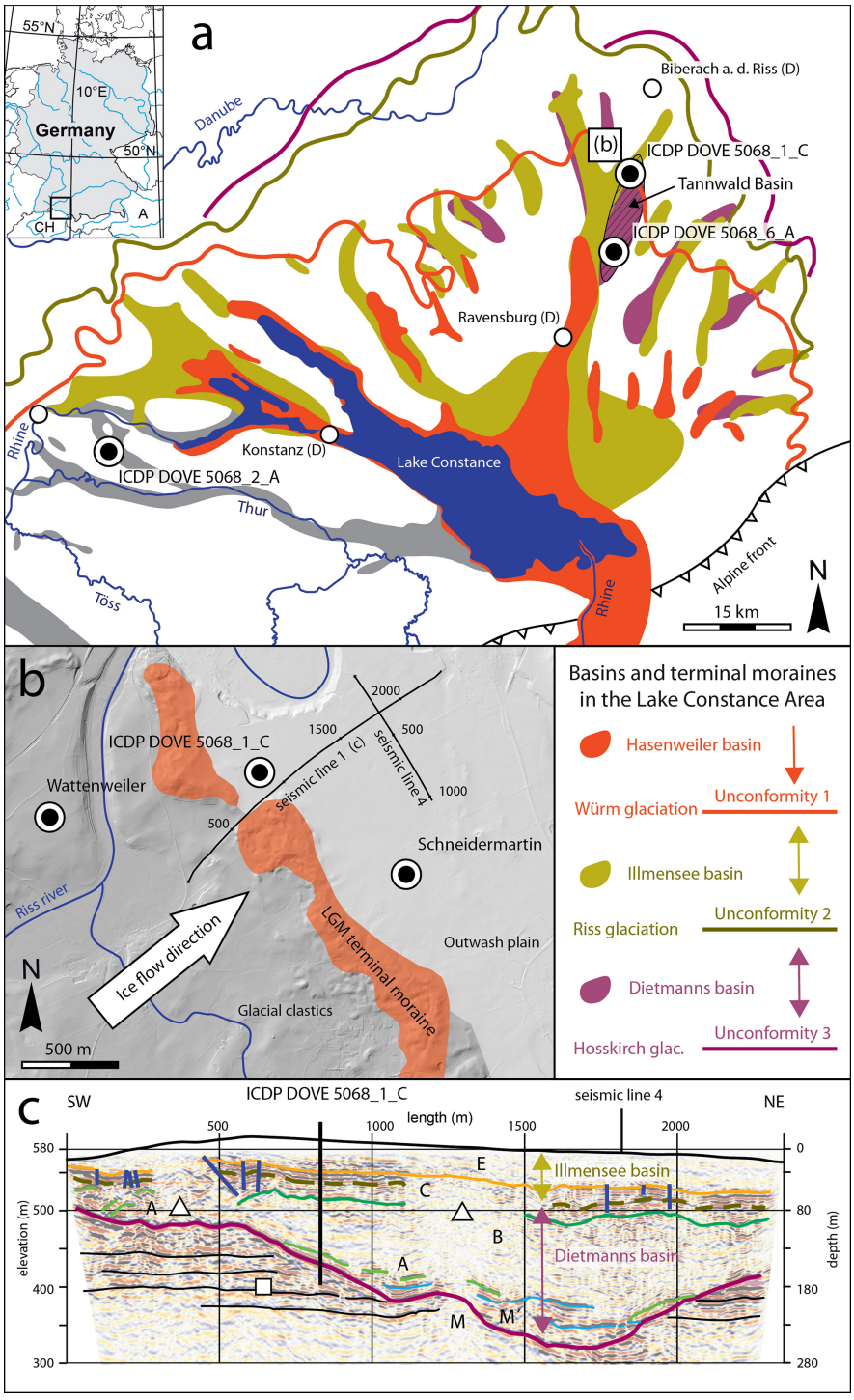

Figure 1. **(a)** Map illustrating the Quaternary overdeepened structures within the German (differentiated) and Swiss (undifferentiated) Lake Constance area of the Rhine glacial landscape in the northern Alpine foreland. The location of the Tannwald Basin is indicated by a black area with hatching. Shown are the maximum ice advances corresponding to the respective glaciations (regional unconformities 1–3); modified after Graf (2009) and Ellwanger et al. (2011). **(b)** Locations of seismic survey and new drill site (ICDP DOVE 5068_1_C) with respect to the outermost terminal moraine of the last glaciation (equivalent to unconformity 2, modified after Burschil et al., 2018). **(c)** Seismic section displaying interpreted geological structures based on the stratigraphy of the Schneidermartin core. Seismic facies abbreviations: M (purple lines) represents molasse, M′ (blue lines) represents slabs of allochthonous molasse, A (light green lines) represents waterlain till, B (dark green lines) represents fine-grained deposits, C (lines of same color as unconformity 2) represents till and sand units, E (orange lines) represents fluvial sand and gravel. Blue vertical line: faults with offsets > 2 m. White square: foresets. White triangle: seismic transparent regions. Modified after Burschil et al. (2018).

Hahne et al., 2012). The Schneidermartin drilling is located just outside the terminal moraine ridge of the LGM (Fig. 1b) and reached the Molasse bedrock at the base of the basin, at 209 m depth. Similar pollen assemblages were identified in the Wattenweiler drilling, situated ∼3500 m northwest of the Schneidermartin drilling within the LGM terminal moraine (Hahne et al., 2012; Ellwanger, 2015). The pollen findings were used to assign the Tannwald Basin to the pre-Holsteinian (pre-MIS 11) advance of the Hosskirch glaciation (Ellwanger et al., 2011). A detailed revision of the sedimentary succession of the Schneidermartin core projected the erosional unconformity 2 of the Riss glaciation (MIS 6) to a depth of 29 m (Ellwanger, 2015; Burschil et al., 2018). Consequently, the Tannwald Basin was interpreted to contain sedimentary deposits representing two generations of basins (Dietmanns Formation, Illmensee Formation) and two glacial cycles (Riss, Hosskirch).

The infill of the Tannwald Basin at the Schneidermartin drilling (Ellwanger et al., 2011) comprises thin layers of sheared fine-grained sediments above the undisturbed Molasse bedrock. These are overlain by a 13 m thick glacially sheared block of Molasse, containing several shear horizons. Based on seismic data, this block has been interpreted as an allochthonous bedrock slab (Burschil et al., 2018). It is overlain by gravel layers with Molasse components, followed by diamictic fines, which were interpreted to represent ice-proximal sediments of the Hosskirch glacial period. Above, a succession of delta bottomsets hosts the previously mentioned pollen assemblages assigned to the Holstein Interglacial. Upcore, these sediments transition into foresets that are capped by a till layer, exhibiting stratification and grading, evolving into a matrix-supported diamict and fines. This layer is separated from topmost coarse gravels, which represent meltwater deposits of the Würm glaciation, by an unconformity.

Five P-wave seismic reflection profiles were acquired in the northeastern section of the Tannwald Basin during 2014/2015 (Burschil et al., 2018). Based on the seismic data and the Schneidermartin drill core description, Burschil et al. (2018) identified six seismic facies and traced them across the five profiles (Fig. 1c). Furthermore, the seismic campaigns revealed a 50 m deep and several 100 m wide depression inside the basin, marking its deepest parts. Several faults with offsets >2 m were identified within the upper 100 m of the basin fill (Burschil et al., 2018). A complementary acquired 3D multicomponent S-wave dataset allowed us to visualize more reflections and lead us to the identification of glacial tectonics, including additional faults and shallow glaciotectonic cuspate–lobate folds (Buness et al., 2020, 2022).

3 Methods

3.1 Drilling operations

Drill site ICDP DOVE 5068_1, located on the western flank of the overdeepened Tannwald Basin, was the first of the DOVE sites to be drilled in April 2021 (Fig. 1c; Anselmetti et al., 2022). To facilitate correlation, it was strategically positioned near the seismic profiles and the Schneidermartin drill site (Fig. 1b). Besides the core drilling ICDP 5068_1_C, two flush drillings (ICDP 5068_1_A and -B), arranged in a triangle with side lengths of 28 m, were drilled to allow for a later cross-hole seismic campaign. The primary challenges encountered during the drilling of the Tannwald Basin were caused by large variations in grain size and the unconsolidated nature of the sediments. To address these challenges, the drilling team adopted a combined approach, utilizing percussion coring techniques down to a depth of 83 m, below which a wireline rotational core system was used that reached the final depth of 166.25 m. For a comprehensive overview of the drilling and logging operations, core-quality assessment, and technical parameters (such as borehole geometry and casing deployment), see the DOVE operational report (DOVE-Phase 1 Scientific Team, 2023a).

The core drilling ICDP DOVE 5068_1_C successfully retrieved 200 individual core sections, each stored within opaque PVC liners with an inner diameter of 104 mm. The overall recovery rate was 95 %, some core loss occurred primarily in unconsolidated coarse gravels and cobbles above 39 m depth. Additionally, the unconsolidated nature of the sediments led to the mobilization and partial loss of sandy and fine sediments, for example at depths between 70 and 115 m. Both at the drill site and university storage facilities, the cores were refrigerated at 3–5 °C.

3.2 Core logging and sampling

The core workflow defined in the DOVE project follows mostly the guidelines developed during the Quaternary drilling campaign of the National Cooperative for the Disposal of Radioactive Waste of Switzerland (e.g., Schuster et al., 2020), which has been successfully applied in numerous drilling campaigns within the Swiss Alpine foreland (e.g., Gegg et al., 2021; Schaller et al., 2023). We conducted non-destructive, whole-core scanning to measure wet bulk density and magnetic susceptibility, using a multi-sensor core logger (MSCL; Geotek Ltd.) at 5 mm resolution. Any disturbed segments encountered during drilling or described in the lithological analysis were later manually excluded. A baseline correction was applied to the magnetic susceptibility data. Subsequently, the cores were split into archive and working halves (A-half and W-half) under subdued orange light to facilitate luminescence dating at a later stage.

The initial core description (ICD) was carried out on the A-half with a primary focus on specific sedimentological ob-

servations, including grain size, character of contacts (e.g., erosional or deformed), clast characteristics (e.g., shape and roundness), clast-surface features (e.g., striations and calcite precipitations), and sedimentary structures (e.g., cross-bedding, lamination, and grading). High-resolution line-scan images were generated with the Geotek scanner to support the ICD. Additionally, we conducted minimally invasive measurements using a vane-shear tester to systematically estimate the undrained shear strength, where the sediment was suitable (i.e., dominantly sand or finer). We selected specific cores, primarily those suspected to contain ice-contact sediments, for X-ray computed tomography (CT) scanning at the Institute of Forensic Medicine, University of Bern. Subsequently, observations from geophysical logs, ICD, and CT scans were integrated to define lithotypes, following Eyles et al. (1983) and Schaller et al. (2023). On the basis of the sedimentary characteristics and context, the lithotypes were grouped into seven lithofacies assemblages (LFAs). These LFAs then serve as building blocks to establish three lithostratigraphic units, which in turn constitute the foundation of the geological interpretation.

The W-half was used for destructive sampling under subdued orange light, while all cores were otherwise stored in lightproof tubular film. Geochemical samples were taken immediately upon opening the cores at a 1 m resolution. These samples were also used to determine water content. Subsequently, the fine fraction (< 63 µm) of the geochemical samples was analyzed for their carbon content, including total organic carbon (TOC) and total inorganic carbon (TIC), using a Thermo Scientific Flash 2000 Smart (Thermo Fisher, Waltham, MA, USA). The concentrations of carbonates and organic matter (weight percent) were calculated by multiplying TIC and TOC values by the stoichiometric factors of 8.3 and 1.8, respectively (Meyers and Teranes, 2001). Potential downcore variations in carbonate phases, such as the dolomite/calcite ratio, were, however, not accounted for. For further information on the curated samples, analysis, and data, see the operational dataset (DOVE-Phase 1 Scientific Team, 2023b) and explanatory remarks (DOVE-Phase 1 Scientific Team, 2023c).

4 Identification and interpretation of lithotypes and lithofacies associations

Seventeen lithotypes (facies codes in italic) were identified in the ICDP DOVE 5068_1_C core (Fig. 2), 11 of these follow those introduced by Schaller et al. (2023), while 6 lithotypes are unique to the Tannwald drill core. These lithotypes are presented as core photos (Figs. 3 and 4) and detailed descriptions in the Appendix (Table A1). The broad range of lithofacies encountered in the ICDP DOVE 5068_1_C core was reduced by grouping commonly associated lithofacies into seven lithofacies associations (LFAs; Fig. 2 and Table 1).

The bottom of the ICDP DOVE 5068_1_C core consists of moderately consolidated, partly friable sand- and siltstones, and marls, all representing Molasse bedrock (*B*, Fig. 3a). The Molasse was identified as the Upper Marine Molasse (tOM according to the nomenclature of Ellwanger, 2015; Bachmann et al., 1987) as opposed to the interpretation of the seismic data (Upper Freshwater Molasse; Burschil et al., 2018). A sharp, planar bedrock contact at 155.90 m depth marks the erosional base of the Tannwald overdeepening in the core.

LFA1 is located directly above the bedrock and predominantly comprises both unconsolidated (Fig. 3b) and consolidated (Fig. 3c) Molasse bedrock rafts (*Mgt*). Glauconite grains identify the bluish sand of the unconsolidated Molasse rafts as Upper Marine Molasse (Fischer, 1987). The consolidated Molasse rafts show in situ crushing and brecciation. The Molasse bedrock rafts are intercalated and locally sheared into stratified diamicts (*Dms*). *Dms* of LFA1 contains glacially striated clasts of Alpine lithologies and substantial amounts of friable bedrock fragments. LFA1 is defined by low density ($2\ \mathrm{g\ cm^{-3}}$) and shear-strength values below 50 kPa of the unconsolidated Molasse bedrock rafts. The deformation structures and weak mechanical properties are interpreted as evidence of the shearing of subglacial till and bedrock rafts (Benn and Evans, 1996; Hiemstra and van der Meer, 1997; Buechi et al., 2017). Carbonate content reaches below 20 wt %, which further reflects the incorporation of local Molasse sediments into LFA1. Therefore, LFA1 is classified as a Type B glaciotectonite (Benn and Evans, 1996; Evans et al., 2006).

LFA2 comprises brownish-colored, matrix-supported, massive, and stratified diamicts (*Dmm, Dms*) associated with well-sorted, fining-upward sediments that contain frequent dropstones (*Flr(d), Fl(d), Sl*). The stratified fines located between the basal diamicts do not exhibit macroscopic deformation features at the core scale. The number of dropstones generally increases near the diamicts, indicating the presence of floating ice (Bennett et al., 1996; Eyles et al., 1983). Both dropstones and diamicts frequently contain clasts with glacial striations, providing further evidence for the proximity of the glacier. Even though the organic matter content is very low (mostly < 0.5 wt %) throughout the core, it abruptly increases from 0.1 to 0.3 wt % at the emplacement of the matrix-supported diamicts (*Dmm*; Fig. 3d) of LFA2. Furthermore, *Dmm* exhibits both high values of density ($2.4\ \mathrm{g\ cm^{-3}}$) and shear strength (200–270 kPa), with low water content (10 %–13 %). A similar shift of shear-strength values measured in drill cores from a glacial overdeepening has previously been interpreted as the result of temporary ice loading (Anselmetti et al., 2010; Dehnert et al., 2012). Alongside frequent glacial striations, this observation likely indicates subglacial lodgement processes. Consequently, *Dmm* is interpreted as subglacial till (Evans et al., 2006), suggesting that LFA2 was emplaced subglacially or submarginally with intermittent glacier–bed coupling. The association with stratified fines (*Flr(d), Fl(d)*) and diamicts (*Dms*) further sug-

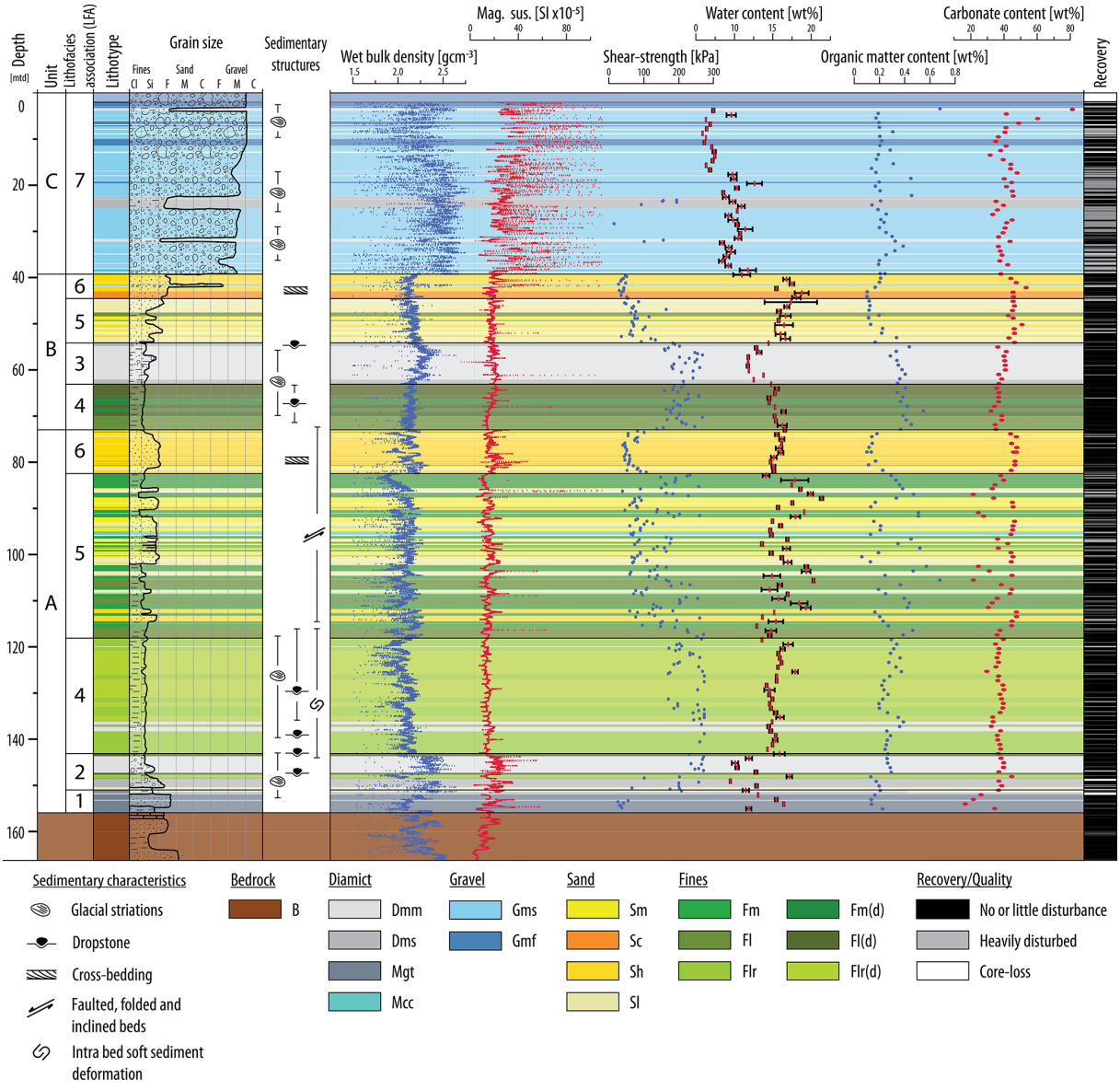

Figure 2. Summary profile of the ICDP DOVE 5068_1_C core with sedimentary characteristics and acquired petrophysical data.

gest deposition during ice–bed decoupling in confined subglacial cavities or infilling of accommodation space created under a floating glacier tongue (Ravier et al., 2014; Buechi et al., 2017).

LFA3 consists of fine-grained *Dmm* deposits of dark grey color with frequently occurring glacially striated clasts (Figs. 2, 3e). The *Dmm* deposits show increasing density upcore (peak at 56 m; 2.4 g cm^{-3}), which reflects a gradual increase in clast size upcore (Fig. 2). Upcore-increasing shear strength (peak at 57 m; 270 kPa) additionally indicates increasing compaction. Water content reaches its lowest values of 14 % at 58 m. Thus, LFA3 is interpreted to be similar to LFA2 as a mud-dominated subglacial till (Evans et al., 2006). The fine-grained character and dark grey color are attributed to the predominant incorporation of underlying glaciolacustrine deposits.

LFA4 consists of fine-grained deposits with gradual laminations and beds, often containing dropstones (*Flr, Flr(d), Fl, Fl(d)*; Fig. 4d, g, c, f) and rarely interbedded with soft, dark-colored, and fine-grained diamicts (*Dmm*, Fig. 3e). Frequent glacial striations on both dropstones and diamicts suggest the proximity of a glacier. The diamicts show low density values (2.2 g cm^{-3}) and relatively low shear strength (compared to the overlying fines) and are interpreted as subaqueous debris flows with a proglacial sediment source (Eyles et al., 1983; Mulder and Alexander, 2001). LFA4 is interpreted as deposits from an ice-contact proglacial lake. The fines of LFA4 at around 70 m depth of the ICDP DOVE

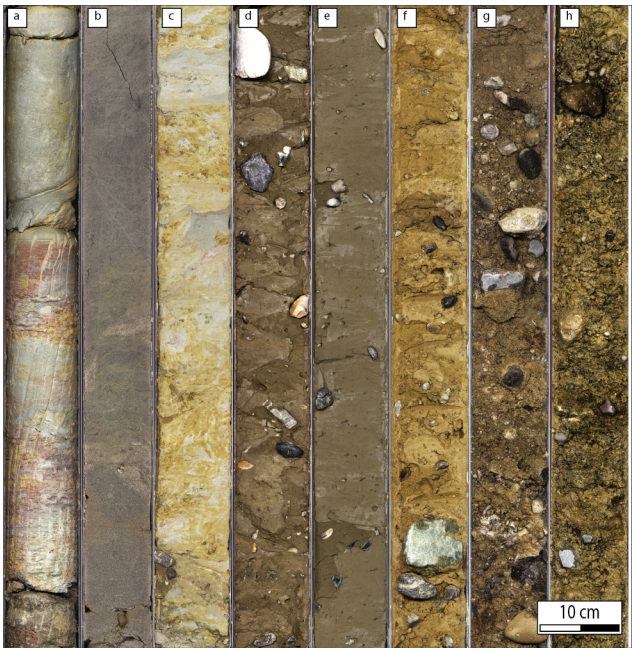

Figure 3. Line-scan images of cores (1 m sections), showing representative lithotypes. **(a)** *B*: interbedded mottled siltstone and sandstone of the Molasse bedrock (163–164 m). **(b)** *Mgt*: unconsolidated and deformed (faulted) medium sand of the Molasse bedrock (153–154 m). **(c)** *Mgt*: consolidated and deformed Molasse siltstones and sandstones associated with small amounts of diamict (mélange type) (152–153 m). **(d)** *Dmm*: highly consolidated, brownish-colored diamict with both Alpine and Molasse clasts (144–145 m). **(e)** *Dmm*: soft, fine-grained, dark-colored diamict (57–58 m). **(f)** *Dms*: soft, light-colored diamict (23–24 m). **(g)** *Gms*: moderately sorted gravel with sandy matrix (10–11 m). **(h)** Gmf: poorly sorted gravel with silty and sandy matrix, likely partly washed out during coring (10–11 m).

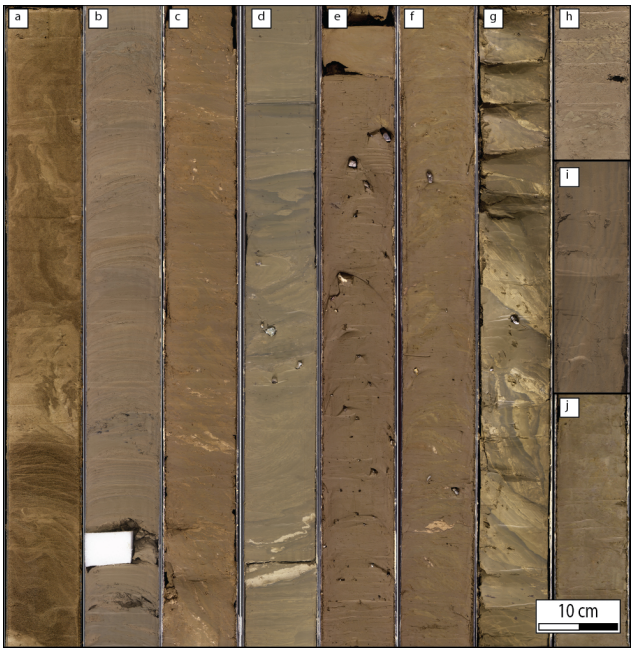

Figure 4. Line-scan images of cores (1 and 0.5 m sections) showcasing representative lithotypes. **(a)** *Sh/Sc*: partly deformed (homogenized), brownish-colored, (cross-)bedded fine to medium sand (78–79 m). **(b)** *Sh/Sl*: dark-colored, fine sand interbedded with dark silt and clay laminae (53–54 m). **(c)** *Fl*: mottled laminations in clay and silt (lighter greenish and darker grey shades) with bright sand laminae and sand lenses (106–107 m). **(d)** *Flr*: deformed silt and clay rhythmites of varying thicknesses (126–127 m). **(e)** *Fm(d)*: massive fines with dropstones (66–67 m). **(f)** *Fl(d)*: mottled lamination in clay and silt with sandy laminae, soft sediment deformation and dropstones (64–65 m). **(g)** *Flr(d)*: highly consolidated rhythmites with dropstones and strong soft sediment deformation (118–119 m). **(h)** *Mcc*: fine to medium sand with horizontally aligned silt and clay lenses (107–107.5 m). **(i)** *Sl*: oversteepened beds of laminated fine sand (94–94.5 m). **(j)** *Fm*: massive fines (84.5–85 m).

5068_1_C core show a slight upcore-increasing trend in density and shear strength (if a trend is visible at all), while water content decreases upcore. Increasing amounts of dropstones upcore illustrate the shift from more distal, well-sorted clay and silt facies to a proximal, dropstone-dominated facies with frequent glacial striations. This typical upward succession can be interpreted, similarly to LFA2 and LFA3, as evidence of glacial approaching and overriding. However, the trend in density and shear strength might alternatively result from an upcore decrease in clay content. Multiple meter-thick beds of fine-grained lake sediments (*Flr(d)*) at a depth of 119–115 m show similar petrophysical characteristics and are moreover above-average consolidated (Fig. 4g). This also suggests compaction from ice contact, indicating a glacial advance (Anselmetti et al., 2010; O'Regan, 2010; Dehnert et al., 2012). The fines in the lower part of the core locally exhibit soft-sediment deformation along several horizons, ranging from centimeter-thick slumps to meter-thick deformed sections (Fig. 4d). Deformation mechanisms include both faulting and folding and, within water-saturated fines on a depositional slope in subglacial to proglacial beds, likely indicate gravitational slumping (Visser et al., 1984).

LFA5 is characterized by intercalated meter-thick successions of stratified and massive fine-grained deposits (*Fm, Fl*; LFA5.1) and greyish-colored, partly laminated sands (*Sm, Sl*; LFA5.2). The intercalation results in varying density values and a significant scatter in shear-strength values in beds of cohesive fines and uncohesive sands. Carbonate content varies between 20 wt % and 40 wt %, indicating varying sediment sources (Alpine and Molasse origin). Post-sedimentary deformation occurs throughout LFA5 is in the form of folding, faulting, and inclined bedding. *Fm* and *Fl* are interpreted as the product of turbidity currents and suspension settling in an ice-proximal lake (Eyles et al., 1993; Smith and Ashley, 1985), while the sand-dominated facies is attributed to density flows (Mulder and Alexander, 2001) and subaqueous channel fills in a higher energy setting. The repeated shifts between LFA5.1 and LFA5.2 are attributed to

transitions to a more proximal or laterally shifted deltaic setting (Dehnert et al., 2012). The dark grey laminations in the sand beds (Fig. 4b) suggest that this process occurs not only on the meter scale but also on the centimeter scale. The post-sedimentary deformation features along multiple failure surfaces, which are likely the result of reduced slope stability during interglacial periods. A similar phenomenon of slope instability that resulted from geomorphological changes during rapid deglaciation has been documented by Fernandes et al. (2020) in the Central Pyrenees. Furthermore, LFA5 contains horizontally aligned, decimeter-thick beds of mud-clasts, which are interpreted as reworked fine lacustrine sediments eroded by subaquatic mass movements (Li et al., 2017). These beds were also identified as mud-clast conglomerates (*Mcc*; Fig. 4h) in the ICDP_5068_2 core (Schaller et al., 2023).

LFA6 is characterized by well-sorted, massive, and stratified sands (*Sh, Sc*) of brownish color that are weakly consolidated and rarely interbedded with moderately sorted gravel (*Gms*; Fig. 3e). LFA6 is strongly deformed in the lower part of the core, mainly through steep to near-vertical bedding (Fig. 2). These sands and gravels are interpreted as glaciodeltaic deposits, formed by underflows from the retreating glacier front during deglaciation (Buechi et al., 2018). This interpretation is supported by a change in color (Fig. 4a), indicating a shift in the primary sediment source of basinal fines.

LFA7 consists of moderately sorted gravels with sand-dominated matrix (*Gms*) and poorly sorted gravels with predominantly fine-grained matrix (*Gmf*; both LFA7.1) with intercalated soft matrix-supported light-colored diamicts (*Dmm, Dms*; LFA7.2). Both the gravels and the diamicts frequently show glacially striated clasts, which indicate a glacier-proximal depositional environment. Thus, LFA7 is interpreted as proglacial fluvial and glaciofluvial sediments, representing alternating meltwater outwash and subaerial debris flows, possibly sourced in ice-marginal and supraglacial sediments (e.g., Lawson, 1982; Buechi et al., 2018). *Dmm* and *Dms* exhibit comparatively low shear-strength values that support interpretation of a non-subglacial origin (< 200 kPa). Thus, they partly exhibit characteristics of subglacial till (massive nature, glacial striations), but they lack consolidation (low density and shear strength). Thus, diamicts of LFA7 are interpreted as short-distance redeposition by slumping of diamicts, originally deposited at the LGM glacier front on the inclined outwash plain (Fig. 1b; Ellwanger et al., 2011). *Gmf* likely represents sedimentation in a more chaotic setting, possibly during a more proximal glacier position or during floods (Eyles et al., 1983; Siegenthaler and Huggenberger, 1993). The upcore-increasing occurrence of *Gmf* correlates with an increase in carbonate content and occurrence of cobble-sized clasts, reflected in an increase in density (Fig. 2), which might indicate an overall shift to a more ice-marginal position in a fluvial and glaciofluvial proglacial outwash plain.

5 Discussion

The lithostratigraphic and petrophysical observations of the sedimentary infill in the Tannwald Basin are integrated with existing seismic data (Burschil et al., 2018; Buness et al., 2020, 2022), morphostratigraphic data, and previously published drill-core data (Ellwanger et al., 2011; Hahne et al., 2012). To facilitate this integration, the Quaternary sedimentary infill was categorized into three lithostratigraphic units: A, B, and C (Fig. 2). These units represent distinct episodes of basin infill separated by stratigraphic breaks (Figs. 5 and 6).

The facies evolution in Unit A is interpreted as basin erosion and subglacial traction processes (LFA1 and LFA2; Fig. 5a), followed by ice-proximal sedimentation in a proglacial lake (LFA4; Fig. 5b), and eventually a glacier retreat leading to the formation of a stacked delta succession (LFA5 and LFA6; Fig. 5c). The bedrock rafts of LFA1 can be correlated with mobilization and transport of much larger (> 10 m) rafts reported from the Schneidermartin core (Ellwanger et al., 2011; Hahne et al., 2012) and seismic facies M′ of the seismic survey at deeper positions of the Tannwald Basin (Burschil et al., 2018; Fig. 6). The overlying LFA2 was probably still emplaced in a subglacial to submarginal setting, as indicated by the intimate association of subglacial traction till with sorted fines and stratified diamicts. The interbedding is likely to represent first a coupled and then a decoupled ice–bed interface, as a result of an oscillation of the ice-margin position, intermittent floating of the glacier tongue, or opening and closing of more confined subglacial cavities (Fig. 5a). LFA2 correlates with seismic facies A on the western slopes of the Tannwald Basin (Burschil et al., 2018; Fig. 6). The overlying LFA4 represents typical fine-grained, dropstone-bearing basin fill observed in ice-contact proglacial lake, representing turbidity flows on a subaqueous fan (Fig. 5b). They can be correlated with finer basin-floor bottomsets of the Schneidermartin drill core 1 km SW further away and seismic facies B (Ellwanger et al., 2011; Burschil et al., 2018; Fig. 6). The organic matter content does not indicate interglacial sediments, suggesting the filling of the overdeepening under still periglacial conditions, which is a common phenomenon (Gegg and Preusser, 2023). Individual beds of above-average consolidated fines at the top of LFA4 might result from compaction by ice contact, indicating glacial advance (Anselmetti et al., 2010; O'Regan, 2010; Dehnert et al., 2012). However, the role the glacier played within this lake remains an open question, especially because of the lack of coarse-grained deposits that are expected at the front of a moving glacier. One possible explanation might be the reported inability of such re-advances to carve basins into fine-grained, soft lake sediments with low permeability (e.g., Menzies, 1989). The onset of delta propagation might be associated with continuing and larger-scale gravitational slumping on the depositional slopes of the basin, leading to faulted and folded sediment beds. This correlates with the

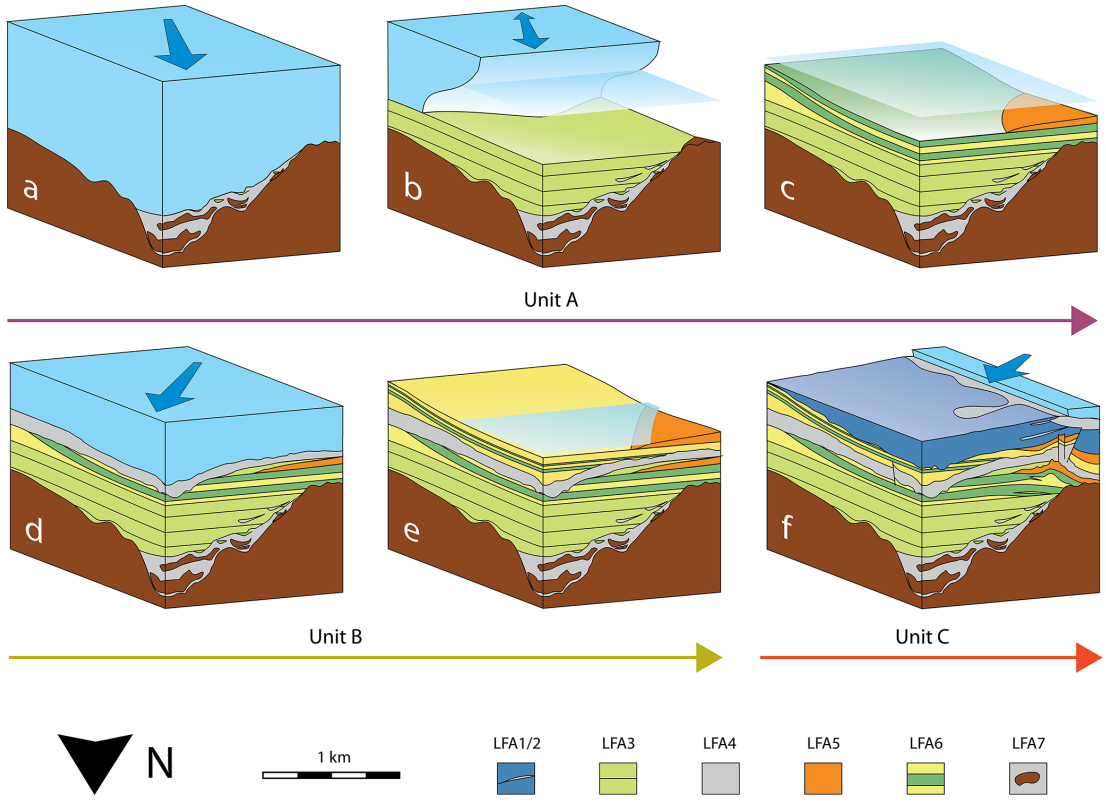

Figure 5. Schematic block diagrams to illustrate the geological evolution of the Tannwald Basin. Glacier ice is illustrated in light blue, water level in transparent light blue, and (oscillating) ice-flow direction with dark blue (bi)directional arrows. **(a)** Advancing glacier from S (Hosskirch glaciation), basin erosion and transport of bedrock rafts and subglacial diamict, filling of subglacial cavities at decoupled ice–bed interfaces. **(b)** Ice-contact sedimentation in proglacial lake with mass movements on basin slopes. **(c)** Glacier retreat and stacked delta formation. **(d)** Glacier re-advance from SW (Riss glaciation) and erosion of second-order inlaid basin. **(e)** Glacier retreat and stacked delta formation. **(f)** Glacier advance from SW (Würm advance, LGM), emplacement of LGM terminal moraine with mass movements on outwash plain, glaciotectonic deformation of sedimentary strata of Unit A.

transition from fine-grained bottomsets to foresets inferred from the Schneidermartin core at the top of seismic facies B (Ellwanger et al., 2011; Burschil et al., 2018; Fig. 6). The facies evolution from LFA5 to LFA6 with fluvial channel fills of different color indicates the transition to a more proximal sediment source, for example, by development of alluvial fans by more local, secondary stream-networks after glacial retreat (Fig. 5c). Finally, Unit A is identified as the Dietmanns Formation (Ellwanger et al., 2011; Hahne et al., 2012).

Facies evolution of Unit B indicates glacier re-advance, likely coupled with secondary shallow basin erosion (LFA4 and LFA3; Fig. 5d), subsequent glacier retreat, and, in analogy to Unit A, delta formation (LFA5 and LFA6; Fig. 5e). In contrast to the Schneidermartin core, where coarsening-upward foresets announce glacier advance (Ellwanger et al., 2011), the ICDP DOVE 5068_1_C core shows the transition back to fine-grained lacustrine sediments. The characteristics (dropstone occurrences, density) of LFA4 indicate gradual glacier advance, infilled into a newly eroded, possibly rather shallow, basin, stacked on top of the main valley fill (Fig. 5d). This is supported by the fact that overlying LFA3 correlates with unconformity 2 (Fig. 1c) and can be followed in the seismic profiles of Burschil et al. (2018) from the Schneidermartin core at ∼ 30 m depth (Ellwanger et al., 2011) to the ICDP DOVE 5068_1_C core at ∼ 60 m depth (Fig. 6). Hence, Unit B is identified as the Illmensee Formation (Ellwanger et al., 2011; Hahne et al., 2012).

Unit C indicates the development of a fluvial and glaciofluvial proglacial outwash plain with mass movements from the close glacier margin (LFA7; Fig. 5f). LFA7 morphologically correlates with the outwash plain associated with the LGM terminal moraine ∼ 100 m to the southwest of the ICDP DOVE 5068_1_C drilling (Figs. 1b, c and 6). The basal contact of LFA7 can be followed in the seismic profiles of Burschil et al. (2018) to the Schneidermartin core (Ellwanger et al., 2011), where it correlates to the topmost 22 m of fluvial coarse gravels with diamicts. The decreased thickness at the Schneidermartin drilling might be due to the greater distance from the LGM terminal moraine. The LGM glacier,

https://doi.org/10.5194/sd-33-191-2024

Table 1. Summary table of lithofacies associations (LFAs).

Lithofacies association		Facies codes	Short description	Base contact	Interpretation
LFA1 Diamicts with bedrock fragments/rafts		*Mgt, Dms*	Tectonically sheared bedrock fragments and matrix-supported stratified diamict of brownish color ranging to Molasse color	Sharp	Glaciotectonized bedrock, proto-till
LFA2 Diamicts with sorted interbeds		*Dmm, Dms, Flr(d), Fl(d), Sl*	Brownish-colored and highly consolidated diamict with glacial striations intercalated with graded sand, silt and clay with lamination and frequent dropstone occurrences	Gradual	Subglacial till with subglacial cavity fills
LFA3 Matrix-rich diamicts		*Dmm*	Dark-colored fine-grained consolidated massive diamict	Unclear	Subglacial till
LFA4 Laminated silt and clay with diamictic interbeds		*Flr, -(d),Fl, -(d), Fm, -(d), Dmm*	Well-sorted dark-colored silt and clay with laminations and frequent dropstones, rarely associated with dark-colored fine-grained soft massive diamict	Gradual	Proglacial lake deposits with rare proglacial subaqueous debris flows
LFA5 Distal fan deposits	LFA5.1	*Fm, Fl*	Well-sorted massive to crudely laminated fines	Sharp or gradual	Distal fan deposits
	LFA5.2	*Sm, Sl*	Moderately sorted dark-colored sands with repeated laminae and beds of dark-colored silt and clay	Sharp or gradual	Distal to proximal fan deposits
LFA6 Proximal fan deposits		*Sh, Sc, Gms*	Well sorted brownish-colored cross-bedded and horizontally bedded sands with gravel interbed	Gradual	Proximal fan or subaqueous channels deposits
LFA7 Gravels with interbedded diamicts	LFA7.1	*Gms, Gmf*	Moderately to poorly sorted gravels	Sharp	Glaciofluvial outwash
	LFA7.2	*Dmm, Dms*	Light-colored fine- and coarse-grained soft diamicts	Sharp	Terrestrial debris flows

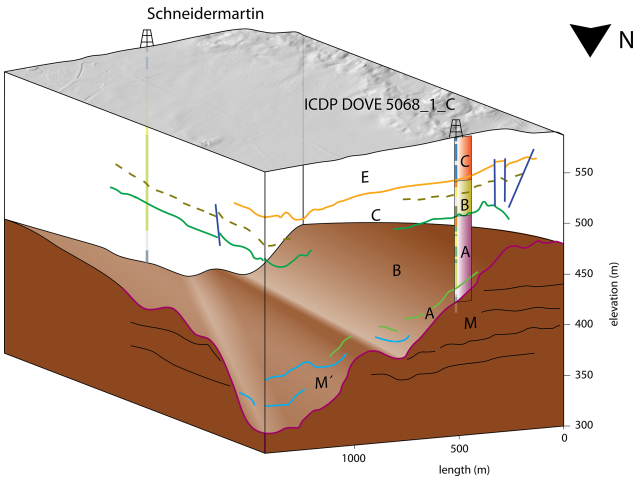

Figure 6. 3D block image showing simplified core profiles (of DOVE 5068_1_C (supplemented with the lithostratigraphic units of this study) and Schneidermartin (Ellwanger et al., 2011)) and their spatial relationship to seismic lines 1 (front) and 4 (left side) including the seismic facies (capital letters and colored lines; see Fig. 1c for legend; Burschil et al., 2018). Inferred bedrock morphology in brown, modern topography in grey.

which evidently created push-moraines in the Lake Constance area (Ellwanger et al., 2011), caused cuspate–lobate folding that was documented in 60 m depth in the vicinity of the ICDP DOVE 5068_1_C drilling (Buness et al., 2022). Seismic reflections of seismic line 1, however, seem to be displaced and inclined at an even greater depth of ∼ 100 m (Fig. 1c). This effect can be correlated to sedimentary deformation in the form of faulting, folding, and oversteepening of sedimentary strata in LFA5 and LFA6 of Unit A (Figs. 2 and 6). Hence, glaciotectonic deformation caused by the Würm (LGM) glacial advance presents an alternative explanation to syn-sedimentary gravitational slumping. The resulting stresses might have further contributed to the above-average consolidation and severe deformation of fines at the interface of LFA4 and LFA5 of Unit A, as well as the mottled character of lamination of fines throughout Unit A.

6 Conclusions

Drilling the overdeepened Tannwald Basin revealed key geological and sedimentological features, including a basal 5.4 m thick glacial shear zone of deformed bedrock as well as recurrent ice-contact sediments. Frequent evidence of sediment deformation indicates the pivotal role of gravitational and glaciotectonic processes on the western slope of the basin. Detailed sedimentological investigations, combined with petrophysical data from the ICDP DOVE 5068_1_C core, led to the definition of seven lithofacies associations that were grouped into three lithostratigraphic units. Unit A represents an initial basin infill cycle following subglacial erosion and deformation, followed by the development of a delta. Unit B provides evidence for a glacier re-advance, once again followed by the development of a delta similar to Unit A. Unit C indicates the development of a glacier-proximal glaciofluvial outwash plain. Hence, the sedimentary sequence of the Tannwald Basin reflects a multi-phase stacked infill, indicative of at least three distinct glacial advances. However, without independent age control, the timing and relevance (glacial fluctuations or independent glaciations) of these advances remains uncertain.

The identification of potential ice-contact sediments (subglacial till) and indirect evidence of glacier overriding (sediment deformation and compaction) are crucial to interpret glacial sequences (not only within the Tannwald Basin). This task is particularly challenging in overdeepened basins, often accessed through drilling, which limits the scale and lateral continuity of observations and has rarely been carried out in detail (e.g., Buechi et al., 2017). In this context, 3D analysis, such as computer tomography (CT) scanning, will provide a powerful tool to identify and quantify sedimentological features and systematically characterize potential ice-contact sediments. To address the architecture of the sedimentary infill at the drill site, particularly in terms of shear-wave anisotropy and its sedimentological significance, a high-resolution cross-hole seismic survey has been conducted. Furthermore, luminescence and cosmogenic nuclide dating offer the potential of numerical age determination. The availability of such data will allow for an integration of the results into the broader context of the glacial evolution of the Lake Constance amphitheater.

Appendix A: Lithofacies description

Table A1. Summary table with the 17 lithotypes identified in the Tannwald drill core presented, along with their corresponding sedimentological descriptions and interpretations. Respective core photos are shown in Figs. 3 and 4.

No: *abbreviation* core photo	Lithofacies	Description	Interpretation
1: *B* Fig. 3a	Molasse bedrock	Strongly to moderately consolidated siltstones and sandstones with decimeter-thick marl sequences.	Upper Freshwater Molasse (tOS) as found in the study area in previous drillings (Ellwanger et al., 2011) and seismic survey (Burschil et al., 2018)
2: *Dmm* Fig. 3d, e	Diamict, massive	Matrix-supported and poorly sorted diamict, slightly to very sandy silt matrix (70 %–95 %) and occasional cobbles; angular to rounded components with glacial striations, Alpine and local Molasse clast lithologies	(i) Subglacial traction till (Evans et al., 2006) or (ii) terrestrial or subaqueous cohesive debris flows (Mulder and Alexander, 2001; Eyles et al, 1983)
3: *Dms* Fig. 3f	Diamict, stratified	Matrix-supported to clast-supported and poorly sorted diamict, bedded by centimeter- to decimeter-thick variations in matrix composition and clast size; bedding locally inclined or graded; with slightly to very sandy silt matrix (50 %–95 %) and occasional cobbles; angular to rounded components with glacial striations, Alpine and local Molasse clast lithologies (strongly varying proportions)	Melt-out till (Evans et al., 2006) or proximal hyperconcentrated density flow deposits (Mulder and Alexander, 2001)
4: *Mgt* Fig. 3b, c	Mélange	Consolidated and unconsolidated Molasse sand- and siltstone fragments showing in situ crushing and brecciation.	Deformed bedrock rafts (Benn and Evans, 1996; Hiemstra and van der Meer, 1997)
5: *Mcc* Fig. 4h	Mud-clast conglomerate	Horizontally aligned accumulations of well-sorted fines in a coarser, mostly sandy matrix; often show soft sediment deformation	Reworked fine lacustrine sediments eroded by subaquatic mass movements (e.g., Li et al., 2017)
6: *Gms* Fig. 3g	Gravel, sandy	Clast-supported and moderately sorted gravel with cobbles and fine sandy matrix; massive to crudely bedded; subangular to rounded components, Alpine and Molasse clast lithologies, locally glacial striations (33.09–32.28 m depth).	Distal fluvial to glaciofluvial deposits
7: *Gmf* Fig. 3h	Gravel, silty	Clast-supported and poorly sorted gravel with cobbles and silty coarse sand matrix (prone to coring-induced deformation); massive; subangular to rounded components, Alpine and Molasse clast lithologies	Proximal fluvial to glaciofluvial deposits
8: *Sm*	Sand, massive	Well-sorted fine to medium sand; massive to crudely bedded by localized millimeter- to centimeter-thick variations in silt content and dominant grain-size fraction	Hyperconcentrated density flow deposits (Mulder and Alexander, 2001)

Table A1. Continued.

No: *abbreviation* core photo	Lithofacies	Description	Interpretation
9: *Sh* Fig. 4a, b	Sand, horizontally bedded	Well to moderately sorted fine to medium sand; bedded by centimeter- to decimeter-thick variations in silt content and dominant grain-size fraction, locally with silt and clay laminae	Subaquatic channel fills
10: *Sc* Fig. 4a	Sand, cross-bedded	Well-sorted fine to medium sand; centimeter-thick cross-bedding by silt content and variations in dominant grain-size fraction	Subaquatic channel fills
11: *Sl* Fig. 4h	Sand, laminated	Well-sorted fine to medium sand, laminated (mottled) by varying silt content and dominant grain-size fraction ranging from silty sand up to silt and clay	Proximal turbidity deposits (Bouma, 1962).
12: *Fm* Fig. 4j	Fines, massive	Very well-sorted silt and clay, massive to locally crudely interbedded by fine sand laminae	Suspension settling (Eyles et al., 1993).
13: *Fm(d)* Fig. 4e	Fines, massive, dropstones	Fm with dropstones locally showing glacial striations	Suspension settling in a proglacial lake with ice rafting (Bennett et al., 1996).
14: *Fl* Fig. 4c	Fines, laminated	Very well-sorted clay and silt bedded by millimeter- to centimeter-thick variations in dominant grain-size reflected in slight changes of color	Distal sedimentation of turbidity currents in a proglacial lake (Smith and Ashley, 1985).
15: *Fl(d)* Fig. 4f	Fines, laminated, dropstones	...with dropstones locally showing glacial striations	Distal sedimentation of turbidity currents in a proglacial lake with ice rafting (Bennett et al., 1996)
16: *Flr* Fig. 4d	Fines, laminated, rhythmites	Very well-sorted clay and silt bedded by normal graded laminae and beds with strongly varying thickness (mm to dm thick) of varying dominant grain-size fraction ranging from fine sand to clay	Proximal turbidity deposits (Eyles et al., 1993; Bouma, 1962: Bouma divisions C–E)
17: *Flr(d)* Fig. 4g	Fines, laminated, rhythmites, dropstones	...with dropstones showing glacial striations	Proximal turbidity deposits floating in a proglacial lake with ice rafting (Eyles et al., 1983).

Data availability. The DOVE operational dataset is published under https://doi.org/10.5880/ICDP.5068.001 (DOVE-Phase 1 Scientific Team et al., 2023b) together with the operational report (https://doi.org/10.48440/ICDP.5068.001, DOVE-Phase 1 Scientific Team et al., 2023a) and the explanatory remarks (https://doi.org/10.48440/ICDP.5068.002, DOVE-Phase 1 Scientific Team et al., 2023c). Furthermore, the dataset is accessible via the ICDP website: https://www.icdp-online.org/projects/by-continent/europe/dove-switzerland/ (ICDP, 2024). Information on the project and the data is also available on the ICDP DOVE project website: https://www.icdp-online.org/projects/by-continent/europe/dove-switzerland (DOVE-Phase 1 Scientific Team, 2024).

Author contributions. FP and FSA played a pivotal role in conceptualizing the research project, project management, and coordination. BS and DT were drill site geologists, and BS performed the ICD. SS performed the data preprocessing and preparation. LG, MWB, and UWS provided valuable insights into the theoretical framework and methodology used in this study. Their guidance significantly influenced the research approach. All authors contributed to the writing of the manuscript and editing process.

Competing interests. The contact author has declared that none of the authors has any competing interests.

Disclaimer. Publisher's note: Copernicus Publications remains neutral with regard to jurisdictional claims made in the text, published maps, institutional affiliations, or any other geographical representation in this paper. While Copernicus Publications makes every effort to include appropriate place names, the final responsibility lies with the authors.

Acknowledgements. We would like to express gratitude to the International Scientific Continental Drilling Program (ICDP) for their support during drilling and for providing access to the online database "mDIS". Special thanks to the drilling firm "H. Anger's Söhne", particularly Mirko Huber and the dedicated drilling crew, including Jürgen Pröhl, Markus Schiek, J. Achler, Mohammad Alhamad, Hsaan Alsasihl, Asabdi, Peter Goor, Frank Hapke, Zoltan Mihalti, Zoltan Olah, Jens Täubert, Lutz Tonne, and Peter Toth, who skillfully navigated challenging sedimentary conditions and provided essential on-site infrastructure. We highly appreciate the cooperation of the local authorities of the municipality of Ingoldingen in the district of Biberach, particularly Roland Wersch, Jürgen Schell, and Reiner Traub. Their support for the drilling project and granting access to refrigerated rooms was instrumental. Thanks are due to the Leibniz Institute for Applied Geophysics (LIAG) for their crucial involvement in the project, including the pre-drilling seismic survey and downhole logging in all three holes. In particular, we thank Thomas Burschil and Hermann Buness for providing important seismic data. LIAG's contribution of technical infrastructure for scientific operations on site, as well as outreach efforts to schools and local events, is appreciated. We would also like to thank Merlin Kamke for documenting our work through photography. Special recognition goes to Julijana Gajic, Patrizia Ruffiner, and Aaron Alexander Hutter for their efforts in processing and analyzing the TIC and TOC samples. Lastly, my gratitude to the entire DOVE science team for their collaborative contributions that have enriched the research experience and contributed to the project's success. We thank the two reviewers and the editors for constructive reviews.

Financial support. This research has been funded by the ICDP, the Deutsche Forschungsgemeinschaft (DFG, grant nos. KR2073/3-1, BU 2467/1-2, GA749/5-1, BU2467/3-1, BU 3894/2-1, BU3894/3-1, and PR 957/6-1), Nagra, ENSI, LGRB, LFU, LIAG, BOKU Vienna, University of Freiburg, and the University of Bern.

Review statement. This paper was edited by Nadine Hallmann and reviewed by two anonymous referees.

References

Alley, R. B., Cuffey, K. M., Evenson, E. B., Strasser, J. C., Lawson, D. E., and Larson, G. J.: How glaciers entrain and transport basal sediment: physical constraints, Quaternary Sci. Rev., 16, 1017–1038, 1997.

Alley, R. B., Cuffey, K. M., and Zoet, L. K.: Glacial erosion: status and outlook, Ann. Glaciol., 60, 1–13, https://doi.org/10.1017/aog.2019.38, 2019.

Anselmetti, F. S., Drescher-Schneider, R., Furrer, H., Graf, H. R., Lowick, S. E., Preusser, F., and Riedi, M. A.: A 180,000 years sedimentation history of a peri-Alpine overdeepened glacial trough (Wehntal, N-Switzerland), Swiss J. Geosci., 103, 345–361, https://doi.org/10.1007/s00015-010-0041-1, 2010.

Anselmetti, F. S., Bavec, M., Crouzet, C., Fiebig, M., Gabriel, G., Preusser, F., Ravazzi, C., and DOVE scientific team: Drilling Overdeepened Alpine Valleys (ICDP-DOVE): quantifying the age, extent, and environmental impact of Alpine glaciations, Sci. Dril., 31, 51–70, https://doi.org/10.5194/sd-31-51-2022, 2022.

Bachmann, G. H., Müller, M., and Weggen, K.: Evolution of the molasse basin (Germany, Switzerland), Tectonophysics, 137, 77–92, https://doi.org/10.1016/0040-1951(87)90315-5, 1987.

Benn, D. I. and Evans, D. J.: The interpretation and classification of subglacially-deformed materials, Quaternary Sci. Rev., 15, 23–52, https://doi.org/10.1016/0277-3791(95)00082-8, 1996.

Bennett, M. R., Doyle, P., and Mather, A. E.: Dropstones: their origin and significance, Palaeogeogr. Palaeocl., 121, 331–339, https://doi.org/10.1016/0031-0182(95)00071-2, 1996.

Bouma, A. H.: Sedimentology of some Flysch deposits: a graphic approach to facies interpretation, Elsevier, Amsterdam, the Netherlands, https://lib.ugent.be/catalog/rug01:000978747 (last access: 12 December 2023), 1962.

Buechi, M. W., Frank, S. M., Graf, H. R., Menzies, J., and Anselmetti, F. S.: Subglacial emplacement of tills and meltwater deposits at the base of overdeepened bedrock troughs, Sedimentology, 64, 658–685, https://doi.org/10.1111/sed.12319, 2017.

Buechi, M. W., Graf, H. R., Haldimann, P., Lowick, S. E., and Anselmetti, F. S.: Multiple Quaternary erosion and infill cycles in overdeepened basins of the northern Alpine foreland, Swiss

J. Geosci., 111, 133–167, https://doi.org/10.1007/s00015-017-0289-9, 2018.

Burschil, T., Buness, H., Tanner, D. C., Wielandt-Schuster, U., Ellwanger, D., and Gabriel, G.: High-resolution reflection seismics reveal the structure and the evolution of the Quaternary glacial Tannwald Basin, Near Surf. Geophys., 16, 593–610, 2018.

Buness, H., Burschil, T., and Tanner, D. C.: Imaging glacial sediments and tectonics with a small-scale 3-D reflection seismic survey, 26th European Meeting of Environmental and Engineering Geophysics, 7–8 December 2020, online, 1, 1–4, https://doi.org/10.3997/2214-4609.202020094, 2020.

Buness, H., Tanner, D. C., Burschil, T., Gabriel, G., and Wielandt-Schuster, U.: Cuspate-lobate folding in glacial sediments revealed by a small-scale 3-D seismic survey, J. Appl. Geophy., 200, 104614, https://doi.org/10.1016/j.jappgeo.2022.104614, 2022.

Cook, S. J. and Swift, D. A.: Subglacial basins: Their origin and importance in glacial systems and landscapes, Earth-Sci. Rev., 115, 332–372, https://doi.org/10.1016/j.earscirev.2012.09.009, 2012.

Dehnert, A., Lowick, S. E., Preusser, F., Anselmetti, F. S., Drescher-Schneider, R., Graf, H. R., Heller, F., Horstmeyer, H., Kemna, H. A., Nowaczyk, N. R., Züger, A., and Furrer, H.: Evolution of an overdeepened trough in the northern Alpine Foreland at Niederweningen, Switzerland, Quaternary Sci. Rev., 34, 127–145, https://doi.org/10.1016/j.quascirev.2011.12.015, 2012.

Doppler, G., Kroemer, E., Rögner, K., Wallner, J., Jerz, H., and Grottenthaler, W.: Quaternary stratigraphy of southern Bavaria, EandG Quaternary Sci. J., 60, 23, https://doi.org/10.3285/eg.60.2-3.08, 2011.

DOVE-Phase 1 Scientific Team, Anselmetti, F. S., Beraus, S., Buechi, M. W., Buness, H., Burschil, T., Fiebig, M., Firla, G., Gabriel, G., Gegg, L., Grelle, T., Heeschen, K., Kroemer, E., Lehne, C., Lüthgens, C., Neuhuber, S., Preusser, F., Schaller, S., Schmalfuss, C., Schuster, B., Tanner, D. C., Thomas, C., Tomonaga, Y., Wieland-Schuster, U., and Wonik, T.: Drilling Overdeepened Alpine Valleys (DOVE) – Operational Report of Phase 1, (ICDP Operational Report), GFZ German Research Centre for Geosciences, Potsdam, 70 pp., https://doi.org/10.48440/ICDP.5068.001, 2023a.

DOVE-Phase 1 Scientific Team, Anselmetti, F. S., Beraus, S., Buechi, M. W., Buness, H., Burschil, T., Fiebig, M., Firla, G., Gabriel, G., Gegg, L., Grelle, T., Heeschen, K., Kroemer, E., Lehne, C., Lüthgens, C., Neuhuber, S., Preusser, F., Schaller, S., Schmalfuss, C., Schuster, B., Tanner, D. C., Thomas, C., Tomonaga, Y., Wieland-Schuster, U., and Wonik, T.: Drilling Overdeepened Alpine Valleys (DOVE) – Operational Dataset of DOVE Phase 1, GFZ Data Services [data set], https://doi.org/10.5880/ICDP.5068.001, 2023b.

DOVE-Phase 1 Scientific Team, Anselmetti, F. S., Beraus, S., Buechi, M. W., Buness, H., Burschil, T., Fiebig, M., Firla, G., Gabriel, G., Gegg, L., Grelle, T., Heeschen, K., Kroemer, E., Lehne, C., Lüthgens, C., Neuhuber, S., Preusser, F., Schaller, S., Schmalfuss, C., Schuster, B., Tanner, D. C., Thomas, C., Tomonaga, Y., Wieland-Schuster, U., and Wonik, T.: Drilling Overdeepened Alpine Valleys (DOVE) – Explanatory remarks on the operational dataset, ICDP Operational Dataset – Explanatory Remarks, GFZ German Research Centre for Geosciences [data set], Potsdam, 34 pp., https://doi.org/10.48440/ICDP.5068.002, 2023c.

DOVE-Phase 1 Scientific Team: DOVE – What is DOVE?, https://www.dove-icdp.eu/ (last access: 26 June 2024), 2024.

Dürst Stucki, M. and Schlunegger, F.: Identification of erosional mechanisms during past glaciations based on a bedrock surface model of the central European Alps, Earth Planet. Sc. Lett., 384, 57–70, https://doi.org/10.1016/j.epsl.2013.10.009, 2013.

Dürst Stucki, M., Reber, R., and Schlunegger, F.: Subglacial tunnel valleys in the Alpine Foreland: an example from Bern, Switzerland, Swiss J. Geosci., 103, 363–374, https://doi.org/10.1007/s00015-010-0042-0, 2010.

Ellwanger, D.: Lithostratigraphische Entwicklung des baden-württembergischen Rheingletschergebietes: übertiefte Becken- und Moränenlandschaft, LGRB-Fachbericht 2015/4a & 4b, Landesamt für Geologie, Rohstoffe und Bergbau (RP Freiburg, Baden-Württemberg), 2015.

Ellwanger, D., Bibus, E., Bludau, W., Kösel, M., and Merkt, J.: Baden-Württemberg, in: Das Quartär Deutschlands: 255–295, edited by: Benda, L., Berlin, Stuttgart, New York, https://www.schweizerbart.de/publications/detail/artno/001199531 (last access: 12 December 2023), 1995.

Ellwanger, D., Wielandt-Schuster, U., Franz, M., and Simon, T.: The Quaternary of the southwest German Alpine Foreland (Bodensee-Oberschwaben, Baden-Württemberg, Southwest Germany), EandG Quaternary Sci. J., 60, 22, https://doi.org/10.3285/eg.60.2-3.07, 2011.

Evans, D. J. A., Phillips, E. R., Hiemstra, J. F., and Auton, C. A.: Subglacial till: Formation, sedimentary characteristics and classification, Earth-Sci. Rev., 78, 115–176, https://doi.org/10.1016/j.earscirev.2006.04.001, 2006.

Eyles, C. H., Eyles, N., and França, A. B.: Glaciation and tectonics in an active intracratonic basin: the Late Palaeozoic Itararé Group, Paraná Basin, Brazil, Sedimentology, 40, 1–25, https://doi.org/10.1111/j.1365-3091.1993.tb01087.x, 1993.

Eyles, N., Eyles, C. H., and Miall, A. D.: Lithofacies types and vertical profile models; an alternative approach to the description and environmental interpretation of glacial diamict and diamictite sequences, Sedimentology, 30, 393–410, https://doi.org/10.1111/j.1365-3091.1983.tb00679.x, 1983.

Fernandes, M., Oliva, M., and Vieira, G.: Paraglacial slope failures in the Aran valley (Central Pyrenees), Quaternary Int., 566, 24–38, https://doi.org/10.1016/j.quaint.2020.07.045, 2020.

Fiebig, M.: Pleistozäne Ablagerungen im süddeutschen und im neuseeländischen Alpenvorland – ein Vergleich, Doctoral dissertation, Albert-Ludwigs-Universität Freiburg im Breisgau, 122 pp., https://freidok.uni-freiburg.de/inst/2040 (last access: 12 December 2023), 1995.

Fiebig, M., Herbst, P., Drescher-Schneider, R., Lüthgens, C., Lomax, J., and Doppler, G.: Some remarks about a new Last Glacial record from the western Salzach foreland glacier basin (Southern Germany), Quaternary Int., 328–329, 107–119, https://doi.org/10.1016/j.quaint.2013.12.048, 2014.

Fischer, H.: Excess K-Ar ages of glauconite from the Upper Marine Molasse and evidence for glauconitization of mica, Geol. Rundsch., 76, 885–902, 1987.

Gegg, L. and Preusser, F.: Comparison of overdeepened structures in formerly glaciated areas of the northern Alpine foreland and northern central Europe, E&G Quaternary Sci. J., 72, 23–36, https://doi.org/10.5194/egqsj-72-23-2023, 2023.

Gegg, L., Deplazes, G., Keller, L., Madritsch, H., Spillmann, T., Anselmetti, F. S., and Buechi, M. W.: 3D morphology of a glacially overdeepened trough controlled by underlying bedrock geology, Geomorphology, 394, 107950, https://doi.org/10.1016/j.geomorph.2021.107950, 2021.

Geyer, O. F., Gwinner, M. P., Geyer, M., Nitsch, E., and Simon, T.: Geologie von Baden-Württemberg, Schweizerbart, 117–118, https://scholar.archive.org/work/5g5oa6bb5jdl3mztto7wpiv3bi/access/wayback/https://journals.wlb-stuttgart.de/ojs/index.php/sh/article/download/2880/2924 (last access: 12 December 2023), 2011.

Graf, H. R.: Stratigraphie von Mittel- und Spätpleistozän in der Nordschweiz. Beiträge zur Geologischen Karte der Schweiz (N.F.), 168, Landesgeologie, Swisstopo, 198 pp., https://doi.org/10.3285/eg.58.1.02, 2009.

Hahne, J., Ellwanger, D., Franz, M., Stritzke, R., and Wielandt-Schuster, U.: Pollenanalytische Untersuchungsergebnisse aus dem baden-württembergischen Rheinsystem Oberrheingraben, Hochrhein, Oberschwaben – eine Zusammenfassung des aktuellen Kenntnisstandes, LGRB Info, 26, 119–154, https://produkte.lgrb-bw.de/docPool/c618_data.pdf (last access: 12 December 2023), 2012.

Hiemstra, J. F. and van der Meer, J. J. M.: Pore-water controlled grain fracturing as an indicator for subglacial shearing in tills, J. Glaciol., 43, 446–454, https://doi.org/10.3189/S0022143000035036, 1997.

Huuse, M. and Lykke-Andersen, H.: Overdeepened Quaternary valleys in the eastern Danish North Sea: morphology and origin, Quaternary Sci. Rev., 19, 1233–1253, https://doi.org/10.1016/S0277-3791(99)00103-1, 2000.

ICDP: Drilling Overdeepened Alpine Valleys, https://www.icdp-online.org/projects/by-continent/europe/dove-switzerland/ (last access: 26 June 2024), 2024.

Lämmermann-Barthel, J., Neeb, I., Hinderer, M., Ellwanger, D., and Frechen, M.: Sediment budget of Pliocene and Quaternary unconsolidated deposits of the Rhine Glacier area, Swiss Midlands and the Upper Rhine Graben, in: EGS-AGU-EUG Joint Assembly, 13554, https://www.researchgate.net/profile/Inge-Neeb/publication (last access: 12 December 2023), 2003.

Lawson, D. E.: Mobilization, movement and deposition of active subaerial sediment flows, Matanuska Glacier, Alaska, J. Geol., 90, 279–300, https://doi.org/10.1086/628680, 1982.

Li, S., Li, S., Shan, X., Gong, C., and Yu, X.: Classification, formation, and transport mechanisms of mud clasts, Int. Geol. Rev., 59, 1609–1620, https://doi.org/10.1080/00206814.2017.1287014, 2017.

Menzies, J.: Subglacial hydraulic conditions and their possible impact upon subglacial bed formation, Sediment. Geol., 62, 125–150, https://doi.org/10.1016/0037-0738(89)90112-7, 1989.

Meyers, P. A. and Teranes, J. L.: Sediment Organic Matter, in: Tracking Environmental Change Using Lake Sediments: Physical and Geochemical Methods, edited by: Last, W. M. and Smol, J. P., Springer Netherlands, Dordrecht, 239–269, https://doi.org/10.1007/0-306-47670-3_9, 2001.

Mulder, T. and Alexander, J.: The physical character of subaqueous sedimentary density flows and their deposits, Sedimentology, 48, 269–299, https://doi.org/10.1046/j.1365-3091.2001.00360.x, 2001.

O'Regan, M., Jakobsson, M., and Kirchner, N.: Glacial geological implications of overconsolidated sediments on the Lomonosov Ridge and Yermak Plateau, Quaternary Sci. Rev., 29, 3532–3544, https://doi.org/10.1016/j.quascirev.2010.09.009, 2010.

Pomper, J., Salcher, B. C., Eichkitz, C., Prasicek, G., Lang, A., Lindner, M., and Götz, J.: The glacially overdeepened trough of the Salzach Valley, Austria: Bedrock geometry and sedimentary fill of a major Alpine subglacial basin, Geomorphology, 295, 147–158, https://doi.org/10.1016/j.geomorph.2017.07.009, 2017.

Preusser, F., Drescher-Schneider, R., Fiebig, M., and Schlüchter, C.: Re-interpretation of the Meikirch pollen record, Swiss Alpine Foreland, and implications for Middle Pleistocene chronostratigraphy, J. Quaternary Sci., 20, 607–620, https://doi.org/10.1002/jqs.930, 2005.

Preusser, F., Reitner, J. M., and Schlüchter, C.: Distribution, geometry, age and origin of overdeepened valleys and basins in the Alps and their foreland, Swiss J. Geosci., 103, 407–426, https://doi.org/10.1007/s00015-010-0044-y, 2010.

Preusser, F., Graf, H. R., Keller, O., Krayss, E., and Schlüchter, C.: Quaternary glaciation history of northern Switzerland, E&G Quaternary Sci. J., 60, 21, https://doi.org/10.3285/eg.60.2-3.06, 2011.

Ravier, E., Buoncristiani, J. F., Clerc, S., Guiraud, M., Menzies, J., and Portier, E.: Sedimentological and deformational criteria for discriminating subglaciofluvial deposits from subaqueous ice-contact fan deposits, A Pleistocene example (Ireland), Sedimentology, 61, 1382–1410, https://doi.org/10.1111/sed.12111, 2014.

Schaller, S., Buechi, M. W., Schuster, B., and Anselmetti, F. S.: Drilling into a deep buried valley (ICDP DOVE): a 252 m long sediment succession from a glacial overdeepening in northwestern Switzerland, Sci. Dril., 32, 27–42, https://doi.org/10.5194/sd-32-27-2023, 2023.

Schlüchter, C.: The most complete Quaternary record of the Swiss Alpine Foreland, Palaeogeogr. Palaeocl., 72, 141–146, https://doi.org/10.1016/0031-0182(89)90138-7, 1989.

Schuster, B., Amschwand, D., Huber, M. L., Madritsch, H., Deplazes, G., and Büchi, M.: Quaternary Borehole QBO Kleinandelfingen-Laubhau (QKLA), Data Rep., https://boris.unibe.ch/id/eprint/167486 (last access: 12 December 2023), 2020.

Schwenk, M. A., Schläfli, P., Bandou, D., Gribenski, N., Douillet, G. A., and Schlunegger, F.: From glacial erosion to basin overfill: a 240 m-thick overdeepening–fill sequence in Bern, Switzerland, Sci. Dril., 30, 17–42, https://doi.org/10.5194/sd-30-17-2022, 2022.

Siegenthaler, C. and Huggenberger, P.: Pleistocene Rhine gravel: deposits of a braided river system with dominant pool preservation, Geol. Soc., London, Special Publications, 75, 147–162, 1993.

Smith, N. D. and Ashley, G. M.: Proglacial lacustrine environments, in: Glacial Sedimentary Environments, edited by: Ashley, G. M., Shaw, J., and Smith, N. D., SEPM Short, 16, 135–215, 1985.

Visser, J. N. J., Colliston, W. P., and Terblanche, J. C.: The origin of soft-sediment deformation structures in Permo-Carboniferous glacial and proglacial beds, South Africa, J. Sediment. Res., 54, 1183–1196, https://doi.org/10.1306/212F8594-2B24-11D7-8648000102C1865D, 1984.

Sci. Dril., 33, 207–218, 2024
https://doi.org/10.5194/sd-33-207-2024

Scientific Drilling
Open Access

Workshop report: Afar Dallol Drilling – ONset of sedimentary processes in an active rift basin (ADD-ON)

Anneleen Foubert[1], Derek Keir[2,3], Balemwal Atnafu[4], Tesfaye Kidane[5], and the ADD-ON Workshop Consortium✚

[1]Department of Geosciences, University of Fribourg, Fribourg, 1700, Switzerland
[2]School of Ocean and Earth Science, University of Southampton, Southampton SO143ZH, UK
[3]Dipartimento di Scienze della Terra, University of Florence, Florence, 50121, Italy
[4]School of Earth Sciences, Addis Ababa University, Addis Ababa, 1176, Ethiopia
[5]Department of Environmental Science and Geology, Wayne State University, Detroit, MI 48201, USA
✚A full list of authors appears at the end of the paper.

Correspondence: Anneleen Foubert (anneleen.foubert@unifr.ch)

Received: 31 January 2024 – Revised: 22 April 2024 – Accepted: 19 June 2024 – Published: 30 August 2024

Abstract. Rifts and rifted margins form when continents break apart and shape the continent-to-ocean transition on much of our planet. The sedimentary basins that result from continental rifting host unique sedimentary archives of palaeo-environmental and palaeo-climatic change required to understand complex natural processes. Rifts and rifted margins are key sites for natural resources (e.g. geothermal and hydrogen potential, critical metal resources, and CO_2 storage) and have an important societal relevance in the mitigation of geohazards such as earthquakes and volcanic activity. However, knowledge on the tectonic structure, sedimentary architecture, rapid palaeo-environmental change, fluid flow and hydrothermal circulation, deep subsurface biosphere, and their impacts on biogeochemical fluxes in rift basins remains poorly understood. Considering their large scientific potential and societal relevance, understanding the formation and architecture of rifts and rifted margins is now critical. The Afar rift is a world-class natural field lab where continental breakup can be directly observed. The northern part of Afar, the Danakil Depression, especially represents a unique snapshot in space and time when the continent ruptures and new seafloor and adjacent rifted margins form. However, deep subsurface records are missing in the basin. The ADD-ON project aims at deep drilling in the Danakil Depression to provide a unique sedimentary record in an active rift basin paced by global environmental fluctuations and their interplay with volcanic and tectonic events. To explore drilling targets and address scientific drilling objectives, an International Continental Scientific Drilling Program (ICDP) workshop was organized in Addis Ababa, Ethiopia, in August 2023. In total, 64 participants from 10 countries and all career stages respecting diversity and inclusion joined the workshop. They represented a wide range of scientific disciplines including government agencies, industry, local universities, and communities to discuss the overall ADD-ON science plan during several workshop sessions. One target drilling site has been flagged, covering the unique Pleistocene full syn-rift sedimentary record in the Danakil Depression. This unique sedimentary archive will allow us to (1) unravel complex palaeo-environmental change in a rift basin, (2) understand incipient and intermittent dynamics through punctuated volcano-tectonic events in a rift transitioning from continental rifting towards seafloor spreading and adjacent rifted margin development, (3) test the origin and limits of life in the deep biosphere under poly-extreme conditions, (4) better understand fluid flow and fluid–sediment interaction in an active hydrothermal system, and (5) use the drilling site to develop a downhole Earth observatory to improve hazard-related monitoring capacity (earthquakes, gas/fluid flux, ground motion).

Published by Copernicus Publications on behalf of the IODP and the ICDP.

1 Introduction

Since the early days of the continental drift theory, the Afar Triangle developed into the archetypal field lab where the breakup of continents and potential future ocean spreading can be subaerially observed and studied. The Afar Depression is situated at the boundaries of the Nubian, Arabian, and Somalian plates and forms a triple junction related to the opening of the Afro-Arabian rift system (McKenzie et al., 1970; Viltres et al., 2020). The Danakil Depression is the northern portion of the Afar Depression, bordered by the western plateau and the Danakil Horst to the east. Rifting in the region started in the Oligocene, with extension localizing in the Danakil Depression since Middle to Late Miocene times due to the rotation of the Danakil Block (Arrata Microplate) (Rime et al., 2023) (Fig. 1).

Kinematic modelling supported by geological and geophysical observations suggest the Danakil Depression has formed in faulted, stretched, and thinned continental crust that has been heavily modified by mafic intrusions and flow of volatiles (Bastow and Keir, 2011; Rime et al., 2023). This, in combination with the potentially thick, young syn-rift evaporites and basaltic lava flows in a near-sea-level basin, makes it one of the few modern analogues for the development of a classic magma-rich rifted margin (Bastow et al., 2018; Rime et al., 2023). Accelerated subsidence rates in the central axis of the Danakil Depression over at least the last 120 kyr, resulted in the accumulation of an exceptional stratigraphic and sedimentary record (Foubert et al., 2018; Rime et al., 2024). Several cycles of marine flooding with transgression of the Red Sea into the Danakil Depression resulted in the formation of kilometre-thick evaporite successions in the subsurface of the depression composed of halite intercalated with gypsum, anhydrite, and potash-bearing deposits of economic significance (Warren, 2016; Rime et al., 2024). With that, the Danakil Depression is one of the youngest salt giants on planet Earth. The central part of the Danakil Depression hosts the Dallol volcano formed through the direct interaction between magmatism and sedimentary processes. The associated hydrothermal brine pools, sulfuric acidic springs, and fumaroles form an ideal test case to understand the limits of life in poly-extreme conditions (Belilla et al., 2019). This unique set of geo-physico-chemical conditions may open a new window on the origin of life and function as an analogue for potential extra-terrestrial life. As such, the Danakil Depression is a unique setting in which the interplay between tectonic, sedimentary, volcanic, fluid flow, and environmental processes during the formation of a magmatic rifted continental margin can be studied.

1.1 Historical backbone

Research during the last 2 decades largely focused on tectonics, volcanology, and geophysics to understand mechanisms and controls of rifting. Only a few studies dating back nearly half a century ago focused on the sedimentary deposits and mostly on the rich record of northern Afar. They were initiated as a result of early potash exploration (Holwerda and Hutchinson, 1968; Bannert et al., 1971) and resulted in the first structural and stratigraphic mapping of the area (e.g. Bannert et al., 1971; Brinckmann and Kürsten, 1971; Barberi et al., 1971; Varet et al., 1975; Bonatti et al., 1971). Then, little was done until 2013, with the start of reconnaissance field actions in northern Afar exploring the carbonate sedimentary record at the basin margins (COCARDE research networking programme) (Atnafu et al., 2015). Recently, projects such as SERENA ("Sedimentary Record of the northern Afar: Insights in the flooding history of the Danakil Depression", 2016–2022) and CONNECT ("Paleo-Connectivity and Paleo-Hydrological change in an initial rift basin", 2023–2027) started to focus on the unique Middle to Late Pleistocene and Holocene sedimentary archive (Atnafu et al., 2015; Foubert et al., 2021, 2018; Jaramillo-Vogel et al., 2019) and have resulted in new geological maps of the wider Afar region and the Danakil Depression (Rime et al., 2022a, b, 2023). More recent exploration and exploitation surveys led by the potash industry during the last decade resulted in an additional set of subsurface data, which have been further scientifically explored within the framework of the above-mentioned research projects (e.g. Rime et al., 2024; Bastow et al., 2018; Hurman et al., 2023).

1.2 Unique syn-rift sedimentary record: the need for drilling

In the Danakil Depression, pre-Cambrian, Palaeozoic, and Mesozoic pre-rift series are diachronously overlain by Palaeogene to Neogene Afar flood basalts or trap volcanics ranging from basalts to alkaline rhyolites (Barberi and Varet, 1970; Watts et al., 2020), followed and intertwined with Cenozoic syn-rift sediments (Fig. 2a). Syn-rift sediments are characterized by fluvio-lacustrine siliciclastic sediments since the Neogene (Belekiya and Sabba formations). The Middle to Late Pleistocene record witnessed episodic marine flooding and desiccation resulting in the deposition of marine carbonate sediments at the margins (Zariga Formation) and evaporites in the centre of the depression (Dallol Formation) (Atnafu et al., 2015; Foubert et al., 2018; Jaramillo-Vogel et al., 2019). Currently, the surface of the Danakil Depression, featuring elevations as low as 120 m b.s.l., is covered by lacustrine sediments, seasonal terminal saline lakes, saline pans and geothermal pools.

Available industrial core sections provide relatively good constraints on the expected lithologies and allow for correlations with carbonate outcrops at the margin of the depression (Rime et al., 2023, 2024) (Fig. 2b). Seismo-stratigraphic interpretations, based on industrial seismic section, core, and borehole data, evidence the presence of evaporite units until the depth of about 800 m below the Dallol salt pan (e.g. Bastow et al., 2018; Foubert et al., 2018; Hurman et al., 2023).

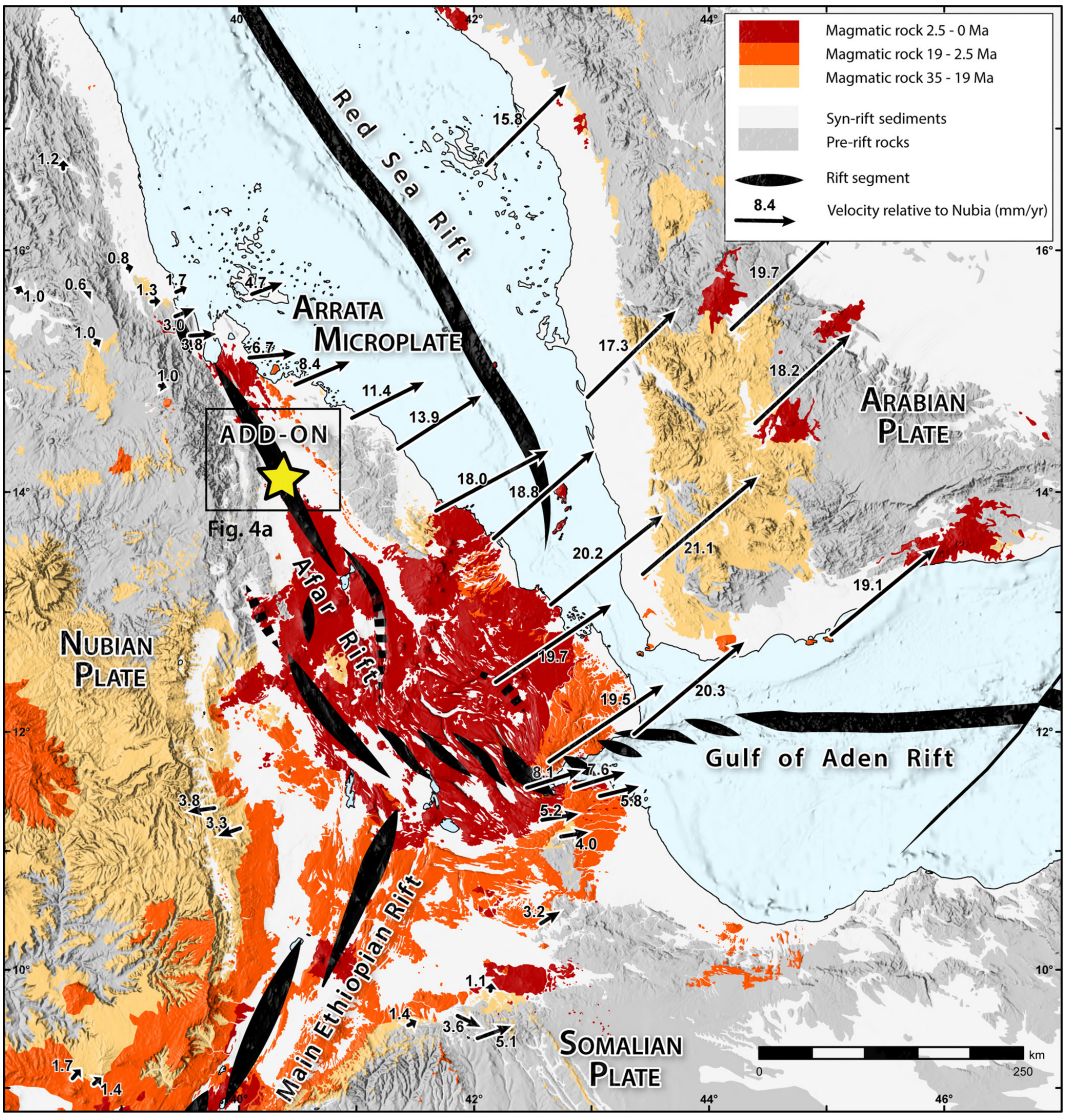

Figure 1. Afro-Arabian rift system with indication of the Red Sea Rift, Gulf of Aden Rift, Main Ethiopian Rift, and the Afar Rift. The central Afar domain is mainly characterized by magmatic rocks, while the northern Afar represents a unique archive of syn-rift sediments. Yellow star represents ADD-ON drilling location. Modified after Rime et al. (2023).

However, to date no sedimentary records are available from the central part of the rift basin filled with more than 2.2 km of sediments which record the basin evolution.

2 Workshop structure

After funding was granted in 2020, a first online International Continental Scientific Drilling Program (ICDP) ADD-ON workshop was initiated from 29 to 30 June 2021 with 70 participants from 10 countries and representatives from the ICDP Operational Support Group (OSG). This workshop resulted in a first set of scientific ADD-ON drilling objectives and a selection of drilling scenarios that served as a base for subsequent discussions. To keep momentum during the COVID-19 era, a European Geosciences Union (EGU) splinter meeting was held on 25 May 2022. The in-presence ICDP ADD-ON workshop was finally organized from 28 to 31 August 2023 in Addis Ababa, Ethiopia, at the Ambassador Hotel and at Addis Ababa University (Fig. 3). The workshop was attended by 64 participants from Ethiopia, Germany, United Kingdom, USA, Switzerland, France, Italy, Belgium, Israel, and Japan. More than half of the participants were from Ethiopia, including scientists and delegates from Addis Ababa University, Addis Ababa Science and Technology University, Mekelle University, and Semera University. There were representatives from the potash, geothermal, and petroleum exploration sectors; the national and regional government; and a number of non-government agencies active

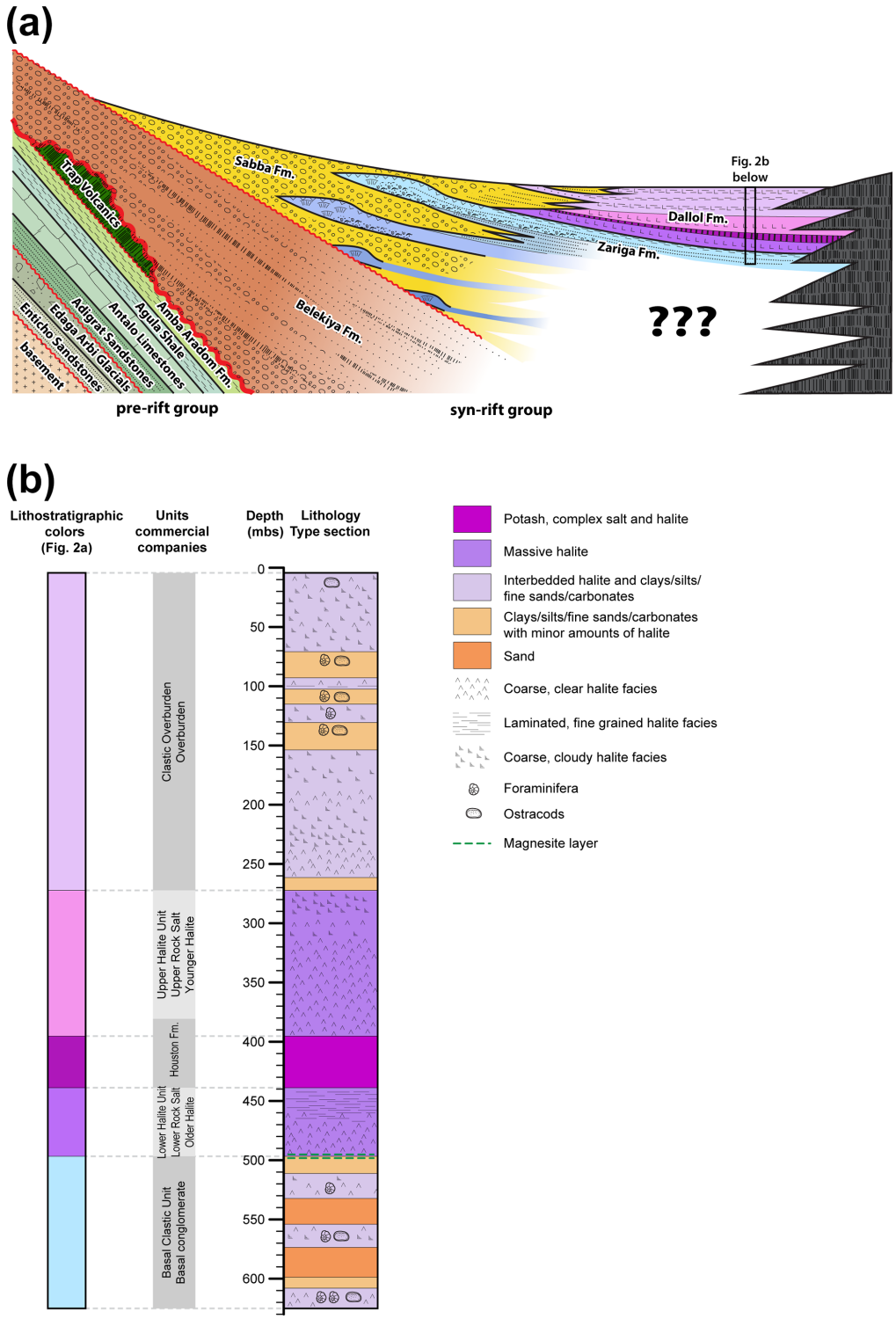

Figure 2. **(a)** W–E cross-section through the Danakil Depression indicating pre-rift and syn-rift sediments (Belekiya Formation, Sabba Formation, Zariga Formation, and Dallol Formation). Please note that this schematic cross-section only represents the lithostratigraphy. Structural features (faults, fractures) are not represented. **(b)** Lithology of the upper syn-rift sedimentary record. The upper units are mainly consisting of an alternation of halite and clay/silt ("Clastic Overburden"), below which there is a thick unit of mainly halite ("Upper Halite Unit"). This is followed by a layer of potash-bearing minerals ("Houston Formation"), another major halite unit ("Lower Halite Unit"), and then sandstones locally enriched by anhydrite ("Basal Clastic Unit"). Those sandy units can be correlated, based on seismic sections, with the carbonate outcrops (Zariga Formation) at the margins of the depression and identified as belonging to the Middle to Late Pleistocene (Foubert et al., 2018; Rime et al., 2024).

in the Afar region. The principal investigators (PIs) encouraged the participation of early-career scientists by inviting around 20 post-graduate (both local and international MSc and PhD) students. A wide range of disciplines was represented and included sedimentology, stratigraphy, structural geology, volcanology, geochemistry, geophysics, hydrology, palaeo-climate, biology, biogeochemistry, and engineering.

The official workshop opening started with a meet-and-greet event and an ice-breaker event on 28 August 2023. Formal sessions started on 29 August with welcome addresses by the ADD-ON PI team, delegates from the Ethiopian Ministry of Mines, and Addis Ababa University, as well as an introduction to the ICDP from the ICDP executive director. The first scientific session set the state of the art for geological, sedimentological, basin dynamics, and biological background of the Danakil Depression. The afternoon sessions opened with lightning talks on research background and interests by workshop attendees, followed by talks on industrial drilling experience in Ethiopia from the potash, geothermal, and petroleum industries. The day concluded with a presentation by the ICDP OSG on guidelines for writing a full drilling proposal, followed by an open discussion around the 25 posters presented by workshop attendees.

The 30 August started with presentations by the PI team on the draft science plan and three potential drilling strategies followed by discussions on science objectives and drilling strategy by all workshop participants during break-out sessions of three groups with a balanced mix of disciplines, background, and experience. The second half of the morning was devoted to discussions on the societal relevance of the drilling project and opened with a presentation on the hydrogeology in Afar and an overview of the permanent seismic monitoring network managed by Addis Ababa University. Further talks included local Afar community-based schemes that promote education about, and sustainable development of, geothermally sourced energy compatible with their lifestyle and culture (the green geothermal village concept). After an introduction on core, sample, and data handling; ICDP geophysical downhole logging capability; and gas/fluid monitoring, a second break-out session was organized in the afternoon. Groups that were organized by broad discipline (stratigraphy, biology, palaeo-climate, tectonics, volcanology) discussed required sampling material, analyses, and datasets. A geophysics/monitoring group discussed post-drilling downhole and surface geophysical monitoring infrastructure. The day finished with a final discussion on matching funds, funding resources, and time plan for the compilation of the full drilling proposal. Future avenues were explored for an integrative cross-border regional seismic monitoring initiative and a LEAP (Ocean Drilling Legacy Assets Project) initiative for including existing Deep Sea Drilling Project (DSDP) and Ocean Drilling Program (ODP) core records in the Red Sea and Gulf of Aden.

On 31 August, the full ICDP ADD-ON team made a trip through Addis Ababa with a visit to Unity Park and the National Museum of Ethiopia. The day finished at Addis Ababa University with a session on education and public outreach as well as possible links with local education activities inside and outside the academic environment. Key delegates in the discussion were from Addis Ababa University, Semera University, and Mekelle University (Ethiopia). Local MSc and PhD students from Addis Ababa University were invited to join the session and participate in the discussion. Different ideas on how to actively involve local Afar communities and Afar authorities in the drilling project were levered, as well as the potential of recognizing Danakil as a national heritage site.

3 Drilling site

The ADD-ON project aims at deep drilling in the Danakil Depression to provide a unique sedimentary record in an active rift basin paced by global environmental fluctuations and their interplay with volcanic and tectonic events. During the ADD-ON workshops, different drilling sites have been discussed along a basinal transect going from west to east (Fig. 4). Due to financial and technical constraints, it has been decided to only focus on one drilling site in the central part of the Danakil Depression between the Dallol volcano and the Erta Ale volcanic range, i.e. Dallol-01A. This strategic choice avoids major faults and fault zones, as well as gas pockets. The target depth is 2.2 km, aiming to intercept the full syn-rift sedimentary record through continuous coring until the rift basement (Fig. 4). Available site survey data at the potential drill site show the presence of four distinct seismo-stratigraphic units covering the Middle-to-Upper Pleistocene to Holocene ($\sim$ 500 kyr) (Fig. 4). After drilling, we aim to keep the hole open for seismic monitoring and develop a downhole Earth observatory.

4 ADD-ON project strategy

During the workshop discussion, five thematic challenges were flagged, covering the major aim and objectives of the ADD-ON drilling project: the understanding of rapid palaeo-environmental change in rift settings, unravelling the complex interaction between basin dynamics and volcanics, unveiling the deep geo-biosphere in poly-extreme environments, characterizing hydrothermal systems and mineral resources in active rift settings, and developing a downhole Earth observatory to monitor seismic and volcanic hazards (Fig. 5). These are outlined below.

4.1 Rapid palaeo-environmental change in rift settings

Rift basins are characterized by heterogeneous sedimentation patterns varying at very short temporal scale, resulting in complex palaeo-environmental change. The interaction and feedback between tectonics, surface processes, volcanic events, climate variations, and eustasy on sediment

Figure 3. Impressions from the workshop discussions, presentations, and group picture of the workshop participants at Addis Ababa, Ethiopia.

flux, sediment deposition, and basin dynamics explain their complex stratigraphic architecture. Drilling in the Danakil Basin will provide keys to understand the complex palaeo-environmental change in a rift basin near breakup and how this is modulated by climate, tectonic, and volcanic events.

Until now, only the more recent desiccation record has been recovered from the central part of the basin, while outcrops at the basin margin witnessed at least four flooding cycles during which the Red Sea transgressed into the basin. It is hypothesized that the four flooding cycles represent a high-resolution record of approximately 500 kyr. However, how these cycles of flooding and desiccation are expressed in the central Danakil Basin is not known. Having the full syn-rift sedimentary record will help to understand complex sedimentation patterns since the onset of rifting, including the complex transitional phase from continental sedimentation towards the first marine incursion events.

Sedimentation rates in the Danakil Depression are not well constrained due to the lack of deep subsurface data. Detailed stratigraphy will allow for calculating sedimentation rates and their variability through time. This will help to constrain and quantify the non-linear sedimentation rates in an active rift setting.

The last desiccation cycle in the Danakil Depression resulted in the formation of thick halite units (Rime et al., 2024). However, the formation mechanisms of these evaporites as well as the palaeo-hydrological balance of the basin are poorly constrained. Understanding how the Danakil evaporites may form a deep subsurface salt giant remains debatable. Understanding the formation of those evaporites will also help us to understand other salt giants on planet Earth, e.g. the Messinian.

Finally, having access to the high-resolution palaeo-environmental record in the Danakil Depression may also elucidate new insights into regional palaeo-climatic change, especially precipitation patterns, in northeast Africa, influenced by global monsoonal variations and Atlantic driven oscillations. Palaeo-climatic records in northern Afar are lacking – despite it being a critical zone in the corridor between Africa and Eurasia. The combined effects of climate change and the volcano-tectonic evolution of the Afar may have had an influence on the out-of-Africa migration of *Homo sapiens*.

4.2 Interaction between basin dynamics and volcanism

The Danakil Depression is a unique zone where the final transition from continental rifting to seafloor spreading is well

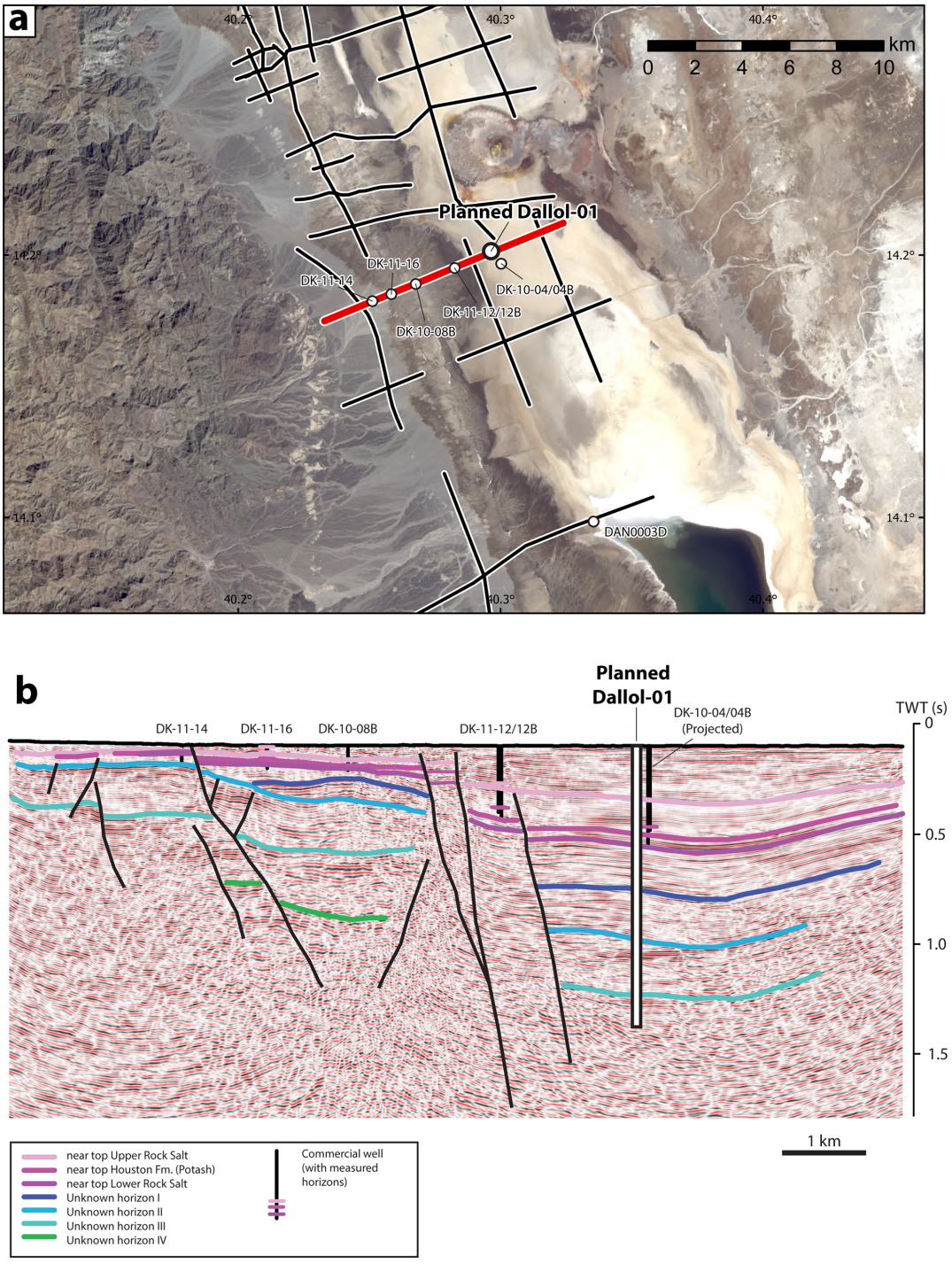

Figure 4. **(a)** Location of the ADD-ON drilling site Dallol-01 (Landsat-8 image). Red line indicates the location of the seismic profile presented in panel **(b)**. **(b)** Seismic section with an indication of the planned drilling site Dallol-01. Seismic profile provided by former Allana Potash Ltd.

exposed subaerially. Constraints from the drill core will significantly aid the interpretation of other datasets such as the surface geology and subsurface seismic images of the basin. Combined datasets will show a 4D picture of how the tectonics and magmatic/volcanic processes unfold in space and time during the final stages of splitting a continent. This will provide key insights to interpret the structure and processes that form magmatic rifted passive margins flanking much of the oceans.

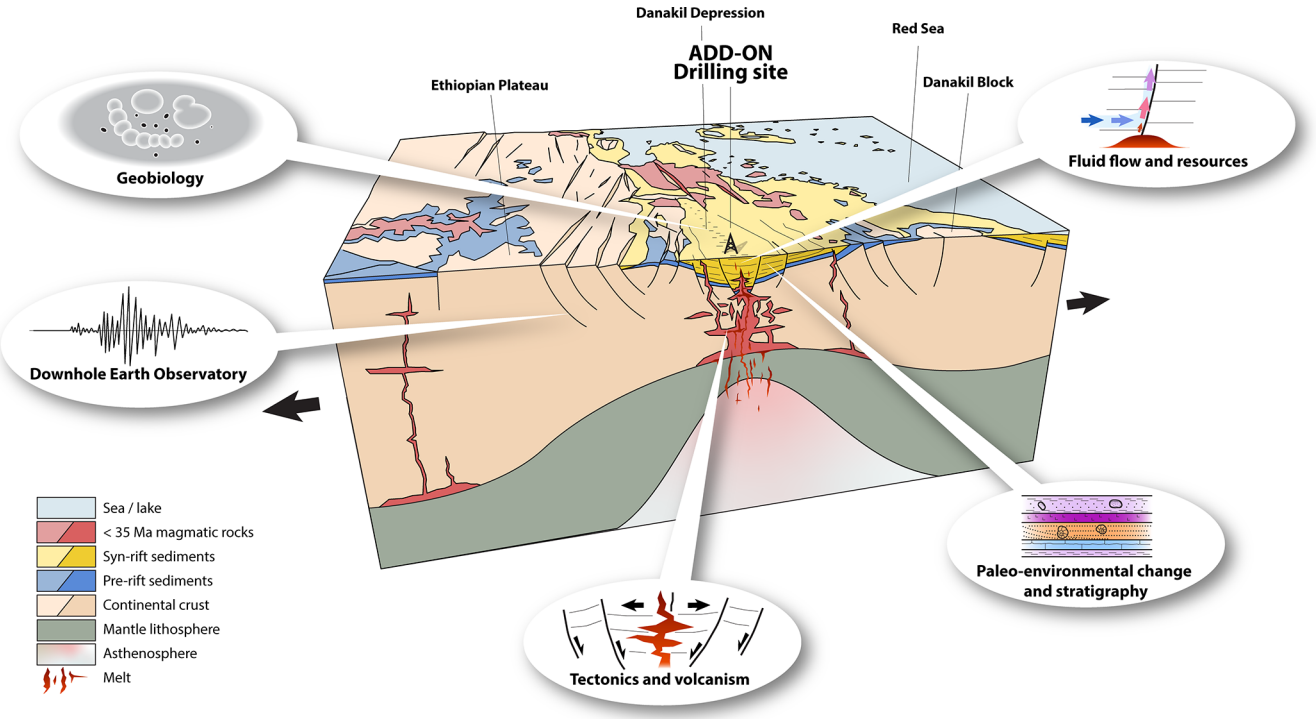

Figure 5. ADD-ON block diagram synthesizing the main objectives of the ADD-ON project.

Traditionally, it was thought that extension via magma intrusion increases during the breakup process (e.g. Ebinger, 2005). However, recent studies of the Danakil Basin show evidence of significant subsidence caused by plate thinning and faulting and thus contradicting standard models (Bastow and Keir, 2011; Rime et al., 2023). A well-dated core record will directly constrain subsidence rates and enable quantitative interpretation of fault slip rates from subsurface seismic images, as well as modelling of associated plate thinning. We will address when did rapid subsidence and fault slip rates initiate and how do these processes vary in space and time.

In addition to the longer-term evolution of basins during the rift to drift transition being uncertain, the short-term interaction between faulting, subsidence, volcanism, sea level, and the sedimentary environment is not well understood. The development of a unique sedimentary record will enable us to develop conceptual and numerical modelling schemes to address what is the sedimentary record of short-term episodic events (volcanic eruptions, earthquakes, flooding) and how do these interact with long-term rift processes.

4.3 Geo-biosphere in poly-extreme environments

The unique Dallol brines and associated hydrothermal fields in the Danakil Depression are ideal natural labs to (1) understand the limits of life in poly-extreme conditions; (2) discriminate biotic from abiotic signatures, using those areas for deriving implications for habitability and life in extra-terrestrial environments; and (3) study the role of archaea and bacteria in mediating mineral precipitation and dissolution. At this stage, it is not yet fully deciphered how extreme halophiles evolved their unique adaptations and if they are also present in brines in the deep anoxic subsurface. Brines and evaporites in the Dallol–Danakil region impose physicochemical, biophysical, and biochemical stress on life that has not been experienced and studied in detail before. Moreover, the interactions of the deep halophilic biosphere with the geosphere are to be unveiled, as well as how metabolic processes affect elemental and biogeochemical cycles.

Having access to the core records will allow us to understand the deep unknown biosphere experiencing poly-extreme conditions, testing the limits of life and opening up a window on the origin of life and/or life in extra-terrestrial environments. Moreover, the recovered pristine records will allow us to study how the deep biosphere interacts with brine circulation in an active rift hydrothermal system.

4.4 Hydrothermal systems and resources

The Danakil Basin has one of the most vigorous hydrothermal systems globally (e.g. Varet, 2017), with fumaroles, hot springs, steam vents, and hot grounds common in the rift and on its flanks. Previous studies suggest the region has all the key component conditions for the development of high-enthalpy geothermal fields, including shallow magmatic heat sources, fault and fracture permeability, and po-

tential aquifers from infiltration of meteoric water from the Ethiopian Plateau into the basement and Mesozoic to Quaternary sediments. However, we lack subsurface petrophysical observations including rock, microfracture, fluid properties, and heat flow data to build realistic models of ground water and hydrothermal fluid flow. The data from the core will constrain how fluid flow in the basin impacts the sedimentary record and fracture/fault evolution. Data from the core should also be combined with other datasets (such as surface gas/fluid flux and chemistry, microseismicity, and surface deformation), along with surface geology, as key inputs to 3D models of fluid and heat flow and geochemical exchanges. The active hydrothermal circulation through evaporites also raises the possibility of commercially viable concentrations of metals such as lithium that are required for global society to transition to renewable green sources of energy. Overall, drilling will allow us to understand better active high-enthalpy geothermal systems and associated green-energy-related resources and directly determine whether there is a major deep aquifer in the basin.

4.5 Hazards: towards a downhole Earth observatory

The Danakil region is seismically and volcanically active, and it experiences ground deformation caused by tectonic, magmatic, hydrothermal, and anthropogenic processes (Pagli et al., 2012; Battaglia et al., 2021; La Rosa et al., 2023). Specifically, we aim to understand where and when earthquakes, ground deformation, and fluid flow occur and what controls these processes, gaining a better understanding of controls and links between these processes to improve forecasts and manage the associated hazards.

After the drilling phase is complete, we aim to use the new borehole site as a platform for a downhole Earth observatory for improved capacity in Ethiopia for short and permanent long-term monitoring of seismic activity, ground deformation, and gas/fluid flux. To this end, a permanent broadband borehole seismometer should be installed in the borehole, combined with a surface GPS station, which will use real-time data transfer into the national monitoring centre at the Addis Ababa Geophysical Observatory. During drilling, we plan to populate the basin with temporary dense networks of these instruments for improved spatial mapping.

5 Societal relevance and public outreach

A major component of the workshop involved presentations and open discussions about the societal relevance of ADD-ON; who the stakeholders in the project are; and how to effectively engage with them before, during, and after the project. Potential stakeholders such as the Energy Office of the Afar National Regional Government; the Afar Geothermal Alternative Power (AGAP) company; representatives from the potash and geothermal sectors; and representatives from the universities of Addis Ababa, Mekelle, and Semera universities led the conversation.

ADD-ON is a research project led by academics with a strong desire and need to engage with local communities. Opportunities were identified to link with ongoing community-based projects to exploit geothermal systems in ways not normally pursued by traditional large-scale commercial projects. The intensive time required to develop and implement the project in the field has offered and offers opportunities to invest in sustainable-geoscience-related educational activities/material for local government, schools, and commercial activities including geo-tourism. The universities expressed a strong desire to use the links, knowledge, data, and drill site developed through ADD-ON to strengthen student training in subsurface characterization as well as using the drill site as a future focus for a field camp, along with archiving core samples and downhole data locally. Using the borehole post-drilling to permanently house a downhole seismometer, linked real-time to the national earthquake monitoring system, provides a mechanism to help support ongoing maintenance of the drill site and also aids hazard and risk assessment for the Afar region.

ADD-ON will further deliver knowledge directly relevant to the wider economic and societal development in Afar and Ethiopia. Deep drilling offers an opportunity to identify and better quantify potential water aquifers, and it also informs on the hydrothermal fluid flow needed for commercial-scale development of geothermal energy. Deep drilling is of direct interest to potash exploration, since the project aims to characterize past marine flooding cycles and therefore potentially identify deeper potash deposits or tap into metal resources key for the global green transition.

Data availability. The map data used in this paper are available at https://doi.org/10.5281/zenodo.7351643 (Rime et al., 2022a) and https://doi.org/10.5281/zenodo.7351765 (Rime et al., 2022b). The seismic profile and core data presented in the paper are courtesy of former Allana Potash Ltd and the Ministry of Mines, Ethiopia.

Team list. ADD-ON Workshop Consortium: In-presence workshop participants: Bekele Abebe (Addis Ababa University, Addis Ababa, Ethiopia), Bahru Asegahegn (University of Cologne, Cologne, Germany), Abate Melaku Assen (Addis Ababa University, Addis Ababa, Ethiopia; University of St Andrews, St Andrews, UK), Balemwal Atnafu (Addis Ababa University, Addis Ababa, Ethiopia), Atalay Ayele (Addis Ababa University, Addis Ababa, Ethiopia), Ian Bastow (Imperial College London, London, UK), Gemechu Bedassa (Addis Ababa Science and Technology University, Addis Ababa, Ethiopia), Behailu Birhanu (Addis Ababa University, Addis Ababa, Ethiopia), Samuel Chernet (Addis Ababa University, Addis Ababa, Ethiopia; Technische Universität Dresden, Dresden, Germany), Alban Cheviet (Université de Franche-Comté, Besançon, France), Addis Hailu Endeshaw (University of Fribourg, Fribourg, Switzerland), Anneleen Foubert (Uni-

versity of Fribourg, Fribourg, Switzerland), Christophe Galerne (MARUM – Centre for Marine Environmental Sciences, University of Bremen, Bremen, Germany), Ermias Filfilu Gebru (University of Fribourg, Fribourg, Switzerland; Addis Ababa University, Addis Ababa, Ethiopia), Mekbib Fekadu Gelaw (Addis Ababa University, Addis Ababa, Ethiopia), Worash Getaneh (Addis Ababa University, Addis Ababa, Ethiopia), Miruts Hagos (Mekelle University, Mekelle, Ethiopia), Henok Haile (Geotest Engineering, Houston, USA), Binyam Hailu (Addis Ababa University, Addis Ababa, Ethiopia), Katja Heeschen (ICDP, GFZ German Research Centre for Geosciences, Potsdam, Germany), Gareth Hurman (University of Southampton, Southampton, UK), William Hutchison (University of St Andrews, St Andrews, UK), Kazuo Kawasaki (University of Toyama, Toyama, Japan), Derek Keir (University of Florence, Florence, Italy; University of Southampton, Southampton, UK), Tesfaye Kidane (Wayne State University, Detroit, USA), Alessandro La Rosa (University of Pisa, Pisa, Italy), Purificación López Garcia (CNRS, Université Paris-Saclay, Paris, France), Lisa McNeill (University of Southampton, Southampton, UK), David Moreira (CNRS, Université Paris-Saclay, Paris, France), Ameha Muluneh (Addis Ababa University, Addis Ababa, Ethiopia; GFZ German Research Centre for Geosciences, Potsdam, Germany), Haileyesus Negga (University of Fribourg, Fribourg, Switzerland; Addis Ababa University, Addis Ababa, Ethiopia), Carolina Pagli (University of Pisa, Pisa, Italy), Valentin Rime (University of Fribourg, Fribourg, Switzerland), Charlotte Spencer-Jones (Durham University, Durham, UK), Amdemichael Tadesse (Free University of Brussels, Brussels, Belgium), Tsedenya Tafesse (University of Newcastle, Newcastle, UK), Jacques Varet (Geo2D, Orleans, France), Nicolas Waldmann (University of Haifa, Haifa, Israel), Emma Watts (University of Southampton, Southampton, UK), Gezahegn Yirgu (Addis Ababa University, Addis Ababa, Ethiopia), Frank Zwaan (GFZ German Research Centre for Geosciences, Potsdam, Germany), Damenu Adefris (Debre Berhan University, Debre Birhan, Ethiopia), Yasin Kadir Ali (Geology, Semera University, Semera, Ethiopia), Serawit Amene (New Africa Global Energy, Addis Ababa, Ethiopia), Belay Yonas Bekele (Circum Minerals, Addis Ababa, Ethiopia), Marco Bohnhoff (ICDP exec. director, GFZ German Research Centre for Geosciences, Potsdam, Germany), Yitemgeta Fantu (Tulu Moye Geothermal, Addis Ababa, Ethiopia), Ismael Ali Gardo (Afar Geothermal Alternative Power Co., Semera, Ethiopia), Tadesse Mamo (Tulu Moye Geothermal, Addis Ababa, Ethiopia), Wonde Megdelawit (Addis Ababa University, Addis Ababa, Ethiopia), Aklilu Tekka (Tulu Moye Geothermal, Addis Ababa, Ethiopia), Gebreegziabher Mekonen Wube (EthioPotash, Addis Ababa, Ethiopia), Yasin Hanfire Yasin (Afar Energy Office, Semera, Ethiopia).

Online workshop participants: Catherine Beck (Hamilton College, Hamilton, USA), Simon Blondel (University of Oslo, Oslo, Norway), Cindy De Jonge (ETH Zürich, Zurich, Switzerland), Francesco Dela Pierre (University of Turin, Turin, Italy), Markus Fischer (University of Potsdam, Potsdam, Germany), Verena Foerster (University of Cologne, Cologne, Germany), Luis Gilbert (University of Barcelona, Barcelona, Spain), Annett Junginger (University of Tübingen, Tübingen, Germany), Said Kamrani (ICDP, GFZ German Research Centre for Geosciences, Potsdam, Germany), Electra Kotopoulou (Université Paris-Saclay, Paris, France), Cindy Kunkel (ICDP, GFZ Potsdam, Potsdam, Germany), Sylvie Leroy (CNRS, Sorbonne University, Paris, France), José Maria López-Garcia (Instituto Geológico y Minero de España, Palma de Mallorca, Spain), Stefano Lugli (Universita di Modena e Reggio Emilia, Bologne, Italy), Craig Magee (University of Leeds, Leeds, UK), Inka Meyer (University of Ghent, Ghent, Belgium), Mengesha Million (Addis Ababa University, Addis Ababa, Ethiopia), Alexis Nutz (Cerege, Aix-Marseille Université, Marseille, France), Yayso Omer (Semera University, Semera, Ethiopia), Lisa Park Boush (University of Connecticut, Storrs, USA).

Author contributions. All co-authors contributed to the text and figures that resulted in the submission of a full ICDP proposal and this workshop report. AF, DK, BaA, and TK chaired the workshop as the scientific committee. BaA, TK, WG, BB, AHE, and HN acted as the local workshop organizing committee. AF and DK wrote the workshop report with involvement especially from the following co-authors: VR and AF worked actively on Figs. 1, 2, 3, 4, and 5 (visualization and data analysis). HN provided the picture material for Fig. 3. TK, BaA, PLG, and KH revised and edited the manuscript. All ADD-ON workshop participants contributed with discussions and intellectual input. AF, DK, BaA, and TK were responsible for the funding acquisition of the ICDP workshop grant and supervised the project.

Competing interests. The contact author has declared that none of the authors has any competing interests.

Disclaimer. Publisher's note: Copernicus Publications remains neutral with regard to jurisdictional claims made in the text, published maps, institutional affiliations, or any other geographical representation in this paper. While Copernicus Publications makes every effort to include appropriate place names, the final responsibility lies with the authors.

Acknowledgements. We thank the local organization committee of the ADD-ON workshop and especially Haileyesus Negga, Addis Endeshaw, and Behailu Birhanu. We acknowledge the state-of-the-art presentations by Valentin Rime, Jacques Varet, and Purificación López Garcia. The Ministry of Mines (Ethiopia), the vice president for R&D transfer (Addis Ababa University, Ethiopia), and the Energy Office of the Afar Regional Government are acknowledged for their support for the ADD-ON workshop and drilling initiative. The potash mining companies (namely EthioPotash and Circum Minerals), Tulu Moye Geothermal, and New Africa Global Energy are thanked for their active participation and contribution to the workshop with technical drilling and logistical expertise. Henok Haile is especially thanked for his technical support with respect to drilling in the Danakil Depression. The moderators and reporters of the break-out sessions, namely Bahru Asegahegn, Atalay Ayele, Ian Bastow, Samuel Chernet, William Hutchison, Ameha Muluneh, Lisa McNeill, David Moreira, Caroline Pagli, Amdemichael Tadesse, Nicolas Waldmann, and Frank Zwaan, are thanked for having chaired the sessions and reported on the discussions. Ismael Ali Gardo (Afar Geothermal Alternative Power company and the associated Afar Pastoralist Development Association (APDA)), Atalay Ayele, Behailu Birhanu, and Jacques Varet are es-

pecially acknowledged for their contributions to the societal relevance of the ADD-ON project. The universities of Addis Ababa, Semera, and Mekelle, as well as the students from the School of Earth Sciences, Addis Ababa University (Ethiopia), are thanked for their participation and active contribution in the workshop session on education and outreach. The ICDP Team, especially Katja Heeschen and Cindy Kunkel, are thanked for their full operational support during the workshop organization.

Information on the ADD-ON project is available at http://www.afardalloldrilling.com (last access: 22 August 2024) and https://www.icdp-online.org/projects/by-continent/africa/afar-ethiopia/ (last access: 22 August 2024).

Financial support. This research has been supported by the Helmholtz-Zentrum Potsdam – Deutsches GeoForschungsZentrum GFZ (ICDP Workshop Proposal 11-2020 ADD-ON). Additional financial contributions have been provided through the SNF (Swiss National Science Foundation) projects SERENA 200021_163114 and CONNECT 200020_212903.

Review statement. This paper was edited by Tomoaki Morishita and reviewed by two anonymous referees.

References

Atnafu, B., Kidane, T., Foubert, A., Jaramillo-Vogel, D., Schaegis, J.-C., and Henriet, J.-P.: Reading history in Afar, EOS, 96, 12–15, 2015.

Bannert, V. D., Brinckmann, J., Käding, K. C., Knetsch, G., Kürsten, M., and Mayrhofer, H.: Zur Geologie der Danakil-Senke: Nördliches Afar-Gebiet, NE-Äthiopien, Geol. Rundsch., 59, 409–443, 1971.

Barberi, F. and Varet, J.: The Erta Ale volcanic range (Danakil depression, northern afar, ethiopia), Bulletin Volcanologique, 34, 848–917, 1970.

Barberi, F., Giglia, G., Marinelli, G., Santacroce, R., Tazieff, H., and Varet, J. with collaboration of Bonatti, E., Borsi, S., Cheminée, J. L., Faure, H., Ferrara, G., Martini, M., and Chèdeville, E.: Carte Géologique de la Dépression des Danakil (1 : 500 000), GEOTECHNIP, CNRS/CNR, 1971.

Bastow, I. D. and Keir, D.: The protracted development of the continent–ocean transition in Afar, Nat. Geosci., 4, 248–250, https://doi.org/10.1038/ngeo1095, 2011.

Bastow, I. D., Booth, A. D., Corti, G., Keir, D., Magee, C., Jackson, C. A.-L., Warren, J., Wilkinson, J., and Lascialfari, M.: The development of late-stage continental breakup: Seismic reflection and borehole evidence from the Danakil Depression, Ethiopia, Tectonics, 37, 2848–2862, https://doi.org/10.1029/2017TC004798, 2018.

Battaglia, M., Pagli, C., and Meuti, S: The 2008–2010 subsidence of Dallol volcano on the spreading Erta Ale Ridge: InSAR observations and source models, Remote Sens., 13, 1991, https://doi.org/10.3390/rs13101991, 2021.

Belilla, J., Moreira, D., Jardillier, L., Reboul, G., Benzerara, K., López-García, J. M., Bertolino, P., and López-Archilia,López-García, P.: Hyperdiverse archaea near life limits at the polyextreme geothermal Dallol area, Nature Ecology & Evolution, 3, 1552–1561, https://doi.org/10.1038/s41559-019-1005-0, 2019.

Bonatti, E., Emiliani, C., Ostlund, G., and Rydell, H.: Final desiccation of the Afar rift, Ethiopia, Science, 172, 468–469, 1971.

Brinckmann, J. and Kürsten, M.: Stratigraphie und Tektonik der Danakil-Senke (NE-Aethiopien), Beih. Geol. Jb., 116, 5–86, 1971.

Ebinger, C.: Continental break-up: the East African perspective, Astron. Geophys., 46, 2–16, https://doi.org/10.1111/j.1468-4004.2005.46216.x, 2005.

Foubert, A., Kidane, T., and Atnafu, B.: Stepping stones towards an unique archive in the Danakil Basin, EGU General Assembly 2018, 18–13 April 2018, Vienna, Austria, https://www.geophysical-research-abstracts.net/ (last access: 26 August 2024), 2018.

Foubert, A., Kidane, T., Keir, D., Atnafu, B., and ADD-ON Team, T. I.: Afar Dallol Drilling – ONset of sedimentary processes in an active rift basin (ADD-ON): Scientific drilling targets in the Afar (Ethiopia), EGU General Assembly 2021, online, 19–30 April 2021, EGU21-14486, https://doi.org/10.5194/egusphere-egu21-14486, 2021.

Holwerda, J. G. and Hutchinson, R. W.: Potash-bearing evaporites in the Danakil area, Ethiopia, Econ. Geol., 63, 124–150, https://doi.org/10.2113/gsecongeo.63.2.124, 1968.

Hurman, G. L., Keir, D., Bull, J. M., McNeill, L. C., Booth, A. D., and Bastow, I. D.: Quantitative analysis of faulting in the Danakil Depression Rift of Afar: The importance of faulting in the final stages of magma-rich rifting, Tectonics, 42, e2022TC007607, https://doi.org/10.1029/2022TC007607, 2023.

Jaramillo-Vogel, D., Foubert, A., Braga, J. C., Schaegis, J. C., Atnafu, B., Grobety, B., and Kidane, T.: Pleistocene sea-floor fibrous crusts and spherulites in the Danakil Depression (Afar, Ethiopia), Sedimentology, 66, 480–512, https://doi.org/10.1111/sed.12484, 2019.

La Rosa, A., Raggiunti, M., Pagli, C., Keir, D., Wang, H., and Ayele, A.: Extensional earthquakes in the absence of magma in northern Afar: Insights from InSAR, Geophys. Res. Lett., 50, e2023GL102826, https://doi.org/10.1029/2023GL102826, 2023.

McKenzie, D. P., Davies, D., and Molnar, P.: Plate tectonics of the Red Sea and east Africa, Nature, 226, 243–248, https://doi.org/10.1038/226243a0, 1970.

Pagli, C., Wright, T. J., Ebinger, C. J., Yun, S. H., Cann, J. R., Barnie, T., and Ayele, A.: Shallow axial magma chamber at the slow-spreading Erta Ale Ridge, Nat. Geosci., 5, 284–288, https://doi.org/10.1038/ngeo1414, 2012.

Rime, V., Foubert, A., Atnafu, B., and Kidane, T.: Geological map of the Afar Depression, Zenodo [data set], https://doi.org/10.5281/zenodo.7351643, 2022a.

Rime, V., Foubert, A., Atnafu, B., Kidane, T.: Geological map of the southern Red Sea and western Gulf of Aden region, Zenodo [data set], https://doi.org/10.5281/zenodo.7351765, 2022b.

Rime, V., Foubert, A., Ruch, J., and Kidane, T.: Tectonostratigraphic evolution and significance of the Afar Depression, Earth-Sci. Rev., 244, 104519, https://doi.org/10.1016/j.earscirev.2023.104519, 2023.

Rime, V., Negga, H., Fentimen, R., El Khorh, A., Pirkenseer, C., Schaegis, J.C., Hajdas, I., Adatte, T., Atnafu, B., Kidane, T., and Foubert, A.: Late Pleistocene to Holocene evaporites in the

Danakil Depression: a modern salt giant analogue, Sedimentology, in review, 2024.

Varet, J.: Geology of Afar (East Africa), Springer, https://doi.org/10.1007/978-3-319-60865-5, 2017.

Varet, J., Barberi, F., Borsi, S., Cheminée, J. L., Giglia, G., Marinelli, G., Santacroce, R., Stieltjes, H., Tazieff, H., La Volpe, L., Lirer, L., Di Paola, M., Demange, J., Black, R., Morton, W., Gasse, F., Taieb, M., and Chèdeville, E.: Geological map of central and southern Afar (1 : 500 000), GEOTECHNIP, CNRS/CNR, 1975.

Viltres, R., Jónsson, S., Ruch, J., Doubre, C., Reilinger, R., Floyd, M., and Ogubazghi, G.: Kinematics and deformation of the southern Red Sea region from GPS observations, Geophys. J. Int., 221, 2143–2154, https://doi.org/10.1093/gji/ggaa109, 2020.

Warren, J. K.: Evaporites: A compendium, Springer, Berlin, p. 1854, ISBN 978-3-319-13511-3, 2016.

Watts, E. J., Gernon, T. M., Taylor, R. N., Keir, D., Siegburg, M., Jarman, J., Pagli, C., and Gioncada, A.: Evolution of the Alu-Dalafilla and Borale volcanoes, Afar, Ethiopia, J. Volcanol. Geoth. Res., 408, 107094, https://doi.org/10.1016/j.jvolgeores.2020.107094, 2020.

Sci. Dril., 33, 219–236, 2024
https://doi.org/10.5194/sd-33-219-2024

Scientific Drilling
Open Access

Active seismic surveys for drilling target characterization in Ossola Valley: International Continental Scientific Drilling Program (ICDP) project Drilling the Ivrea–Verbano zonE (DIVE) phase I

Andrew Greenwood[1,2], György Hetényi[1], Ludovic Baron[1], Alberto Zanetti[3], Othmar Müntener[1], and the MOS field team[+]

[1]Institute of Earth Sciences, University of Lausanne, Lausanne, 1015, Switzerland
[2]Chair of Applied Geophysics, Montanuniversität Leoben, Leoben, 8700, Austria
[3]Dipartimento di Scienze della Terra e dell'Ambiente, University of Pavia, Pavia, Italy
[+]A full list of authors appears at the end of the paper.

Correspondence: Andrew Greenwood (andrew.greenwood@unileoben.ac.at)

Received: 24 September 2023 – Revised: 8 June 2024 – Accepted: 19 June 2024 – Published: 2 September 2024

Abstract. Drilling target locations of the International Continental Scientific Drilling Program (ICDP) project Drilling the Ivrea–Verbano zonE (DIVE) have been initially proposed based on geological knowledge of surface outcrops and the structural context of the Ivrea–Verbano zone (IVZ) and of the Insubric Line. For the determination of the exact locations of drilling sites as well as for drilling geometry planning, we have carried out a series of active seismic experiments to image the subsurface at high resolution. The two drilling sites of project DIVE in Ossola Valley, one near Ornavasso and the other in Megolo di Mezzo, in the central part of the Ivrea–Verbano zone have been surveyed with site-specific velocity models and a seismic data processing chain. The findings have been interpreted in relation with the outcropping structures. These suggest a reasonable continuity from the surface. They also guide the planned borehole orientations: near-vertical at DT-1B (Ornavasso) into the tightly folded Massone Antiform and at 15–20° from the vertical in Megolo across a flank of the broad Proman Anticline. The seismic surveys indicate that the sedimentary overburden is up to 50 m deep at the specific drill sites and can be minimized by relocating the proposed locations. The seismic surveys also indicate that the center of the Ossola Valley contains about 550 m of sedimentary infill, defining the interface of bedrock and Quaternary glacial sediments at about 300 m below sea level.

1 Introduction

The geology of the Ivrea–Verbano zone (IVZ) has been extensively studied for over a century and is arguably one of the most complete exhumed cross sections of the lower continental crust (LCC) and its transition into the uppermost mantle (Fig. 1) in the world. Consequently, these exposed sections in the Western Alps of Italy have been a prime locality to gain insights into the composition, structure, and evolution of the continental lithosphere from surface samples (e.g., Brodie and Rutter, 1987; Fountain, 1989; Quick et al., 1995). Furthermore, prominent geophysical anomalies observed over the IVZ, such as seismic, gravimetric, and magnetic anomalies, have sparked worldwide interest (e.g., Niggli, 1946; Berckhemer, 1968; Lanza, 1982; Kissling et al., 1984; Kissling, 1993; The ECORS-CROP Gravity Group, 1989; The ECORS-CROP DSS Group, 1989; Diehl et al., 2009; Lu et al., 2018; Scarponi et al., 2020, 2021). The common interpretation of the causative structure is a sliver of the Adriatic lower crust and upper mantle, the so-called Ivrea Geophysical Body (IGB), which was finally exhumed during the collision with the European plate (e.g., Schmid et al., 2017).

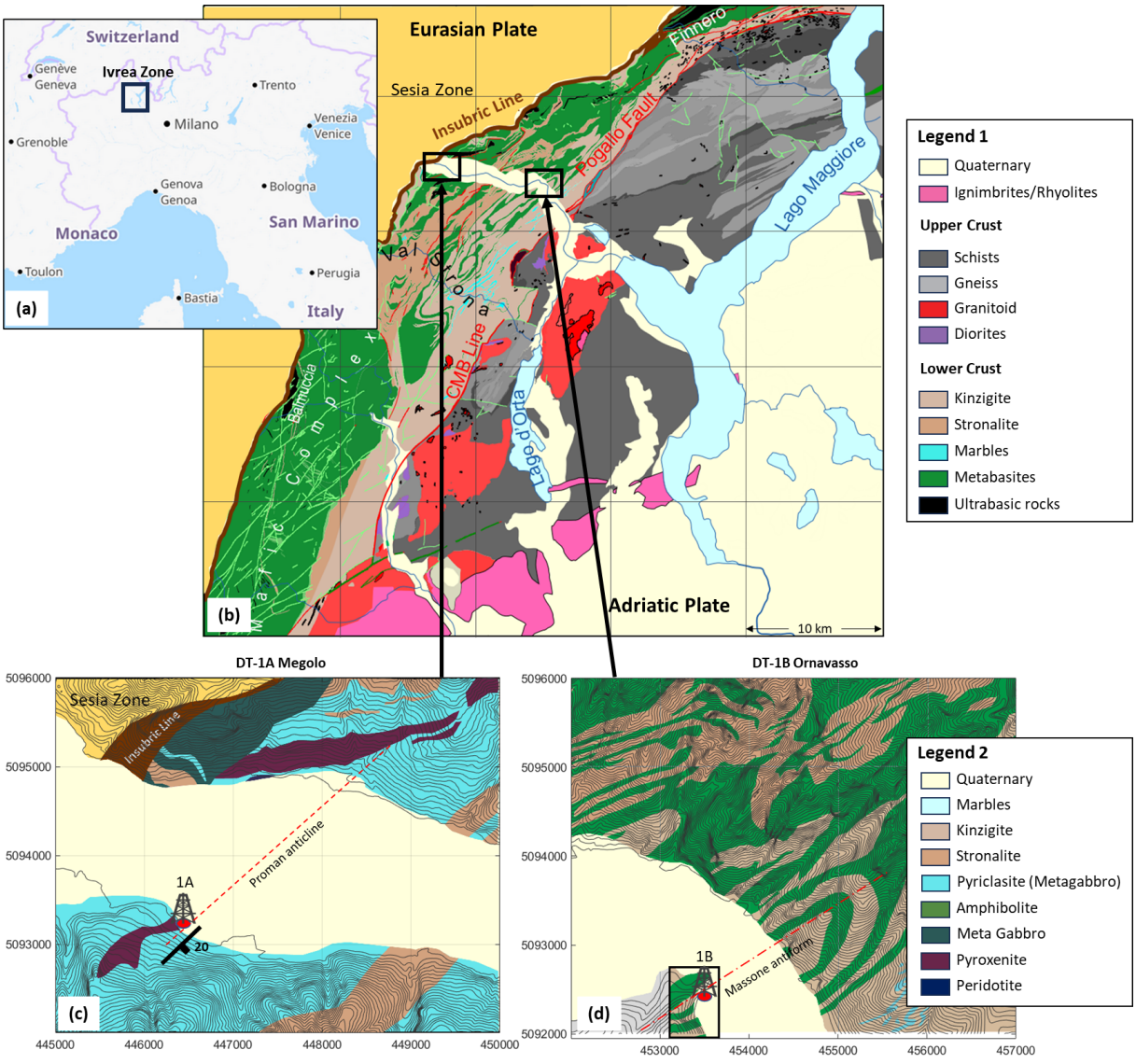

Figure 1. **(a)** Location of the Ivrea–Verbano zone (black rectangle) in Italy. (© OpenStreetMap contributors 2024. Distributed under the Open Data Commons Open Database License (ODbL) v1.0.) **(b)** Overview of the IVZ geology (modified from Brack et al., 2010), with the Insubric Line as the major boundary between the Adriatic and Eurasian plates. Marked by black rectangles are the locations of geologic maps enhanced in panels **(c)** and **(d)**. Refer to Legend 1 for the geologic unit description of **(b)**. Geologic units of the Sesia zone west of the Insubric Line are not shown. Panels **(c)** and **(d)** show the local geology (modified after Burlini, 2008) of the DT-1A and DT-1B drill sites. The proposed drill locations are marked by red dots and a drill rig symbol. The Sesia zone geologic units and the Insubric Line mylonites are not fully described. Refer to Legend 2 for the geologic unit description for areas in panels **(c)** and **(d)**. The dashed red line indicates the strike of the Proman Anticline, which dips ESE at 20°in Megolo. The dotted–dashed red line indicates the orientation of the Massone Antiform axial plane. The southern geology in panel **(c)** and the insert in panel **(d)** have been mapped by DIVE.

Based on the intense interest in deepening our understanding of the lower crust, the Drilling the Ivrea–Verbano zonE (DIVE) project has been approved and co-funded by the International Continental Scientific Drilling Program (ICDP). Drilling is the only way to analyze the deepest, non-exposed portions of the IVZ crustal sections in a continuous manner by means of fresh rock cores. Using this method, the DIVE project aims at unraveling long-standing fundamental questions on the nature of the LCC and the characteristics of the underlying physical and chemical rock properties across a broad range of spatial scales and investigating potential microbiological niches; these will ultimately provide unique insights into the architecture of the LCC and the processes that have formed it. For a detailed description and motivations to initiate project DIVE, we refer to Pistone et al. (2017). Scientific drilling is planned to have two phases.

DIVE phase II, in the future, is planned to be in Sesia Valley (Liu et al., 2021; Ryberg et al., 2023), with the promising target of drilling through the crust–mantle transition zone, the Moho (Fig. 1), whereas the approved and funded DIVE phase I plans to drill two boreholes that are 1 km in length, DT-1A (5071-1A, IGSN ICDP5071EH10001; Müntener, 2024a) and DT-1B (5071-1B, IGSN ICDP5071EH30001; Müntener, 2024b), into two portions of an archetypal lower crustal section in the central IVZ (Fig. 1) that have been selected primarily based on the geological structure (see details in Pistone et al., 2017). The recovered rock cores in combination with a comprehensive downhole logging program and high-resolution geophysical studies will significantly advance our knowledge with respect to the geological information collected at the surface.

In preparation for the borehole location and orientation as well as for post-drilling interpretation of the DIVE phase I, a set of active seismic surveys has been planned with the aim to image the subsurface structure at and around the targeted borehole locations. This is highly needed to cover the gap in spatial scales between the regional geophysical structure (known from broadband seismology and gravity results) on the 1–10 km scale and the future borehole geophysics dataset at the 0.1–1 m scale. Furthermore, although the surface geological structure is mapped in detail and topographic relief and deformed structure allow for some level of downward extrapolation, it is essential to perform an actual site characterization by high-resolution active seismic methods. This was planned not only with the departure hypothesis that surface geology is reasonably continuable downward and to verify that there are no unexpected subsurface discontinuities at the drilling target locations, but also to precisely locate and optimally orient the borehole for the DIVE scientific targets to be reached, such as reaching the deepest structural layers possible during drilling.

With these objectives in mind, the corresponding active seismic surveys have been carefully planned and completed. These investigations concentrate on transects within the Ossola Valley to characterize the vicinity of the DT-1A and DT-1B drill hole locations in Megolo and Ornavasso (Fig. 1), respectively. Here we present the results of our so-called MicrO-SEIZE (SEismic imaging of the Ivrea ZonE; MOS) active seismic campaigns. The observations are discussed with respect to the prevailing structure and planning of the drilling operations. An ancillary goal is to determine the bedrock–Quaternary sediment interface, which provides additional constraints when defining the precise drill sites. The overall findings will ultimately serve for the interpretation of the rich program of borehole geophysical results of both drill holes.

2 Geological setting of DIVE phase I drilling targets

The central IVZ consists of highly variable amphibolite to granulite facies rocks (e.g., Schmid and Wood, 1976; Sills, 1984), dominated by garnet-bearing metasediments, enriched in U, Th, and K, intercalated with minor marble and mafic rocks (e.g., Redler et al., 2012) and locally cut by alkali syenites, carbonatites, and ultramafic pipes (e.g., Schaltegger et al., 2015; Galli et al., 2019; Garuti et al., 2001). It is characterized by large-scale folds, Permian to Jurassic high-temperature shear zones, low-grade Alpine deformation, and past partial melting represented by migmatites (e.g., Rutter et al., 2007; Ewing et al., 2015; Wyatt et al., 2022). The dominant Paleozoic deformation was responsible for the formation of large-scale folds (Massone Antiform; Rutter et al., 2007), whilst Alpine tilting resulted in the general orientation of the foliation that dips steeply northeast or southwest. Previous deformation is documented by small- to large-scale tight folds (Candoglia Antiform; Rutter et al., 2007). Alpine shortening and back-thrusting followed by dextral strike-slip deformation caused the formation of the large-scale Proman Anticline (Schmid, 1967; Rutter et al., 2007), localized greenschist facies fabrics, cataclasites, and pseudotachylytes (Obata and Karato, 1995; Souquière and Fabbri, 2010; Pittarello et al., 2012; Garde et al., 2015).

The Ornavasso borehole is expected to intersect the pre-Permian dominantly felsic heterogeneous upper part of the lower crust in the hinge of the tightly folded Massone Antiform. Site surveys indicate that intercalations of amphibolite facies, metasedimentary, and metamafic rocks are present and there is a reasonable chance to investigate the transition into denser rock types. At Megolo, an inclined borehole is planned to intersect the Proman Anticline, a pre-Permian part of the continental lower crust characterized by peridotite–gabbro–metasedimentary interfaces, dipping approximately 20° east-southeast. Together, these two sites will provide a comprehensive section of Ivrea LCC lithologies and may encounter the transition into deeper mantle rocks.

3 MicrO-SEIZE surveys

MicrO-SEIZE (MOS) surveys were conducted over a period of 12 d in mid- to late June 2019, utilizing a 26 000 lb (12 247 kg) EnviroVibe 2™ vibrator source. A total of four seismic reflection surveys, one in Megolo, two in Ornavasso (Ornavasso primary, OP; Ornavasso secondary, OS), and a transect crossing from Premosello–Chiovenda south toward Megolo (PCM), make up the database (Fig. 2). The Ossola Valley is a deep glacial valley bounded by steep (ca. 25–30 degree), densely vegetated mountain flanks. Consequently, the valley hosts agricultural pastures, the Toce River, major arterial roads, water canals, and rail lines, which impose major constraints on seismic survey design and generate anthropogenic noise. In addition to these constraints and to avoid drilling thick Quaternary sedimentary overburden, the DT-

1A and DT-1B drill sites are located very close to the valley sides, further complicating the coverage obtainable with surface seismic arrays. Nonetheless, survey planning utilized existing roads, pathways, and open grass fields to cover as much area as possible around the borehole sites, to reduce the environmental impact on cultivation, and to ease operation logistics. In the Megolo survey, between 446750 and 447000 m E (Fig. 2b), in order to maintain better geophone coupling, it was decided to plant geophones along an old disused highway, whilst the EnviroVibe followed the current road, which navigates over a large stormwater culvert spanned by a bridge and gentle ramps.

Seismic equipment and operational support for the surveys were supplied by the Montanuniversität Leoben (MUL), the University of Lausanne (UNIL), the University of Pavia, the University of Trieste, and the vibrator source supplied by Geo2X SA. Geophones with a nominal resonant frequency of 15 Hz were used in conjunction with two cabled distributed seismic systems: (1) SUMMIT X One™ system, with 240 channels (MUL) nominally spaced at 10 m along in lines and (2) Geometrics Geode system (UNIL and Geo2X), with 144 channels nominally spaced at 5 m deployed along supplementary and crosslines. The EnviroVibe produced a broadband vibroseis sweep of 12.5 to 150 Hz over 12 s. The seismic records were recorded at 1 kHz with a 4 s correlation time. This ensured the recording of both low-velocity layers of variable thickness and steeply dipping (greater than 45°) reflections that may have been produced by far-offset source points. A Pelton vibrator controller and a GISCO radio trigger were used to synchronize the vibrator sweep and the two seismic acquisition systems. A summary of acquisition parameters is provided in Table 1.

In the anticipation of complex and steeply dipping structures, the surveys were designed to capture potentially 3D cross-dipping reflections whilst maintaining a wide-angle reflection profile orthogonal to the strike of the target structures, the Proman and Massone antiforms. This is achieved using the crossed array method (Figs. 2 and 3), whereby the principle seismic coverage across strike is attained along a central (2D) receiver line, the in line, with long offsets of up to approximately 2 km and complemented by shorter orthogonal crosslines to help constrain structural dips oblique to strike. Vibrator points (VPs) were along both the in- and crosslines, and along nearby farm tracks where possible. This greatly increases the common-midpoint (CMP) coverage, providing a sparse 3D coverage (Fig. 3). Where large segments of profile have co-located sources and receivers, the fold is as high as 70, and up to 195 in the center of the OP profile. Figure 3c shows linear areas of high fold in orthogonal orientations due to the crossed array method.

In addition to the aforementioned MOS surveys, a very shallow penetrating seismic survey, nanO-SEIZE, utilizing a 1.5 m geophone separation and a 35 kg ELVIS VII portable vibrator (Table 1) was conducted to extend the northwest extent of the OS profile. This allowed a very near-surface characterization of the immediate vicinity of the DT-1B drill site by placing a high density of sources and receivers up to the adjoining cliff face.

4 Processing

A standard processing sequence for the MOS datasets is applied based on parameters derived from P-wave reflection processing of the PCM transect. Importantly, this transect is processed first to understand the overlying Quaternary sedimentary cover in the Ossola Valley. Moreover, the PMC profile is the simplest of the profiles to process due to the horizontal layering of the valley infill, and it is relatively noise-free due to the profile being somewhat away from roads, railways, and the Toce River. Following this, processing flows are adapted to the more complex scenarios in Megolo and Ornavasso.

Processing typically involved the following procedures:

- vibroseis correlation (pilot trace),
- applying geometry to the seismic records (UTM 32 coordinate system),
- bad trace editing,
- trace conditioning and amplitude corrections (bandpass filtering, spherical divergence correction, and trace equalization),
- vertical stack (stacking of shot records),
- spiking deconvolution,
- crooked-line common-midpoint (CMP) binning,
- first-break picking and refraction analysis,
- static corrections,
- S-wave removal (time-variant bandpass filtering and $f-k$ filtering),
- first arrival removal (top mute),
- normal moveout (NMO) correction and CMP stacking (NMO stack),
- velocity modeling,
- post-stack filtering and amplitude corrections.

The conditioned NMO stacked sections are then reviewed for the refinement of processing parameters and updating velocity models. Subsequently, flow procedures are re-run and pre- and/or post-stack time migration applied to the resulting NMO-corrected data. RadexPro© professional seismic processing software is used to process all MOS data, and

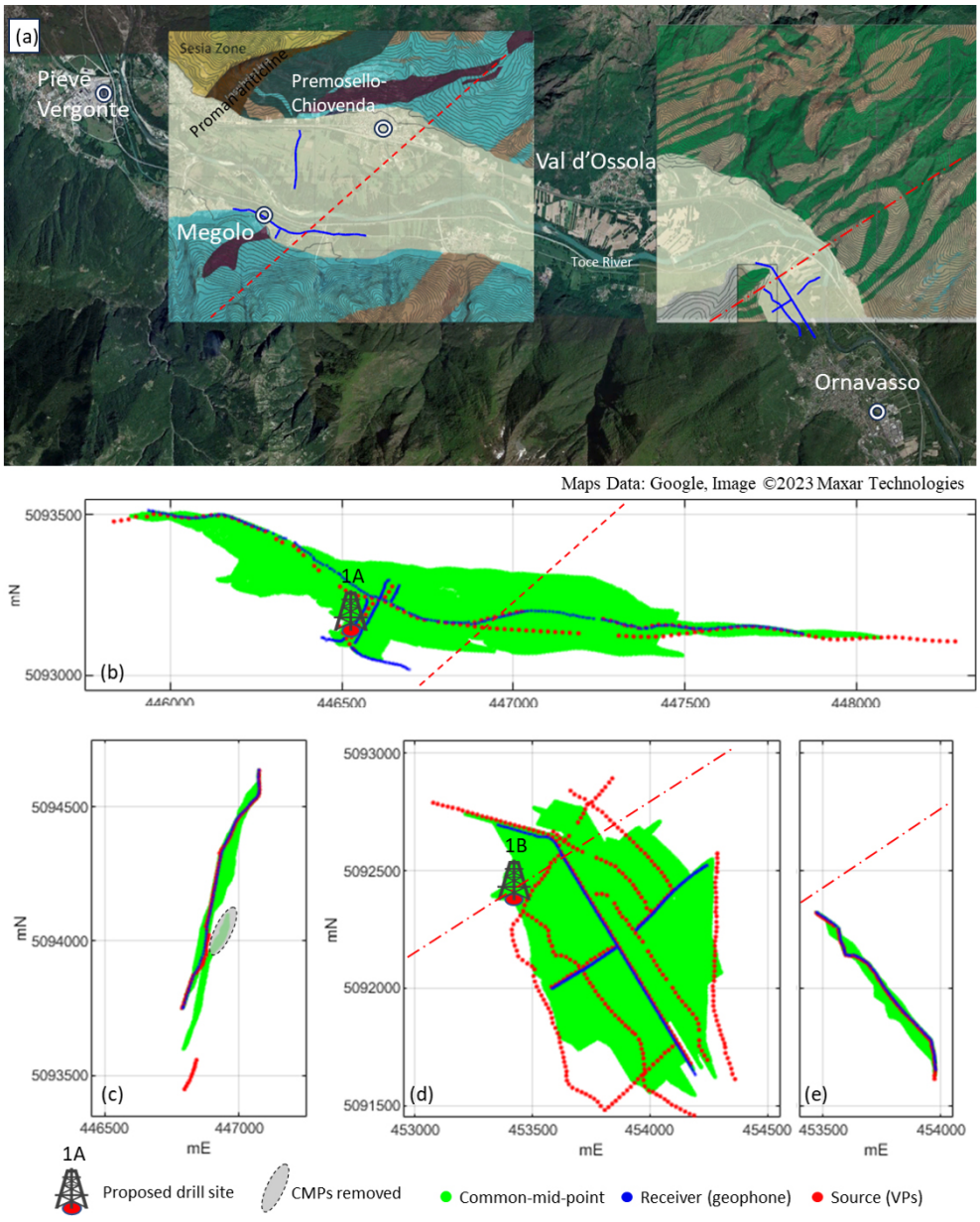

Figure 2. **(a)** Location of the MOS active seismic surveys within the Ossola Valley. Seismic receiver lines are indicated by blue lines and the geology overlay maps and lithologies are as described in Fig. 1. Common-midpoint (CMP) maps for **(b)** the Megolo primary (MP) profile, **(c)** the Premosello Chiovenda–Megolo (PCM) profile, **(d)** the Ornavasso primary (OP) profile, and **(e)** the Ornavasso secondary (OS) line. CMPs are shown as green dots, whereas source and receiver locations are displayed as red and blue dots, respectively. For reference, the Proman Anticline and Massone Antiform are indicated by dashed and dotted–dashed red lines, respectively (refer to Fig. 1). CMPs that were removed from the Premosello–Megolo profile processing are indicated with a dashed grey oval. **(d)** displays the crossed array method whereby the receiver lines are approximately orthogonal to each other and oriented to be orthogonal and parallel to the main strike.

MATLAB© scripts are used to develop 3D velocity models outside of RadexPro. Additional profile-specific processing, such as static corrections and velocity modeling, are described in the following sections along with the results of each profile.

5 Results

5.1 Data quality and refraction analysis

Data quality for the MOS profiles is mixed, whereby the near offsets are generally of good quality and far offsets strongly affected by constant road noise. This is improved by sweeping twice (or more) at each VP. However, in the MP pro-

Table 1. Acquisition parameters.

Profile	Megolo	Ornavasso primary	Ornavasso secondary	Premosello transect	nanO-SEIZE
Spread type	Static – crossed array	Static – crossed array	Static – 2D	Static – 2D	Static – 2D
Number of channels	340	294	79	78	96
In line	195	142	79	78	96
X line	48 + 72 + 13 + 12	65 + 87	–	–	–
Receiver type	15 Hz, 1C	15 Hz, 1C	15 Hz, 1C	15 Hz, 1C	15 Hz, 1C
Spacing in line	10 m	10 m	12 m	12 m	1.5 m
Spacing X line	5 m	5 m	–	–	–
Source	26 000 lb (12 247 kg) EnviroVibe 2	26 000 lb (12 247 kg) EnviroVibe 2	26 000 lb (12 247 kg) EnviroVibe 2	26 000 lb (12 247 kg) EnviroVibe 2	35 kg ELVIS portable vibrator
Source spacing	20 m	20 m	12 m	12 m	1.5 m
Source points	126	394	80	88	96
In line	110	176	80	78 + 10 far offset	96
X line	11	16 + 11	–	–	–
Sweep parameter	12 s, linear, 12–150 Hz	12 s, linear, 12–150 Hz	12 s, linear, 12–150 Hz	12 s, linear, 12–150 Hz	
Sample rate	1 ms	1 ms	1 ms	1 ms	0.5 ms
Record length	12 + 4 s	12 + 4 s	12 + 4 s	12 + 4 s	10 + 1 s
Sweeps per source point	2–4	2–3	1–2	1–2	2
Near-offset/skid	0 m/2 m	0 m/2 m	0 m/2 m	0 m/2 m	0 m/0.5 m
Maximum offset	2192 m	1590 m	848 m	929–1218 m	125 m
Recording instrument					
In line	SUMMIT X	SUMMIT X	SUMMIT X	SUMMIT X	GEODE
X line	SUMMIT X and GEODE	SUMMIT X and GEODE	–	–	–

file, both source and geophone coupling were variable due to the diversion around the aforementioned stormwater culvert. This resulted in variable data quality, data gaps, and low fold between 446750 and 447000 m E. In an exemplary example of good data from the OS profile collected away from noise sources, seismic refraction energy reaches the far offsets, and near-surface reflections are clearly observed between 100 and 300 ms in the raw shot records (Fig. 4). However, shot records over crystalline rock, such as the northwest end of the OP profile, no such reflections are observed.

The first-break arrival times of refracted phases were manually picked for each profile and displayed in MATLAB for quality control. This, in general, showed very linear refracted phases within the valley, which is consistent with a topographically flat and homogeneous sedimentary cover. Simple refraction analysis using the generalized reciprocal method (Palmer, 1981) (Easy Refraction module; RadexPro) is performed and results in a simple two-layer case, with average velocities of 200 and 1520 m s^{-1}, respectively, for the two layers (Fig. 5b). It should be noted in Fig. 5a that the refracted phase already arrives at the nearest receivers, indicating a very shallow interface. The two layers are interpreted to be dry and saturated sediments, respectively. The non-saturated zone above is on average only approximately 5–10 m thick (Fig. 5) and agrees with the approximate height above the nearby Toce River. Thus, the elevation and refraction static corrections were negligible for all areas. Deeper, second refractive layers, in general, were not observed, except in the MP profile, and this supports the assumption of thick valley sediment infill away from steeply dipping valley walls.

5.2 Velocity modeling

Velocity models are developed for each profile and are presented with the results of each profile. The classic 1D velocity semblance analysis of NMO-corrected CMP panels (e.g., Yilmaz, 2001) is not applied, as the nominal 10 m receiver separation used results in poor imaging of the first 50–100 m (100–200 ms two-way travel time). However, the basic principle of applying NMO corrections in a series of velocity panels to determine the correct stacking velocity

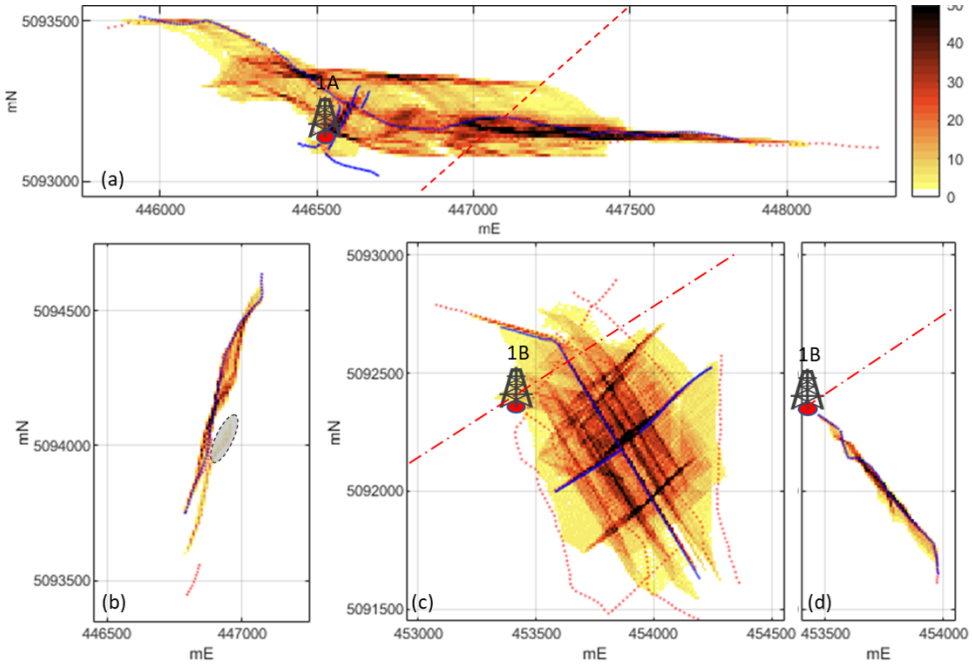

Figure 3. Fold maps for **(a)** Premosello, **(b)** Megolo primary profile, **(c)** Ornavasso primary profile, and **(d)** Ornavasso secondary profile. Source and receiver locations are defined by red and blue dots, respectively, and the relative location of DT-1A and DT-1B are shown. Fold is calculated for a 10 × 10 m bin size. The color bar indicates the fold of each bin. All fold values higher than 50 are indicated in black.

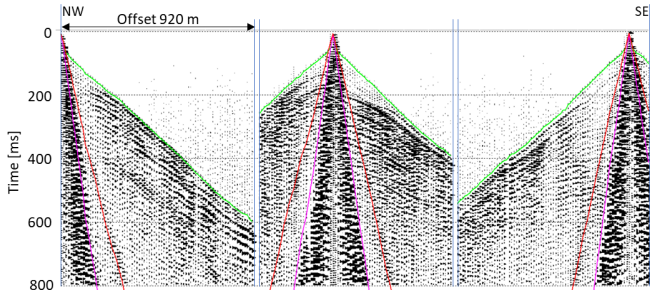

Figure 4. Exemplary shot records without topographic correction from the OS profile, annotated with the first arrivals (green), the airwave arrival (330 m s^{-1} red), and the very slow ground roll (200 m s^{-1} magenta). The vertical axis is two-way-travel-time in milliseconds. Only the first 800 ms out of 4000 is shown. Trace normalization has been applied for display.

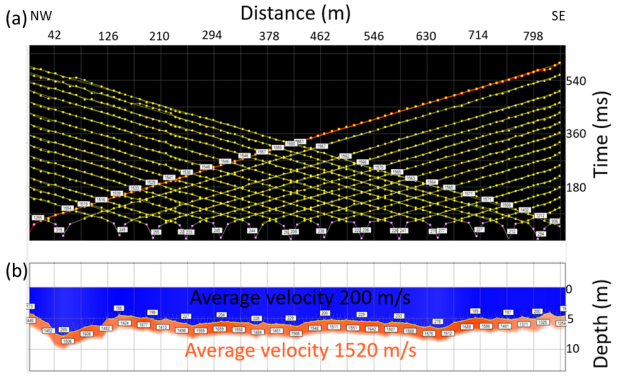

Figure 5. Generalized reciprocal method of refraction analysis from the OS profile. **(a)** First-arrival offset-travel-time curves from every fifth source point of the Ornavasso secondary profile. **(b)** Two-layer velocity model derived from travel time curves in panel **(a)**.

is applied. To resolve the uppermost sediment layer, velocities from the refraction analysis are used as a starting point, and constant-velocity stacks (CVS) using a small range of velocities (1400–1600 m s^{-1} at 20 m s^{-1} intervals) centered around the first refractor velocity (determined in the previous section) are applied to the data. For the PCM profile, the optimal near-surface stacking velocity is 1480 m s^{-1}, which is slightly slower than the average refractor velocity observed in the OS profile. To resolve horizontal reflectors below 100 ms, a series of velocity gradients is then trialed. A gradient of 0.00167 m s^{-1} is found to coherently resolve horizontal reflectors at times up to 500 ms (ca. 500 m) and is used for subsequent velocity models for the valley sediments and delineating the sedimentary basement contact. From this contact, more advanced velocity models are developed to account for the crystalline crustal rocks. In general, higher-velocity areas are graphically picked from the basement contact and a gradient is applied to smooth the boundary. Various boundary gradients and upper velocity limits are tested. The upper velocity in the PCM and OS profiles that returns the best images is 5500 m s^{-1}. These simple 2D models accu-

rately resolve the sedimentary basement contact in the PCM, OP, and OS profiles, which are generally perpendicular to the basement contact. However, the MP profile is (sub)parallel to the local valley walls, which dip to the north, and the Proman Anticline, which dips to the west. Thus, a 3D velocity model is developed for the MP profile.

5.3 Premosello–Chiovenda to Megolo

To increase the CMP coverage of the PCM profile in the south, where access is restricted (Fig. 2b), far-offset VPs are acquired past the termination of the geophone line. These long-offset VPs are offset from the projected receiver line, resulting in laterally offset CMP positions. To reduce the effects of the non-collocated CMPs, a selection of the offset-CMPs is removed before stacking. Results from the PCM profile are shown in Fig. 6. These consist of an NMO stack and a pre-stack time migration (PSTM) section, derived using a gradient velocity model, as described in Sect. 5.2. A weathered crystalline contact with a velocity of 4500 m s^{-1}, which increases to 6000 m s^{-1}, has been assumed (Fig. 6b). The sections are converted from time to depth (T2D) using only the gradient velocity, thus preserving the depth to the base of the valley. The velocity model is considered reliable, as reflectors within the Quaternary sediments are well imaged and typically flat-lying, with many coherent reflections down to 500 m, i.e. the base of the sediments (Fig. 6c). These sedimentary reflections often show local variation and changes in continuity, indicating potential movement within the sediments and paleo-erosion surfaces (e.g., ca. 100 ms highlighted in green). Shallow reflections in the southern end of the profile are affected down to approximately 300 ms by the large and lateral displacement of CMPs. Automatic NMO stretch-muting has also been applied in the upper portion of this zone and along the profile, reducing the resolution in the upper 50–100 ms. The sedimentary bedrock interface is generally well imaged (highlighted), indicating a wide U-shaped valley, the center of which is at approximately a 300 m profile distance, which is equivalent to the center of the Ossola Valley at this location.

PSTM imaging (Fig. 6d) improves the coherency of the Quaternary sediment crystalline interface and structure of the U-shape valley. Coherent reflections below this contact within the crystalline basement, however, are not observed, and migration smiles dominate below 600 m.

5.4 Megolo

The Megolo DT-1A drill hole is planned to intersect a crystalline rock sequence of garnet-bearing metagabbros, charnockitic granites, pyroxenites, and potentially peridotites within the IVZ. The dominant metagabbro (pyriclasite in Fig. 1d) dips approximately 20° east-southeast and forms part of the Proman Anticline (Fig. 1c). The survey consists of a central 2.3 km long receiver line (in line, across strike) that follows the F. M. Beltrami Road which connects Megolo to Pieve Vergonte and Ornavasso and a section of old disused road that crosses a water channel to the east of Megolo di Fondo as well as two closely spaced short crosslines placed within the nominated DT-1A drill site (Fig. 7a).

5.4.1 X line

Along the crosslines, the data are of extremely high quality due to the short offsets and excellent coupling of both the EnviroVibe and geophones, with a shallow dipping reflection that is very apparent in the raw data (Fig. 7b). The data are processed to produce a simple depth-converted NMO stack (Fig. 7c). Again, due to stretch-muting and the survey geometry, the upper 100 m of the section has poor resolution. However, the processed stack locates the prominent reflector at 45–50 m depth below the proposed drilling location dipping approximately 30° toward north-northeast. This is interpreted as the contact between the Quaternary sediments and metagabbros of the valley basement rocks, which outcrop some tens of meters south of the drill site (Fig. 2). When this section is placed in line with the PCM transect (Fig. 8), it is obvious that the dipping reflector conforms with the glacial valley structure seen in the PCM transect. Again, reflections within the crystalline basement rocks are not well observed, partially due to the short extent of the crossline profile, although it is expected that more energy is transmitted through the Quaternary sediment–crystalline basement interface in this area due to the better coupling and thinner sedimentary cover.

5.4.2 In line

Refraction depths and velocities varied from west to east with variable near-surface conditions. Additionally, the western end of the profile is slightly topographically elevated and crosses over a shoulder protruding from the southern valley flank.

Refraction analysis of the Megolo in line profile is shown in Fig. 9. This clearly shows the elevated high-velocity section in the west corresponding to the subsurface extension of the southern valley flank, the slow valley sediments in the center, and a higher-velocity near-surface feature at the eastern end of the profile. Corresponding elevation and refraction static corrections are applied to the inline dataset. Processed results are shown in Fig. 10 and consist of NMO, PSTM, and post-stack time migration (PostSTM) sections presented in two-way travel time. Within these processed sections, the contact at the base of the Quaternary sediments is reasonably well mapped and agrees with the refraction analysis (Fig. 9) and the assumption that the crystalline rock is closer to surface in the west and gently dips to the east. At the eastern end of the profile, a shallow horizontal reflector is prominent in the PSTM image (Fig. 10b and e), coinciding with the higher-velocity zone exposed in the refraction analysis. Here

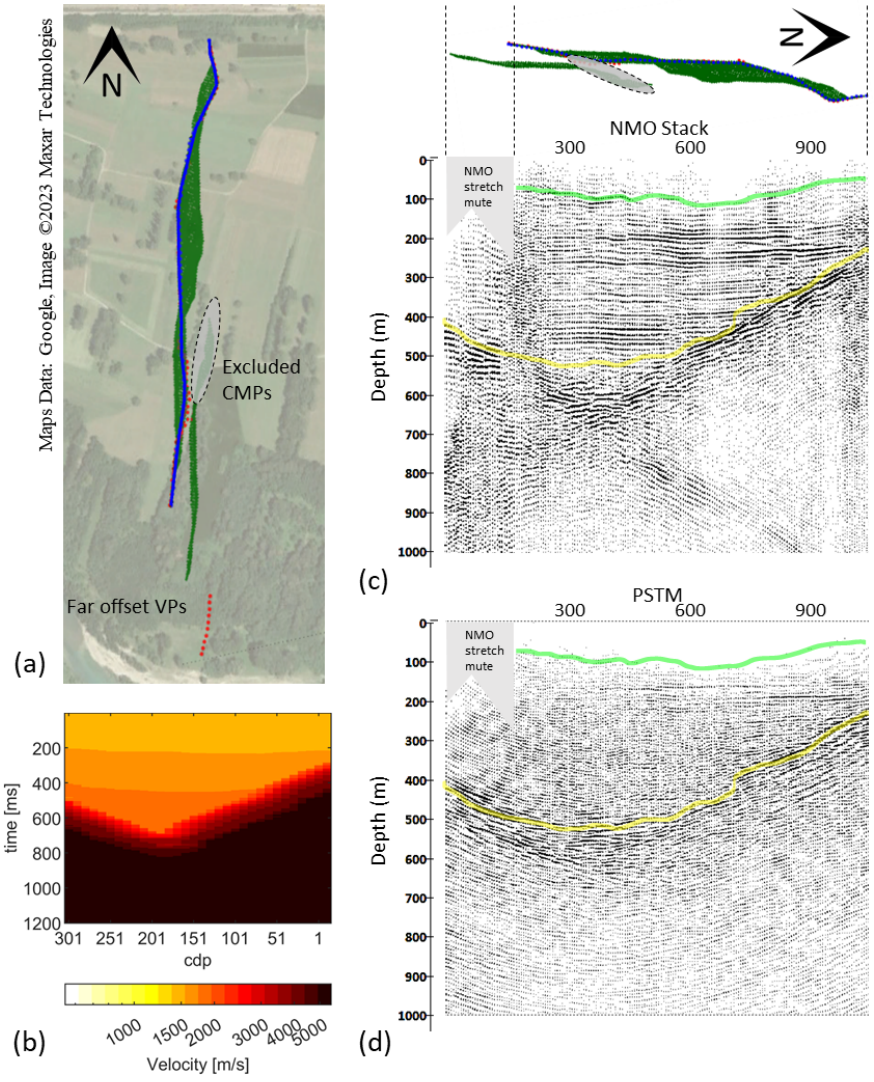

Figure 6. Premosello–Chiovenda-to-Megolo seismic section. **(a)** CMP map overlaying the aerial photo showing the extent of the receivers (blue dots) and source points (red dots), CMPs (green dots), and CMPs that are excluded from the stack (grey oval). **(b)** Velocity model showing a gradient from 1480–1850 m s^{-1} down to 500 ms in the sedimentary deposits and a weathered contact from 4500 to 6000 m s^{-1}. **(c)** NMO stack derived from the velocity model in panel **(b)**. The survey geometry is displayed above the profile indicating where the out-of-plane CMPs have a negative influence on the stack and where fold decreases at the edges of the profile. **(d)** Pre-stack time migration derived from velocity model. **(b)** Low-fold and offset CMPs in the south end of the profile result in many migration smiles. The green line indicates a potential paleo-surface within the Quaternary sediments, whilst the yellow line is the contact between the sediments and valley basement rocks.

a complex overburden is also observable. Within the crystalline rock, there is little reflection energy received, and each of the processed sections reveals different seismic features. The NMO stack maps the strong reflection from the sedimentary basement well, indicating discontinuities and terminations (Fig. 10a and d). Below this, however, the stack is particularly bland. The PostSTM profile (Fig. 10b and e) similarly shows little below the Quaternary–basement contact and progressively smears the seismic energy into smiles beyond 500 ms, an artifact of the migration process due to a lack of coherent reflectors being present. However, the seismic character is consistent for approximately 400 ms below the sediment contact, indicating a shallow dip to the east. The PSTM profile (Fig. 10c and f) over-migrates the near-surface, with many smiles evident; however, a weaker shallow (100 ms) reflector in the east has become more coherent (marked with a blue arrow Fig. 10d–f), and the dipping seismic character has been enhanced in the west updip of the origin of the crystalline rock.

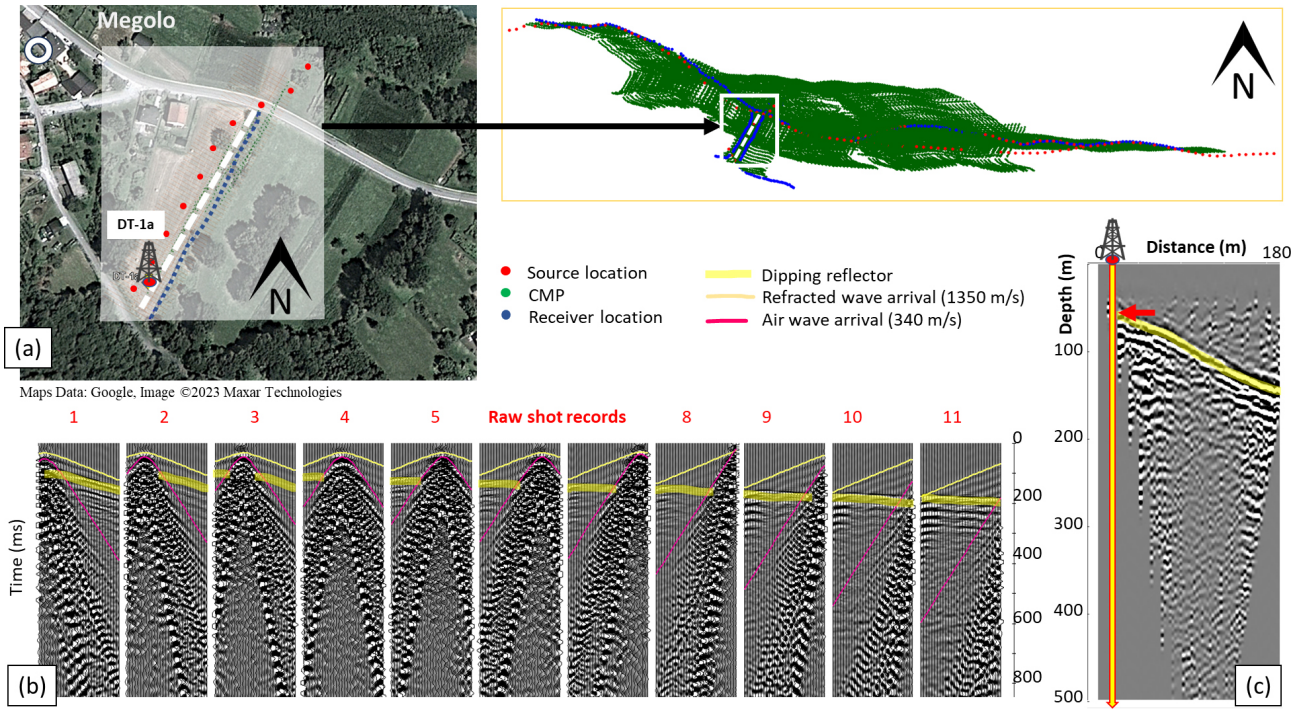

Figure 7. Megolo high-resolution (5 m geophone spacing) crossline profile. **(a)** Plan view of DT-1A site area and the short crossline. **(b)** Raw shot records after correlation of the vibroseis sweep. The first-arrival (yellow), airwave (magenta), and shallow dipping reflector (highlighted in yellow) are clearly visible. **(c)** NMO reflection profile after simple processing. A near-surface dipping reflector (highlighted in yellow) has been imaged at a depth of 45 m, dipping at 30° to the north.

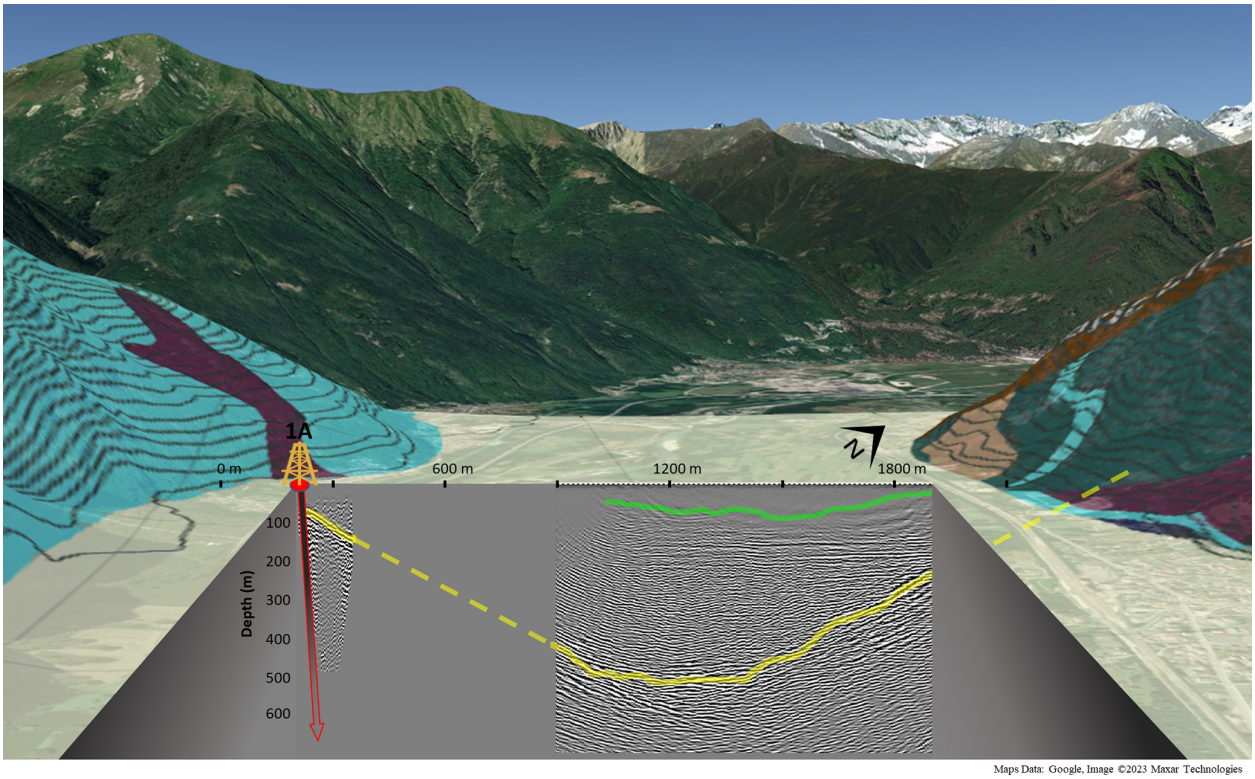

Figure 8. Premosello–Chiovenda-to-Megolo transect and Megolo crossline profile projected into a cut-through of the Ossola Valley. The geology, yellow, and green lines are as described in Figs. 1, 5, and 6.

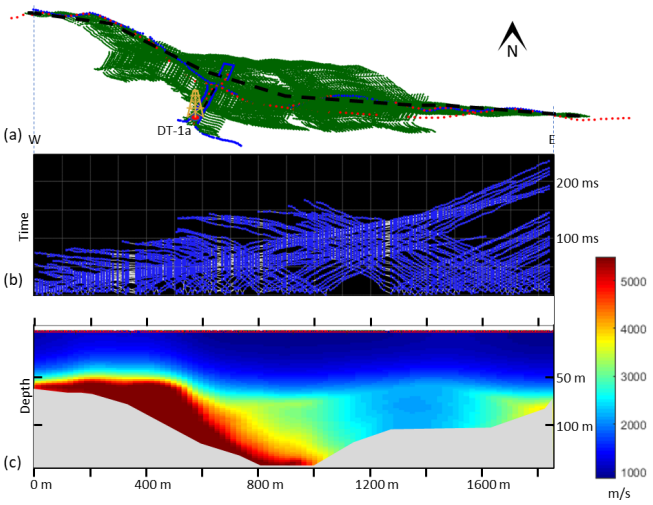

Figure 9. Megolo refraction tomography analysis. **(a)** CMP (green) plot of the Megolo survey, including data from all receiver lines (blue). The refraction profile is taken along the main receiver line approximated by the dashed black line. **(b)** Travel time plot of the first arrivals for all shot records along the main profile. **(c)** Travel time tomography results showing very slow sediments (blue) overlying fast hard rocks (red) in the west and a valley structure to the east with faster sediments. Grey-shaded area depicts the area with no ray-path coverage.

The strong velocity contrast between the sediments and crystalline rocks distorts T2D-converted images and imposes an interface in the depth–velocity model; thus, a 20° southeast dipping smoothed velocity gradient (1500 to 6500 m s^{-1}) from the base of the sediments until 2500 ms is used. Depths to the Quaternary–metagabbro contact are assumed accurate, although depths below this are likely underestimated and features within the crystalline rocks deeper than indicated.

An attempt at improving imaging within the crystalline basement is made using the MOS sparse 3D seismic data collected. To generate a 3D depth–velocity model representative of the sedimentary cover and basement topography, the valley boundary is determined from aerial photographs (Google Earth) and topographic maps, and the slope of the valley determined in the short crossline is used to extend the crystalline structure below ground level. A lack of coherent reflectors within the crystalline rock mass prevents the performance of a classic semblance velocity analysis, and a velocity of 7000 m s^{-1} is used as a representative metagabbro velocity. This velocity is established by a field sample analysis and values from the literature (e.g., Khazanehdari et al., 2000; Salisbury et al., 2003; Weiss et al., 1999). To avoid preimposed sharp boundaries in reflection images, the velocity model is smoothed. The complete 3D depth–velocity model is shown as depth slices in Fig. 11a–d.

Additional processing is applied to the NMO data using the 3D velocity model developed, predictive deconvolution to remove near-surface multiples, and post-stack FX deconvolution to improve coherency of reflection events. The advanced processing greatly improves imaging of the sedimentary crystalline basement contact, sedimentary layering, and the structural dip of the metagabbro facies. This image (Fig. 12) is offset approximately 100 m north of the planned DT-1A location and inserted into a combined topographic and geologic collage.

5.5 Ornavasso

The DT-1B drill hole at Ornavasso targets the center of the tightly folded Massone Antiform (Fig. 1) to intersect metasediments; amphibolite; and, potentially, metagabbro units. An irregular sparse 3D survey pattern was used (Fig. 2), consisting of a long central primary receiver line across strike, two short receiver crosslines, and multiple VP lines on and around the receiver lines wherever access was possible. Near the end of the MOS campaign, a second 2D line, progressing away from the DT-1B drill site and parallel to the OP line as well as a short very high-resolution profile (nanO-SEIZE) across the DT-1B drill site were acquired. The drill site is located within close proximity to a near-vertical cliff face, exposing metasediments and amphibolites.

5.5.1 Secondary line

The OS profile is processed first due to its high data quality, as it is away from the main road, and its proximity to DT-1B. The imaging results are shown in Fig. 13. The results clearly show multiple flat-lying to sub-horizontal reflectors in the first 250 ms. These are associated with the valley sediments, which seemingly do not reach the northwest edge of the profile and roughly terminate at a 45° angle from the start of the profile (Fig. 13a and b). This termination line is the basis for a simple steeply dipping layer velocity model (Fig. 13c), assuming that the crystalline valley walls are directly to the west-northwest of the profile. This velocity model is applied to produce time-to-depth-converted NMO, PSTM, and Post-STM profiles (Fig. 13d and e). Each profile shows different seismic features, with the sediment layers having been enhanced in the migration profiles; however, due to the lack of seismic coverage at the edge of the profile, the migration process smears energy at the edge of the profile and falsely enhances dipping events, and the seismic characteristics pertaining to the terminating western edge are easier to interpret in the NMO stack. A broader-scale interpretation of the OS profile is conducted using the results of the nanO-SEIZE and OP profiles.

5.5.2 The nanO-SEIZE profile

The nanO-SEIZE profile is a short, very high-resolution (Table 1) north-northwest extension of the OS profile up to the cliff edge of the DT-1B drill site. The resulting NMO pro-

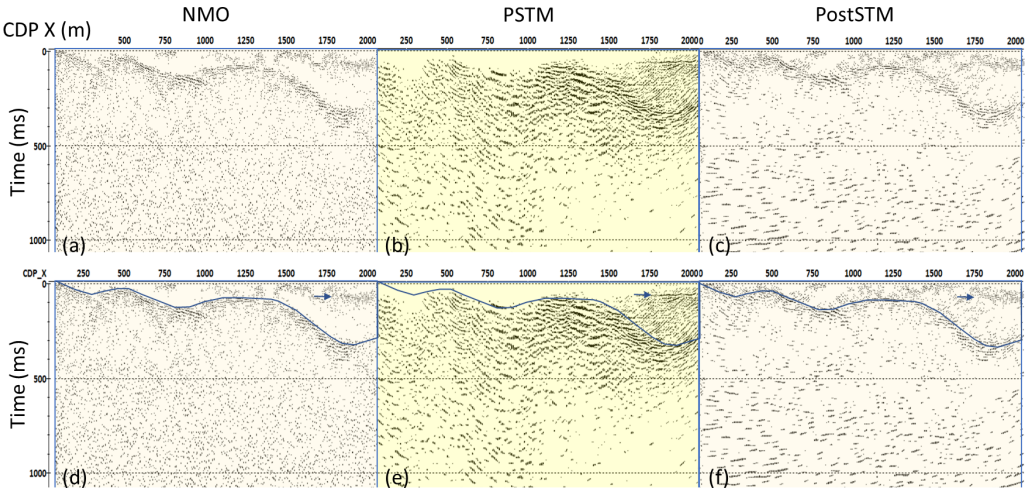

Figure 10. **(a)** NMO stack, **(b)** PSTM, and **(c)** PostSTM profiles of the Megolo inline seismic survey. Panels **(d)**, **(e)**, and **(f)** show annotated plots in panels **(a)**, **(b)**, and **(c)**, which show the depth to the local crystalline basement rocks (blue line). A shallow reflector within the sediment cover is indicated by a blue arrow. Note that the profiles are shown oriented west to east, as acquired in the field.

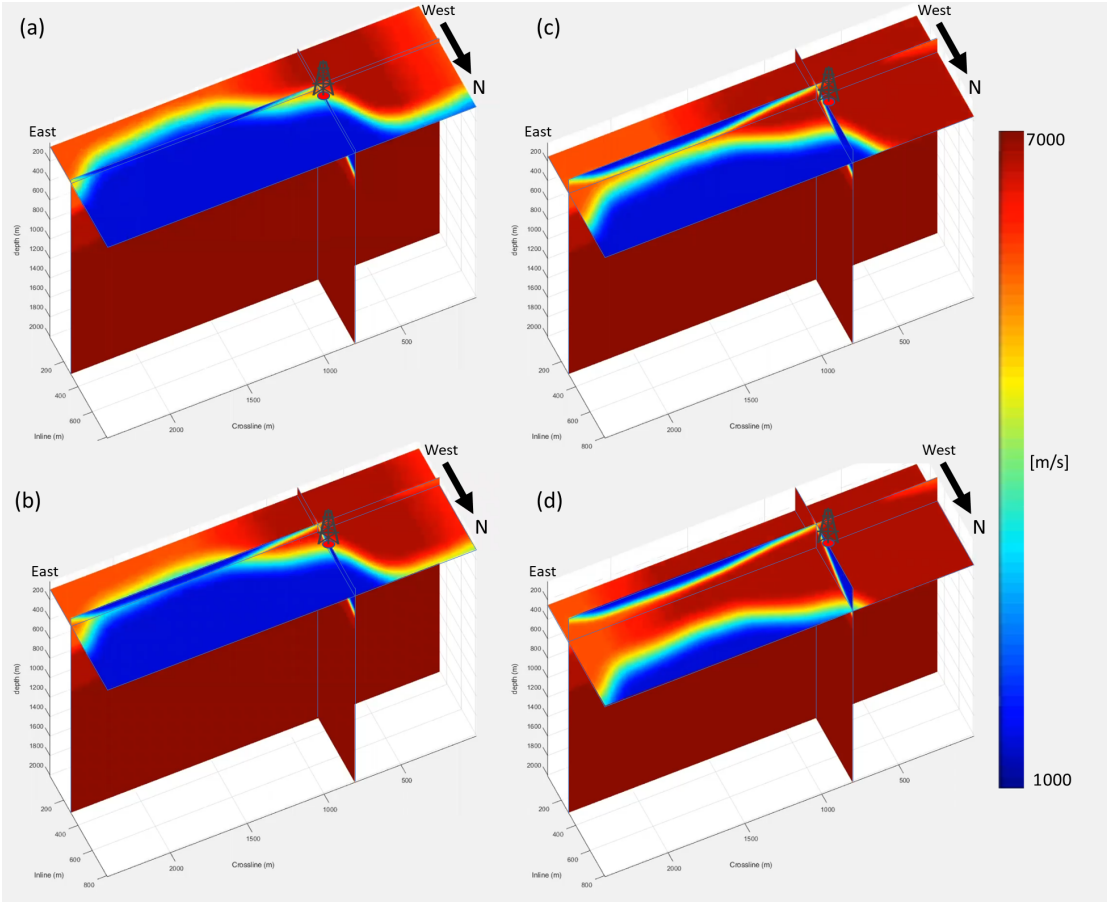

Figure 11. **(a)** Depth slices through the Megolo 3D depth velocity model showing the near-surface 50 m topology transition from slow (blue) valley sediments to fast (red) metagabbro–pyriclasite rocks. The valley walls are modeled as dipping 30° to the north, as indicated by the sediment–metagabbro interface (yellow contour) progressing northward in depth slices of **(b)** 100 m, **(c)** 200 m, and **(d)** 300 m. Also modeled are the westward dipping metagabbros, with a gradient from 6000–7000 m s^{-1} (light red to dark red) also visible in panels **(b)**, **(c)**, and **(d)**. The velocity model is displayed as oriented obliquely east to west looking from the Ossola Valley to the south.

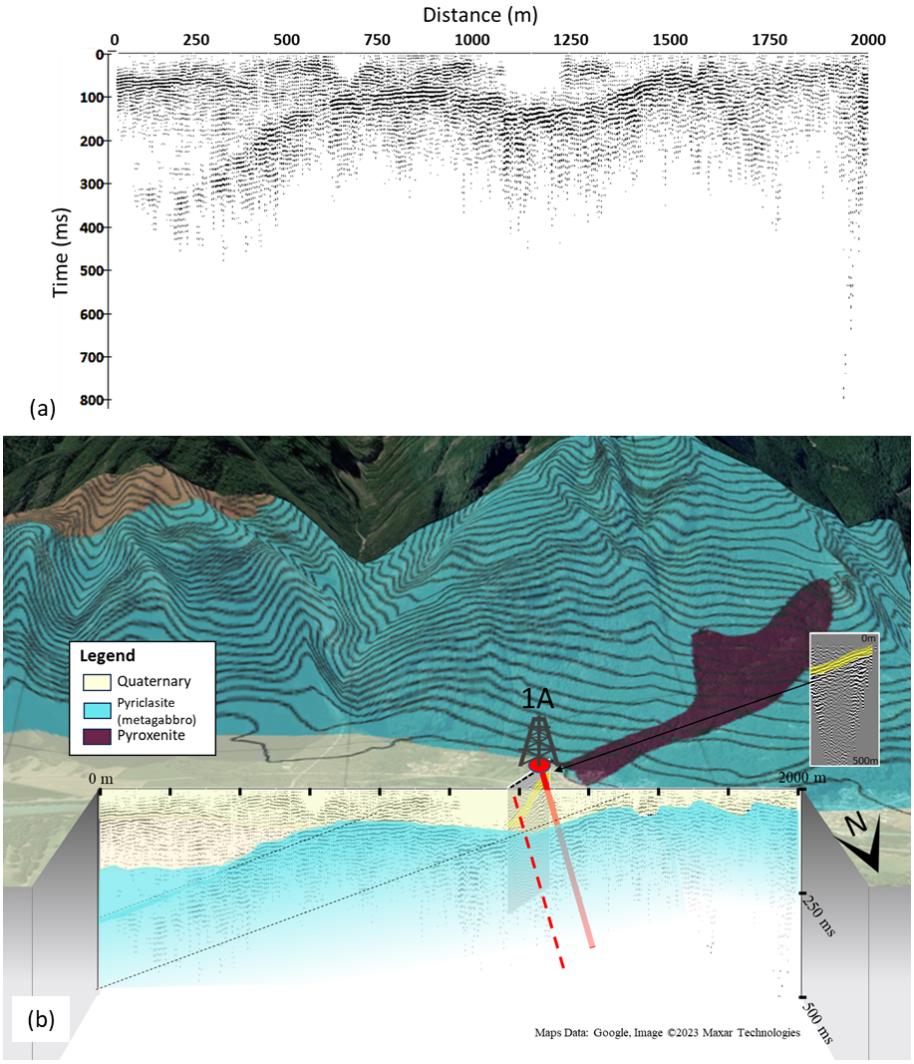

Figure 12. **(a)** Megolo primary profile using the 3D velocity model developed, predictive deconvolution to remove near-surface multiples, and post-stack FX deconvolution to improve coherency of reflection events. **(b)** Megolo in line, post-processed, time-to-depth-converted NMO stack, inlaid onto the Ossola Valley with 3D topography and geology displayed. The general dip of the metagabbro (dashed light-grey line) conforms with the prominent dip of the metagabbro mapped at approximately 21°. For reference, the Megolo crossline profile (refer to Fig. 6) is displayed as an insert (right) and as an inlay in oblique view to the primary inline. The location and orientation of the proposed of DT-1A drill path are indicated as a solid red line, and its location, relative to the inline profile, is indicated as a dashed red line.

file is shown in Fig. 14. Thickness of the sedimentary cover at DT-1B is indicated as being 30–50 m thick at 40 m profile distance (Fig. 14c). Additionally, it is ascertained that the near-surface crystalline rock dips at approximately 22° and then terminates at about 100 m profile distance, where an internal reflection within the crystalline structure is observed. This termination indicates a very steep progression of the valley walls at this location. A high-energy near-surface reflection causing a large step in the near-surface reflections is evident in the data between 0 and 12 m. This is interpreted to be a block or rock debris from the adjacent cliff face. Many diffraction tails observed as very steeply dipping events are evident in the profile and indicate the presence of either near-surface point sources, such as buried boulders, or sharp edges.

Combining the results of the nanO-SEIZE and OS profiles in Fig. 15a shows a very good continuation of the near-surface reflections and agreement of the general interpretations observed in both profiles. These observations are also supported by the results of the OP profile.

5.5.3 Primary line

The OP profile is processed using crooked-line geometry with a swath of 50 m to increase the CMP fold with data from nearby VPs. Although data quality suffered from traf-

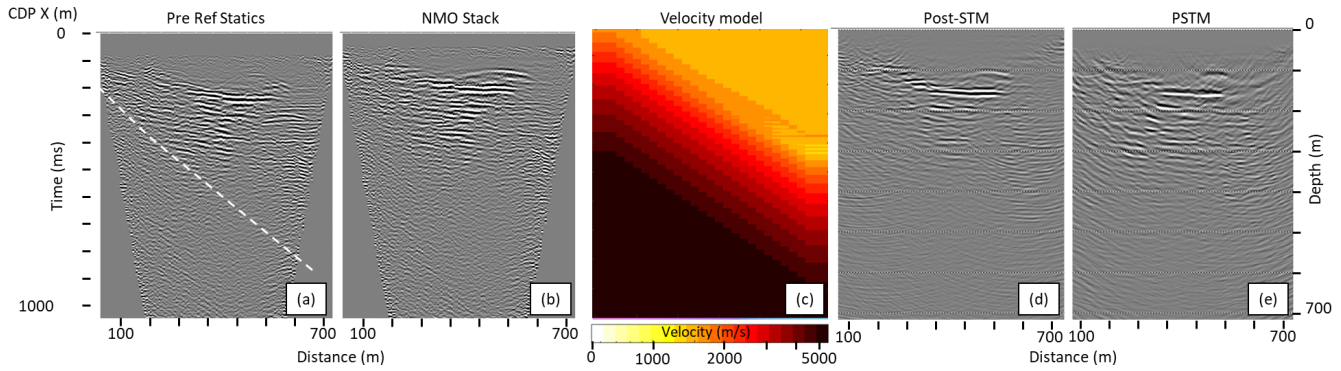

Figure 13. Ornavasso secondary profile constant velocity NMO stack **(a)** before and **(b)** after the application of refraction statics; **(c)** smooth-gradational-dipping (45°) velocity model for stacking, migration, and T2D conversion; and **(d)–(e)** T2D-converted PostSTM and PSTM profiles after the application of the velocity model in panel **(c)**.

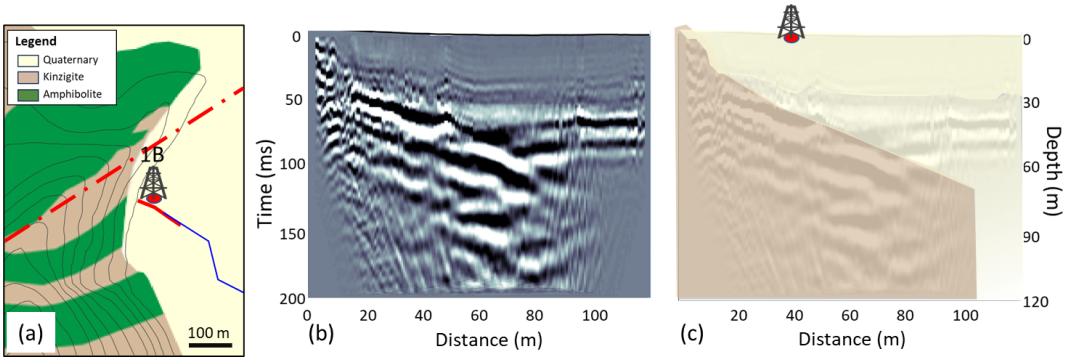

Figure 14. Results of the nanO-SEIZE profile collected at 1.5 m geophone spacing using an ELVIS VII wheelbarrow 35 kg vibrator. **(a)** Planned location of DT-1B in relation to the Massone Antiform (Fig. 1) and steep topography. **(b)** CMP stack. **(c)** Interpretation overlay showing the depth extent of Quaternary sediments (yellow) and underlying kinzigite.

fic noise and required significant trace editing, energy from the EnviroVibe over two sweeps is sufficient to maintain energy for up to 1200 m offsets. Elevation and refraction static corrections were minimal, as the Ornavasso site is in a flat open part of the Ossola Valley (Figs. 1 and 2). Processing adapted the parameters and velocity model determined from the OS profile. The results are similar to that of the OS profile, with, however, some lateral coverage over the outcropping Massone Antiform. The OP and OS T2D NMO profiles have been interpreted together in Fig. 15, whereby the assumed lithologies of the Massone Antiform have been overlaid. There is a clear termination, observed as a change in seismic character, of the Quaternary valley sediments at the western end of the profiles where metasedimentary rocks outcrop. The sediments within the valley are largely horizontal, showing local variability and character changes with depth. There is seemingly no sharp reflector at the Quaternary metasediment interface like that observed in the PMC transect. This is likely due to a steeper profile of the valley walls. The crystalline section is indicated by a change in seismic character, with the presence of scattered energy and lack of specular reflections. Inference of any lithological changes within this section is speculative and interpretation can only be guided by a priori knowledge (expected geology) and the existence of diffraction events such as those highlighted by the arrows in Fig. 15a, which is evidence of steeply dipping irregular surfaces. Like the depth observations in Megolo, the smoothed gradational velocity model used for T2D conversion in Ornavasso is assumed to have accurately determined the depth of the Quaternary sediments; however, any observations within the crystalline section are underestimated in depth.

6 Discussion and limitations

A large contrast in the seismic response between the Quaternary valley sediments and the Permian basement metasediments is observed throughout the MOS profiles. Within the sedimentary infill, horizontal reflectors are prominent, and one would expect a simple infill of the last glacial cycle to be preserved; however, the layering is quite irregular and onlapping horizontally, which is indicative of thick lacustrine proglacial sediments from preserved older fills and evidence of paleochannels from the Toce River meandering. These soft

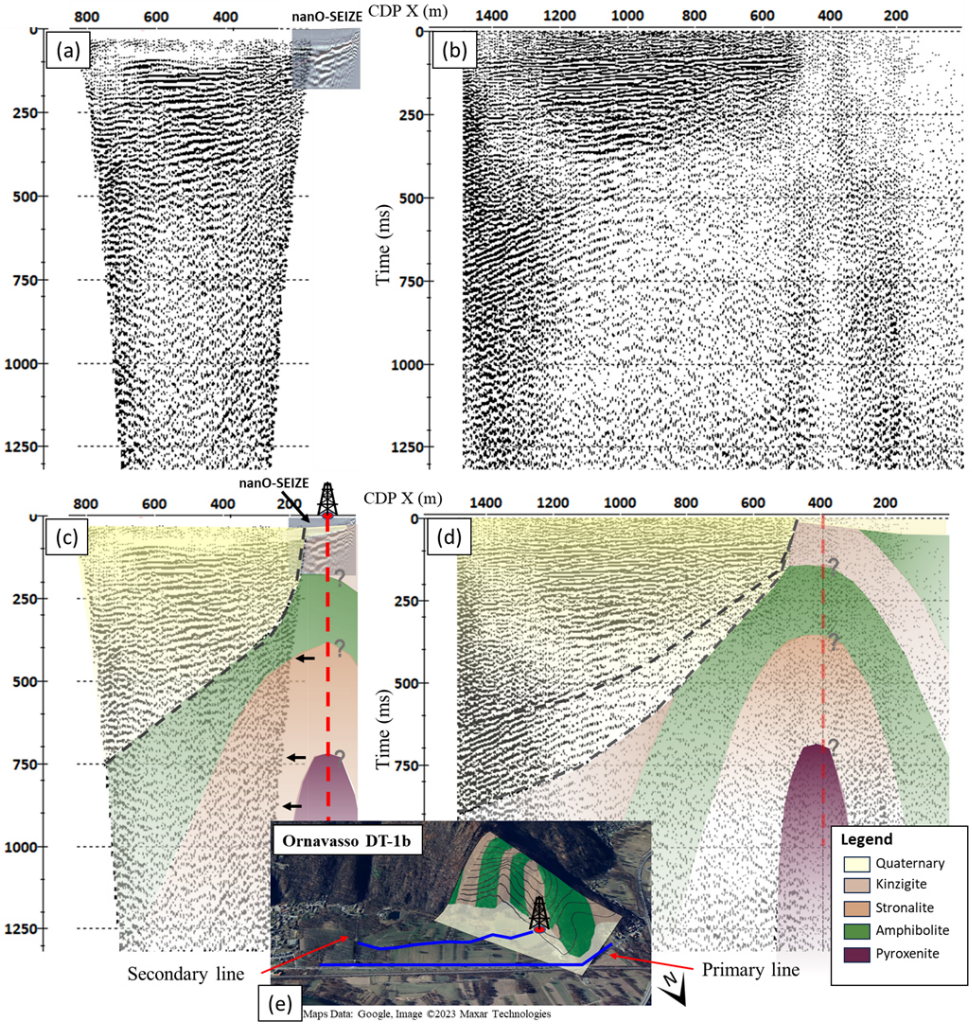

Figure 15. Reflection profiles of **(a)** the Ornavasso secondary and nanO-SEIZE profiles and **(b)** the Ornavasso primary profile after CMP stacking. Panels **(c)** and **(d)** include an interpretation overlay showing the Quaternary sediments as yellow, whilst the expected crystalline sequences of the Massone Antiform are shown as green, pink, and purple colors (Legend 2). The dashed black lines indicate the boundary between the valley sediments and Massone Antiform units. Black arrows in panel **(c)** identify diffraction tails that are synonymous with a steeply dipping irregular surface. For reference, the geographic location of the seismic lines is indicated in panel **(e)**, with DT-1A located at the near-vertical western boundary of the secondary line.

sediments are in high acoustic impedance (AI) contrast to the basement rocks, resulting in a strong reflection at the contact, which is well observed in the PMC transect as well as the Megolo crossline extension. The shape is consistent with a wide U-shaped glacial valley with its trough at the center of the Ossola Valley, and the bottom is estimated at approximately 550 m (e.g., ∼ 300 m b.s.l.). However, whilst the high AI sedimentary–basement boundary results in a clear definition of the glacial valley, there is a lack of coherent specular reflections within the basement rocks, which is problematic in the MOS data and quite typical of crystalline environments (e.g., Salisbury et al., 2003). The problem is primarily due to the very low AI contrast of conformable boundaries within the lower crustal Ivrea rocks, which generate very weak reflections, with reflection coefficients of less than 0.05 for Ivrea metagabbros and metasediments (Barberini et al., 2007). Accordingly, very low-reflectivity features within the crystalline basement will need to be extensively laterally continuous, at least a Fresnel zone width (ca. 200 m at 50 Hz, 5500 m s^{-1}, and 500 m in depth), and be no more than moderately dipping (ca. 35°) to be observed within the seismic sections. Such events can only be observed in the primary Megolo profile, where the Proman Anticline is known to be broad and dipping approximately 20° east-southeast. This is observed in the western end of the profile, where the target rocks are closer to the surface and exhibit a shallow east-dipping fabric. Any highly dipping (> 45°) metasedimentary layering, such as that expected in the Massone Antiform,

cannot be significantly imaged by the surface seismic reflection method below shallow depths. In such instances, we rely on secondary geological features within the crystalline basement rocks to ascertain the geological structure. Only features with high contrast to the surrounding rock mass are expected to produce observable reflections, such as cataclastic and fault zones, large open fractures or fracture sets, or sharp terminations. Sharp terminations are recognized by diffraction tails, such as those detected in the western edge of the Ornavasso secondary profile, and anomalies such as small fault/joint offsets or apexes and terminations of continuous reflectors may be evident in the Ornavasso primary profile through the recognition of weak diffraction events. However, there are no shallow-dipping strong, short, continuous reflectors observed in any of the crystalline sections in all profiles, indicating that there are likely no major cataclastic zones, faults, or fracture planes with open porosity at shallow angles. We, however, cannot exclude the possibility of such zones and structures at high angles. These commonly exhibit as dislocated reflections (faults), often separated with null-energy zones. Small dislocations, with very limited null zones, can be observed in the MP profile (Fig. 12a), and it would be reasonable to assume the presence of high-angle faults and fractures in Megolo.

7 Conclusions

The high-resolution MicrO-SEIZE active seismic campaigns have been carried out to characterize the subsurface structure at two planned borehole locations of the ICDP project DIVE. The processed and interpreted profiles have confidently imaged the Quaternary sediment–basement contact of the Ossola Valley, placing the base of the valley at approximately 550 m depth at its center and clearly showing the continuation of the topographic slopes observed at the adjacent mountain flanks, which are sloping at approximately 25–30°. The sediments within the valley show signs of several proglacial fill cycles older than the last glacial cycle. The sediments in Ossola Valley have a relatively low velocity (1500–1800 m s^{-1}), which cause a large acoustic impedance contrast at the contact point with the underlying crystalline crustal rocks. Below this contact, the majority of sections show little to no specular reflections due to the very low AI contrast of Ivrea rocks. Shallow dipping reflectors that would suggest large open-fracture or fault systems are not observable; however, a steeply dipping structure is not imaged with the geometry of the surveys, and the existence of steep faults or fractures cannot be excluded. However, such features are not thought to be extensive, and it is reasonable to consider that the lithological progression is in continuous succession of the geological structures mapped at the surface at both sites, i.e., at DT-1B (Ornavasso; narrow antiform) and at DT-1A (Megolo; dipping layers).

Sedimentary overburden is established to be at least 30–50 m at the Ornavasso and Megolo drill sites, respectively. At DT-1B (Ornavasso), the seismic survey has prompted moving the borehole location approximately 20 m closer to the exposed bedrock cliff in order to minimize the Quaternary overburden and to approach the axis of the narrow Massone Antiform. At DT-1A (Megolo), the borehole location plan is confirmed and the seismic survey results are the primary subsurface constraint to orient the borehole's inclination to be at 15–20° in order to orthogonally cross the flank of the broad Proman Anticline and reach the deepest layers of the crust.

Future deployment of longer seismic profiles and larger seismic sources may aid the delineation of the broader geology in the area; however, these are not necessary to plan the borehole geometries, which are determined and agreed on, and enable the start of drilling. Further analysis of the MOS seismic data with respect to fracture reflectivity, and anisotropy effects of metasedimentary layering will be conducted after the rock-core physical property analysis (density and P- and S-wave velocity), borehole geophysics, seismic analysis while drilling, and seismic anisotropy modeling become available. Conversely, the MOS seismic database will also help interpret the forthcoming comprehensive borehole logging program's dataset. Passive seismic data from the DIVEnet monitoring network, which are composed of 12 continuously operated stations over 2 years, covering an area of up to 10 km distance around the boreholes, may further aid the interpretation at a broader scale.

Code availability. All data have been processed with RadExPro commercial seismic processing software. 3D velocity models were generated in MATLAB using generic MATLAB functions. The MATLAB script is available upon request from the author.

Data availability. The data collected within the DIVE project are available to the scientific community. Seismic raw data are available at https://doi.org/10.5880/ICDP.5071.002 (Greenwood et al., 2024).

Team list. Nicolò Barago (University of Trieste, Trieste, Italy), Ludovic Baron (University of Lausanne, Lausanne, Switzerland), Davide Berno (University of Pavia, Pavia, Italy), Florian Bleibinhaus (University of Leoben, Leoben, Austria), Mattia Bonazzi (University of Pavia, Pavia, Italy), Lorenzo Candioti (University of Lausanne, Lausanne, Switzerland), Andrew Greenwood (University of Lausanne, Lausanne, Switzerland), Steve Henchoz (Geo2X SA, Yverdon-les-Bains, Switzerland), György Hetényi (University of Lausanne, Lausanne, Switzerland), Gerado Maurizio (University of Trieste, Trieste, Italy), Valentin Métraux (Geo2X SA, Yverdon-les-Bains, Switzerland), Alexis Neven (University of Lausanne, Lausanne, Switzerland), Gerald Raymond (University of Lausanne, Lausanne, Switzerland), Alberto Roselli (Geo2X SA, Yverdon-les-Bains, Switzerland), Matteo Scarponi (University of Lausanne, Lausanne, Switzerland), Edith Sotelo (University of Lausanne, Lau-

sanne, Switzerland), Thomas Tsaner (Geo2X SA, Yverdon-les-Bains, Switzerland).

Author contributions. AG designed and planned the survey, coordinated and led the data acquisition, processed the data, and prepared the paper. GH led the implementation of the survey, coordinated and participated in the acquisition, and assisted with paper preparation. LB assisted in survey design and implementation, data acquisition, and processing. AZ arranged all permissions and land access, contributed to the implementation of the study, and gave feedback on the paper. OM, contributed to the implementation of the study and gave input and assistance with paper preparation.

Competing interests. The contact author has declared that none of the authors has any competing interests.

Disclaimer. Publisher's note: Copernicus Publications remains neutral with regard to jurisdictional claims made in the text, published maps, institutional affiliations, or any other geographical representation in this paper. While Copernicus Publications makes every effort to include appropriate place names, the final responsibility lies with the authors.

Acknowledgements. We would like to acknowledge the Swiss National Science Foundation for the support (grant nos. PP00P2_157627 and PP00P2_187199) as part of project OROG3NY that funded the field campaign.

Financial support. This research has been supported by the Swiss National Science Foundation (grant nos. PP00P2_157627 and PP00P2_187199).

Review statement. This paper was edited by Ulrich Harms and reviewed by Christopher Juhlin and one anonymous referee.

References

Barberini, V., Burlini, L., and Zappone, A.: Elastic properties, fabric and seismic anisotropy of amphibolites and their contribution to the lower crust reflectivity, Tectonophysics, 445, 227–244, https://doi.org/10.1016/j.tecto.2007.08.017, 2007.

Berckhemer, H.: Topographie des "Ivrea-Körpers" abgeleitet aus seismischen und gravimetrischen Daten, Schweiz Mineral. Petrogr. Mitt., 48, 235–246, 1968.

Brack, P., Ulmer, P., and Schmid, S.: A crustal magmatic system from Earth mantle to the Permian surface: Field trip to the area of lower Valsesia and val d'Ossola (massiccio dei Laghi, Southern Alps, Northern Italy), Swiss Bull. Angew. Geol., 15, 3–21, 2010.

Brodie, K. H. and Rutter, E. H.: Deep crustal extensional faulting in the Ivrea Zone (N-Italy), Tectonophysics, 140, 193–212, https://doi.org/10.1016/0040-1951(87)90229-0, 1987.

Burlini, L.: Parco Nazionale Val Grande: Carta geologica (1 : 25'000), ETH Zurich, Zurich, 2008.

Diehl, T., Husen, S., Kissling, E., and Deichmann, N.: High resolution 3-D P-wave model of the Alpine crust, Geophys. J. Int., 179, 1133–1147, https://doi.org/10.1111/j.1365-246X.2009.04331.x, 2009.

Ewing, T. A., Rubatto, D., Beltrando, M., and Hermann, J.: Constraints on the thermal evolution of the Adriatic margin during Jurassic continental break-up: U–Pb dating of rutile from the Ivrea–Verbano Zone, Italy, Contrib. Mineral Petrol., 169, 1–22, https://doi.org/10.1007/s00410-015-1135-6, 2015.

Fountain, D. M.: Growth and modification of lower continental crust in extended terrains: The role of extension and magmatic underplating, in: Properties and Processes of Earth's Lower Crust, edited by: Mereu, R. F., Mueller, S., and Fountain, D. M., AGU Monograph series, 51, 287–299, AGU, Washington DC, https://agupubs.onlinelibrary.wiley.com/doi/10.1029/GM051p0287 (last access: 22 August 2024), 1989.

Galli, A., Grassi D., Sartori G., Gianola O., Burg J. P., and Schmidt M. W.: Jurassic carbonatite and alkaline magmatism in the Ivrea zone (European Alps) related to the breakup of Pangea, Geology, 1, 199–202, https://doi.org/10.1130/G45678.1, 2019.

Garde, A. A., Boriani, A., and Sørensen, E. V.: Crustal modeling of the Ivrea-Verbano zone in northern Italy re-examined: coseismic cataclasis versus extensional shear zones and sideways rotation, Tectonophys, 662, 291–311, https://doi.org/10.1016/j.tecto.2015.04.003, 2015.

Garuti, G., Bea, F., Zaccarini, F., and Montero, P.: Age, geochemistry and petrogenesis of the ultramafic pipes in the Ivrea Zone, NW Italy, J. Petrol., 42, 433–457, https://doi.org/10.1093/petrology/42.2.433, 2001.

Greenwood, A., Hetényi, G., and Baron, L.: Active seismic surveys for drilling target characterisation in Ossola valley, ICDP expedition 5071, DIVE phase I (Drilling the Ivrea-Verbano zonE) seismic dataset, GFZ Data Services [data set], https://doi.org/10.5880/ICDP.5071.002, 2024.

Khazanehdari, J., Rutter, E. H., and Brodie, K. H.: High-pressure-high-temperature seismic velocity structure of the midcrustal and lower crustal rocks of the Ivrea-Verbano zone and Serie dei Laghi, NW Italy, J. Geophys. Res., 105, 13843–13858, https://doi.org/10.1029/2000JB900025, 2000.

Kissling, E.: Deep structure of the Alps: What do we really know?, Phys. Earth Planet. Int., 79, 87–112, https://doi.org/10.1016/0031-9201(93)90144-X, 1993.

Kissling, E., Wagner, J. J., and Mueller, S.: Three-dimensional gravity model of the northern Ivrea-Verbano zone, in: Geomagnetic and gravimetric studies of the Ivrea zone, edited by: Wagner, J. J. and Mueller, S., 53–61 pp., Swiss Geophys. Comm., Kümmerly & Frey, Neuchâtel, 1984.

Lanza, R.: Models for interpretation of the magnetic anomaly of the Ivrea body, Géologie Alpine, 58, 85–94, 1982.

Liu, Y., Greenwood, A., Hetényi, G., Baron, L., and Holliger, K.: High-resolution seismic reflection survey crossing the Insubric Line into the Ivrea-Verbano Zone: Novel approaches for interpreting the seismic response of steeply dipping structures, Tectonophysics, 816, 229035, https://doi.org/10.1016/j.tecto.2021.229035, 2021.

Lu, Y., Stehly, L., and Paul, A.: High-resolution surface wave tomography of the European crust and uppermost mantle from

ambient seismic noise, Geophys. J. Int., 214, 1136–1150. https://doi.org/10.1093/gji/ggy188, 2018.

Müntener, O.: IGSN ICDP5071EH10001 (5071_1_A): Borehole: rock from Megolo (Val d'Ossola) (ICDP DIVE Project), near Verbano-Cusio-Ossola, Italy, GFZ Data Services, https://doi.org/10.60510/ICDP5071EH10001, 2024a.

Müntener, O.: IGSN ICDP5071EH30001 (5071_1_B): Borehole: rock from Ornavasso (Val d'Ossola) (ICDP DIVE Project), near Verbano-Cusio-Ossola, GFZ Data Services, https://doi.org/10.60510/ICDP5071EH30001, 2024b.

Niggli, E.: Über den Zusammenhang zwischen der positiven Schwereanomalie am Südfuss der Westalpen und der Gesteinszone von Ivrea, Eclogae Geol. Helv., 39, 211–220, 1946.

Obata, M. and Karato, S.: Ultramafic pseudotachylyte from the Balmuccia peridotite, Ivrea-Verbano zone, northern Italy, Tectonophys, 242, 313–328, https://doi.org/10.1016/0040-1951(94)00228-2, 1995.

Palmer, D.: An introduction to the generalized reciprocal method of seismic refraction interpretation, Geophysics, 46, 1508–1518, https://doi.org/10.1190/1.1441157, 1981.

Pistone, M., Müntener, O., Ziberna, L., Hetényi, G., and Zanetti, A.: Report on the ICDP workshop DIVE (Drilling the Ivrea–Verbano zonE), Sci. Dril., 23, 47–56, https://doi.org/10.5194/sd-23-47-2017, 2017.

Pittarello, L., Pennacchioni, G., and Di Toro, G.: Amphibolite-facies pseudotachylytes in Premosello metagabbro and felsic mylonites (Ivrea Zone, Italy), Tectonophy, 580, 43–57, https://doi.org/10.1016/j.tecto.2012.08.001, 2012.

Quick, J. E., Sinigoi, S., and Mayer, A.: Emplacement of mantle peridotite in the lower continental crust, Ivrea-Verbano Zone, northwest Italy, Geology, 23, 739–742, https://doi.org/10.1130/0091-7613(1995)023<0739:EOMPIT>2.3.CO;2, 1995.

Redler, C., Johnson, T. E., White, R. W., and Kunz, B.: Phase equilibrium constraints on a deep crustal metamorphic field gradient: Metapelitic rocks from the Ivrea Zone (NW Italy), J. Metam. Geol., 30, 235–254, https://doi.org/10.1111/j.1525-1314.2011.00965.x, 2012.

Rutter, E. H., Brodie, K. H., James, T., and Burlini, L.: Large scale folding in the upper part of the Ivrea-Verbano zone, J. Struct. Geol., 29, 1–17, https://doi.org/10.1016/j.jsg.2006.08.013, 2007.

Ryberg, T., Haberland, C., Wawerzinek, B., Stiller, M., Bauer, K., Zanetti, A., Ziberna, L., Hetényi, G., Müntener, O., Weber, M. M., and Krawczyk, C. M.: 3-D imaging of the Balmuccia peridotite body (Ivrea–Verbano zone, NW-Italy) using controlled source seismic data, Geophys. J. Int., 234, 1985–1998, https://doi.org/10.1093/gji/ggad182, 2023.

Salisbury, M. H., Harvey, C. W., Matthews, L., Eaton, D. W., and Milkereit, B.: The acoustic properties of ores and host rocks in hardrock terranes, Hardrock seismic exploration, SEG, 9–19, https://doi.org/10.1190/1.9781560802396.ch1, 2003.

Scarponi, M., Hetényi, G., Berthet, T., Baron, L., Manzotti, P., and Petri, B., et al.: New gravity data and 3D density model constraints on the Ivrea geophysical body (Western Alps), Geophys. J. Int., 222, 1977–1991, https://doi.org/10.1093/gji/ggaa263, 2020.

Scarponi, M., Hetényi, G., Plomerová, J., Solarino, S., Baron, L., and Petri, B.: Joint seismic and gravity data inversion to image intra-crustal structures: the Ivrea Geophysical Body along the Val Sesia profile (Piedmont, Italy), Front. Earth Sci., 9, 671412, https://doi.org/10.3389/feart.2021.671412, 2021.

Schaltegger, U., Ulianov, A., Müntener, O., Ovtcharova, M., Peytcheva, I., Vonlanthen, P., Vennemann, T., Antognini, M., and Girlanda, F.: Megacrystic zircon with planar fractures in miaskite-type nepheline pegmatites formed at high pressures in the lower crust (Ivrea Zone, southern Alps, Switzerland), Am. Mineral., 100, 83–94, https://doi.org/10.2138/am-2015-4773, 2015.

Schmid, S. M., Kissling, E., Diehl, T., van Hinsbergen, D. J. J., and Molli, G.: Ivrea mantle wedge, arc of the Western Alps, and kinematic evolution of the Alps-Appenines orogenic system, Swiss J. Geosci., 110, 581–612, https://doi.org/10.1007/s00015-016-0237-0, 2017.

Schmid, R.: Zur Petrographie und Struktur der Zone Ivrea-Verbano zwischen Valle d'Ossola und Valle Grande, Schweiz Mineral. Petrogr. Mitt., 47, 935–1117, 1967.

Schmid, R. and Wood, B. J.: Phase relationships in granulitic metapelites from the Ivrea-Verbano zone (Northern Italy), Contrib. Mineral Petrol, 54, 255–279, 1976.

Sills, J. D.: Granulite facies metamorphism in the Ivrea zone, N.W. Italy, Schweiz Mineral Petrograph. Mitt., 64, 169–191, 1984.

Souquière, F. and Fabbri, O.: Pseudotachylites in the Balmuccia peridotite (Ivrea Zone) as markers of the exhumation of the southern Alpine continental crust, Terra Nova, 22, 70–77, https://doi.org/10.1111/j.1365-3121.2009.00918.x, 2010.

The ECORS-CROP Deep Seismic Sounding Group: Mapping the Moho of the Western Alps by wide-angle reflection seismics, Tectonophysics, 162, 193–202, https://doi.org/10.1016/0040-1951(89)90243-6 , 1989.

The ECORS-CROP Gravity Group: Gravity modeling along the ECORS-CROP vertical seismic reflection profile through the Western Alps, Tectonophysics, 162, 203–218, https://doi.org/10.1016/0040-1951(89)90244-8, 1989.

Weiss, T., Siegesmund, S., Rabbel, W., Bohlen, T., and Pohl, M.: Seismic Velocities and Anisotropy of the Lower Continental Crust: A Review, in: Seismic Exploration of the Deep Continental Crust, edited by: Gajewski, D. and Rabbel, W., Pure and Applied Geophysics (PAGEOPH), Birkhäuser, Basel, https://doi.org/10.1007/978-3-0348-8670-3_6, 1999.

Wyatt, D. C., Smye, A. J., Garber, J. M., and Hacker, B. R.: Assembly and Tectonic Evolution of Continental Lower Crust: Monazite Petrochronology of the Ivrea-Verbano Zone (Val Strona di Omegna), Tectonics, 41, e2021TC006841, https://doi.org/10.1029/2021TC006841, 2022.

Yilmaz, Ö.: Seismic data analysis: Processing, inversion, and interpretation of seismic data, Society of Exploration Geophysicists , https://doi.org/10.1190/1.9781560801580, 2001.

Sci. Dril., 33, 237–248, 2024
https://doi.org/10.5194/sd-33-237-2024

Scientific Drilling
Open Access

A comprehensive crosshole seismic experiment in glacial sediments at the ICDP DOVE site in the Tannwald Basin

Sarah Beraus[1,2], Thomas Burschil[3], Hermann Buness[1], Daniel Köhn[4], Thomas Bohlen[5], and Gerald Gabriel[1,2]

[1]LIAG Institute for Applied Geophysics, Stilleweg 2, 30655 Hannover, Germany
[2]Section Geology, Institute of Earth System Sciences (IESW), Leibniz University Hannover, Callinstraße 30, 30167 Hannover, Germany
[3]Federal Institute for Geosciences and Natural Resources, Stilleweg 2, 30655 Hannover, Germany
[4]Institute for Geosciences, Christian-Albrechts-Universität zu Kiel, Otto-Hahn-Platz 1, 24118 Kiel, Germany
[5]Geophysical Institute, Karlsruhe Institute of Technology, Hertzstraße 16, 76187 Karlsruhe, Germany

Correspondence: Sarah Beraus (sarah.beraus@leibniz-liag.de)

Received: 29 January 2024 – Revised: 15 July 2024 – Accepted: 16 August 2024 – Published: 11 October 2024

Abstract. Glaciers have shaped the Alpine landscape by carving deep valleys and depositing sediments to form overdeepened basins. Understanding these processes provides information on the evolution of the climate and landscape. One such overdeepened structure is the Tannwald Basin (ICDP site 5068_1) north of Lake Constance, which was formed by the Rhine Glacier in several glacial cycles. In order to study these sediments and their seismic properties down to about 160 m depth, we conducted seismic crosshole experiments between three boreholes, obtaining compressional (P) wave data. The P-wave data are generated by a sparker source and recorded by a 24-station hydrophone string. We present the data acquisition and review our approach for future optimization, suggesting a finer time sampling interval and a separate registration of borehole and surface receivers. Travel-time tomography of the P-wave first-arrival picks under geostatistical constraints yields initial subsurface models. The tomograms correlate well with cased-hole sonic logs and the lithology derived from the core of one of the boreholes. These results will be further investigated in future research, which will include full-waveform inversion (FWI) to obtain high-resolution subsurface models.

1 Introduction

Within the International Continental Scientific Drilling Program (ICDP) project 5068 “Drilling Overdeepened Alpine Valleys” (DOVE), we study overdeepenings in the Alps in order to understand climate and landscape evolution in Quaternary times. The valleys were excavated by glacial erosion and form elongated structures that usually correspond to the recent ice flow directions. Typically, these structures are quickly filled by various deposits. These deposits may then be eroded again by another glacial advance. The sedimentary infill of the valleys results in a complex system of aquifers with different permeabilities, so groundwater levels can vary greatly within short distances. Knowledge of the sedimentary structure is therefore crucial for water supply and shallow geothermal facilities. The rather soft sediments also play a decisive role in local site effects of earthquakes, which are common in the Alpine region. The DOVE project addresses these topics through a suite of geological, geochemical, geotechnical, and geophysical methods that heavily depend on the information obtained from cores as well as in and around the boreholes that were drilled for the project (Anselmetti et al., 2022).

At site 5068_1, the Tannwald Basin in southern Germany, not just one but three boreholes were drilled to conduct seismic crosshole experiments. Our seismic crosshole measurements are unique in that, to our knowledge, this acquisition geometry has never been used to investigate glacial sedi-

ments at depths down to about 160 m. However, the method is commonly used in the industry to investigate and characterize oil and gas reservoirs at depths greater than 500 m (Van Schaack et al., 1995; Bauer et al., 2005; Zhang et al., 2012; Liu et al., 2012) as well as geothermal sites (Martuganova et al., 2022; Gaucher et al., 2020); von Ketelhodt et al. (2018) applied the method to study aquifers in the upper 40 to 50 m by travel-time tomography.

Surface seismic methods, where the source frequencies are usually limited to below 200 Hz and strongly attenuated by the low-velocity weathering layer, which prevents high frequencies from penetrating the subsurface when shot at the surface, often lack the desired resolution. Crosshole seismic methods, which deploy high-frequency sources and receivers below the surface, can thus bridge the resolution gap between borehole methods (core analysis and logging) and surface seismic data. In addition, the transmission geometry samples horizontal travel paths, while surface seismic acquisition geometries predominantly treat vertical travel paths of seismic waves and local heterogeneities impair amplitude-variation-with-offset/angle (AVO/AVA) methods. This often prevents the study of complex geology, including the phenomenon of seismic anisotropy.

Here, we present the crosshole experiments we conducted in a glacially overdeepened basin of the Rhine Glacier. By a comprehensive discussion of the strengths and limitations of the data, we aim to encourage the application and improve the implementation of crosshole tomography in other projects. We are convinced that such measurements can provide crucial high-resolution information on sediment structures that cannot be derived from surface measurements. This is corroborated by the results of isotropic travel-time tomography, which can be linked to geological features observed in the lithology of the boreholes, demonstrating the value of the data.

2 Study site: 5068_1 (Tannwald)

Our study area is ICDP site 5068_1 in the Tannwald Basin and located about 45 km north of Lake Constance (Fig. 1a). The Tannwald Basin is a distal glacially overdeepened valley of the Rhine Glacier that is about 1 km wide and up to 250 m deep, and it is part of the Lake Constance amphitheater. According to Ellwanger et al. (2011), the Rhine Glacier incised into the Tertiary Upper Freshwater Molasse and the Upper Marine Molasse down below the fluvial base level during the Hosskirchian. Subsequently, the sediments transported in the glacial system refilled the basin during the Middle to Late Pleistocene. The study site lies beyond the maximum ice extent and thus beyond the terminal moraine of the Last Glacial Maximum (LGM) (Burschil et al., 2018).

Prior to drilling, the LIAG Institute for Applied Geophysics carried out intense pre-site surveys using surface seismic methods. These included five compressional wave (P-wave) seismic reflection lines distributed over the northeastern part of the basin. Using the high-resolution surface seismic data, Burschil et al. (2018) were able to characterize the sediments by reflection seismic imaging and facies characterization. A 3D survey at the drill site revealed additional faults and a glaciotectonic feature referred to as cuspate–lobate folding, which provides information on local stress regimes in the past (Buness et al., 2022). Based on the information from the seismic profiles, ICDP drilling site 5068_1 was selected.

In comparison to the other DOVE sites, at site 5068_1 not just one but three boreholes (sites 5068_1_A, 5068_1_B, and 5068_1_C; hereafter referred to as A, B, and C) were drilled, all of which reached the base of the Quaternary overdeepened basin between 153 and 158 m depth (DOVE-Phase 1 Scientific Team et al., 2023b; Schuster et al., 2024). The boreholes are cased with a PVC pipe with a diameter of 80 mm. The backfill consists of bentonite and filter sand (DOVE-Phase 1 Scientific Team et al., 2023b). The boreholes are arranged in an isosceles triangle with short edges of 28 m that are oriented in N–S and W–E directions (Fig. 1b). This setup was found to be optimal for conducting seismic crosshole experiments in the glacial sediments. A detailed description of the drilling and the core recovered from borehole C can be found in Schuster et al. (2024) and DOVE-Phase 1 Scientific Team et al. (2023b, c). Cuttings from the flush drilling of boreholes A and B and core catcher information from the cored borehole C provided a preliminary lithology at each borehole location (Fig. 2; lithology: Bennet Schuster, personal communication, 2021). The top layer consists of gravel, followed by mainly fines (silt/clay), interrupted by some sand layers in the cored borehole C, indicating that the sand was flushed out during the flush drilling of boreholes A and B. In addition, wireline logging data were acquired by LIAG during and after drilling (DOVE-Phase 1 Scientific Team et al., 2023b), providing information such as the borehole trajectories (Fig. 1b).

3 Seismic crosshole experiments

3.1 Data acquisition

High-resolution P-wave data were acquired in all three borehole planes, i.e., AB, BC, and AC (Figs. 1b and 2), in two surveys. The first survey covered the shorter borehole planes between boreholes A and B and boreholes B and C, and the second survey covered the longer borehole plane between boreholes A and C. In both surveys, we used a sparker source in boreholes A and B, which requires a high-voltage power supply that is powered by a generator. The seismic waves were recorded with a 24-station hydrophone string. The hydrophones are omnidirectional pressure sensors which are spaced every 2 m along the receiver string. Both the source and the receiver string rely on them being placed below the groundwater level (GWL) (Table A1 in AppendixA) and be-

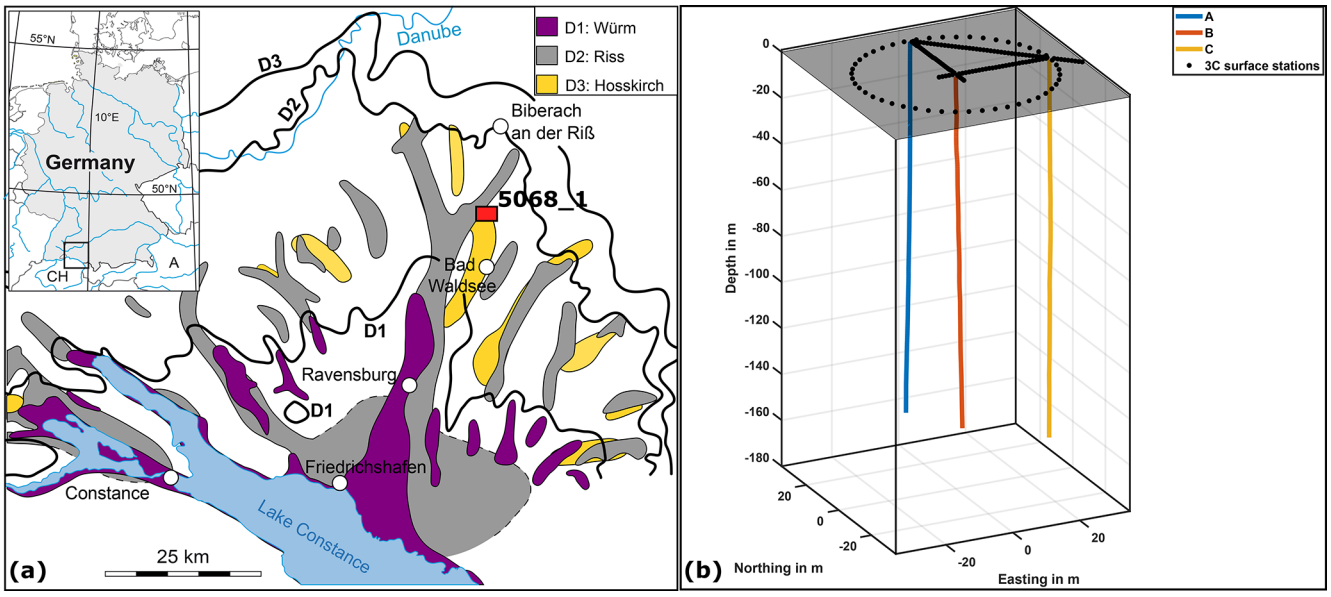

Figure 1. **(a)** Location of the overdeepened Tannwald Basin and extent of the Rhine Glacier in the Quaternary in the northern Alpine Foreland (modified after Ellwanger et al., 2011). ICDP drill site 5068_1 is marked in red. **(b)** 3D view of the borehole trajectories and the locations of the 3C geophones at the surface. The circle has a radius of 28 m around borehole B.

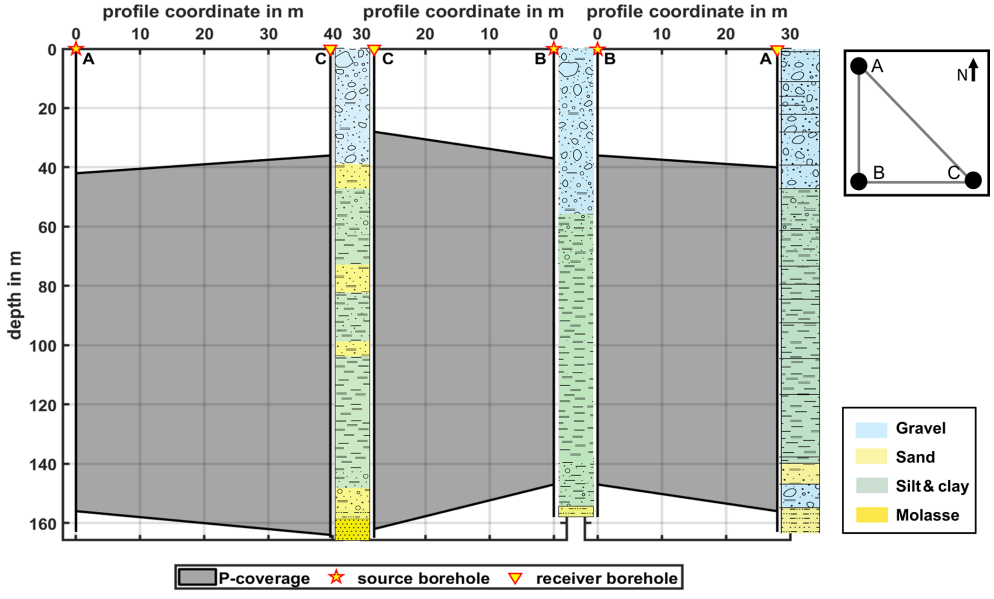

Figure 2. Survey coverage of the crosshole experiments (adapted from Beraus et al., 2023). The source and receiver depths were limited by the groundwater level and the buoyancy of the drilling mud remaining in the boreholes after drilling. Note that plane AC was acquired in a separate survey as compared with the P-wave data from the shorter planes.

ing free to move laterally at depth, i.e., not coupled to the borehole walls. The shot and receiver depths are listed in Table 1. We shot eight times at each position to increase the signal-to-noise ratio (SNR). For the two short borehole planes, we chose a time sampling interval of 0.5 ms to ensure the required measurement progress. For the long plane between A and C, we decreased the time sampling interval to 0.125 ms.

Furthermore, we deployed up to 112 three-component (3C) geophones at the surface. For the short plane measurements, we placed the stations every 1 m (plane BC) and every 2 m (plane AB) along the profiles connecting the wells to improve the polar coverage and, thus, the area of the bore-

Table 1. P-wave acquisition coverage of plane AB, plane BC, and plane AC. The source and receiver spacing within the layouts is 2 m. Layouts with double letters, e.g., "aa", are referred to as the staggered scheme. The effective receiver spacing is 1 m. Note that for layout 3b of plane AC the planned receiver positions (in brackets) differ from the actual positions because the string was not moved downwards. The uncertainties of source and receiver positions are discussed in Sect. 3.3.

	Plane AB		Plane BC			Plane AC	
Layout	Receiver depth (in m)	Source depth (in m)	Receiver depth (in m)	Source depth (in m)	Source spacing (in m)	Receiver depth (in m)	Source depth (in m)
L1a	40–86	36–64	28–74	37–125	2	36–82	42–121
L1aa	40–86	37–91					
L1b	41–87	37–65	29–75	37–125	2	37–83	42–122
L1bb	41–87	38–92					
L2a	63–109	38–136	76–122	60–146	1	71–117	42–156
L2aa	63–109	63–109					
L2b	64–110	37–137	77–123	61–146	1	72–118	42–156
L2bb	64–110	64–106					
L3a	109–155	66–147	115–161	66–147	1	118–164 (117–163)	74–156
L3b	110–156	67–147	116–162	67–147	1	118–164	74–156

hole plane that is illuminated by the seismic waves. Additionally, we set up 48 receivers evenly distributed in a circle of radius 28 m around borehole B to sample the seismic wave field with azimuth. In the additional P-wave survey for plane AC, we deployed 56 three-component geophones along a line starting 1 m from the shot borehole A and going in the direction of the receiver borehole C with a spacing of 1 m. The surface station locations compiled from all surveys are shown in Fig. 1b, and the crosshole survey coverage is depicted in Fig. 2. We acquired approximately 40 GB of data in about 10 working days with a crew of three to four using borehole and surface receivers.

3.2 Raw data

The P-wave data have an overall excellent signal-to-noise ratio regarding environmental noise. However, they are also characterized by two distorting features: first by tube waves, which are often the most significant noise in crosshole sparker surveys (Daley, 1977), and second by aliasing (Fig. 3).

The tube waves, which appear as linear noise in both the shot gathers and the receiver gathers, mask other late arrivals because of their high amplitudes. The steeply dipping events in the shot gathers (Fig. 3a) are associated with tube waves that originate at discontinuities in the source borehole and have velocities of about 1430 m s^{-1}, depending on the casing and formation discontinuities (Galperin et al., 2012). In the receiver gathers (Fig. 3b), the waves forming the linear events either travel through the subsurface and are then converted to tube waves at the receiver well or have already propagated as tube waves through the source well, radiated towards the receiver borehole, and are converted to tube waves once again. These waves can also be identified in the frequency–wavenumber (denoted fk) spectrum of the data (Fig. 4), where they appear as separate lines originating from $k = 0$. Tube waves can be removed, e.g., by fk or $\tau - p$ filtering.

In order to prevent temporal aliasing, an anti-aliasing filter was applied during recording. However, it deteriorates the data quality in such a way that the P-wave first arrivals are not sharp but show precursors. These precursors are also offset-dependent and become stronger the shorter the source–receiver distance is. Spatial aliasing, caused by the source and receiver spacing of 1 m, however, could not be avoided, such that seismic events dip in two different directions simultaneously.

The fk spectrum of the field data from plane BC (Fig. 4) shows that most of the energy is concentrated in a triangle that is symmetrical to the frequency axis at $k = 0$. However, a considerable amount of energy is aliased at about 270 Hz, resulting in a wrap-around effect in the fk spectrum. In addition, we can identify unusually dipping events in the fk spectrum that originate at the minimum and maximum wavenumbers.

The frequency spectra from plane BC (Fig. 5a and b, red) show large peaks below 20 Hz. Another significant peak can be found at about 200 Hz. The cumulative spectrum, i.e., the normalized sum of the spectra of all shots, has its overall maximum at 345 Hz. Frequencies at 830 Hz, which corresponds to 83 % of the Nyquist frequency, are attenuated by −3 dB by the anti-aliasing filter applied during acquisition. Frequencies above 650 Hz already contribute less than 50 % to the signal energy. The normalized amplitude spectra of plane AB (Fig. 5a and b, orange) show a narrower peak at around 200 Hz and higher values at high frequencies. For plane AC (Fig. 5c and d, purple), where a finer sampling interval of 8 kHz was used, we observe several peaks below 500 Hz in the amplitude spectrum and another peak at about 1100 Hz. Frequencies above 1500 Hz contribute less than 30 % to the signal energy.

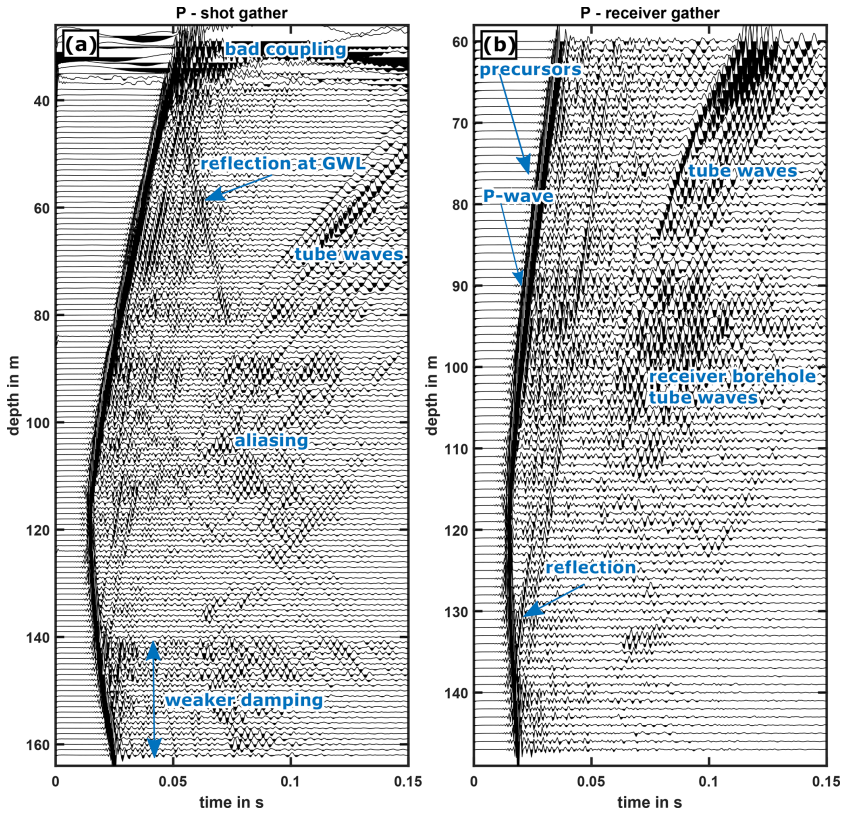

Figure 3. **(a)** Raw shot gather at 122 m depth with strong shot borehole tube waves. The top few stations were outside the water column in the receiver borehole C, resulting in long-period noise. **(b)** Raw trace-normalized P-wave receiver gather at 122 m depth with strong shot borehole tube waves and a weak receiver borehole tube wave.

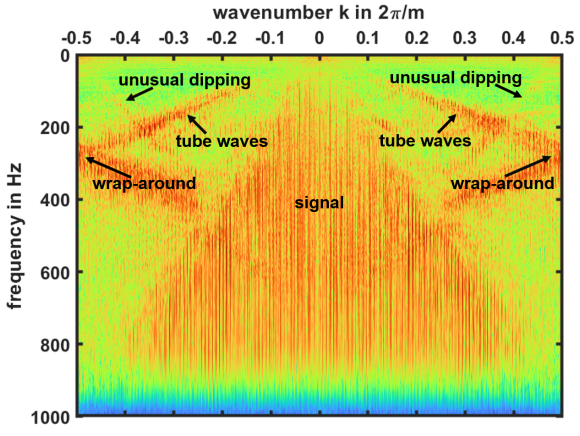

Figure 4. fk spectra of P-wave sparker data from plane BC showing tube wave energy, a wrap-around effect, and unusually dipping events originating at the minimum and maximum wavenumbers. For presentation purposes, we plot the spectrum to the power of 0.1 and apply a 95 percentile clip to the color map.

3.3 Discussion

In retrospect, we recommend focusing the P-wave surveys solely on the high-resolution imaging using horizontal travel paths and disregarding anisotropy investigations to reduce the number of shot positions required to obtain a proper angular coverage. Instead, a finer temporal sampling of at least 8 kHz would have ensured sharp phase onsets. For the longer plane between boreholes A and C, which was measured in a separate survey after the data were acquired in the short planes, the temporal sampling was reduced to 0.125 ms, which was sufficient to record the entire frequency range of the signal (Fig. 5) and thus sharp first arrivals.

To reduce the listening time, i.e., the time it takes to send the data to the computer, and with the intention of imaging by travel-time inversion methods as opposed to reflection imaging, we would reduce the total recording time to 800 ms. This would be sufficient to record first arrivals and reflections in our crosshole setting with short borehole spacings of 28 and 40 m (Liu et al., 2012). Later arrivals are too attenuated in the sediments to be visible in the data. Consequently, the recording time was adjusted in the acquisition of data in the plane between boreholes A and C. In addition, we would record the data at the surface seismic stations independently of the crosshole data, as the additional 336 channels are the main factor in the long listening time.

Although we additionally deployed 3C geophones along profiles at the surface between the boreholes, these data are

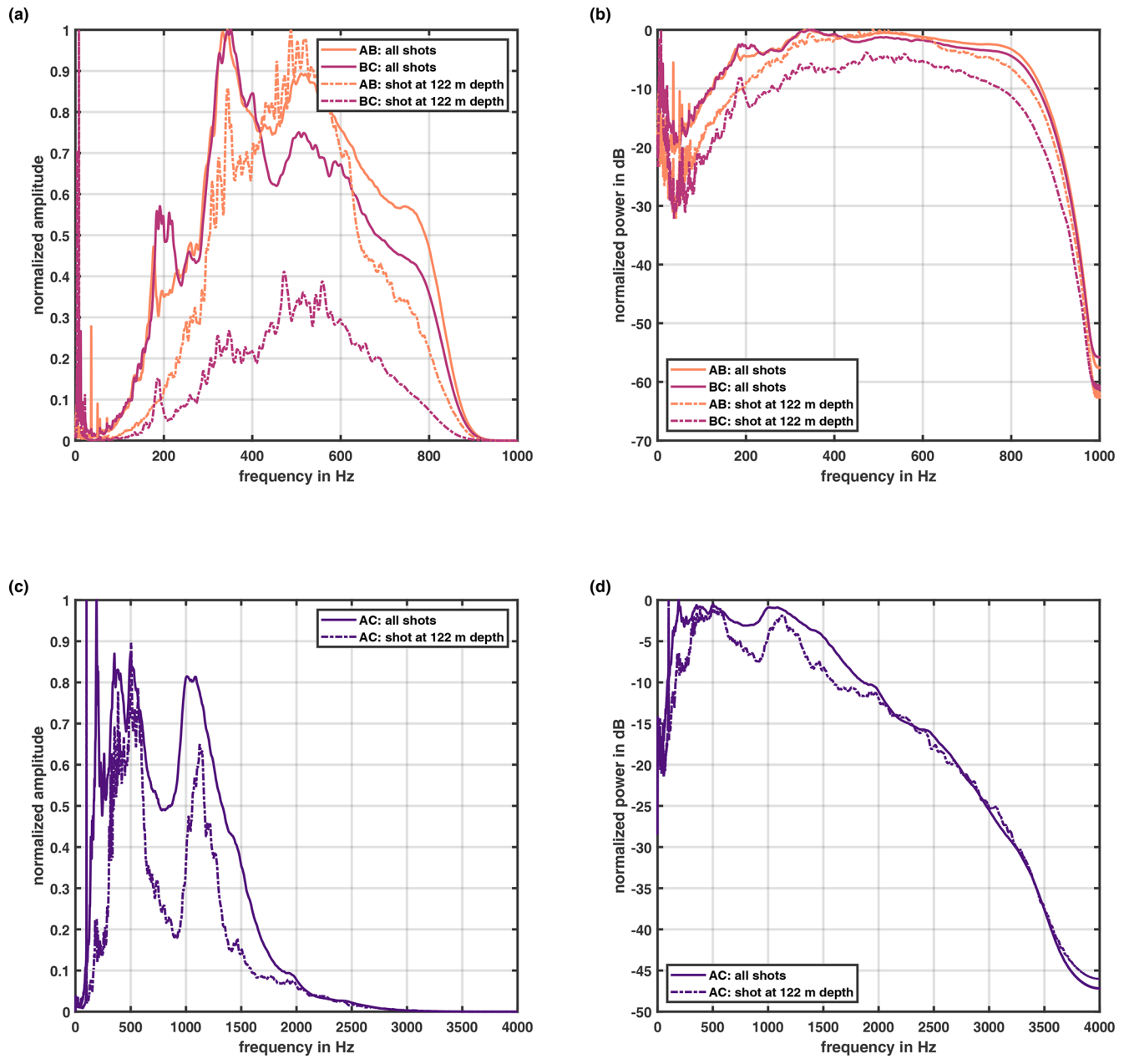

Figure 5. Frequency spectra for P-wave sparker data from planes AB, BC (both panels **a** and **b**), and AC **(c, d)**. **(a, c)** Normalized amplitude spectrum. **(b, d)** Normalized power spectrum. The solid lines represents the frequency content of the entire dataset; the dashed line represents that of the traces recorded for the shots at 122 m depth.

not expected to be able to fully compensate for the limited angular coverage of the crosshole data due to the noise level caused by environmental noise. This includes factors such as vehicles passing directly by the site, trains commuting in the nearby river valley, and agricultural and forestry operations – all of which also cause a significant amount of downtime.

Regarding the noise identified in the fk spectra of the P-wave data, we interpret the unusually dipping events at the minimum and maximum wavenumbers in the fk spectrum as related to the interlacing of the receiver strings according to Watanabe et al. (2005). However, definitive verification is not possible, because we do no see systematic shifts in every second receiver depth. It seems reasonable to conclude that this is a display problem as a consequence of the temporal undersampling.

To avoid the spatial aliasing, a source and receiver spacing of 0.1 m would have been necessary. Thus, the depth errors of the borehole tools would be of a similar magnitude or even greater. These location errors include cable extension (up to 0.1 m), erroneous depth markers (up to $\pm$0.1 m), and smaller

errors (up to 0.05 m) due to clamping of the source and the receiver string. For the three to five deepest shot positions in borehole B, we estimate a position error of up to 0.5 m due to buoyancy caused by remaining drilling mud, depending on both the depth and the type of source and receiver.

4 Travel-time analysis

4.1 First arrival travel-time tomography and resolution test

In order to obtain preliminary subsurface models based on the P-wave first arrivals from the sparker data, we perform travel-time tomography. The method uses the phase picks and the acquisition geometry to invert the subsurface model. Synthetic travel times are computed based on Dijkstra's shortest path method, using secondary nodes to improve accuracy, as detailed by Giroux and Larouche (2013). Given the highly nonlinear nature of this geophysical inversion problem, an iterative optimization approach is employed to minimize the misfit between the field data and the simulated data. Here, we apply the damped Gauss–Newton algorithm with global regularization (Günther et al., 2006), which is implemented in the inversion code pyGIMLi (Rücker et al., 2017). It minimizes the objective function

$$\Phi = \Phi_{\mathrm{d}}(\boldsymbol{m}) + \lambda\,\Phi_{\mathrm{m}}(\boldsymbol{m}) \rightarrow \min, \tag{1}$$

where $\Phi_{\mathrm{d}}(\boldsymbol{m})$ is the data misfit and where $\Phi_{\mathrm{m}}(\boldsymbol{m})$ is the model sharpness. The parameter λ is the damping or trade-off parameter, which controls the relationship between data fit and model smoothness. Once the optimal model parameter updates, $\delta\boldsymbol{m}$, have been identified, the algorithm updates the model on an unstructured mesh after each iteration step until it reaches the abort criterion. The latter is defined as the χ^2 value, which is construed as the mean of the sum of the squared data errors weighted by the misfit. Thus, reaching this criterion avoids both overfitting and underfitting of the data.

Since we expect a predominantly horizontally layered structure, we also apply geostatistical constraints to the inversion. This additional regularization uses the model covariance matrix to define a correlation ellipse, which is construed over the horizontal and vertical correlation lengths and the dip with respect to the horizontal direction (Jordi et al., 2018). Here, we choose a horizontal correlation length of 50 m and a vertical correlation length of 5 m for all three borehole planes without any dip.

We choose the initial model as the slowness, p, of the median apparent P-wave velocity, i.e., $p = 1/1935\,\mathrm{m\,s^{-1}}$, derived from the data of the borehole plane AC. The damping or trade-off parameter, λ, is set to 2000 so that the inversion quickly reaches the target data fit, and any systematic pattern in the residuals is removed.

Furthermore, we check the resolution of the tomography by means of a synthetic test model with 5 m thick layers (Fig. 6a and c), which differ in their velocity by 5 %. We forward calculate the travel times between the sources and receivers based on the model with a relative noise level of 1 % and an absolute noise level of 0.125 and 0.5 ms, corresponding to the respective temporal sampling interval and estimated picking error. Afterwards, we use a homogeneous initial model of $2050\,\mathrm{m\,s^{-1}}$ and perform an inversion with the same parameters used to invert the field data.

4.2 Tomography results

The resolution test shows that 5 m thick layers could be well distinguished in plane AC using an unstructured mesh with a triangular area of $2\,\mathrm{m^2}$ (Fig. 6a) if we assumed the actual picking error of this part of the dataset. The inverted high-velocity layers are thicker than the low-velocity layers (Fig. 6b), except in the central part at about 110 m depth, where the low-velocity layers are thicker. Furthermore, the layers extend all the way from the sources to the receivers. Nevertheless, a high-velocity zone is also recovered near the source positions. For plane BC (Fig. 6c), the layers are less well resolved in terms of the velocity contrast and their planar interfaces, which appear convex above 90 m depth (Fig. 6d). In general, layers that are above and below the sensor depth range are not resolved.

The inversion runs of the field data stop after a few iterations because they reach the abort criterion of $\chi^2 < 1$ (i.e., the inverted models explain the data within the assigned error of 0.5 ms). Figure 7 shows the obtained velocity distributions (tomograms) for all three borehole planes. The areas that remain white are those that are not traversed by the simulated seismic rays.

All tomograms in Fig. 7 show a low-velocity ($< 1800\,\mathrm{m\,s^{-1}}$) structure at the very top of the model down to about 54 m (label a). In plane AC, this low-velocity zone is interrupted by a layer of a slightly higher velocity at about 40 m depth (b). Below this, we can identify an approximately 9 m thick layer with P-wave velocities of above $2000\,\mathrm{m\,s^{-1}}$ that extends over all three planes (c). This is followed by another layer, about 5 m thick, with a velocity of about $1900\,\mathrm{m\,s^{-1}}$ (d). At depths from about 75 m down to about 138 m, we see more layers, but they are not continuous in their extent or their velocities. Distinctive features in this depth range are a low-velocity zone at about 90 m depth, which is concentrated near borehole C and more pronounced in plane AC (e), and a high-velocity zone between 110 and 120 m depth on the same side of plane AC (f). Below 138 m, the tomograms show a high-velocity zone of about $2300\,\mathrm{m\,s^{-1}}$ (g), followed by a layer, about 5 m thick, with velocities of $2200\,\mathrm{m\,s^{-1}}$ (h). The former is more concentrated on the source sides of the short planes, while it is continuous in the long plane. The overall highest velocities are found at the bottom of the model with velocities of up to almost $2600\,\mathrm{m\,s^{-1}}$ (i).

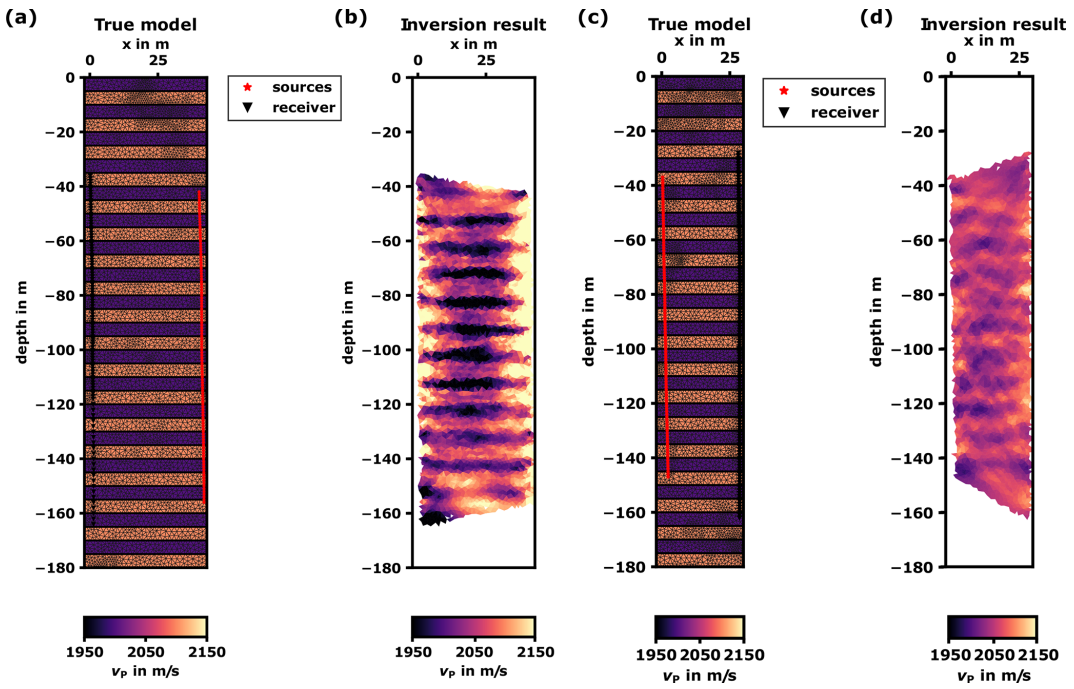

Figure 6. **(a)** Layered model for synthetic inversion test for plane AC. Fine lines show the modeling and inversion mesh. **(b)** Result of inversion of the forward modeled data from panel **(a)** including an absolute noise level of 0.125 ms. High-velocity layers appear thicker in the inversion result than low-velocity layers. **(c)** Layered model for synthetic inversion test for plane AC. Fine lines show the modeling and inversion mesh. **(d)** Result of inversion of the forward modeled data from panel **(c)** including an absolute noise level of 0.5 ms.

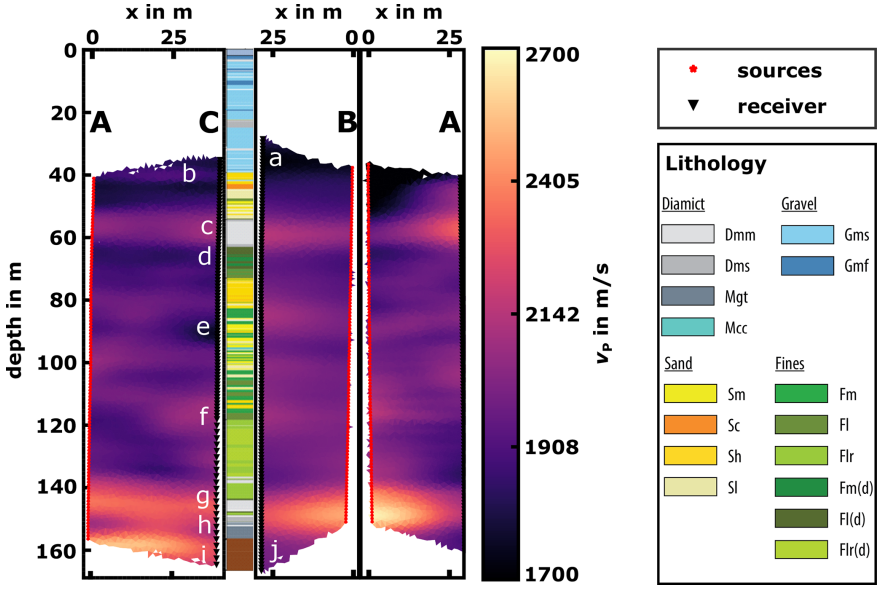

Figure 7. P-wave travel-time tomography velocity models and final lithology from the cored borehole C (Schuster et al., 2024). Receivers are marked by black triangles and sources by red stars. The *x* refers to the profile coordinate in Fig. 2.

From the tomograms of the field data inversion, P-wave velocity profiles are extracted along the borehole trajectories. They reasonably match the cased-hole sonic logs (Fig. 8), where the samples represent an averaged value over 0.5 m and which are smoothed over 5 m to make the datasets comparable. Along well A, the long-period trend is consistent. The profiles obtained from the long plane AC look like a further smoothed version of the sonic log. The profile from the shorter plane BA fits both the sonic log and the other profile at intermediate depth, but it has an overall trend from too fast

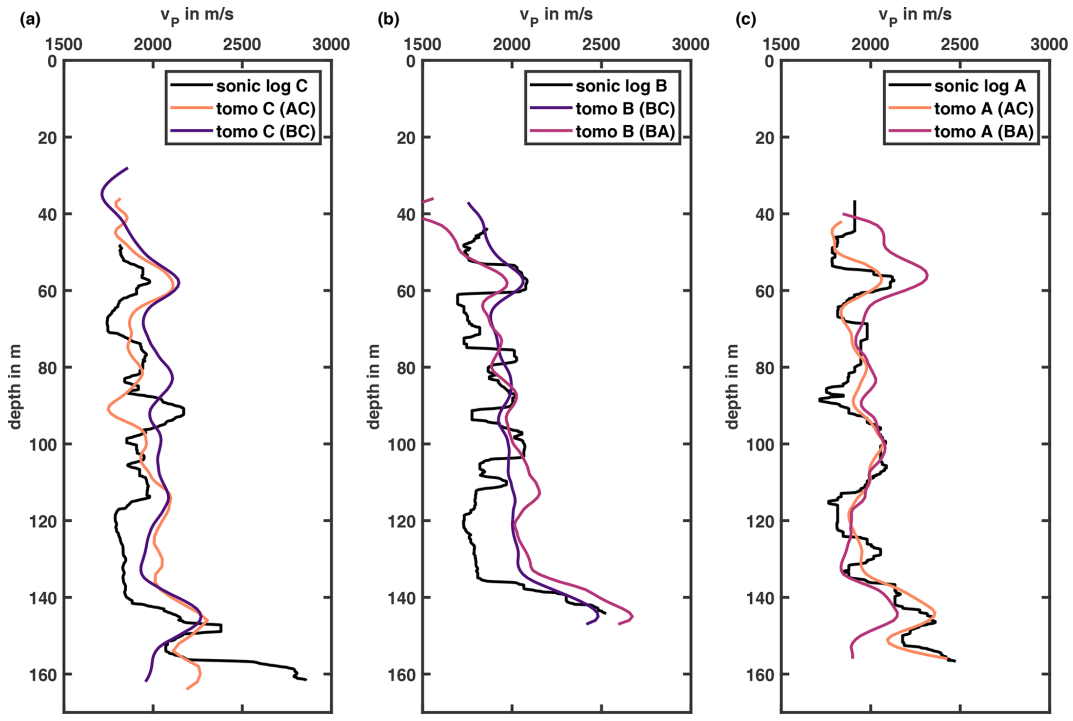

Figure 8. P-wave velocity profiles from smoothed wireline sonic logs vs. profile from travel-time tomography model for borehole C **(a)**, borehole B **(b)**, and borehole A **(c)**.

to too slow from top to bottom. For borehole C, we observe a greater discrepancy between the tomography profiles and the sonic log, including an anticorrelation at about 90 m depth. There, the log indicates a high-velocity zone, while the tomograms show a low-velocity zone. Moreover, the velocity profiles from the tomograms exhibit a shift of approximately 200 m s^{-1} towards higher velocities at depths of about 55 to 145 m. Furthermore, the low-velocity zone at depths from 114 to 144 m forms a less pronounced contrast than that observed in the sonic log. Additionally, the tomograms indicate a reduction in P-wave velocity at depths below 160 m, in contrast to the sonic log, which shows a strong increase of about 1000 m s^{-1}. The velocity variations along borehole B are considerably less pronounced in the tomograms than in the sonic log, so many minima and maxima cannot be identified and correlated. The tomography profiles also show a trend of increasing velocity with depth, which is not evident in the sonic log above 135 m. Nevertheless, the velocities are of a comparable magnitude.

4.3 Discussion

The resolution test confirms that we can distinguish layers of 5 m thickness with 5 % velocity difference. However, the high-velocity layers become thicker as the rays prefer to minimize the travel time. First-arrival travel-time tomography therefore favors arrivals from fast media. Thus, the low-velocity zones are sampled less densely with respect to the phase arrival picks and appear thinner, especially when the geostatistical regularization is applied, which effectively smooths the velocity field over 5 m in the vertical direction. Furthermore, the larger error estimate of the short planes results in a poorer resolution. However, the bending effect on the layers in the upper part cannot be observed in the field data tomography results of planes AB or BC.

Comparing the tomograms of the long plane AC with the two short planes AB and BC, the former shows more details, while the latter depict smoother velocity distributions. This can be explained by the higher picking accuracy of about a factor of 4 in plane AC, where a 4 times finer time sampling interval was chosen. The effect becomes evident when we compare the low- and intermediate-velocity zones above the high-velocity layer located at about 54 m (Fig. 7c). While the horizontally bedded sand layer (Sh) just below 40 m depth can be identified in plane AC as a zone of intermediate velocities (b), this is not the case in the two shorter planes. However, the weakly decreasing velocities in the layer towards borehole C might also indicate that the geostatistical regularization distributes the intermediate velocity information further than it actually reaches. The tomogram of plane BC also suggests that the layer might not continue into the direction of the plane but is interrupted by low-velocity material, which is not present in plane AC. This explanation is further supported by the tomogram of plane AB, where we see an intermediate-velocity zone close to borehole A but a low-velocity zone close to borehole B, indicating that the

structure is interrupted halfway between borehole A and B, i.e., in the north–south direction. The complete absence of the intermediate-velocity zone, despite the correlation with the sand layer in the core, leads us to assume that the sand reaches only very little into plane BC and is smoothed out by the regularization. The shallow part of the tomograms from the short planes should be treated with care not only because of the coarse time sampling interval, but also because of the higher noise level at the shallow source and receiver positions. The high-velocity layer (c) below the just discussed shallow part clearly corresponds to a diamict found in the core at depths of about 54 to 63 m and extents over all three borehole planes. The next low-velocity layer (d) is associated with the fines found in the core. The discontinuities and velocity changes in depths from 75 to 138 m indicate a complex subsurface structure, which is confirmed by the alternating layers of sand and fines in the core lithology. Again, plane AC shows larger velocity contrasts, while the tomogram of plane AB depicts the layering down to about 118 m very well, including the layer boundary with the layers of only fines. The continuous high-velocity layer (g) at the bottom of the model correlates well with the massive diamict (Dmm). The thick low-velocity zone at the bottom of the short layers (j) is mostly an artifact of the smoothing, limited ray coverage, source mislocations due to the buoyancy of the remaining drilling mud in borehole B, and again inaccurate picks due to both the temporal sampling interval and the increased noise level because of the inert fluid at the bottom of the boreholes. In plane AC, this intermediate-velocity zone (h) is much thinner and correlates with the mélange (Mgt) "consisting of consolidated and unconsolidated molasse, sandstone, and siltstone fragments showing in situ crushing and brecciation" according to Schuster et al. (2024). The high-velocity layer at the very bottom (i) of plane AC eventually shows the molasse bedrock. A comprehensive sedimentological interpretation of the core lithology can be found in Schuster et al. (2024).

The overall trend of the profiles from the sonic logs and the tomographic models is similar (Figs. 7 and 8). The larger variations along boreholes C and B suggest that the formation close to those boreholes shows more variation than along borehole A. This near-field effect is well sampled by the sonic log, which inspects only a few decimeters of the formation around the borehole. The crosshole experiment, on the other hand, covers the plane between the boreholes and is sensitive to structures from the entire Fresnel volume with a radius of about 5 m. Furthermore, the geostatistical regularization with its horizontally extended correlation ellipse favors the inversion of layered structures and leads to smoothing of the velocity field. Differences in the velocity profiles obtained from different planes are related to picking inaccuracies, the geostatistical regularization, and location errors of the tools. The former is most obvious for borehole A, where the good-quality data from plane AC give an impressive fit to the sonic data, while the temporally undersampled data from plane BA show a larger deviation. In general, deviations of the velocity profiles at minimum and maximum depth are related to the reduced ray coverage in the tomography.

5 Conclusions and outlook

The crosshole data acquisition showed that the sparker source excites seismic waves with frequencies in the order of kilohertz (kHz). Therefore, the wave field has to be sampled very finely both in time and space, which increases the acquisition time and requires precise shot and receiver positioning. In this context, we discerned that the low-pass filter effect of the glacial sediments is much smaller than estimated from literature and anticipated during survey planning. We can clearly identify these effects in the data in the form of aliasing effects. Furthermore, the data are dominated by first-arrival P-waves and strong tube wave noise.

The travel-time tomography models, which show discontinuous layers in intermediate depths despite the application of a geostatistical regularization assuming horizontal layering, depict complex seismic wave fields indicating a heterogeneous basin infill. This is also reflected in the highly variable GWL over short distances of less than 40 m.

The velocity profiles extracted from the tomography models along the trajectory of the boreholes are in good agreement with the available sonic log data and the lithology of borehole C. However, we believe that this preliminary result can be further improved by full-waveform inversion (FWI), which considers not only the arrival time of a seismic phase, but also the entire waveform. This will require a thorough removal of the tube waves, yet it will increase the resolution to the decimeter scale, thereby bridging the gap between conventional surface seismic and core-scale information. Together with additional information from the core, the seismic subsurface models will be geologically interpreted.

Appendix A: Groundwater levels

Table A1. Groundwater level (GWL) changes in boreholes A, B, and C during the time of the crosshole campaigns. Due to the instruments in the boreholes, the GWL in B and C was only measured at the beginning and the end of the survey. Note: NA represents not available.

Date (dd.mm.yyyy)	A	B	C
22.03.2022	42.18	35.30	28.60
23.03.2022	42.37	35.34	28.80
24.03.2022	38.05	34.92	28.50
25.03.2022	38.39	34.46	28.01
26.03.2022	38.72	35.56	27.98
31.03.2022	43.40	35.59	27.88
01.04.2022	43.30	40.24	30.75
03.05.2022	42.22	35.62	27.81
05.05.2022	42.17	NA	NA
06.05.2022	42.14	NA	NA
07.05.2022	42.09	NA	NA
13.05.2022	41.97	38.25	30.76
06.10.2022	40.59	36.04	27.91
12.10.2022	41.70	36.54	28.93

Data availability. Upon completion of the project, the seismic data is accessible via the GFZ data services (https://doi.org/10.5880/ICDP.5068.002, Beraus et al., 2024). The DOVE operational dataset is published under https://doi.org/10.5880/ICDP.5068.001 (DOVE-Phase 1 Scientific Team et al., 2023a), together with the operational report (https://doi.org/10.48440/ICDP.5068.001, DOVE-Phase 1 Scientific Team et al., 2023b) and the explanatory remarks (https://doi.org/10.48440/ICDP.5068.002, DOVE-Phase 1 Scientific Team et al., 2023c).

Author contributions. TBu, HB, and DK developed the project concept. GG manages and coordinates the project. SB and HB were involved in the data acquisition. SB processed the data, prepared the figures, and wrote the manuscript. All authors contributed to the discussion of the data, as well as the structure and editing of the manuscript.

Competing interests. The contact author has declared that none of the authors has any competing interests.

Disclaimer. Publisher's note: Copernicus Publications remains neutral with regard to jurisdictional claims made in the text, published maps, institutional affiliations, or any other geographical representation in this paper. While Copernicus Publications makes every effort to include appropriate place names, the final responsibility lies with the authors.

Acknowledgements. We thank the International Continental Drilling Program (ICDP) for their continued support and funds for the drilling of the three boreholes at site 5068_1. The seismic crosshole equipment was rented from Geotomographie GmbH, Neuwied. A special thanks to the technical staff of LIAG-S1 (Jan Bayerle, Sven Wedig, and Jan Bergmann Barrocas) as well as our student assistant Kim Ripke for their vigorous support in the field. Further thanks go to Thomas Grelle and Carlos Lehne (LIAG-S5) for acquiring the logging data. Preprocessing of the data was done using an academic license of Shearwater's Reveal software and the open-source code BIRGIT. Many thanks to Thomas Günther and Nico Skibbe for the exchange on pyGIMLi that was used to create the travel-time tomography models.

Financial support. This research has been funded by the Deutsche Forschungsgemeinschaft (grant nos. BU 3894/2-1, BU 2467/3-1, and KO 6375/1-1).

Review statement. This paper was edited by Ulrich Harms and reviewed by two anonymous referees.

References

Anselmetti, F. S., Bavec, M., Crouzet, C., Fiebig, M., Gabriel, G., Preusser, F., and Ravazzi, C.: Drilling Overdeepened Alpine Valleys (ICDP-DOVE): Quantifying the age, extent, and environmental impact of Alpine glaciations, in: Scientific drilling: reports on deep earth sampling and monitoring, Sapporo: IODP, 31, 51–70, https://doi.org/10.15488/13635, 2022.

Bauer, K., Pratt, R., Weber, M., Ryberg, T., Haberland, C., and Shimizu, S.: Mallik 2002 cross-well seismic experiment: project design, data acquisition, and modelling studies, in: Scientific Results from the Mallik 2002 Gas Hydrate Production Research Well Program, Mackenzie Delta, Northwest Territories, Canada, edited by: Dallimore, S. R. and Collett, T. S., vol. 585 of GSC Bulletin, Geological Survey of Canada, 14 pp., ISBN 978-0-660-19339-7, 2005.

Beraus, S., Burschil, T., Buness, H., Köhn, D., Bohlen, T., and Gabriel, G.: Can We Detect Seismic Anisotropy in Glacial Sediments Using Crosshole Seismics?, European Association of Geoscientists & Engineers, vol. 2023, 1–5, https://doi.org/10.3997/2214-4609.202320174, 2023.

Beraus, S., Buness, H., Bayerle, J., Bergmann Barrocas, J., Wedig, S., Ripke, K., and Gabriel, G.: Crosshole seismic data at ICDP site 5068_1, GFZ German Research Centre for Geosciences [data set], https://doi.org/10.5880/ICDP.5068.002, 2024.

Buness, H., Tanner, D. C., Burschil, T., Gabriel, G., and Wielandt-Schuster, U.: Cuspate-lobate folding in glacial sediments revealed by a small-scale 3-D seismic survey, J. Appl. Geophys., 200, 104614, https://doi.org/10.1016/j.jappgeo.2022.104614, 2022.

Burschil, T., Buness, H., Tanner, D., Wielandt-Schuster, U., Ellwanger, D., and Gabriel, G.: High-resolution reflection seismics reveal the structure and the evolution of the Quaternary glacial Tannwald Basin, Near Surf. Geophys., 16, 593–610, https://doi.org/10.1002/nsg.12011, 2018.

Daley, P. F.: Reflection and transmission coefficients at the interface between two transversely isotropic media, B. Seismol. Soc. Am., 67, 661–675, https://doi.org/10.1785/BSSA0670030661, 1977.

DOVE-Phase 1 Scientific Team, Anselmetti, F. S., Beraus, S., Buechi, M., Buness, H., Burschil, T., Fiebig, M., Firla, G., Gabriel, G., Gegg, L., Grelle, T., Heeschen, K., Kroemer, E., Lehne, C., Lüthgens, C., Neuhuber, S., Preusser, F., Schaller, S., Schmalfuss, C., Schuster, B., Tanner, D. C., Thomas, C., Tomonaga, Y., Wieland-Schuster, U., and Wonik, T.: Drilling Overdeepened Alpine Valleys (DOVE) – Operational Dataset of DOVE Phase 1, GFZ German Research Centre for Geosciences [data set], https://doi.org/10.5880/ICDP.5068.001, 2023a.

DOVE-Phase 1 Scientific Team, Anselmetti, F. S., Beraus, S., Buechi, M. W., Buness, H., Burschil, T., Fiebig, M., Firla, G., Gabriel, G., Gegg, L., Grelle, T., Heeschen, K., Kroemer, E., Lehne, C., Lüthgens, C., Neuhuber, S., Preusser, F., Schaller, S., Schmalfuss, C., Schuster, B., Tanner, D. C., Thomas, C., Tomonaga, Y., Wieland-Schuster, U., and Wonik, T.: Drilling Overdeepened Alpine Valleys (DOVE) – Operational Report of Phase 1, ICDP Operational Report, GFZ German Research Centre for Geosciences, https://doi.org/10.48440/ICDP.5068.001, 2023b.

DOVE-Phase 1 Scientific Team, Anselmetti, F. S., Beraus, S., Buechi, M. W., Buness, H., Burschil, T., Fiebig, M., Firla, G., Gabriel, G., Gegg, L., Grelle, T., Heeschen, K., Kroemer, E., Lehne, C., Lüthgens, C., Neuhuber, S., Preusser, F., Schaller, S., Schmalfuss, C., Schuster, B., Tanner, D. C., Thomas, C., Tomonaga, Y., Wieland-Schuster, U., and Wonik, T.: Drilling Overdeepened Alpine Valleys (DOVE) – Explanatory remarks on the operational dataset, GFZ German Research Centre for Geosciences, https://doi.org/10.48440/ICDP.5068.002, 2023c.

Ellwanger, D., Wielandt-Schuster, U., Franz, M., and Simon, T.: The Quaternary of the southwest German Alpine Foreland (Bodensee-Oberschwaben, Baden-Württemberg, Southwest Germany), E&G Quaternary Sci. J., 60, 22, https://doi.org/10.3285/eg.60.2-3.07, 2011.

Galperin, E. I., Nersesov, I. L., and Galperina, R. M.: Borehole Seismology and the Study of the Seismic Regime of Large Industrial Centres, Springer Science & Business Media, ISBN 978-94-009-4510-4, 2012.

Gaucher, E., Azzola, J., Schulz, I., Meinecke, M., Dirner, S., Steiner, U., and Thiemann, K.: Active cross-well survey at geothermal site Schäftlarnstraße, Researchgate, https://www.researchgate.net/publication/348232434_Active_cross-well_survey_at_geothermal_site_Schaftlarnstrasse (last access: 2 October 2024), 2020.

Giroux, B. and Larouche, B.: Task-parallel implementation of 3D shortest path raytracing for geophysical applications, Comput. Geosci., 54, 130–141, https://doi.org/10.1016/j.cageo.2012.12.005, 2013.

Günther, T., Rücker, C., and Spitzer, K.: Three-dimensional modelling and inversion of dc resistivity data incorporating topography – II. Inversion, Geophys. J. Int., 166, 506–517, https://doi.org/10.1111/j.1365-246X.2006.03011.x, 2006.

Jordi, C., Doetsch, J., Günther, T., Schmelzbach, C., and Robertsson, J. O.: Geostatistical regularization operators for geophysical inverse problems on irregular meshes, Geophys. J. Int., 213, 1374–1386, https://doi.org/10.1093/gji/ggy055, 2018.

Liu, J., Zeng, X., Xia, J., and Mao, M.: The separation of P- and S-wave components from three-component crosswell seismic data, J. Appl. Geophys., 82, 163–170, https://doi.org/10.1016/j.jappgeo.2012.03.007, 2012.

Martuganova, E., Stiller, M., Norden, B., Henninges, J., and Krawczyk, C. M.: 3D deep geothermal reservoir imaging with wireline distributed acoustic sensing in two boreholes, Solid Earth, 13, 1291–1307, https://doi.org/10.5194/se-13-1291-2022, 2022.

Rücker, C., Günther, T., and Wagner, F. M.: pyGIMLi: An open-source library for modelling and inversion in geophysics, Comput. Geosci., 109, 106–123, https://doi.org/10.1016/j.cageo.2017.07.011, 2017.

Schuster, B., Gegg, L., Schaller, S., Buechi, M. W., Tanner, D. C., Wielandt-Schuster, U., Anselmetti, F. S., and Preusser, F.: Shaped and filled by the Rhine Glacier: the overdeepened Tannwald Basin in southwestern Germany, Sci. Dril., 33, 191–206, https://doi.org/10.5194/sd-33-191-2024, 2024.

Van Schaack, M., Harris, J. M., Rector, J. W., and Lazaratos, S.: High-resolution crosswell imaging of a West Texas carbonate reservoir; Part 2, Wavefield modeling and analysis, Geophysics, 60, 682–691, https://doi.org/10.1190/1.1443807, 1995.

von Ketelhodt, J., Fechner, T., Manzi, M., and Durrheim, R.: Joint-Inversion of Cross-Borehole P-waves, horizontally and vertically polarised S-waves: Tomographic data for hydrogeophysical site characterisation, Near Surf. Geophys., 16, 529–542, https://doi.org/10.1002/nsg.12010, 2018.

Watanabe, T., Shimizu, S., Asakawa, E., Kamei, R., Matsuoka, T., Watanabe, T., Shimizu, S., Asakawa, E., Kamei, R., and Matsuoka, T.: Preliminary assessment of the waveform inversion method for interpretation of cross-well seismic data from the thermal production test, JAPEX/JNOC/GSC et al. Mallik 5L-38 gas hydrate production research well, in: Scientific Results from the Mallik 2002 Gas Hydrate Production Research Well Program, Mackenzie Delta, Northwest Territories, Canada, edited by: Dallimore, S. R. and Collett, T. S., vol. 585 of GSC Bulletin, Geological Survey of Canada, https://eurekamag.com/research/023/399/023399500.php (last access: 2 October 2024), 2005.

Zhang, F., Juhlin, C., Cosma, C., Tryggvason, A., and Pratt, R. G.: Cross-well seismic waveform tomography for monitoring CO_2 injection: a case study from the Ketzin Site, Germany, Geophys. J. Int., 189, 629–646, https://doi.org/10.1111/j.1365-246X.2012.05375.x, 2012.

Sci. Dril., 33, 249–266, 2024
https://doi.org/10.5194/sd-33-249-2024

Scientific Drilling
Open Access

International Continental Scientific Drilling Program (ICDP) workshop on the Fucino paleolake project: the longest continuous terrestrial archive in the MEditerranean recording the last 5 Million years of Earth system history (MEME)

Biagio Giaccio[1], Bernd Wagner[2], Giovanni Zanchetta[3], Adele Bertini[4], Gian Paolo Cavinato[1], Roberto de Franco[1], Fabio Florindo[5], David A. Hodell[6], Thomas A. Neubauer[7], Sebastien Nomade[8,9], Alison Pereira[9], Laura Sadori[10], Sara Satolli[11], Polychronis C. Tzedakis[12], Paul Albert[13], Paolo Boncio[11], Cindy De Jonge[14], Alexander Francke[15], Christine Heim[2], Alessia Masi[10], Marta Marchegiano[16], Helen M. Roberts[17], Anders Noren[18], and the MEME team✚

[1]Istituto di Geologia Ambientale e Geoingegneria, IGAG-CNR, 00015 Monterotondo, Rome, Italy
[2]Institute of Geology and Mineralogy, University of Cologne, Cologne, Germany
[3]Dipartimento di Scienze della Terra, University of Pisa, Pisa, Italy
[4]Dipartimento di Scienze della Terra, Università degli Studi di Firenze, Firenze, Italy
[5]Istituto Nazionale di Geofisica e Vulcanologia, Rome, Italy
[6]Department of Earth Sciences, University of Cambridge, Cambridge, CB2 3EQ, United Kingdom
[7]SNSB – Bavarian State Collection for Paleontology and Geology, Munich, Germany
[8]Laboratoire de Sciences du Climat et de l'Environnement, CEA, UMR 8212, UVSQ, IPSL, Gif-sur-Yvette, France
[9]Laboratory GEOPS, Université de Paris-Saclay, Gif-sur-Yvette, France
[10]Dipartimento di Biologia Ambientale, Sapienza Università di Roma, Rome, Italy
[11]Dipartimento di Ingegneria e Geologia, Università degli Studi G. d'Annunzio di Chieti–Pescara, Chieti–Pescara, Italy
[12]Environmental Change Research Centre, Department of Geography, University College London, London, WC1E 6BT, United Kingdom
[13]Department of Geography, Swansea University, Swansea, SA2 8PP, United Kingdom
[14]Biogeoscience Group, Geological Institute, ETH Zurich, Zurich, Switzerland
[15]School of Physics, Chemistry, and Earth Sciences, Faculty of Science, Engineering and Technology, University of Adelaide, Adelaide, SA 5005, Australia
[16]Departamento de Estratigrafía y Paleontología, Universidad de Granada, 18002 Granada, Spain
[17]Department of Geography and Earth Sciences, Aberystwyth University, Aberystwyth, SY23 3DB, United Kingdom
[18]Continental Scientific Drilling Facility, University of Minnesota, Minneapolis, MN 55455, USA
✚A full list of authors appears at the end of the paper.

Correspondence: Biagio Giaccio (biagio.giaccio@cnr.it)

Received: 2 August 2024 – Revised: 9 October 2024 – Accepted: 11 October 2024 – Published: 16 December 2024

Abstract. During the last 5 million years (Pliocene–Holocene), the Earth climate system has undergone a series of marked changes, including (i) the shift from the Pliocene warm state to the Pleistocene cold state with the intensification of Northern Hemisphere glaciation; (ii) the evolution of the frequency, magnitude, and shape

of glacial–interglacial cycles at the Early Middle Pleistocene Transition (∼ 1.25–0.65 Ma); and (iii) the appearance of millennial-scale climate variability. While much of this paleoclimate narrative has been reconstructed from marine records, relatively little is known about the impact of these major changes on terrestrial environments and biodiversity, resulting in a significant gap in the knowledge of a fundamental component of the Earth system. Long, continuous, highly resolved, and chronologically well-constrained terrestrial records are needed to fill this gap, but they are extremely rare. To evaluate the potential of the Fucino Basin, central Italy, for a deep-drilling project in the framework of the International Continental Scientific Drilling Program (ICDP), 42 scientists from 14 countries and 32 institutions met in Gioia dei Marsi, central Italy, on 24–27 October 2023 for the ICDP-supported MEME (the longest continuous terrestrial archive in the MEditerranean recording the last 5 Million years of Earth system history) workshop. The existing information and unpublished data presented and reviewed during the workshop confirmed that the Fucino Basin fulfils all the main requisites for improving our understanding of the mode and tempo of the Plio-Quaternary climatic–environmental evolution in a terrestrial setting at different spatial and temporal scales. Specifically, the combination of the seismic line evidence with geochronological and multi-proxy data for multiple sediment cores consolidated the notion that the Fucino Basin infill (i) is constituted by a sedimentary lacustrine succession continuously spanning at least 3.5 Myr; (ii) has a high sensitivity as a paleo-environmental–paleoclimatic proxy; and (iii) contains a rich tephra record that allows us to obtain an independent, high-resolution timescale based on tephrochronology. Considering the typical half-graben, wedge-shaped geometry of the basin, four different potential drilling targets were identified: MEME-1, located in the middle of the basin, should reach the base of the Quaternary infill at ∼ 500 m depth; MEME-2, located west of MEME-1, has sedimentation rates that are lower, with the base of the Pliocene–Quaternary at ∼ 600 m depth; MEME-3b has the same target as MEME-2 but is located further west, where the base of the Pliocene–Quaternary should be reached at ∼ 300 m; and MEME-3a (∼ 200–300 m depth) is located, for tectonic purposes, on the footwall of the basin master fault. Overall, the MEME workshop sets the basis for widening the research team and defining the scientific perspectives and methodological approaches of the project, from geophysical exploration to the development of an independent chronology and to the acquisition of multi-proxy records, which will contribute to the preparation of the full MEME proposal.

1 Introduction

During the last 5 million years, from the Early Pliocene to the Holocene, the Earth system has undergone a series of prominent changes in its abiotic and biotic components. Overall, global climate shifted from the Pliocene warm state to the Pleistocene cold state (Filippelli and Flores, 2009; Haywood et al., 2009; Lisiecki and Raymo, 2007; Westerhold et al., 2020) with changes in global ice volume and atmospheric greenhouse gas concentrations (Fig. 1). Global mean temperatures during the Pliocene were ∼ 2–3 °C higher than during the pre-industrial Holocene (Haywood et al., 2009), peaking at temperatures up to 4 °C higher (e.g. Haywood et al., 2016) during the so-called mid-Pliocene Warm Period (mPWP; 3.26–3.02 Ma), with atmospheric carbon dioxide values ranging between 350–550 ppm (Stap et al., 2016; de la Vega et al., 2020; Guillermic et al., 2022) (Fig. 1) and a global sea level that was likely to be 12–20 m higher than today (Miller et al., 2020). In light of these climatic features, the Pliocene (and, in particular, the mPWP) represents a potential analogue for current and future anthropogenic global warming scenarios (Haywood et al., 2020; Allan et al., 2021; Burke et al., 2018).

Later, during the Pliocene–Pleistocene transition (PPT), the Northern Hemisphere glaciation intensified (Ravelo et al., 2004; Westerhold et al., 2020) (Fig. 1), and Earth's climate entered a new stage dominated by the quasi-periodic expansion and contraction of the major Northern Hemisphere ice sheets, driven by variations in the Earth's axial inclination and orbital geometry (Milankovitch, 1941) that affect the seasonal and latitudinal distribution of incoming solar radiation. However, the frequency, amplitude, and shape of the glacial–interglacial cycles were not uniform, and the ∼ 41 kyr periodicity that dominated the first part of the Early Pleistocene gradually turned into the longer ∼ 100 kyr high-amplitude and strongly saw-toothed cycles seen during the Early Middle Pleistocene Transition (EMPT; Head and Gibbard, 2015) between ca. 1.25 and 0.65 Ma (e.g. Berends et al., 2021) (Fig. 1). In addition to orbital-scale variability, North Atlantic and polar records revealed the extreme and pervasive nature of millennial-scale climate variability over the last 1.5 Myr (McManus et al., 1999; Jouzel et al., 2007; Barker et al., 2011; Raymo et al., 1998; Hodell et al., 2008, 2023b; Naafs et al., 2013; Hodell et al., 2023a).

The most relevant information and data for many of these events and processes that have marked the overall evolution of the Earth's climatic system during the last 5 Myr are derived from marine records (Ronge et al., 2020; Westerhold et al., 2020). However, the knowledge that can be gained from these records is reliant on astronomical tun-

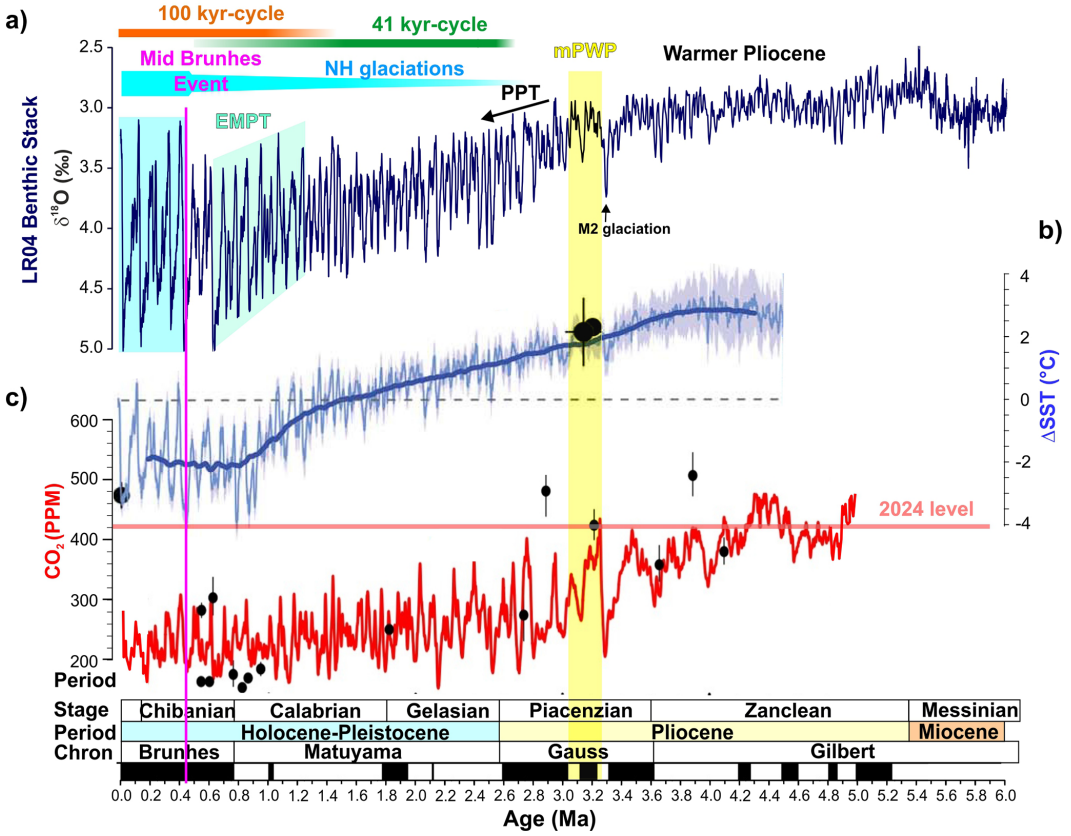

Figure 1. Main features and evolutionary processes of the last 5 million years of climate history. **(a)** LR04 benthic δ^{18}O stack from Lisiecki and Raimo (2005). **(b)** Global sea surface temperature change (ΔSST) from Clark et al. (2024) (light blue represents 1σ uncertainty, while the long-term average is in dark blue). Black circles represent ΔSSTs for the Pliocene KM5c interglaciation, the mid-Piacenzian stage (36), and the Last Glacial Maximum. **(c)** Simulated (red line) and δ11B-based (black dots) atmospheric CO_2 concentrations from Stap et al. (2016). Abbreviations: PPT – Pliocene–Pleistocene transition, M2 glaciation – Marine Isotope Stage (MIS) M2 (3.312–3.264 Ma) glaciation, mPWP – mid-Pliocene Warm Period, EMPT – Early Middle Pleistocene Transition.

ing for its chronological framework, largely lacking independent radiometric constraints and, apart from a few exceptions, missing the terrestrial dimension. Some of the knowledge gaps are targeted by recent or proposed IODP (International Ocean Discovery Program) projects, such as IODP Expedition 397 to the Iberian Margin; Expedition 401, which is constituted by the study of the Mediterranean–Atlantic Gateway Exchange since the Late Miocene; or IODP Proposal 1006, which focuses on the Mediterranean–Black Sea Gateway Exchange (see https://www.iodp.org/proposals/active-proposals, last access: 18 October 2024). Ice core records, on the other hand, provide high-resolution chronological and environmental information from the terrestrial realm, but they are limited to the last $\sim$ 800 kyr and to polar regions (Jouzel et al., 2007).

From the terrestrial realm, lake sediments have shown the potential to provide long, highly resolved, and precisely dated records, shedding light on climate-driven ecosystem and biodiversity changes. Outstanding examples of lake sediment records from Eurasia are the Pliocene–Pleistocene records of Baikal and El'gygytgyn (Williams et al., 1997; Melles et al., 2012; Fig. 3). Lake Baikal was the first record drilled within the framework of the ICDP (International Continental Scientific Drilling Program) in the mid-1990s, and research on this material is still ongoing (Alexander Prokopenkov, personal communication, 2023). On the other hand, the record from Lake El'gygytgyn nicely demonstrated a polar amplification of climate extremes that has not otherwise been documented in marine records so far (Melles et al., 2012). From the Mediterranean region, which is characterized by high biodiversity and a high human population today, ICDP drilling targets have included the Dead Sea, Lake Van, and Lake Ohrid (Fig. 3a). Although these records have broadened our general understanding of changes in ecosystems (Sadori et al., 2016; Donders et al., 2021), biodiversity, and endemism (Wilke et al., 2020), they are limited to $\sim$ 1.4 Ma and do not cover the PPT and, in particular, the mPWP.

In the framework of western Eurasia, the Pliocene–Quaternary lacustrine successions hosted in the central

Apennine intermountain tectonic depressions (e.g. Galadini et al., 2003) are among the few sedimentary archives that can fill these knowledge gaps back to the mPWP, or even beyond, in an unprecedented way. Indeed, the high sensitivity of these archives to climatic change and the occurrence of a rich record of $^{40}Ar/^{39}Ar$ dated tephras from the adjacent ultra-potassic peri-Tyrrhenian volcanic centres (Figs. 2, 3) are well documented (e.g. Giaccio et al., 2015a; Regattieri et al., 2015, 2016, 2019; Mannella et al., 2019; Bertini et al., 2023). However, many of the central Apennine Pliocene–Quaternary successions are discontinuous and often cover only relatively short intervals.

The Fucino Basin, which is the largest basin in the core of the central Apennine (Figs. 2, 3), is an exception. According to our present knowledge, it is the only central Apennine basin hosting a continuous and well-resolved lacustrine succession from the Early Pliocene to historical times (e.g. Cavinato et al., 2002), unique in the European realm. New (unpublished) tephrochronological paleomagnetic and pollen data of a 270 m long sediment core from the marginal part of the basin, coupled with high-resolution seismic data, suggest that the sediment succession in the lake may reach back to ∼ 3.0–3.5 Ma. Furthermore, recent investigations reported the presence of ∼ 130 volcanic ash layers in a composite ∼ 98 m long sediment core (Fig. 3c–d) from the Fucino Basin spanning the last 430 kyr (Giaccio et al., 2017, 2019; Monaco et al., 2021, 2022; Leicher et al., 2023, 2024). They confirmed the outstanding potential of this sedimentary succession to provide us with the most intensely and independently dated record of the entire Mediterranean region, setting benchmarks in the regional tephrostratigraphic framework, as well as in dating global climato-stratigraphic and paleomagnetic event boundaries (Fig. 4). Although high-resolution investigations of the Fucino Basin are limited at present to the last 430 kyr, evidence from the discontinuous successions of the adjacent basins of Sulmona and L'Aquila (Figs. 1, 3) indicate that the occurrence of tephra layers extends to as far back as at least 2 Ma (Bertini et al., 2023); volcanological records from Pontine Island (Fig. 3b) indicate that explosive activity in the region can extend back to 4.2 Ma (Conte et al., 2016). Therefore, its long and continuous geological history and its proximity to peri-Tyrrhenian volcanic centres (distance: 100 to 150 km; Fig. 3b) indicate that the Fucino Basin is ideally located to provide an exceptional record of Pliocene–Quaternary environmental changes underpinned by a precisely dated $^{40}Ar/^{39}Ar$-based chronological framework.

Ultimately, the aim of MEME is to gain insights into the mode and tempo of Pliocene–Quaternary climatic–environmental changes at different spatial (e.g. from global climate variability to regional tectonics and explosive volcanism) and temporal (long-term, orbital, and millennial–centennial climate variability) scales by extending the independently dated $^{40}Ar/^{39}Ar$ chronology of the Fucino lacustrine record back into the Pliocene. In particular, the Fucino chronology can eventually provide a template for key marine sequences such as the new IODP Expedition 397 Site U1385 on the Iberian Margin, extending to ∼ 5.3 Ma (http://publications.iodp.org/proceedings/397/397title.html, last access: 22 September 2024). In addition, the Fucino record has the potential to form a bridge between IODP initiatives focusing on the Mediterranean–Atlantic Gateway Exchange (IODP Expedition 401) and the Mediterranean–Black Sea Gateway Exchange (IODP Proposal 1006; see https://www.iodp.org/proposals/active-proposals, last access: 14 September 2024) while offering a continental perspective on changes in climate and biodiversity. By using suitable paleoclimatic proxies and/or globally synchronous events (e.g. cosmogenic nuclide peaks related to the geomagnetic field reversal), the tephrochronology from Fucino Basin can eventually also be transferred to the Antarctic ice core records, potentially providing a radioistopically based timescale for investigating the EMPT at this iconic site (e.g. https://www.beyondepica.eu/en/publications/beyond-epica-publications/, last access: 8 August 2024). Finally, the project will offer basic new data on the tectonic evolution of the Apennine, where Fucino represents a pivotal area, being of the largest and most tectonically continuous active Quaternary basins. In order to explore the suitability of the Fucino sedimentary succession for a deep-drilling project in the framework of the ICDP and, thus, to unlock its full potential, an ICDP-supported workshop took place in Gioia dei Marsi (Fig. 3c) on 24–27 October 2023.

2 Current knowledge and potential of the Fucino sedimentary succession

2.1 Geological and climatic setting of the Fucino Basin

The Fucino Basin is a morpho-tectonic extensional basin located in central Italy at ∼ 650 m a.s.l. It is surrounded by Mesozoic to Cenozoic carbonate platform rocks that constitute the highest peaks of the central Apennine (Fig. 2), which hosted mountain glaciers during glacial periods (e.g. Giraudi and Giaccio, 2015). In historical times, the Fucino Basin hosted Lake Fucinus, which covered a surface area of ∼ 150 km^2 until the first partial drainage took place during the 1st–2nd century CE. At the end of the 19th century, the drainage of the basin was completed.

At present, the Fucino Basin is characterized by a Mediterranean climate with warm and dry summers, a mean annual temperature of ∼ 12.5 °C, and an average annual precipitation from 600 to 750 mm in the plains to 900 to 1200 mm in the piedmont zone (e.g. Lionello et al., 2006). From middle spring to early autumn, monthly average temperatures are over 10 °C, peaking in July and August (18 to 21 °C). From early autumn to middle spring, monthly average temperatures are below 10 °C, with January being the coldest month (−5 to −2 °C; e.g. Mannella et al., 2019).

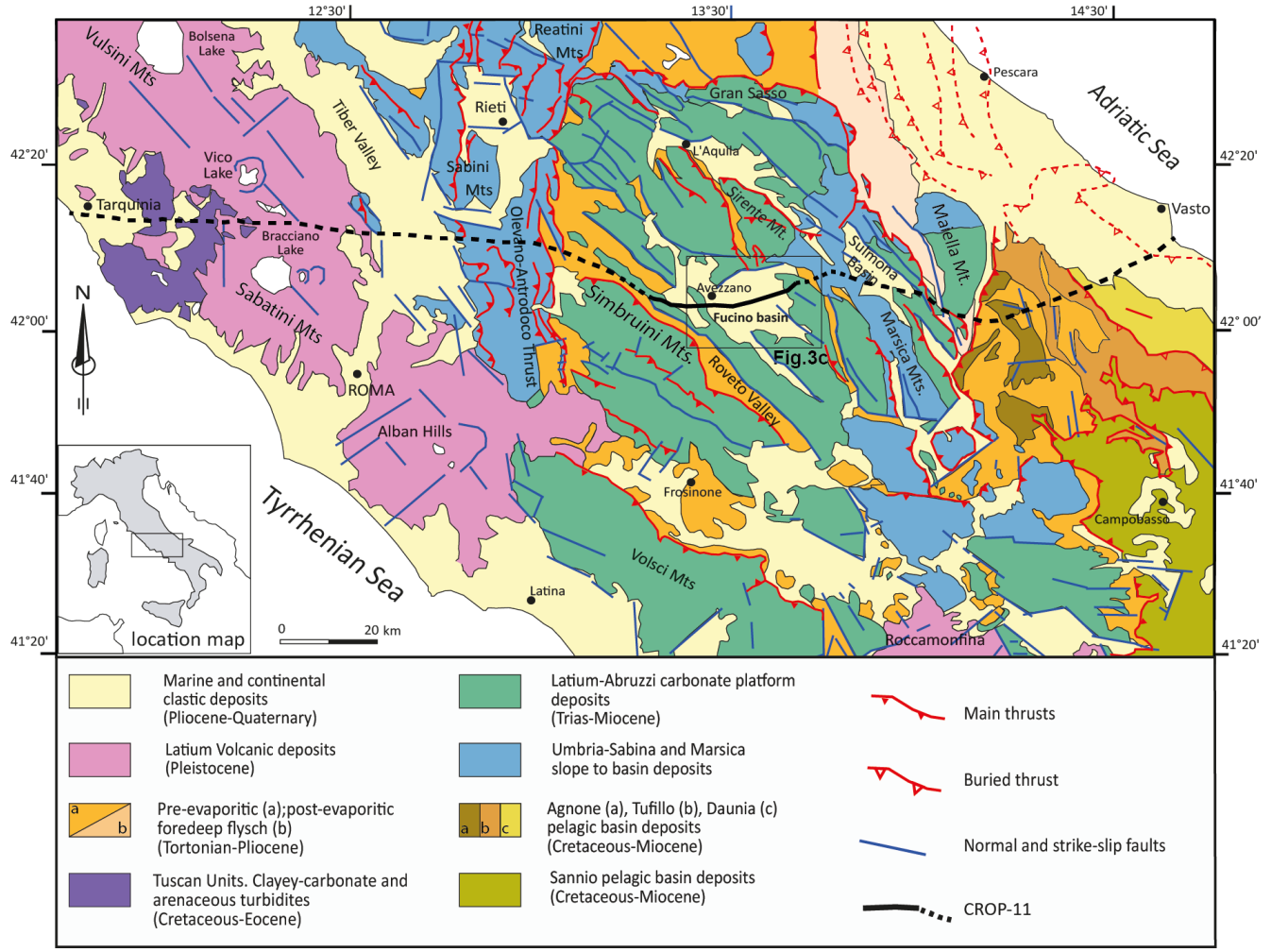

Figure 2. Geological map of central Italy, with the location of the Fucino Basin (from Caielli et al., 2023).

The opening and the Pliocene–Pleistocene evolution of the Fucino Basin were driven by the two main transversal normal fault systems of the Tremonti fault and the San Benedetto-Gioia dei Marsi (SB-GdM) fault system (Fig. 3a; Cavinato et al., 2002). The SB-GdM fault system is composed of three 110–140° N primary segments subtended in relation to their 130–140° N hanging-wall synthetic and antithetic splays (Fig. 3c; Galadini and Galli, 2000). The SB-GdM fault is currently active and was responsible for the most devastating central Italian earthquake that occurred on 13 January 1915 (M_w 7.0, Io 11 MCS grade; ~33 000 fatalities; e.g. Galli et al., 2016).

The subsurface architecture of the Fucino Basin is well defined by 11 commercial and scientific seismic lines that cross the basin, both longitudinally and transversely with respect to the NW–SE trends of the tectonic structures composing the SB-GdM fault (Fig. 3c; Cavinato et al., 2002; Patacca et al., 2008; Patruno and Scisciani, 2021; Mancinelli et al., 2021; Caielli et al., 2023). The seismic lines depict a half-graben geometry with increasing thickness of the Pliocene–Quaternary sedimentary infilling from the west to the east (i.e. toward the SB-GdM) and from the northwestern and southwestern tips of the SB-GdM fault to its central part, which is the depocentre of the basin, located a few kilometres northwest of San Benedetto village (Fig. 3c). Specifically, Cavinato et al. (2002) distinguished four unconformity-bounded seismic facies: Meso-Cenozoic substratum (Seq. 1), Messinian flysch deposits (Seq. 2), Pliocene continental deposits (Seq. 3), and Quaternary continental deposits (Seq. 4), separated by the major unconformities A, B, and C (Fig. 3d). In the depocentre, Seq. 4 forms a well-defined and regularly stratified sedimentary wedge that will be targeted within the MEME deep-drilling project. In particular, the E–W-trending line 1, crossing the depocentre of the basin, shows that no significant tectonic deformations or sedimentary unconformities affect Seq. 4, which, in this sector of the basin, reaches a maximum two-way travel time of ~700 ms, equivalent to a thickness of ~700 m (Cavinato et al., 2002) (Fig. 3d). More

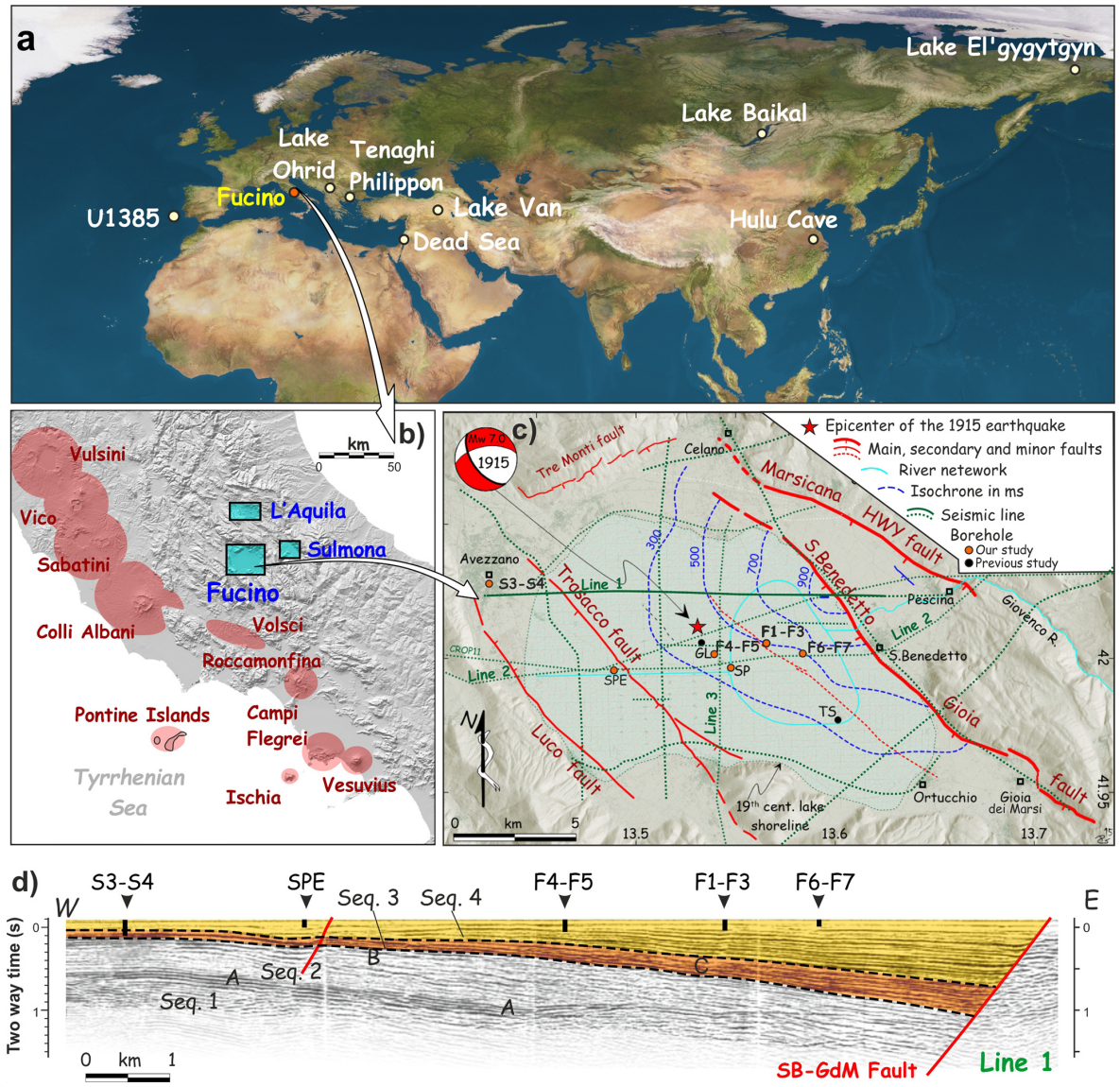

Figure 3. Reference map of the Fucino Plain with a representative seismic line crossing the basin. **(a)** The Fucino Basin in the context of some relevant Northern Hemisphere ICDP and IODP sites and other reference Quaternary paleoclimatic records, including the quoted U1385 core, Lake Ohrid, Tenaghi Philippon, L'Aquila Basin, Sulmona Basin, Lake Baikal, and Lake El'gygytgyn. **(b)** Details of the location of the Fucino Basin relative to the peri-Tyrrhenian volcanic systems of central-southern Italy. **(c)** Fucino Basin with locations of recently investigated sediment cores F1–F3 , F4–F5, F6–F7, SP, SPE, and Avezzano S3–S4 (Giaccio et al., 2015b, 2017, 2019, and unpublished data) and of previously investigated sediment cores. Isochrones of the Plio-Quaternary basin infill, traces of seismic lines (the solid one is that shown in panel **d**), Quaternary master faults responsible for the asymmetrical (half-graben) geometry of the basin, and the epicentre of the last strong earthquake (1915 CE) are also shown. The continuous green line represents the traces of the seismic profiles shown in panel **(c)**. The village of Gioia dei Marsi, where the workshop took place, is located in the southeastern corner. **(d)** Seismic line 1 showing the internal architecture of the Pliocene–Quaternary continental deposits of the Fucino Basin along a W–E profile. The projected locations of the S3–S4, SPE, F3–F4, F1–F3, and F6–F7 boreholes are marked. Seq. 1: Meso-Cenozoic marine carbonate; Seq. 2: Messinian foredeep sediments; Seq. 3: Pliocene lacustrine–fluvial deposits; Seq. 4: Quaternary lacustrine–fluvial deposits A, B, C (main unconformities). This figure and its information were compiled with modifications from Cavinato et al. (2002), Galli et al. (2012), Patacca et al. (2008), Giaccio et al. (2019), and Monaco et al. (2021).

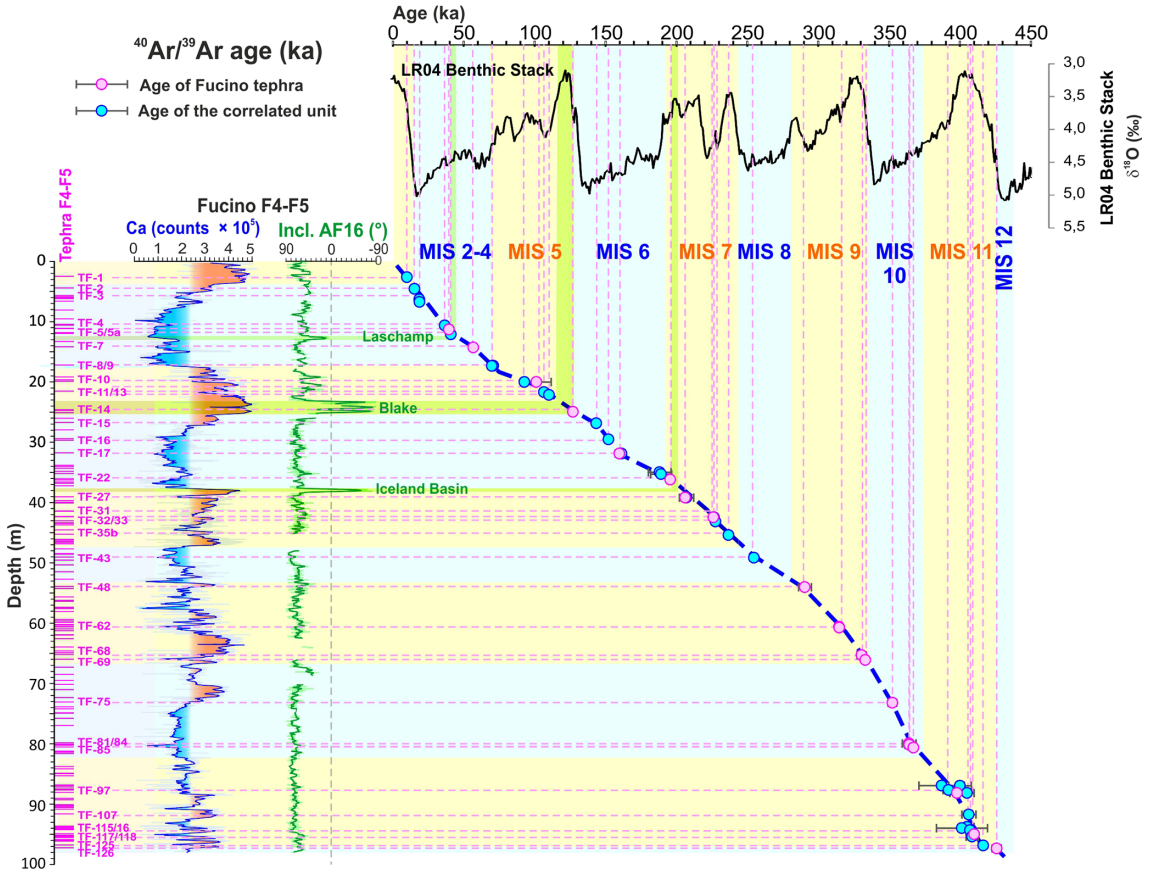

Figure 4. Tephrochronology, selected proxy data, and general chronological framework for the F1–F3 and F4–F5 (see location in Fig. 3c) composite records (from Giaccio et al., 2017, 2019; Mannella et al., 2019; Monaco et al., 2021, 2022; Leicher et al., 2023, 2024) in relation to the LR04 (Lisiecki and Raymo, 2004).

details of the existing high-resolution seismic lines are provided in Sec. 3.2.2. Several holes have been drilled in the Fucino half-graben basin for scientific and geotechnical purposes in the past decades (Fig. 3a). The longest of these boreholes is the 200 m long GeoLazio core (GL in Fig. 3c), for which only sparse geochronological and stratigraphic data exist (e.g. Follieri et al., 1986, 1991; Narcisi, 1994). More recently, four new sediment cores (F1–F3, F4–F5, F6–F7, and Avezzano S3–S4) were retrieved from the Fucino Basin, allowing more detailed insights into the stratigraphic and chronologic framework of its sedimentary infill.

2.2 Results from the deep-drilling pre-siting investigations: F1–F3, F4–F5, and F6–F7 sediment cores

In the framework of an international consortium, a ~ 82 m long sediment succession from the eastern-central area of the Fucino Basin (F1–F3 in Fig. 3c) was recovered in June 2015. The aims of the consortium were as follows: (i) assess the lithology and continuity of the lacustrine sedimentary succession; (ii) document the presence of widespread tephra layers mandatory for regional to extra-regional correlations and their suitability for ^{40}Ar/^{39}Ar dating; (iii) evaluate the mean sedimentation rate and, thus, the potential temporal extent of the Fucino lacustrine succession; and (iv) explore the sensitivity of different paleoclimatic proxies for this site. With the same aims, but on a longer time interval, a second, 98 m long sediment succession was retrieved in 2017 from a different area of the basin within the project FUTURE, funded by the Italian Research Ministry (MUR, PRIN 2017, grant no. 20177TKBXZ_003, coordinator Giovanni Zanchetta). Here, based on seismic line evidence, the sedimentation rate was expected to be lower than at the F1–F3 drill site (Fig. 3c). Collected sediments from both drillings were all fine-grained lacustrine sediments (Giaccio et al., 2017, 2019).

Multi-proxy investigations, including tephrochronology (geochemical analyses and ^{40}Ar/^{39}Ar dating); paleomagnetic analyses; scanning XRF (X-ray fluorescence) element geochemistry; $CaCO_3$ content analyses; carbon, nitrogen, and sulfur (CNS) analyses; $\delta^{18}O_{calcite}$ analyses; and pollen analyses, have been carried out and are ongoing on both sediment successions. Tephrochronological results, based on ^{40}Ar/^{39}Ar dating of K-rich crystals extracted from Fucino

tephras and robust geochemical correlation with the well-dated proximal counterparts, indicate that the F1–F3 and F4–F5 successions span the last ∼ 190 and ∼ 430 kyr, respectively. Mean sedimentation rates are on the order of ∼ 0.43 mm yr^{-1} for F1–F3 and ∼ 0.23 mm yr^{-1} for F4–F5 (Giaccio et al., 2017, 2019). Detailed information on MIS 12-11, MIS 10-9, MIS 8-7, and MIS 7-1 tephrostratigraphy is reported by Monaco et al. (2021), Leicher et al. (2023, 2024), Monaco et al. (2022), and Giaccio et al. (2017). Overall, ∼ 130 tephra layers have been detected for both successions, 40 of which were either directly dated or correlated to their respective proximal, dated units, resulting in the richest and most intensely dated Middle–Upper Pleistocene Mediterranean tephra record (Fig. 4). Preliminary paleomagnetic data documented Laschamp, Blake, and Iceland basin geomagnetic excursions (Giaccio et al., 2019, Fig. 4). Published proxy data, e.g. scanning XRF element geochemistry and CNS data, show the high sensitivity of the Fucino sediment in providing high-resolution paleoenvironmental records as a regional expression of the orbital- and millennial- to centennial-scale climate variability (Mannella et al., 2019; Monaco et al., 2022). Ongoing pollen analyses of the interglacials documented in the Fucino succession, carried out as part of PhD projects at La Sapienza Università di Roma (MIS 12-11c, Vera-Polo et al., 2024) and the University College of London (MIS 5e-MIS 1) and as part of the NERC project VARING (Polychronis C. Tzedakis, coordinator) (MIS 9e and MIS 7e-a), reveal a close correspondence with climate changes recorded in deep-sea cores from the Iberian Margin (e.g. see Tzedakis et al., 2018).

In early 2022, two additional overlapping and ca. 33 m long cores (F6–F7) were retrieved to the east of the F1–F3 drilling site, where a higher sedimentation rate was expected. Preliminary results of the ongoing investigation confirmed that the depths of some marker tephras recognized in cores F6–F7 are deposited 2 times and 4 times deeper than the equivalent layers recognized in F1–F3 and F4–F5, respectively.

Overall, the results of the multi-proxy investigation on the F1–F3 and F4–F5 sediment successions confirm the great potential of the Fucino succession in providing us with detailed proxy records of the last 430 kyr supported by a robust chronology based on high-precision $^{40}Ar/^{39}Ar$ dating, which enables an exploration of the role of climate drivers, avoiding any circularity that may arise from astronomical tuning. Moreover, the independent Fucino chronology can eventually be transferred to sediment sequences from the Iberian Margin on the basis of paleoclimatic alignments using homologue terrestrial proxies (e.g. pollen), documenting the vegetation response to abrupt climate change (see, for example, Tzedakis et al., 2018; Regattieri et al., 2019; Bajo et al., 2020).

3 The MEME workshop

3.1 Participants and motivation

The MEME workshop was attended by 42 scientists (Fig. 5) from 14 countries and 32 institutions, as summarized in Table 1.

The main aims of the MEME workshop were as follows:

i. evaluate the existing seismic data and discuss the potential to extend the seismic information with new profiles to better define the basin architecture, ensuring the feasibility of an ICDP drilling project;

ii. discuss the existing stratigraphic, dating, and paleoclimatic–environmental data of the Fucino sediment succession and their potential for reaching the aims of the MEME project;

iii. based on (i) and (ii), determine overarching scientific objectives and establish and plan for further investigations in preparation for a full ICDP drilling proposal;

iv. discuss drilling logistics and cost estimates mandatory for the full proposal;

v. based on (ii), identify scientific aspects not yet covered by the current team and propose invitations to additional selected experts;

vi. establish a well-coordinated interdisciplinary ICDP research group.

3.2 Programme and discussion

3.2.1 Sessions 1 and 2: state of the art

During the afternoon of 24 October, the research teams involved in past and ongoing studies on the Fucino Basin provided short presentations about the current results and methods relevant to a potential deep-drilling campaign. These included (i) a summary of the state of the art with regard to previous and ongoing investigations in the Fucino Basin (Biagio Giaccio); (ii) a general overview on the Italian Pliocene–Quaternary volcanism in the framework of the complex Mediterranean geodynamic setting (Sandro Conticelli); (iii) a discussion regarding the tectonic architecture of the sedimentary infill of the Fucino Basin (Gian Paolo Cavinato); and (iv) a general overview of the FUTURE (FUcino uniTes QUaternary REcords) project (Giovanni Zanchetta), including the main results of $^{40}Ar/^{39}Ar$ geochronology (Sebastien Nomade), tephrostratigraphy (Niklas Leicher), pollen (Chronis Tzedakis, Alessia Masi), and mitochondrial DNA and lipid (Cindy De Jonge) investigations performed during the project.

Finally, Fabio Florindo and Adele Bertini presented the unpublished lithostratigraphical, $^{40}Ar/^{39}Ar$, paleomagnetic, and pollen data from the Avezzano S3–S4 sediment core,

Table 1. Participants of the MEME ICDP workshop.

ICDP-supported	Affiliation	Country
Adele Bertini	University of Florence	Italy
Gian Paolo Cavinato	National Research Council	
Giulia Cheli	University of Pisa	
Fabio Florindo	Istituto Nazionale di Geofisica e Vulcanologia	
Biagio Giaccio	National Research Council	
Luigi Improta	Istituto Nazionale di Geofisica e Vulcanologia	
Alessia Masi	Sapienza University of Rome	
Eleonora Regattieri	National Research Council	
Laura Sadori	Sapienza University of Rome	
Giovanni Zanchetta	University of Pisa	
Christine Heim*	University of Cologne	Germany
Niklas Leicher	University of Cologne	
Mathias Vinnepand	Leibniz Institute for Applied Geophysics	
Bernd Wagner	University of Cologne	
Leon Clarke	Manchester Metropolitan University	UK
Alice Paine	Oxford University	
Helen Roberts	Aberystwyth University	
Chronis Tzedakis	University College London	
Dustin White	University of York	
Paul Albert	Swansea University	
Alison Pereira*	Paris-Saclay University	France
Sebastien Nomade	CEA-CNRS-UVSQ	
Cindy De Jonge	ETH Zurich	Switzerland
Camille Thomas	University of Bern	
Marta Marchegiano	University of Granada	Spain
Jose Eugenio Ortiz Menendez	Universidad Politécnica de Madrid	
Sofia Pechlivanidou	University of Bergen	Norway
Grisha Fedorov	National Academy of Sciences of the Republic of Armenia	Armenia
Ivan Razum	Croatian Natural History Museum	Croatia
Vitor Azevedo	Trinity College Dublin	Ireland
Julieta Massaferro	National Scientific and Technical Research Council	Argentina
Alexander Franke*	University of Adelaide	Australia
Martin Danisik	Curtin University	
Anders Noren	University of Minnesota	USA
Elizabeth Niespolo*	Princeton University	
Deniz Cukur	Korea Institute of Geoscience and Mineral Resources	South Korea
Other participants		
Paolo Boncio	University “G. D’Annunzio” of Chieti–Pescara	Italy
Edi Chiarini	Istituto Superiore per la Protezione e Ricerca Ambientale	
Angelo Cipriani	Istituto Superiore per la Protezione e Ricerca Ambientale	
Sandro Conticelli	University of Florence – National Research Council	
Roberto De Franco	National Research Council	
Roberto Martini	Private company – Drilling engineering design	

* Unable to attend, contribution presented by colleagues.

Figure 5. MEME workshop participants at the panoramic-view stop during the short field trip on 26 October. The Fucino paleolake basin can be seen in the background. All participants gave their consent for the publication of the group photo.

continuously cored until a depth of ∼ 185 m and discontinuously reaching ∼ 270 m. This core was recovered from the western margin of the basin in 2019 as part of a project concerning seismic microzonation led by the University of Chieti–Pescara (Paolo Boncio coordinator) (for location, see Fig. 3). These preliminary data consistently provided evidence for a very long, though discontinuous, terrestrial record, likely extending back to ∼ 3.0–3.5 Ma.

3.2.2 Combining geophysical, stratigraphic, and chronological information to estimate the integrity and temporal extent of the Plio-Quaternary lacustrine succession

The interpretation of the available seismic reflection profile across the Fucino Basin allowed us to highlight a wedge-shaped basin fill architecture and stratigraphy. The best image of the wedge-shaped architecture of the Fucino Pliocene–Quaternary continental infill is shown in a high-resolution E–W seismic line (line 1, Figs. 3d, 5). Line 1 highlights the Pliocene–Quaternary growth geometry of the strata characterized by continuous eastward-divergent reflectors across the SB-GdM fault plane, indicating a Pliocene–Quaternary sedimentary accumulation in a fault-controlled basin (Fig. 6). In the eastern part of seismic line 1, the total thickness of Pliocene–Quaternary deposits along the hanging wall of the SB-GdM fault can be estimated to be 0.9–1.0 s two-way time (TWT), corresponding to ∼ 900–1000 m sediment thickness (Fig. 6).

According to the seismic stratigraphy and tectonic setting of the basin, the tectonic subsidence has been very low at the Avezzano drilling site. Specifically, seismic line 1 reveals that the town of Avezzano coincides with the thinner part of the sedimentary wedge that characterizes the architecture of the Fucino sedimentary infilling (Fig. 6). The Avezzano S3–S4 drilling site is, in fact, far from the Tremonti and SB-GdM fault systems (Fig. 6), which were and are responsible, at different times and in different ways, for the opening and evolution of the Fucino Basin (Cavinato et al., 2002), thus resulting in limited accommodation space and highly condensed, as well as possibly discontinuous, sedimentary succession. In agreement with this tectonic–sedimentary framework, the tephrochronological, paleomagnetic, and pollen evidence indicates that the 270 m long Avezzano sediment core could span the last 3.5 Myr, with a resulting mean sedimentation rate of 0.08 mm yr^{-1}, i.e. a rate much lower than the accumulation rates in the cores drilled closer to the SB-GdM fault (Fig. 6).

While the Avezzano core has provided an opportunity to explore the temporal extent of the Fucino sediment succession within a short stratigraphic interval, confirming the extraordinarily long history of sediment accumulation in the basin, its marginal setting and lithology, also including intervals of relatively coarse sediments, contradict a complete and continuous sediment succession that is stratigraphically and lithologically suitable for high-resolution investigation. Nevertheless, the Avezzano S3–S4 sediment core can be used to calibrate seismic line 1 by translating the chronological information from this succession towards the depocentre (Fig. 6). Accordingly, at the sites F6–F7, F4–5, and F1–F3, the same stratigraphic time interval recorded in the Avezzano S3–S4 core should be represented by ∼ 800, ∼ 700 and ∼ 500 m thick successions, respectively, reaching ∼ 1000 m or more in the depocentre (SRmax. in Fig. 6). Therefore, at these sites, the Plio-Quaternary sedimentary successions should be more expanded (up to 1 order of magnitude), more highly re-

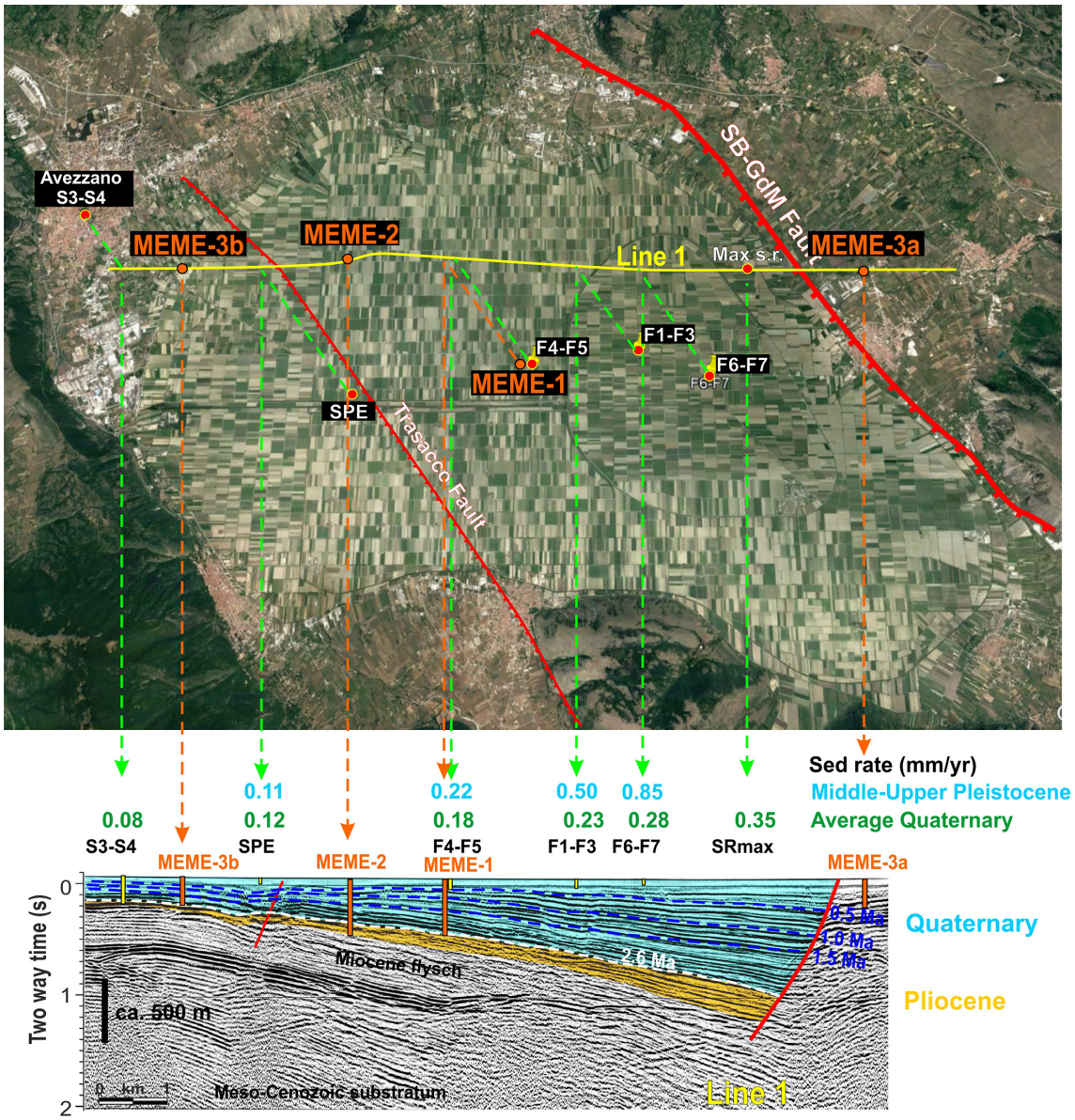

Figure 6. Aerial view of the Fucino Basin (© Google Maps), with the locations of the investigated Fucino sediment cores F1–F3, F4–F5, F6–F7, SPE, and S3–S4 (Giaccio et al., 2015b, 2017, 2019, author's unpublished data) and stratigraphical–chronological calibration of the seismic line 1 using the constraints provided by the Avezzano S3–S4 core.

solved, and characterized by finer sediments with respect to the Avezzano S3–S4 core. Thus, it should be ideally suited to recovering a complete succession for detailed and high-resolution multi-proxy investigations.

3.2.3 Concluding remarks for sessions 1 and 2

In summary, the evidence presented in sessions 1 and 2 shows that the Fucino Basin fulfils all the main requisites for achieving the aims of the MEME project to improve our understanding of the mode and tempo of the Plio-Quaternary climatic–environmental evolution at different spatial and temporal scales. This evidence includes the following:

1. long and continuous sedimentation of fine lacustrine sediments since at least 3.5 Ma;

2. high sensitivity of the paleo-environmental–paleoclimatic multi-proxies, with regional and extra-regional relevance;

3. an independent, high-resolution timescale based on tephrochronology.

3.3 Session 3: participant self-presentation

A total of 20 contributions were presented during session 3, with topics ranging from geophysical exploration, drilling operations, and geochronological methods to physical and bio-geochemical proxies (Table 2).

3.4 Field trip

On the morning of 26 October, a short field trip headed by Paolo Boncio and Gian Paolo Cavinato took place. During the field trip, the main morpho-tectonic features of the eastern side of the Fucino Basin (Fig. 6), some outcrops of the SB-GdM fault system affecting recent deposits, and the co-seismic fault scarp related to the 1915 earthquake were shown.

3.5 General discussion

Based on current insights into the subsurface of the Fucino paleolake and the paleo-environmental information recorded, the general discussion included the following topics:

1. overarching scientific and societal objectives of the MEME project;
2. location, depth(s) of the borehole(s), and technical and management aspects, reflecting the constraints of scientific and societal needs;
3. involvement of the public and private companies;
4. matching funds and compositions of the Co-PI and Co-I teams.

3.5.1 Objectives

Recovering and investigating a long continuous succession from Fucino Basin will provide unprecedented insights into the evolution of the Earth system during the Pliocene–Quaternary, i.e. the last 3.0–3.5 Myr.

Our proposed multi-method dating approach, including direct $^{40}Ar/^{39}Ar$, tephrochronology, zircon double-dating, luminescence and amino acids, and a multi-proxy analysis of sediment physical and bio-geochemical properties, has the potential to provide a detailed radiometric chronology for reconstructing the timing and dynamics of the Pliocene–Quaternary geo-bio-environmental and climatic processes independently of any a priori assumptions regarding response times to climate forcing and feedbacks. By studying the interaction between climate and environmental changes, these insights will allow a better understanding of the impact of ongoing and future climatic–environmental changes in the highly populated Mediterranean area. Eventually, the Fucino record will be linked to reference marine records by constructing a tephro-stratigraphic and pollen stratigraphic lattice.

The specific objectives of the deep drilling into the Fucino Basin are outlined below.

A. Stratigraphy, paleoclimate, and biodiversity

A1. Event stratigraphy

We assemble a regional to global stratigraphic reference record deep into the Pliocene, including and combining a unique time series of orbital- to millennial-scale climate events and cycles and tephrostratigraphic and magnetostratigraphic cosmogenic nuclide events.

A2. Sequence, timing, duration, and dynamics of Pliocene–Quaternary climatic events

i. We reconstruct climate conditions during the warm Pliocene and during the transition to the colder Pleistocene.

ii. We evaluate the timing and differences of the terminations of glacial periods;

iii. We assess interglacial structures, namely their internal variability, initiation, development, and demise.

iv. We constrain hydrological changes in the central Mediterranean at times of sapropel formation, specifically their links to low- and high-latitudes climate.

v. We explore millennial-scale variability during glacial times within the central Mediterranean.

vi. We evaluate the longitudinal influence of changes in North Atlantic circulation patterns by means a west–east transect including the records of U1385; Fucino; Lake Ohrid; Tenaghi Philippon; and, potentially, other records across the Eurasian continent, including the Lake Baikal record.

A3. Changes in terrestrial ecosystems and biodiversity across main climatic transitions and events since the late Pliocene

i. We reconstruct the response of Mediterranean environments and biomes to global changes during the warm Pliocene, including the mPWP; the progressive expansion of the Northern Hemisphere ice sheets during the Plio-Pleistocene transition; and the change in periodicity, magnitude, and shape (symmetrical vs. asymmetrical) of the glacial–interglacial cycles during the EMPT and after the Mid-Brunhes Event.

ii. We establish the timing and causes of the progressive extinction of forest species in the Mediterranean.

iii. We consider the intra-lacustrine diversity dynamics of different biological groups through time.

Table 2. List of the participant presentations in session 3.

Name	Presentation title
Luigi Improta	A new high-resolution seismic reflection experiment in the Fucino Basin acquisition geometry and data quality
Sofia Pechlivanidou	From surface processes modeling to high-resolution drilling record resolving key controls on sediment production and stratigraphic development in active rifts
Deniz Cukur	Geophysics
Anders Noren	Drilling operations
Elizabeth Niespolo[1]	$^{40}Ar/^{39}Ar$ geochronology
Paul Albert	Tephra (cryptotephra) studies
Vitor Azevedo	Tephrochronology – machine learning models
Ivan Razum	Statistical treatment of tephra data
Martin Danisik	Zircon double-dating applied to tephras
Helen Roberts	Luminescence dating of calcite
Dustin White	Malacology and amino acid dating
Alice Pine	New geochemical proxies
Alexander Franke[2]	Novel (trace metal) isotope methods to infer Quaternary environmental change
Leoan Clarke	Bio-geochemistry
Eleonora Regattieri	Stable isotope and other geochemical proxies
Marta Marchegiano	Carbonate clumped isotope ($\Delta 47$) paleothermometry
Jose E. Ortiz Menendez	Organic molecules, amino acid geochronology, and lipid biomarkers
Grisha Fedorov	Sedimentology
Mathias Vinnepand	Sediment physical properties
Julieta Massaferro	Paleoecology, insects

[1] Not attending, presented by Biagio Giaccio. [2] Not attending, presented by Bernd Wagner.

iv. We generate a reference site of a vegetation-based record to assess the paleo-environmental background for early hominin migration and occupation in western Eurasia.

B. Geodynamics

B1. Volcanology and magmatic evolution

i. We reconstruct the history and recurrence time of explosive volcanism in the peri-Tyrrhenian region.

ii. We define the chronology and timing of the transition between the calc-alkaline and ultra-potassic (late Pliocene–earliest Pleistocene) peri-Tyrrhenian volcanism.

iii. We explore the possible relation between glacio-eustatic sea level change and explosive peri-Tyrrhenian volcanism.

iv. We evaluate the evolutionary petrological processes as related to the mantle–crust magma source dynamics.

v. We assess the impact of the large explosive eruptions on local- and regional-scale ecosystems.

B2. Tectonics

i. We consider the tempo and dynamics of the opening and development of the Fucino Basin in relation to the surrounding fault systems in the framework of the Mediterranean geodynamic field.

ii. We conduct an assessment of seismic hazards in relation to seismic amplification phenomena.

3.5.2 Location and depth of drilling(s) and technical and management aspects

Parallel drilling is needed and envisaged to obtain a continuous sediment succession. Drilling in the area of the maximum sedimentation rate would be the best location to obtain a full, expanded (∼ 1000 m deep drill hole; SRmax in Fig. 6), and continuous succession of the Fucino lacustrine infill, providing the ideal setting for very high-resolution investigations. Despite these eligible conditions, this option was noted to be challenging to the drilling engineers because of the necessary casing strings, the mud composition for pressure control, the borehole stability, and the management of swelling clays. Altogether, much higher costs and risks are associated with this approach. However, the basin fill architecture (Figs. 3d and 6) offers an alternative option with multiple shallower drill holes drilled along an east–west transect, each of which recovers a section of the basin fill.

In order to overcome drilling-related risks and to provide a cost-efficient drilling operation, the participants discussed three drilling sites with different targets and maximum drill depths of < 500 m. The first selected drilling site, MEME-1, is in the central part of the basin, not far from F4–F5 site. Here, according to the seismic reflection data, the base of the lacustrine succession should be around 500 m depth (Fig. 6).

The second site, MEME-2, is further to the west, where sedimentation rates are lower (Fig. 6). Here, a drilling of ∼ 500 m would allow us to recover almost the entire sediment succession down to the bedrock and to provide the full Pliocene–Quaternary history of the Fucino Basin, although this would be at a lower resolution compared to MEME-1. A further site was considered for tectonic purposes. It could be shallower (200–300 m) and located on the footwall of the SB-GdM fault system, where relatively low sedimentation rates are expected (MEME-3a; Fig. 6).

Depending on the outcomes of MEME-1 and MEME-2, as a contingency plan, the third shallower drilling could be also placed further toward the MEME-2 site, where, according to seismic data, the whole Quaternary or Pliocene–Quaternary succession should be recovered in 200–300 m (MEME-3b, Fig. 6). This option is relevant in terms of the strategy and success of the MEME project as, in case of technical problems at MEME-1 and MEME-2, MEME-3b would warrant recovering the whole lacustrine succession and would thus reach the target of the MEME project, although this would be with a shorter sediment core, which, theoretically, is technically easier to recover.

Based on the experience from past drilling campaigns in the Fucino Basin, the optimal approach will include the use of soft-sediment coring tools deployed in numerous ICDP lake-drilling campaigns for the upper ∼ 200 m at each site, with standard industry tools used for the remainder of each profile. Budget estimates produced by local drilling contractors provide the basis for this plan, with additional costs to be added for soft sediment coring.

3.5.3 Societal, economic, and industrial aims

Scientific deep drilling has not only scientific and economic relevance but also a great educational potential.

A local professional photographer and videographer participated in the workshop to discuss the best strategies for engaging the local community and identifying effective communication channels for spreading the news. Workshop participants were interviewed to create a video explaining the importance of the Fucino Basin and the MEME research project in layperson's terms, which was then sent to the local press; uploaded to YouTube; and shared on social media platforms such as X, Instagram, and Facebook. A short report of the workshop, including the future research plan, was shared with the Italian National Research Center that published it on their website.

In the future, we plan to involve both the local community and the general public in our research. This will be done at different levels. For the local community, preliminary meetings will be planned in cooperation with local authorities and organizations to illustrate the aims and the methods of the research.

During the drilling operation, visits to the drilling site will be organized for local schools and committees. To involve the general public, we also plan to have a media release for every step of the project, both through local and national press avenues and through the use of social networks. In addition, as many of the PIs are enrolled in universities, specific field trips and training involving university students from bachelor level to PhD level will be planned prior to, during, and after the drilling.

MEME drilling will also give the opportunity to measure the local geothermal gradient and to evaluate the potential for low-enthalpy geothermal resources, eventually with the use of the holes for pivotal heat exchanger systems. Moreover, after drilling, the borehole(s) will be equipped with specific probes to measure geochemical parameters such as conductivity, pH, Eh, dissolved CO_2, and temperature in addition to facilitating water sampling. These geochemical parameters may indeed constitute indicators of seismic cycles or even earthquake precursors (Skelton et al., 2014).

3.5.4 Time frame, Co-PI and Co-I team, and matching funds

The workshop included small-group and whole-group discussions regarding potential sources of funding available to supplement the costs of scientific drilling and also of funding to support post-drilling science. The steps and timeline involved in preparing a full proposal for submission to the ICDP for deep drilling in the Fucino paleolake were considered. In order to develop a well-coordinated research programme and to prepare an ICDP full proposal, the participants committed themselves to providing all the information required to support more detailed project planning, includ-

ing (i) a detailed budget plan; (ii) a detailed operations plan, including a permission plan with a list of authorities to be contacted; (iii) a project management plan; (iv) a plan for data and sample management and long-term core curation; and (v) an education and outreach plan.

The constitution of the Co-PI and Co-I teams was discussed with regard to the proposers of the workshop, as well as with the participants as a whole, considering the contributions and the interests of the workshop participants. All participants agreed on modifications to the PI- and Co-PI teams to meet the ICDP balance requirements and to support equality, diversity, and inclusion (e.g. gender, age, nationality, expertise).

4 Concluding remarks

The ICDP-supported MEME workshop provided the opportunity to enlarge the spectrum of expertise, opening new research perspectives for the geophysical exploration needed for the drilling site location and for the development of a multi-method and independent chronology, consisting of $^{40}Ar/^{39}Ar$; tephrostratigraphy; paleomagnetism; U series; luminescence and amino acid dating methods; and multi-proxy records, such as sediment physical properties, stable isotopes, clumped isotopes, inorganic and organic biogeochemistry, pollen, and insects. As a matter of fact, the Fucino sedimentary archive brought into focus the broad interests expressed by participants, who enthusiastically expressed their commitment to continue collaborating, either as Co-PIs or Co-Is or as external collaborators. Therefore, the next steps will be the constitution of the Co-PI and Co-I teams together with collecting the data and information needed for the writing of a full MEME proposal.

Data availability. No data sets were used in this article.

Team list. Vitor Azevedo (Trinity College Dublin, Dublin, Ireland), Leoan Clarke (Manchester Metropolitan University, Manchester, UK), Giulia Cheli (University of Pisa, Pisa, Italy), Edi Chiarini (Istituto Superiore per la Protezione e Ricerca Ambientale, Rome, Italy), Angelo Cipriani (Istituto Superiore per la Protezione e Ricerca Ambientale, Rome, Italy), Sandro Conticelli (University of Florence – National Research Council, Florence–Rome, Italy), Deniz Cukur (Korea Institute of Geoscience and Mineral Resources, Daejeon, South Korea), Grisha Fedorov (National Academy of Sciences of the Republic of Armenia, Yerevan, Armenia), Luigi Improta (Istituto Nazionale di Geofisica e Vulcanologia, Rome, Italy), Niklas Leicher (University of Cologne, Cologne, Germany), Martin Danisik (Curtin University, Perth, Australia), Julieta Massaferro (National Scientific and Technical Research Council, Bariloche, Argentina), Elizabeth Niespolo (Princeton University, Princeton, New Jersey, USA), Jose E. Ortiz Menendez (Universidad Politécnica de Madrid, Madrid, Spain), Alice Paine (University of Oxford, Oxford, UK), Sofia Pechlivanidou (University of Bergen, Bergen, Norway), Ivan Razum (Croatian Natural History Museum, Zagreb, Croatia), Eleonora Regattieri (IGG-National Research Council, Pisa, Italy), Camille Thomas (University of Bern, Bern, Switzerland), Mathias Vinnepand (Leibniz Institute for Applied Geophysics, Leibniz, Germany), Dustin White (University of York, York, UK)

Author contributions. Conceptualization: BG, BW, GZ, LS, and PCT. Methodology, validation, formal analysis, investigation, data curation, and writing (original draft preparation): BG, BW, GZ, AB, GPC, RdF, FF, SN, AP, LS, SS, and PCT. Writing (review and editing) and visualization: BG, BW, GZ, AB, GPC, RdF, FF, DAH, TAN, SN, AP, LS, SS, PCT, PA, PB, CDJ, AF, CH, AM, MM, HMR, and AN. All the authors have read and agreed to the published version of the paper. In addition to the named co-authors of this paper, the MEME team includes all the people mentioned in the Team list, whose participation in the workshop contributed to the generation of ideas presented in this report.

Competing interests. The contact author has declared that none of the authors has any competing interests.

Disclaimer. Publisher's note: Copernicus Publications remains neutral with regard to jurisdictional claims made in the text, published maps, institutional affiliations, or any other geographical representation in this paper. While Copernicus Publications makes every effort to include appropriate place names, the final responsibility lies with the authors.

Acknowledgements. We thank Ulrich Harms, Head of the Operational Support Group (OGS) of the ICDP, for his precious suggestions and support to the organization and management of the workshop. Bernd Zolitschka and an anonymous reviewer provided useful comments and suggestions that improved this report.

Review statement. This paper was edited by Hendrik Vogel and reviewed by Bernd Zolitschka and one anonymous referee.

References

Allan, R. P., Hawkins, E. , Bellouin, N. and Collins, B. IPCC: Summary for Policymakers, in: Climate Change: The Physical Science Basis, Contribution of Working Group I to the Sixth Assessment Report of the Intergovernmental Panel on Climate Change, edited by: Masson-Delmotte, V., Zhai, P., Pirani, A., Connors, S. L., Péan, C., Berger, S., Caud, N., Chen, Y., Goldfarb, L., Gomis, M. I., Huang, M., Leitzell, K., Lonnoy, E., Matthews, J. B. R., Maycock, T. K., Waterfield, T., Yelekçi, O., Yu, R., and Zhou, B., Cambridge University Press, 3–32, ISBN 978-92-9169-163-0, 2021.

Bajo, P., Drysdale, R. N., Woodhead, J. D., Hellstrom, J. C., Hodell, D., Ferretti, P., Voelker, A. H. L., Zanchetta, G., Rodrigues, T., Wolff, E., Tyler, J., Frisia, S.,and Spötl, C., and Fallick, A. E.:

Persistent influence of obliquity onice age terminations since the Middle Pleistocene transition, Science, 367, 1235–1239, 2020.

Barker, S., Knorr, G., Edwards, R. L., Parrenin, F., Putnam, A. E., Skinner, L. C., Wolff, E., and Ziegler, M.: 800,000 years of abrupt climate variability, Science, 334, 347–351, 2011.

Berends, C. J., Kohler, P., Lourens, L. J., and van de Wal, R. S. W.: On the cause of the mid-Pleistocene transition, Rev. Geophys., 59, e2020RG000727, https://doi.org/10.1029/2020RG000727, 2021.

Bertini, A., Arcangeli, P., Bragagni, A., Casalini M., Cifelli, F., Conte, A. M., Conticelli, S., Cosentino, D., Deino, Alan, Di Salvo, S., Giaccio, B., Gliozzi, E., Huang, H., Iorio, M., Marchegiano, M., Mattei, M., Mondati, G., Nocentini, M., Petrelli, M., Regattieri, E., Sagnotti, L., Spadi, M., Tallini, M., and Zanchetta, G.: Before the Early Middle Pleistocene Transition: insights on the environmental variability and explosive activity in central Italy during the 1.5-2.1 Ma interval from the L'Aquila Basin lacustrine record, in: INQUA 2023, 14–20 July 2023, Sapienza University of Rome, Italy, Abstract, 16, Session 3, 2023.

Burke, K. D., Williams, J. W., Chandler, M. A., Haywood, A. M., Lunt, D. J., and Otto-Bliesner, B. L.: Pliocene and Eocene provide best analogs for near-future climates, P. Natl. Acad. Sci. USA, 115, 13288–13293, 2018.

Caielli, G., Maffucci, R., De Franco, R., Bigi, S., Parotto, M., Mollica, R., Gaudiosi, I., Simionato, M., Romanelli, M., De Marchi, N., and Cavinato, G. P.: Fucino basin structure revealed by the tomography and the reusing of the CROP11 seismic data, Tectonophysics, 865, 230043, https://doi.org/10.1016/j.tecto.2023.230043, 2023.

Cavinato, G. P., Carusi, C., Dall'Asta, M., Miccadei, E., and Piacentini, T.: Sedimentary and tectonic evolution of Plio–Pleistocene alluvial and lacustrine deposits of Fucino Basin (central Italy), Sediment. Geol., 148, 29–59, 2002.

Clark, P. U., Shakun, J. D., Rosenthal, Y., Köhler, P., and Bartlein, P. J.: Global and regional temperature change over the past 4.5 million years, Science, 383, 884–890, 2024.

Conte, A. M., Perinelli, C., Bianchini, G., Natali, C., Martorelli, E., and Chiocci, F. L.: New insights on the petrology of submarine volcanics from the Western Pontine Archipelago (Tyrrhenian Sea, Italy), J. Volcanol. Geoth. Res., 327, 223–239, 2016.

de la Vega, E., Chalk, T. B., Wilson, P. A., Bysani, R. P., and Foster, G. L.: Atmospheric CO_2 during the Mid-Piacenzian Warm Period and the M2 glaciation, Scientific Reports, 10, 11002, https://doi.org/10.1038/s41598-020-67154-8, 2020.

Donders, T., Panagiotopoulos, K., Koutsodendris, A., Bertini, A., Mercuri, A. M., Masi, A., Combourieu-Nebout, N., Joannin, S., Kouli, K., Kousis, I., Peyron, O., Torri, P., Florenzano, A., Francke, A., Wagner, B., and Sadori, L.: 1.36 million years of Mediterranean forest refugium dynamics in response to glacialinterglacial cycle strength, P. Natl. Acad. Sci. USA, 118, e2026111118, https://doi.org/10.1073/pnas.2026111118, 2021.

Filippelli, G. M. and Flores, J. A.: From the warm Pliocene to the cold Pleistocene: A tale of two oceans, Geology, 37, 959–960, 2009.

Galadini, F. and Galli, P.: Active tectonics in the central Apennines (Italy) – input data for seismic hazard assessment, Nat. Hazards, 22, 225–270, 2000.

Galadini, F., Messina, P., and Giaccio, B., Sposato, A.:Early uplift history of the Abruzzi Apennines (central Italy): Available geomorphological constraints, Quatern. Int., 101–102, 125–135, 2003.

Galli, P., Messina, P., Giaccio, B., Peronace, E., and Quadrio, B.: Early Pleistocene to Late Holocene activity of the Magnola Fault (Fucino Fault System, central Italy), B. Geofis. Teor. Appl., 53, 435–458, 2012.

Galli, P., Giaccio, B., Messina, P., and Peronace, E.: Three magnitude 7 earthquakes on a single fault in central Italy in 1400 years, evidenced by new palaeoseismic results, Terra Nova, 28, 146–154, 2016.

Giaccio, B., Regattieri, E., Zanchetta, G., Nomade, S., Renne, P. R., Sprain, C. J., Drysdale, R. N., Tzedakis, P. C., Messina, P., Scardia, G., Sposato, A., and Bassinot, F.; Duration and dynamics of the best orbital analogue to the present interglacial, Geology, 43, 603–606, 2015a.

Giaccio, B., Regattieri, E., Zanchetta, G., Wagner, B., Galli, P., Mannella, G., Niespolo, E., Peronace, E., Renne, P. R., Nomade, S., Cavinato, G. P., Messina, P., Sposato, A., Boschi, C., Florindo, F., Marra, F., and Sadori, L.: A key continental archive for the last 2 Ma of climatic history of the central Mediterranean region: A pilot drilling in the Fucino Basin, central Italy, Sci. Dril., 20, 13–19, https://doi.org/10.5194/sd-20-13-2015, 2015b.

Giaccio, B., Niespolo, E. M., Pereira, A., Nomade, S., Renne, P. R., Albert, P. G., Arienzo, I., Regattieri, E., Wagner, B., Zanchetta, G., Gaeta, M., Galli, P., Mannella, G., Peronace, E., Sottili, G., Florindo, F., Leicher, N., Marra, F., and Tomlinson, E. L.: First integrated tephrochronological record for the last ∼190 kyr from the Fucino Quaternary lacustrine succession, central Italy, Quaternary Sci. Rev., 158, 211–234, https://doi.org/10.1016/j.quascirev.2017.01.004, 2017.

Giaccio, B., Leicher, N., Mannella, G., Monaco, L., Regattieri, E., Wagner, B., Zanchetta, G., Gaeta, M., Marra, F., Nomade, S., Palladino, D. M., Pereira, A., Scheidt, S., Sottili, G., Wonik, T., Wulf, S., Zeeden, C., Ariztegui, D., Cavinato, G. P., Dean, J. R., Florindo, F., Leng, M. J., Macrì, P., Niespolo, E., Renne, P. R., Rolf, C., Sadori, L., Thomas, C., and Tzedakis, P. C.: Extending the tephra and palaeoenvironmental record of the Central Mediterranean back to 430 ka: A new core from Fucino Basin, central Italy, Quaternary Sci. Rev., 225, 106003, https://doi.org/10.1016/j.quascirev.2019.106003, 2019.

Giraudi, C. and Giaccio, B.: Middle Pleistocene glaciations in the Apennines, Italy: new chronological data and preservation of the glacial record, Geological Society, London, Special Publications, 433, 161–178, https://doi.org/10.1144/SP433.1, 2015.

Guillermic, M., Misra, S., Eagle, R., and Tripati, A.: Atmospheric CO_2 estimates for the Miocene to Pleistocene based on foraminiferal $\delta^{11}B$ at Ocean Drilling Program Sites 806 and 807 in the Western Equatorial Pacific, Clim. Past, 18, 183–207, https://doi.org/10.5194/cp-18-183-2022, 2022.

Haywood, A. M., Dowsett, H. J., Valdes, P. J., Lunt, D. J., Francis, J. E., and Sellwood, B. W.: Introduction. Pliocene climate, processes and problems, Philos. T. Roy. Soc. A, 367, 3–17, 2009.

Haywood, A. M., Dowsett, H., and Dolan, A.: Integrating geological archives and climate models for the mid-Pliocene warm period. Nat Commun 7, 10646, https://doi.org/10.1038/ncomms10646, 2016.

Haywood, A. M., Tindall, J. C., Dowsett, H. J., Dolan, A. M., Foley, K. M., Hunter, S. J., Hill, D. J., Chan, W.-L., Abe-Ouchi, A., Stepanek, C., Lohmann, G., Chandan, D., Peltier, W. R., Tan, N., Contoux, C., Ramstein, G., Li, X., Zhang, Z., Guo, C., Nisancioglu, K. H., Zhang, Q., Li, Q., Kamae, Y., Chandler, M. A., Sohl, L. E., Otto-Bliesner, B. L., Feng, R., Brady, E. C., von der Heydt, A. S., Baatsen, M. L. J., and Lunt, D. J.: The Pliocene Model Intercomparison Project Phase 2: large-scale climate features and climate sensitivity, Clim. Past, 16, 2095–2123, https://doi.org/10.5194/cp-16-2095-2020, 2020.

Head, M. J. and Gibbard, P. L.: Early–Middle Pleistocene transitions: linking terrestrial and marine realms, Quatern. Int., 389, 7–46, 2015.

Hodell, D. A., Channell, J. E., Curtis, J. H., Romero, O. E., and Röhl, U.: Onset of "Hudson Strait" Heinrich events in the eastern North Atlantic at the end of the middle Pleistocene transition (~ 640 ka)?, Paleoceanography, 23, PA4218, https://doi.org/10.1029/2008PA001591, 2008.

Hodell, D. A., Abrantes, F., Alvarez Zarikian, C. A., and the Expedition 397 Scientists: Expedition 397 Preliminary Report: Iberian Margin Paleoclimate. International Ocean Discovery Program, https://doi.org/10.14379/iodp.pr.397.2023, 2023a.

Hodell, D. A., Crowhurst, S. J., Lourens, L., Margari, V., Nicolson, J., Rolfe, J. E., Skinner, L. C., Thomas, N. C., Tzedakis, P. C., Mleneck-Vautravers, M. J., and Wolff, E. W.: A 1.5-million-year record of orbital and millennial climate variability in the North Atlantic, Clim. Past, 19, 607–636, https://doi.org/10.5194/cp-19-607-2023, 2023b.

Jouzel, J., Masson-Delmotte, V., Cattani, O., Dreyfus, G., Falourd, S., Hoffmann, G., Minster, B., Nouet, J., Barnola, J. M., Chappellaz, J., Fischer, H., Gallet, J. C., Johnsen, S., Leuenberger, M., Loulergue, L., Luethi, D., Oerter, H., Parrenin, F., Raisbeck, G., Raynaud, D., Schilt, A., Schwander, J., Selmo, E., Souchez, R., Spahni, R., Stauffer, B., Steffensen, J. P., Stenni, B., Stocker, T. F., Tison, J. L., Werner, M., and Wolff, E. W.: Orbital and millennial Antarctic climate variability over the past 800,000 years, Science, 317, 793–796, 2007.

Leicher, N., Giaccio, B., Pereira, A., Nomade, S., Monaco, L., Mannella, G., Galli, P., Peronance, E., Palladino, D. M., Sottili, G., Zanchetta, G., and Wagner, B.: Central Mediterranean tephrochronology between 313 and 366 ka: New insights from the Fucino palaeolake sediment succession, Boreas, 52, 240–271, 2023.

Leicher, N., Monaco, L., Giaccio, B., Nomade, S., Pereira, A., Mannella, G., Wulf, S., Sottili, G., Palladino, D., Zanchetta, G., and Wagner, B.: Central Mediterranean tephrochronology for the time interval 250–315 ka derived from the Fucino sediment succession, Boreas, 53, 164–185, https://doi.org/10.1111/bor.12637, 2024.

Lionello, P., Malanotte-Rizzoli, P., Boscolo, R., Alpert, P., Artale, V., Li, L., Luterbacher, J., May, W., Trigo, R., Tsimplis, M., Ulbrich, U., and Xoplaki, E.: The Mediterranean climate: an overview of the main characteristics and issues, Developments in Earth and Environmental Sciences, 4, 1–26, https://doi.org/10.1016/S1571-9197(06)80003-0, 2006.

Lisiecki, L. E. and Raymo, M. E.: A Pliocene-Pleistocene stack of 57 globally distributed benthic δ^{18}O records, Paleoceanography 20, PA1003, https://doi.org/10.1029/2004PA001071, 2005.

Lisiecki, L. E. and Raymo, M. E.: Plio–Pleistocene climate evolution: trends and transitions in glacial cycle dynamics, Quaternary Sci. Rev., 26, 56–69, 2007.

Mancinelli, P., Scisciani, V., Patruno, S., and Minelli, G.: Gravity modelling reveals a Messinian foredeep depocenter beneath the intermontane Fucino Basin (Central Apennines), Tectonophysics, 821, 229144, https://doi.org/10.1016/j.tecto.2021.229144, 2021.

Mannella, G., Giaccio, B., Zanchetta, G., Regattieri, E., Niespolo, E. M., Pereira, A., Renne, P. R., Nomade, S., Leicher, N., Perchiazzi, N., and Wagner, B.: Palaeoenvironmental and palaeohydrological variability of mountain areas in the central Mediterranean region: A 190 ka-long chronicle from the independently dated Fucino palaeolake record (central Italy), Quaternary Sci. Rev., 210, 190–210, 2019.

McManus, J. F., Oppo, D. W., and Cullen, J. L.: A 0.5-million-year record of millennial-scale climate variability in the North Atlantic, Science, 283, 971–975, 1999.

Melles, M., Brigham-Grette, J., Minyuk, P. S., Nowaczyk, N. R., Wennrich, V., DeConto, R. M., Anderson, P. M., Andreev, A. A., Coletti, A., Cook, T. L., Haltia-Hovi, E., Kukkonen, M., Lozhkin, A. V., Rosén, P., Tarasov, P., Vogel, H., and Wagner, B.: 2.8 million years of Arctic climate change from Lake El'gygytgyn, NE Russia, Science, 337, 315–320, 2012.

Milankovitch, M. R.: Canon of Insulation and the ice-Age Problem, Serb. Acad. Special Publ. 132, Belgrade, 1941.

Miller, K. G., Browning, J. V., Schmelz, W. J., Kopp, R. E., Mountain, G. S., and Wright, J. D.: Cenozoic sea-level and cryospheric evolution from deep-sea geochemical and continental margin records, Science Advances, 6, eaaz1346, https://doi.org/10.1126/sciadv.aaz1346, 2020.

Monaco, L., Palladino, D. M., Gaeta, M., Marra, F., Sottili, G., Leicher, N., Mannella, G., Nomade, S., Pereira, A., Regattieri, E., Wagner, B., Zanchetta, G., Albert, P. G., Arienzo, I., D'Antonio, M., Petrosino, P., Manning, C. J., and Giaccio, B.: Mediterranean tephrostratigraphy and peri-Tyrrhenian explosive activity reevaluated in light of the 430–365 ka record from Fucino Basin (central Italy), Earth-Sci. Rev., 220, 103706, https://doi.org/10.1016/j.earscirev.2021.103706, 2021.

Monaco, L., Leicher, N., Palladino, D. M., Arienzo, I., Marra, F., Petrelli, M., Nomade, S., Pereira, A., Sottili, G., Conticelli, S., D'Antonio, M., Fabbrizio, A., Jicha, B. R., Mannella, G., Petrosino, P., Regattieri, E., Tzedakis, P. C., Wagner, B., Zanchetta, G., and Giaccio, B.: The Fucino 250–170 ka tephra record: New insights on peri-Tyrrhenian explosive volcanism, central mediterranean tephrochronology, and timing of the MIS 8-6 climate variability, Quaternary Sci. Rev., 296, 107797, https://doi.org/10.1016/j.quascirev.2022.107797, 2022.

Naafs, B. D. A., Hefter, J., and Stein, R.: Millennial-scale ice rafting events and Hudson Strait Heinrich (-like) Events during the late Pliocene and Pleistocene: a review, Quaternary Sci. Rev., 80, 1–28, 2013.

Patacca, E., Scandone, P., Di Luzio, E., Cavinato, G., and Parotto, M.: Structural architecture of the central Apennines: interpretation of the CROP 11 seismic profile from the Adriatic coast to the orographic divide, Tectonics, 27, TC3006, https://doi.org/10.1029/2005TC001917, 2008.

Patruno, S. and Scisciani, V.: Testing normal fault growth models by seismic stratigraphic architecture: The case of the Pliocene-

Quaternary Fucino Basin (Central Apennines, Italy), Basin Res., 33, 2118–2156, https://doi.org/10.1111/bre.12551, 2021.

Ravelo, A. C., Andreasen, D. H., Lyle, M., Olivarez Lyle, A., and Wara, M. W.: Regional climate shifts caused by gradual global cooling in the Pliocene epoch, Nature, 429, 263–267, 2004.

Raymo, M. E., Ganley, K., Carter, S., Oppo, D. W., and McManus, J.: Millennial-scale climate instability during the early Pleistocene epoch, Nature, 392, 699–702, 1998.

Regattieri, E., Giaccio, B., Zanchetta, G., Drysdale, R.N., Galli, P., Nomade, S., Peronace, E., and Wulf, S.: Hydrological variability over the Apennines during the Early Last Glacial precession minimum, as revealed by a stable isotope record from Sulmona basin, Central Italy, J. Quaternary Sci., 30, 19–31, 2015.

Regattieri, E., Giaccio, B., Galli, P., Nomade, S., Peronace, E., Messina, P., Sposato, A., Boschi, C., and Gemelli, M.: A multiproxy record of MIS 11–12 deglaciation and glacial MIS 12 instability from the Sulmona Basin (central Italy), Quaternary Sci. Rev., 30, 19–31, 2016.

Regattieri, E., Giaccio, B., Mannella, G., Zanchetta, G., Nomade, S., Tognarelli, A., Perchiazzi, N., Vogel, H., Boschi, C., Drysdale, R.N., Wagner, B., Gemelli, M., and Tzedakis, P.: Frequency and dynamics of millennial-scale variability during Marine Isotope Stage 19: Insights from the Sulmona Basin (central Italy), Quaternary Sci. Rev., 214, 28–43, 2019.

Ronge, T. A., Nürnberg, D., and Tiedemann, R.: Plio-Pleistocene Variability of the East Pacific Thermocline and Atmospheric Systems, Paleoceanography and Paleoclimatology, 35, e2019PA003758, https://doi.org/10.1029/2019PA003758, 2020.

Sadori, L., Koutsodendris, A., Panagiotopoulos, K., Masi, A., Bertini, A., Combourieu-Nebout, N., Francke, A., Kouli, K., Joannin, S., Mercuri, A. M., Peyron, O., Torri, P., Wagner, B., Zanchetta, G., Sinopoli, G., and Donders, T. H.: Pollen-based paleoenvironmental and paleoclimatic change at Lake Ohrid (south-eastern Europe) during the past 500 ka, Biogeosciences, 13, 1423–1437, https://doi.org/10.5194/bg-13-1423-2016, 2016.

Shackleton, N. J., Hall, M. A., and Vincent, E.: Phase relationships between millennial-scale events 64,000–24,000 years ago, Paleoceanography, 15, 565–569, 2000.

Skelton, A., Andrén, M., Kristmannsdóttir, H., Stockmann, G., Mörth, C.-M., Sveinbjörnsdóttir, Á., Jónsson, S., Sturkell, E., Guðrúnardóttir, H. R., Hjartarson, H., Siegmund, H., and Kockum, I.: Changes in groundwater chemistry before two consecutive earthquakes in Iceland, Nat. Geosci., 7, 752–756, 2014.

Stap, L. B., de Boer, B., Ziegler, M., Bintanja, R., Lourens, L. J., and van de Wal, R. S.: CO_2 over the past 5 million years: Continuous simulation and new δ^{11}B-based proxy data, Earth Planet. Sc. Lett., 439, 1–10, 2016.

Tzedakis, P. C., Drysdale, R. N., Margari, V., Skinner, L. C., Menviel, L., Rhodes, R. H., Taschetto, A. S., Hodell, D. A., Crowhurst, S. J., Hellstrom, J. C., Fallick, A. E., Grimalt, J. O., McManus, J. F., Martrat, B., Mokeddem, Z., Parrenin, F., Regattieri, E., Roe, K., and Zanchetta, G.: Enhanced climate instability in the North Atlantic and southern Europe during the Last Interglacial, Nat. Commun., 9, 1–14, 2018.

Vera-Polo, P., Sadori, L., Jiménez-Moreno G., Masi, A., Giaccio, B., Zanchetta, G., and Tzedakis, P. C.: Wagner, B. Climate, vegetation, and environmental change during the MIS 12-MIS 11 glacial-interglacial transition deduced from a high-resolution pollen analysis from the Fucino Basin, Palaeogeogr. Palaeocl., 655, 112486, https://doi.org/10.1016/j.palaeo.2024.112486, 2024

Westerhold, T., Marwan, N., Drury, A. J., Liebrand, D., Agnini, C., Anagnostou, E., Barnet, J. S. K., Bohaty, S. M., De Vleeschouwer, D., Florindo, F., Frederichs, T., Hodell, D. A., Holbourn, A. E., Kroon, D., Lauretano, V., Littler, K., Lourens, L. J., Lyle, M., Pälike, H., Röhl, U., Tian, J., Wilkens, R. H., Wilson, P. A., and Zachos, J. C.: An astronomically dated record of Earth's climate and its predictability over the last 66 million years, Science, 369, 1383–1387, 2020.

Wilke, T., Hauffe, T., Jovanovska, E., Cvetkoska, A., Donders, T., Ekschmitt, K., Francke, A., Lacey, J. H., Levkov, Z., Marshall, C. R., Neubauer, T. A., Silvestro, D., Stelbrink, B., Vogel, H., Albrecht, C., Holtvoeth, J., Krastel, S., Leicher, N., Leng, M. J., Lindhorst, K., Masi, A., Ognjanova-Rumenova, N., Panagiotopoulos, K., Reed, J. M., Sadori, L., Tofilovska, S., Van Bocxlaer, B., Wagner-Cremer, F., Wesselingh, Frank P., Wolters, V., Zanchetta, G., Zhang, X., and Wagner, B.: Deep drilling reveals massive shifts in evolutionary dynamics after formation of ancient ecosystem, Science Advances, 6, eabb2943, https://doi.org/10.1126/sciadv.abb2943, 2020.

Williams, D. F., Peck, J., Karabanov, E. B., Prokopenko, A. A., Kravchinsky, V., King, J., and Kuzmin, M. I.: Lake Baikal record of continental climate response to orbital insolation during the past 5 million years, Science, 278, 1114–1117, 1997.